COMBUSTION
AND
FLAME

QUARTERLY JOURNAL OF THE COMBUSTION INSTITUTE

VOLUME III

Editor-in-Chief
SIR ALFRED EGERTON

Editor
BERNARD LEWIS (U.S.A.)

Editorial Board

L. Deffet (BELGIUM)
W. Jost (GERMANY)
P. Laffitte (FRANCE)
J. W. Linnett (U.K.)
P. Lloyd (U.K.)
J. P. Longwell (U.S.A.)
F. E. Marble (U.S.A.)
W. T. Olson (U.S.A.)
D. T. A. Townend (U.K.)
S. Yagi (JAPAN)
E. F. M. van der Held (NETHERLANDS)

LONDON
BUTTERWORTHS SCIENTIFIC PUBLICATIONS
1959

COMBUSTION & FLAME

Quarterly Journal of The Combustion Institute

Editorial Professor Ubbelohde's Editorial of a year ago ended by conveying good wishes for the service that this Journal could give to 'a very ancient but still very lively branch of science'. We regret that owing to pressure of other work he could not carry on as Editor for this side of the Atlantic but are grateful for the good start that he has given to the Journal.

An Editor is much concerned with 'material-in-hand'. The early part of last year was a lean period: authors were busily preparing papers for the Seventh Symposium of the Combustion Institute which was held in London and Oxford, 27 August to 3 September. There were some papers which did not come within the scope of the Symposium discussions, and so some of these were added to the 'material-in-hand' for the Institute's Journal instead of the Symposium Volume. This helped the Editor to maintain the flow of original papers published in the Journal without having recourse to more review articles than are desirable. An occasional review article, however, can be very useful. The tide has now turned and until the next Symposium is imminent, there will no doubt be plenty of good 'material-in-hand', and the Editor will endeavour to keep publication delay as short as possible. The Eighth Symposium is to be held in September 1960 in Pasadena.

The Institute's Journal is becoming the main international channel for publication of original scientific work in the field of combustion and allied subjects. Slightly more than half the papers published last year came from the U.S.A. and contributions have come from Canada and France as well as Great Britain. The Editor also welcomes the Letters received for publication, another feature which has increased during the year. He takes the opportunity to thank Dr W. A. Kirkby for continuing to supply the columns apportioned to 'Recent Developments and Notes' which are much appreciated by readers of the Journal. The Editors believe that the Journal is providing members of the Combustion Institute with information as well as being the means by which original work can be published and they will therefore be glad to receive notice of forthcoming meetings and other items of combustion interest for prompt insertion in the Journal.

The main event in the past year was the Symposium, and we were glad to publish immediately in the September issue the brief summary of the discussions, prepared by G. J. Minkoff and his collaborators, particularly for the information of those who were not able to participate. The Symposium volume is expected next month; the issue of preprints of the papers to those attending the Symposium has made it easier to publish the volume without too much delay. The Symposia volumes collect together

04902

original papers on selected aspects of combustion science and if they are to serve their purpose there should be as little delay in publication as possible. Some may incline to the view that the function of a symposium is to provide a forum for exchange of views and discussion of 'growth boundaries' of the science and that current research work should be published mainly through the normal channels, such as in this Journal: others emphasize the importance of the Symposia volumes as a convenient and continuing compendium of information summarizing the progress of the subject. At present, owing greatly to the initiative of Dr BERNARD LEWIS the subject is very much better served than it used to be in regard to means of publication. It needs to be, for the interests are very wide throughout industry as well as in many branches of science. Original work in the field of combustion still appears in quite a wide range of journals and it would surely be more convenient for workers in the field if the scatter were not so wide. The Journal of the Institute and the Symposia volumes could well become the main channel, thereby making it easier to gather the threads of information which together weave the fabric of knowledge.

The tools now available are making a great impact on the progress of understanding of the processes of combustion. The mass spectrograph and gas chromatography replace speculation by fact in the study of the products formed during oxidation of hydrocarbons and other substances. Even the rapid reactions preceding inflammation can be investigated. Optical methods, however, continue to be highly effective in providing information not only about laminar flame propagation but also for the examination of shock waves and detonation phenomena.

During the past year, there were several papers in the Journal which illustrate the importance of the tools. There was, for example, C. R. YOKLEY and R. E. FERGUSON's paper on the cool flame oxidation of propane in which gas chromatography has sorted out the eighteen or so products formed. A good example of the value of optical methods is found in the paper by W. E. KASKAN on 'hydroxyl concentrations in rich hydrogen–air flames held on porous burners'. There will no doubt be many more papers during the coming year which will illustrate the harvesting of information by the newer methods of reaping now available.

A. C. Egerton

Pre-ignition and Ignition Reactions of the Propagatively Reacting System Magnesium–Sodium Nitrate–Laminac

VIRGINIA D. HOGAN and SAUL GORDON

The thermal ignition of the propagatively burning system magnesium–sodium nitrate–Laminac was studied with respect to the thermal parameters of ignition, propagative burning and the reaction mechanisms responsible for these phenomena. Differential thermal analysis, thermogravimetry and determinations of the time to ignition as a function of temperature were employed. On a basis of these experimental data, a mechanism is postulated for the ignition reactions of the ternary system in which the thermal degradation products of the styrenated polyester binder, Laminac, play a decisive role. It is noteworthy that the sodium nitrate decomposes only as far as sodium nitrite when ignition takes place under differential thermal analysis conditions, i.e. at atmospheric pressure and under no confinement.

THE system 54 per cent magnesium–36 per cent sodium nitrate–10 per cent Laminac approximates an empirically developed standard pyrotechnic illuminant composition[1]. In this investigation, the thermal ignition of this propagatively burning system was studied with respect to the thermal parameters of ignition, propagative burning and the reaction mechanisms responsible for these phenomena. The experimental techniques of differential thermal analysis (DTA), thermogravimetry and determinations of the time to ignition as a function of temperature were used to examine various binary and ternary mixtures of magnesium, sodium nitrate, Laminac and a carbonaceous residue obtained from the pyrolysis of Laminac. This approach was suggested by previous thermoanalytical studies of propagatively reacting systems[2, 3]. Differential thermal analyses furnish data relative to the absorption or evolution of heat as a result of any physicochemical reaction characteristic of the sample under study, while thermogravimetric curves yield data concerning any physical or chemical reactions that are accompanied by weight changes. The experimental values of the time to ignition were used to calculate an energy of activation for ignition. On a basis of the experimental data, a mechanism is postulated for the ignition reactions of the system.

EXPERIMENTAL

Reagents

Sodium nitrate, analytical reagent grade (Mallinckrodt Chemical Works) average particle size, 62 microns; atomized magnesium, 98·0 per cent free metallic magnesium[1] (Golwynne Chemical Co.) average particle size, 160 microns; Laminac 4116, a polyester resin crosslinked with styrene (American Cyanamid Co.); and carbon obtained as a solid black residue when polymerized Laminac was heated at 450°C in a muffle furnace.

Approximately 50 g of each composition investigated was prepared from the weighed ingredients; samples for individual determinations were taken from the bulk supply. These compositions are listed in *Table 1*.

Table 1

Class	*Percentage composition*			
	Mg	$NaNO_3$	*Laminac*	*Carbon*
Binaries	(I) 22·2†	77·8	—	—
	(II) 60 *	40	—	—
	84·4*	—	15·6	—
	—	87·6‡	—	12·4
	—	78·3*	21·7	—
Ternaries	11·8§	82·4	—	5·8
	54 *	36	10	—

*As in the item.
†Stoichiometric for $Mg+NaNO_3 \rightarrow MgO+NaNO_2$.
‡Stoichiometric for $NaNO_3+C \rightarrow NaNO_2+CO$.
§Stoichiometric for $Mg+2NaNO_3+C \rightarrow MgO+CO+2NaNO_2$.

Apparatus and procedures

Thermogravimetry consists of continuously weighing a sample as it is heated at a constant temperature or to elevated temperatures at a constant rate so that weight changes are continuously recorded as a function of time or temperature. The apparatus and procedures employed have been described[3]. Only the individual ingredients were studied by this technique due to the possibility of damage to the balance resulting from a sudden ignition. DTA involves heating the sample under study together with a thermally inert reference material to elevated temperatures at a constant rate while continuously recording the temperature difference between them as a function of sample temperature or time. The time-base apparatus was described by S. GORDON and C. CAMPBELL[5], while the temperature-base apparatus was described by V. HOGAN, S. GORDON and C. CAMPBELL[6]. A nominal heating rate of 15°C per minute was used consistently. The reaction temperatures obtained by these techniques agree within five degrees. Measurements of the time to ignition as a function of temperature were used to determine the thermal parameters of the propagative ignition for the four binary fuel–oxidant and the two ternary mixtures. The method and apparatus have been described[2]*.

RESULTS AND DISCUSSIONS

Since thermogravimetric curves are quantitative representations of weight changes, they can be related to the chemical and physical changes taking place in a sample as it is heated and can often be used to determine the nature of the products. These studies show that all three ingredients undergo thermal reactions involving weight changes. The thermogravimetric curves which plot weight change in milligrammes as a function of furnace temperature in degrees centigrade are illustrated in *Figure 1*. Sodium nitrate exhibits a weight loss from 700° to 1 000°C which corresponds to complete conversion to sodium oxide. The curve also shows a point of inflection at about 850°C due to the concurrent decomposition of the intermediate product, sodium nitrite. Magnesium shows a continuous gain in weight which begins at about 625°C and continues on past the maximum temperature. The curve varies in slope, becoming perceptibly steeper at 650°C and markedly less steep at 680°C. This weight gain is attributed to the successive formation of magnesium nitride and magnesium oxide. Polymerized Laminac first shows a continuous weight loss extending from about 100° to 500°C which markedly changes in slope at 350°C. This loss is followed by another loss ending at 625°C which represents a loss in weight equivalent to the initial weight of the sample. It has been confirmed that the polymer is thermally degraded to carbon which is completely oxidized[5].

---

*All the experimental determinations were made in air at ambient pressure.

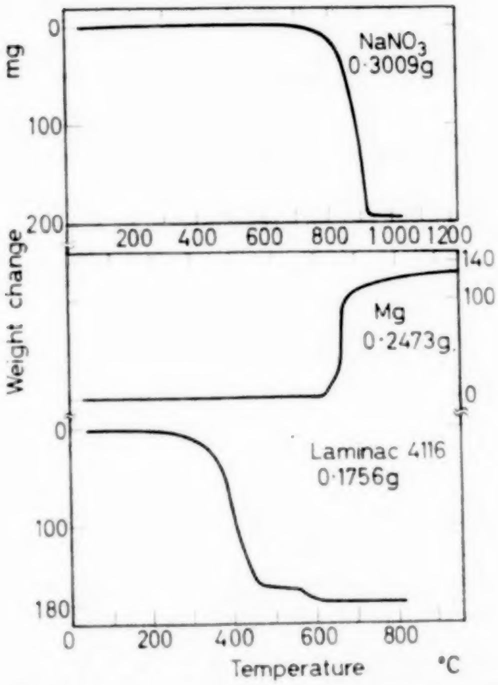

Figure 1. Thermogravimetric curves for ingredients sodium nitrate, magnesium and Laminac

Differential thermal analyses were run on the ingredients and all of the mixtures, with differential temperature plotted on the ordinate and sample temperature or time on the abscissa. The zero of differential temperature is placed at the centre of the record so that exothermal reactions are plotted as upward deflections and endothermal reactions are plotted as downward deflections. For the samples run on a time base, the vertical lines crossing the curves at one minute intervals are reference timing marks and the deflections are curvilinear because of the construction of the recorder.

The DTA curves for the ingredients are illustrated in *Figure 2*. The only thermal effects exhibited by sodium nitrate are endothermic crystalline transition at 270°C immediately followed by endothermic fusion at 308°C. The differential thermogram of magnesium shows a double exothermic peak beginning at about 565°C which may be due to the formation of magnesium nitride or magnesium oxide on the surface of the metal, or to reaction with the glass tube. The double peak culminates in the endothermic fusion of magnesium. The DTA curve of polymerized Laminac displays only one broad endothermic band beginning at about 250°C with a peak temperature of 371°C. However, it appears as though several overlapping reactions are responsible for the heat absorption. At 305°C, a colourless liquid condenses on the upper part of the sample tube. At 332°C, a pale yellow liquid is observed refluxing with sparse white fumes. At 366°C, there are dense white fumes escaping from the tube. At 479°C, after the endotherm is over, the sample gives off dense yellow fumes and some charring is observed in the tube.

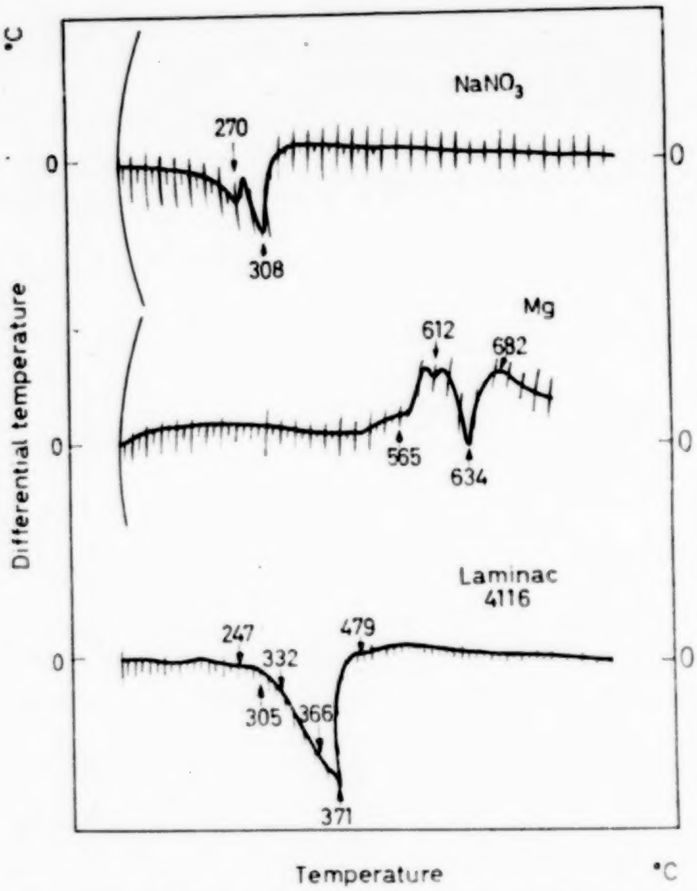

Figure 2. DTA curves for ingredients sodium nitrate, magnesium and Laminac

As shown in *Figure 3*, the binary fuel mixture magnesium–Laminac gives DTA evidence of the thermal decomposition of the Laminac present by several shallow endotherms prior to the sharply endothermic fusion of magnesium. The magnesium fusion endotherm is followed by an exothermal reaction, probably the oxidation of molten magnesium. The absence of any exothermal peak prior to magnesium fusion suggests that, although the Laminac does not react with the bulk of the metal, it protects the solid magnesium from reaction with air. The four binary fuel–oxidant mixtures ignite. For all the ignitable sodium nitrate compositions run on the time-base apparatus, the endotherms corresponding to the crystalline transition of sodium nitrate are very small because only very small samples were used. The fuel rich system 60–40 magnesium–sodium nitrate, curve II, used in the items ignites at 560°C. The DTA curve shows the endothermic crystalline transition of sodium nitrate at 265°C and its fusion at 305°C in addition to the sharply exothermic ignition. The stoichiometric mixture, curve I, for the reaction $Mg + NaNO_3 = MgO + NaNO_2$, containing only 22 per cent magnesium, ignites at 613°C and displays endotherms at 270° and 310°C which are caused by the crystalline transition and fusion of sodium nitrate, respectively. Sodium nitrate–Laminac ignites with an apparently small evolution of heat at 417°C that may be due to a combination of small sample size and formation of gaseous products. The differential thermogram exhibits the crystalline transition of sodium nitrate at 268° and its fusion at 297°C. A broad, shallow endotherm, during which a colourless, and then a yellow liquid condense on the sample tube, culminates in ignition. The sodium nitrate–carbon system exhibits the crystalline transition of sodium nitrate successively followed by sodium nitrate fusion and then ignition at 467°C.

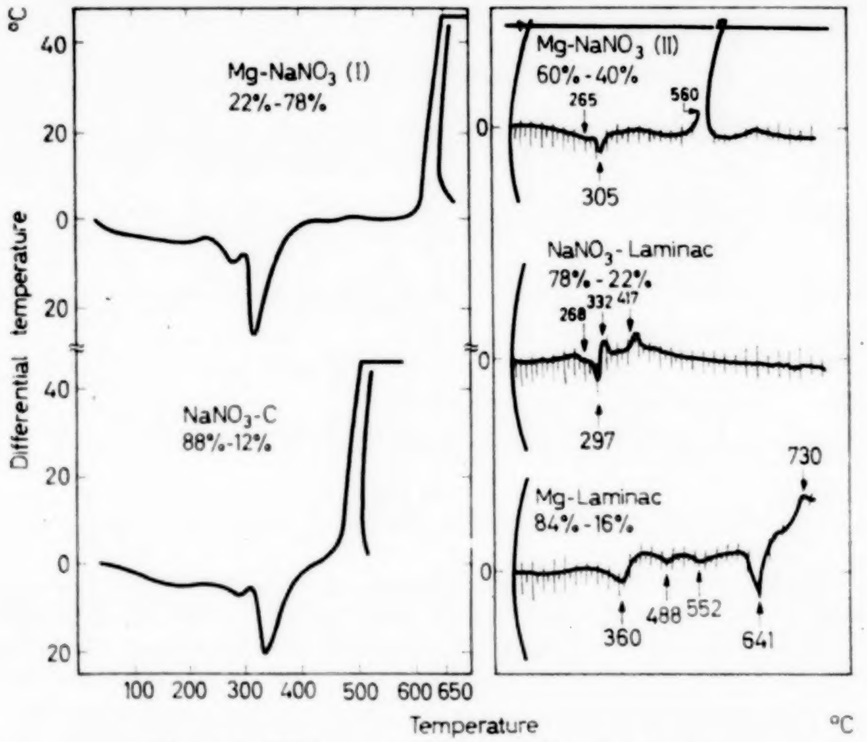

Figure 3. DTA curves for the five binary mixtures

DTA curves for the two ternary compositions are shown in ***Figure 4***. The mixture containing magnesium, sodium nitrate, and carbon is very similar to the sodium nitrate–carbon binary mixture; that is, it ignites at 455°C immediately following the crystalline transition and fusion of the sodium nitrate. The mixture containing magnesium–sodium nitrate–Laminac ignites at 489°C. The first thermal phenomena observed are the crystalline transition and fusion of sodium nitrate at 270°C and 299°C, respectively. There is a small, sharp exothermal reaction beginning at 373°C and another beginning at 450°C with peak temperatures of 405° and 485°C, respectively. Ignition occurs as the system is recovering from the second exothermal reaction.

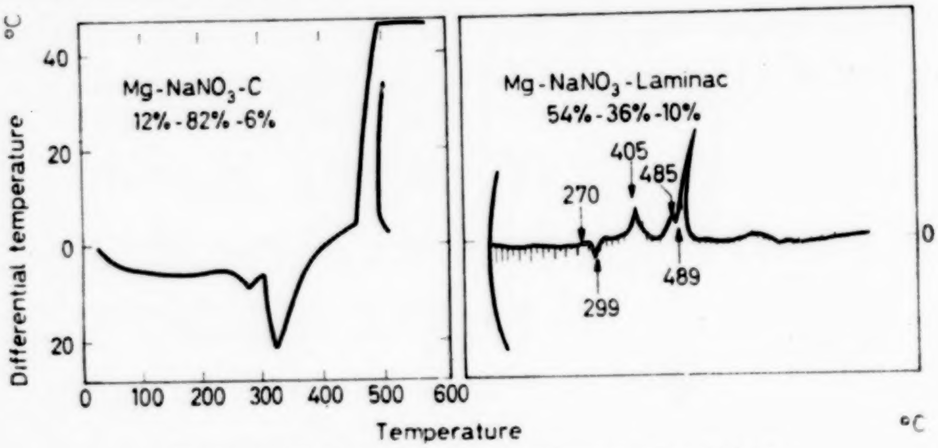

Figure 4. DTA curves for the two ternary compositions

It was not feasible to write pre-ignition or combustion reactions for the systems containing Laminac due to the complexity of the polymer and the uncertainty of its combustion products. Under DTA conditions, it seems most probable that magnesium reacts with sodium nitrate to form magnesium oxide and sodium nitrite, since x-ray examination of solid residues indicates that these are the only products found after ignition. X-Ray examination of solid residues from sodium nitrate–Laminac differential thermal analyses showed only sodium nitrite and unreacted sodium nitrate. It is interesting to note that sodium carbonate, which would be a logical product if Laminac were oxidized to carbon dioxide, was not found. Furthermore, neither sodium oxide nor metallic sodium, products found when sodium nitrate is ignited with a fuel in a closed bomb, were detected in any of these residues. From the DTA and thermogravimetric data we can conclude that ignition occurs between molten sodium nitrate and either solid magnesium in the absence of Laminac, or thermal degradation products of Laminac whenever it is present. This is analogous to the pre-ignition and ignition behaviour of the magnesium–barium peroxide–calcium resinate system[3].

Thermal parameters for ignition can be discussed quantitatively in terms of the time to ignition for the various ignitable compositions as a function of the temperature at which the ignition takes place. ΔE_a, the energy of activation for ignition, is the amount of energy required to raise a mole of the system in its ignition temperature range to a point where it will initiate a propagative reaction. ΔE_a can be calculated from these data, assuming that the time to ignition is reciprocally related to the specific reaction rate of the limiting ignition reaction in the Arrhenius rate equation[2].

A plot of the logarithm of the time to ignition versus the reciprocal of the absolute temperature at which the ignition takes place should give a straight line of slope $\Delta E_a/2{\cdot}3R$ and intercept B/A, where B/A is a constant and R is the universal gas constant.

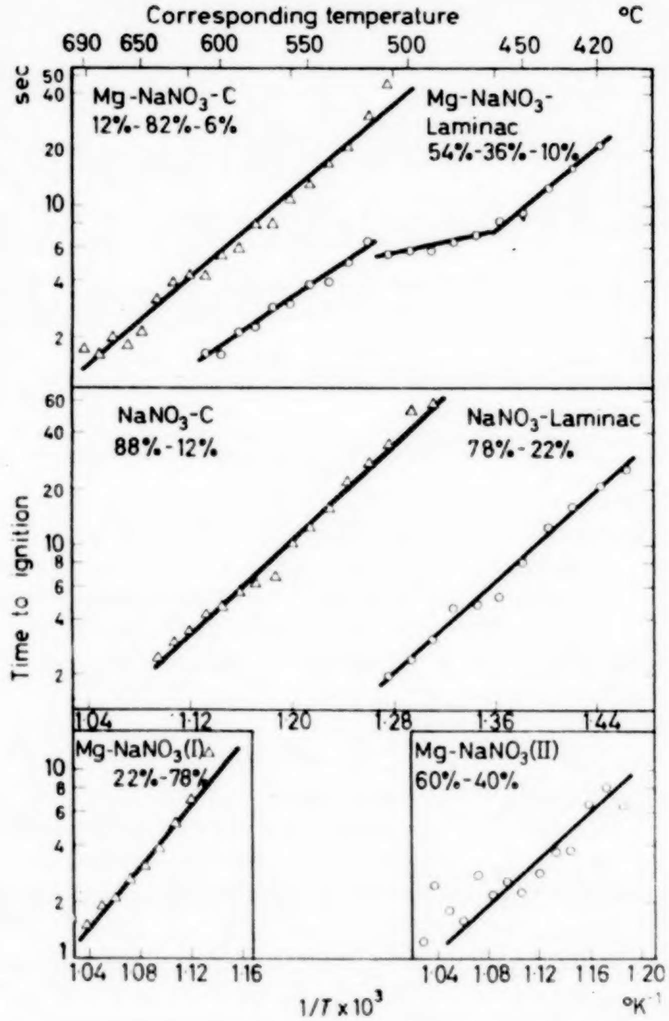

Figure 5. Ignition time/temperature plots for six ignitable compositions

Figure 5 shows these curves for the six ignitable compositions. On the basis of these experimental data*, it was concluded that the thermal degradation products of Laminac determine the ignition parameters for compositions containing this organic material. Within the temperature range 410° to 510°C, some initial degradation product or products of Laminac other than carbon react propagatively with sodium nitrate producing a system which has a single energy of activation for ignition of 28 kcal/mole. This material is not the black carbonaceous residue obtained

---

*Summarized in *Table 2*.

by heating polymerized Laminac to 450°C in a muffle furnace, since a mixture of this residue and sodium nitrate, although it has a similar activation energy, 29 kcal/mole, doesn't begin to ignite until the temperature reaches 490°C. When magnesium is present, the Arrhenius plot for the ternary composition containing the carbonized residue shows that ignition occurs over essentially the same temperature range, 500° to 700°C, as for the sodium nitrate–carbon system, with a similar activation energy, 26 kcal/mole. However, the metal-rich ternary composition containing Laminac is more complex. In the temperature range 420° to 460°C, ignition must be due to an initial thermal degradation product of Laminac not carbon, since the sodium nitrate–Laminac mixture is the only other system which ignites in this temperature range. Furthermore, the activation energies for the two systems are similar, viz. 25 kcal/mole for the ternary composition and 28 kcal/mole for sodium nitrate–Laminac. The region 470° to 510°C seems to be one of transition, since the apparent value of 7 kcal/mole for the activation energy for ignition is quite low for a chemical reaction. Activation energies of this order of magnitude are usually found in cases where the rate-controlling step is a physical process such as surface diffusion. In the temperature range 520° to 610°C, another decomposition product of Laminac seems to be responsible for the propagative reaction, with an activation energy of 20·5 kcal/mole. The ignition temperature range is similar to that observed with carbonized Laminac compositions but the activation energy for ignition in this ternary composition is significantly lower than that of both the sodium nitrate–carbon system and the magnesium–sodium nitrate–carbon system, 29 and 26 kcal/mole, respectively. These different reactions exhibited by the ternary system in the two higher temperature regions may be due to products formed by the thermal degradation of Laminac in the presence of magnesium.

Table 2.

Composition	*Ignition temperature range (°C)*	ΔE_a *(kcal/mole)*	*Intercept value B/A (sec)*
Mg–$NaNO_3$ *I* (22–78)	600 *to* 690	37	$0{\cdot}51 \times 10^{-8}$
Mg–$NaNO_3$ *II* (60–40)	570 *to* 700	28	40×10^{-8}
Mg–$NaNO_3$*	570 *to* 630	32	$6{\cdot}4 \times 10^{-8}$
$NaNO_3$–C	490 *to* 640	29	19×10^{-8}
$NaNO_3$–*Laminac*	410 *to* 510	28	$3{\cdot}2 \times 10^{-8}$
Mg–$NaNO_3$–C	500 *to* 700	26	160×10^{-8}
Mg–$NaNO_3$–*Laminac*	420 *to* 460	25	23×10^{-8}
	470 *to* 510	7	71×10^{-3}
	520 *to* 610	20·5	12×10^{-6}

*Taken from results reported by E. S. FREEMAN and S. GORDON'.

It was not within the scope of this study to investigate the ignition reactions of the decomposition products of Laminac. Laminac 4116 resin is a complex polyester containing phthallic acid, maleic acid and propylene glycol, crosslinked with styrene. That a great number of degradation products are obtained from the pyrolysis in air of such a complex material has been substantiated by a kinetic study of the thermal decomposition of Laminac[7]. The derivative thermogravimetric plot, *Figure 6*, indicates that there are three main reaction zones in the thermal decomposition of Laminac 4116 in air. The major reaction occurs from 275° to 450°C, with smaller reactions occurring before and after it. The major reaction zone corresponds to the largest weight loss seen on the thermogravimetric curve. The last reaction, which is the oxidation of carbon, occurs at a lower temperature in the kinetic study because a much slower heating rate than that used in this investigation was employed.

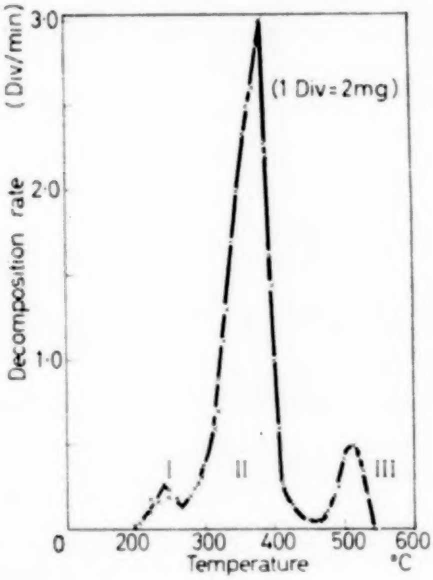

Figure 6. Kinetic study plot for thermal decomposition of Laminac in air

The temperature range and activation energies observed for the metal–oxidant systems indicate that they play little, if any, part in the ignition of the ternary compositions. The mixture containing 22 per cent magnesium, *Figure 5*, curve I, ignites at temperatures from 600° to 690°C with an activation energy of 37 kcal/mole; in contrast to an ignition temperature range of 500° to 700°C and an activation energy of 26 kcal/mole for the ternary composition magnesium–sodium nitrate–carbon which contains a comparable amount of magnesium. The metal-rich binary system, II, ignites very erratically over a temperature range of 570° to 700°C with an activation energy of 28 kcal/mole, calculated from the line shown. This is in contrast to the high ignition temperature region of the metal-rich ternary composition magnesium–sodium nitrate–Laminac which extends from 520° to 610°C and has an activation energy for ignition of 20·5 kcal/mole. The extremely erratic behaviour of this binary system, 60–40 magnesium–sodium nitrate, is probably due to the large particle size (160 microns) and the high percentage of the magnesium. With this large amount of metal present, the coarse fuel particles tend to separate out forming a non-homogeneous mixture of variable composition*.

---

*A calculation of the limiting activity of the powdered metal fuel in the stoichiometric composition, based on the theoretical interpretation previously described[3, 8], shows excellent agreement between the theoretical and experimental values of $0{\cdot}7 \times 10^{-5}$ and $0{\cdot}3 \times 10^{-5}$, respectively.

In conclusion, the combustion of the illuminant composition proceeds via a pre-ignition reaction between molten sodium nitrate and some thermal degradation product of Laminac. This reaction furnishes sufficient heat to ensure ignition and combustion of the magnesium and sodium nitrate which is the light-producing reaction.

Pyrotechnics Chemical Research Laboratory,
Picatinny Arsenal, Dover, N.J.

(*Received June 1958*)

REFERENCES

[1] Nolan, W. J. and Dorfman, H. 'Development of improved illuminant for illuminating shell, 105 mm, M314A1.' *Picatinny Arsenal tech. Rep. No. 2027* (May 1954)

[2] Gordon, S. and Campbell, C. 'Pre-ignition and ignition reactions of the pyrotechnic system zinc–hexachlorobenzene–potassium perchlorate.' *Fifth Symposium (International) on Combustion*, pp 277–284. Reinhold: New York, 1955

[3] Hogan, V. and Gordon, S. 'Pre-ignition and ignition reactions of the system barium peroxide–magnesium–calcium resinate.' *J. phys. Chem.* 61 (1957) 1401

[4] Purchase Description, PA–PD–265, 21 March 1953. 'Powders, Metal, Atomized (for use in ammunition).'

[5] Gordon, S. and Campbell, C. 'Differential thermal analysis of inorganic compounds. Nitrates and perchlorates of the alkali and alkaline earth groups and their subgroups.' *Analyt. Chem.* 27 (1955) 1102

[6] Hogan, V., Gordon, S. and Campbell, C. 'Differential thermal analysis and thermogravimetry applied to potassium perchlorate–aluminum–barium nitrate mixtures.' *Analyt. Chem.* 29 (1955) 306

[7] Anderson, D. A. and Freeman, E. S. 'The kinetics of the thermal degradation of the synthetic styrenated polyester, Laminac 4116. *J. appl. Polymer Sci.* 1 (1959) in press.

[8] Freeman, E. S. and Gordon, S. 'The application of the absolute rate theory to the ignition of propagatively reacting systems. The thermal ignition of the systems lithium nitrate–magnesium, sodium nitrate–magnesium.' *J. phys. Chem* 60 (1956) 867

Transition Probability Parameters of Molecular Spectra arising from Combustion Processes

R. W. Nicholls, P. A. Fraser and W. R. Jarmain

The dependence of intensity distributions in molecular spectra upon (a) *source conditions and* (b) *molecular constants (particularly transition probabilities) is discussed briefly. Knowledge of transition probabilities is essential to the interpretation of spectral intensities in terms of source conditions. Arrays of Franck-Condon factors* $q_{v'v''}$, *which are closely related to relative vibrational transition probabilities,* $p_{v'v''}$, *have been computed upon a Morse model and are presented for a comprehensive range of band systems of significance in combustion processes for the molecules* C_2, CN, B_2, BO, BH, BN, OH, O_2, NO, PbO. *Where available, values of smoothed relative vibrational transition probabilities* $p_{v'v''}$ *and band intensities at infinite temperatures* $I_{\infty v'v''}$ *are also given.*

DURING the past decade the *qualitative* aspects of combustion spectroscopy, which are primarily concerned with identification of features in the spectra of luminosities from combustion sources, have been increasingly supplemented by more *quantitative* aspects of spectroscopy by which the physical conditions existing in the luminous gases may be inferred from the intensities of their spectra. This trend is seen in papers of previous combustion symposia and also in the monographs of A. G. GAYDON and H. G. WOLFHARD[1-3].

The experience of astrophysics has been duplicated somewhat in combustion spectroscopy by the increasing recognition of a great lack of oscillator strengths and transition probabilities for important features of combustion spectra. Without such transition probabilities little significant quantitative progress can be made towards the interpretation of intensities of spectra arising from combustion sources in terms of excitation conditions and processes which maintain them.

In this paper therefore relative transition probabilities and related data for molecular band systems which are of importance in combustion have been gathered together. In most cases the data have been newly calculated and for a few systems the information, which had originally been published elsewhere, has been included for the sake of completeness.

In the next section there is a brief discussion of the parameters which control the intensity in emission of molecular bands. The third section presents the results, mostly in tabular form, and in the fourth a brief discussion is given.

INTENSITIES IN MOLECULAR SPECTRA

General concepts

In this section, the factors which control the band intensities (in emission) of molecular electronic spectra will be defined and discussed.

The integrated intensity $I_{v'v''}$ of the v'–v'' molecular electronic band emitted from an optically thin layer of gas is given by

$$I_{v'v''} = K N_{v'} P_{v'v''} E_{v'v''} \quad \ldots.[1]$$

$N_{v'}$ is the concentration of emitting molecules in the upper level v', $P_{v'v''}$ is the transition probability of the v'–v'' transition; that is $N_{v'v''} P_{v'v''}$ is the number of radiative v'–v'' transitions made per second per cubic centimetre. $E_{v'v''}$ is the energy change in the v'–v'' transition and K is a constant which takes account of units and of the detection geometry.

It is well known[1] that

$$P_{v'v''} = (64\pi^4/3h^4c^3) E^3_{v'v''} \left| \int \psi_{v'} R_e(r) \psi_{v''} \, dr \right|^2 \quad \ldots.[2]$$

where the relative vibrational transition probability $p_{v'v''}$ is defined as

$$p_{v'v''} = \left| \int \psi_{v'} R_e(r) \psi_{v''} \, dr \right|^2 \quad \ldots.[3]$$

$\psi_{v'}$ and $\psi_{v''}$ are the vibrational wave functions for the v' and v'' levels respectively. $R_e(r)$ is the electronic transition moment[4] of the transition and r is the internuclear separation.

The customary assumption of approximate constancy of $R_e(r)$ across a band system has been found to be invalid in a significant number of cases (see below). In fact variations across a band system by a factor of 2 have been found in some cases. Using a procedure suggested by P. A. FRASER[5], equation 3 may be rewritten to take account of the variation of electronic transition moment with internuclear separation as follows

$$p_{v'v''} = R_e^2(\bar{r}_{v'v''}) \left| \int \psi_{v'} \psi_{v''} \, dr \right|^2 = R_e^2(\bar{r}_{v'v''}) \, q_{v'v''} \quad \ldots.[4]$$

where

$$q_{v'v''} = \left| \int \psi_{v'} \psi_{v''} \, dr \right|^2 \quad \ldots.[5]$$

and

$$\bar{r}_{v'v''} = \int \psi_{v'} r \psi_{v''} \, dr \Big/ \int \psi_{v'} \psi_{v''} \, dr \quad \ldots.[6]$$

The overlap integral square $q_{v'v''}$ has been called the Franck–Condon factor by D. R. BATES[6] and exerts a dominant influence upon the relative vibrational transition probability and thus upon the distribution of intensity in a band system. The r-centroid $\bar{r}_{v'v''}$ is a unique value of internuclear separation which may be associated with a band and has been discussed fully elsewhere[7].

Equation 1 may then be rewritten as

$$I_{v'v''} = K N_{v'} E^4_{v'v''} p_{v'v''} \quad \ldots.[7]$$

or as

$$I_{v'v''} = K N_{v'} E^4_{v'v''} R_e^2(\bar{r}_{v'v''}) \, q_{v'v''} \quad \ldots.[8]$$

In these equations $I_{v'v''}$ may be assumed to have been measured, $E_{v'v''}$, $p_{v'v''}$, $R_e(r)$, $\bar{r}_{v'v''}$, $q_{v'v''}$ are (in principle) known molecular constants, and $N_{v'}$ is controlled by the physical excitation conditions in the luminous gas.

Thus in principle $N_{v'}$ may be inferred from a knowledge of the other parameters.

Unfortunately ignorance of $p_{v'v''}$, $q_{v'v''}$ and $R_e(r)$ often prevents the unambiguous determination of source conditions from measured intensities. Thus efforts have been made in a number of laboratories during recent years to determine $R_e(r)$ and arrays of $p_{v'v''}$ and $q_{v'v''}$ for band systems of importance.

Franck–Condon factors $q_{v'v''}$

Franck–Condon factors $q_{v'v''}$ as defined in equation 5 have been calculated by analytical and numerical means by a number of workers for a variety of band systems (and often for a fragmentary number of bands per system) since the pioneer work of J. FRANCK[8], E. U. CONDON[9] and E. HUTCHISSON[10, 11]. This work has been summarized elsewhere[12, 13].

P. A. FRASER and W. R. JARMAIN[14–16] have developed a method by which Franck–Condon factor arrays may be evaluated for Morse models of molecular oscillators with a relatively small amount of tedious computation. Franck–Condon factor arrays (including the tables of this paper) have been calculated for some 40 band systems by this method using desk calculators in the early work, and FERUT, the electronic computer at the University of Toronto for the later work[17–20].

Finally it may be mentioned that three-dimensional plots of $q_{v'v''}$ are also instructive in visualizing the gross change in band intensities across a system[21].

Determination of smoothed relative vibrational transition probabilities

From equation 7 it would appear that $p_{v'v''}$ could be simply determined *band by band* for v''-progressions from $I_{v'v''}/E^4_{v'v''}$. However, as more intense bands can be measured with greater precision than less intense bands, variability in the accuracy of the $p_{v'v''}$ values thereby derived occurs. Fraser[5] has therefore suggested the following method which enables the determination to be made first of the variation of $R_e(r)$ with r and thus secondly of smoothed values of $p_{v'v''}$ $[=R_e^2(\bar{r}_{v'v''})\,q_{v'v''}]$.

It is clear from equation 8 that a plot of $(I_{v'v''}/q_{v'v''}\ E^4_{v'v''})^{1/2}$ versus $\bar{r}_{v'v''}$ will be an indication for each v'' progression (v' = constant) of the variation of $R_e(r)$ with r. The plots for neighbouring progressions partly overlap in r. This allows an objective rescaling to compensate for the variation of $N^{1/2}_{v'}$ which places each v' = constant segment upon the same ordinate scale. The resulting set of points, through which a smooth curve may be fitted, represents the variation of $R_e(r)$ with r across the range of r which is significant to the band system in question. *All* of the measured and calculated data for every band contribute to the $R_e(r)$ curve in this procedure, and thus an array of $p_{v'v''}$, calculated from equation 4, for the band system in this case will presumably not have the same variability in precision which is inherent in an array of $I_{v'v''}/N_{v'}E^4_{v'v''}$.

The procedure of Fraser has been followed for some 20 band systems[22–27] and large variation of $R_e(r)$ with r has been obtained in some cases. In these cases the smoothed $p_{v'v''}$ array is perceptibly different from the $q_{v'v''}$ array.

Insofar as the practical application of equations 7 and 8 are concerned, it is clear that, in addition to tables of $p_{v'v''}$ (when available) and $q_{v'v''}$, tables of $p_{v'v''}E^4_{v'v''}$ ($\sim p_{v'v''}/\lambda^4_{v'v''}$) or $q_{v'v''}E^4_{v'v''}$ ($\sim q_{v'v''}/\lambda^4_{v'v''}$) would be of value. $p_{v'v''}E^4_{v'v''}$ is sometimes called the intensity $I_{\infty v'v''}$ at infinite temperature, for at infinite temperature all $N_{v'}$ become equal. In cases where $R_e(r)$ is unknown, a useful approximation (which can be quite crude in some cases) proportional to $I_{\infty v'v''}$ is given by $q_{v'v''}/\lambda^4_{v'v''}$.

RESULTS

Table 1 lists the band systems of this paper together with the basic molecular constants with which the following calculations were made.

Franck–Condon factors $q_{v'v''}$

The Franck–Condon factor arrays for each band system have been computed using a Morse model for the molecular oscillator in both the upper and lower states for each system. The method of Fraser and Jarmain[14, 15], with perturbation improvement[16], was employed. In most cases the calculations were made using the generously provided facilities of the electronic computer FERUT at the University of Toronto.

Relative vibrational transition probabilities $p_{v'v''}$

For a number of band systems, intensity measurements are available and in each of these cases the procedure referred to above has been followed to determine the form of $R_e(r)$ and thereby to obtain an array of smoothed $p_{v'v''}$.

Intensities at infinite temperature

Arrays of $p_{v'v''}/\lambda^4_{v'v''}$ have been calculated where available, and in other cases arrays of $q_{v'v''}/\lambda^4_{v'v''}$ have been calculated, on a scale which sets one of the most intense bands in each case at 100.

The data are presented in alphabetical order in *Tables 2* to *20*, using a multiple entry $v'v''$ array for each band system. The band systems were in part selected from those collected in Gaydon's recent monograph[2] to which a few systems of boron-containing molecules have been added. No data are included for band systems of CH and NH, in all of which the change of equilibrium internuclear separation is very small (thus q_{00}, q_{11}, q_{22}, . . . are all very nearly unity, and all others negligible); for all of which there is doubt as to the applicability of the Morse oscillator model; and further for which, in view of the $\omega_e x_e$ values of the states, the method of Fraser and Jarmain[14–16] is not appropriate (if one were to assume a Morse model). Data for the Fourth Positive System of CO have not been included, for the significant bands occur at large values ($\sim$ 10 to 20) of vibrational quantum numbers. For such large quantum numbers the approximate method is not appropriate, and results would be extremely model-sensitive owing to the large number of oscillations in the integrand of the overlap integral.

Table 1. Band systems and basic constants*

Table	*Molecule*	*Transition*		*State*	ω_e	$\omega_e x_e$	r_e
2	B_2		$A^3\Sigma_u^- - X^3\Sigma_g^-$	$A^3\Sigma_u^-$	937·4	2·6	1·625
				$X^3\Sigma_g^-$	1051·3	9·4	1·589
3	BH		$B^1\Sigma^+ - A^1\Pi$	$B^1\Sigma^+$	(2400)	(65)	1·2149
				$A^1\Pi$	(2344)	(129)	1·2257
4	BN		$A^3\Pi - X^3\Pi$	$A^3\Pi$	1317·5	14·9	1·326
				$X^3\Pi$	1514·6	12·3	1·281
5	BO	*β*	$B^2\Sigma^+ - X^2\Sigma^+$	$B^2\Sigma^+$	1280·3	10·07	[1·311]
6		*Combination*	$B^2\Sigma^+ - A^2\Pi_i$	$A^2\Pi_i$	1260·7	11·157	1·3524
7		*α*	$A^2\Pi_i - X^2\Sigma^+$	$X^2\Sigma^+$	1885·44	11·769	1·2049
8	C_2	*Mulliken*	$d^1\Sigma_u^+ - a^1\Sigma_g^+$	$d^1\Sigma_u^+$	1829·57	13·97	1·2378
9		*Deslandres d'Azambuja*	$c^1\Pi_g - b^1\Pi_u$	$c^1\Pi_g$	1809·1	15·81	1·2730
10		*Phillips*	$b^1\Pi_u - a^1\Sigma_g^+$	$b^1\Pi_u$	1608·33	12·14	1·3180
11		*Fox–Herzberg*	$B^3\Pi_g - X^3\Pi_u$	$a^1\Sigma_g^+$	1855·63	14·08	1·2422
12		*Swan*	$A^3\Pi_g - X^3\Pi_u$	$B^3\Pi_g$	1106·56	39·26	1·5350
				$A^3\Pi_g$	1788·22	16·44	1·2660
				$X^3\Pi_u$	1641·35	11·67	1·3117
13	CN	*Violet*	$B^2\Sigma^+ - X^2\Sigma^+$	$B^2\Sigma^+$	2164·13	20·25	1·1506
14		*Red*	$A^2\Pi_i - X^2\Sigma^+$	$A^2\Pi_i$	1814·43	12·883	1·2327
				$X^2\Sigma^+$	2068·705	13·144	1·1718
15	NO	*β*	$B^2\Pi - X^2\Pi$	$B^2\Pi$	1037·7	7·603	1·415
16		*γ*	$A^2\Sigma - X^2\Pi$	$A^2\Sigma$	2371·3	14·48	1·0637
				$X^2\Pi$	1903·9	13·97	1·151
17	O_2	*Schumann–Runge*	$B^3\Pi_u^- - X^3\Sigma_g^-$	$B^3\Pi_u$	700·36	$8{\cdot}002_3$	$1{\cdot}60_4$
				$X^3\Sigma_g^-$	1580·361	12·073	1·20739
18	OH	*Violet*	$A^2\Sigma^+ - X^2\Pi$	$A^2\Sigma^+$	2319·9	52·0	1·012
				$X^2\Pi_i$	2720·9	44·2	0·9699
19	PbO		$D - X^1\Sigma^+$	D	530·5	2·92	(2·048)
20			$A - X^1\Sigma^+$	A	451·7	3·33	(2·098)
				$X^1\Sigma$	721·8	3·70	1·922

*All the numerical data and notation are as in *Table 39*, pp 501–581 of ref. 4.

Table 2. B_2: $(A^3\Sigma_u^- - X^3\Sigma_g^-)$ *system*

$v' \diagdown v''$	0	1	2	3
0	3272·8 0·92 100	— 0·08$_0$	0·00$_3$	—
1	3176·5 0·08$_2$ 10	3283·4 0·80 86	0·13	0·01
2	0·00$_2$	3187 0·13 16	3292·7 0·75 80	0·16

Legend

$\lambda_{v'v''}$ (A)
$q_{v'v''}$
$q_{v'v''}/\lambda^4_{v'v''}$

Table 3. BH: $(B^1\Sigma^+ - A^1\Pi)$ *system*

$v' \diagdown v''$	0	1	2
0	3415 0·99 100	0·01	—
1	0·01	3396 0·95 98	0·06
2		0·07	0·88

Legend

$\lambda_{v'v''}$ (A)
$q_{v'v''}$
$q_{v'v''}/\lambda^4_{v'v''}$

Table 4. **BN**: ($A^3\Pi$–$X^3\Pi$) *system*

$v' \diagdown v''$	0	1	2	3	4
0	3599·2 $0{\cdot}75_9$ 100	3803·2 $0{\cdot}21_5$ 23	$0{\cdot}02_5$	$0{\cdot}00_2$	
1	3439·7 $0{\cdot}20_1$ 32	3625·6 $0{\cdot}38_4$ 49	3829·3 $0{\cdot}33_8$ 35	$0{\cdot}07_1$	$0{\cdot}00_7$
2	$0{\cdot}03_5$	3467·4 $0{\cdot}29_2$ 45	3653·2 $0{\cdot}14_7$ 18	3856·1 0·38 38	0·13
3	$0{\cdot}00_5$	$0{\cdot}08_7$	3496·3 $0{\cdot}29_8$ 44	3681·8 $0{\cdot}02_9$ 4	$0{\cdot}35_7$

Legend

$\lambda_{v'v''}$ (Å)†

$q_{v'v''}$

$q_{v'v''}/\lambda^4_{v'v''}$

†$\lambda_{v'v''}$ for *R* heads of $B^{11}N$.

Table 5. BO : β ($B^2\Sigma^+$–$X^2\Sigma^+$) *system*

$v' \backslash v''$	0	1	2	3	4	5	6	7	8
0	2331·3 $0{\cdot}20_4$ 75	2437·1 $0{\cdot}32_4$ 100	2551·4 $0{\cdot}26_0$ 67	2675·3 $0{\cdot}13_8$ 29	2809·9 $0{\cdot}05_4$ 9	2956·6 $0{\cdot}16_1$ 2	$0{\cdot}00_4$	$0{\cdot}00_1$	
1	2264·8 $0{\cdot}31_1$ 129	2364·5 $0{\cdot}07_2$ 25	2472 $0{\cdot}02_5$ 7	2588 $0{\cdot}17_1$ 42	2713·8 $0{\cdot}20_8$ 42	2850·6 $0{\cdot}13_3$ 22	2999·7 $0{\cdot}05_7$ 8	$0{\cdot}01_8$	$0{\cdot}00_4$
2	2203·0 0·25 116	$0{\cdot}18_0$	2398·5 $0{\cdot}16_1$ 53	2507·7 $0{\cdot}03_5$ 10	2625·5 $0{\cdot}02_8$ 6	2753·4 $0{\cdot}15_3$ 29	2892·2 $0{\cdot}17_8$ 28	3043·6 $0{\cdot}11_2$ 14	3209·3 $0{\cdot}04_7$ 5
3	$0{\cdot}14_1$	2234·6 $0{\cdot}14_4$ 63	2330·4 0·04 15	2433·3 0·06 19	2544·3 $0{\cdot}11_5$ 30	2664·1 $0{\cdot}00_7$ 2	2793·9 $0{\cdot}05_4$ 10	2934·9 $0{\cdot}15_9$ 23	3088·6 $0{\cdot}15_4$ 18
4	$0{\cdot}06_2$	$0{\cdot}18_7$	$0{\cdot}13_6$	$0{\cdot}11_2$	0	2581·6 $0{\cdot}09_8$ 24	2703·4 $0{\cdot}06_5$ 13	$0{\cdot}00_2$	2978·5 $0{\cdot}09_8$ 13

Legend

$\lambda_{v'v''}$ (*A*)
$q_{v'v''}$
$q_{v'v''}/\lambda^4_{v'v''}$

Table 6. **BO**: *Combination system* ($B^2\Sigma^+ - A^2\Pi_i$)

$v' \diagdown v''$	0	1	2	3	4	5
0	5201·1 A_1 $0{\cdot}77_8$ 100	(5552) $0{\cdot}17_7$ 18	5916·2 B_1 $0{\cdot}03_6$ 3	$0{\cdot}00_7$	$0{\cdot}00_2$	0
1	4881·2 A_1 $0{\cdot}20_9$ 35	5195 $0{\cdot}43_8$ 56	(5550) $0{\cdot}24_4$ 25	5895·3 B_1 $0{\cdot}07_9$ 6	$0{\cdot}02_2$	$0{\cdot}00_6$
2	4576·5 A_1 $0{\cdot}01_3$ 3	4881·2 $0{\cdot}34_9$ 58	5189·3 A_1 $0{\cdot}22_0$ 29	5493·7 B_1 $0{\cdot}24_4$ 25	$0{\cdot}11_4$	$0{\cdot}04_1$
3	0	4580·8 B_1 $0{\cdot}03_6$ 8	4881·2 A_1 $0{\cdot}43_3$ 72	5184·7 $0{\cdot}09_1$ 12	$0{\cdot}20_9$	$0{\cdot}13_5$
4		0	$0{\cdot}06_7$	$0{\cdot}47_3$	$0{\cdot}02_5$	$0{\cdot}16_0$
5			$0{\cdot}00_1$	$0{\cdot}10_5$	$0{\cdot}48_0$	$0{\cdot}00_1$

Legend

$\lambda_{v'v''}$ (A)*

$q_{v'v''}$

$q_{v'v''}/\lambda^4_{v'v''}$

---

*Wavelengths in parentheses estimated from ref. 32.

Table 7. BO: α $(A^2\Pi_i–X^2\Sigma+)$ system

$v' \diagdown v''$	0	1	2	3	4	5	6	7	8
0	4250·4 $0{\cdot}03_7$ 11	4615·4 $0{\cdot}13_4$ 28	5043·5 $0{\cdot}22_7$ 33	5551·5 $0{\cdot}24_4$ 24	6165·4 $0{\cdot}18_1$ 12	$0{\cdot}10_5$	$0{\cdot}04_6$	$0{\cdot}01_6$	$0{\cdot}00_5$
1	4037·4 $0{\cdot}10_7$ 38	4365·9 $0{\cdot}18_9$ 49	4746·9 $0{\cdot}09_6$ 18	$0{\cdot}00_1$	$0{\cdot}05_5$	$0{\cdot}15_7$	$0{\cdot}17_8$	$0{\cdot}12_4$	$0{\cdot}06_2$
2	3848·7 $0{\cdot}16_5$ 71	4145·5 $0{\cdot}10_7$ 34	$0{\cdot}00_0$	$0{\cdot}08_8$	$0{\cdot}10_1$	$0{\cdot}01_1$	$0{\cdot}02_9$	$0{\cdot}12_7$	$0{\cdot}16_3$
3	3679·1 $0{\cdot}18_3$ 94	3950·5 $0{\cdot}01_9$ 7	$0{\cdot}06_1$	$0{\cdot}08_2$	0	$0{\cdot}07_2$	$0{\cdot}08_7$	$0{\cdot}00_4$	$0{\cdot}03_2$
4	3526·8 $0{\cdot}16_4$ 100	$0{\cdot}00_3$	$0{\cdot}09_7$	$0{\cdot}00_5$	$0{\cdot}06_1$	$0{\cdot}05_7$	$0{\cdot}00_2$	$0{\cdot}07_7$	$0{\cdot}06_7$
5	3389·1 $0{\cdot}12_7$ 91	$0{\cdot}04_0$	$0{\cdot}05_6$	$0{\cdot}02_1$	$0{\cdot}06_8$	0	$0{\cdot}07_0$	$0{\cdot}03_0$	$0{\cdot}01_4$
6	$0{\cdot}08_8$	$0{\cdot}08_2$	$0{\cdot}00_9$	$0{\cdot}06_7$	$0{\cdot}01_1$	$0{\cdot}04_9$	$0{\cdot}03_4$	$0{\cdot}01_5$	$0{\cdot}06_9$
7	$0{\cdot}05_6$	$0{\cdot}10_1$	$0{\cdot}00_3$	$0{\cdot}06_3$	$0{\cdot}00_7$	$0{\cdot}05_7$	$0{\cdot}00_2$	$0{\cdot}06_2$	$0{\cdot}00_5$
8	$0{\cdot}03_3$	$0{\cdot}09_6$	$0{\cdot}02_8$	$0{\cdot}02_6$	$0{\cdot}04_4$	$0{\cdot}01_4$	$0{\cdot}04_2$	$0{\cdot}02_0$	$0{\cdot}02_7$

Legend

$\lambda_{v'v''}$ (A)*
$q_{v'v''}$
$q_{v'v''}/\lambda^4_{v'v''}$

*Wavelengths of Q_2 heads quoted.

Table 8. C_2: *Mulliken* ($d^1\Sigma_u^+ - a^1\Sigma_g^+$) *system*

$v' \diagdown v''$	0	1	2	3	4	5	6	7	8
0	2312·7 0·99$_7$ 100	0·00$_3$	0						
1	0·00$_3$	2314·0 0·99$_1$ 99	0·00$_5$						
2		0·00$_6$	2315·4 0·98$_6$ 98·5	0·00$_7$					
3			0·00$_8$	2316·8 0·98$_1$ 97·7	0·00$_9$	0·00$_2$			
4			0·00$_1$	0·01$_1$	0·97$_6$	0·01$_1$	0·00$_2$		
5				0	0·01$_2$	0·97$_2$	0·01$_1$	0·00$_3$	
6					0·00$_1$	0·01$_4$	0·96$_8$	0·01$_2$	0·00$_4$
7						0·00$_2$	0·01$_6$	0·96$_5$	0·01$_3$
8							0·00$_3$	0·01$_7$	0·96$_2$

Legend

$\lambda_{v'v''}$ (*A*)*
$q_{v'v''}$
$q_{v'v''}/\lambda^4_{v'v''}$

*Wavelengths from ref. 33

Table 9. C_2: *Deslandres d'Azambuja* ($c^1\Pi_g$–$b^1\Pi_u$) *system*

$v' \backslash v''$	0	1	2	3	4	5
0	3852·2 0·73$_9$ 100	4102·3 0·21$_4$ 22	0·04$_0$	0·00$_6$	0·00$_1$	
1	3607·3 0·23$_3$ 41	3825·6 0·36$_5$ 51	4068·1 0·29$_1$ 32	0·08$_9$	0·01$_9$	0·00$_3$
2	3399·7 0·02$_7$ 6	3592·9 0·35$_1$ 63	0·15$_5$	4041·8 0·29$_3$ 33	0·13$_1$	0·03$_7$
3	0·00$_1$	3398·1 0·06$_6$ 15	3587·6 0·39$_7$ 71	0·04$_9$	4026·9 0·25$_7$ 29	0·16$_2$
4	0	0·00$_4$	3405·1 0·11$_1$ 25	3599·3 0·40$_1$ 71	0·00$_6$	0·20$_7$
5		0	0·00$_9$	3431·9 0·15$_6$ 33	3617·9 0·38$_1$ 66	0·00$_1$
6			0	0·01$_6$	0·20$_1$	3689 0·34$_9$ 56

Legend

$\lambda_{v'v''}$ (*A*)
$q_{v'v''}$
$q_{v'v''}/\lambda^4_{v'v''}$

Table 10. C_2: *Phillips* $(b^1\Pi_u - a^1\Sigma_g^+)$ *system*

$v' \diagdown v''$	0	1	2	3	4	5	6
0	$0{\cdot}41_4$	$0{\cdot}40_0$	$0{\cdot}15_3$	$0{\cdot}03_0$	$0{\cdot}00_3$		
1	10107 $0{\cdot}33_1$ 96	$0{\cdot}00_8$	$0{\cdot}29_5$	$0{\cdot}27_0$	$0{\cdot}08_5$	$0{\cdot}01_3$	$0{\cdot}00_1$
2	8750·8 $0{\cdot}16_1$ 82	$0{\cdot}17_5$	$0{\cdot}05_6$	$0{\cdot}12_3$	$0{\cdot}30_5$	$0{\cdot}15_0$	$0{\cdot}02_9$
3	7714·6 $0{\cdot}06_2$ 53	8980·5 $0{\cdot}19_9$ 92	$0{\cdot}03_8$	$0{\cdot}14_2$	$0{\cdot}02_2$	$0{\cdot}27_4$	$0{\cdot}21_0$
4	$0{\cdot}02_1$	7907·7 $0{\cdot}12_4$ 95	$0{\cdot}14_0$	$0{\cdot}00_1$	$0{\cdot}16_2$	$0{\cdot}00_1$	$0{\cdot}20_7$
5	$0{\cdot}00_7$	$0{\cdot}05_9$	8108·2 $0{\cdot}14_4$ 100	$0{\cdot}06_2$	$0{\cdot}03_3$	$0{\cdot}12_6$	$0{\cdot}03_1$
6	$0{\cdot}00_2$	$0{\cdot}02_4$	$0{\cdot}09_4$	$0{\cdot}12_2$	$0{\cdot}01_2$	$0{\cdot}07_8$	$0{\cdot}07_1$

Legend

$\lambda_{v'v''}$ (A)
$q_{v'v''}$
$q_{v'v''}/\lambda^4_{v'v''}$

Table 11. C_2: *Fox–Herzberg* ($B^3\Pi_g$–$X^3\Pi_u$) *system*

$v' \diagdown v''$	0	1	2	3	4	5	6	7	8
0	$0{\cdot}00_2$	$0{\cdot}01_4$	2731·5 $0{\cdot}05_3$ 37	2855 $0{\cdot}12_4$ 74	2987 $0{\cdot}20_2$ 100	3129 $0{\cdot}24_1$ 99	3283 $0{\cdot}21_3$ 72	$0{\cdot}13_7$	$0{\cdot}06_1$
1	$0{\cdot}00_6$	$0{\cdot}03_6$	2656·3 $0{\cdot}09_7$ 77	2772·1 $0{\cdot}14_1$ 94	2896·4† $0{\cdot}10_2$ 57	$0{\cdot}01_5$	$0{\cdot}02_9$		
2	$0{\cdot}01_1$	2486·3* $0{\cdot}05_5$ 57	2589 $0{\cdot}10_6$ 93	2698·8 $0{\cdot}07_9$ 59	$0{\cdot}00_3$	$0{\cdot}06_8$			
3	$0{\cdot}01_7$	2429·9* $0{\cdot}06_7$ 76	2527·9 $0{\cdot}08_7$ 84	$0{\cdot}02_0$	$0{\cdot}02_9$				
4	$0{\cdot}02_3$	2378·2* $0{\cdot}07_2$ 90	$0{\cdot}05_7$	0	$0{\cdot}08_9$				
5	$0{\cdot}02_7$	$0{\cdot}07_3$	$0{\cdot}03_0$	$0{\cdot}01_5$					
6	$0{\cdot}03_1$	$0{\cdot}06_5$	$0{\cdot}01_1$	$0{\cdot}04_2$					
7	$0{\cdot}03_3$	$0{\cdot}05_5$							
8	$0{\cdot}03_5$								

Legend

$\lambda_{v'v''}$ (*A*)
$q_{v'v''}$
$q_{v'v''}/\lambda^4_{v'v''}$

*These bands are incorrectly assigned as (2, 0) (3, 0) (4, 0) in refs 2 and 30, see ref. 31.
†This band wavelength incorrectly given as 2996·4 A.U. in refs 2 and 30, see ref. 31.

Table 12. C_2: *Swan* ($A^3\Pi_g$–$X^3\Pi_u$) *system**

$v' \diagdown v''$	0	1	2	3	4	5
0	5165 $0{\cdot}73_1$ 100 100	5636 $0{\cdot}21_1$ 28·9 20	6191 $0{\cdot}04_2$ 5·8 3	$0{\cdot}00_7$	$0{\cdot}00_1$	
1	4737 $0{\cdot}23_7$ 32·4 46	5129 $0{\cdot}36_3$ 49·7 51	5586 0·28 38·3 28	6122 $0{\cdot}08_8$ 12 6	0·02	$0{\cdot}00_5$
2	4383 0·02 3·3 6	4715 $0{\cdot}35_6$ 48·7 70	5098 $0{\cdot}16_2$ 22·2 23	5541 0·28 38·3 29	6060 $0{\cdot}12_4$ 17 9	6677 $0{\cdot}03_0$ (∼1·5)
3	0·00	4371 0·06 8·2 16	4698 $0{\cdot}40_5$ 55·4 81	$0{\cdot}05_7$	5502 $0{\cdot}26_3$ 36 28	
4	0·00	0·00	4365 $0{\cdot}09_7$ 13·3 26	4685 $0{\cdot}42_7$ 58·4 86		

Legend

$\lambda_{v'v''}$ (*A*)
$q_{v'v''}$
$p_{v'v''}$
$I_{\infty\, v'v''}$

---

*See refs 25 and 18.

Table 13. CN: *Violet* $(B^2\Sigma^+ - X^2\Sigma^+)$ *system**

$v' \backslash v''$	0	1	2	3
0	3883·4 0·92 100 100	4216·0 0·07$_4$ 5·8 4·2	4606·1 0·00$_5$ 0·3 0·15	0·00
1	3590·4 0·07$_9$ 12 16	3871·4 0·78$_7$ 88 89	4197·2 0·12$_1$ 9·4 7	4578 0·01$_4$ 0·9 0·5
2	0·00$_1$	3585 0·13$_7$ 21 29	3861·9 0·69$_1$ 79 81	4181·0 0·14$_7$ 11 8
3	0·00	0·00$_3$	3583·9 0·18$_0$ 28 39	3854·7 0·62$_5$ 74 76

Legend

$\lambda_{v'v''}$ (A)
$q_{v'v''}$
$p_{v'v''}$
$I_{\infty\, v'v''}$

*See refs 25 and 18.

Table 14. CN: *Red* ($A^2\Pi$–$X^2\Sigma$) *system*

$v' \diagdown v''$	0	1	2	3	4	5	6	7	8
0	10933 $0{\cdot}49_9$ 100 100	14074 $0{\cdot}37_0$ 75·2 27	$0{\cdot}11_1$	$0{\cdot}01_8$	$0{\cdot}00_2$	—			
1	9148·3 $0{\cdot}32_1$ 63·6 130	11247 $0{\cdot}04_6$ 9·2 8	$0{\cdot}34_9$ 71	$0{\cdot}22_3$	$0{\cdot}05_5$	$0{\cdot}00_7$	$0{\cdot}00_1$		
2	7876·4 $0{\cdot}12_6$ 24·7 92	9392·5 $0{\cdot}24_2$ 48 88	$0{\cdot}01_2$ 2·4	$0{\cdot}20_9$ 42·5	$0{\cdot}28_6$	$0{\cdot}10_6$	$0{\cdot}01_8$	$0{\cdot}00_2$	
3	6927·6 $0{\cdot}04_0$ 7·7 48	8067 $0{\cdot}19_5$ 38·4 84	$0{\cdot}10_0$ 19·9	$0{\cdot}90_0$ 18·2	$0{\cdot}08_2$ (16·7)	$0{\cdot}29_4$	$0{\cdot}16_1$	$0{\cdot}03_5$	$0{\cdot}00_4$
4	6191·7 $0{\cdot}01_1$ 2·1 20	7091 $0{\cdot}09_4$ 18·4 104	8272 $0{\cdot}18_4$ 36·1 110	$0{\cdot}01_6$ 3·1	$0{\cdot}15_0$ 3·03	$0{\cdot}01_3$ (2·6)	$0{\cdot}25_6$	$0{\cdot}21_0$	$0{\cdot}05_8$
5	5606·7 $0{\cdot}00_3$ (0·55) 8	6332·2 $0{\cdot}03_6$ 6·9 61	7259 $0{\cdot}13_4$ 26·2 135	8485 $0{\cdot}12_5$ 24·6 68	$0{\cdot}00_2$ 0·42	$0{\cdot}15_8$ 32	$0{\cdot}00_2$ (0·37)	$0{\cdot}19_3$	$0{\cdot}24_7$
6	5129·7 $0{\cdot}00_1$ (0·13) 3	5730·2 $0{\cdot}01_2$ 2·3 30	6478·7 $0{\cdot}06_7$ 13 105	7435 $0{\cdot}14_3$ 28 131	8708 $0{\cdot}05_9$ 11·7 29	$0{\cdot}03_2$ 6·4	$0{\cdot}12_5$ 25·4	$0{\cdot}02_9$ (5·9)	$0{\cdot}12_4$
7	4732·7 —	5239·3 $0{\cdot}00_4$ (0·68) 13	5858·2 $0{\cdot}02_8$ 5·3 64	6631·6 $0{\cdot}09_5$ 18·5 137	$0{\cdot}12_3$ 24·1	$0{\cdot}01_5$ 2·9	$0{\cdot}07_2$ 14·5	$0{\cdot}07_6$ 15·3	$0{\cdot}07_0$ (14·4)
8	0	4832·6 $0{\cdot}00_1$	5347·5 $0{\cdot}01_0$ (1·9) 33	5992·6 $0{\cdot}04_8$ 9·4 104	6792·5 $0{\cdot}11_1$ 21·5 144	$0{\cdot}08_6$ 16·8	0 0	$0{\cdot}10_0$ 20·1	$0{\cdot}03_1$ 6·4
9	0	4488·8 0	4835·8 $0{\cdot}00_3$	5473·3 $0{\cdot}02_1$ (4) 64	6133·0 $0{\cdot}06_9$ 13·3 134	6961 $0{\cdot}10_9$ 21·1 128	$0{\cdot}04_6$ 8·9	$0{\cdot}01_1$ 2·1	$0{\cdot}10_6$ 21·2

Legend

$\lambda_{v'v''}$ (*A*) (R_2 head)
$q_{v'v''}$*
$p_{v'v''}$†
$I_{\infty\, v'v''}$

*These are substantially the same as those of A. WYLLER.

†See ref. 26

Table 15. NO: β ($B^2\Pi$–$X^2\Pi$) *system**

$v' \diagdown v''$	4	5	6	7	8	9	10	11	12	13
0	2623 $0{\cdot}02_5$ $0{\cdot}01_9$ 26	2751 $0{\cdot}05_7$ $0{\cdot}05_2$ 52	2888·9 $0{\cdot}10_2$ $0{\cdot}08_8$ 80	3039 $0{\cdot}14_7$ $0{\cdot}13_2$ 99	3202·5 $0{\cdot}17_4$ $0{\cdot}16_6$ 100	3381·4 $0{\cdot}17_0$ $0{\cdot}17_0$ 83	3578 $0{\cdot}13_8$ $0{\cdot}14_6$ 56	3794·7 $0{\cdot}09_4$ $0{\cdot}10_4$ 32	4034·8 $0{\cdot}05_3$ $0{\cdot}62_2$ 15	
1		2675·5 $0{\cdot}11_1$ $0{\cdot}08_8$ 109	2806 $0{\cdot}11_3$ $0{\cdot}09_4$ 96	2947 $0{\cdot}06_9$ $0{\cdot}06_0$ 51	— $0{\cdot}01_4$ $0{\cdot}01_5$ —	— $0{\cdot}00_4$ $0{\cdot}00_4$ —	3451·5 $0{\cdot}05_1$ $0{\cdot}05_2$ 23	3652·8 $0{\cdot}11_7$ $0{\cdot}12_5$ 45	3874·5 $0{\cdot}15_0$ $0{\cdot}17_0$ 48	4120·75 $0{\cdot}13_2$ $0{\cdot}15_8$ 35
2			2728·6 $0{\cdot}02_6$ $0{\cdot}02_1$ 24	— $0{\cdot}00_1$ $0{\cdot}00_1$ —	3006·7 $0{\cdot}03_8$ $0{\cdot}03_4$ 26	3164·1 $0{\cdot}08_9$ $0{\cdot}08_4$ 53	3335·5 $0{\cdot}05_8$ $0{\cdot}05_7$ 29	— $0{\cdot}01_3$ $0{\cdot}01_4$ —	— $0{\cdot}01_0$ $0{\cdot}01_1$ —	3956·3 $0{\cdot}07_8$ $0{\cdot}09_0$ 23

Legend

$\lambda_{v'v''}$ (A) (Average of R heads of sub-bands)
$q_{v'v''}$
$p_{v'v''}$
$I_{\infty\, v'v''}$

---

*See ref. 27.

Table 16. NO: γ *($A^2\Sigma$–$X^2\Pi$) system**

$v' \diagdown v''$	0	1	2	3	4	5	6	7	8
0		2366·7 $0{\cdot}26_3$ $0{\cdot}02_7$ 40	2474·9 $0{\cdot}23_7$ $0{\cdot}07_3$ 93	2591·6 $0{\cdot}16_1$ $0{\cdot}09_7$ 100	2717·7 $0{\cdot}09_1$ $0{\cdot}09_1$ 77	2854·6 $0{\cdot}04_6$ $0{\cdot}06_6$ 46	3003·2 $0{\cdot}02_1$ $0{\cdot}04_1$ 23	3170·7 $0{\cdot}00_9$ $0{\cdot}02_3$ 10	
1			— $0{\cdot}00_1$ 0 0	2443·5 $0{\cdot}07_1$ $0{\cdot}01_7$ 23	2554 $0{\cdot}13_4$ $0{\cdot}06_0$ 75	2675·2 $0{\cdot}13_4$ $0{\cdot}11_5$ 104	2805·6 $0{\cdot}09_9$ $0{\cdot}12_8$ 96	2947 $0{\cdot}06_2$ $0{\cdot}10_8$ 67	
2				2312·9 $0{\cdot}07_7$ $0{\cdot}00_3$ 4	— $0{\cdot}00_1$ 0 0	2520 $0{\cdot}03_3$ $0{\cdot}01_4$ 16	2634·9 $0{\cdot}08_7$ $0{\cdot}06_3$ 60	2759·5 $0{\cdot}10_5$ $0{\cdot}11_8$ 95	2893 $0{\cdot}09_0$ $0{\cdot}14_3$ 95

Legend

$\lambda_{v'v''}$ (*A*) (Average of ${}^0P_{12}$ and P_2 heads)
$q_{v'v''}$
$p_{v'v''}$
$I_{\infty\, v'v''}$

*See ref. 27.

Table 17(a). O_2: *Schumann–Runge* ($B^3\Pi_u$–$X^3\Sigma_g^-$) *system*

$v' \diagdown v''$	0	1	2	3	4	5
0	2030 $2{\cdot}3_1(-9)$ $2{\cdot}0_8(-8)$ 0·001	$6{\cdot}2_5(-8)$	$8{\cdot}1_2(-7)$	0	0	
1	1998 $2{\cdot}6_9(-9)$ $2{\cdot}7_6(-7)$ 0·02	$6{\cdot}6_4(-7)$	$7{\cdot}8_4(-6)$	0	0	
2	1971 $1{\cdot}6_4(-7)$ $1{\cdot}4_8(-6)$ 0·1	$3{\cdot}6_9(-6)$	$5{\cdot}6_1(-5)$	0	$0{\cdot}00_1$	
3	1947 $6{\cdot}9_0(-7)$ $5{\cdot}8_4(-6)$ 0·4	$1{\cdot}4_2(-5)$	$1{\cdot}3_9(-4)$	$0{\cdot}00_1$	$0{\cdot}00_4$	
4	1924 $2{\cdot}2_8(-6)$ $2{\cdot}6_4(-5)$ 1·9	$4{\cdot}3_2(-5)$	$3{\cdot}8_0(-4)$		*G.F.*	*G.F.*
5	1902 $6{\cdot}3_0(-6)$ $5{\cdot}6_7(-5)$ 4·3	1960 $8{\cdot}4_8(-5)$	2021 $8{\cdot}6_4(-4)$	2084	2151	2221
6	1882 $1{\cdot}5_0(-5)$ $1{\cdot}2_6(-6)$ 10	1938 $2{\cdot}3_7(-4)$	*G.F.* $1{\cdot}7_1(-3)$	2060	2125	2193
7	1863 $3{\cdot}1_8(-5)$ $3{\cdot}4_6(-4)$ 29	1918 $4{\cdot}6_2(-4)$	— $3{\cdot}0\ (-3)$	2038	2101	2168
8	1846 $6{\cdot}1_2(-5)$ $5{\cdot}8_8(-4)$ 51	1900 $8{\cdot}1_2(-4)$	— $4{\cdot}8_0(-3)$	2017	2080	
9	1830 $1{\cdot}0_8(-4)$ $1{\cdot}1_1(-3)$ 99	$1{\cdot}3_2(-3)$	$7{\cdot}0_7(-3)$			
10	1816 $1{\cdot}8_0(-4)$ $1{\cdot}3_5(-3)$ 124	$2{\cdot}0_2(-3)$	$9{\cdot}7_2(-3)$			
11	1803 $2{\cdot}7_9(-4)$ — —	$2{\cdot}8_9(-3)$	$1{\cdot}2_5(-2)$			
12	1792 $4{\cdot}1_6(-4)$ — —	$3{\cdot}9_4(-3)$	$1{\cdot}5_4(-2)$			
13	1782 $5{\cdot}8_8(-4)$ — —	$5{\cdot}1_3(-3)$	$1{\cdot}8_2(-2)$			
14	1774 $7{\cdot}9_5(-4)$ — —	$6{\cdot}4_2(-3)$	$2{\cdot}0_4(-2)$			
15	1768 $1{\cdot}0_4(-3)$ $2{\cdot}0_4(-3)$	$7{\cdot}7_4(-3)$	$2{\cdot}2_2(-2)$			

Legend 17(a)

$\lambda_{v'v''}$*
$q_{v'v''}$†
$p_{v'v''}$‡
$I_{\infty v'v''}$§

See footnotes on *Table 17*(b).

Table 17(b). O_2 : *Schumann Runge* ($B^3\Pi_u - X^3\Sigma_g^-$) *system (continued)*

$v' \diagdown v''$	5	6	7	8	9	10	11	12	13	14
0	0	$0\cdot00_1$	$0\cdot00_2$	$0\cdot00_6$	(2780) $0\cdot01_5$ 26	2871 $0\cdot02_9$ 45	2984 $0\cdot05_0$ 66	3104 $0\cdot07_6$ 86	3233 $0\cdot10_2$ 98	3370 $0\cdot12_3$ 100
1	$0\cdot00_1$	$0\cdot00_4$	$0\cdot01_2$	2615 $0\cdot02_5$ 56	2705 $0\cdot04_6$ 90	2815 $0\cdot06_8$ 114	2924 $0\cdot08_4$ 121	3040 $0\cdot08_2$ 101	$0\cdot06_0$	$0\cdot02_8$
2	$0\cdot00_5$	(2410) $0\cdot01_3$ 41	2481 $0\cdot02_8$ 78	2570 $0\cdot04_9$ 118	2664 $0\cdot06_7$ 140	(2810) $0\cdot06_9$ 117	$0\cdot04_9$	$0\cdot01_8$	$0\cdot00_3$	$0\cdot01_1$
3	(2320) $0\cdot01_1$ 40	(2370) $0\cdot02_6$ 86	(2470) $0\cdot04_6$ 130	$0\cdot06_1$	$0\cdot05_7$	$0\cdot03_2$	$0\cdot00_5$	$0\cdot00_3$	$0\cdot02_8$	$0\cdot04_9$

$v' \diagdown v''$	15	16	17	18	19	20	21
0	3517 $0\cdot13_2$ 90	3673 $0\cdot12_7$ 74	3841 $0\cdot10_9$ 53	4021 $0\cdot08_5$ 35	4215 $0\cdot05_9$ 20	$0\cdot03_7$	$0\cdot02_1$
1	$0\cdot00_4$	3583 $0\cdot00_3$ 2	3742 $0\cdot02_8$ 15	3913 $0\cdot06_5$ 29	4096 $0\cdot09_6$ 36	4292 $0\cdot10_8$ 34	$0\cdot09_8$
2	3357 $0\cdot04_1$ 34	3510 $0\cdot06_2$ 43	$0\cdot05_3$	$0\cdot02_3$	3987 $0\cdot00_1$ 0	4173 $0\cdot01_0$ 3	4373 $0\cdot04_4$ 13
3	$0\cdot04_0$	$0\cdot01_1$	$0\cdot00_1$	$0\cdot02_4$	$0\cdot05_3$	$0\cdot05_3$	$0\cdot02_4$

Legend

$\lambda_{v'v''}$*

$q_{v'v''}$†

$q_{v'v''}/\lambda^4_{v'v''}$§

*Wavelengths in parentheses estimated from M. W. FEAST's spectra.

†See refs 18, 19. Note: 2·2, (−6) = 2·2, × 10⁻⁶.

‡See ref. 25 where $R_e(r)$ and $p_{v'v''}$ were calculated from R. W. DITCHBURN and D. W. O. HEDDLE's[37] measurement of band oscillator strength $f_{v'v''}$. $R_e(r)$ was determined from a plot of $(f_{v'v''}/q_{v'v''})^{1/2}$ versus $\bar{r}_{v'v''}$ rather than from the correct $(\lambda_{v'v''} f_{v'v''}/q_{v'v''})^{1/2}$. Recalculation has shown that owing to the small (300A.U.) wavelength spread of the $v'' = 0$ progression the difference between these is not great.

§$I_\infty = p_{v'v''}/\lambda^4_{v'v''}$ given for $v'' = 0$ progression; $q_{v'v''}/\lambda^4_{v'v''}$ given where possible (100 at 0,14) for rest. The scales of $I_{\infty\, v'v''}$ [*17(a)*] and $q_{v'v''}/\lambda^4_{v'v''}$ [*17(b)*] are different.

Table 18. OH: *Violet* ($A^2\Sigma$–$X^2\Pi$) *system**

$v' \diagdown v''$	0	1	2	3	4
0	3064 $0{\cdot}90_7$ 100 100	3428 $0{\cdot}08_9$ $0{\cdot}3$ $0{\cdot}2$	$0{\cdot}00_3$		
1	2811 $0{\cdot}08_6$ $23{\cdot}1$ 33	3122 $0{\cdot}71_6$ 60 56	3484 $0{\cdot}18_6$ $0{\cdot}1$ $0{\cdot}1$	$0{\cdot}01_2$	
2	$0{\cdot}00_6$	2875 $0{\cdot}16_9$ $36{\cdot}6$ 47	3185 $0{\cdot}51_4$ $31{\cdot}3$ 27	$0{\cdot}28_0$	$0{\cdot}03_2$
3	0	$0{\cdot}02_3$	2945 $0{\cdot}23_7$ $42{\cdot}3$ 50	3254 $0{\cdot}32_1$ $13{\cdot}4$ 11	$0{\cdot}32_9$
4	—	$0{\cdot}00_3$	$0{\cdot}05_4$	$0{\cdot}25_3$	

Legend

$\lambda_{v'v''}$ (A)
$q_{v'v''}$
$p_{v'v''}$
$I_{\infty\, v'v''}$

*See refs 25 and 19.

Table 19. PbO: (D–$X^1\Sigma^+$) *system*

$v' \diagdown v''$	0	1	2	3	4	5	6
0	3320·7 $0{\cdot}13_0$ 45	3401·9 $0{\cdot}27_8$ 87	3485·7 $0{\cdot}28_4$ 80	$0{\cdot}18_4$	$0{\cdot}08_4$	$0{\cdot}00_8$	$0{\cdot}00_2$
1	3264·4 $0{\cdot}24_9$ 92	3341·8 $0{\cdot}14_0$ 47	0	$0{\cdot}10_5$	3594·2 $0{\cdot}20_6$ 52	$0{\cdot}17_1$	$0{\cdot}08_8$
2	3209·2 $0{\cdot}25_3$ 100	$0{\cdot}00_1$	$0{\cdot}12_5$	3442·8 $0{\cdot}09_3$ 28	0	$0{\cdot}09_9$	$0{\cdot}18_3$
3	$0{\cdot}18_2$	$0{\cdot}05_7$	$0{\cdot}10_1$	$0{\cdot}00_8$	$0{\cdot}12_1$	$0{\cdot}04_7$	$0{\cdot}01_2$
4	$0{\cdot}10_4$	$0{\cdot}14_1$	$0{\cdot}00_6$	$0{\cdot}10_4$	$0{\cdot}02_6$	$0{\cdot}04_8$	$0{\cdot}10_4$

Legend

$\lambda_{v'v''}$ (A)

$q_{v'v''}$

$q_{v'v''}/\lambda^4_{v'v''}$

Table 20. PbO: $(A\text{–}X^1\Sigma)$ *system*

$v' \diagdown v''$	0	1	2	3	4	5	6	7	8
0	5068·8 $0{\cdot}02_3$ 15	$0{\cdot}09_1$	5459·4 $0{\cdot}17_5$ 81	5677·8 $0{\cdot}21_9$ 87	5910·7 $0{\cdot}14_4$ 68	6160·5 $0{\cdot}08_3$ 41	6427·7 $0{\cdot}04_0$ 20	$0{\cdot}01_6$	
1	$0{\cdot}07_3$	5138·2 $0{\cdot}16_9$ 100	5311·1 $0{\cdot}13_3$ 68	$0{\cdot}02_8$	$0{\cdot}00_6$	$0{\cdot}07_8$	6550·7 $0{\cdot}14_7$ 40	$0{\cdot}15_1$	$0{\cdot}10_3$
2	$0{\cdot}14_1$	$0{\cdot}13_1$	$0{\cdot}01_1$	$0{\cdot}03_7$	5617·6 $0{\cdot}10_6$ 44	$0{\cdot}06_0$	$0{\cdot}00_1$	6342 $0{\cdot}03_6$ 9	$0{\cdot}11_1$
3	$0{\cdot}17_6$	$0{\cdot}04_5$	$0{\cdot}02_5$	$0{\cdot}09_6$	$0{\cdot}02_4$	$0{\cdot}15_2$	$0{\cdot}08_5$	$0{\cdot}06_3$	6433·6 $0{\cdot}00_3$ 1
4	$0{\cdot}17_4$	$0{\cdot}00_3$	$0{\cdot}08_5$	$0{\cdot}03_3$	$0{\cdot}01_7$	$0{\cdot}07_8$	$0{\cdot}02_0$	$0{\cdot}01_4$	$0{\cdot}07_7$
5	$0{\cdot}14_5$	$0{\cdot}02_1$	$0{\cdot}07_8$	$0{\cdot}00_1$	$0{\cdot}07_1$	$0{\cdot}01_7$	$0{\cdot}02_4$	$0{\cdot}06_5$	$0{\cdot}01_1$

Legend

$\lambda_{v'v''}$ (A)

$q_{v'v''}$

$q_{v'v''}/\lambda^4_{v'v''}$

DISCUSSION

The Condon 'parabolae'[9] which are the loci of the most intense bands relative to their neighbours may readily be traced upon the tables. In three-dimensional plots[21] the Condon parabolae lie upon the ridges of the $q_{v'v''}$ surfaces.

For band systems for which no information is yet available for $p_{v'v''}$, and thus for $I_{\propto v'v''}$, the Franck–Condon factors $q_{v'v''}$ and $q_{v'v''}/\lambda^4_{v'v''}$ respectively may be used as approximations. This latter procedure should, however, be employed with some reservations as neglect of the variation of $R_e(r)$ with r could lead in some cases to considerable error as may be seen in tables in which both $p_{v'v''}$ and $q_{v'v''}$ are given.

An example of the use of $p_{v'v''}$ tables in flame spectroscopy may be seen in the recent work of G. V. MARR[28, 29].

This work has been supported in part by the Defence Research Board of Canada through Research Grant No. DRBC 5001–15, in part by the Geophysical Research Directorate of the U.S. Air Force Cambridge Research Centre under Contract AF 19(604)–1718, and in part by The National Research Council of Canada which generously made computing time available upon FERUT.

We wish to acknowledge the cooperation of the Computation Centre, University of Toronto, and especially to thank Miss D. Goulding of that Centre, without whose generous help the computations could not have been made. Dr G. P. Henderson, formerly of the Department of Mathematics of this University, wrote a large part of the computer programme, and his assistance is gratefully acknowledged.

Department of Physics,
University of Western Ontario,
London, Ontario

(*Received April 1958*)

REFERENCES

[1] GAYDON, A. G. *Spectroscopy and Combustion Theory*, 2nd ed. Chapman and Hall: London, 1948

[2] GAYDON, A. G. *The Spectroscopy of Flames*. Chapman and Hall: London, 1957

[3] GAYDON, A. G. and WOLFHARD, H. G. *Flames, Their Structure, Radiation and Temperature*. Chapman and Hall: London, 1953

[4] HERZBERG, G. *Spectra of Diatomic Molecules*, 2nd ed. Van Nostrand: New York, 1950

[5] FRASER, P. A. *Canad. J. Phys.* 32 (1954) 575

[6] BATES, D. R. *Mon. Not. R. astr. Soc.* 112 (1952) 614

[7] NICOLLS, R. W. and JARMAIN, W. R. *Proc. Phys. Soc. Lond. A* 69 (1956) 253

[8] FRANCK, J. *Trans. Faraday Soc.* 21 (1925) 536

[9] CONDON, E. U. *Phys. Rev.* 28 (1926) 1192

[10] HUTCHISSON, E. *Phys. Rev.* 36 (1930) 410

[11] HUTCHISSON, E. *Phys. Rev.* 37 (1931) 45

[12] NICHOLLS, R. W., *The Airglow and the Aurorae*, pp 302–323. Edited by E. B. Armstrong and A. Dalgarno. Pergamon: New York, 1956

[13] NICHOLLS, R. W. *Ann. Géophys.* In press

[14] FRASER, P. A. and JARMAIN, W. R. *Proc. phys. Soc. Lond. A* 66 (1953) 1145

[15] JARMAIN, W. R. and FRASER, P. A. *Proc. phys. Soc. Lond. A* 66 (1953) 1153

[16] FRASER, P. A. *Proc. phys. Soc. Lond. A* 67 (1954) 939

[17] JARMAIN, W. R., FRASER, P. A. and NICHOLLS, R. W. *Astrophys. J.* 118 (1953) 228

[18] Fraser, P. A., Jarmain, W. R. and Nicholls, R. W. *Astrophys. J.* 119 (1954) 286
[19] Jarmain, W. R., Fraser, P. A. and Nicholls, R. W. *Astrophys. J.* 122 (1955) 55
[20] Fraser, P. A., Nicholls, R. W. and Jarmain, W. R. In preparation
[21] Nicholls, R. W. *J. chem. Phys.* 24 (1956) 1104
[22] Turner, R. G. and Nicholls, R. W. *Canad. J. Phys.* 32 (1954) 460
[23] Turner, R. G. and Nicholls, R. W. *Canad. J. Phys.* 32 (1954) 475
[24] Wallace, L. V. and Nicholls, R. W. *J. atmos. terr. Phys.* 7 (1955) 101
[25] Nicholls, R. W. *Proc. phys. Soc. Lond.* 69 (1956) 741
[26] Dixon, R. N. and Nicholls, R. W. *Canad. J. Phys.* 36 (1958) 127
[27] Robinson, D. and Nicholls, R. W. *Proc. phys. Soc. Lond.* In press
[28] Marr, G. V. *Canad. J. Phys.* 35 (1957) 1265
[29] Marr, G. V. *Canad. J. Phys.* 35 (1957) 1275
[30] Pearse, R. W. B. and Gaydon, A. G. *The Identification of Molecular Spectra.* 2nd ed. Wiley: New York, 1950
[31] Phillips, J. G. *Astrophys. J.* 110 (1949) 73
[32] Mulliken, R. S. *Phys. Rev.* 25 (1925) 259
[33] Rosen, B. (Editor). *Données Spectroscopiques concernant les Molécules Diatomiques.* Hermann: Paris, 1951
[34] Wyller, A. *Astrophys. J.* In press
[35] Feast, M. W. *Proc. phys. Soc. Lond. A* 62 (1949) 114
[36] Garton, W. R. S. and Feast, M. W. *Nature, Lond.* 165 (1950) 281
[37] Ditchburn, R. W. and Heddle, D. W. O. *Proc. Roy. Soc. Lond. A* 226 (1954) 509

Combustion and Flame—R. W. Nicholls, P. A. Fraser, W. R. Jarmain—26

The Source of the Continuum in Carbon Monoxide–Hydrogen–Air Flames

W. E. KASKAN

The source of the continuum from flames containing carbon monoxide and oxygen has been investigated by measuring both the emission intensity and [OH] *in the flame gases from rich carbon monoxide–hydrogen–air flames. The concentrations of carbon monoxide are calculated from the water gas equilibrium and those of oxygen atoms are calculated from the measured* [OH]. *It is shown that the light-producing step involves a reaction between a carbon monoxide molecule and an oxygen atom with a rate constant of* $2{\cdot}7\times10^{-19}$ *cm*^{3}/*molecule sec. In the range of conditions employed the continuum amounts to about 95 per cent of the radiation. It is shown that the rate of decay of radicals is not much affected by the presence of carbon monoxide and carbon dioxide.*

THE source of the blue radiation from flames containing carbon monoxide and oxygen has been a subject of investigation for many years. The work up to quite recently has been reviewed by A. G. GAYDON[1]. This radiation consists of a continuum extending from below 3 000 Å throughout the visible and beyond, with a maximum in the blue, plus some superimposed structure generally referred to as the carbon monoxide flame bands. These have not as yet been satisfactorily analysed. In high temperature flames, in addition to these there can also be observed the Schumann–Runge bands of oxygen[2], as well as another band system of the oxygen molecule[3]. The continuum and flame bands are most intense in carbon monoxide flames but can also be observed in hydrocarbon–air flames, and hydrogen–air flames to which carbon dioxide has been added[1]. In other words, they are characteristic of flames containing carbon and oxygen.

Most of the previous work has been directed towards an understanding of the flame bands. However, at not too low a pressure the bulk of the radiation is associated with the continuum. For example, in explosions at (initially) 100 to 200 mm, R. H. KNIPE and A. S. GORDON[4] estimate that the continuum represents about 90 per cent of the energy radiated. On the other hand, the intensity of the bands relative to that of the continuum has been reported to increase with decreasing pressure and temperature[5]. H. P. BROIDA and A. G. GAYDON have reported the bands alone in a discharge at 3 mm[6].

The present paper is concerned only with the continuum. Gaydon has suggested that it arises from the reaction

$$CO + O \rightarrow CO_2 + h\nu \qquad \ldots.[1]$$

where the state of the CO_2 molecule is not necessarily specified, but CO and O are in their ground states. On the other hand, G. A. HORNBECK has suggested that the continuum may come from the radiative recombination of two oxygen atoms[2].

In a previous paper it was shown that part of the radiation from lean hydrogen–air flame gases to which some nitric oxide had been added was due to the radiative recombination

$$NO + O \rightarrow NO_2 + h\nu \qquad \ldots.[2]$$

and a rate constant for the reaction was determined[7]. This conclusion was in accord with other work[8, 9] and the value for the rate constant was in good agreement with that determined by F. KAUFMAN[10] who added nitric oxide to oxygen atoms produced by a discharge. The similarity between reactions 1 and 2 suggested that it might be possible to ascertain the source of the carbon monoxide flame continuum by the technique used for the nitric oxide–oxygen continuum. In the latter case the experiments were done in flames which were not hot enough to decompose the nitric oxide[11] appreciably, and the oxygen atom concentration was calculated from the measured hydroyxl concentration assuming equilibration of the reaction

$$2OH \rightleftharpoons H_2O + O \qquad \ldots.[3]$$

[OH] was measured spectroscopically by the line absorption technique[12]*. The knowledge of both [NO] and [O] allowed a direct comparison of the light intensity and the product [NO][O], with the result that reaction 2 was shown to be the light-producing reaction.

A similar situation exists with respect to reaction 1, or for that matter the recombination of two oxygen atoms, in rich flames containing carbon monoxide. As long as the temperature is sufficiently high to ensure that the water gas equilibrium is maintained, [CO] can be calculated from the known stoichiometry and the temperature. This together with the measurement of [OH] should suffice to determine the light-producing reaction.

EXPERIMENTAL

Except for the wavelength at which the emission was measured, the equipment and techniques were identical with those previously described[7, 12, 13]. Light intensity was measured at 4 345 Å. This wavelength was chosen because it was essentially at the peak of the curve of the response of the system to the continuum and also because it was in a valley between two of the flame bands. This was desirable since it was expected that the behaviour of the flame bands might be different from that of the underlying continuum.

In addition to the measurements of intensity, the spectrum was scanned from 3 200 to 6 000 Å under the various conditions employed. The scanning was done with slits with a band pass of 10 Å, but a single scan of a very bright flame using slits with a band pass of only 0·4 Å showed no obvious difference in the relative intensities of the bands and the continuum. A check for self-absorption using a mirror behind the flame was made at 4 345 Å in a relatively luminous flame and none was observed.

---

*In equation 7 of ref. 12 the factor of 4 in the expression for the partition function which corrects for the spin and λ doubling of the $^2\Pi$ state was accidentally omitted. Both here and in ref. 12 the correct expression was used to calculate [OH].

As before[7, 12] the flames were burned on cooled porous metal burners, and an annular sheath of nitrogen was provided to prevent the formation of a diffusion flame between the hot gas and the atmosphere. Both [OH] and the light intensity were measured as a function of distance from the burner. For atmospheric pressure flames the first measurement was at 2 mm from the burner and subsequent measurements were made at 2 mm intervals. For the low pressure flames measurements were made at intervals of 3·18 mm ($\frac{1}{8}$ in.). Temperatures were measured with silica-coated Pt/Pt–10% Rh thermocouples and corrected for radiation loss[13]. Considerable care was taken to measure the emission and [OH] at the same distances from the burner, and to ensure that the volume elements being studied were parallel to the burner surface. The system sensitivity was checked during each run with a constant intensity radioactively excited phosphor disc. The hydrogen used was 99·9 per cent pure (nitrogen impurity) and carbon monoxide, 99·5 per cent pure (hydrogen and nitrogen impurities) the air was taken from cylinders maintained at 2 000 lb/in^2.

RESULTS

(a) *Spectrum*

It was not intended in this work to make a study of the spectrum *per se*, but a few observations may be noted. Assuming that the flame bands were essentially resolved from the continuum under all of the conditions reported on here, about 95 per cent of the light energy was in the continuum. There was no marked change in this proportion with change in temperature or pressure from 0·158 to 1 atmosphere, but there did seem to be a slight strengthening of the bands relative to the continuum at the lower pressures. This statement can only be made qualitatively, since the photocell noise was always appreciable relative to the structure, and sometimes just as large.

In agreement with A. G. GAYDON and F. GUEDENEY[14] the violet end of the spectrum was strengthened with increasing temperature. This was shown by choosing one spectral distribution (neglecting the structure) as a standard and fitting this curve to the other spectra at 4 200 Å. It was found that all of the spectra had the same spectral distribution from 4 200 Å and above, and that only below this was the enhancement noticeable.

The spectral distribution of the continuum (neglecting the flame bands) from a flame at 1 900°K is shown in *Figure 1*, together with similar data reported by Knipe and Gordon[4]. The two curves were normalized at 5 600 Å. The agreement is only fair, especially since Knipe and Gordon's flames were at considerably higher temperature which should have given a distribution relatively stronger toward the violet.

(b) *Light intensity as a function of* [OH]

As before, [OH] was always found to be a maximum nearest the burner, and to decay downstream. The behaviour of the emission was similar. This fact allowed several observations to be made on each flame under conditions of essentially constant temperature and gross composition.

Some pertinent data for the five runs made are given in *Table 1*. The second to fourth columns give the unburnt gas composition and the fifth to eighth columns give the burnt gas composition calculated from the data given by B. LEWIS and G. VON ELBE[15] and the unburnt composition. The burnt gas compositions are simply those given by the water gas equilibrium and are not corrected for the amount of material tied up in the excess radical concentrations since the latter are relatively small. The next four columns give the maximum gas temperature, the pressure, and the cold gas velocity, and the length of the optical path. The thirteenth column gives the maximum hydroxyl concentration found, the fourteenth the ratio of this to the equilibrium concentration, and the next column gives the distance from the burner at which $[OH]_{max.}$ was determined. These are in all cases the minimum distances at which measurements were made.

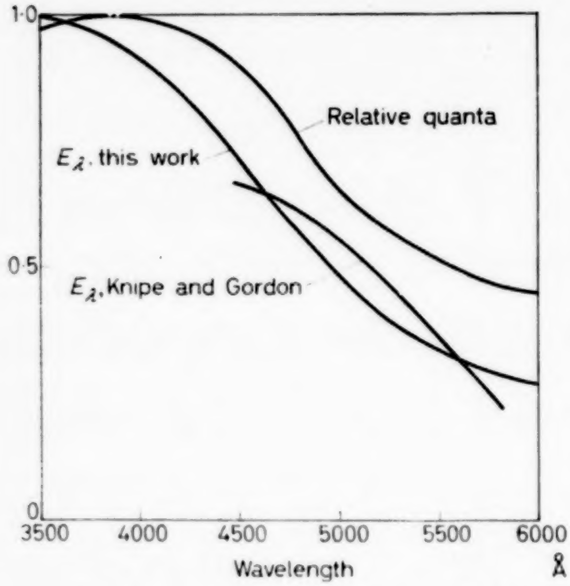

Figure 1. Intensity distribution in the carbon monoxide–oxygen continuum in terms of relative energy per unit wavelength interval and relative number of quanta per unit wavelength interval

Table 1

Run	*Unburnt gas composition, moles per mole of air*			*Burnt gas composition mole fraction*				*T*	*P*
	H_2	CO	CO_2	H_2	H_2O	CO	CO_2	°*K*	*atm*
1	0·226	0·260	—	0·014	0·162	0·039	0·165	1535	1
2	0·077	0·507	—	0·0054	0·0505	0·115	0·254	1880	1
3	0·469	—	0·211	0·016	0·303	0·019	0·124	1565	1
4	0·294	0·252	—	0·036	0·187	0·064	0·124	1520	0·325
5	0·193	0·410	—	0·0235	0·115	0·109	0·185	1520	0·158

Run	V_{25} *cm/s*	*l* *cm*	$[OH]_{max.} \times 10^{-16}$ *molecules per cm*^{3}	$\frac{[OH]_{max.}}{[OH]_{equ.}}$	*z* *mm*	$\frac{[H]}{[OH]}$	k_5 [M] *cm*^{3}*/mole sec* $\times 10^{-13}$
1	13·0	6·0	0·149	345	2·0	3·26	0·6
2	29·2	6·0	0·472	39	2·0	1·65	0·3
3	31·0	6·0	0·284	250	2·0	1·86	0·8
4	32·0	7·5	0·142	100	3·0	7·8	0·12
5	41·2	7·5	0·127	1650	4·6	7·7	0·04

The penultimate column gives the ratio of [H] to [OH], assuming the equilibration of the reaction

$$\mathrm{OH}+\mathrm{H}_2 \rightleftharpoons \mathrm{H}_2\mathrm{O}+\mathrm{H} \qquad \ldots.[4]$$

The last column gives (approximately) the rate constants for the reaction

$$\mathrm{M}+\mathrm{H}+\mathrm{H} \rightarrow \mathrm{H}_2+\mathrm{M} \qquad \ldots.[5]$$

which were calculated as described in ref. 12.

In each of the three one-atmosphere runs the gas temperature at all distances from the burner was essentially the temperature given in *Table 1*. In runs 4 and 5, however, temperature rises of 70° and 100°C respectively took place in the distance between the first and last measurements. The compositions in *Table 1* are given for the maximum temperature, which is the one listed.

As pointed out initially, the most likely light-producing reaction is reaction 1. This reaction leads to the prediction that the light intensity per unit volume should be proportional to the product [CO] [O] so that in the present case

$$I/l\,[\mathrm{CO}] \propto [\mathrm{O}] = [\mathrm{OH}]^2\,K_3/[\mathrm{H}_2\mathrm{O}] \qquad \ldots.[6]$$

where I is the intensity measured as described and l is the length of the optical path in centimetres. Thus a log/log plot of $I/l\,[\mathrm{CO}]$ against $[\mathrm{OH}]\{(K_3/[\mathrm{H}_2\mathrm{O}])\}^{\frac{1}{2}}$ should be a straight line with a slope of 2. In *Figure 2* are shown all the data from the five runs described in *Table 1* plotted in this way. For runs 1 to 3 the quantity $(K_3/[\mathrm{H}_2\mathrm{O}])^{\frac{1}{2}}$ was a constant during the run since the temperature was essentially constant, but for the other two runs the variation in temperature from point to point

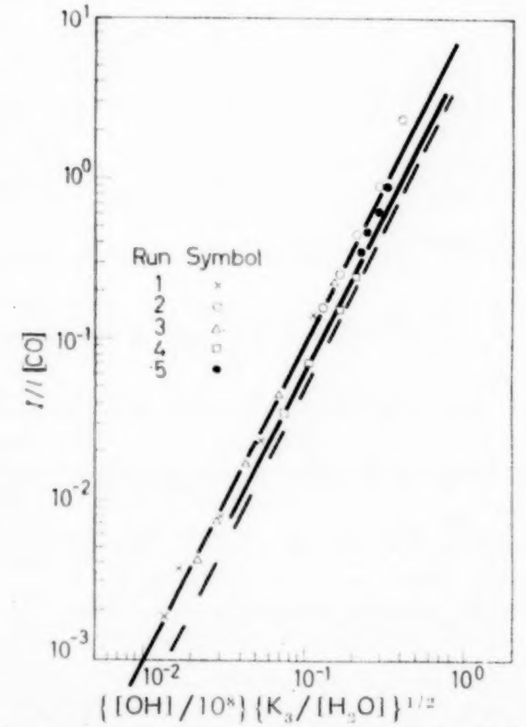

Figure 2. Intensity of emission in 10 Å wide band at 4 345 Å per unit path length per unit CO *concentration as a function of the 1/2 power of oxygen atom concentration as calculated from* [OH]. *Concentrations in units of 10^{16} molecules/cm³ Data for runs given in Table 1. Broken line is that on which data on the two full lines would fall if pressure broadening of hydroxyl lines were taken into account.*

was taken into account in calculating this factor. The two full lines in *Figure 2* are drawn with a slope of 2 through the one atmosphere data and through the data for run 4, respectively. It can be seen that the two sets of data fit the two lines very well. The fit of the data from run 5 to the line for run 4 is not as good, and this will be discussed later. Considering only the first four runs, the fact that the two lines do not coincide is undoubtedly due to the fact that the hydroxyl lines are actually somewhat pressure broadened[16]. The assumption of a pressure broadening parameter $a' = 0{\cdot}3$ would cause all of the data for the first four runs to fall essentially on a single line, the broken line in *Figure 2*. This value for a' is in good agreement with the value of 0·25 deduced from a similar disparity in the study of the nitric oxide–oxygen continuum[7].

DISCUSSION

Before considering the light-producing reaction in more detail, the validity of the calculations of [CO] and of [O] should be examined. Recent work in this laboratory has shown that the establishment of the water gas equilibrium by reaction 4 and by the reaction

$$\mathrm{CO + OH \rightleftharpoons CO_2 + H} \qquad \ldots .[7]$$

is very rapid and essentially complete near the flame zone for flames of the temperatures used here[17]. Thus there seems to be little doubt that we are justified in assuming the water gas equilibrium to be established and in thus calculating [CO].

In the previously referred to work on the nitric oxide–nitrogen continuum[7], only lean flames were examined. It was shown that in the flame gases in this temperature range, reaction 3 and its reverse as written were probably fast enough to effect the equilibration at the [OH] concentrations observed. It was pointed out that whether or not this was so, the equilibration represented by reaction 3 would undoubtedly be catalysed by H and H_2 via the pair of reactions[18]

$$\mathrm{OH + H_2 \rightleftharpoons H_2O + H} \qquad \ldots .[4]$$

$$\mathrm{OH + H \rightleftharpoons H_2 + O} \qquad \ldots .[8]$$

Thus it appears certain, in the rich flames used here with their relatively high H and H_2 concentrations, that it is valid to calculate [O] from [OH] by assuming the equlibration of reaction 3.

Although the data for the first four runs in *Figure 2* are consistent with the demands of reaction 1, it remains to be shown that there is no other possible reaction which would do as well. The data show that in any run the light intensity is proportional to $[\mathrm{OH}]^2$, since [CO] and I are both constant. The other molecules and atoms which are expected to be present in excess of the equilibrium are H, O and O_2. The concentration of H is undoubtedly proportional[7, 12, 18] to [OH] and that of O and of O_2 to $[\mathrm{OH}]^2$. Considering these species then, the only other combinations which could both lead to an $[\mathrm{OH}]^2$ dependence of the light intensity and to a reaction with sufficient energy to emit the continuum are: (*a*) two H atoms; (*b*) H plus OH; (*c*) O plus H_2. There is an additional restriction on these reactions; they must involve carbon monoxide or carbon dioxide as a third body, since the emission is characteristic of flames containing carbon monoxide or carbon dioxide, and in the present experiments the magnitudes of the concentrations of all of the species in possibilities (*a*) to (*c*) are not particularly changed when either carbon monoxide or carbon dioxide is added to the hydrogen–air system.

From the data given in *Table 1* and in *Figure 2* it is easy to show that none of the three possibilities can account for the data. Thus we can conclude that the reaction certainly involves a carbon monoxide molecule plus an oxygen atom. Furthermore, there is no effect of pressure. The relative displacement of the one-atmosphere data and the low-pressure data is most easily explained by the assumption of some pressure broadening of the OH lines. In any case, it certainly does not represent the pressure effect to be expected if reaction 1 involved a third body, since the value of $I/I[\mathrm{CO}]$ at a constant $\{[\mathrm{OH}](K_3/[\mathrm{H_2O}])\}^{\frac{1}{2}}$ would then have been proportional to pressure, which it clearly is not.

There are two ways in which a reaction between carbon monoxide and oxygen to produce light at a rate independent of pressure could take place. The first and most obvious is by reaction 1 as written. The other is by the set of reactions

$$\mathrm{CO+O+M \rightarrow CO_2^* + M} \qquad \dots .[9]$$

$$\mathrm{CO_2^* + M \rightarrow CO_2 + M} \qquad \dots .[10]$$

$$\mathrm{CO_2^* \rightarrow CO_2} + h\nu \qquad \dots .[11]$$

Assuming that the first two of these are rapid compared with the time scale of the experiments, the steady state approximation can be applied at any level above the burner. Thus

$$\mathrm{d}[\mathrm{CO_2^*}]/\mathrm{d}t = 0 = k_9[\mathrm{M}][\mathrm{CO}][\mathrm{O}] - (k_{10}[\mathrm{M}] + k_{11})[\mathrm{CO_2}]^* \qquad \dots .[12]$$

and

$$I = k_{11}[\mathrm{CO_2}]^* = \{k_{11}k_9[\mathrm{M}]/(k_{10}[\mathrm{M}] + k_{11})\}[\mathrm{CO}][\mathrm{O}] \qquad \dots .[13]$$

Equation 13 gives an intensity proportional to the product [CO] [O] and independent of pressure provided only that k_{10} [M] is always much larger (i.e. by a factor of ten or more) than k_{11}. k_{11} is of course the transition probability. The present data are not capable of distinguishing between the two possibilities, reaction 1 as opposed to the set 9 to 11. The latter alternative is more restrictive than the former and thus is probably not to be preferred. All that can be said with certainty is that it has been proved that the light-producing reaction involves an oxygen atom and a carbon monoxide molecule.

The data in *Figure 2* for run 5 deviate from the expected behaviour in the direction of too much emission for a given value of $\{[\mathrm{OH}](K_3/[\mathrm{H_2O}]\}^{\frac{1}{2}}$. There seems to be a tendency for the data to approach the expected behaviour as the gases pass downstream (direction of decreasing emission and [OH]). The flame of run 5 was characterized by, among other things, the fact that the zone of most rapid reaction was most nearly approached in the measurements. In general it is certainly true that as measurements are made farther and farther upstream the assumptions made in deriving equation 6 must ultimately break down. It is felt that the small discrepancy noted in this flame is due to just this fact, namely that the measurements were made too close to the zone of rapid reaction and equation 6 no longer holds exactly because insufficient time has been allowed for the various reactions to equilibrate. However, it is clear that equation 6 is obeyed approximately.

The fact that no temperature dependence was found is probably mostly accidental and results from the choice made of wavelength for observation. Since the strengthening of the blue end of the spectrum described by Gaydon and Guedeney[14] was also observed by us, it seems likely that at a shorter wavelength a temperature effect would have been noticed. This point is worthy of further study. Of course, under the conditions of our experiments, an activation energy for radiation at 4 345 Å of only two or three kilocalories per mole could have gone unnoticed.

Leaving out any temperature dependence, the data obtained allow an estimate to be made of the rate constant for the light-producing reaction. By comparison with a tungsten strip filament lamp operating at a known temperature, it was established that, at the point on the broken line in *Figure 2* at $I/I[\mathrm{CO}] = 1{\cdot}0$ the gas was radiating at a rate of $1{\cdot}5 \times 10^{10}$ quanta per sec per cm^3 into the total solid angle in the 10 Å band at 4 345 Å. The unit of concentration of carbon monoxide in the function $I/I[\mathrm{CO}]$ was taken as 10^{16} molecules per cm^3. At this same point the oxygen atom concentration is 2×10^{15} atoms/cm^3.

From the curve in *Figure 1* giving the relative number of quanta per unit wavelength interval as a function of wavelength, it can be determined that the total number of quanta radiated from 3 500 to 6 000 Å is 194 times the number in the above 10 Å band. It is clear from *Figure 1* that not all the quanta have been counted, but from the shape of the curve and from other information on the extent of the continuum[1] it would seem to be a reasonable guess that the ratio of all the quanta to those counted at 4 345 Å is about 400. This number combined with the rate of emission in the 10 Å band and the oxygen and carbon monoxide concentrations leads to a value for k_1 of $2{\cdot}7 \times 10^{-19}$ cm^3/molecule sec. This may be compared with the value of 2×10^{-18} for k_2 derived previously. Assuming that this is k_1, dividing by the collision number gives a value of about 5×10^{-10} for the probability of radiation per collision. On dividing this by the time of a collision, say 10^{-13} or 10^{-14} sec, a probability for spontaneous emission of the order of 10^3 is obtained, corresponding to a somewhat forbidden transition.

Considering again the set of reactions 9 to 11, if k_9 and k_{10} have values appropriate for very efficient three- and two-body processes respectively, then the ratio k_9/k_{10} becomes about 10^{-21}, and k_{11} is about 10^4, not too different from the value deduced for reaction 1. Furthermore, the product $k_{10}[\mathrm{M}]$ in this work would always be larger than k_{11}. Thus it is still not possible to choose between the two alternatives.

It should be pointed out in this connection that a similar argument can be made for the nitric oxide–oxygen atom continuum. It is less plausible here because the rate constants at one atmosphere and at one or two millimetres have been found to be not too different[7, 10].

To conclude the discussion of the continuum, the fact that the continuum has been shown to involve carbon monoxide provides a relatively easy spectroscopic method for the determination of carbon monoxide concentrations provided that [O] can be measured. Thus the findings presented here allow a purely spectroscopic study of the high temperature oxidation of carbon monoxide in lean flames, where [O] is known to be calculable from [OH][7]. Such a study has been made and will be reported in a subsequent paper.

Although it was not the purpose of these experiments to provide information on the radical decay process, this aspect of the work will be dealt with briefly. In *Table 1* the rates of decay have been expressed as $k_5[M]$, following the treatment in an earlier paper[12] where k_5 is the rate constant for the three-body recombination of H atoms

$$H + H + M \rightarrow H_2 + M \qquad \ldots.[5]$$

These data have been included here mainly for comparison with the other data. However, the conditions under which the runs in *Table 1* were made were for the most part not such as to allow reliable conclusions to be drawn concerning the rate constants for the recombination reactions. It will be recalled that $k_5[M]$ was obtained from

$$k_5[M] = \{[H_2O]/2K_4[H_2]\}\, d(1/[OH])/dt \qquad \ldots.[14]$$

where K_4 is the equilibrium constant for reaction 4. This expression was derived assuming that the rate constants for equations 5 and for 15

$$H + OH + M \rightarrow H_2O + M \qquad \ldots.[15]$$

were equal, that only H and OH had to be accounted for, and that $[H] \gg [OH]$. Furthermore, it was shown that the effect of diffusion was quite appreciable in the slower flames, such as run 1 (*Table 1*).

Of the runs in *Table 1*, all of them were plotted reasonably well according to equation 14 except for the last. For this one the rate constant in *Table 1* was obtained from the last two points. Of these five runs only run 3 was done under conditions which were suitable, and even this run was poor because the [H]/[OH] ratio was not very large. The rate constant for this run is most nearly equal to those obtained previously. The oxygen concentrations calculated from [OH] in run 2 are of the order of [OH], a fact which should tend to reduce materially the rate of decay of hydroxyl, which was observed. In the two low-pressure runs diffusion should have been fairly important and in both of these again the calculated oxygen concentrations are relatively high. In general, however, the values for $k_5[M]$ are not markedly different from those in rich hydrogen–air flames, which suggests that the rates of reactions 15 and 5 are not materially affected by the presence of carbon monoxide and carbon dioxide.

The author wishes to acknowledge the aid of W. W. Crotty in carrying out the experiments.

G.E. Research Laboratory,
Schenectady, N.Y.

(*Received June 1958*)

REFERENCES

[1] GAYDON, A. G. *The Spectroscopy of Flames*, Chap. 6. Chapman and Hall: London, 1957

[2] HORNBECK, G. A. *Third Symposium (International) on Combustion, Flame and Explosion Phenomena*, p 501. Williams and Wilkins: Baltimore, 1949

[3] HORNBECK, G. A. and HOPFIELD, H. S. *J. chem. Phys.* 17 (1949) 982

[4] KNIPE, R. H. and GORDON, A. S. *J. chem. Phys.* 23 (1955) 2097

[5] GAYDON, A. G. *Proc. Roy. Soc. A* 182 (1943) 199

[6] BROIDA, H. P. and GAYDON, A. G. *Trans. Faraday Soc.* 49 (1953) 1190

[7] KASKAN, W. E. *Combustion & Flame* 2 (1958) 286

[8] GAYDON, A. G. *loc. cit.* p 70

[9] JAMES, C. G. and SUGDEN, T. M. *Nature, Lond.* 175 (1955) 252

[10] KAUFMAN, F. *J. chem. Phys.* 28 (1958) 352

[11] FENIMORE, C. P. and JONES G. W. *J. phys. Chem.* 61 (1957) 654

[12] KASKAN, W. E. *Combustion & Flame* 2 (1958) 229

[13] KASKAN, W. E. *Sixth Symposium (International) on Combustion*, p 134. Reinhold: New York, 1957

[14] GAYDON, A. G. and GUEDENEY, F. *Trans. Faraday Soc.* 51 (1955) 894

[15] LEWIS, B. and VON ELBE, G. *Combustion, Flames and Explosions of Gases*, p. 742. Academic Press: New York, 1951

[16] KASKAN, W. E. *J. chem. Phys.* 28 (1958) 729

[17] FENIMORE, C. P. and JONES, G. W. *J. phys. Chem.* 62 (1958) 1578

[18] BULEWICZ, E. M., JAMES, C. G. and SUGDEN, T. M. *Proc. Roy. Soc. A* 235 (1956) 89

Excess Radical Concentrations and the Disappearance of Carbon Monoxide in Flame Gases from Some Lean Flames

W. E. Kaskan

Both the concentrations of hydroxyl and the intensities of the carbon monoxide–oxygen continuum have been measured in a series of lean hydrogen–carbon monoxide–air, hydrogen–carbon dioxide–air and ethylene–air flames burning on cooled porous metal burners. Since the continuum is known to come from a reaction of carbon monoxide and oxygen and since [O] *is calculable under some conditions at least from* [OH], *these measurements effectively determine* [CO]. *It is shown that above 1 500° K the relationship of emitted intensity to* [OH] *is consistent with a scheme involving the equilibration of the reaction*

$$CO + OH \rightleftharpoons CO_2 + H$$

as well as the first three reactions in the hydrogen–oxygen scheme. Because of this equilibration it is concluded that above 1 500° K excess carbon monoxide concentrations disappear by a recombination process rather than by an oxidation process. It is shown that this recombination process is probably the same one which operates in lean hydrogen–air flames in the absence of carbon monoxide and carbon dioxide.

In a previous paper[1] it was shown that the continuum emitted by flames containing carbon monoxide and oxygen arises from a reaction between a carbon monoxide molecule and an oxygen atom. This reaction is probably

$$CO + O \rightarrow CO_2 + h\nu \qquad \ldots.[1]$$

where carbon monoxide and oxygen are both in their ground states but the state of carbon dioxide is not specified and is presumed to be irrelevant to the subject of this paper. A rate constant was deduced for reaction 1.

This finding suggests the possibility of studying the high temperature oxidation of CO in flame gases by a purely spectroscopic technique. Since the emitted light as measured in the previous paper[1] is proportional to the product [CO] [O] and since [O] can be calculated from the measured [OH] and the equilibrium constant for the reaction[2]

$$2OH \rightleftharpoons H_2O + O \qquad \ldots.[2]$$

it should be possible by combining the measurements to determine [CO]. Reaction 2 was previously shown to be equilibrated at least down to about 1 500°K in flame gases from lean hydrogen–air flames held on porous burners, by means of the nitric oxide test for oxygen atoms[2].

The work on the high temperature water-catalysed oxidation of carbon monoxide is in need of clarification. Flame sampling studies in lean flames have shown that the decay of CO is apparently first order in carbon monoxide[3–5] and this was interpreted by C. P. Fenimore and G. W. Jones[3] in terms of a free radical mechanism involving the reaction

$$CO + OH \rightarrow CO_2 + H \qquad \ldots.[3]$$

Furthermore, in the absence of any other information, these authors assumed in their treatment that [OH] was constant, i.e. independent of distance from the burner, which allowed them to use a steady state treatment of the data. However, recent developments have caused two serious difficulties to arise with respect to this interpretation. In the first place the finding that hydroxyl concentrations are generally higher than equilibrium in flame gases and that they decay downstream[2] shows that one cannot assume a steady state if reaction 3 is to be retained. The second difficulty is that reaction 3 is so fast in both directions at high temperatures[4] that it is questionable whether one is justified in assuming that it goes only in the forward direction.

Thus, as is also pointed out by C. P. FENIMORE and G. W. JONES[5], if their rate constant for reaction 3 is combined with their observed [CO] and the equilibrium [OH] (a lower limit as will be shown in this paper) the resulting rate is much higher than the rate of carbon monoxide disappearance observed by them for the higher temperature runs. Similarly the rate of the reverse reaction calculated from the known $[CO_2]$ and the equilibrium [H] is relatively large.

This condition, where the actual forward and reverse rates are considerably larger than the net rate for the reaction, is precisely that required for equilibration. Under these circumstances the concentrations of these four species are related, to an approximation which depends on the relative magnitudes of the actual rates as compared with the net rate, as they are at equilibrium by the relationship

$$[H][CO_2]/[OH][CO] = K_3 \qquad [4]$$

where K is the equilibrium constant.

In a previous paper[2] it was shown, by means of the nitric oxide test for oxygen atoms, that in a variety of lean hydrogen–air flames the reaction

$$2OH \rightleftharpoons H_2O + O \qquad \ldots [2]$$

was equilibrated in the flame gases. This reaction is formally equivalent to the difference of the reactions

$$OH + H_2 \rightleftharpoons H_2O + H \qquad \ldots [5]$$

$$O + H_2 \rightleftharpoons OH + H \qquad \ldots [6]$$

If the assumption is made, as a hypothesis to be tested by its success in interpreting the data, that these two reactions are each equilibrated and likewise the reaction

$$H + O_2 \rightleftharpoons OH + O \qquad \ldots [7]$$

there is obtained a system of four equations of the form of equation 4 by means of which the concentrations of carbon monoxide, hydrogen, and oxygen and hydrogen atoms can be expressed in terms of [OH], $[H_2O]$, $[CO_2]$ and $[O_2]$. These are:

$$[CO] = \frac{K_5}{K_3 K_7 K_6} \frac{[OH]^2 [CO_2]}{[H_2O][O_2]} \qquad \ldots [8]$$

$$[H_2] = \frac{[OH]^2}{K K [O_2]} \qquad \ldots.[9]$$

$$[O] = K \frac{[OH]^2}{[H_2O]} \qquad \ldots.[10]$$

$$[H] = \frac{K}{K K} \frac{[OH]^3}{[H_2O][O_2]} \qquad \ldots.[11]$$

As above, the expressions can be expected to apply with increasing accuracy with an increasing ratio of the actual rates, forward and reverse, of reactions 3 and 5–7 to the net rates.

The formulation of the problem embodied in equations 4 and 8–11, involving as it does many assumptions not easily justified, would not be too meaningful except for the fact that it allows a very simple test to be made of its validity. Since, as has been pointed out above, under some conditions equation 10 is satisfied and since the intensity of the blue continuum is proportional to the product [CO][O], then from equations 8 and 10

$$I \propto [CO][O] = [OH]^4 \left[\frac{K}{K K} \frac{[CO_2]}{[H_2O]^2[O_2]}\right] \qquad \ldots.[12]$$

where I is the intensity of the continuum as measured previously and where the constant of proportionality is known. It should be noted that equation 12 can only be derived by assuming that all four reactions 3 and 5–7 are equilibrated.

Equation 12 predicts that insofar as the equilibration is maintained, the intensity of emission should be proportional to the fourth power of [OH] multiplied by the expression in brackets in equation 12. Conversely, insofar as this relationship between [OH] and the emission intensity is found to hold, this will be evidence that under those conditions the equilibration scheme is valid and the concentrations of the various species in excess can be calculated from the measured [OH] by means of equations 8 to 11.

The objective of the work reported here was principally to learn whether equation 12 was satisfied under any conditions in lean flames containing hydrogen and carbon, and if so to delineate roughly this range of conditions. In addition it was intended to see what further light could be thrown on the rate and mechanism of the disappearance of excess carbon monoxide in the flame gases.

EXPERIMENTAL

The technique and equipment were identical with those used previously[1, 2, 7]. Lean flames were burned on flat porous metal burners and measurements of [OH] and of the intensity of emission in a 10 Å wide band at 4 345 Å were made as a function of distance from the burner. As before, care was taken to ensure that [OH] and the intensity were measured at as nearly as possible the same level, and that the sheet of gas being observed was as nearly parallel to the burner as possible. Measurements were generally made between 1·5 and 11 mm from the burner at atmospheric pressure, and from 3 to 17 mm from the burner at reduced pressure. The system sensitivity to the emitted light was checked during each run by comparison with a radioactively excited phosphor disc. (The lifetime of the exciting material is 25 years, so that constancy of light output was assured.) Temperatures were measured with silica-coated Pt/Pt-10% Rh thermocouples[8] and a few checks were made against the rotational temperatures of hydroxyl as determined by absorption. The agreements were within 100°C or better. [OH] was determined from the measured temperature and the absorption of a single line, either $P_1 5$ or $Q_1 12$. The latter line was used at high hydroxyl concentrations in order that the absorption should not be so strong.

In a few of the high temperature flames some emission by hydroxyl was detectable under the conditions in which absorption was being determined. This never amounted to more than a few per cent of the intensity of the light from the source, and it was corrected for where necessary.

All flames were burnt with air, and the fuels were mixtures of hydrogen plus carbon monoxide, or hydrogen plus carbon dioxide, and in one flame, ethylene. In the latter case, the spectrum near 4 345 Å was scanned to ensure that CH radiation had died out before measurements were made. The hydrogen was electrolytic, 99·9 per cent pure (nitrogen impurity); the carbon monoxide was 99·5 per cent pure (hydrogen and nitrogen impurities); the carbon dioxide was 99·5 per cent pure (air and water vapour impurities); the ethylene was C.P. grade, 99·5 per cent pure; and the air used was relatively dry, being taken from cylinders which were kept charged to 2 000 lb/in^2.

RESULTS

As before[1, 2, 7] [OH] near the flame was always found to be higher than equilibrium and to decay downstream; plots of 1/[OH] against time were generally good straight lines. *Table 1* summarizes the conditions of the runs and the hydroxyl concentrations observed. Columns 2 to 5 give the cold gas composition, and the next three columns give the cold gas velocity, pressure and maximum flame temperature. In the ninth column are the maximum hydroxyl concentrations observed, and in the tenth the distance from the burner at which $[\mathrm{OH}]_{\max}$ was found, which in all of the cases is the minimum beam–burner distance. The eleventh column gives the ratio of $[\mathrm{OH}]_{\max}$ to the equilibrium concentration as calculated from the data given by B. LEWIS and G. VON ELBE[9]. The last column gives a rate constant for the decay of OH which as before is defined simply by

$$k_{\mathrm{OH}} = \tfrac{1}{2}\,\mathrm{d}\,\{1/[\mathrm{OH}]\}/\mathrm{d}t \qquad \ldots\ldots [13]$$

These are given principally for the purpose of comparison with the data on lean hydrogen–air flames in ref. 2, where it was shown that the decay rates of hydroxyl were consistent with a reaction bimolecular in OH.

The spectrum was scanned for almost all of the flames, and for many of them it was scanned at more than one level. The results were as with the rich flames[1]. The intensity of the flame bands relative to that of the continuum was not dependent on composition, temperature or pressure.

An enhancement of the intensity of the violet end of the spectrum was found at the higher temperatures[10]. The intensity distribution for any flame was independent of distance from the burner (i.e. intensity).

The intensity of emission in all cases fell off rapidly as the gases passed downstream from the flame. The data on the emission intensity as related to hydroxyl concentrations are given in *Figures 1* and *2* in the form required

Table 1

Run	*Unburnt gas composition, moles/mole air*				V_{25}	P
	H_2	CO	CO_2	*Other*	*cm/s*	*atm*
6				0·0574 (C_3H_8)	28·2	1
7	0·158	0·158			44·3	1
8	0·158	0·158			25·5	1
9	0·158	0·158			16·3	1
10	0·026	0·287			6·63	1
11	0·358		0·095		60·5	1
12	0·358		0·095		35·2	1
13	0·256		0·0865		18·2	1
14	0·152	0·122			11·3	1
15	0·324	0·062		1·015 (N_2)	21·2	1
16	0·153	0·062			10·7	1
17	0·1983	[illegible]			30·0	0·38
18	0·0878	0·0815			33·5	0·38
19	0·297	0·061			29·8	0·304

Run	T K	$[OH]_{max}$ $\times 10^{-16}$	z *mm*	$\frac{[OH]_{max}}{[OH]_{eqm}}$	$10^{13}\,k_{OH}$ *cm³/molecule sec*
6	2000	1·20	1·5	2·77	0·12
7	1900	1·06	1·5	3·3	0·12
8	1820	0·682	1·5	3·0	0·25
9	1640	0·451	1·5	6·4	0·64
10	1660	0·286	2·0	8·8	0·20
11	1870	0·915	2·0	2·6	0·25
12	1750	0·570	2·0	3·25	0·35
13	1510	0·260	2·0	7·2	1·0
14	1550	0·299	2·0	7·5	0·6
15	1510	0·304	2·0	17·2	0·45
16	1440	0·270	2·0	15·2	0·8
17	1670	0·393	3·0	11·9	0·20
18	1660	0·341	4·6	10·8	0·30
19	1670	0·397	2·9	22·2	0·15

by equation 12. In both figures the logarithm of the emission per centimetre of path length is plotted against the logarithm of [OH] times the one-fourth root of the quantity in large brackets on the RHS of equation 12. The values of the latter quantity, by which the values of [OH] are multiplied, are given for each run in the figures. These are the values computed for the maximum temperature. In the low pressure runs, temperature rises of as much as 140° C took place over the region of observation, and in these cases the effect of temperature on the multiplier was taken into account. The concentrations in this expression were computed assuming complete oxidation of carbon dioxide and water vapour. In *Figure 1* are all of the data on one atmosphere, and the line has been drawn with the slope of 4, which is required by equation 12. This same line has been

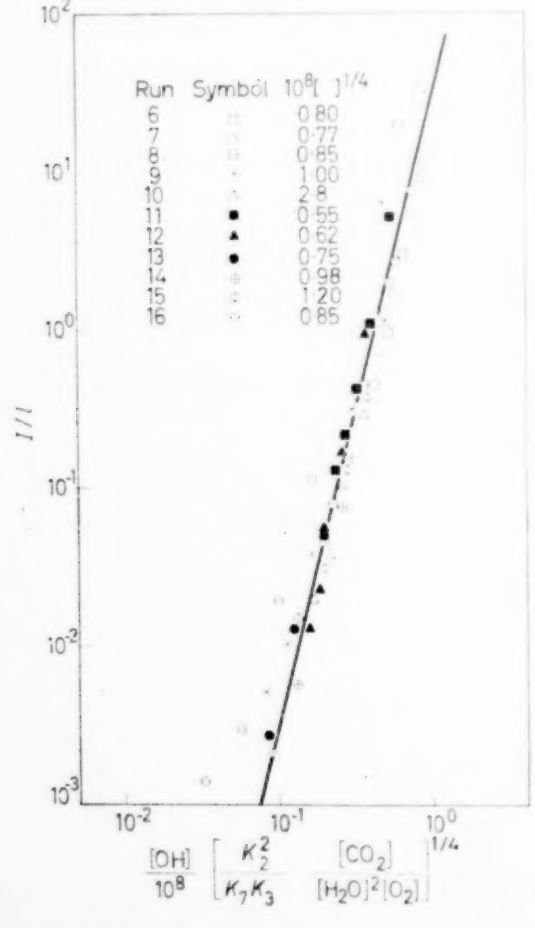

Figure 1. Intensity of emission at 4 345 Å per centimetre path length as a function of the one-fourth power of the product [CO] [O] *as calculated from the measured* [OH]. *Concentrations in molecules/cm³. The factor by which* [OH] *was multiplied is given for each run*

drawn in ***Figure 2***, which shows both the data in low pressure lean flames (open symbols) and the data for the three rich atmospheric pressure runs described in the previous paper[1]. The rich data were originally plotted in the form $I/I[CO]$ against $\{[OH](K_2/[H_2O])\}^{\frac{1}{2}}$, since [CO] was calculable from the stoichiometry and the water gas equilibrium. For the purposes of ***Figure 2***, these data have been replotted in the form of I/I against the quantity $\{K_2[CO][OH]^2/[H_2O]\}^{\frac{1}{4}}$ to put them in the same form as the present data.

Apart from errors in the measurements of temperature and of [OH] which were discussed in some detail in an earlier paper[7], there are two sources of error peculiar to the present experiments which should be mentioned. The first is the fact that for the lowest values of I, the signal to noise ratio was as low as three giving a corresponding loss of precision.

The second arises from the fact that the gradient of emission intensity was generally quite large, especially at atmospheric pressure. On the average about a hundred-fold decrease in intensity occurred in the 10 mm distance in which measurements were made. It is felt that the burner position could be set to within 0·1 or 0·2 mm, but since [OH] and *I* were measured in separate operations, a difference in level of 0·4 mm for any datum is conceivable. In addition to this, there was some irregular wandering of the optical path relative to the burner due presumably to the long optical path involved and its sensitivity to temperature changes, lack of complete rigidity of the system, etc. It is felt that these effects could cause much of the scatter seen in the figures.

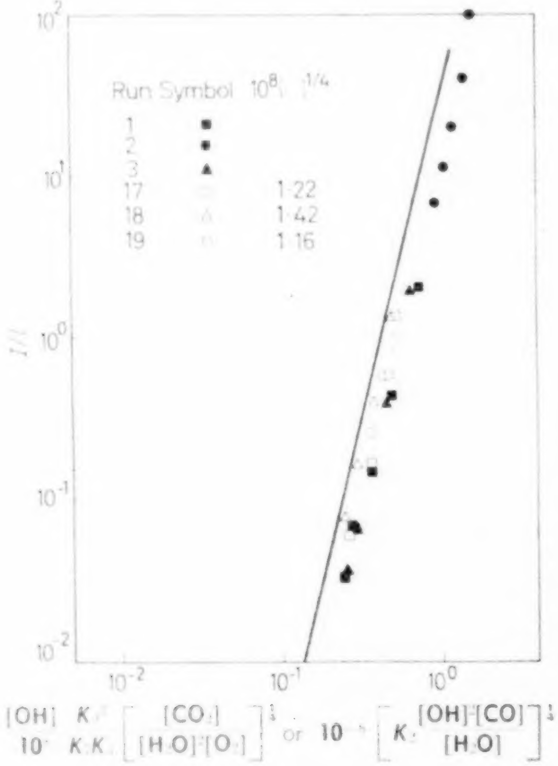

Figure 2. *Intensity of emission at 4 345 Å per centimetre of path length as a function of: (a) for lean runs 17, 18 and 19, the one-fourth power of the product* [CO] [O] *as calculated from the measured* [OH]; *the factor by which* [OH] *was multiplied is given for each run: (b) for rich runs 1, 2 and 3 the same function as in (a) but only* [O] *calculated from* [OH], *and* [CO] *calculated from water gas equilibrium. Data for runs 1, 2 and 3 taken from the like numbered runs in ref. 1. Concentrations in molecules/cm*^{3}

DISCUSSION

Considering first the atmospheric pressure data in *Figure 1*, it is seen that in spite of the considerable scatter all of the data conform roughly to the straight line over a wide range of intensity. A more detailed examination of *Figure 1* reveals two particular causes of the scatter. In the first place, run 16 which had the lowest temperature (1 440° K), seems to be anomalous and this may represent the breakdown of the assumptions made of the equilibration of reactions 3 and 5–7. At the other end of the scale it can be seen that the measurement nearest the burner in any particular run was often too high in intensity. This is possibly due to the fact that these measurements were always in the region of the highest gradient of emission intensity, and the measurement is weighted too heavily by the more luminous gases near the flame. On the other hand, it is clear that as measurements are made farther and farther upstream, the equilibration scheme must eventually break down. If both the first points in each run and the points for the lowest temperature run are disregarded, the agreement of the remaining data with the straight line is very good.

Turning to *Figure 2*, the data on the lean flames conform to the line as expected: they lie parallel to the line but displaced in the direction and by roughly the amount to be expected from the pressure broadening effect discussed earlier[1, 2]. The data for the rich flames, however, are even more displaced. Clearly part of this difference lies in the fact that for rich flames [CO] is calculable *a priori* and is therefore unaffected by the error in assuming no line broadening, whereas [CO] in lean flames is calculated from [OH] by equation 8 and is so affected. It does seem, however, that this consideration cannot account for the whole of this displacement.

At first glance it might appear that this discrepancy arises from an error in the heat of formation of hydroxyl, ΔH_f (OH), since in lean flames one depends on this quantity in calculating [CO] from [OH] and in rich flames the calculation of [CO] is independent of the thermodynamics of hydroxyl formation. A detailed examination of this possibility shows that in this respect our results are completely independent of ΔH_f (OH). There is a cancellation of errors due to the fact that on the one hand the calculated concentration of hydroxyl is a function of ΔH_f (OH) and the thermodynamic properties of water vapour and oxygen, and on the other hand, the concentration of carbon monoxide in equilibrium with hydroxyl according to reaction 3 is a function of ΔH_f (OH) and the thermodynamic properties of water vapour, oxygen and carbon dioxide. In effect the calculation of [CO] from [OH] and equation 8 amounts to a comparison of the thermodynamic properties of carbon monoxide with those of water vapour, oxygen and carbon dioxide, from which ΔH_f (OH) can be cancelled.

The discrepancy consists then of the fact that for a given level of emission the product [CO][O] as calculated in lean flames is not as large as the rich flame data show that it should be. Since both sets of data have in common the calculation of [O] from [OH] by equation 10, this amounts to saying that the [CO] calculated from equation 8 is too small by perhaps 10 or 20 per cent and this cannot be ascribed to an error in the thermodynamics of hydroxyl formation. It would appear that the only possible explanation is that the integrated absorption coefficients of the hydroxyl lines are too low. If they were increased by 5 or 10 per cent, an amount probably within the experimental error of the determination by O. OLDENBERG and F. F. RIEKE[11], then the square of [OH] for any given amount of absorption would be increased by 10 to 20 per cent and [CO] in the lean flames would be calculated in agreement with the rich data.

To sum up the observations on the emission of light, it is felt that these experiments show that the assumption of the equilibration of reactions 3 and 5–7 in the lean flame gases is valid down to at least 1 500° K, and possibly not much lower, depending no doubt on the stoichiometry and pressure. As long as this equilibration is maintained, concentrations of carbon monoxide, hydrogen and oxygen atoms and hydrogen molecules are calculable from the measured [OH] by equations 8 to 11. In *Table 2* are given the results of such calculations for some of the runs, all for the maximum observed [OH]. As can be seen from the table, the concentrations of these species are often comparable to that of hydroxyl. However, as the gases pass downstream all of these concentrations fall off more rapidly than [OH] so that eventually the hydroxyl concentration exceeds that of any of the others.

Table 2. Concentrations, 10 [illegible] *× molecules/cm^3*

Run	$[OH]_{eq}$	$[OH]_{max}$	$[O]_{max}$	$[CO]_{max}$	$[H_2]_{max}$	$[H]_{max}$
6	0·434	1·2	0·39	2·26	0·47	0·168
8	0·227	0·68	0·148	0·72	0·186	0·040
9	0·070	0·45	0·106	0·42	0·133	0·026
10	0·0325	0·285	0·235	1·72	0·047	0·036
14	0·040	0·30	0·060	0·119	0·053	0·0093
18	0·0315	0·34	0·24	0·21	0·071	0·046
19	0·0179	0·40	0·126	0·35	0·52	0·152

Insofar as this equilibration is maintained, the disappearance of carbon monoxide from the flame gases is not an oxidation in the ordinary meaning of the word, but rather the result of a recombination process. This follows from the fact that as long as equilibration is maintained it is possible, in a way exactly analogous to the case of carbon monoxide-free hydrogen–air flames[2, 7, 10], to define a function of the concentrations of the species in excess of equilibrium which has zero time dependence if only reactions 3 and 5–7 are operative. This function is

$$F_{CO} = [OH] + 2[CO] + 2[O] + 2[H_2] + 3[H] \qquad \ldots .[14]$$

Since this function cannot decrease due to the above four reactions, it can only decrease as a result of other, presumably recombination, reactions.

The disappearance of the radicals in carbon monoxide-free lean hydrogen–air flames has already been discussed[7]. When carbon monoxide is added to the system, the pool of radicals and molecules in excess of equilibrium which must disappear in order to reach complete equilibrium becomes larger by the amount of carbon monoxide given by equation 8, as has been demonstrated here. In addition to this, the presence of carbon monoxide may provide additional reaction paths by which this disappearance may take place.

The only reaction which it appears plausible to introduce would be a three-body recombination of carbon monoxide and oxygen to form a molecule of carbon dioxide in some unspecified state, but from which the carbon dioxide eventually finds its way to the ground state. (This cannot be the light-producing reaction 1, which is too slow to account for any appreciable decrease in carbon monoxide.) However, such a three-body recombination would probably be relatively slow, since oxygen atoms were generally not present in very large concentrations in the flames used here. Thus, one might expect that the decay of the radicals would go on at about the same rate in the presence of carbon monoxide as in its absence, only more slowly since the carbon monoxide present must also be disposed of.

The data in *Table 1* bear this out. The rate constants k_{OH} are generally smaller than those in corresponding hydrogen air flames[2], but of the same order of magnitude. On the other hand, the flames in this work are generally of smaller burning velocity, so that the larger diffusion effects may tend to obscure the relationship. In any case it does seem, that the recombination process is not changed much if at all by the presence of carbon monoxide.

The findings and conclusions reported here are at variance with reported work on the water-catalysed high temperature oxidation of carbon monoxide[3-5]. Not only are the proposed mechanisms different, but the rates of carbon monoxide disappearance deduced here are generally not first order in [CO]. All of the work of Fenimore and Jones was in the temperature region in which one should expect the equilibration scheme to hold (except possibly the relatively hydrogen-free flames for which we have not obtained any data). The conditions of run 6 (*Table 1*) were very similar to a run made with ethylene air by Fenimore and Jones. For this flame the two sets of data, $[CO]_{OH}$ calculated from equation 8 on the one hand, and [CO] determined directly by sampling* on the other, are shown plotted together in *Figure 3*. The $[CO]_{OH}$ calculated from [OH] is about three times that from the sampling experiments (without correcting for the line width effect or the low f number) and the plot of $\log[CO]_{OH}$ against time is not a straight line. However, in the range of distance from the burner which both sets of data have in common, the slope of an average line drawn through the $[CO]_{OH}$ data agrees fairly well with that drawn through the sampling data. Apart from the difference in magnitudes then it appears that the two sets of observations are not contradictory.

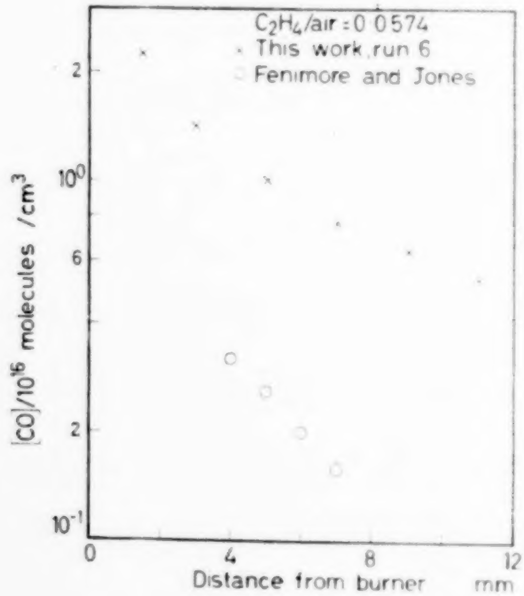

Figure 3. Comparison of concentration of carbon monoxide as a function of distance from the burner for the conditions of run 6 (Table 1)

---

*We are indebted to Dr Fenimore for supplying the data used in making this comparison.

Similar comparisons could not be made with the data of Friedman and Cyphers, since their flames were all at too low a pressure to be conveniently handled in our equipment: that is, our burner is only three inches in diameter and at such low pressures as used by Friedman and Cyphers the flame becomes too thick. It should be pointed out though that if reaction 3 is to be used as the carbon monoxide-oxidizing step in cases where the problem is really oxidation and not recombination, a knowledge of the hydroxyl concentration and its variation is indispensable to an interpretation of the data.

The results obtained here by optical methods point out a difficulty with sampling techniques which may not be generally appreciated but which is clearly apparent in a recent study of sampling by C. HALPERN and F. W. RUEGG[10]. This problem consists of the fact that whereas the analysis of samples withdrawn from flames are found to consist only of stable species, both our experiments and purely equilibrium considerations show that under some conditions the concentrations of radicals (particularly OH in lean flames) in the gases sampled are larger than the concentrations of some of the stable species for which a chemical analysis can be made. The question then is, what happens to these radicals and where do they appear in the product? Discharge tube work[11] shows that under conditions similar to those one might expect to obtain in a sampling system the hydrogen contained in the products from dissociated water vapour appears mainly as H_2. If similar conditions do prevail in a sampling experiment where the gases before sampling contain more OH than H_2, then clearly the analysis of H_2 in the samples obtained are meaningless unless the fate of OH and H in the sampling system are established by some independent means. Similarly, one can speculate on the fate of OH and of CO in an experiment in which the gases before sampling contain as much OH as CO. In this connection it is worth pointing out that the equilibration which has been shown here to obtain in the flame gases above 1 500°K implies that the water gas equilibrium is established in the flame gases. That is, in the lean flame gases the H_2/CO ratio is that given by the water gas equilibrium even though carbon monoxide and hydrogen are not in equilibrium with carbon dioxide and oxygen on the one hand and water vapour and oxygen on the other. In general then it can be said that care should be exercised in interpreting the results of sampling experiments whenever the component analysed for is such that its equilibration with unstable species in the flame gases is possible.

The author wishes to acknowledge the many helpful discussions he has had with Drs C. P. Fenimore and G. E. Moore, and also the aid of W. W. Crotty in the experimental work.

G.E. Research Laboratory,
Schenectady, N.Y.

(Received July 1958)

REFERENCES

[1] KASKAN, W. E. *Combustion & Flame* 3 (1959) 39
[2] KASKAN, W. E. *Combustion & Flame* 2 (1958) 286
[3] FENIMORE, C. P. and JONES, G. W. *J. phys. Chem.* 61 (1957) 651
[4] FRIEDMAN, R. and CYPHERS, J. A. *J. chem. Phys.* 23 (1955) 1875

[5] Friedman, R. and Cyphers, J. A. *J. chem. Phys.* 25 (1956) 448
[6] Fenimore, C. P. and Jones, G. W. *J. phys. Chem.* 62 (1958) 1578
[7] Kaskan, W. E. *Combustion & Flame* 2 (1958) 229
[8] Kaskan, W. E. *Sixth Symposium (International) on Combustion*, p 134. Reinhold: New York, 1957
[9] Lewis, B. and von Elbe, G. *Combustion, Flames and Explosions of Gases*, p 742. Academic Press: New York, 1951
[10] Gaydon, A. G. and Guedeney, F. *Trans. Faraday Soc.* 51 (1955) 894
[11] Oldenberg, O. and Rieke, F. F. *J. chem. Phys.* 6 (1938) 439
[12] Bulewicz, E. M., James, C. G. and Sugden, T. M. *Proc. Roy. Soc.* *A* 235 (1956) 89
[13] Halpern, C. and Ruegg, F. W. *J. Res. Nat. Bur. Stand.* 60 (1958) 29
[14] Jones, R. A. and Winkler, C. A. *Canad. J. Chem.* 29 (1951) 1010

Theory of Flame Propagation

Y. B. ZELDOVICH and G. I. BARENBLATT

Previous work on steady state propagation of flat flames is reviewed and various mathematical techniques are contrasted. In the numerical evaluation of the velocity of uniform propagation of flames, the effects of varying parameters, heat loss and chain reactions are considered, leading to analysis of stability of propagation. Limits of validity are given.

THE propagation of flame can be expressed in terms of a heat transfer equation, which refers to the transmission of heat in the zone of combustion, and a group of diffusion equations, which define transfer of the reactants, intermediate products and final products of the reaction taking place in the combustion zone. Those parts of such equations which represent generation of heat and production or decomposition of substances during the process of combustion are derived from reaction kinetics. They are expressed as a summation of the effects of progressive concentration of numerous components n_i of the burning mixture on certain operators $\Phi_i(T)$ dependent only on the temperature of the burning mixture. A complete system of equations corresponding to the case of the flat flame can be found for example in the work of C. F. CURTISS *et al.*[1].

Many investigations[1–5] have been devoted to the study of steady state propagation of flat flames. In this case, the corresponding solutions of the basic equations have the following form:

$$n_i(x - V_n t), \quad T(x - V_n t)$$

where, as before, n_i is the concentration of component i of the burning mixture, T is the temperature of the mixture and V_n is the velocity of flame propagation which is unknown. Thus with this form of solution the basic equations of the problem change into ordinary differential equations containing V_n as the unknown parameter. Strictly speaking, for the condition of linear flame propagation to exist, it is essential that in the cold mixture the velocity of reaction shall be zero. Otherwise, burning mixture which is initially at a sufficiently large distance from the front of the flame will have reacted fully before the front reaches it.

This condition at first appears to contradict the usually accepted Arrhenius exponential relation between the velocity of reaction and temperature. In actual fact, however, with the high activation energies arising in the majority of cases, the velocity of reaction in the cold mixture is lower by several orders of magnitude than the velocity of reaction in the zone where rapid combustion occurs. Thus the distance at which the mixture could actually burn out before the arrival of the flame front would have to be of astronomical size. Considering the practical aspects of the experiment therefore, the condition of zero reaction velocity in the cold mixture, i.e. $\Phi(T_0)=0$ where T_0 is the temperature of the cold mixture, can generally be accepted as highly accurate. With the same degree of accuracy, it may be taken that $\Phi(T)=0$ not only when $T=T_0$ but also in the neighbourhood of $T=T_0$, i.e. when $T_1 > T > T_0$. Under this condition, T_1 is of small significance provided that $\Phi(T_1) \ll \Phi_{\max}$.

It is worth noting that, instead of the condition of zero reaction velocity in the cold mixture, some authors[8] proposed the so-called condition of 'cold porous plug' which supposes that at the outer boundary of the burning zone a small but finite quantity of heat is absorbed. It seems to us that this condition is not very clear from the physical point of view. We wish to stress that the steady state in the propagation of flame represents an intermediate asymptotic solution of a group of unsteady state equations for propagation of flat flame for a time interval which is large in comparison with the period of stabilization but small in comparison with the period of combustion of all the matter present in the reaction vessel.

At the present time, the only case for which there is a rigorous analysis of the condition of steady state propagation is that when the composition of mixture can be described in terms of temperature T and concentration n of one of the components and when the diffusion coefficient D in the mixture is equal to the heat transfer coefficient κ. For this case, in the work of D. A. FRANK-KAMENETSKY and one of the authors[3,4], it was shown that under the conditions of steady propagation the total enthalpy remains constant, i.e.

$$cT+Qn \equiv \text{constant} \qquad \ldots.[1]$$

where c is the specific heat of the mixture and Q is the heat of reaction. From equation 1 it can be seen that, in this case, the roles of temperature and concentration are similar. It should be noted that B. LEWIS and G. VON ELBE[9] assumed constant total enthalpy by way of a hypothesis* in their explicit assumption concerning the thermal character of the reaction.

In fact, the constant total enthalpy is not dependent on the character of the reaction and when $D \neq \kappa$ it cannot arise. Using equation 1 it is possible to eliminate concentration terms from the steady state equation in order to evaluate the temperature

$$V_0\frac{\mathrm{d}t}{\mathrm{d}\xi}+\frac{\mathrm{d}}{\mathrm{d}\xi}\left(\kappa\frac{\mathrm{d}T}{\mathrm{d}\xi}\right)+\frac{Q}{\rho c}\Phi(n,T)=0 \qquad \ldots.[2]$$

where $\xi=x-V_0t$ and $\Phi(n,T)$ represent velocity of reaction. Taking also the usual equation showing an increase along the coordinate ξ, equation 2 can be reduced to an equation of the first order which is more suited to detailed investigation. The transformation to the first order simplifies investigation and evaluation of the parameter V_0.

---

*Lewis and von Elbe correlated constant enthalpy with the problem of stability of flame propagation supposing that under conditions of maximum enthalpy the flame is unstable. In actual fact, analysis[10] of the question of stability of flames with heat transmission and diffusion taking place shows that the flame becomes unstable as a result of unbalanced conditions, namely, when $D > \kappa$, which corresponds to the case of minimum enthalpy.

A rigorous mathematical proof of the existence and uniform character of the steady state propagation for the case when $D=\kappa$ has been published[5].

In this work, and in agreement with the statements above, it was assumed that the relation between the velocity of reaction and the prevailing temperature

$$z=(T-T_0)/(T_\infty-T_0)$$

where T_∞ represents the temperature of the burnt mixture, can be obtained after elimination of the concentration terms using equation 1 for constant enthalpy. This can be represented approximately, as shown in *Figure 1*,

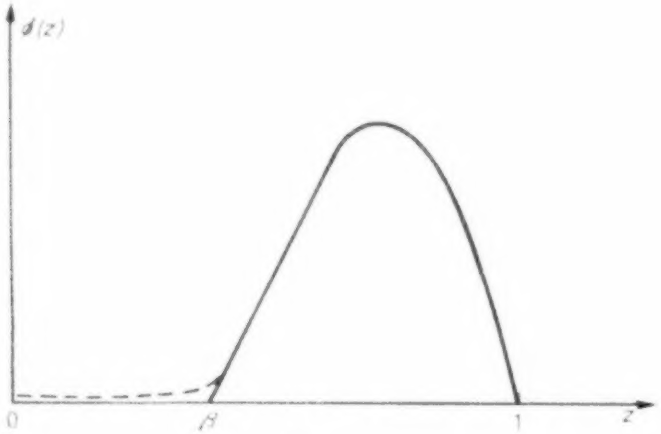

Figure 1

by the continuous curve (the dotted line represents the real shape of the function). Thus the function $\Phi(n, T)=\Phi(z)$ is exactly equal to zero when $0 \leq z \leq \beta$ where $\beta=(T_i-T_0)/(T_\infty-T_0)$ and this becomes equal to zero when $z=1$ and is positive when $\beta < z < 1$.

In our previous work[3] another simple method of numerical calculation of flame propagation was introduced. Further, for an important practical case when the velocity of reaction is appreciable, at temperatures close to the temperature of the burnt mixture, a simple asymptotic formula was given[3,4] for evaluation of velocity of uniform propagation of flame

$$V_0=\frac{1}{\rho}\left\{\frac{2\lambda}{cn_0}\int_0^1 \varphi(z)\,\mathrm{d}z\right\}^{\frac{1}{2}} \qquad \ldots.[3]$$

where λ is thermal conductivity of the mixture, ρ the density, and n_0 is concentration of the main component of the mixture. As shown before[5], the integration of equation 3 can be based not on an approximate expression of the velocity of reaction but on a true one.

In more complex cases, where $D=\kappa$ cannot be applied, or where, on the basis of constant enthalpy, one cannot obtain an expression for concentration of the reactants as a function of temperature because several initial reactions are taking place simultaneously, in order to calculate the steady state propagation of flame different authors adopted different methods.

Thus, the method of numerical integration of equations describing steady state propagation[6], different variations of the method of successive approximations for the equation of steady state propagation, and several other methods have been used. A survey of these methods is given in a recent paper by T. VON KÁRMÁN[7].

However, with more than one unknown, the analysis of the system of ordinary differential equations of steady state flame propagation appears to be extremely complicated.

We feel that in such cases, the most suitable method is that of numerical integration of the corresponding unsteady state equation (i.e. of a group of equations with partial derivatives) under initial conditions, automatically securing entry to the steady state propagation, if such exists. This method

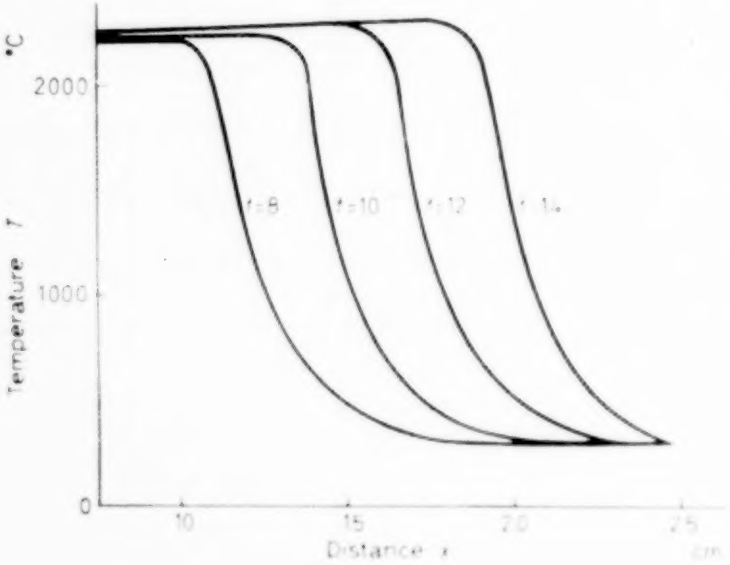

Figure 2(a)

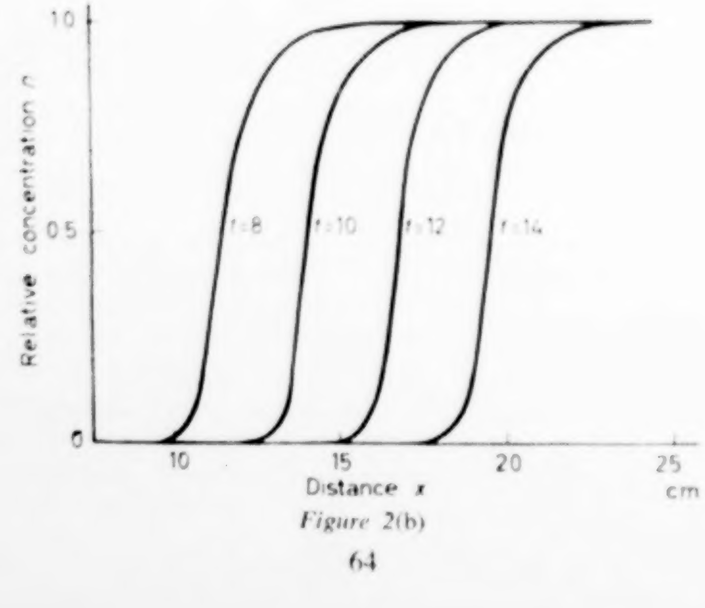

Figure 2(b)

is also suitable for numerical evaluation of the condition of ignition. It is necessary to integrate over a time interval for which entry to steady state will take place, with a sufficient degree of accuracy. Initially, this method was introduced in the very interesting publications of D. B. Spalding[11, 12]. In what follows, we shall consider the application of this method to calculation of several idealized systems, the general analytical investigation in this case being too difficult.

NUMERICAL EVALUATION OF THE VELOCITY OF UNIFORM PROPAGATION OF FLAMES

In this section, using several idealized models, we shall consider the effect of numerous factors on the steady state propagation of flame. The numerical calculations were carried out under the guidance of N. M. Zueva to whom the authors express their gratitude.

(1) *Effect of κ/D ratio*

Assuming that the composition of the mixture can be described by the concentration n of the main component and that there are no heat losses, the system of basic relationships is of the following form:

$$\left.\begin{aligned} \frac{\partial n}{\partial t} &= \frac{\partial^2 n}{\partial x^2} - zn\exp(-E/RT) \\ \frac{\partial T}{\partial t} &= \alpha\frac{\partial^2 T}{\partial x^2} + \frac{Q}{c}zn\exp(-E/RT) \end{aligned}\right| \qquad \ldots\ldots[4]$$

where $\alpha = \kappa/D$, $x = y/D$ and y is the coordinate taken at right angles to the flame front. The boundary conditions are

$$\left.\begin{aligned} x &\to \infty, \quad n = 1, \quad T = T_0 \\ x &\to -\infty, \quad n = 0, \quad T = T_0 + Q/c \end{aligned}\right| \qquad \ldots\ldots[5]$$

Numerical calculations were carried out for $T_0 = 300°C$, $Q/c = 2 \times 10^3$, $E/R = 1.5 \times 10^4$ and $z = 10^6$. The coefficient α was taken to have the following values: 0·5, 1·0, 2·0 and 10·0. Note that when $\alpha = 1$

$$(T - 300)/2000 + n = 1$$

and therefore the problem reduces to one equation. Entry into steady state of propagation for $\alpha = 2·0$ is shown in *Figure 2*. *Figure 3* shows the displacement of several isotherms when $T = 1000$, $T = 1500$ and $T = 2000$. It can be seen here that a rapid approach to uniform propagation takes place. *Figure 4* shows the variation of the value of $(T - 300)/2000 + n$ with different values of α under the conditions of already established uniform propagation. The curve shows that when $\alpha \neq 1$ the total enthalpy reaches a maximum or a minimum value in the zone of rapid reaction depending on whether α is greater or smaller than unity. In *Figure 5* the dotted line shows the relation between the velocity of propagation of flames and the parameter α.

When $\alpha = 1$ the velocity of flame propagation was found to be 0·71 whereas according to the approximate formula 3 the value for this variable is equal to 0·67. As our calculations indicate (*Figure 5*), when $0·5 < \alpha < 2$, V_n is directly proportional to $\alpha = \kappa/D$. Thus, since the coordinates x and y are related by $x = y/D$, we find that the actual velocity of propagation is proportional to αD, i.e. κ/D, which is in complete agreement with the approximate theory published previously.

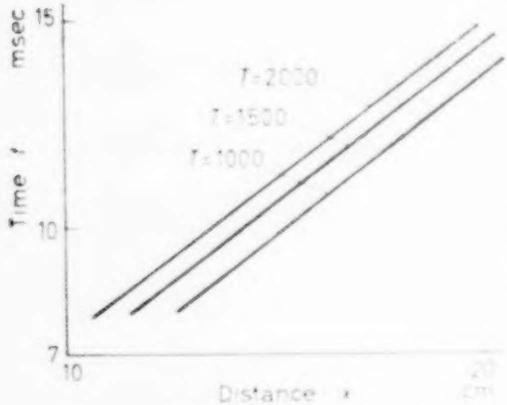

Figure 3

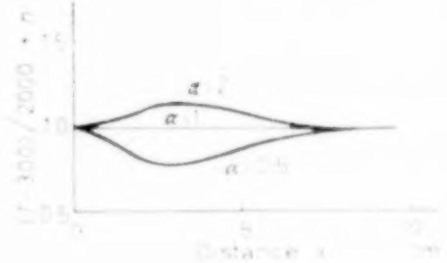

Figure 4

(2) *Effect of heat loss*

We shall now consider a more complicated case where composition of the mixture is a function of temperature as well as of concentration of the main component and when heat losses are encountered.

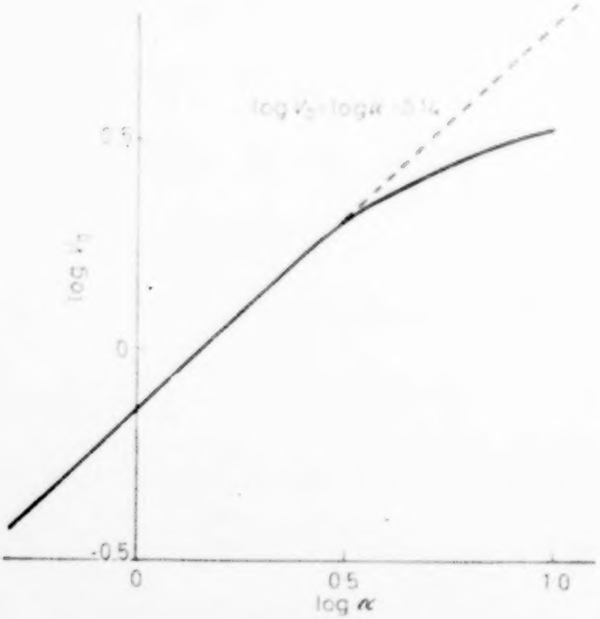

Figure 5

In the presence of a heat loss, even when $z = 1$, the temperature and concentration are no longer related by an algebraic equation. The system of basic equations is now of the following form:

$$\left.\begin{aligned} \frac{\partial n}{\partial t} &= \frac{\partial^2 n}{\partial x^2} - zn\exp(-E/RT) \\ \frac{\partial T}{\partial t} &= \frac{\partial^2 T}{\partial x^2} + \frac{Q}{c} zn\exp(-E/RT) - b(T - T_0) \end{aligned}\right\} \quad \ldots\ldots[6]$$

where the boundary conditions and the values of the parameters z and E/R remain the same as in the previous case.

An approximate physical theory of flame propagation in the presence of heat loss was proposed earlier by one of the authors. It was shown then that the steady state exists when b does not exceed a certain critical value b_{cr}, and a method was given for approximate evaluation of this parameter. It was shown that the loss of heat decreases the velocity of flame propagation V so that

$$V_{\text{[illegible]}} = V_{\text{[illegible]}} \ (1/e) \quad \ldots\ldots[7]$$

From the approximate theory presented in this publication it follows that, when $b = b_{cr}$, the maximum temperature $T_{\text{[illegible]}}$ could be evaluated from the following equation

$$T_{\text{[illegible]}} = T_{\text{[illegible]}} - R(T_{\text{[illegible]}})^2/E \quad \ldots\ldots[8]$$

Our calculations have shown that $b_{cr} = 0{\cdot}012$. When $b = 0{\cdot}015$ entry into the steady state cannot occur and the combustion subsides (see *Figure 6*), but when $b = 0{\cdot}012$ the steady state can be realized (*Figure 7*).

Approximate theoretical estimates showed that $b_{cr} = 0{\cdot}0175$. The calculation carried out confirms the values of $V_{\text{[illegible]}}$ as previously

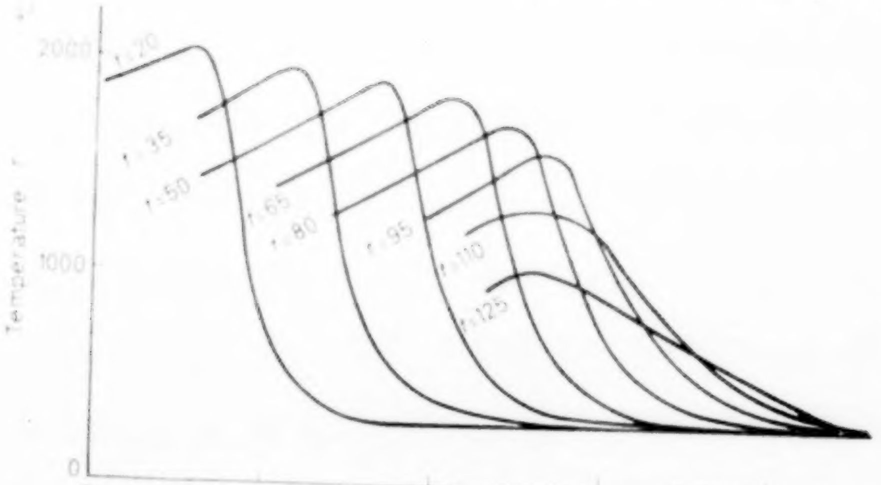

Figure 6

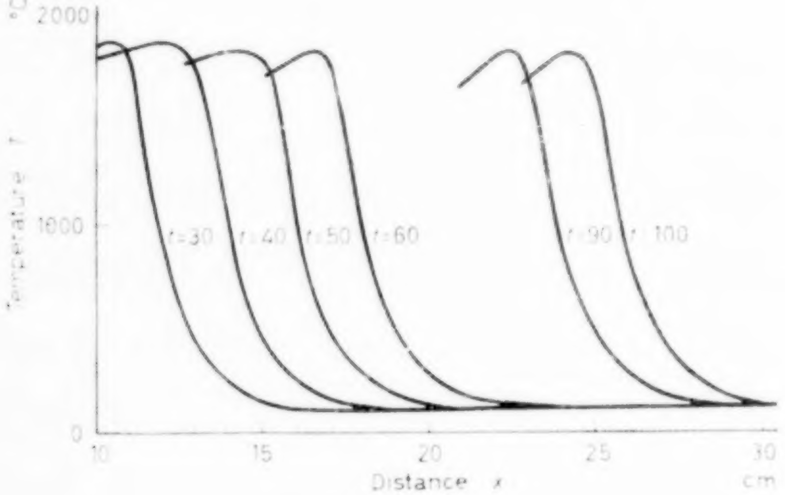

Figure 7(a)

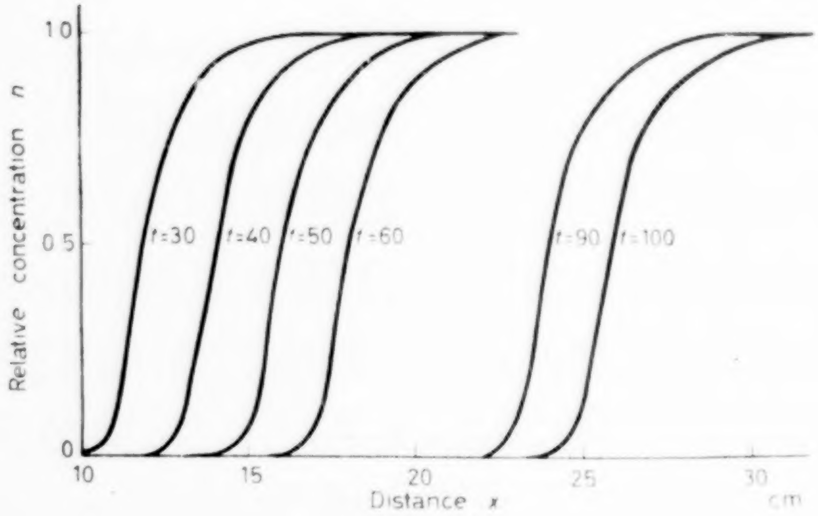

Figure 7(b)

predicted[13]. For $b=0{\cdot}012$ we find $V_u=0{\cdot}39$ when $V_{u,\,b=0}/e^{1/2}=0{\cdot}43$. Equation 8 affords further confirmation. In actual fact $T_{\max}$ is found to be 1 980°C when $b=0{\cdot}012$ so that

$$T_{\max,\,(b=0)}-T_{\max,\,(b=0{\cdot}012)}=2\,300-1\,980=320^\circ\mathrm{C}$$

whereas according to equation 8 $T_{\max,\,(b=0{\cdot}012)}$ is equal to 1 950° and therefore

$$T_{\max,\,(b=0)}-T_{\max,\,(b=0{\cdot}012)}=2\,300-1\,950=350^\circ\mathrm{C}$$

Thus, the calculated value of $T_{\max,\,(b=0)}-T_{\max,\,(b=0{\cdot}012)}$ deviates only by 10 per cent from the corresponding value predicted by the theory.

(3) *Chain reaction*

We shall assume here that the reaction takes place with formation of an intermediate product which plays the role of an autocatalyst for the active centres and that there are no heat losses. Further we shall assume that the conversion of the initial reactants into intermediate products takes place with evolution of a small quantity of heat whereas the change of the active centre into the final products of reaction is associated with evolution of a large quantity of heat, and that the velocity of this reaction depends very little on the temperature.

The conversion of the reactants into the active centres takes place only when the reactants and the active centres are present together. Further, it is very important that increase in the number of active centres is possible only at sufficiently high temperatures.

Thus the present assumptions of the problem differ from the rather less realistic assumptions of isothermal chain propagation of flames. From the above, the basic group of equations takes the following form:

$$\left.\begin{aligned} \frac{\partial n}{\partial t} &= \frac{\partial^2 n}{\partial x^2} - zan\exp(-E/RT) \\ \frac{\partial a}{\partial t} &= \frac{\partial^2 a}{\partial x^2} + zan\exp(-E/RT) - ha \\ \frac{\partial T}{\partial t} &= \frac{\partial^2 T}{\partial x^2} + \frac{Q}{c}ha \end{aligned}\right\} \quad \ldots . [9]$$

where a is the concentration of the intermediate product; n, as before, is the concentration of the starting material and the remaining symbols have their previously stated meanings. Clearly, an increase in the number of active centres can occur only if the RHS of the second of the above equations 9 applies, this being true if

$$T > E/R\ln(nz/h) > E/R\ln(n_0 z/h)$$

In the investigation of the propagation, it is necessary to find the solution for the group of equations 9 to satisfy the following boundary conditions: when $x \to \infty$ (cold mixture) $T = T_0$, $n = 1$, $a = 0$, and when $x \to -\infty$ (far behind the flame front) the reaction should cease. Further, it is easy to imagine that the process would terminate at low concentrations of the initial reactants, even at high temperatures, because the number of chain ruptures [product ha] would exceed the number of chain initiations [product $zan\exp(-E/RT)$] so that $a \to 0$ while n tends rapidly to a limiting value which is less than $T_0 + Q/c$. In the final composition of the mixture, therefore, a certain quantity of unburnt material occurs and this can be predicted by solving the equations. It is necessary to note that the condition of steady state propagation exists only when h is smaller than its critical value $h_{\text{crit.}}$ which must be also determined. We shall take the following initial conditions:

$$\left.\begin{aligned} &x > 0, \quad n = 1, \quad a = 0, \quad T = T_0 \\ &x \leq 0, \quad n = 0, \quad a = a_0, \quad T = T_0 + Q(1 - a_0)/c \end{aligned}\right\} \quad \ldots . [10]$$

The above conditions were so chosen as to comply with the following identity

$$(T - T_0)/(Q/c) + n + a = \text{constant} = 1 \qquad \ldots.[11]$$

which permits consideration of two equations instead of three.

Equation 11 expresses the law of stability of the total enthalpy although it is insufficient to express the concentration of both components of the mixture as a function of temperature. The problem reduces now to investigation of the onset of the steady state determination of the final degree of incomplete combustion and the value of h_{st}. *Figure 8* shows

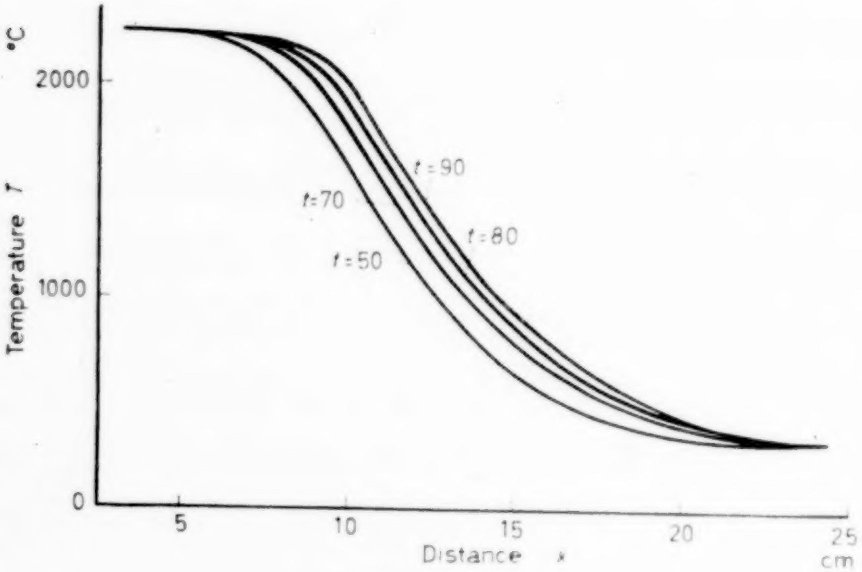

Figure 8(a)

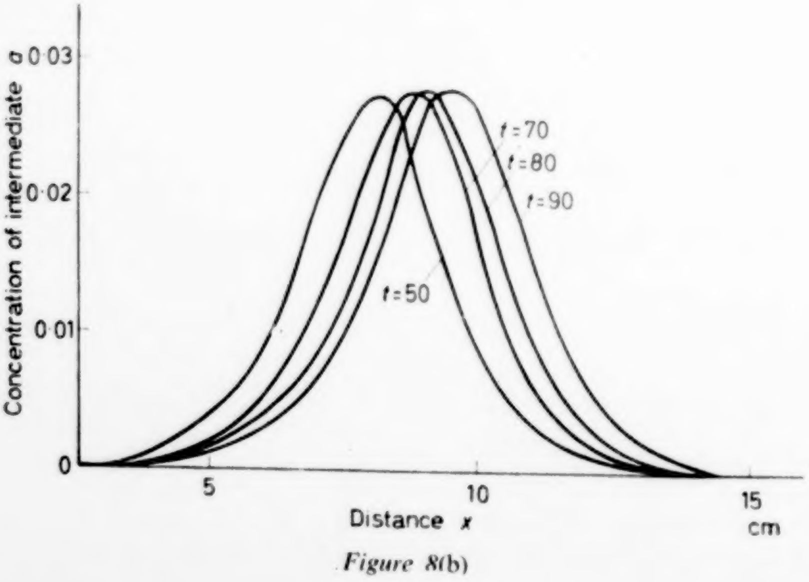

Figure 8(b)

the onset of the steady state propagation when $a_0 = 0{\cdot}05$, $h = 0{\cdot}5 < h_{crit}$ while the concentration of the main component far behind the flame front was found to be 0·02. *Figure 9* shows degeneration of the initial distribution of the active centres and quenching of the reaction when $a_0 = 0{\cdot}05$, $h = 0{\cdot}75 > h_{crit}$. Trial estimations show that $h_{crit} \approx 0{\cdot}7$.

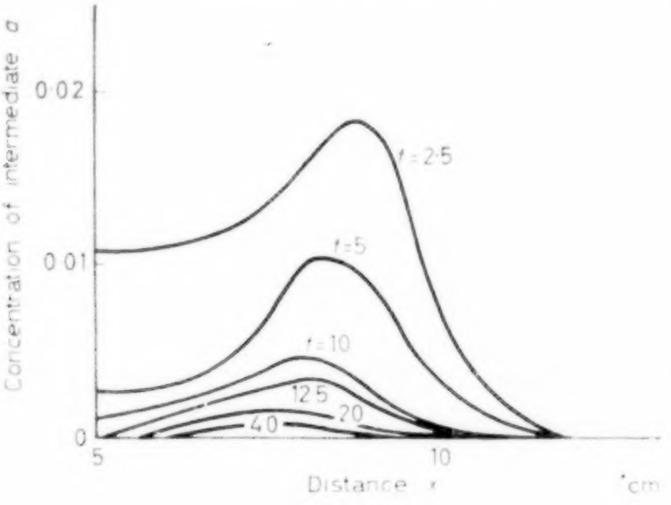

Figure 9

The method quoted above is suitable also for analysis of more complex mechanisms of reaction by evaluating the velocity of steady state flame propagation for these reactions.

STABILITY OF STEADY STATE PROPAGATION OF FLAMES

As follows from the above, in the assumption of the similarity between the roles of concentration and temperature, in the case when $\alpha = 1$, thermal propagation of flat flames can be described by the following equations:

$$\frac{\partial T}{\partial t} = \kappa \frac{\partial^2 T}{\partial x^2} + \varphi(z), \quad z = \frac{(T - T_0)}{(T_\infty - T_0)} \qquad \ldots.[12]$$

where the function $\varphi(z)$ satisfies the conditions stated initially. The steady state solution of this equation corresponds to the condition of uniform propagation of flame and has the following form:

$$T = \overline{T}(\xi), \quad \xi = x - V_0$$

where the velocity V_0 can be determined only from the conditions $\overline{T}_{(-\infty)} = T_\infty$, $\overline{T}_{(\infty)} = T_0$ and the function $\overline{T}(\xi)$ satisfies the equation

$$-V_0 \frac{d\overline{T}}{d\xi} = \kappa \frac{d^2 T}{d\xi^2} + \varphi(z) \qquad \ldots.[13]$$

Thus, investigation of the stability of propagation of flames is equivalent under present assumptions to the determination of the stability of the stationary solutions of equation 12 which correspond to a given value of V_0.

When the gas mixture undergoes combustion without heat loss under the condition of similarity between concentration and temperature, and when the phenomenon of flame propagation can be described by one equation, the stability of the stationary solutions appears intuitively as unquestionable. Recently, however, the question of stability of flames in a unidimensional problem with one equation was investigated by J. B. ROSEN[14] who concluded that instability is possible and used an 'approximate criterion of stability', etc. We feel that the conclusions of Rosen are based on incorrect appraisal of the condition of instability. As given below, evaluation of the stability of steady state propagation shows that for one equation in a unidimensional problem the conditions are always stable.

The results presented below were first published by the authors[15]; after this work was published it was found that the earlier work of J. M. RICHARDSON[16] gave similar results by other methods.

For the investigation of stability we shall assume that the initial distribution corresponds to the following stationary solution with a certain small addition in the form of $\varepsilon\varphi(x)$, where ε is a small parameter and $\varphi(x)$ is a limited function equal to zero over a certain portion of the x axis, while the resulting temperature distribution can be expressed in the form:

$$T(x,t)=T(\xi)+u(x,t)=T(\xi)+U(\xi,t) \qquad \ldots.[14]$$

and

$$U(\xi,0)=u(x,0)=\varepsilon\varphi(x)$$

Determination of the stability, on account of the invariant formulation of the problem as regards displacement along the x axis, should be also invariant as regards its change. Thus, from the point of view of establishment of the asymptotic stationary state, it is not necessary that after the perburbation, the distribution should tend to the unperturbed, stationary solution; on the contrary, it is fully sufficient for this distribution to tend to a stationary solution $\overline{T}(\xi+a)$ displaced along the coordinate. Here a is a certain quantity which is directly proportional to the small parameter ε so that $a=b\varepsilon$. Thus, the stationary solution $T(\xi)$ can be regarded as stable if the perturbed distribution of temperature can be represented as

$$T(x,t)=\overline{T}(\xi+b\varepsilon)+z(\xi,t) \qquad \ldots.[15]$$

where $z(\xi,t)\rightarrow 0$ when $t\rightarrow\infty$, when quantity b is necessary. Resolving $\overline{T}(\xi+b\varepsilon)$ followed by the small parameter $b\varepsilon$ and neglecting terms of the expression which are of higher order than one, equation 15 can be expressed as

$$T(x,t)=\overline{T}(\xi)+b\varepsilon\overline{T}'(\xi)+z(\xi,t) \qquad \ldots.[16]$$

In the work of Rosen[14] an ordinary evaluation of the asymptotic stability is taken so that the stationary solution $T(\xi)$ is regarded as stable if the perturbed solution is of the form

$$T(x,t)=\overline{T}(\xi)+z(\xi,t) \qquad \ldots.[17]$$

where $z(\xi,t)\rightarrow 0$ when $t\rightarrow\infty$.

From the expressions quoted above this evaluation appears a little too rigid. In fact, in order to ensure stability, decay of combustion of all the components present is not necessary but only of those components which are orthogonal with respect to $T'(\xi)$. Changing the variables to $\xi = x - V_u t$, t, equation 12 can be expressed as

$$\frac{\partial T}{\partial t} - V_u \frac{\partial T}{\partial \xi} = \kappa \frac{\partial^2 T}{\partial \xi^2} + \phi \qquad \ldots . [18]$$

Now, assuming in this equation that $T = T(\xi) + U(\xi, t)$, using components of the first order only and the equation which is satisfied by $T(\xi)$, we obtain for $U(\xi, t)$

$$\frac{\partial U}{\partial t} - V_u \frac{\partial U}{\partial \xi} = \kappa \frac{\partial^2 U}{\partial \xi^2} + \phi'\{T(\xi)\}\, U \qquad \ldots . [19]$$

Separating the variables in this equation, to seek a solution of equation 19 in the form $U(\xi, t) = \theta(t)\, X(\xi)$, we obtain

$$U = c \exp(-\lambda t)\, \psi(\xi, \lambda) \qquad \ldots . [20]$$

where the function $\psi(\xi, \lambda)$ is a complementary function of the equation

$$V_u \frac{d\psi}{d\xi} + \kappa \frac{d^2\psi}{d\xi^2} + [\phi'\{T(\xi)\} + \lambda]\, \psi = 0 \qquad \ldots . [21]$$

This becomes equal to zero when $\xi = \pm\infty$ and normalized in one way or another. Thus the proof of stability now reduces to the proof that all complementary values of the operator

$$-\left(V_u \frac{d}{d\xi} + \kappa \frac{d^2}{d\xi^2} + \phi'\{\bar{T}(\xi)\} \right) \qquad \ldots . [22]$$

are positive. It should be noted that zero is taken deliberately as a complementary value of the operator 22 so long as, in agreement with the above, when $\lambda = 0$ equation 21 is satisfied by the function $cT'(\xi)$ which becomes equal to zero when $\xi = \pm\infty$. On account of continuity of the function, $T(\xi)$ cannot become zero at any finite point along the ξ axis. Assuming that

$$\psi(\xi, \lambda) = \chi(\xi, \lambda) \exp(-V_u \xi / 2\kappa)$$

equation 21 can be expressed as

$$\kappa \chi''(\xi, \lambda) + [\lambda + \phi'\{\bar{T}(\xi)\} - V_u^2/4\kappa]\, \chi(\xi, \lambda) = 0 \qquad \ldots . [23]$$

which corresponds to the operator

$$-\kappa \frac{d^2}{d\xi^2} + \phi\{\bar{T}(\xi)\} - V_u^2/4\kappa \qquad \ldots . [24]$$

It is clear that $T'(\xi) \exp(V_u \xi / 2\kappa)$ is a complementary function of operator 24 which becomes zero when $\xi = \pm\infty$ and does not become zero anywhere along the interval $(-\infty, \infty)$.

As is known, the complementary function which has no zero value anywhere except at the extremities corresponds to the lower real value. Therefore $\lambda = 0$ becomes the lower real value of the operators 22 and 24, i.e. the negative real values for these operators do not exist. Hence, the steady state distribution of temperature is stable.

We wish to add that assuming perturbed distribution of temperature, which is expressed by the basic equation 12, we have, in effect, assumed similarity between concentration and temperature under perturbed conditions. In general, considering the equations for concentration and temperature, we find that the total enthalpy differs from a constant by a small quantity, which introduces a rapidly decreasing term on the RHS of the linear equation 19 and does not change the range of validity of the corresponding differential operator or the validity of the conclusion as regards stability of the stationary solution.

Petroleum Institute,
Academy of Sciences,
Moscow, U.S.S.R.

(*Received September 1958*)

REFERENCES

[1] Curtiss, C. F., Hirschfelder, J. O. and Campbell, D. E. *Fourth Symposium (International) on Combustion*. Williams and Wilkins: Baltimore, 1953
[2] Kolmogorov, A. N., Pietrovski, I. G. and Piskunov, N. S *Bull. M.G.U.*, Sec. A., Vol. 1, No. 6. O.N.T.I.: Moscow, 1937
[3] Zeldovich, Y. B. and Frank-Kamenetsky, D. A. *Zh. fiz. Khim., Mosk.* 12 (1938) 100
[4] Zeldovich, Y. B. and Frank-Kamenetsky, D. A. *Dokl. Akad. Nauk SSSR* 19 (1938) 693
[5] Zeldovich, Y. B. *Zh. fiz. Khim., Mosk.* 22 (1948) 27
[6] Hirschfelder, J. O. and Curtiss, C. F. *J. chem. Phys.* 17 (1949) 1076
[7] von Kármán, T. and Penner, S. S. *Selected Combustion Problems, I.* AGARD: Butterworths: London, 1954
[8] von Kármán, T. *Sixth Symposium (International) on Combustion*. Reinhold: New York, 1957
[9] Lewis, B. and von Elbe, G. *J. chem. Phys.* 2 (1934) 537
[10] Zeldovich, Y. B. *Theory of Combustion and Detonation of Gases*. Academy of Sciences: Moscow, 1944
[11] Spalding, D. B. *Aircr. Engng* 25 (1953) 264
[12] Spalding, D. B. *Phil. Trans. A* 249 (1956) 1
[13] Zeldovich, Y. B. *Zh. eksp. teor. Fiz.* 11 (No. 1) (1941)
[14] Rosen, J. B. *J. chem. Phys.* 22 (No. 4) (1954) 733, 743 and 750
[15] Barenblatt, G. I. and Zeldovich, Y. B. *Appl. Math. Mech., Leningr.* 21 (No. 6) (1957)
[16] Richardson, J. M. *Fourth Symposium (International) on Combustion*. Williams and Wilkins: Baltimore, 1953

The Low-temperature Vapour-phase Oxidation of cyclo*Hexane*

D. H. ALLEN, F. H. GARNER, R. LONG and J. R. TODD

The vapour-phase oxidation of cyclohexane at temperatures below 450°C has been studied in a flow type apparatus and the products of oxidation have been examined by methods which include gas chromatography. Polarographic methods have been used to investigate the nature of the peroxides present. The reactions taking part in the oxidation process are discussed in the light of the products obtained.

THE complexity of the oxidation of hydrocarbons in the gas phase is well known. Several excellent reviews have recently been published[1-3] and it is unnecessary to examine here either the experimental results or the nature of the elementary reactions which have been suggested as playing a part in such oxidation.

It is usual to distinguish between 'low-temperature' and 'high-temperature' oxidation. The former occurs below about 400° to 450°C and cool flames and negative temperature coefficients of reaction are often observed. It is generally believed that the peroxidic intermediates are of prime importance in 'low-temperature' oxidation and that the decomposition of either peroxy radicals or of peroxides themselves determines the subsequent course of the reactions.

Rather surprisingly in view of the extensive literature on the paraffins, little information is available concerning the vapour-phase oxidation of the *cyclo*paraffins and alkyl *cyclo*paraffins although several studies have been been made of their liquid-phase oxidation.

EXPERIMENTAL

The *cyclo*hexane used was the Spectroscopic Grade, supplied by British Drug Houses Ltd. It was 'peroxide free' and no impurity could be detected by gas chromatography using a dinonyl phthalate column. H. E. MORRIS'S[4] test also indicated that it was free from benzene.

The flow method of studying the reaction was adopted as this enables larger quantities of intermediate products of oxidation to be collected than can be obtained by sampling in the static method.

Nitrogen and oxygen passed through reducing valves and fine-control needle valves to capillary flowmeters kept at 30°C in a constant temperature bath. These capillary flowmeters were calibrated initially for each gas by means of a soap bubble flowmeter.

Hydrocarbon was introduced into the nitrogen stream by means of a 'Microdoser'[5] also kept in a constant temperature bath at 30°C. The rate of delivery could be controlled accurately by regulating the current flowing through the electrolytic cell. The liquid hydrocarbon displaced by electrolytic gas was evaporated continuously into the preheated nitrogen stream. The relative rates of flow of nitrogen and oxygen were adjusted so that the hydrocarbon was effectively provided with the stoichiometric proportion of air.

The Pyrex reaction vessel was enclosed inside a furnace controlled at a steady temperature to within ± 1 °C. A number of reaction vessels, differing only in length, could be used to vary the residence time. The incoming streams of oxygen, and nitrogen plus hydrocarbon vapour, after being preheated to reaction temperature in the front part of the furnace, were mixed and passed through a nozzle (1 mm diameter) located tangentially at the entrance to the reaction vessel. This ensured that the gases were well mixed and the swirling motion imparted to them eliminated stagnant pockets of gas.

The oxidation products were rapidly removed through a capillary tube (2 mm bore) heated to 150 °C to minimize condensation. Condensation was effected by passing the vapours through four consecutive condensing bottles cooled by crushed solid carbon dioxide packed into Dewar flasks.

A standard procedure was adopted in each experiment. As the exothermic oxidation resulted in a temperature rise in the reaction vessel, trial and error adjustments had to be made in order to carry out a run at any predetermined temperature.

ANALYTICAL METHODS

When the separate volumes of the hydrocarbon and aqueous phases of the oxidation products were required, the products were drained from the condensing bottles into a semimicro burette, the dead space of which had previously been filled with water. After measurement, the products were transferred to a volumetric flask, the condensing bottles and burette were rinsed with methanol (the washings being added to the flask), and the volume was made up with methanol. Methanol unified the two phases and had little effect on the subsequent analyses. Aliquot portions of this solution were used for analysis.

(1) *Total peroxides*

Peroxide determinations were always carried out as soon as possible to eliminate decomposition.

(a) *Colorimetric method*—The colorimetric method of C. D. WAGNER *et al.*[6] depends on measurement of the depth of colour of ferric thiocyanate produced by the oxidation of an acidified solution in methanol of ferrous thiocyanate.

The depth of colour of the solution was measured by an EEL photoelectric colorimeter (using an Ilford No. 404 green filter), calibration being effected by the use of hydrogen peroxide solutions of known concentration.

(b) *Iodometric method*—An iodometric method based upon that of J. P. WIBAUT *et al.*[7] was also used.

(2) *Formaldehyde*

S. B. SCHRYVER'S[8] colorimetric method was employed. The depth of colour produced by the reaction with phenylhydrazine hydrochloride in acid solution in the presence of potassium ferricyanide was measured by means of the photoelectric colorimeter (Ilford No. 404 green filter). Calibration was carried out using solutions of formaldehyde of known concentration.

(3) *Total aldehydes and ketones*

The hydroxylamine hydrochloride method of O. WIDMAIER and F. MAUSS[9] was used, with bromo-phenol-blue as indicator during titration of the liberated hydrochloric acid. To obtain the concentration of aldehydes and ketones it was necessary to subtract the concentration of acids in the sample, which was determined separately.

(4) *Carboxylic acids*

Standard 0·1 N sodium hydroxide solution was added to a sample and after standing the excess was titrated with standard hydrochloric acid using phenolphthalein as indicator.

(5) *Individual aldehydes and ketones*

In some cases the 2,4-dinitrophenylhydrazones were prepared by C. ALLEN'S method[10]. The derivatives were filtered off, washed with 2 N hydrochloric acid and dried *in vacuo* over phosphorus pentoxide. They were then dissolved in chloroform and separated on a chromatographic column of silica gel prepared by the method of B. GORDON *et al.*[11]. Development was carried out with gradually increasing concentrations of ether in petroleum ether and the eluted fractions were evaporated to dryness.

The crystals of the separated derivatives were crushed and ground with liquid paraffin. Their infra-red (i.r.) spectra were obtained using a Grubb–Parsons double-beam spectrometer, and these were compared with those of the pure 2,4-dinitrophenylhydrazones published by J. ROSS[12].

(6) *Unsaturated compounds*

These were estimated by the method of M. N. DAS[13] which depends on the reaction between mercuric acetate, methanol and unsaturated compounds.

(7) *Phenol*

The method of M. B. ETTINGER *et al.*[14] was employed. This involves measuring the depth of the orange-red coloration produced when 4-amino antipyrine and potassium ferricyanide are mixed in the presence of phenol. The photoelectric colorimeter (Ilford No. 404 green filter) was used, calibration being carried out with solutions containing known small concentrations of phenol.

(8) *Application of gas chromatography to products of oxidation*

The apparatus used was the Griffin V.P.C. apparatus which employs a katharometer as a detector.

(a) *Hydrocarbon phase*—Adequate separation of the individual constituents of a sample (0·005 to 0·03 ml) was obtained by using a column (6 ft in length) of dinonyl phthalate on 52/85 mesh firebrick. This column gave a better separation than did one of dinonyl phthalate on 'Celite 545' which was used initially.

Individual constituents of the mixture were identified by measuring their retention volumes (retention time × gas flow rate) and comparing these with those determined for a series of substances suspected to be likely constituents, under the same experimental conditions. (The retention volumes relative to that for a standard substance were actually used.)

The identity of a constituent was confirmed by analysing a mixture of the hydrocarbon phase to which a small amount of the suspected substance had been added. If the original identification was correct then a similar chromatogram, with an enlarged peak for the substance in question, was obtained. If incorrect, the chromatogram obtained showed an extra peak.

Quantitative analysis was carried out by using the internal normalization method.

(b) *Aqueous phase*—Difficulty was experienced in the chromatographic analysis of the aqueous phase of the oxidation products because of the preponderance of water. Several methods of removing the water were tried, but without success; for example, using anhydrous sodium sulphate it was found that the residual organic liquid adhered to the large excess of sodium sulphate and could not be separated.

Distillation proved effective in giving a distillate with a reduced water content, but decomposition of the peroxides in the sample occurred and this would inevitably result in some change in composition. Triethylene glycol was adopted as the stationary phase on graded crushed firebrick. This gave a good separation of the water peak from those due to other constituents of the distillate.

Experimental data were obtained on the retention volumes of aldehydes, ketones, etc., to aid in the identification of the constituents of the sample under investigation. The use of relative instead of absolute retention volumes was employed in order to decrease any error due to small variations in column temperature. Where there was doubt about the identity of a substance responsible for a peak the method of adding some of the suspected substance was adopted.

The method used enabled aldehydes and ketones in the aqueous phase to be identified. The internal normalization method, however, could not be used for quantitative analysis of the more complex aqueous phase. The quantitative determination of the constituents was based upon the experimental observation that at a fixed temperature for a given column and stationary phase, there is a simple empirical relationship between the quantity of a substance introduced, the corresponding peak area in the chromatogram and the nitrogen flow rate. This relationship was determined for each substance separately and the results used to calculate the composition of each fraction of the aqueous phase examined.

The aqueous phase was distilled, as already mentioned, and the distillate to 90° C and the residue were analysed. The volumes of the fractions were carefully determined at each stage and measured samples introduced into the vaporizer of the gas chromatography unit by means of an 'Agla' micrometer syringe. Sharp symmetrical peaks were measured geometrically and those which showed rounding and tailing-off were measured by means of a planimeter.

As already mentioned the disadvantage inherent in this method of analysis is that distillation, with decomposition of peroxide, would inevitably cause some change in composition of the mixture.

The total aldehydes and ketones by the hydroxylamine hydrochloride method should equal the sum of the aldehydes and ketones determined individually. Reasonably good agreement was, in fact, obtained, the former value being 0·22 g equiv./g mol. *cyclo*hexane and the latter, 0·25 g mol./g mol. *cyclo*hexane.

(9) *Application of polarography*

Analysis of the total peroxide concentration of the products indicated well-defined maxima at about 350° and 385° C. In order to find out more about the nature of the peroxides formed at these temperatures several oxidation experiments of 3 h duration were carried out and the products subjected to polarographic analysis; the aqueous and hydrocarbon layers being studied separately.

A Tinsley polarograph was employed and a 0·1 M solution of lithium sulphate was used as the supporting electrolyte. Where necessary a dilute solution of α-naphthol was used as a maximum suppressor. Dissolved oxygen was removed from the solutions prior to analysis by bubbling nitrogen through, for periods of up to 15 minutes. The values of the half-wave potentials were referred to the mercury pool anode.

RESULTS

(1) *Effect of temperature on concentrations of oxidation products*

The oxidation of *cyclo*hexane was studied in a series of experiments over the temperature range 300° to 420° C with a constant residence time of 1·2 sec using a reaction vessel 1 in. (2·5 cm) in length. The products were analysed for peroxides, total aldehydes and ketones, formaldehyde, acids, phenol and unsaturated compounds. The resulting curves illustrating the variation in concentration of these products with temperature are reproduced in *Figures 1, 2, 3* and *4*.

The points on the products versus temperature curves were deliberately obtained at temperatures in a random order and thus the scatter of adjacent points about the mean curves gives some indication of the reproducibility. When a new reaction vessel was used the results only became consistent after a number of oxidation experiments when the surface of the vessel had settled down to a steady condition.

The peroxide concentrations determined by the iodometric method are consistently higher than those obtained by the colorimetric method. It is known that formaldehyde forms an addition compound with hydrogen peroxide and it is considered that the iodometric method gives a better

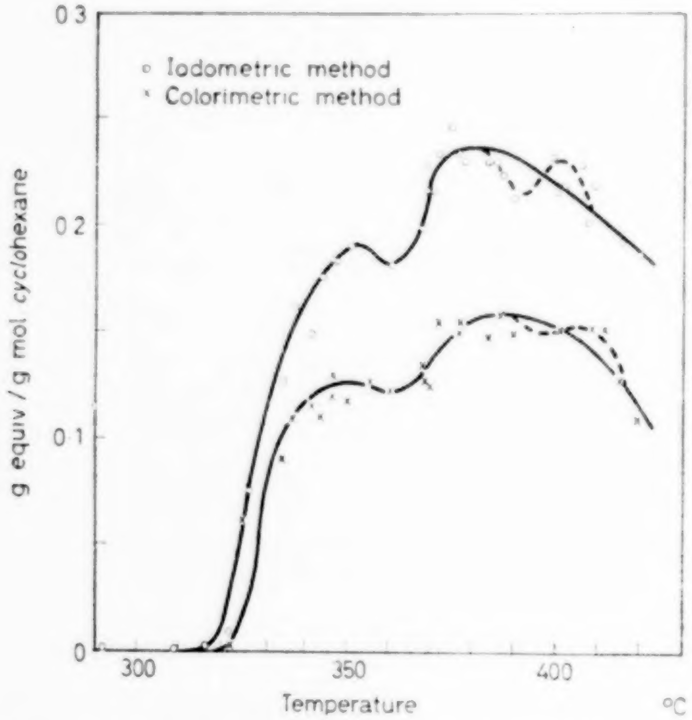

Figure 1. Effect of temperature on concentration of peroxides (residence time 1·2 sec)

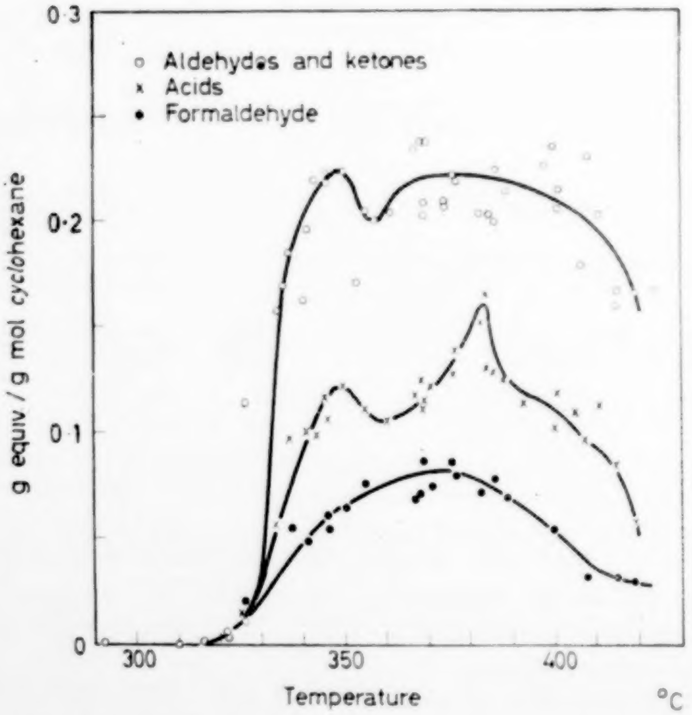

Figure 2. Effect of temperature on concentration of total aldehydes and ketones, acids, and formaldehyde respectively

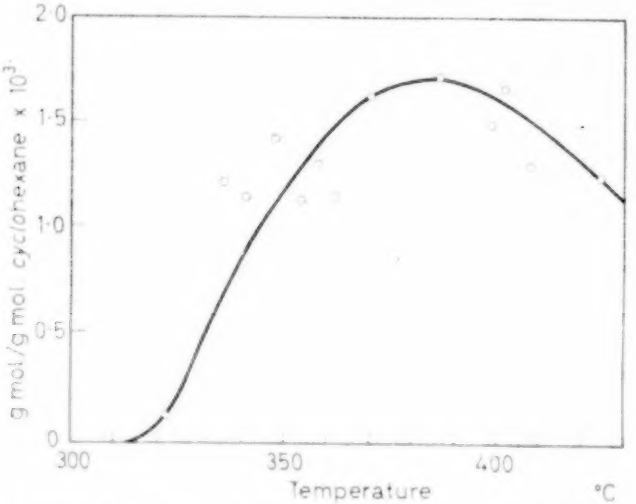

Figure 3. Effect of temperature on concentration of phenol

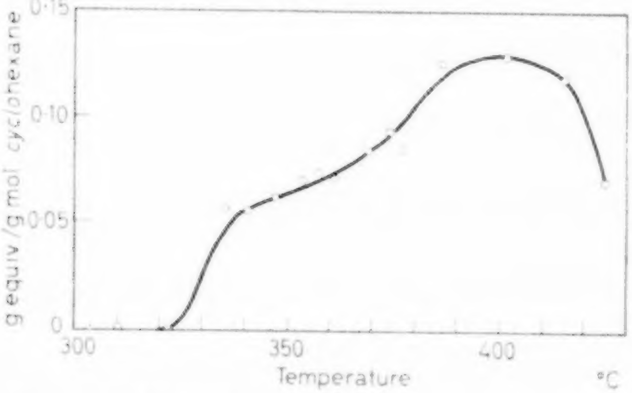

Figure 4. Effect of temperature on concentration of unsaturateds

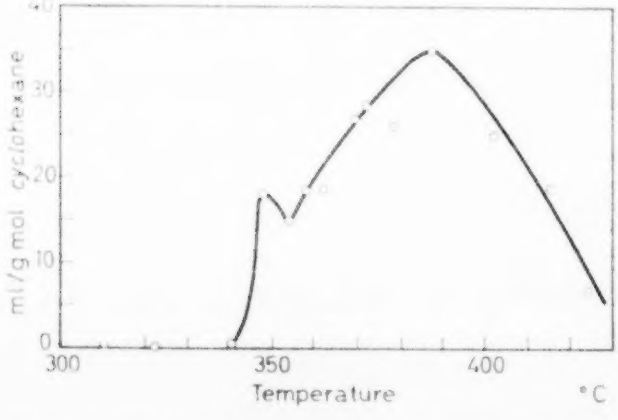

Figure 5. Effect of temperature on volume of aqueous phase produced

estimate of the total peroxide since the solution is boiled during this method of analysis and the addition compound will be decomposed.

Prior to the work on polarographic analysis a further series of 36 oxidation experiments was carried out, using a Pyrex reaction vessel* with a surface/volume ratio of 2·7 cm^{-1} and a residence time of 6 sec. This confirmed that the first two peaks in the curves of peroxide concentration versus temperature occur at approximately 350° and 385°C respectively, whilst a third peak at *ca.* 425°C is more clearly evident (*Figure 6*).

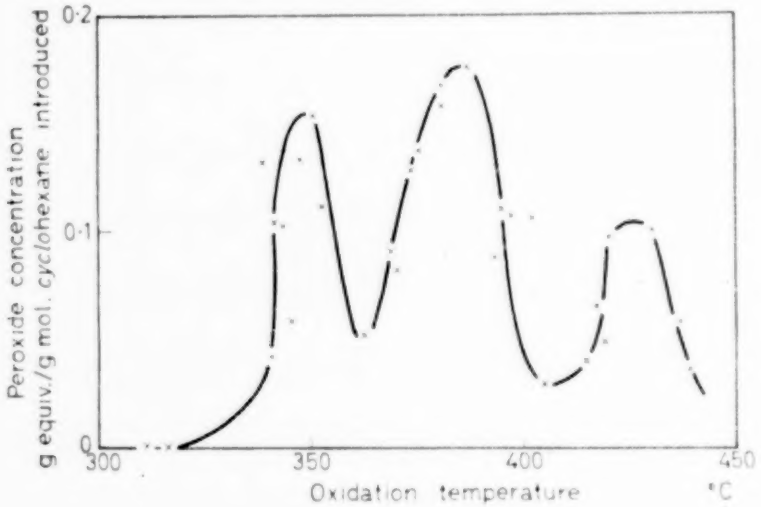

Figure 6. Effect of temperature on concentration of peroxides (residence time 6 sec—iodometric method)*

Table 1

Product	*Temperature corresponding to peak concentration*	*Maximum product concentration g equiv./g mol. cyclohexane*
	°C	
Peroxides		
(1) *colorimetric method*	350	0·13
	383	0·16
(2) *iodometric method*	350	0·19
	383	0·23
Aldehydes and ketones	350	0·22
	383	0·22
Formaldehyde	375	0·08
Acids	350	0·12
	383	0·16
Phenol	383	0·0017
Unsaturateds	350 (*inflection*)	0·065
	395	0·13

---

*This reaction vessel (5·5 in. in length) gave lower peroxide concentrations than those obtained in the series of experiments on effect of residence time, possibly due to a change in the nature of the surface with time.

Oxidation began at about 320° C and weak cool flames were detected up to 350° C. The occurrence of peak concentrations of products is summarized in *Table 1*.

(2) *Effect of residence time*

The oxidation of *cyclo*hexane was studied in a series of Pyrex reaction vessels 1, 2, 5½ and 8 in. in length at a constant reaction temperature of 383° C (which corresponds to the maximum yield of products in the previous work). In this way the concentration of products obtained at different residence times can be examined.

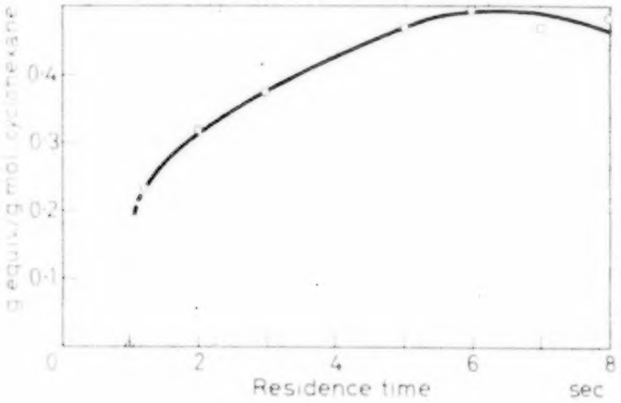

Figure 7. Effect of residence time on concentration of peroxides (iodometric method)

With a residence time of less than 1 sec no oxidation can be detected. The concentrations of peroxides, total aldehydes and ketones, and acids, all reach maxima with a residence time of 6 sec and then decrease with further increase in residence time (*Figures 7, 8* and *9*).

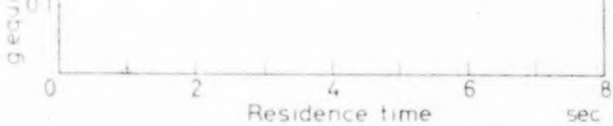

Figure 8. Effect of residence time on concentration of total aldehydes and ketones

(3) *Identification of individual aldehydes*

Chromatographic separation of the 2,4-dinitrophenylhydrazones and examination of the i.r. spectra of the separated derivatives showed the presence of formaldehyde, acetaldehyde and propionaldehyde together with traces of three fractions of higher molecular weight which have not been identified. The amount of ketones formed is small.

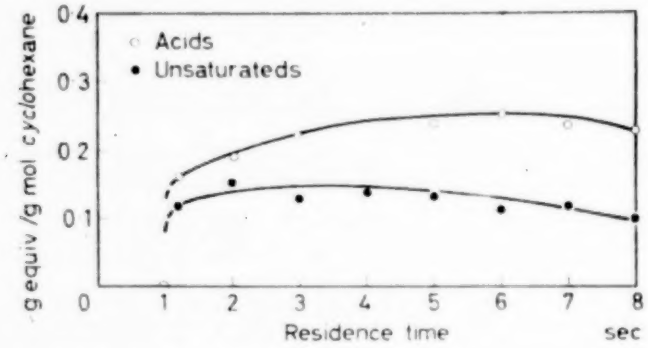

Figure 9. Effect of residence time upon concentration of acids and unsaturateds

(4) *Individual aldehydes and ketones by gas chromatography*

0·045 g mol. of *cyclo*hexane was oxidized at 383 °C with a residence time of 6 sec in the 8 in. (20·3 cm) vessel.

Total volume of aqueous phase =3·35 ml
Aqueous phase subjected to distillation =2·30 ml
Volume of distillate =0·30 ml
Volume of distillate corrected to total volume of aqueous phase =0·3 × 3·35/2·30 0·44 ml
Residue from distillation =2·0 ml
Residue corrected to total volume of aqueous phase =2·0 × 3·35/2·3 =2·9 ml

Details of the chromatographic analysis of these fractions are included in *Table 2*. (Triethylene glycol on graded crushed firebrick was the stationary phase.) A typical chromatogram is reproduced in *Figure 10*.

The yields of the individual aldehydes and ketones detected in the products of oxidation at 383 °C are given in *Table 3*. Formaldehyde was estimated separately by the colorimetric method as it did not give a reliable quantitative elution peak.

Table 2

Sample	*Column temp. °C*	*Nitrogen flow rate l./h*	*Constituent*	*Peak area cm²*	*g mol/g mol cyclohexane*
0·05 ml of fresh aqueous phase	100	1·2	cyclo*Hexane* *Acetaldehyde* *Acetone* *MEK** *Methyl n-propyl ketone*	*poorly separated*	
0·05 ml of distillate	50	1·2	*Acetaldehyde* *Acetone* *MEK* *Propionaldehyde*	7·02 4·90 3·47 1·17	0·096 0·019 0·012 0·017
0·05 ml of residue	100	1·2	*Acetaldehyde*	0·265	0·025

*Methylethyl ketone.

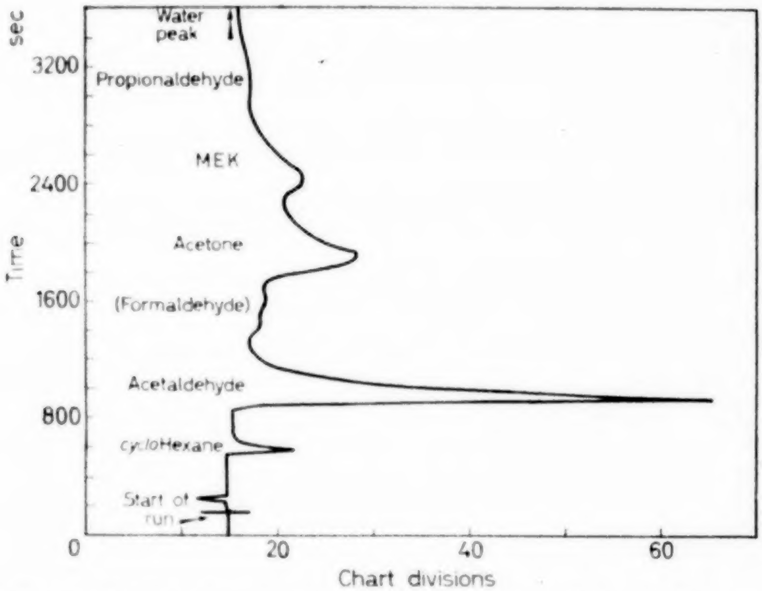

Figure 10. Gas chromatogram for 0·05 ml of distillate. Column—triethylene glycol on firebrick C. 22 at 50°C; nitrogen flow rate: 1·2 l./h

(5) *Analysis of hydrocarbon phase of oxidation products by gas chromatography*

*cyclo*Hexane was oxidized with a residence time of 6 sec in the vessel 8 in. in length over a range of temperature of from 314° to 480°C.

The hydrocarbon phase of the oxidation products is found to consist of *cyclo*hexane, *cyclo*hexene and benzene only, in relative amounts depending on the temperature of oxidation.

A typical chromatogram is reproduced in *Figure 11*.

From the analysis of each sample the composition of the hydrocarbon phase and the mols of each constituent per mol. of *cyclo*hexane introduced

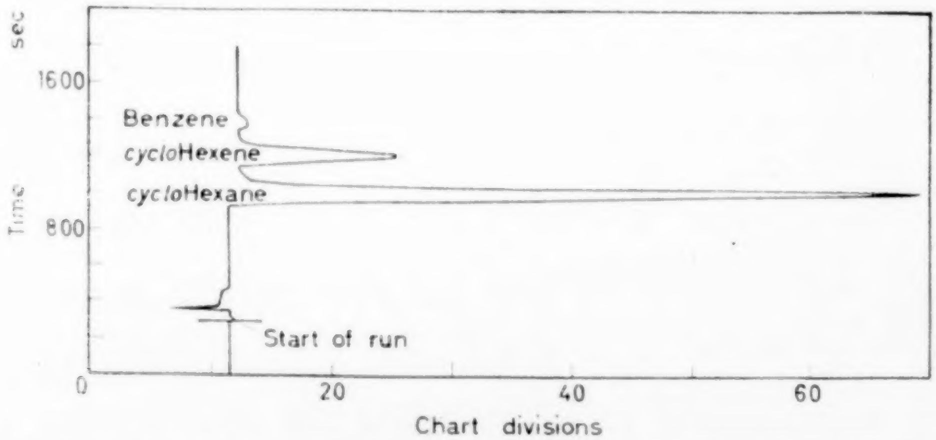

Figure 11. Gas chromatogram for hydrocarbon phase of products of oxidation at 364°C. Column—dinonyl phthalate on 'Celite 545' at 55°C; nitrogen flow rate: 1·6 l./h

into the reaction vessel have been calculated. The resulting curves relating the *cyclo*hexene, benzene and unreacted *cyclo*hexane per mol. of *cyclo*hexane introduced, and *cyclo*hexene and benzene per mol. of hydrocarbon phase, to the temperature of oxidation are shown in *Figures 12, 13* and *14*.

In order to ascertain whether any of the products might be due to pyrolysis rather than to oxidation, a series of experiments was carried out. No *cyclo*hexene, benzene or any substance other than *cyclo*hexane was detected in the attempted pyrolysis at the temperatures previously used in the oxidation experiments. M. LETORT and M. NICLAUSE[15] and C. F. CULLIS, C. N. HINSHELWOOD and M. F. R. MULCAHY[16] have pointed out that pyrolysis is sometimes induced by small amounts of oxygen. However, in the present case attempted pyrolysis in the presence of 0·1 of the stoichiometric proportion of oxygen was unsuccessful so that apparently no pyrolysis takes place during the low-temperature oxidation of *cyclo*hexane.

Table 3

Substance	*Yield* *g mol/g mol* cyclo*hexane*	*Percentage of total carbonyl*
Formaldehyde	0·080	32
Acetaldehyde	0·121	48
Propionaldehyde	0·017	7
	0·218	87
Acetone	0·019	7·5
MEK	0·012	4·7
Methyl n-*propyl ketone*	0·002	0·8
	0·033	13
Total	0·251	100

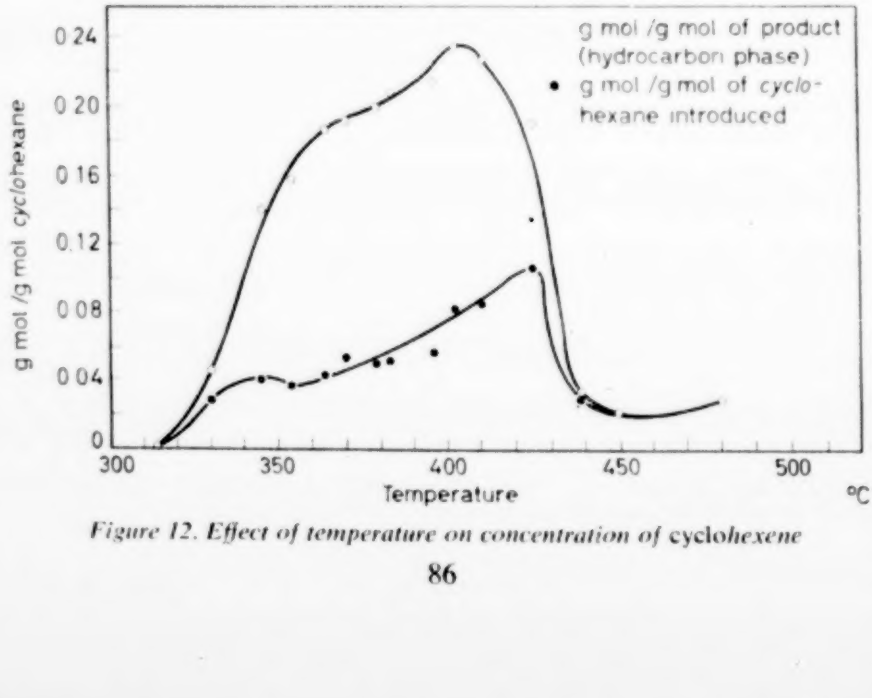

Figure 12. Effect of temperature on concentration of cyclo*hexene*

RESULTS OF POLAROGRAPHIC ANALYSIS

(1) *Temperature of oxidation 385°C*

(a) *Upper (hydrocarbon) layer of products*—Previous work carried out and reference to the literature indicated that peroxides, including hydrogen peroxide, are all reduced at the dropping mercury electrode at applied potentials less negative than −1·5 V. In order to study this region polarograms were obtained over the range 0 to −1·6 V with a sensitive galvanometer setting. A typical result is shown in *Figure 15* where two distinct waves are visible. A number of repeat analyses indicated that $E_{\frac{1}{2}}$ for the first wave varies between −0·35 and −0·38 V whilst $E_{\frac{1}{2}}$ for the second wave varies over the range −1·20 to −1·30 V. The values of the half-wave potentials are referred to the mercury pool anode.

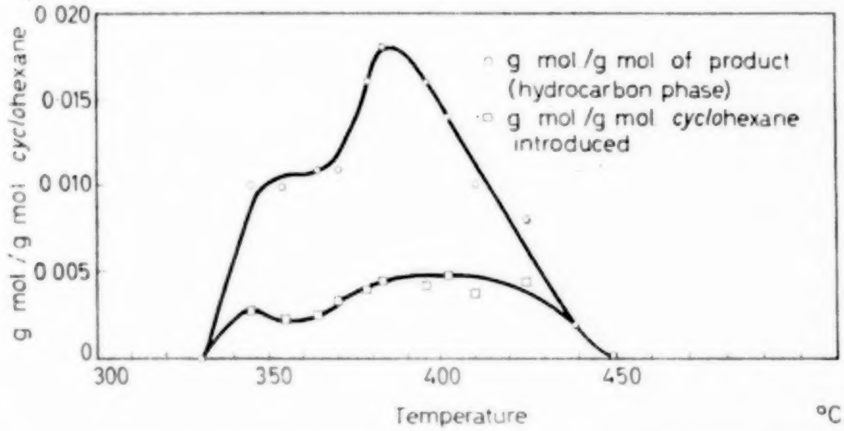

Figure 13. Effect of temperature on concentration of benzene

(b) *Lower (aqueous) layer of products*—*Figure 16* is a typical polarogram obtained from analysis of a sample of the lower (aqueous) layer of products from the oxidation of *cyclo*hexane at 385°C.

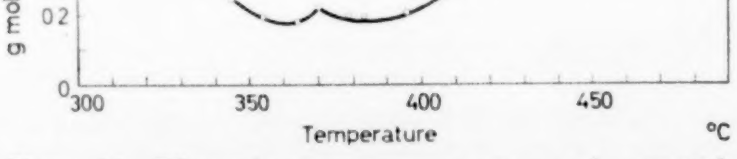

Figure 14. Effect of temperature on amount of unreacted cyclo*hexane*

Four distinct waves are visible and the results of duplicate analyses on the products from two different oxidation experiments are given in *Table 4*.

Table 4

	Wave number in sequence	$E_{\frac{1}{2}}$ *V*	i_d *(μA)*
(*i*)	1	−1·32	12·0
	2	−1·63	32·0
	3	−2·0	8·0
	4	−2·22	34·0
(*ii*)	1	−1·33	12·0
	2	−1·62	31·0
	3	−2·0	10·0
	4	−2·22	34·0

It can be seen that the results are consistent and this is confirmed by many experimental results.

(2) *Temperature of oxidation 350°C*

(a) *Upper (hydrocarbon) layer of products*—The peroxide region was studied by obtaining polarograms over the range 0 to −1·6 V with a sensitive galvanometer setting. A typical result is shown in *Figure 17* where two waves are visible. Accurate interpretation is difficult, but results indicate that the values of $E_{\frac{1}{2}}$ for the first wave vary over the range −0·35 to −0·40 V.

(b) *Lower (aqueous) layer of products*—*Figure 18* is a typical polarogram obtained from analysis of a sample of the lower (aqueous) layer of products from the oxidation of *cyclo*hexane at 350°C.

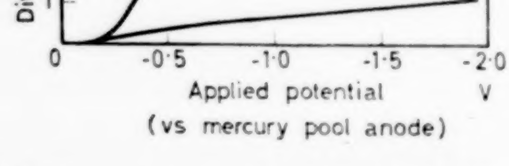

Figure 15. Polarogram of hydrocarbon phase of products of oxidation at 385°C; 0·1 ml products; supporting electrolyte 0·1 M Li_2SO_4; *α-naphthol as maximum suppressor*

Five waves are visible and the results of duplicate analyses are given in *Table 5*.

(3) *Identification of individual constituents*

(a) *Upper (hydrocarbon) layer of products*—Two distinct waves are visible in the region in which peroxides are reduced at the dropping mercury electrode. The first at a value of $E_{\frac{1}{2}}$ of −0·35 V (approx.) is in the region typical of organic peroxides and hydroperoxides whilst the second with $E_{\frac{1}{2}} = -1{\cdot}20$ to $-1{\cdot}30$ V suggests that hydrogen peroxide is responsible for its appearance.

In order to ascertain whether hydrogen peroxide is present, a further study was made. A yellow colour was obtained with titanic sulphate solution. This test is specific for hydrogen peroxide but is not quantitative in the presence of formaldehyde.

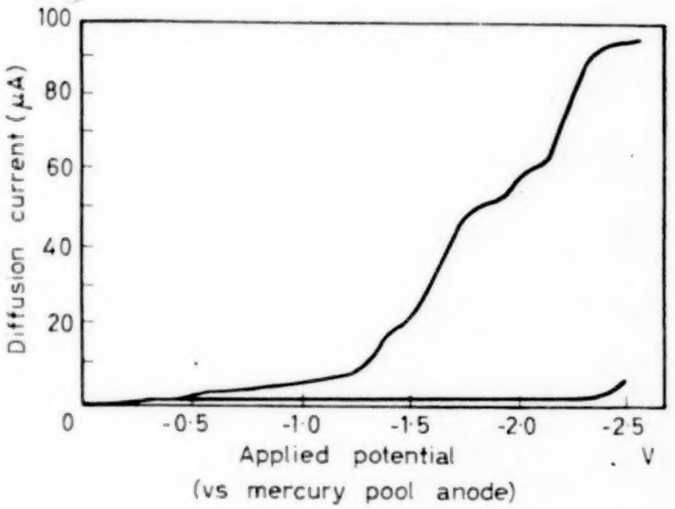

Figure 16. Polarogram of aqueous phase of products of oxidation at 385°C; 0·03 ml products; supporting electrolyte 0·1 M Li_2SO_4; *α-naphthol as maximum suppressor*

Table 5

	Wave number in sequence	$E_{\frac{1}{2}}$ *V*	i_d (μ*A*)
(*i*)	1	−1·30	7·0
	2	−1·60	15·0
	3	−1·88	4·5
	4	−2·04	3·5
	5	−2·22	14·0
(*ii*)	1	−1·30	9·0
	2	−1·60	14·0
	3	−1·86	5·0
	4	−2·03	3·5
	5	−2·22	13·5

The use of the lanthanum reagent in alkaline solution[17] provides a specific test for hydrogen peroxide and peroxidic compounds which are in equilibrium with it. Addition of lanthanum acetate and lithium hydroxide precipitates a basic lanthanum peroxide when added to solutions containing hydrogen peroxide. Alkyl hydroperoxides are unaffected.

Figure 19 illustrates the effect of the reagent on the polarogram of a solution of hydrogen peroxide and it can be seen that the wave due to hydrogen peroxide is completely eliminated, the resulting curve being identical with that of the residual current of the supporting electrolyte.

Treatment of samples of the upper (hydrocarbon) layer of products with the lanthanum reagent was not successful in completely eliminating the wave corresponding to $E_{\frac{1}{2}}$ of $-1{\cdot}20$ to $-1{\cdot}30$ V. This may be due to the fact that because of the low concentration and the high galvanometer sensitivity required, the succeeding wave causes interference. The presence of hydrogen peroxide is, however, inferred from the result obtained with the titanium reagent.

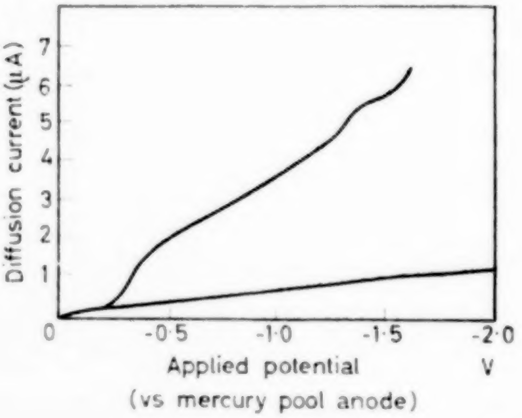

Figure 17. Polarogram of hydrocarbon phase of products of oxidation at 350°C; 0·1 ml products; supporting electrolyte 0·1 M Li_2SO_4 *α-naphthol as maximum suppressor*

It is considered that the first wave in the polarogram at $E_{\frac{1}{2}} = -0{\cdot}35$ V is probably due to the presence of a hydroperoxide. The oxidation of *cyclo*hexane in the vapour phase might be expected to lead to two possible hydroperoxides, *cyclo*hexyl hydroperoxide and *cyclo*hexene hydroperoxide, as we have seen that appreciable quantities of *cyclo*hexene are present. In order to study this further, a fraction of *cyclo*hexene boiling above 85°C was taken and submitted to polarographic analysis. No wave was obtained over the potential range of 0 to −1·6 V. The sample was then heated to 35°C and oxygen was bubbled through it while it was irradiated by a mercury vapour lamp. This continued with shaking for four hours. Under these conditions E. H. FARMER and A. SUNDRALINGHAM[18] obtained *cyclo*hexene hydroperoxide.

A small sample was then submitted to polarographic analysis and a wave at a value of $E_{\frac{1}{2}}$ of −0·35 V was found.

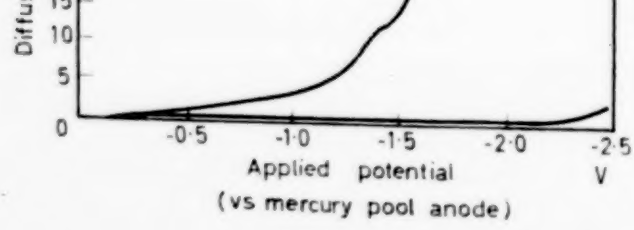

Figure 18. Polarogram of aqueous phase of products of oxidation at 350°C; 0·03 ml products; supporting electrolyte 0·1 M Li_2SO_4; *α-naphthol as maximum suppressor*

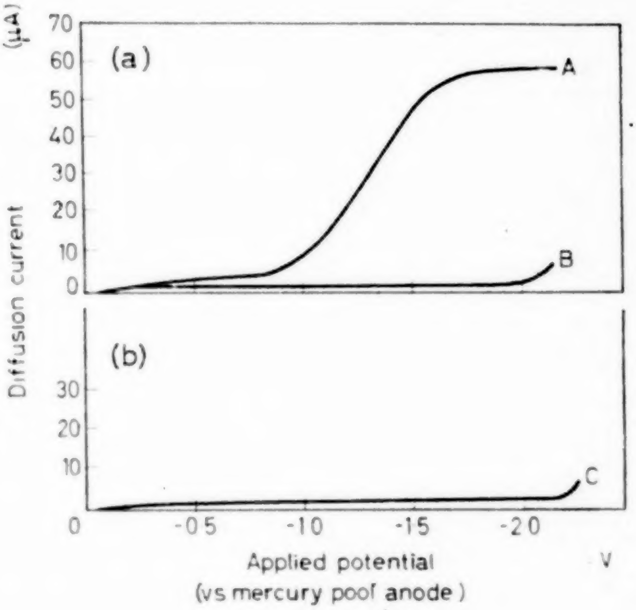

Curve A: Polarogram of H_2O_2 *solution.*
Curve B: After treatment with lanthanum reagent.
Curve C: Residual current of supporting electrolyte.

Figure 19. Effect of lanthanum reagent on polarogram of hydrogen peroxide; supporting electrolyte 0·1 M Li_2SO_4*; α-naphthol as maximum suppressor*

Figure 20 is the polarogram obtained on analysis of a mixture of the oxidized *cyclo*hexene with hydrogen peroxide.

Two waves are visible at −0·35 and −1·19 V, the result being rather similar to that obtained for the sample of the hydrocarbon layer of the oxidation products of *cyclo*hexane. The values of the half-wave potentials agree well, indicating the presence of a hydroperoxide (probably *cyclo*hexene hydroperoxide) and hydrogen peroxide in the latter.

(b) *Lower (aqueous) layer of products*—Analysis of the lower (aqueous) phase of the products of oxidation gave polarograms showing four distinct waves with oxidation at 385°C and five waves with oxidation at 350°C. The substance responsible for the wave at a value of $E_{\frac{1}{2}}$ of −1·88 V, in the latter case, has not been identified.

The wave at $E_{\frac{1}{2}}$ of −1·32 V was shown to be due to hydrogen peroxide. Addition of titanic sulphate solution to a sample of the products gave a yellow coloration whilst treatment with the lanthanum reagent led to

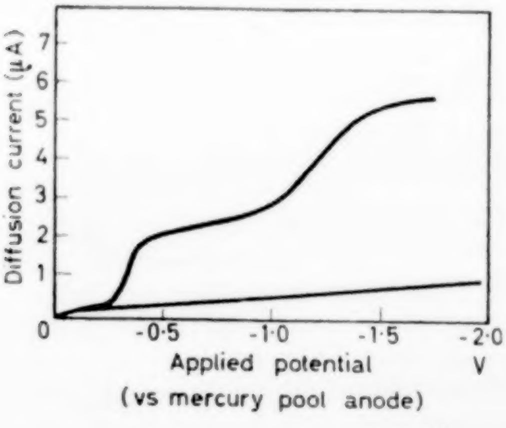

Figure 20. Polarogram of 'oxidized' cyclo*hexene plus hydrogen peroxide; supporting electrolyte 0·1* M Li_2SO_4*; α-naphthol as maximum suppressor*

complete elimination of the wave in question as indicated in *Figure 21*. *Figure 19* shows a typical polarogram for a solution of hydrogen peroxide with a wave at a value of $E_{\frac{1}{2}}$ of $-1{\cdot}30$ V. Comparison of the other half-wave potentials obtained in the polarograms of the aqueous layer of products with those of known substances suggests the presence of the substances listed in *Table 6*.

Further results, not presented here, indicate that the wave heights and values of $E_{\frac{1}{2}}$ are very consistent for the products from different oxidation experiments at the same temperature. This suggests that the method could be used for the quantitative estimation of aldehydes in the products.

Table 6

Oxidation products	*Known substances*	
$E_{\frac{1}{2}} = -1{\cdot}63\,V$	*Acrolein*	$E_{\frac{1}{2}} = -1{\cdot}62\,V$*
$E_{\frac{1}{2}} = -2{\cdot}03\,V$	*Formaldehyde*	$E_{\frac{1}{2}} = -2{\cdot}03\,V$
$E_{\frac{1}{2}} = -2{\cdot}22\,V$	*Acetaldehyde*	$E_{\frac{1}{2}} = -2{\cdot}23\,V$

*However, cf. footnote to *Table 7*.

(4) *Estimation of relative amounts of hydrogen peroxide and hydroperoxide*

The wave heights cannot be measured with great accuracy because of the complexity of the polarograms. However, it is interesting to consider the relative concentrations of hydrogen peroxide and hydroperoxide at the temperatures 385° and 350°C.

The total peroxide was determined by the iodometric method and the concentration of hydrogen peroxide by measurement of the wave height with a value of $E_{\frac{1}{2}} = -1{\cdot}32$ V and reference to a calibration curve of concentration versus wave height. The concentration of 'other peroxide' was taken to be the difference between the above values.

Table 7 gives the concentrations of the peroxides at the two temperatures corresponding to the principal peaks in the plot of peroxide concentration versus temperature. The ratio of 'free' hydrogen peroxide/total peroxide thus increases from $\frac{2}{3}$ to $\frac{3}{4}$ as the temperature of oxidation rises from 350° to 385°C.

DISCUSSION

At the outset it must be emphasized that no pyrolysis occurs, therefore the oxidation mechanism must be able to explain the presence of *cyclo*hexene and benzene as well as the oxygenated products.

The relatively high temperature at which the oxidation of *cyclo*hexane occurs in the present work (viz. 320°C approx.) agrees with the observations of E. W. J. Mardles[19], W. F. Hoot and K. A. Kobe[20] and G. R. Plumb[21]. The ignition diagram obtained by J. H. Burgoyne, T. L. Tang and D. M. Newitt[22] suggests that oxidation might be observed at a temperature as low as 270°C in the region of the first cool flame lobe. Long ignition delays have been noted, however, in this region and consequently observable oxidation is not to be expected in a flow apparatus with residence times of the order of those used in the present work.

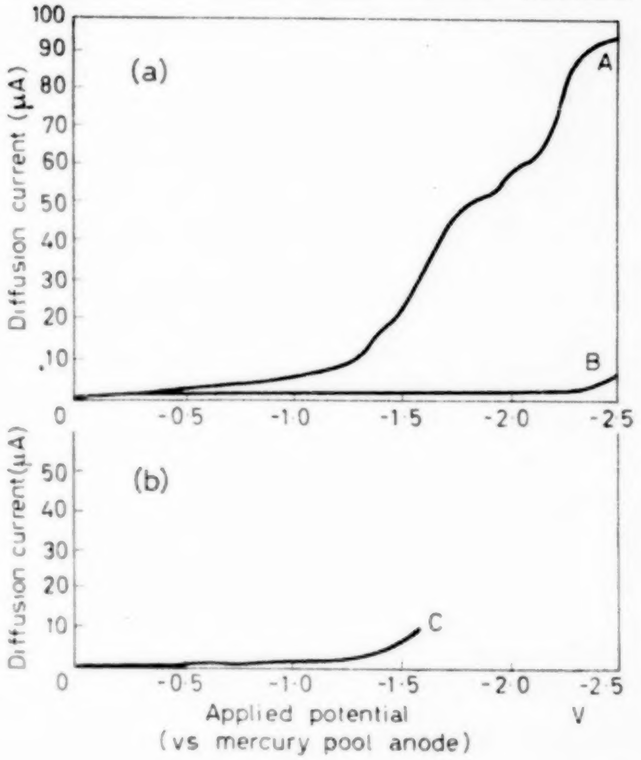

Curve A: Polarogram of aqueous phase of products (0·03 ml) of oxidation at 385° C.
Curve B: Residual current curve of supporting electrolyte.
Curve C: Polarogram after treatment with lanthanum reagent.

Figure 21. Effect of lanthanum reagent on polarogram of aqueous phase of products of oxidation at 385° C; supporting electrolyte 0·1 M Li_2SO_4*; ml products; α-naphthol as maximum suppressor*

Two main peaks are observable in the plots of concentration versus temperature for certain substances, viz. total aldehydes and ketones, acids, unsaturateds, *cyclo*hexene and benzene. With total peroxides, a third peak at about 425° C is indicated.

Table 7†

Expt No.	*Oxidation temp. °C*	*'Free'* H_2O_2 *concentration g equiv./g mol.* cyclo*hexane*	*'Other peroxide' concentration g equiv./g mol.* cyclo*hexane*	*Percentage* H_2O_2	*Percentage 'Other peroxide'*
59	385	0·085	0·022	79	21
61	385	0·081	0·026	76	24
62	385	0·080	0·027	75	25
63	385	0·085	0·022	79	21
64	350	0·069	0·033	68	32
65	350	0·069	0·033	68	32

†More recent work on the polarographic examination of the products of oxidation of *n*-heptane suggests that the wave with $E_{\frac{1}{2}} = -1{\cdot}63$V may be due to an addition compound of hydrogen peroxide with some other oxidation product—possibly an aldehyde. This implies that the values obtained by subtracting the concentrations of 'free' hydrogen peroxide from the total peroxide concentrations, i.e. 'other peroxide', represent hydroperoxide together with hydrogen peroxide addition compound. The hydroperoxide concentrations may thus be considerably less than the values indicated in the last column of *Table 7*.

F. E. MALHERBE and A. D. WALSH[23] have suggested that the oxidation of *cyclo*hexane occurs by the usual scheme:

$$C_6H_{12} + O_2 \rightarrow C_6H_{11}\cdot + HO_2\cdot$$

$$C_6H_{11}\cdot + O_2 \rightarrow C_6H_{11}O_2\cdot$$

$$C_6H_{11}O_2\cdot + C_6H_{12} \rightarrow C_6H_{11}OOH + C_6H_{11}\cdot$$

They suggest further, however, that the peroxide reacts with oxygen in two distinct temperature ranges, the lower corresponding to attack at a tertiary C—H bond and the upper to attack at a secondary C—H. This might explain the existence of the two lobes in the low-temperature region of the ignition diagram for this hydrocarbon. However, the existence of three peaks in the peroxide versus temperature curves suggests that this explanation is unlikely.

The results obtained by gas chromatography in the present work indicate that the aldehydes and ketones in the products of oxidation are the same as those detected in the products of oxidation of *n*-heptane[24], but in slightly smaller amounts. This observation, together with the fact that no cyclic aldehydes or ketones are found, indicates that the *cyclo*hexane ring is broken at an early stage. This supports the earlier work of F. H. GARNER, R. LONG and R. G. TEMPLE[25] on the oxidation of methyl*cyclo*hexane.

This latter work has recently been interpreted by Tipper[2] and by Bawn[3] in terms of decomposition of the peroxy radical with ring splitting, thus

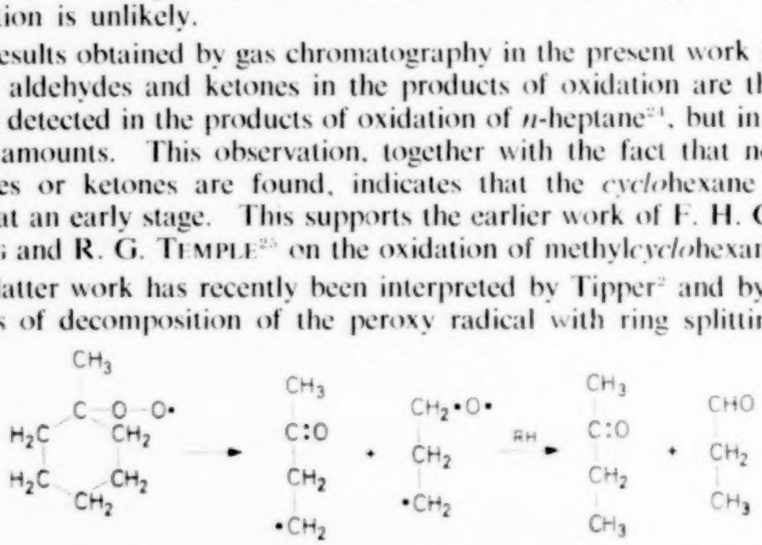

In the present work with *cyclo*hexane, the corresponding breakdown of the peroxy radical must explain the presence of acetone, methylethyl ketone and methyl-*n*-propyl ketone as well as aldehydes, in the products. Some of the latter may well be derived from alkyl radicals and higher aldehydes by oxidative degradation. Decomposition of the *cyclo*hexyl peroxy radical may involve splitting of the ring in two places which would account for the above ketones.

The unusually large amount of carbon dioxide formed during the oxidation of *cyclo*pentane at 400°C has recently led Tipper[2] to suggest that some may be produced directly in the decomposition of *cyclo* $C_5H_9O_2$• radicals, i.e.

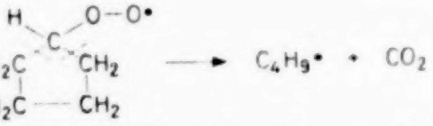

In the present work no gas analyses have been made so that no comment can be made concerning the source of carbon monoxide and carbon dioxide usually found in gaseous products of oxidation. Appreciable amounts of *cyclo*hexene are detected in the products of oxidation and *cyclo*hexene comprises the major part of the unsaturateds. The curves for *cyclo*hexene and benzene formation versus temperature both show peaks in the regions of 350°C and 390° to 425°C. These temperature regions are roughly similar to those at which peaks occur for peroxides and other oxidation products. The concentrations of *cyclo*hexene and benzene in the products both decline rapidly between 400° and 460°C. These observations suggest that *cyclo*hexene and subsequently benzene are formed by the reaction of the original *cyclo*hexane with radicals involved in the oxidation chain.

Several elementary reactions, by which olefin formation occurs, appear to be possible, viz.

(*a*) Decomposition of peroxy radical

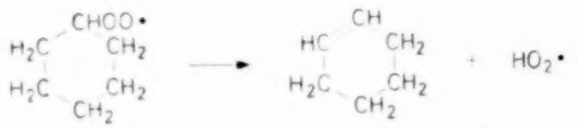

(*b*) Oxygen attack on the *cyclo*hexyl radical

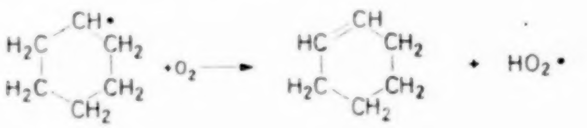

C. N. SATTERFIELD *et al.*[26] have explained the formation of propylene during the oxidation of propane by (*b*) whilst more recently I. R. MCGOWAN and C. F. H. TIPPER[27] have suggested such reactions as the source of *cyclo*pentene detected during the oxidation of *cyclo*pentane.

Other possible but less likely reactions which would lead to olefin formation are:

$$C_6H_{11}OO\cdot + C_6H_{12} \rightarrow C_6H_{11}OOH + C_6H_{11}\cdot$$

$$C_6H_{11}OO\cdot + C_6H_{11}\cdot \rightarrow C_6H_{11}OOH + C_6H_{10}$$

It seems likely that the benzene originates from the *cyclo*hexene but the mechanism is obscure. Further abstraction of hydrogen might lead to *cyclo*hexadiene (although this has not been detected) and finally to benzene. The latter might possibly be formed by successive disproportionation reactions from *cyclo*hexene.

The *cyclo*hexene and benzene formed are themselves oxidized. *cyclo*-Hexene is more resistant to oxidation than *cyclo*hexane[22, 28] but as the polarographic work indicates, there is some hydroperoxide, probably *cyclo*hexene hydroperoxide

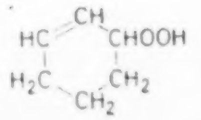

That oxidation of benzene occurs too is indicated by the traces of phenol found in the products. Several workers[29–31] have demonstrated that *cyclo*hexane is a promoter of the oxidation of benzene to phenol and Plumb[21] has shown that this applies even in the low temperature region.

The main peroxide present in the products is hydrogen peroxide. This may be formed by the reaction

$$RH + HO_2\cdot \rightarrow H_2O_2 + R\cdot$$

the $HO_2\cdot$ radical having been produced as suggested earlier.

It must not be forgotten that many of the early products of the oxidation of *cyclo*hexane, in particular the aldehydes, will themselves be subjected to oxidative degradation.

Department of Chemical Engineering,
University of Birmingham

(Received October 1958)

REFERENCES

[1] VON ELBE, G. *Fifth Symposium (International) on Combustion*. p 79. Reinhold: New York, 1955
[2] TIPPER, C. F. H. *Quart. Rev. chem. Soc., Lond.* 11 (1957) 313
[3] BAWN, C. E. H. 'Reactions of free radicals in the gas phase'. p 65. *Spec. Publ. chem. Soc., Lond. No. 9* (1957)
[4] MORRIS, H. E., STILES, R. B. and LANE, W. H. *Analyt. Chem.* 18 (1946) 294
[5] KING, R. O. and DAVIDSON, R. R. *Canad. J. Res. A* 21 (1943) 65
[6] WAGNER, C. D., LAWRENCE, H. L. and PETERS, E. D. *Analyt. Chem.* 19 (1947) 980
[7] WIBAUT, J. P., VAN LEEUWEN, H. B. and VAN DER WAL, B. *Rec. Trav. chim. Pays-Bas* 73 (1954) 1033
[8] SCHRYVER, S. B. *Proc. Roy. Soc. B* 82 (1910) 226
[9] WIDMAIER, O. and MAUSS, F. *Rev. Inst. Franç. Pét.* 3 (1948) 151 and 183
[10] ALLEN, C. *J. Amer. chem. Soc.* 52 (1930) 2955
[11] GORDON, B., WOPAT, F., BURNHAM, H. and JONES, L. *Industr. Engng Chem. (Anal.)* 23 (1951) 1754
[12] ROSS, J. *Analyt. Chem.* 25 (1953) 1287
[13] DAS, M. N. *Analyt. Chem.* 26 (1954) 1086
[14] ETTINGER, M. B., RUSHHOFT, C. C., and LISHKA, R. J. *Analyt. Chem.* 23 (1951) 1783
[15] LETORT, M. and NICLAUSE, M. *Rev. Inst. Franç. Pét.* 4 (1949) 319
[16] CULLIS, C. F., HINSHELWOOD, C. N. and MULCAHY, M. F. R. *Proc. Roy. Soc. A* 196 (1949) 160
[17] BRUSCHWEILER, H. and MINKOFF, G. J. *Analyt. chim. Acta* 12 (1955) 186
[18] FARMER, E. H. and SUNDRALINGHAM, A. *J. chem. Soc.* (1942) 121
[19] MARDLES, E. W. J. *Trans. Faraday Soc.* 27 (1931) 681
[20] HOOT, W. F. and KOBE, K. A. *Industr. Engng Chem. (Industr.)* 47 (1955) 776
[21] PLUMB, G. R. *Ph.D. Thesis.* University of Birmingham, 1955
[22] BURGOYNE, J. H., TANG, T. L. and NEWITT, D. M. *Proc. Roy. Soc. A* 174 (1940) 379
[23] MALHERBE, F. E. and WALSH, A. D. *Trans. Faraday Soc.* 46 (1950) 824 and 835
[24] ALLEN, D. H. *Ph.D. Thesis.* University of Birmingham, 1957
[25] GARNER, F. H., LONG, R. and TEMPLE, R. G. *Trans. Faraday Soc.* 49 (1953) 1193; *Fuel, Lond.* 32 (1953) 117
[26] SATTERFIELD, C. N. and WILSON, R. E. *Industr. Engng Chem. (Industr.)* 46 (1954) 1001
SATTERFIELD, C. N. and REID, R. C. *Fifth Symposium (International) on Combustion*, p 511. Reinhold: New York, 1955
[27] McGOWAN, I. R. and TIPPER, C. F. H. *Proc. Roy. Soc. A* 246 (1958) 52 and 64
[28] ESTRADÈRE, S. quoted by JOST, W. *Explosion and Combustion Processes in Gases*, p 465. (Trans. CROFT, H. O.) McGraw-Hill: New York, 1946
[29] DENTON, W., DOHERTY, H. and KRIEBLE, R. *Industr. Engng Chem. (Industr.)* 42 (1950) 777
[30] DONALD, M. and GROVER, J. 'Proceedings of the Conference on Oxidation Processes'. *Chem. Engng Sci.* 3 (1954) (Spec. Suppl.) 31
[31] DARLINGTON, M. E. *Ph.D. Thesis.* University of London, 1956

Model Investigations into the Factors affecting the Mixing of Gas and Air in Coke Oven Flues

V. JAYARAMAN*, C. HULSE and M. W. THRING

The length of the heating flame in a coke oven flue is governed only by the mixing of the gas and the air, but the factors that govern such mixing are not clear. This model work is an attempt to establish these for the case of rich (coke oven) gas firing. It has been found that a wide range of flame lengths can be obtained for the same flow rates by employing burners and airports of different cross sectional area. A scale theory is put forward to render the model results applicable to actual systems. The theory has been roughly confirmed for a particular case, by carrying out full scale trials in an operating coke oven flue. Work on further confirmation is in hand at Sheffield.

THERE are two major problems in obtaining uniform heating of the walls of a vertical-flue coke oven. The temperature uniformity along the length of the oven wall depends on the distribution of the gas and the air to the various flues, while that along the height is dependent on the length of the heating flames in the flues. The distribution problem has engaged the attention of coke oven designers for a long time, and a large measure of success can be said to have been achieved in perfecting the distribution. The problem of the flame length has, however, not been satisfactorily solved to this date.

This work is an attempt to analyse this latter problem from an aerodynamic point of view. The only other work, done along similar lines, is described in two papers[1, 2], but there are no useful conclusions. The approach is based on the facts that the flame in the coke oven flue is a diffusion flame and that the combustion is subject to a dynamic régime: that is, the combustion rate at the prevailing high temperatures is decided essentially by the rate at which the fuel and the air are brought together.

Investigations have been carried out on a cold model, under conditions of a fair degree of dynamic similarity, and partial confirmation of the model results has been obtained on an actual flue. Only the case of rich gas firing is dealt with.

MODEL WORK

Similarity criteria

A 1/10 scale model of a twinflue of a typical Underjet compound coke oven was built in Perspex (*Figure 1*). Calculations show that the dimensions of modern flues and the rates of carbonization in modern practice (i.e. the flow rates of the heating gases in the flues) are such that the Reynolds number in the flues, DV/ν, is of the order of 700 where D is the hydraulic mean diameter of the flue, V the actual gas velocity and ν the hot gas kinematic viscosity in the same set of units. The volume of air normally employed for combustion is about 6 n.ft^3 per n.ft^3 of coke oven gas, representing 30 per cent excess air. For a coke oven gas specific gravity of 0·4, the mass ratio of air and gas in a coke oven flue therefore becomes 15. Working with water or air as the model fluid at a Reynolds number of 700 in the flue, the total flow being divided in the ratio 1 : 15 between the burner and the two airports, the effect of various factors on the mixing was studied. In particular, the areas of the burner and the airports were varied over a wide range (*Figure 2*).

---

*V. Jayaraman, Ph.D., A.M.Inst.F., is now with the Thermal Engineering Department, Tata Locomotive and Engineering Co. Ltd, Jamshedpur, India

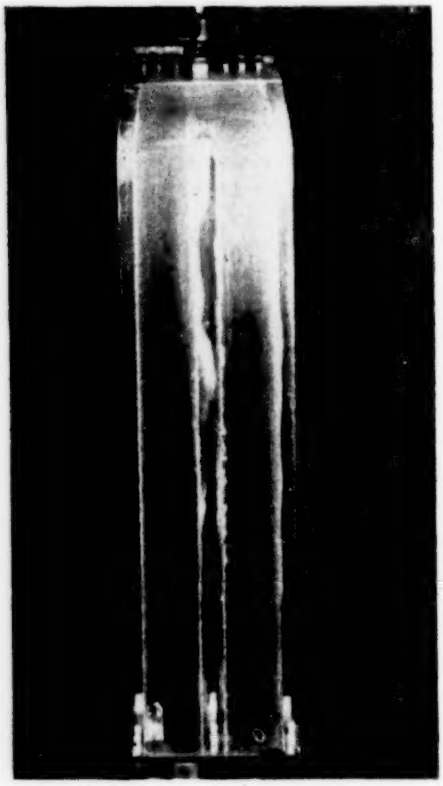

Figure 1. Perspex model of a twin-flue

Buoyancy effects, known to exist in the hot system, could not be simulated on the cold model, since this would require the use of miscible fluids of greatly different densities, which are not easily available.

Photographs of flow patterns

A number of flow patterns, corresponding to various burner diameter–airport size combinations, were first photographed with water as the model fluid (*Figure 3*). For the dimensions of the model, the Reynolds number of 700 fixed the total flow at 28·4 gall/h of water at 10°C. This was appropriately divided among the 'gas' and the 'air' streams. Flow visualization was achieved by employing a very dilute (but deeply coloured) solution of malachite green in water, for the stream representing the gas.

Mixing measurements

Using air as the model fluid, the 'gas' stream being mixed with a small quantity of nitrous oxide as a tracer, many of the arrangements of the water model were then examined quantitatively to obtain the rate of mixing in each case, by analysing the nitrous oxide concentration at various points with the help of an infra-red gas analyser. For the same Reynolds number, with the air model, the velocity has to be greater, since the kinematic viscosity of air is greater. The flow is calculated to be 48·8 ft^3/h of air at 10 °C.

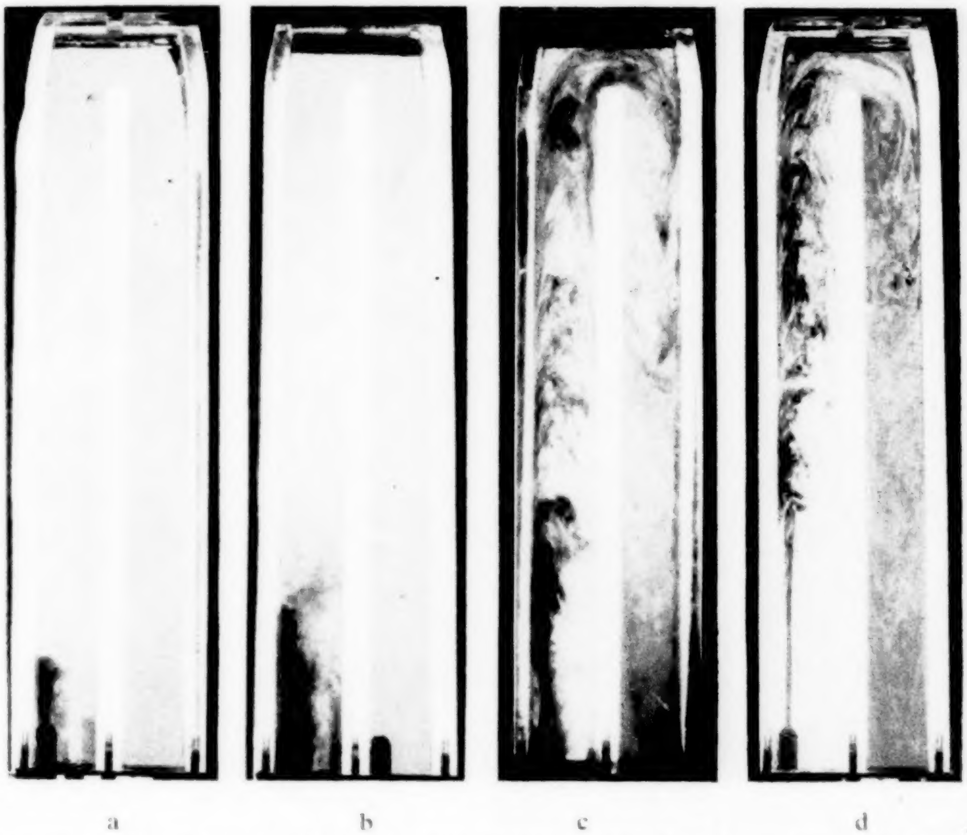

Figure 2. Flame lengths obtainable with various airport sizes for a burner 4·00 mm in diameter. (a) *Each airport 7·70 mm sq.* (b) *Each airport 10·25 mm sq.* (c) *Each airport 13·40 mm sq.* (d) *Each airport 15·80 mm sq.*

From the nitrous oxide concentration at various points in the model, contours were drawn showing lines of equal mixing in the model. The line along which the gas-air mixture is stoichiometric may be taken to represent the flame front, and the highest point on this line therefore gives the height of the flame.

Conclusions from the model work

(*1*) The sizes of the gas and air inlets to the flue have the greatest effect on mixing. A wide range of mixture rates, i.e. flame lengths, can be obtained for the same flow rates by employing burners and airports of different cross sectional area.

(*2*) As a rule, for any given burner diameter, increasing the size of the airports leads to longer flames. *Figures 2*(a) (4·00, 7·70)*, *2*(b) (4·00, 10·25), *2*(c) (4·00, 13·40) and *2*(d) (4·00, 15·80) illustrate this effect on a particular burner, 4·00 mm in diameter. *Figure 4*(a) gives the flame lengths (derived from mixing measurements) against the airport size for various burners, while *Figure 4*(b) gives flame length versus burner diameter for the different airport sizes. Contours similar to those of *Figure 3* represent the general nature of the flow pattern usually obtained.

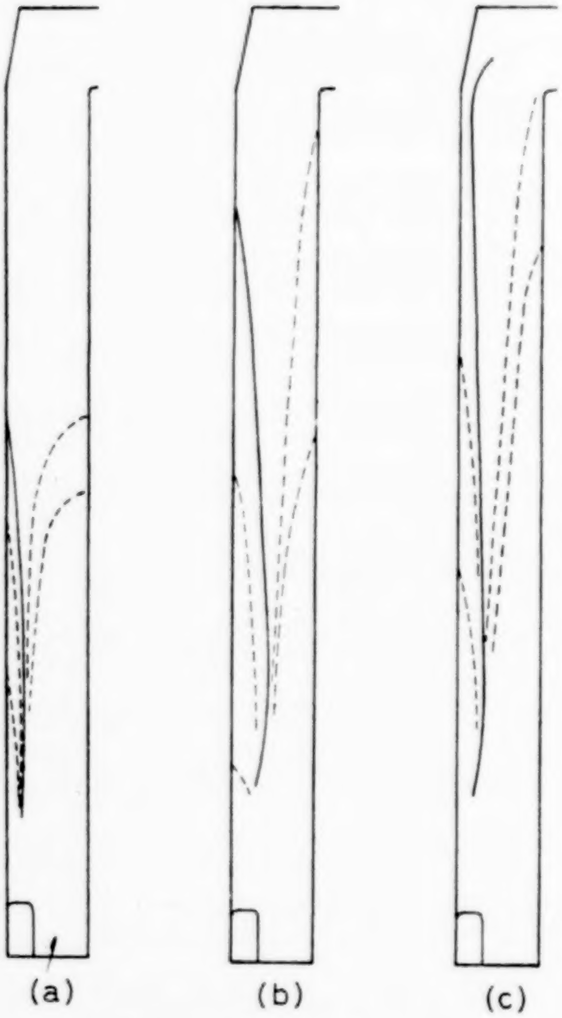
(a) (b) (c)

Figure 3. Concentration (mixing) contours obtained with various airport sizes for different burners using water: (a) *1·75 mm diameter burner, airport size 15·80 mm sq. each;* (b) *3·14 mm diameter burner, airport size 13·40 mm sq. each;* (c) *3·14 mm diameter burner, airport size 15·80 mm sq. each*

(*3*) The effect of factors like excess air percentage, spacing of the airports with respect to the burner, entry conditions, etc., is, within limits, secondary.

INTERPRETATION OF THE MODEL RESULTS

The observations on the model, summarized by *Figure 4*, can be explained at least partly as follows.

---

*Values in parentheses are the burner diameter and the airport side, respectively, in millimetses.

As the air streams enter the flue, a certain amount of recirculation takes place due to the sudden increase in cross sectional area, and if the gas stream has enough momentum to break through this return flow, without itself getting broken up to any appreciable degree, the mixing is thereafter slow. Such recirculation of the air stream would normally be less the bigger the proportion of the flue area occupied by the airports, and the chances of the gas stream breaking up while passing through are less. This explains why the mixing is delayed with bigger airports for any given burner diameter (*Figure 4*).

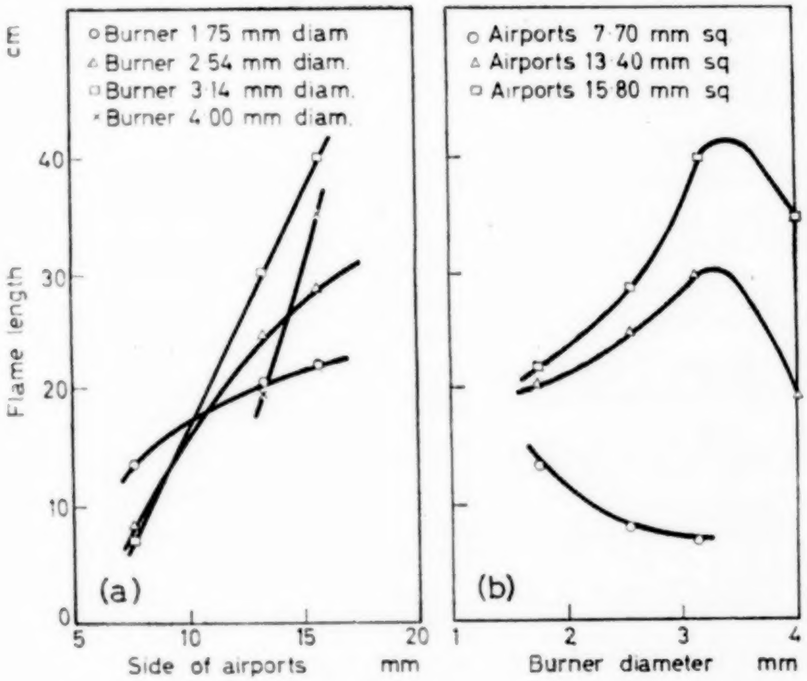

Figure 4(a). Flame length versus airport size for various burners
Figure 4(b). Flame length versus burner diameter for various airport sizes

As regards the gas stream, there are two opposing considerations. For a given mass flow, burners of smaller diameter pass streams of greater momenta, which must have a greater capacity to break through the return air flow. Smaller burners, however, also lead to more turbulent gas streams, which of themselves have a tendency to break up and recirculate. The mean is struck by a burner which produces enough momentum while, at the same time, keeping turbulence down to the necessary extent. The crossing of the lines in *Figure 4* can be attributed to this.

SCALE THEORY

The question of formulating a scale theory becomes difficult in this case. In view of the low Reynolds numbers involved, the recirculation of the air stream would probably be controlled mainly by the Reynolds numbers in the system, while the breaking through of the gas stream would depend on its momentum, the extent of dispersal depending again on the turbulence level, as determined by the Reynolds number. Mixing is the net result of these various factors.

In the absence of a suitable theory, which can adequately take into account all these factors, and in view of the predominant effect of Reynolds numbers on the process of mixing, it is suggested that any model flow pattern can be reproduced substantially in full scale if:

(*1*) the Reynolds numbers in the burner and the airports in full scale are made equal to those on the model (in addition to the Reynolds number in the main chamber being the same in both cases), and

(*2*) the mass ratio of air and gas flows is also the same on the model as on full scale.

These two requirements can be shown to lead to the relations:

$$D_g = K\, d_g\, \mu_c / \mu_g \qquad \ldots . [1]$$

$$D_a = K\, d_a\, \mu_c / \mu_a \qquad \ldots . [2]$$

where D is the full scale linear dimension, d the linear dimension on the model, K the scale factor and μ the absolute viscosity. Subscripts $_a$, $_c$ and $_g$ refer to air, combustion products and gas respectively.

Since μ_c is greater than μ_g and μ_a (the difference depends largely on the difference between T_c, T_g and T_a, where T is the temperature), the burner and the airports in full scale would be larger than those obtained by direct scaling up. For example, in a flue ten times as big as the model, the flow pattern of *Figure 3*(b) should be expected to be reproduced not by employing a burner diameter of (3·14 × 10) or 31·4 mm, but by employing one about 65 mm. This is based on μ_g corresponding to 925° C, which has been found independently from actual measurements to be the order of gas temperatures at the burner mouth to be expected in the Underjet design. The airports can be similarly scaled up.

FULL SCALE TRIALS

The purpose of these trials was to establish the flame length in an operating coke oven flue for any known conditions of flow and compare this with the flame length given by the model when run under conditions of dynamic similarity, as expressed by equations 1 and 2. The flame length was established from analysis of quenched gas samples drawn from the flue, by using the formula

$$r = a\left\{\frac{(2CO_2 + 2O_2 + CO) - (mC_mH_{2m} + 2CH_4 + H_2)}{CO_2 + mC_mH_{2m} + CO + CH_4}\right\} + b \qquad \ldots . [3]$$

where CO_2, O_2, etc., refer to the percentages of these gases in the sample. m has been taken as 3 here, and the values of a and b, for a typical coke oven gas, are 1·09 and 2·465 respectively. Similar relations can be derived for any gas from material balances on any three of carbon, oxygen, hydrogen and nitrogen. r is the volume air/gas ratio.

After a series of five trials on a twinflue, it was established that for normal flow rates, the flame length was about 3 ft 6 in. above the burner block. Parallel experiments on the model, using suitable burners and airports to give the same Reynolds numbers as in the flue, showed that the scaled flame lengths given by the model, though not exactly equal (the model flame lengths were 25 per cent shorter), were of the same order. The discrepancy can be explained as being due, among other things, to the fact that buoyancy effects have not been allowed for in the model work.

It was also found from the gas analyses that the stoichiometric mixture was formed about 9 in. below the point where combustion was complete, indicating the presence of an 'unmixedness' factor in the flow pattern. In other words, the flow (despite the low Reynolds numbers) was such that, at any point, the concentration alternated between two values: and at points where it alternated between gas-rich and air-rich mixtures, the final quenched samples contained both combustibles and oxygen. These alternate pockets mix as they move along and burn completely eventually. The point at which all combustion ceases is, really, of interest for the problem of even heating. For comparison with model results, however, the position at which the stoichiometric mixture is formed is the one of interest (a non-cooled probe is adequate for this purpose alone), because the model technique employed here gives only the time-average value of the concentration and cannot throw any light on unmixedness.

CONCLUSIONS

(*1*) It appears to be quite possible to lengthen flames in a coke oven flue sufficiently for higher ovens by a suitable choice of burners and airports. As a rule, in any existing flue design where the flame is short, making the airports bigger should increase the flame length. To what extent the flame would be lengthened for any given increase in airport size, and whether or not the necessary increase in flame length can be achieved by this means alone would depend on the burner diameter. The present work can give this information (*Figure 4*). The results are applicable to all flues of ratio of sides 1·4 (and probably to those flues in the range of side ratio 1·2 to 1·6), where the Reynolds number is 700 ± 150.

(*2*) The scale theory, which is the basis of the above recommendation, has been roughly confirmed for one case. Work on further confirmation is in hand at the University of Sheffield.

(*3*) Rich gas in a coke oven heating system has been found to get quite hot on its way to the flue. In a typical Underjet design, the temperature of the gas rises to between 850 and 1 000°C. The same effects must be expected in the gas gun system, but here the temperatures in the various flues of any heating wall should be expected to be different. The present work indicates that if, for example, the gas temperature in the end flues is 100°C and that at the central flues is 1 000°C, the burners at the end may have to be more than twice as big as those at the centre, to give the same flame lengths.

The work was carried out in the Department of Fuel Technology and Chemical Engineering at the University of Sheffield, under a bursary from Simon-Carves Limited, and grateful thanks are due to this firm for their help.

Department of Fuel Technology
and Chemical Engineering,
University of Sheffield

(Received September 1958)

REFERENCES

[1] AGROSKIN, A. A. and GUBERGRITS, M. Y. *Izvest. Akad. Nauk S.S.S.R., Otdel. tekh. Nauk* (No. 11) (1949) 1626

[2] GUBERGRITS, M. Y. *Ivest. Akad. Nauk S.S.S.R., Otdel. tekh. Nauk* (No. 5) (1950) 695

Recent Developments and Notes

OSCILLATION OF DIFFUSION FLAMES

Investigations of the oscillation of diffusion flames have been described by A. I. Maklakov, using gases and also the vapours of benzene, kerosine and other liquids, under conditions of laminar flow in the ignitable medium [*Zh. fiz. Khim., Mosk.* 30(3) (1956) 708; ***Ref. Zh. Mekh.*** No. 2, 1957, Rev. 1572]. The velocity limit associated with the oscillations depends on the diameter, the material of construction and position of the burner, as well as the nature of the inflammable mixture, but does not depend on the length of the burner. The oscillations were found to be periodic for small fuel consumption and aperiodic for large consumption. The frequency of the periodic oscillations was 10 to 15 hert and is almost independent of the nature of the gas and its consumption, but it decreases somewhat with increase in the diameter of the burner. At velocities lower than the limit it is possible to excite periodic oscillations by means of a concentric flow of nitrogen or carbon dioxide. A qualitative explanation is furnished for the cause of the oscillation phenomenon [Courtesy ***Referativnyi Zhurnal, USSR;*** translation, courtesy Ministry of Supply].

RADIOACTIVE METHOD OF TEMPERATURE DETERMINATION IN FLAMES

G. J. Mullaney has described a method of determining the temperature of flames by X-ray absorption using a radioactive source [***Rev. sci. Instrum.*** 29 (1958) 87]. The source ^{55}Fe was used to measure the density of high-temperature combustion products through a flame zone 6·5 cm long. Premixed propane–oxygen and argon were used for the experiments with a porous metal burner. Temperatures were determined downstream of the main reaction zone in the flame at one atm. Temperature profiles were obtained through the preheated and main reaction zone using the radioactive ^{55}Fe coated on a small platinum wire as a line source.

RADIATION FROM RADICALS IN FLAMES

Studies of radiation from OH, CH and C_2 radicals in laminar and turbulent propane–air and ethylene–air flames have been described by T. P. Clark [*Tech. Note Nat. Adv. Comm. Aero., Wash., No. 4266* (June 1958)]. The radiations from these radicals were isolated with a monochromator and the variation of emitter intensity with equivalence ratio was determined. The ratio of CH and C_2 radiation intensities was found to be a good index of the equivalence ratio in the flame. Turbulent open flames burning on tubes were found to become leaner near the base, but appeared to be burning at the metered equivalence ratio in the turbulent brush. The amount of radiation given off by the flame per unit rate of fuel consumption decreased with increasing average gas-flow velocities and Reynolds numbers. This decrease could not be accounted for by admixture of the secondary air with the turbulent flame brush.

FLAME RESEARCH AT IJMUIDEN

The third conference organized by the French Committee of the Foundation of International Researches on Flames was held in February 1958 and summaries of the papers presented have now been published by M. Rivière [*Flamme et Thermique*, No. 120 (1958) 36], dealing with recent researches carried out at IJmuiden.

M. Malcor, president of the French committee, was chairman of the conference. M. Tissander, engineer at CERCHAR, described the plant for investigating the flames of pulverized coal and M. Kissel, engineer at IRSID, reviewed the development of instruments used for measurements.

M. Loison, director of research at CERCHAR, and M. Tissander reported the results of the first series of experiments with pulverized coal flames. The conditions of these experiments were: Lorraine coal with 39 per cent of volatile matter and 10 per cent of ash; coal supply, 170 kg/h; excess air 10 per cent; temperature of air, primary 80 °C, secondary 400 °C; proportion of primary air, 35 to 75 per cent of the stoichiometric amount; fineness of coal, 70 to 93 per cent through 200 mesh sieve; thermal load of the furnace, 50 to 65 per cent of the total heat input.

The fineness of the coal and the proportion of primary air were found to be the two factors that have an important influence on the development of the combustion process. With the finest coal the volatile matter was released more rapidly and the combustion of the residual coke reduced the length of flame by about 20 per cent for the levels of fineness used. Diminution of the primary air appears to be accompanied by a decided increase in radiation from the early part of the flame. Variation in the speed of the secondary air resulted in very slight effects on the combustion process and flame radiation.

M. Rivière, of IRSID, described the results of the eighth series of experiments on the flames of liquid fuels. These experiments were designed to measure the effect of amount of turbulence of the combustible jet when this is atomized by an auxiliary fluid and the effect of different modes of variation of turbulence. The effect of suspending carbon particles in the fuel on the radiation properties of the flames was also studied. Increase in the turbulence of the jet of pulverized fuel increased the speed of mixing between air and fuel and consequently the rate of combustion at a given distance from the burner. The temperature of the flame was increased and the emissivity reduced due to the more rapid combustion of the carbon particles formed by cracking. Increase in the temperature of atomization air to 315 °C resulted in a slight reduction in the content of carbon particles in the flame and its emissivity. The main advantage in preheating the atomization air is to increase the turbulence and thus the speed of combustion, for a given mass flow of air.

G. Cohen de Lara, of the Société Grenobloise d'Etudes et Applications Hydrauliques and R. Curtet, of the University of Grenoble, described the investigations on recirculation in diffusion flames. Very good agreement between Curtet's theory and the experimental results was found, in that the recirculated combustion products increase from nil near the burner, becoming a maximum, and again nil at the furnace exit. The value of the maximum amount of recirculated products is essentially a function of the ratio of the amount of turbulence of the combustible and the air for combustion.

MM. Husson, Kissel and Rivière, of IRSID, discussed some applications of the IJmuiden researches to the heating of open-hearth furnaces. Two other communications were concerned with high intensity combustion in industrial furnaces and the stability of natural gas flames.

CARBON INDEX OF FUEL GASES

Professor C. Padovani and E. Caffo, of the Stazione Sperimentale per i Combustibili, Milan, have shown how the carbon index, the volume of carbon dioxide produced by the complete combustion of one volume of gas, is a typical characteristic of fuel gases, easily determined experimentally, and can have a practical application in connection with interchangeability formulae [*Riv. Combust.* 12 (1958) 725]. There is a correlation between the mean carbon index and some chemical and physical properties of gaseous hydrocarbon mixtures. This correlation for the calorific value and relative density has generally only a very slight error, and for theoretical air and flue gases the correlation is exact. The hydrocarbons considered were the gaseous members of the methane and ethylene series.

In particular it is shown that the carbon index may be usefully applied to determine the correction coefficients due to the presence of higher hydrocarbons, which P. Delbourg introduced into his latest interchangeability formulae to correct the Wobbe index and the combustion potential.

For these purposes and also for calculating the soot index of aerated or non-aerated flames, computation on the basis of the carbon index may be found not only easier, but more precise than the exact or approximate methods proposed by Delbourg.

GENERAL ELECTRIC COMBUSTION RESEARCH

During 1958 information was distributed from the General Electric Research Laboratory, Schenectady, New York, about three combustion investigations which were being carried out.

Continuing an investigation of the formation of a detonation from a flame it was found that it may occur by two, and possibly more, mechanisms. Experiments have been performed with acetylene–oxygen mixtures in glass tubes, using a rotating-mirror camera for conventional and schlieren streak photography, and for obtaining an image of the luminous wave as it moves past a transverse slit in the otherwise masked tube. It has been shown that in some mixtures the unburnt gas, set in motion by a shock ahead of the flame, can develop a turbulent boundary layer. The estimated Reynolds number, about one million, associated with the formation of this layer is about what is observed for the development of a turbulent boundary layer in flow over flat plates. When the boundary layer is formed, the flame area is greatly increased and it rapidly overtakes the shock, forming the detonation.

Study of the behaviour of the free radicals produced in flames has been pursued for several years at the General Electric Research Laboratory.

New spectroscopic techniques have been developed for the quantitative determination of oxygen atom concentration and reactions among the species O, H and OH have been studied in the burnt gases from flames. Their concentrations on leaving the flame are for most conditions far greater than corresponds to equilibrium with respect to the final products. It has been shown that the decay of O, H and OH and in some cases CO, occurs through relatively slow recombination reactions, requiring three-body collisions, and the rates of such reactions have been measured. In addition, the hypothesis has been confirmed that the other reactions involving these species are so fast that they are at chemical equilibrium on emerging from the flame. The cooled porous plug burner used in this work has proved to be a very convenient and powerful tool for the study of chemical reactions occurring in flames; other high-temperature gas phase reactions have been investigated by appropriate additions to the unburnt gas, using the flame as a homogeneous heating device.

Oxides of nitrogen, even though a minor part of the exhaust of internal combustion engines, play an important role in the chemistry of air pollution. Little is known, however, about the details of the extremely rapid chemical reactions that lead to the formation of such oxides in engines. Recent studies of such reactions have made use of a shock tube as a source of stationary, high-pressure, high-temperature air, making it possible to obtain information that would be difficult or impossible to obtain if an actual engine were used. The shock wave in the tube was used to produce a mass of hot, compressed air, into which liquid fuels of various types were sprayed. Data indicate that the nitric oxide yield varies markedly with the fuel being burned, although most, if not all, of the variation appears to be directly related to the maximum temperature during combustion and its duration.

EXPLOSION AND FIRE HAZARDS IN LIGHTING

The Illuminating Engineering Society has recently published a report entitled 'Lighting in Corrosive, Flammable and Explosive Situations' [*Tech. Rep. Illum. Engng Soc. No. 1* (November 1958)]. This report on the installation of lighting equipment in these hazardous situations is based on a summary of British practice prepared by the National Illumination Committee of Great Britain for presentation to the International Commission on Illumination in 1955, and brought up to date by a panel of the Technical Committee of the I.E.S. Coal mines and explosives manufacturing plants are excluded from consideration. A considerable number of examples is given, from information supplied by various industries, of hazards and the steps taken to deal with them.

MEASUREMENT OF SMOKE

In *Fuel Research 1957* [Department of Scientific and Industrial Research. Her Majesty's Stationery Office: London, 1958] which has recently been issued as the annual report of work at the Fuel Research Station, Greenwich, a description is given of a small portable instrument called the Telesmoke which has been developed for use in place of the Ringelmann chart. In principle, the new instrument consists of a small telescope containing a number of translucent screens, darkened to standard shades, with which smoke can be compared. In one model two screens corresponding to Ringelmann No. 2 and No. 3 shades are fitted in the body of the telescope and arranged so that they are seen, one above the other, in half of the field of view. The image of the smoke is seen directly in the other half and is in the same plane as the screens. The telescope is held so that the screens are seen against the same background as the smoke. The instrument is easy to read and consistent readings are obtained by different observers. It is more convenient to use, but this advantage is not obtained at the expense of accuracy, which is at least as great as that of the Ringelmann chart [see also L. E. Reed, *J. Inst. Fuel*, 32 (1959) 3].

EXHAUST GAS FROM MOTOR ENGINES

It has been reported from the Fuel Research Station, Greenwich, [*Fuel Research 1957*; see previous note] that the first phase of road tests has been completed to determine the effectiveness of a catalytic combustion unit as a means of reducing the amounts of combustible constituents in the exhaust gases from motor vehicles.

It was found that under all conditions of running of a petrol engine, from idling to full load, the temperature of the catalyst was maintained within its active range, even though the carburetter was set to supply a lean mixture whenever the throttle was more than slightly open. The catalyst was effective over the full range of conditions and, on the average, reduced the percentage of carbon monoxide in the exhaust gas by about 85 per cent and the hydrogen by about 80 per cent. The amounts of methane, higher hydrocarbons, and soot were usually reduced by about one half. The percentage of aldehydes, however, was little changed. After the vehicle had covered some 11 000 miles there was a small but definite decrease in the performance of the catalyst.

Polynuclear aromatic hydrocarbons have been extracted from soot from a diesel engine. On chromatographic separation fluoranthene and pyrene were identified as major constituents with chrysene, 1,2-benzpyrene and coronene in much smaller concentrations. Oily matter from the exhaust of a petrol engine was found to contain mainly hydrocarbons, the greater part being C_5 to C_{10} hydrocarbons. Formaldehyde and acetaldehyde have so far been identified in petrol engine exhaust gas.

IMPROVED BOILER EFFICIENCIES

R. Burgholz has described how a particular industrial problem in Germany was solved in connection with the use of a somewhat unsuitable coal on a small boiler plant [*Brennst.-Wärmekr.* 10 (1958) 561]. The plant served a textile factory with dyeing and finishing processes, and large and rapid variations in load on the boiler had to be encountered. The coal was Ibbenburener Ess-Nuss iv, Ostfeld, of low volatile matter content, about 12 per cent, ash content of about 7 to 8·5 per cent. The ash had softening and fusion temperatures of 1 270°C and 1 405°C respectively, in an oxidizing atmosphere, and consequently presented further difficulties.

The satisfactory burning of such coal to meet the above exacting conditions of boiler operation was achieved by a combination of water-cooled flat grates, three-pass boiler and recirculation preheater for high-pressure hot water operation. Boiler efficiencies of about 75·5 per cent were obtained with the preheater in operation for low loads and an average efficiency over the period of a year of about 80 per cent for a wide range of loads.

RECENT TRENDS IN THE INDUSTRIAL USE OF GAS

At the sectional meeting of the World Power Conference held in Canada in September 1958, a paper was read by S. G. ABERDEEN and A. E. TYRRELL, of the North Thames Gas Board, on recent trends in the industrial utilization of gas and a pattern of probable future expansion. In the changing pattern of industrial production high quality and increased amounts are of paramount importance and the increasing adoption of automatic process and product control is vital for such achievement. The principal applications of control techniques are found in the process industries, chemicals, iron and steel, cement, paper, printing and food, and applications will extend wherever production can be organized as a continuous flow of material which responds under control to changes in the conditions of production. Considerable progress is being made by the British gas industry in the development of automatic processing and the authors describe some of the most recent examples of the integration of gas-heated plant into continuous production lines.

In the flame-cutting and profiling of metals town gas is now used in a process which is largely automatic. An electronically controlled oxy–coal gas multi-burner cutting machine can follow the contour of the most complicated drawings with complete accuracy. The production factor for a process of this kind is raised to the highest practicable level, and scrap and the need for labour are kept to a minimum.

The direct application of heat by flames requires that the gas composition shall be controlled and this is achieved by means of a Wobbe Index Recorder with controlling unit which is based on the principle of combining calorific value and specific gravity in a single term. The use of such a controller maintains the Wobbe Index of an air–gas mixture within 1 per cent of a chosen value, independently of the composition of the incoming gas. A recent application of this unit is a hydrogen–nitrogen atmosphere gas plant.

Other recent developments are in connection with continuous steel strip annealing whereby the process can be completed in five minutes as compared with five to seven days for the batch method. In heat treatment furnaces the successful use of high temperature radiant tubes in which the gas burns is one of the most significant changes in furnace design in recent times and has made possible a very desirable trend towards fully automatic atmosphere-controlled heat treatment. The protective atmosphere in the furnace is provided from an external generator and this requires the use of furnaces with gas-tight steel casings and tight mechanically operated doors. In the ceramic industry recent improvements to the continuous tunnel kiln have still further increased its efficiency and research has been directed towards the development of a multi-passage kiln. Tests have indicated that a saving of about one-half of the heat input per ton of load treated, as compared with one ton of load treated in the open-fired continuous tunnel kiln, is probable in practice.

CYCLONE COMBUSTION

For the past ten years work on cyclone combustion as part of a programme of research into solid-fuel firing for gas turbines, has been carried out by the British Coal Utilisation Research Association under an arrangement with the Department of Scientific and Industrial Research. In recent years the gas turbine aspect of the work has assumed less importance and the work has mainly been concerned with studying the performance of the cyclone with a number of British coals of the type widely used for firing power station boilers. A paper of considerable length has now been published by H. R. HOY, A. G. ROBERTS and D. M. WILKINS, describing the more recent work [*J. Inst. Fuel*, 31 (1958) 429 to 457].

The experimental slagging cyclone combustor was 3 ft in diameter and 3 ft high, and was operated with fine coal passing through $\frac{1}{8}$ in. mesh screen, of high ash content, at combustion intensities up to 2 therms/ft^3 h (coal feed rate 1 800 lb/h). The main factors studied were: secondary air velocity; heat input; air/fuel ratio in the combustion chamber; secondary air temperature; fines content of the coal; and fuel type. The main variable of the fuel was ash composition. The chief criteria characterizing the performance of the combustor were: combustion efficiency; heat transfer to the water-cooled surfaces of the combustion chamber; slag recovery, i.e. the proportion of the ash input passing out from the chamber in the form of slag; quantity and carbon content of the dust carried forward with the combustion gases; slag tapping qualities—the ease with which slag flow from the combustion chamber was maintained; conditions of the slag film in the combustion chamber at the end of the test, i.e. the freedom from excessive slag build-up on the walls and floor of the chamber.

The main factor affecting the operation of the combustor was found to be the temperature/viscosity characteristics of the slag and it was further found that these can be characterized by the silica ratio of the ash [silica ratio $= \{SiO_2 \times 100\} / \{SiO_2 +$ equiv. $Fe_2O_3 + MgO + CaO$ (percentages in ash)$\}$]. As the silica ratio increases, the range of operating conditions over which performance is satisfactory narrows, and the upper limit for reliable operation is 72. The experimental combustor could not be operated with coals having ash silica ratio greater than 75.

The outcome of this work is that a vertical slagging cyclone combustor of the size used has been developed under atmospheric pressure conditions to burn low-grade coal with a combustion efficiency of 97 to 98·5 per cent under optimum conditions, and with over 80 per cent of the ash discharged in the form of slag.

Most of the design problems of a cyclone combustor for an open cycle gas turbine appear to have been solved, but the high rate of deposition on surfaces exposed to the combustion gases is likely to be a big deterrent to its use. The chief application of cyclone combustion is almost certain to be for firing large boiler installations and much of the information obtained in this investigation should be applicable for this purpose. In the U.S.A. and Germany there are more than 85 cyclone-fired boilers in operation or under construction, and in the U.K. two are in commercial operation and four others under construction or projected.

SULPHUR TRIOXIDE IN FLUE GASES

The determination of sulphur trioxide in flue gases is important for the problem of corrosion in boiler installations and a number of methods of analysis have been developed in the past few years. One of the most widely used methods is that originally described by P. F. CORBETT [*J. Inst. Fuel*, 24 (1951) 247]. Although improvements and modifications of this method have been made, it easily gives somewhat erratic results and each determination takes about 30 minutes. In an attempt to overcome some of the difficulties inherent in manual methods, P. H. CRUMLEY, H. HOWE and D. S. WILSON have constructed an automatically recording instrument for this purpose at the Fuel Research Station, Greenwich [*J. Inst. Fuel*, 31 (1958) 378]. Corbett's turbidimetric method forms the basis of this new automatic determination. Sulphur trioxide and sulphuric acid vapour in flue gases in the range 10 to 100 p.p.m. by volume are determined by absorbing the trioxide in an *iso*propyl alcohol solution and precipitating it as barium sulphate; the optical density of the suspension is then measured photoelectrically. Tests have shown that the instrument gives results which are more consistent than those normally obtained by earlier methods and a determination takes eight minutes.

FLAME EVALUATOR

A method of studying the influence of flame characteristics on heat transfer in furnaces has been described by A. M. GODRIDGE, G. G. THURLOW and J. WALLIS, of the British Coal Utilisation Research Association [*J. Inst. Fuel*, 31 (1958) 491]. Since departure from full-scale conditions makes direct simulation between model and full scale impossible it was decided not to try to represent a model furnace but to design an appliance to give the required information by as simple a means as possible.

The evaluator furnace which is described consists of a vertical refractory cylinder 40 in. high and 12 in. wide containing a 5 in. diameter chamber in which the gas under test is burnt. The insulating refractory has been selected to give, at the design heat inputs, temperatures in the furnace of the same general value as those measured on industrial plant at the same heat input rates. Provision is made in the refractory wall for the measurement of heat flow, temperature, gas analysis and radiation characteristics of the flame.

Experiments are described in which (*i*) town gas was burnt at two air/fuel ratios, using two nozzle sizes, both under laminar and turbulent diffusion conditions, (*ii*) town gas was burnt at the same rate both as diffusion and premixed flames, (*iii*) town gas and methane were compared, burning at the same heat input rate.

It is concluded that this evaluator furnace can be used to study the characteristics of flames. The length of turbulent flames produced in the furnace are, as far as can be estimated, of the same order as theoretical predictions while the measurements of emissivity can be used to estimate carbon particle concentrations which, again, are in reasonable agreement with direct measurement on other fuels. The combustion mechanisms in the flames in the evaluator appear to be similar to those on larger plant and it is considered by the authors that the effects observed on the apparatus can be used to predict with some confidence the effect of similar changes in fuel or firing procedure on full-scale plant.

In a discussion of the results it is suggested that the inter-relations between (*a*) emissivity and temperature and (*b*) radiation, re-radiation and convection tend to reduce the influence of individual flame characteristics in the final heat flow to the heat-absorbing surfaces. As a working hypothesis it is suggested that the heat transferred from a flame is primarily determined by (*i*) the heat liberated per unit volume of combustion products, (*ii*) the total heat liberated per unit time per unit heat receiving area in the furnace, and (*iii*) the speed of liberation of this heat.

HOMOGENEOUS–HETEROGENEOUS GASEOUS COMBUSTION

Surface catalytic combustion at high temperatures is of great practical interest but there are few data on the course and characteristics of this type of combustion. There are still many uncertainties as to the part played by active surfaces in high-temperature combustion of gases which is often referred to as a homogeneous–heterogeneous process. L. N. **Khitrin** and L. S. **Solovyeva** have examined this process in a paper presented to the 'Seventh Symposium (International) on Combustion, London and Oxford, 1958'. They describe results obtained in the combustion of carbon monoxide–air mixtures in the temperature range 300° to 900°C, flowing in narrow tubes using wall material of quartz, platinum, and copper, which may be regarded as respectively inactive, highly active, and moderately active materials.

The authors point out that in developing a theory of this type of combustion, the transfer of substances taking part in the reaction to the active solid wall must be taken into account. Starting from heterogeneous combustion theory, an equation is developed to express the basic features of the homogeneous–heterogeneous process and this leads to the conclusion that the properties of this process may differ very widely. Depending on the relative values of the reaction velocity constant for the volume reaction and for the surface process, and especially on the diameter of the reaction tube, the catalytic properties of a wall may or may not be felt.

In the combustion of carbon monoxide flowing in tubes, under optimum conditions, when the rate of the surface reaction is very high the role of surface combustion in the overall process is found to be extremely small (at 1 400°C) even for a tube of 10 mm diameter, and only when the diameter is very much less does a sharp increase in the surface combustion ratio occur. For practical purposes this means that in industrial furnaces, even when made of an active refractory material, there is practically no catalytic effect by the walls on the combustion of the gas mixture flowing through the chamber.

The authors discuss the practical difference between the combustion process in a tube and in a bed of particles of catalytically active material, the laws of combustion being qualitatively the same for both these conditions. Combustion in such a bed can be carried out practically, using a small-grain bed, due to a somewhat different value of the diffusion coefficient and the surface combustion may easily predominate in the overall process. In a small-grain bed of very active catalyst particles flameless combustion may lead to a significant increase in the intensity of combustion of a gas.

METHANE OXIDATION

N. S. Enikolopyan discussed in a paper presented to the 'Seventh Symposium (International) on Combustion, London and Oxford, 1958', the kinetics of intermediate and end products of methane oxidation under steady surface conditions of the reaction vessel. The experiments, of the static type, were conducted in an 'aged' tube 40 mm in diameter and of a volume 203 cm³, between 423° and 513°C, at pressures of 100 to 375 mm of mercury, with mixture compositions $CH_4 : O_2 = 1 : 2,\ 1 : 1,\ 2 : 1$.

It was shown that formaldehyde is the only intermediate responsible for degenerate branching and it was further shown that another intermediate product, methyl alcohol, does not affect degenerate branching.

The following scheme of mechanism is proposed:

$$\begin{array}{lllll}
CH_4 & +O_2 & \rightarrow CH_3 & +HO_2 & \ldots.[0] \\
CH_3 & +O_2 & \rightarrow CH_2O & +OH & \ldots.[1] \\
OH & +CH_4 & \rightarrow H_2O & +CH_3 & \ldots.[2] \\
OH & +CH_2O & \rightarrow H_2O & +CHO & \ldots.[2'] \\
CH_2O & +O_2 & \rightarrow HCO & +HO_2 & \ldots.[3] \\
HCO & +O_2 & \rightarrow CO & +HO_2 & \ldots.[4] \\
HO_2 & +CH_4 & \rightarrow H_2O_2 & +CH_3 & \ldots.[5] \\
HO_2 & +CH_2O & \rightarrow H_2O_2 & +CHO & \ldots.[5'] \\
OH & +\text{wall} & \rightarrow \text{destruction} & & \ldots.[6]
\end{array}$$

Reaction 0 is the formation of primary radicals from the initial reactants; 1, 2, 4 and 5 are chain propagation reactions in the oxidation of methane; 3 is a degenerate branching process; 2′ and 5′ are chain propagation reactions in the oxidation of formaldehyde.

Good agreement is shown between the calculated and experimental values of the kinetic parameters for the methane oxidation reactions.

HIGH TEMPERATURE OXIDATION OF METHANE

An experimental derivation of the overall kinetic equation of the oxidation of methane between 700° and 1 100°C is described in a paper by G. I. Kozlov, presented to the 'Seventh Symposium (International) on Combustion, London and Oxford, 1958'. The burning of carbon monoxide was also studied on account of its importance in the oxidation of methane, as well as for the purpose of testing the experimental procedure, since the kinetic characteristics of this reaction are well known.

The gas–air mixture was passed from a cooler at 0°C, used so as to standardize the moisture content, into a three-section quartz reaction vessel. The first section served for preheating the mixture to 200° or 300°C below the reaction temperature. The second section was a quartz tube 1·5 mm in diameter and 60 mm long and in this the mixture was heated rapidly to the reaction temperature before it entered the first probe of the third section, the reaction section. The third section was made of 2·0 mm quartz tubing and consisted of four probes through which the gas passed to be analysed, and these probes also served to accommodate thermocouples for measuring the temperature.

It is concluded that the overall rate of methane combustion is most probably limited up to approximately 1 500°C by the oxidation of methane to carbon monoxide, whereas at higher temperatures the limiting factor must be the combustion of the carbon monoxide formed from the methane, provided the extrapolation of the kinetic equations for the oxidation of methane and carbon monoxide is correct. The kinetic relationships obtained by the author for methane oxidation are in agreement with the experimental data of J. H. BURGOYNE and H. HIRSH [*Proc. Roy. Soc. A* 227 (1954) 73], but the overall kinetic equation proposed for the temperature range 930° to 1 120°C does not agree with that put forward a number of years ago by R. G. W. NORRISH [*Proc. Roy. Soc. A* 150 (1936) 36].

The burning velocity was calculated on the basis of the theory developed by Y. B. ZELDOVICH, D. A. FRANK-KAMENETSKY and N. N. SEMENOV, with the aid of the overall kinetic equation of methane oxidation obtained by the author of the present paper. The values obtained agree well with experimental results up to methane concentrations of approximately 8 per cent in the mixture. There is extremely good agreement between the calculated values at the lower limit of flame propagation and the experimental results of SIR ALFRED EGERTON and S. K. THABET obtained with a flat flame [*Proc. Roy. Soc. A* 228 (1955) 1174].

DETONATION WAVES

An investigation on gaseous detonation waves was described by F. J. MARTIN and D. R. WHITE at the 'Seventh Symposium (International) on Combustion, London and Oxford, 1958', in which two different techniques were used. The mechanics of the formation of detonation waves in acetylene–oxygen mixtures in tubes were studied by means of direct and schlieren photography with a rotating camera, and the structure of detonation waves in hydrogen–oxygen mixtures was examined using a Mach–Zehnder interferometer to determine the density distribution from changes in the refractive index of the gases undergoing reaction.

It is generally accepted that for the development of detonation in a gas mixture the reactant mixture is compressed by a shock wave of sufficient intensity to a condition such that rapid chemical reaction resulting in auto-ignition occurs with a very short induction period. The particular objective of the present research was to discover how such a strong shock required for the propagation of a detonation wave can develop from an ordinary flame which propagates with a velocity only about 1 to 10 m/s relative to the gases immediately ahead of it.

The results obtained point to interaction which occurs in the shock-boundary layer during the transition from deflagration to detonation, being able to cause auto-ignition behind the shock preferentially at the wall even for smooth walls. There is thus provided another mechanism whereby further flame acceleration occurs to strengthen the shock and so develop detonation.

It was further found that hydrogen–oxygen or hydrogen–air detonations at low pressures, 20 to 150 mm of mercury, have irregular fronts, plane only on the average, and departures from being plane increase with the reaction zone thickness. The coupling between the shock front and the reaction zone appears to result in a characteristic instability of the detonation front.

GASEOUS SLOW COMBUSTION

G. Skirrow and C. F. H. Tipper at the 'Seventh Symposium (International) on Combustion, London and Oxford, 1958' discussed some processes in gaseous slow combustion. The purpose of their paper is to suggest a general mechanism for the production of carbon monoxide and carbon dioxide in slow combustion reactions of paraffins, olefins and saturated aldehydes. In addition, possible reasons for the failure of certain systems to comply with the proposed scheme are examined.

A very comprehensive collection of data from the literature is given by these authors showing the CO/CO_2 ratios for a large range of systems and conditions. These data lead to the conclusion that (*i*) for paraffins, olefins and aldehydes, if the relative reactant concentrations are fixed the CO/CO_2 ratio increases with increasing temperature; (*ii*) if the temperature is fixed the ratio decreases as the oxygen/fuel ratio is increased; (*iii*) certain classes of compounds (esters, *cyclo*paraffins higher than *cyclo*propane, and crotonaldehyde) on oxidation may give anomalous CO/CO_2 ratios; (*iv*) high CO/CO_2 ratios are observed for the oxidation of formaldehyde.

It would appear, therefore, that below 400° to 440°C it is unlikely that direct oxidation of carbon monoxide plays a significant part in hydrocarbon combustion reactions.

In the mechanism proposed by these authors it is suggested that from a hydrocarbon during its slow combustion one of the molecular products first formed is an aldehyde. This may be the successor to an earlier peroxide, hydroperoxide or peroxy radical, but the important feature of the present proposal is that the production of this aldehyde precedes the formation of CO or CO_2. On this view, for paraffins and their simply substituted derivatives CO and CO_2 do not come directly from reactions of the radical R (fuel = RH) with oxygen but from the intermediate aldehyde.

$$R'CHO + X \rightarrow R'CO + XH \text{ (X = radical or } O_2) \qquad \ldots [1]$$

$$R'CO \rightarrow R' + CO \qquad \ldots [2]$$

$$R'CO + O_2 \rightarrow CO_2 + \text{products} \qquad \ldots [3]$$

According to this scheme actual attack on the aldehyde must precede the formation of carbon monoxide. Another important aspect of the proposals put forward is that an intimate relationship exists between the production of carbon monoxide, carbon dioxide and carboxylic acids. A detailed examination is given of the proposed mechanism.

CARBON MONOXIDE–OXYGEN FLAMES

A study of lean carbon monoxide–oxygen flames by means of the Egerton–Powling flat-flame burner has been made by **R. Friedman** and **R. G. Nugent** who described the results at the 'Seventh Symposium (International) on Combustion, London and Oxford, 1958'. Some particularly interesting observations were made on the effects produced by adding small proportions of hydrogen or water vapour.

In making earlier studies of lean hydrocarbon–air flames at low pressure with the same technique, it was shown that even in the presence of excess oxygen the carbon monoxide formed as a combustion intermediate is slow to oxidize completely to carbon dioxide. It was in order to study more closely this slow step that the present work with carbon monoxide as the primary fuel was carried out. In these experiments it was found possible to stabilize flames of a reasonable range of composition, between 13 and 18 per cent carbon monoxide, at 30 mm of mercury pressure. At this pressure the flame thickness was 4 to 5 cm which was satisfactory for the measurement of temperature by thermocouples and for the withdrawal of gas samples for analysis.

The following conclusions are drawn from the results. The flame reaction consists of a rapid step, associated with intense luminosity, followed by a much slower process in which the last of the carbon monoxide is consumed. An assumption that the reaction rate decreases linearly with decreasing carbon monoxide concentration does not appear to account for this effect. The temperature was found to be rising through the region of the slower process so the effect cannot be attributed to cooling. At present the explanation of this is not known.

It was observed that hydrogen and water vapour are not interchangeable as additives for lean carbon monoxide–oxygen flames, even though mixture compositions are adjusted to give the same flame temperature. The addition of hydrogen produces a higher burning velocity and a more rapid second-stage reaction, although gas analysis shows that hydrogen is converted to water in the first stage.

L.L.U. TRANSLATIONS BULLETIN

The Department of Scientific and Industrial Research's Lending Library Unit is introducing a new publication under the title *The L.L.U. Translations Bulletin*. It aims to provide British scientists and engineers, who are anxious to have details of current U.S.S.R. research, with up-to-date information on the availability of Russian translations. It will be published monthly and the first issue appeared in January [Her Majesty's Stationery Office, London: price 4*s* (4*s* 5*d* by post). The annual subscription is £2 13*s* 0*d* including postage].

The *Bulletin* contains lists of books, journals and other scientific papers which are now available or which are being translated and will become available in the near future. One section deals with cover-to-cover translations, a scheme for providing a complete Russian technical journal in the English language, and another gives details of the work being carried out by the National Science Foundation in the U.S.A., with whom the L.L.U. collaborates in this translation scheme. Many translations from America are held in London on microfilm and photocopies may be borrowed.

The *Bulletin* also contains articles on new scientific developments in Russia. These can be followed up in detail with the aid of L.L.U.'s comprehensive collection of Russian scientific literature. It is contemplated that in the future the *Bulletin* will cover other language translations.

The Lending Library Unit in London is the nucleus of the new National Lending Library for Science and Technology which will be established at Thorp Arch, near Boston Spa, Yorks, in 1961.

DECIMAL CLASSIFICATION OF ASTRONAUTICS

At the eleventh Congress of the International Astronautical Federation held in Amsterdam in August 1958, a *Decimal Classification of Astronautics* was recommended for general use [*Raketentech. u. Raumfahrtforsch.* 3 (1959) 1]. The classification was originally proposed about ten years ago by Professor Dr E. SÄNGER, who is chairman of the Deutschen Gesellschaft für Raketentechnik und Raumfahrt e.V. Stuttgart, and modifications have been made since then arising out of practical experience. The classification is divided into nine chief groups containing a total of 1 000 divisions.

HEAT TRANSFER CALCULATIONS

Some new methods of approximate solutions of problems of heat transfer by radiation are suggested by A. L. LUBNY-GERTSYK [*J. tech. Phys., Moscow* 2 (6) (1958) 1255; translation of *Zh. tekh. Fiz., Akad. Nauk S.S.S.R.* 27 (6) (1957) 1357 by American Institute of Physics, Inc., New York].

Various problems of heat transfer between radiating gas, stationary or moving, and fixed solid walls are considered.

In the first problem there is a radiating block of grey gas at uniform temperature, either cubical, spherical or cylindrical. Heat is generated at a constant rate within this gas which is surrounded by inert gas enclosed by a solid surface of the same shape as the block of radiating gas. Numerical values of the effective emissivity between the gas and the solid surface are obtained by solving the differential equations of radiant transfer within the gas.

For a selectively absorbing gas, an alternative to Schack's method of calculating total absorption is suggested but not worked out. The method uses a function giving the probability of all absorption coefficients.

Next to be considered is a grey emitting gas filling the space between absorbing tubes which traverse the gas in all directions. The whole is surrounded by an enclosure and numerical results are given for a cylindrical enclosure.

The following problem is the flow of a grey emitting gas along a tube. Mixing and convective heat transfer are neglected. With an assumed form of temperature distribution at any section, the variation of the mean temperature along the tube is obtained numerically by integration of emissions of individual elements.

The final problem is the flow of a grey emitting gas normal to a large plane surface, which may be partly transparent and is pierced by a number of holes to let the gas through. The gas extends to infinity on either side of the plate. Curves are given to calculate the radiant heat transfer to the plate [*Appl. mech. Rev.* 11 (1958) 701; J. E. Davidson, England].

INHIBITION IN GASEOUS COMBUSTION

In the Section de chimie-physique, XVIme Congrès International de l'Union Internationale de Chimie Pure et Appliquée, held in Paris in April 1957, the theme was the combustion of gaseous mixtures. Over forty communications were made by investigators from ten different countries and these were preceded by a plenary conference at which Professor R. G. W. NORRISH, F.R.S., of the University of Cambridge, gave a lecture on his researches on the application of flash photolysis and cine-spectroscopy in the study of combustion reactions. These papers have now been published, together with the discussions on them, as an issue, in the form of a bound volume, of the *Revue de l'Institut Français du Pétrole* [13 (1958) 311–734].

Two papers on the subject of inhibition in the gaseous phase of the combustion of carbon monoxide were presented by H. JAMES and Professor P. LAFFITTE, of the Laboratoire de Chimie Générale, Faculté des Sciences, Paris (*ibid.* 338, 349). The first of these papers, by M. James, deals with a study of flames with very long ignition delays and the application of such investigations to the determination of velocity constants of combustion reactions. Cyanogen was chosen for this investigation as showing at relatively high temperatures and below the normal pressure limits of explosion, a slow combustion process leading to flames which are characterized by very long ignition delays. At the same time cyanogen yields during the slow reaction a few simple combustion products, carbon monoxide, carbon dioxide and nitrogen. The static method of investigation was used and a fairly complete kinetic study of the cyanogen–oxygen reaction is given in the paper.

The second paper, by MM. James and Laffitte, is concerned with the effect of ammonia on the combustion of carbon monoxide–air mixtures, the static method of investigation being again used. The existence of ignition delays was observed at temperatures and pressures at which carbon monoxide–air mixtures ignite without delay. The particular variation of these delay periods leads to an interpretation of the phenomenon as being due to an inhibition of the combustion of carbon monoxide by ammonia and it is further concluded that the three observed pressure limits of explosion are due to particular inhibiting and promoting processes.

COMBUSTION OF MERCAPTANS

C. F. CULLIS and L. C. ROSELAAR, of the Imperial College of Science and Technology, London, presented a paper to the XVIme Congrès International de l'Union Internationale de Chimie Pure et Appliquée, held in Paris in April 1957, describing a research on the slow combustion of methyl and ethyl mercaptans [*Rev. Inst. Franç. Pétrole*, 13 (1958) 466].

The low temperature oxidation of these compounds was studied by a static method and the course of the reactions was followed by means of periodic chemical analysis of the products.

The reaction of both these mercaptans with oxygen begins in the temperature range 200° to 250°C. Many of the characteristic features of hydrocarbon combustion, such as autocatalysis, are only rather weakly developed, and both mercaptans appear to inhibit their own oxidation which is strongly accelerated by oxygen. Sulphur dioxide is the predominant sulphur-containing product, but disulphide formation appears to occur to an appreciable extent in oxygen-lean mixtures. It is concluded that the main oxidation process is initially the removal of hydrogen from the SH group with the production of an RS radical. This radical then reacts with further oxygen giving sulphur dioxide and an alkyl radical R. Subsequent reaction consists essentially of further oxidation of the alkyl radical, the products including acetaldehyde and acetic acid when ethyl mercaptan is reacting with oxygen in defect, and degradation products of acetaldehyde when oxygen is in excess.

W. A. KIRKBY

DECOMPOSITION FLAME OF LIQUID OZONE–OXYGEN MIXTURES IN A TUBE

Dr R. SANDRI writes that in equation 1 on page 349 of the December 1958 issue of *Combustion and Flame*, and in the line immediately following it, x_0 should be replaced by λ_0.

AIR POLLUTION CONTROL ASSOCIATION

The next annual meeting of the Air Pollution Control Association will be held during 22 to 26 June 1959 at the Hotel Statler in Los Angeles, Calif., U.S.A. Planned activities include the presentation of technical papers covering the control of air pollution. Full details are obtainable from the Executive Secretary, A.P.C.A., 4400 Fifth Avenue, Pittsburgh 13, Pa.

THE BRITISH RAILWAYS GAS TURBINE LOCOMOTIVE

The Newsletter of November last sent by the Executive Secretary of the Combustion Institute to the members of the Institute described the holding of the Seventh International Symposium in London and Oxford, England, in a very appreciative and generous manner. There is one statement originating in the symposium programme which for the sake of accuracy should be corrected. The special train provided by British Railways was not drawn by a diesel–hydraulic locomotive but by a 2 500 h.p. gas turbine electric locomotive (supplied to British Railways by British Brown Boveri Ltd, London, and built in Switzerland). It was planned that this locomotive, the first of its kind on British Railways, should draw the train on this occasion; later, however, it was announced that the gas turbine would not be available and that it would be one of the diesel–hydraulic locomotives, a prototype of 80 under construction at Glasgow, which would do duty (as stated in the symposium programme). It was only at the last moment that it was found that the gas turbine locomotive would after all be free for this trip. Many of those who travelled in the train had opportunity to inspect it.

This locomotive is 63 ft long and weighs 115 tons. It is started on diesel oil and after warming up is switched over to burn heavy furnace oil. The power unit consists of gas turbine, compressor, heat exchanger, combustion chamber and geared generator. The traction effort at the wheels during starting is 31 500 lb up to about 21 mile/hour and 8 400 lb at the maximum speed, 90 mile/hour, continuously. There is a single combustion chamber which has a replaceable lining of special steel. The fuel is pumped and sprayed into the chamber by a single centrally located injection nozzle. The combustion air is admitted to the spray through swirl vanes; the high viscosity fuel oil is preheated in a system of tubes placed in the stream of the exhaust gases. As the combustion gases pass down the combustion chamber they are gradually mixed into the excess air until a uniform temperature is reached at the gas turbine inlet.

FUEL

Readers of *Combustion and Flame* may like to know that *Notes* appeared in the January issue of *Fuel* dealing with:

Air pollution in France
American study of air pollution
High-temperature research
Liquid fuels conference
U.S.A. National Fire Codes

Publications

THE SCIENCE OF HIGH EXPLOSIVES

M. A. Cook. *American Chemical Society Monograph No. 139.* New York: Reinhold;
London: Chapman and Hall. 1958. *xv* + 440 *pp.* (*illus.*) 180s

The impetus given to the study of the physics and physical chemistry of explosive functioning by the 1939–45 war has been extended by subsequent military and commercial interest. Although many data have been published in scientific periodicals in recent years a considerable volume has remained in reports of limited availability. The author of this monograph has attempted a wide and up-to-date coverage of the field but has had to rely to a great extent on the work of his group at the University of Utah. The volume and breadth of the information contained in this book are a credit to his energy and enthusiasm.

Professor Cook is as well known for the unorthodoxy of his theoretical interpretation of much of his data as for the experimental ingenuity with which he obtains them. He makes no pretensions to impartiality in the treatment of certain theoretical problems in this book and his exposition of these may confuse the general reader as much as it will exasperate other workers in this field. Nevertheless this is a stimulating and valuable book.

After a brief introductory chapter on the practical application of explosives an excellent survey of modern instrumental techniques is given. Chapter 3 introduces the factors on which the speed of propagation of detonation is known to depend and is intended as an introduction to chapters 4, 5 and 6 which deal with the hydrodynamic theory of the one-dimensional wave, the effect of confinement and of finite reaction rates.

The first part of chapter 4 is a conventional account of the theoretical dependence of detonation speed on the properties of the explosive products and deals briefly but adequately with the utility of various forms of the state equation. The second and larger part, about two thirds of the whole chapter, discusses the von Neumann–Doering–Zeldovich model of detonation structure. This is less satisfactory since it is devoted to a detailed account of the author's personal objections which tend to confuse two separate issues: (*a*) the theoretical behaviour in the vicinity of the CJ plane of the reaction zone and (*b*) the failure to observe experimentally the so-called pressure spike. The NDZ model is well known to represent a limiting case when the shock front can be regarded as separable from the reaction zone and can apply only when the reaction rate and transport properties are small. A more realistic treatment requires the solution of the differential equations of continuity within the reaction zone as has recently been attempted by J. O. Hirschfelder and C. F. Curtiss [*J. chem. Phys.* 28 (1958) 1130].

Chapters 5 and 6 contain a useful account of the author's 'detonation head' theory which appears to correlate satisfactorily many experimental observations on detonation waves in solids. However, free surface velocities (as opposed to plate projection velocities) are not among these and the statement on page 116 that, irrespective of plate impedance, free surface velocities can be extrapolated to a constant value, for zero thickness, of twice the CJ particle velocity of the explosive is incorrect. It overlooks, among others, the experimental results of H. Lawton and I. C. Skidmore [*Disc. Faraday Soc.* 22 (1956) 188]. The figures given in table 1 of this paper clearly demonstrate that when the plate impedance is less than that of the explosive products, the extrapolated free surface velocities exceed the CJ particle velocity. It can be shown that these results fit the free surface velocity/impedance type of relationship, equation 5.24, but not equation 5.30 on page 117.

Chapter 6 recounts the very interesting observations which have been made on the electrical properties of detonating explosives. Subsequent chapters deal with explosive sensitivity, the properties of solids under conditions of explosive attack, shaped charges, blasting action of explosives, the thermodynamics of explosive products and the formation of pressure waves and their damage potential.

The book as a whole contains much useful data together with many new ideas and whilst it will excite criticism it will also excite admiration for the breadth of the author's knowledge of his subject.

G. K. Adams

FAST REACTIONS IN SOLIDS

F. P. Bowden and A. D. Yoffe. London: Butterworths; New York: Academic Press, 1958. *ix + 164 pp. (illus.)* 40s or $7.00

This monograph links up with an earlier publication (1952) by the same authors, on the 'Initiation and Growth of Explosion in Liquids and Solids'. The work described here is mainly an experimental approach, and it deals primarily with the subsequent studies of the writers and their collaborators. It provides convenient access to some of the experimental techniques developed for investigating reactions in solids completed in less than one millisecond, although the monograph does not give technical details about these techniques. High resolution electron microscopy together with electron diffraction has been used to investigate the early stages of decomposition, and fast photography and electronic methods have been employed to follow some of the rapid reactions. Though much in these studies remains incomplete, because of the inherent experimental difficulties and lack of coherent theory particularly of the growth of detonation, the book provides a useful compendium for other workers interested in this field. The monograph gives over two hundred and fifty specific and general references and should undoubtedly fulfil the author's hope that it will prove to be a stimulus for this kind of research.

A. R. Ubbelohde

A DICTIONARY OF NAMED EFFECTS AND LAWS IN CHEMISTRY, PHYSICS AND MATHEMATICS

D. W. G. Ballentyne and L. E. Q. Walker. London: Chapman and Hall, 1958. *v + 205 pp.* 30s

This is an unusual little book giving brief definitions of the laws, effects, theorems, reagents, etc., known by people's names. It does seem that a small reference work of this type on one's own shelf might be much more useful than a more pretentious volume in a less accessible library. There are about 900 entries, averaging less than a quarter of a page each, and for many purposes such brief entries are more useful than a major treatise. Usually, the entries appear accurate and adequate, although in a few cases they seem rather weak; for example, the entries under Raman spectrum and under Fermi Dirac statistics suggest that the authors do not really understand their significance.

The weakness of the book in its present form is that it is not nearly comprehensive enough. Thus, if one checks well-known named effects from the subject index of practically any textbook, one finds that only about half are included. In the reviewer's fields of combustion and spectroscopy, the following items are missing: Birge–Sponer extrapolation, Bunsen burner, Cerenkov radiation, Chapman–Jouguet detonation, Cornu prism, Davy lamp, Diesel engine, Fortrat diagram, Fraunhofer lines, Grashof number, Hugoniot equation, Hund's coupling cases, Kerr cell, Meker burner, Nusselt number, Otto engine, Prandtl number, Russell–Saunders coupling, Saha equation, Stefan Boltzmann law, Swan bands, Venturi duct, Wien's radiation law. While the book is, in principle, very welcome, it will be seen that in its present form it is hardly adequate. One can only hope that it will survive to reach an expanded second edition.

A. G. Gaydon

AXIAL FLOW COMPRESSORS

J. H. Horlock. London: Butterworths, 1958. *xvi + 189 pp. (illus.)* 40*s*

Historians of the development of the gas turbine have often regarded the lack of knowledge of the design and performance of an efficient compressor as the chief obstacle to the early realization of the constant pressure gas turbine. It is, perhaps, this fact which has resulted in the appearance, during the last two decades, of a profusion of literature on the axial flow compressor dealing with both its theoretical and experimental aspects. Therefore, the publication of a work, which may give both the student and the research or design engineer an adequate introduction to this diffuse body of knowledge, should be welcomed, for, until the appearance of this present work, no single book was available which dealt, specifically, with the large fund of knowledge on axial flow compressors.

Any writer who seeks to acquaint his readers with this subject is faced with the problem that many aspects of the theory lean, to a greater or lesser extent, upon the fundamentals of thermodynamics, areo- and hydro-dynamics, and their related mathematical techniques. It is necessary, therefore, to deal with these fundamentals in some way in order that the reader be prepared in advance for their application to the problems of the axial compressor. J. H. Horlock has endeavoured at the outset to present a brief review, in a manner appropriate to the subject, of the equations of motion of liquid flow, of the thermodynamic aspects of the compression process, one-dimensional compressible flow and the use of dimensionless groups, all of which are important for a proper understanding of the axial compressor. However, this treatment should not be regarded as a substitute for the reading that would surely be necessary if the subsequent chapters are to be fully appreciated by one not well acquainted with the basic thermodynamics and fluid dynamics.

The treatment of the subject proper may be divided into three parts: the two-dimensional (i.e. the study of cascades consequent upon the development of annular elements of blade rows into linear arrays), the three-dimensional (namely, the treatment of the blade row as a whole) and, thirdly, the practical and secondary aspects (such as energy losses, secondary flows, surging and the technique of testing).

The design of axial flow compressor blading still rests on the theoretical and experimental knowledge of cascades, which are linear arrangements of straight blades in which the flow is assumed to be two-dimensional, and the would-be designer must be fully conversant with their properties. Both the theoretical lines of attack on this problem (i.e. conformal transformation, with a very brief mention of the theory of this method, also the method of singularities) as well as the experimental and empirical approaches are described. With regard to the correlation of the experimental data derived from cascade tests, the work of Howell, of Carter and also the NACA correlation is covered, although no treatment of the theoretical background to the separation, or loading factor, which is the basis of the former correlations is included. However, this section (and indeed this is true of the whole book) is very well documented with references to the original sources.

The chapters devoted to the three-dimensional flow in complete rows contain most of the recent developments in the theory, to some of which, in particular, the actuator disc theory, the author has personally contributed. In addition, some of the excellent flow visualization work of Herzig, Hansen and Costello, namely, photographs depicting secondary flow in a cascade in non-uniform flow, has been reproduced.

The remainder of the book deals with the problems of rotating stall, surging, blade vibration, experimental techniques of measurement and testing, and a short section on the supersonic axial compressor is included. An Appendix containing a design study for a typical machine has also been added. With regard to the phenomenon of rotating stall, which appears to have been responsible for many blading failures, the work done both in America and at Cambridge is described.

In conclusion, the book may be thoroughly recommended both to the student and to the practising engineer who is interested in this field.

J. W. Railly

Letters to the Editors

Letters to the Editors on points of scientific interest related to combustion and flames are invited. The Editors do not hold themselves responsible for opinions expressed in correspondence. Anonymous contributions cannot be accepted.

The Addition of Air in Stages to a Perfectly Stirred Reactor

SEVERAL investigators have studied premixed combustion systems in order to determine optimum combustion intensities and minimum volumes for completion of the reaction under various conditions. Examples of this work may be found in references 1 to 6. In this Department we are attempting to find the ideal conditions for each individual part of a combustion system so that in the design of a practical system the nearest possible approximations to these optimum conditions may be made. The present note describes a theoretical attempt to discover the optimum mixing conditions for fuel, air, and recirculation products in a non-premixed system. Experimental studies on a one-dimensional flame are being made by Datschefski.

The system theoretically studied here is one in which all the fuel and recirculation products enter Zone 1 of a six-zone reactor along with a proportion of the air, the rest of the air being added to the other five zones (*Figure 1*). The volume required in a reactor of this type to burn one pound of fuel is compared with that of a homogeneous reactor.

THEORY

It is assumed that all mixing processes are so fast that they occupy a negligible volume so that the volume requirements can be calculated from the chemical reaction rate. This is assumed to be given by the following equation[3]

$$\Omega = k' p^2 T^{-3/2} C_F C_O \exp(-E/RT) \qquad \ldots.[1]$$

where Ω = local heat release per unit volume, k' = collision frequency constant, T, p = local temperature and pressure, C_F, C_O = local concentration of fuel and oxygen, E = activation constant, and R = the gas constant.

General assumptions

(*1*) The system works at constant pressure

(*2*) The specific heat of all the gases and fuel vapour per unit mass is 0·27 before and after reaction

(*3*) Weight concentrations may be used

(*4*) Net calorific value of the fuel (kerosine) = 10^4 C.H.U./lb

(*5*) $E/R = 21\,000$°K

(*6*) Air to fuel ratio with 20 per cent excess air = 17 : 1 by weight

(*7*) Inlet air and fuel temperature = 0°C

(*8*) Required final combustion efficiency = 99 per cent

(*9*) Air is introduced at six points along the reactor giving six zones

(*10*) The air, fuel and hot products are perfectly and instantaneously mixed at the beginning of each zone

(*11*) Hot gases are recirculated from the end of Zone 6 to Zone 1

(*12*) No heat lost through the reactor wall

(*13*) Dissociation is neglected.

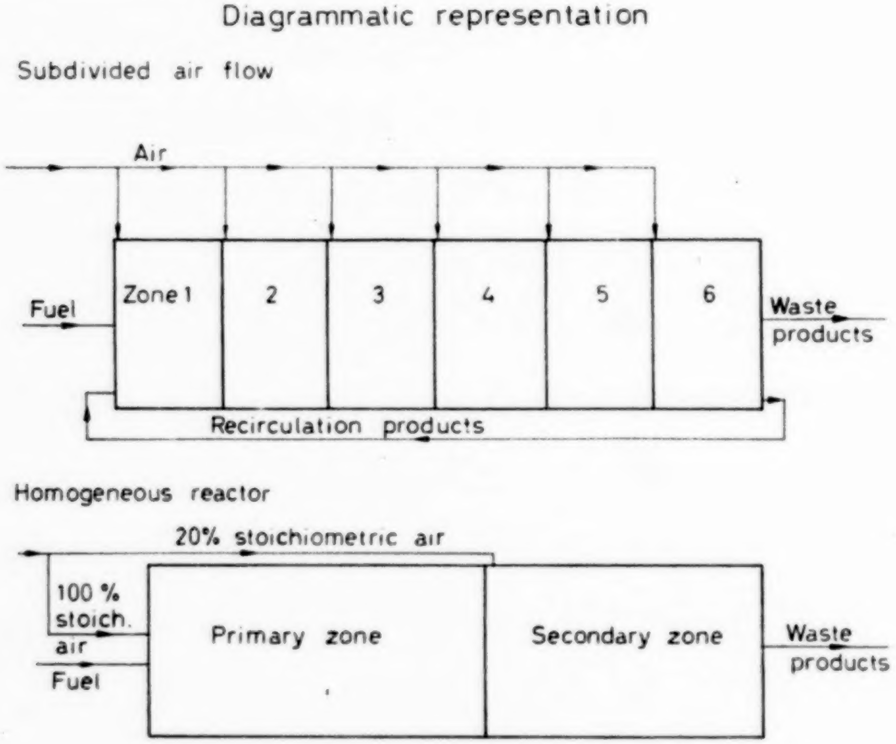
Diagrammatic representation
Subdivided air flow
Air
Fuel
Zone 1
2
3
4
5
6
Waste products
Recirculation products
Homogeneous reactor
20% stoichiometric air
100 % stoich. air
Fuel
Primary zone
Secondary zone
Waste products

Figure 1

With these assumptions we can modify equation 1 so that

$$\Omega = kT^{-3/2}\,\{w_F \,.\, w_A/(w_T)^2\}\,\{\exp(-E/RT)\} \times 10^{12} \qquad \ldots.[2]$$

where w_F = weight of fuel, w_A = weight of air (proportional to weight of oxygen), w_T = total weight, and $k \times 10^{12}$ = a new constant, all at any point. All calculations have been based on an injection rate of 1 lb of fuel per hour.

Calculation of conditions within the zones for three different variations of the reactor

Case 1—

(*a*) 20 per cent of the stoichiometric air is added to each zone

(*b*) Recirculation to Zone 1 = 80 per cent of the total mixture in Zone 1

(*c*) New air is added to the beginning of Zones 2, 3 and 4 as soon as three quarters of the air entering the previous zone has been burnt and to

Zones 5 and 6 when approximately half the fuel from the previous zone has been burnt.

By means of heat and mass balances in stages along the reactor w_A, w_F, w_T and the temperature were calculated for the beginning and end of each zone. For still greater accuracy in the volume determinations these values were also calculated when half the fuel burning in each zone had done so.

Thus w_A, w_F, w_T, $T^{-3/2}$ and $\exp(-E/RT)$ are known at the positions mentioned and the reaction rate can therefore be calculated at these points.

Case 2—The recirculation rate was kept the same as for Case 1 but since some air is being recirculated with the hot products only 10 per cent of the stoichiometric air was added to Zone 1 and 30 per cent was added to Zone 6 when the fuel concentration had fallen to a low value. In this case instead of adding the new air in an arbitrary manner as in Case 1 a plot of Ω against weight of fuel burnt was drawn up for Zone 1 and the new air added when the reaction rate began to fall away rapidly, the process then being repeated for Zone 2 and so on for the subsequent zones. The reaction rate is thus known for the desired positions in each zone.

Case 3—As in Case 2, 10 per cent of the stoichiometric air is added to Zone 1 but now the recirculation products are reduced to 80 per cent of the total mixture in Zone 1 and, instead of adding 30 per cent stoichiometric air to Zone 6, 25 per cent was added to Zones 5 and 6. The fresh air was added to Zones 2, 3, 4 and 5 when three quarters of the air in the previous zone had been burnt (shown to be reasonable from results from Case 2) and to Zone 6 when only 0·05 lb of fuel remained. Calculations were carried out as for Case 1.

Homogeneous reactor—In the primary zone incoming material is instantaneously mixed with four times its own weight of hot combustion products. In this zone 80 per cent of the fuel is burnt at a high reaction rate. The remainder passes into the secondary zone in which burning is completed at a lower average combustion rate.

Two variations were studied: (*a*) all the mixture went into the primary zone; and (*b*) only the stoichiometric mixture entered the primary zone, the 20 per cent excess air being added at the beginning of the secondary zone.

The reaction rate for the primary zone was calculated at four fifths of the adiabatic combustion temperature rise for the incoming material, the concentrations being found from the weights of incoming fuel and air (+ any air in the combustion products) and from the total weight which was five times the weight of incoming material. Calculations for the secondary zone were carried out in a similar manner to those for a zone in Case 1, intermediate values along this zone being calculated for greater accuracy in the volume calculations.

The results obtained are set out in *Tables 1, 2* and *3*.

Calculation of zone volumes

$$\text{Volume of a zone} = w_F \times 10\,000 \times (\overline{1/\Omega}) \qquad \ldots.[3]$$

where w_F = weight of fuel burnt in the zone. It was assumed that $(1/\Omega)$ varied linearly with w_F from the beginning of the zone to the point where half the fuel is burnt in the zone, and from there to the end of the zone.

$$\therefore \overline{\left(\frac{1}{\Omega}\right)} = \frac{1}{4}\left\{\frac{1}{\Omega_0} + \frac{2}{\Omega_{1/2}} + \frac{1}{\Omega_1}\right\} \qquad \ldots.[4]$$

Table 1. Results

	Case 1			Case 2			Case 3		
Zone No.	*Wt fuel burnt lb*	$\left(\frac{1}{\Omega}\right)\times k$ $\frac{C.H.U.}{ft^3}$	*Volume* $\times k$ ft^3	*Wt fuel burnt lb*	$\left(\frac{1}{\Omega}\right)\times k$ $\frac{C.H.U.}{ft^3}$	*Volume* $\times k$ ft^3	*Wt fuel burnt lb*	$\left(\frac{1}{\Omega}\right)\times k$ $\frac{C.H.U.}{ft^3}$	*Volume* $\times k$ ft^3
1	0·2775	0·257	714	0·2055	0·203	417	0·1554	0·1864	290
2	0·22	0·318	700	0·1918	0·256	491	0·189	0·2193	414
3	0·2047	0·565	1157	0·1858	0·366	680	0·2342	0·31	727
4	0·15	0·961	1440	0·192	0·592	1139	0·2458	0·662	1628
5	0·08	1·877	1500	0·16	1·7	2720	0·1256	1·708	2140
6	0·0578		4060	0·531		3830	0·04		2800
			9571			9277			8000

Table 2. Homogeneous reactor

Zone	*Case (a)* *Vol.* $\times k$	*Case (b)* *Vol.* $\times k$
Primary	10 500	4 320
Secondary	4 080	4 080
Total	14 580	8 400

Table 3

System	*Reactor*			*Homogeneous reactor*	
	Case 1	*Case 2*	*Case 3*	*Case (a)*	*Case (b)*
Volume $\times k$ ft^3	9600	9300	8000	14600	8400

where Ω_0 = reaction rate at the beginning of a zone, $\Omega_{1/2}$ = reaction rate when half the fuel to burn in the zone has done so, and Ω_1 = reaction rate at the end of the zone.

Volume of Zone 6—Since Ω falls to a very low value, expression 4 is now no longer accurate. However, in Zone 6, Ω varies linearly with weight of fuel burnt in the zone was derived.

$$\therefore \text{Volume} = \{10^4 w_F/(\Omega_0 - \Omega_1)\}\,\{\ln(\Omega_0/\Omega_1)\} \qquad \ldots.[5]$$

Homogeneous reactor—

Zone 1: A single reaction rate occurs.

$$\therefore \text{Volume} = 0{\cdot}8 \times 10^4/\Omega$$

Zone 2: As the weight of fuel unburnt varies from 0·19 to 0·01 lb it is inaccurate to take mean values of $1/\Omega$. A graph of $1/\Omega$ versus fraction fuel burnt in the zone was derived.

$$\therefore \text{Volume of a zone} = 10^4 \times 0{\cdot}19 \int_0^1 (1/\Omega)\,\mathrm{dF}$$

and using Simpson's rule to calculate the area under the curve

$$\text{Volume} = 10^4 \times 0{\cdot}19 \times \text{area under the curve}$$

Case 3 is superior to Cases 1 and 2 chiefly because of the higher concentrations of fuel in the furnace zones because less dilution has occurred through the addition of a smaller amount of recirculation products. Case (b) of the homogeneous reactor is superior to Case (a) because of its higher reaction rate in the primary zone due to higher temperature and fuel concentration which more than offsets the effect of reduced air concentration.

CONCLUSIONS

Despite the assumptions made, the method described appears adequate for comparing combustion systems under the idealized conditions. The process of splitting the air streams provides a combustion system which compares favourably with the homogeneous reactor of Case (b) and is superior to one of Case (a). The volume in Case 3 is 6 per cent less than that of the better homogeneous reactor and it is most likely that a better example with slightly different recirculation rate, air distribution and positions of air introduction exists. The reason that this system can compare with the homogeneous reactor is that in earlier zones of the furnace the fuel is burnt at a very high rate due to the high temperatures and fuel concentrations caused by having a smaller overall total weight in the zones than in the homogeneous reactor primary zone. A system of this nature will thus burn the first 80 per cent of the fuel more rapidly than a homogeneous reactor but will burn the last 19 per cent of the fuel more slowly because of dilution by the initially added combustion products reducing the fuel concentration as compared with the homogeneous reactor secondary zone. The overall effect is to give a system comparable with the homogeneous reactor and possibly in some cases better, a further advantage being the reasonably small proportion of recirculation products. The problem now would be to mix in the air and hot products instantaneously so as not to waste reactor volume through a slow mixing process.

M. W. THRING
E. G. MASDIN

*Department of Fuel Technology
and Chemical Engineering,
University of Sheffield*

(*Received December 1958*)

REFERENCES

[1] LONGWELL, J. P. and WEISS, M. A. *Industr. Engng Chem.* (*Industr.*) 47 (2) (1955) 1634

[2] BRAGG, S. L. *Aeronaut. Res. Coun. Pap. No. 16170* (*CF272*) (29 September 1953)

[3] BRAGG, S. L. and HOLLIDAY, J. B. *Selected Combustion Problems*, Vol. II, p 270. AGARD; Butterworths: London, 1956

[4] MULLINS, B. P. *Combustion Researches and Reviews 1955*, p 87. Butterworths: London

[5] HERBERT, M. V. *Combustion Researches and Reviews 1957*, p 76. Butterworths: London

[6] SPALDING, D. B. 'Some fundamentals of combustion'. *Gas Turbine Series No. 2*, Chapter 5. Butterworths: London, 1955

On Inductive Break Sparks of High Incendive Power

It is generally accepted that the minimum igniting energy of inductive break sparks is much greater than that of capacitive sparkover discharges for the same explosive mixtures.

Recent work at the Mining Research Establishment has shown that this is only true for existing modes of circuit break between electrodes which are large with respect to the critical size of self-propagating flame kernel, as is the case in the standard breakflash apparatus used in intrinsic safety work[1].

However, when the inductive break spark is produced between electrodes which are small with respect to the critical flame kernel, the minimum igniting energy is drastically reduced and there is evidence that it becomes of the same order as that obtained for capacitive discharges. For an 8·3 per cent methane–air mixture an igniting energy of 0·3 mJ was obtained with thin wire break sparks in an inductive circuit. This is close to B. Lewis and G. von Elbe's value for capacitive sparks[2]. The work was carried out in a cylindrical chamber with an 8·3 per cent methane–air mixture. Thin wires 0·001 in. in diameter and less, were made to carry the current to be interrupted, in a simple series circuit including 24 V battery supply, inductance and resistance. The speed of wire break was made to be about 8 ft/s. It was found that the break must be made to occur about 1 cm or more away from the clamping posts, in order to maintain maximum incendive power. *Table 1* shows comparative results of minimum igniting currents for a 95 mH inductance.

Table 1

Mode of break	*Standard break-flash*	*Stainless steel wire 0·008 in. dia.*	*Stainless steel wire 0·005 in. dia.*	*Stainless steel wire 0·002 in. dia.*	*Stainless steel wire 0·001 in. dia.*	*Platinum wire 0·001 in. dia.*	*Tungsten wire 0·001 in. dia.*
Minimum igniting current mA	185	130	110	100	93	95	82

Table 2

Inductance	*18·5 mH*	*108 mH*	*1·31 H*	*10·8 H*
Minimum igniting current mA	185	78	30	17

Table 2 shows a range of minimum igniting currents versus inductance for 0·001 in. diameter tungsten wire. Some work has been done with separating electrodes and a minimum igniting current of 120 mA was obtained with a 95 mH inductance, and 0·005 in. diameter steel wires separating at high speeds. There is also evidence that the statistical spread of ignition with thin wire breaks is reduced as compared with the larger separating electrodes. This work will be more fully reported subsequently.

The letter is published by permission of Dr W. Idris Jones, Director General of Research in the Scientific Department of the National Coal Board.

I. BERZ

Mining Research Establishment,
Worton Hall,
Isleworth, Middlesex

(Received February 1959)

REFERENCES

[1] *S.M.R.E. Res. Rep. No. 33* November 1951
[2] LEWIS, B. and VON ELBE, G. *J. chem. Phys.* 15 (1947) 798

Hydrocarbon Products from Rich Hydrocarbon Flames

P. H. KYDD

A new type of burner and gas chromatographic analysis of the products of combustion have been used to investigate the formation and decay of non-equilibrium concentrations of hydrocarbon products in the burnt gases of rich hydrocarbon flames. The evidence indicates that excess concentrations of hydrocarbons arise because those fuel molecules which react first in the flame front are oxidized almost completely, consuming all the available oxygen in the process, and leaving a non-equilibrium fraction of the fuel either unchanged or converted to other hydrocarbons and, in some cases, carbon. These products are then attacked at a much lower rate by the oxidation products of the burnt fuel, largely water vapour, and equilibrium is approached. Relative rates of primary oxidation of hydrogen, methane, ethane and ethylene have been determined, and the rates of disappearance of methane and acetylene, the major unburnt products, have been measured.

ONE of the striking features of fuel rich hydrocarbon flames is the presence in the burnt gases of unburnt hydrocarbons in concentrations much larger than those calculated for thermodynamic equilibrium. These products, largely methane, acetylene and ethylene, are found in greatest excess nearest the combustion zone of the flame, and their concentration decays toward equilibrium more or less rapidly in the high temperature gas stream above the flame front.

The rate of this decay is such that one can measure it by sampling and analysing the hot gas stream at various points above the combustion zone. Furthermore, by varying the conditions in the flame, one can infer certain things about the mechanism of formation of these compounds as well as that of their consumption.

EXPERIMENTAL DETAILS

The apparatus employed here is a further development of the porous plate burner[1, 2] used extensively in this laboratory and elsewhere. These burners are useful in that the flame front is quite flat and is fixed in space by the position of the porous plate. In addition, the temperature in the burnt gases may be varied independently of the unburnt gas composition by varying the mass flow rate of unburnt mixture through the plate. Both these characteristics are due to the thermal gradient existing between the flame front and the porous surface, which can be very large. A similar gradient between the hot gases and a porous quenching plate has been used in the present experiments to quench the reaction products for analysis.

This burner is shown in *Figure 1*. The unburnt mixture enters the bottom of the assembly and passes through the first porous plate of sintered copper shot, which is cooled by conduction to a water jacket which surrounds it. As the gas emerges from the plate it burns in a flat, one-dimensional flame front. The distance between this flame front and the second porous plate can be adjusted by placing washers under the latter, which is constructed and cooled similarly to the burner plate. As the gases approach it, they are cooled very rapidly and largely homogeneously. They leave this plate at very nearly the temperature of the cooling water, 100°C, and pass out through the top of the assembly. Plates of 1 in. and 1$\frac{3}{4}$ in. diameter have been used, and the results appear to be independent of burner area. In all cases burner and sample plates of the same diameter were used in an effort to keep the flow one dimensional. The visible flame front is usually very nearly the same area as the burner plate, except for very rich mixtures which give a somewhat smaller flame.

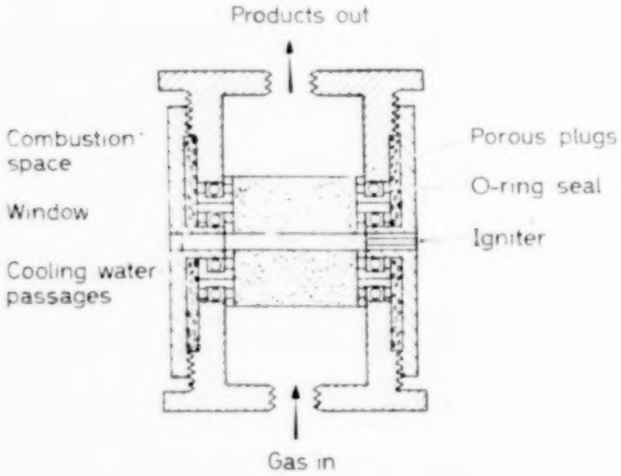
Products out
Combustion space
Window
Cooling water passages
Porous plugs
O-ring seal
Igniter
Gas in

Figure 1. Opposed porous plate burner

This assembly is connected to a Perkin–Elmer Vapor Fractometer, shown in *Figure 2* with the remainder of the gas handling equipment. The unburnt gas composition and flow rate are fixed by critical flow orifices calibrated with the wet test meter. CP hydrocarbons and regular grade oxygen, hydrogen and carbon monoxide were used without purification. After leaving the burner the burnt gases can be sampled direct at 100°C or dried thoroughly first in an ice cooled trap followed by a drierite tube. The flow rate of the dry products is measured with the wet test meter to permit the calculation of mass balances and comparisons between different mixtures.

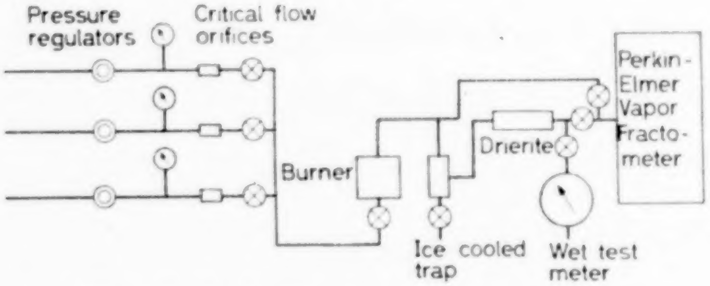
Pressure regulators
Critical flow orifices
Burner
Ice cooled trap
Drierite
Wet test meter
Perkin-Elmer Vapor Fractometer

Figure 2. Gas handling and analysis arrangement

Only a few runs were made with direct sampling. Although the water condensed from methane–oxygen flame products had a pungent smell and contained a small amount of a yellow solid, no high molecular weight products were detected by the Vapor Fractometer. Apparently the materials observed are present in too small an amount to be detected (0·1 per cent or less). Consequently these products were considered to be of minor importance in the present experiments and attention was focused on the lighter products, hydrogen, oxygen, water vapour, carbon monoxide, carbon dioxide, methane, ethane, ethylene and acetylene.

With the exception of water these gases are separated satisfactorily by a 9 ft column of 28–200 mesh Fischer silica gel operated at 100°C. The gases are determined quantitatively by comparing peak heights obtained in a flame product analysis with the heights of corresponding peaks produced by mixtures of the same gases at known partial pressures. Reproducibility from run to run is better than 5 per cent; however, mass balances, computed from the known input flow rates, the product flow rates, and the composition of the products, are consistently low, the deficit being as much as 10 per cent for carbon and 5 per cent for hydrogen and oxygen.

Water is determined by condensing it in the ice cooled trap and measuring the volume of liquid collected in a known time. These results are somewhat less reproducible than those from the Vapor Fractometer, but are estimated to be accurate to 5 per cent.

RESULTS

From the results of these experiments it appears that the excess hydrocarbon concentrations found in the burnt gas arise from the fact that, when a molecule of hydrocarbon fuel is attacked by oxygen, the products of the initial attack are much more easily oxidized than the fuel itself. Thus, in a rich flame, the oxygen is consumed by those molecules of fuel which are attacked first, leading to excess amounts of carbon dioxide and/or water vapour and more or less unburnt fuel, depending on the unburnt mixture ratio.

At the same time that some of the fuel is being oxidized in the flame front the remainder of the fuel is reacting to give an equilibrium assortment of hydrocarbons. This process is initially very rapid, but after the oxidation zone it almost stops, perhaps because it requires oxygen or an oxygen-containing radical.

In the burnt gas above the reaction zone the water gas equilibrium is approached by hydrogen, carbon monoxide, water vapour and carbon dioxide, and the excess hydrocarbon concentrations are oxidized to carbon monoxide and hydrogen by water vapour.

FORMATION OF EXCESS HYDROCARBONS

Most of the experiments reported here were done with flames of equal amounts of methane and oxygen or a carbon to oxygen atom ratio of 0·5 (mole ratio 1·0). In this mixture there is ample oxygen to attack all the fuel, and equilibrium calculations predict vanishingly small amounts of hydrocarbons in the burnt gases. However, quite substantial amounts are found, both with this mixture and with leaner ones. The results obtained in experiments in which increasing amounts of oxygen were added to a constant flow of 9·5 cm/s of methane are plotted in *Figure 3* for distances between burner and quenching plate of 3·0 and 3·5 mm. Here the carbon recovered as hydrocarbons is plotted against the C/O ratio in the unburnt gas, and, except for the results at the leanest compositions, the yields fall on straight lines that extrapolate to zero at C/O = 0·42. The dashed line in *Figure 3* is the yield of carbon as hydrocarbons one would expect if the available oxygen could only consume 0·84 mole of methane per mole of oxygen in the initial combustion, producing products in a higher oxidation state than equilibrium, and leaving the balance of the fuel to appear unchanged or partially converted to other hydrocarbons. Of course, these hydrocarbons are then attacked by the combustion products, so that in the experiments one cannot recover all of the unburnt products; however, the fact that the experimental results are linear and approach the dashed curve as the sample is taken closer to the flame indicate that the amount of fuel which can be attacked by a given amount of oxygen in the combustion wave is kinetically limited and that the remainder of the fuel is not oxidized until later. The upward curvature demonstrated by the points for the leanest composition is the type of behaviour which would be expected throughout the curve if the available oxygen reacted with increasing amounts of methane as the latter becomes more plentiful, rather than being completely consumed by a fixed amount of methane.

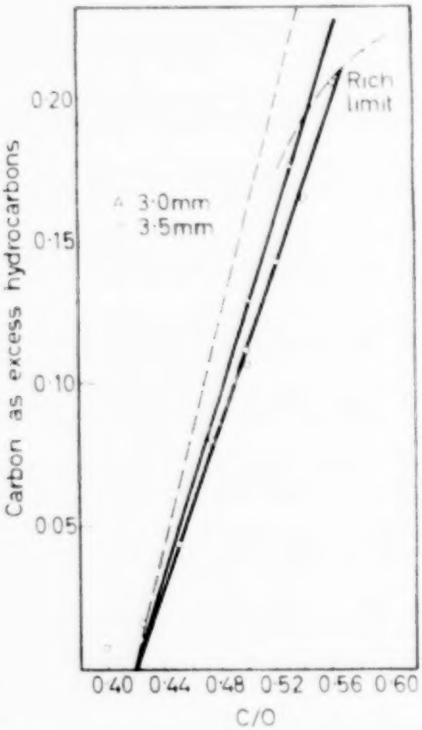

Figure 3. Percentage amount of carbon recovered as hydrocarbons versus C/O ratio in unburnt gas. Solid lines, experimental results at 3·0 and 3·5 mm. Dashed line, calculated amount assuming 1 mole of oxygen completely consumed by 0·84 mole of methane

This conclusion is strengthened by the results of an experiment in which a flame of the above mixture and flow rate was held above a screen fixed

1 cm above the burner surface. This allows one to investigate the preheating zone of the flame. Temperature measurements with a fine thermocouple demonstrated the expected exponential temperature rise in the gas approaching the flame front. Samples were taken with a quartz probe at 1·7 and 1·15 mm below the screen where the temperatures were 530 and 800° K respectively. When analysed on the Vapor Fractometer the first gave a very small amount of hydrogen and approximately 0·1 per cent of carbon dioxide, the second a larger amount of hydrogen and roughly 0·3 per cent of carbon monoxide and 0·3 per cent of carbon dioxide. No hydrocarbons other than methane were observed in either case.

This indicates that very little, if any, pyrolysis of the fuel occurs prior to its oxidation, and that, when this oxidation begins, it proceeds chiefly to the final products despite the large amount of fuel present.

When hydrogen or some other combustible product is added to rich hydrocarbon flames, it will compete for the limited supply of oxygen, increasing the amount of the original fuel in the burnt gas. This increase will be related to the relative rates of oxidation of the two fuels. This is seen qualitatively in the results of a series of experiments in which hydrogen, a mixture of 60 per cent hydrogen and 40 per cent carbon monoxide, and pure carbon monoxide were added to a flame of methane and oxygen with C/O = 0·50. In *Figure 4* the yield of acetylene, which is typical of the other hydrocarbon products, obtained 5·9 mm above the flame is plotted versus the mole ratio of additive to fuel. The acetylene yield increases linearly and rapidly with the addition of hydrogen to the methane–oxygen mixture, and at the same rate when the hydrogen–carbon monoxide mixture

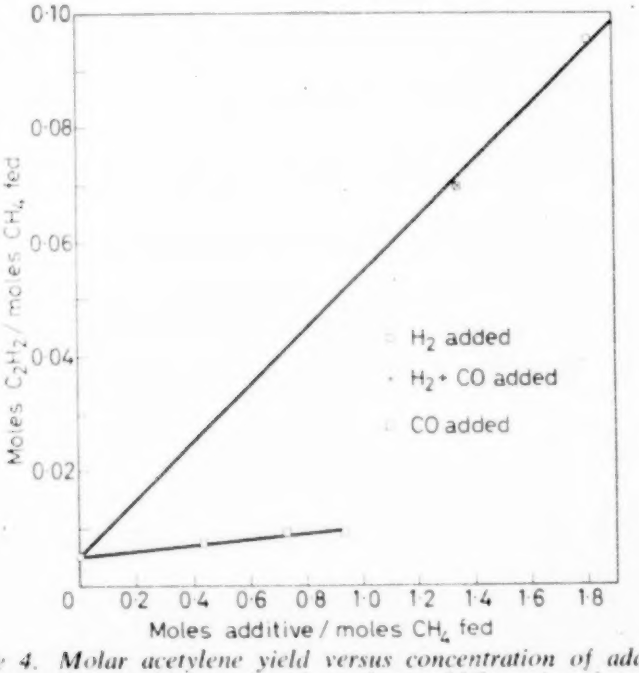

Figure 4. Molar acetylene yield versus concentration of additive. Initial conditions 14·0 cm/s of methane, 14·0 cm/s of oxygen, (C/O = 0·5), samples taken 5·9 mm above flame

is added. When carbon monoxide alone is added, however, only a slight change in the acetylene yield is observed, which can be accounted for by the increased velocity of the gas stream due to the presence of an inert gas. This agrees well with the common observation that hydrogen and mixtures of carbon monoxide with large amounts of hydrogen burn at a similar rate, while carbon monoxide by itself burns at a very much lower rate.

In another series of experiments a single additive was used with a variety of fuels to demonstrate the same effect and obtain a semi-quantitative measure of their relative rates of oxygen consumption. Hydrogen was added to mixtures of methane, ethane and ethylene with oxygen. Flow rates of 9·5 cm/s of methane and 4·75 cm/s of ethane and ethylene were used with 9·5 cm/s of oxygen in all cases, and the products were sampled at a height of 3·5 mm.

Again the amount of carbon recovered as hydrocarbons increases linearly when hydrogen is added, that is, the addition of hydrogen produces the same result as the addition of more fuel. Quantitatively, however, its effect is less because of its lower overall rate of consumption of oxygen relative to the hydrocarbon fuels. The increase in hydrocarbon yield in moles carbon/mole of carbon as fuel due to the addition of one mole of hydrogen/mole of carbon as fuel is given in *Table 1* for the starting mixtures listed.

Table 1

Mixture	*Increase in yield*	$R_{\text{fuel}/\text{H}_2}$
CH_4+O_2	0·29	2·4
$\frac{1}{2}C_2H_6+O_2$	0·16	5·2
$\frac{1}{2}(C_2H_6+H_2)+O_2$	0·16	5·2
$\frac{1}{2}C_2H_4+O_2$	0·10	9·0
$\frac{1}{2}(C_2H_4+2H_2)+O_2$	0·11	8·1

Since the increase in yield (ΔC) is proportional to the overall rate of oxygen consumption by hydrogen, and the remainder of the carbon ($1-\Delta C$) is proportional to the overall rate of oxygen consumption by the fuel, the ratio $R_{\text{fuel}/\text{H}_2}=(1-\Delta C)/\Delta C$ is proportional to the relative overall rates and is given in the table. The increase in reactivity from hydrogen–methane–ethane–ethylene is marked and in the order expected, and the independence of carbon to hydrogen ratio demonstrated.

Experiments were performed at different burner–sample plug spacings with the three hydrocarbons to show differences in the cracking patterns of that part of the fuel passing through the flame unburnt. The amount of carbon recovered as hydrocarbon from a flame of $\frac{1}{2}C_2H_6+O_2$ is about half that recovered from CH_4+O_2 at all sampling positions while $\frac{1}{2}C_2H_4+O_2$ yields no hydrocarbons at all except at very close sampling distances. The major hydrocarbon products in all cases are methane and acetylene. Methane flames produce more methane than acetylene, whereas for ethane and ethylene flames the reverse is true. As hydrogen is added to ethane and ethylene to bring the unburnt mixtures to the same C/H/O ratio as that of CH_4+O_2 the amounts of carbon recovered approach that from methane; however, there is still more acetylene than methane. Ethylene is produced in small and equal amounts by all three systems, and ethane in extremely small amounts at very close plate separations.

DESTRUCTION OF EXCESS HYDROCARBONS

Temperature measurements were performed on the burnt gases between the two porous plates to make possible equilibrium and kinetic calculations on the fate of the hydrocarbons which emerge from the combustion zone. This was done by the sodium line reversal method. The results are not very precise for two reasons. Inequalities in the burner surface, plus the random error of measurement, resulted in a total spread in measured temperatures for a given set of conditions of 60°. Secondly, with the quenching plate in place, there is a fairly strong temperature gradient in the flame, the bottom, immediately above the combustion zone, being as much as 200° hotter than the gas a similar distance from the quenching plate. As the gas approaches the quenching plate still more closely, there is a sudden drastic drop in temperature, the sodium light being extinguished. The temperatures quoted hereafter are mean values measured at the centre of the burner and equidistant from both burner and quenching plate.

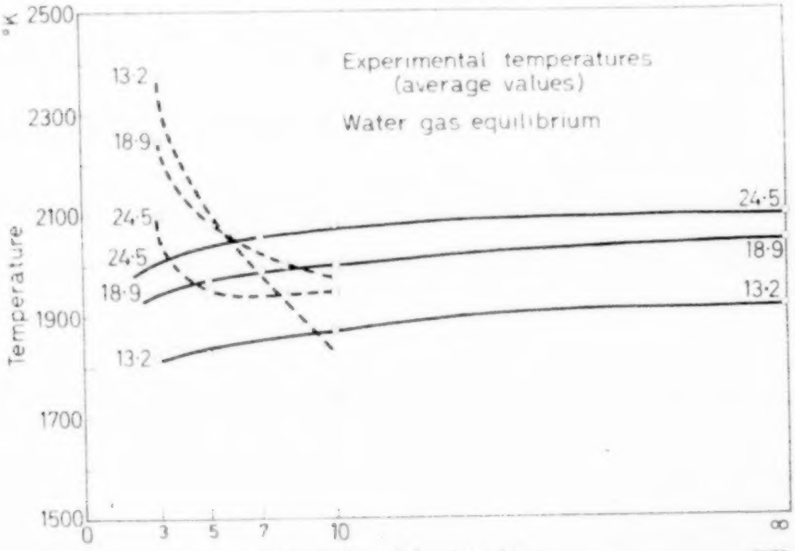

Figure 5. Solid lines are temperatures measured at various plate spacings for flow rates of 13·2, 18·9 and 24·5 cm/s methane–oxygen mixture. Dotted lines are temperatures calculated from product analysis and water gas equilibrium constant

These measurements were carried out on flames of equimolar mixtures of methane and oxygen at unburnt gas flow velocities of 13·2, 18·9 and 24·5 cm/s. Measurements were made with the quenching plate at distances of 3 to 10 mm, as in the sampling experiments, and also with it removed.

The temperature data are presented in *Figure 5*. The adiabatic flame temperature for this mixture[3] is 2650°K, which may be compared with the temperatures measured at infinite plate separation. This demonstrates the effect of reducing the flow rate of the mixture below the normal burning velocity of 122 cm/s, which is allowed by the porous burner. The measured temperatures are compared with temperatures calculated from the concentrations of carbon monoxide, carbon dioxide, hydrogen and water vapour measured under the same conditions and the water gas equilibrium constant. Initially these 'water gas' temperatures are substantially above the measured values, i.e. there is more water vapour or carbon monoxide or less carbon dioxide or hydrogen present than there should be. This is more pronounced with the lowest temperature flame and less so as the temperature is raised. Also the rate of approach to equilibrium is greatest for the highest temperature as one would expect. The fact that the temperatures which the calculated results approach at large plate spacings are uniformly below the measured values may be due to the temperature gradient as the flame gases approach the sample plug, that is, the water gas is equilibrated at the lowest temperature at which the reaction rate is still rapid.

The equilibrium concentrations of all species present in the flame were calculated for a temperature of 2 000° K, pressure of 1 atm, and an initial mixture of equal parts methane and oxygen, i.e. $C/H/O = 1/4/2$. The results obtained are given in *Table 2*.

Table 2

Component	*Partial pressure*	*Component*	*Partial pressure*
H_2	0·376	CH_4	$2{\cdot}3\times10^{-9}$
CO	0·291	C_2H_2	$5{\cdot}3\times10^{-13}$
H_2O	0·291	C_2H_4	$1{\cdot}4\times10^{-15}$
CO_2	0·042	C_2H_6	$7{\cdot}7\times10^{-19}$
O_2	5×10^{-8}		

The most striking fact which emerges from a comparison of this calculated composition and that actually found is the presence of hydrocarbon products at concentrations far above equilibrium.

On the Vapor Fractometer records there was a peak which could have been due to oxygen, nitrogen or argon. This was a constant amount, usually somewhat less than 1 per cent of the dry products. At very close sampling distances the oxygen and fuel concentrations started to rise very rapidly as the flame was quenched strongly. It is very likely that both these observations have no bearing on the products of the flame itself. The rise in oxygen and fuel concentration as the flame was quenched is probably due to unburnt gas eddying around the edge of the flame and entering the sample plug without reacting at all. The flame was observed to shrink in size and flutter slightly under those conditions. The constant apparent oxygen concentration under other conditions is probably due to impurities in the unburnt gases. 1 per cent of nitrogen was found in the CP methane used and 0·5 per cent ($N_2 + A$) in the oxygen, which is nearly enough to explain the observed value. The remainder may well be an edge effect and consequently it has been assumed that oxygen is essentially absent in these flames.

In *Figure 6* the experimentally measured concentrations of the major constituents are plotted as a function of distance above the flame and compared with the calculated equilibrium values. It can be seen that initially the products are formed out of equilibrium and then relax toward it. The chief reaction is the combination of water vapour with excess hydrocarbons to give hydrogen and carbon monoxide with the carbon dioxide concentration essentially constant. The same holds true for the mixtures $C_2H_6 + H_2 + 2O_2$ and $C_2H_4 + 2H_2 + 2O_2$.

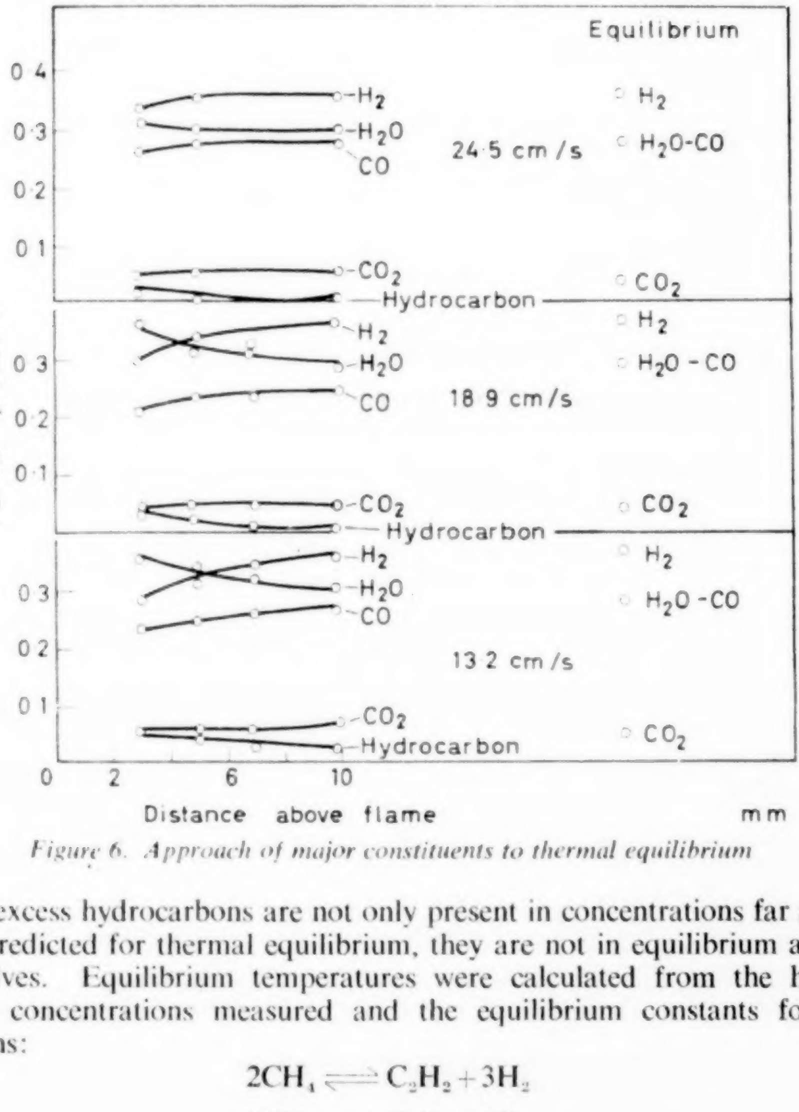

Figure 6. Approach of major constituents to thermal equilibrium

The excess hydrocarbons are not only present in concentrations far above those predicted for thermal equilibrium, they are not in equilibrium among themselves. Equilibrium temperatures were calculated from the hydrocarbon concentrations measured and the equilibrium constants for the reactions:

$$2CH_4 \rightleftharpoons C_2H_2 + 3H_2$$

$$2CH_4 \rightleftharpoons C_2H_4 + 2H_2$$

$$2CH_4 \rightleftharpoons C_2H_6 + H_2$$

For acetylene and ethylene the temperatures calculated are in the neighbourhood of 1 500° K with a slight upward tendency toward the measured flame temperature as the distance above the flame increases.

No significant differences were observed between the results for flames of increasing unburnt flow rate and thus burnt gas temperature, or between flames of methane, ethane and ethylene. Thus in the products of all these flames there is relatively too much methane or too little of the endothermic gases ethylene and acetylene by a very large factor. The concentrations of ethane found are somewhat closer to equilibrium. In methane flames there was too much ethane relative to methane by a factor of 5 for the lowest temperature flame, 2 for the medium temperature, and the ratio was approximately equilibrium at the highest temperature.

It thus appears that the existence and disappearance of the excess hydrocarbons is controlled by chemical kinetics rather than by equilibrium considerations. The fact that a large part of the unburnt methane or other fuel is converted to acetylene with extreme rapidity in the flame front, but stops far short of an equilibrium ratio and never approaches it, indicates that the first very rapid reaction requires an intermediate not present later on, perhaps oxygen or an oxygen-containing radical.

On the assumption that the processes responsible for the disappearance of the major hydrocarbon constituents methane and acetylene are

$$CH_4 + H_2O \longrightarrow CO + 3H_2$$

and

$$C_2H_2 + 2H_2O \longrightarrow 2CO + 3H_2$$

and that they proceed at about the same rate, which appears to be so, the overall reaction is

$$CH_4 + C_2H_2 + 3H_2O \longrightarrow 3CO + 6H_2$$

or

$$-3\Delta(C_2H_2 + CH_4) = -\Delta H_2O = \Delta CO = \tfrac{1}{2}\Delta H_2$$

where Δ stands for the change in concentration from one position above the flame to another. These changes are plotted for the methane–oxygen flames in *Figure 7*, and while the hydrogen and carbon monoxide are produced in the right ratio, and the change in water vapour is approximately three times the change in total hydrocarbon content, the latter is consistently about twice the former, i.e. material is being consumed without appearing elsewhere. However, since the data for ΔH_2, ΔCO and ΔH_2O involve measuring differences between large numbers which are comparable to the limits of error assigned to those numbers, the situation may not be as serious as it seems at first.

With regard to the changes in the concentrations of the hydrocarbons, which are more easily measured, kinetic plots have been constructed for their disappearance without regard to the mechanism of the reaction. That is, since the percentage change in the water concentration is moderate, 10 per cent over the course of the reaction, it has been regarded as constant and only the data for the hydrocarbons themselves plotted.

The disappearance of methane appears to be second order in CH_4. This is shown in *Figure 8* for the three flames for which temperatures were measured. The time scale was determined by computing the burnt gas velocity from the unburnt velocity, assuming a constant temperature in the burnt gas, and using the mole number change from unburnt to burnt gas determined in the analytical work. Then the interplate distances at which concentration measurements were made were divided by the gas velocity to give residence time at high temperature.

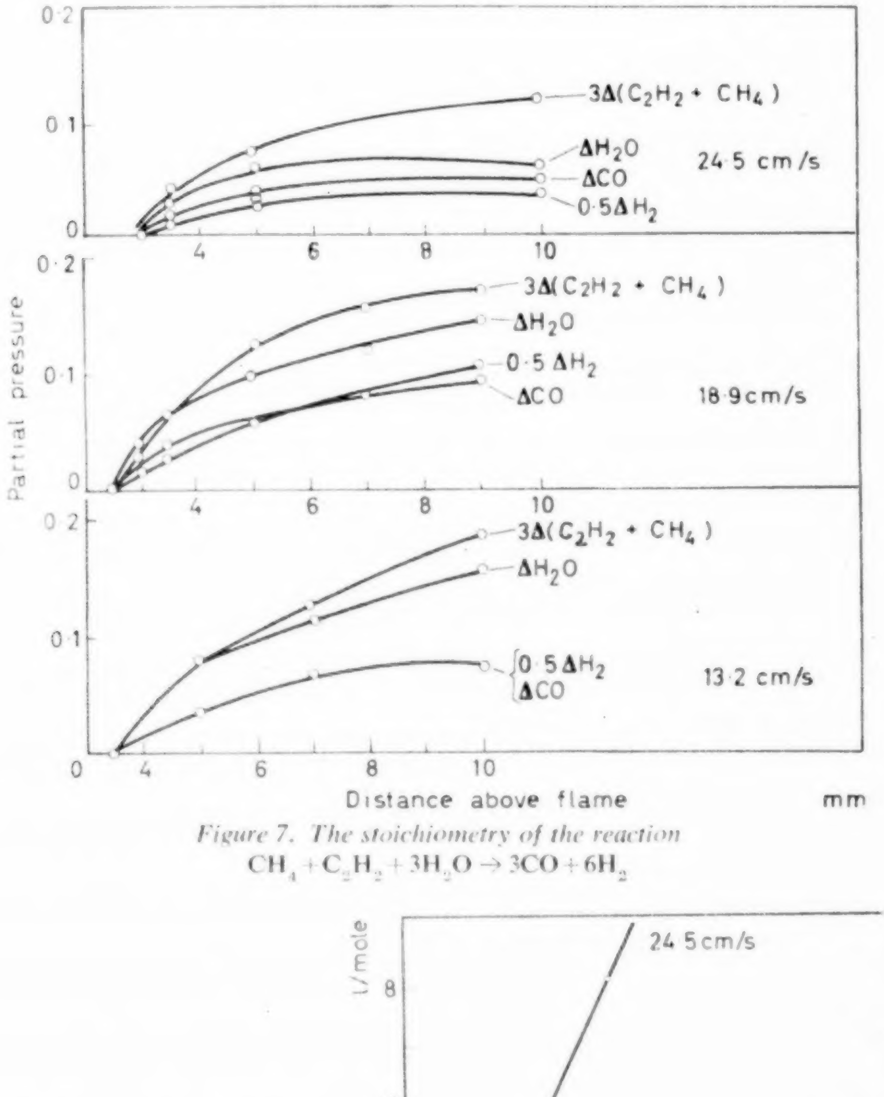

Figure 7. The stoichiometry of the reaction
$CH_4 + C_2H_2 + 3H_2O \rightarrow 3CO + 6H_2$

Figure 8. Second order kinetic plot for disappearance of methane

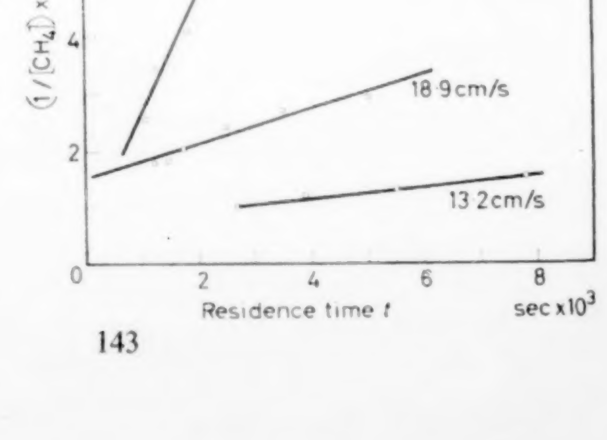

The disappearance of acetylene appears to be first order as shown in *Figure 9*, although some deviation is noted at the highest temperature where the concentrations are quite small. These results have been plotted

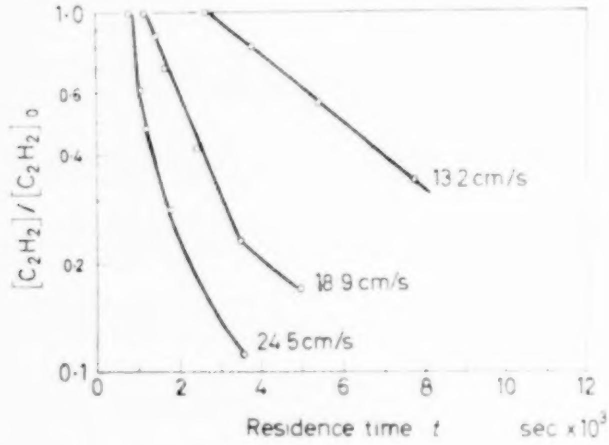

Figure 9. First order kinetic plot for disappearance of acetylene

as log K versus $1/T$ in *Figure 10* and activation energies of 86 kcal for acetylene and 107 kcal for methane determined. The complete rate expressions are:

$$-d[C_2H_2]/dt = 2{\cdot}5 \times 10^{12} [C_2H_2] \exp[-86\,000/RT] \text{ moles/l. sec}$$

and

$$-d[CH_4]/dt = 3 \times 10^{18} [CH_4]^2 \exp[-107\,000/RT] \text{ moles/l. sec}$$

These results may be compared with those of C. P. FENIMORE and

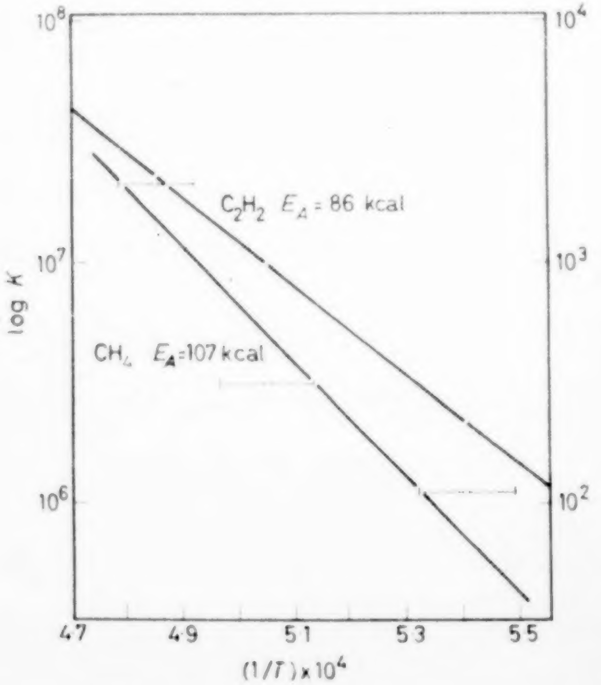

Figure 10. Arrhenius plot of kinetic data

G. W. JONES[4] in which both reactions were found to be first order with the following rate expressions:

$$-\mathrm{d}\ln[\mathrm{C_2H_2}]/\mathrm{d}t = 5\times10^{11}\,[\mathrm{CO_2/CO}]\exp[-76\,000/RT]$$

and

$$\mathrm{d}\ln[\mathrm{CH_4}]/\mathrm{d}t = 3\times10^{16}\,[\mathrm{CO_2/CO}]\exp[-121\,000/RT]$$

The reaction rates predicted by these expressions are almost exactly those found in the present experiments, and the differences in activation energy and choice of reaction order for methane are within the combined limits of experimental error.

In the absence of more detailed information it is difficult to speculate as to the mechanism of these processes. However, since the estimated bond energy of the C—H bond in acetylene[3] is 123 kcal, the same as that for the C≡C triple bond, and the activation energies determined here and by Fenimore and Jones are substantially less than this; it is evident that the mechanism of attack on C_2H_2 does not involve rupturing either of these bonds, but possibly addition to the triple bond followed by further reaction.

In the case of methane in which the estimated C—H bond energy is 103 kcal, direct rupture of one of the bonds is possible, followed by rapid reaction of the methyl radical produced.

The author wishes to express his appreciation to Mr Earl Marx who performed most of the experiments reported herein, and to Drs G. E. Moore, W. E. Kaskan and C. P. Fenimore, for helpful discussions.

G. E. Research Laboratory,
Schenectady, N.Y.

(*Received July 1958*)

REFERENCES

[1] BOTHA, J. P. and SPALDING, D. B. *Proc. Roy. Soc. A*, 1954, **225**, 71
[2] KASKAN, W. E. *Sixth Symposium (International) on Combustion*, p 134. Reinhold: New York, 1957
[3] LEWIS, B. and VON ELBE, G. *Combustion, Flames and Explosions of Gases*, p 416. Academic Press: New York, 1951
[4] FENIMORE, C. P. and JONES, G. W. *G. E. (N.Y.) Res. Lab. Rep. No. 57-RL-1858* (December 1957)
[5] COULSON, C. A. *Valence*, p 201. Clarendon Press: Oxford, 1952

Studies of Perchloryl Fluoride Flames[*]

R. M. LODWIG and J. L. MARGRAVE

Spectroscopic studies on flames of perchloryl fluoride mixtures with hydrogen, methane, ammonia and hydrogen sulphide are reported. The presence of bands attributable to ClO *in some spectra is the only unusual result obtained. Inflammability limits of perchloryl fluoride–natural gas–nitrogen were also determined, and the sources of error in these measurements are discussed briefly. Finally burning velocity data on some methane–perchloryl fluoride mixtures are given.*

PERCHLORYL fluoride was first discovered by A. ENGELBRECHT and H. ATZWANGER[1] in 1952. The preparation and many of the properties of this compound were described by A. ENGELBRECHT and H. ATZWANGER[2] and by G. BARTH-WEHRENALP[3].

In 1957 C. A. NEUGEBAUER and J. L. MARGRAVE[4] found the heat of formation of perchloryl fluoride to be only $-5{\cdot}12$ kcal/mole and not exothermic enough to make ClO_3F thermodynamically stable with respect to the elements. The very low heat of formation together with the stability of potential products in reactions in which perchloryl fluoride serves as an oxidant indicates that the heats of combustion reactions involving perchloryl fluoride should be quite high. The presence of F, Cl and O together in this molecule gives rise to many possibilities of unusual molecular species occurring in the flame gases.

SPECTROSCOPIC STUDIES OF FLAMES WITH METHANE, HYDROGEN, AMMONIA AND HYDROGEN SULPHIDE

Spectrographs and films

Spectroscopic studies were made on various flames involving perchloryl fluoride to determine the molecular species present in the flame gases. The spectral region from 1 850 Å to 7 400 Å was surveyed in emission. No previous work on spectra of flames involving perchloryl fluoride has been reported.

A Hilger quartz spectrograph, Model No. E484, was used in preliminary studies. This spectrograph covered the region from 1 850 Å to about 8 000 Å. The dispersion of this instrument in the ultra-violet (u.v.), about 10 Å/mm at 2 000 Å, is quite adequate, but the dispersion drops to about 300 Å/mm at 6 000 Å in the visible. For more detailed study, a Bausch and Lomb Model II 1·5 m stigmatic grating spectrograph was used. This instrument has a dispersion of about 15 Å/mm in the first order, which includes the region from 3 700 Å to 7 400Å, and a dispersion of about 7·5 Å/mm in the second order, which includes the region from 1 850 Å to 3 700 Å.

---

[*] Abstracted in part from the *Thesis* presented by R. M. LODWIG in partial fulfilment of the requirements for the Master of Science degree, University of Wisconsin, January 1958.

Kodak spectroscopic plates were used with the Hilger spectrograph. Type 103-O plates effectively covered the region below about 5 000 A, and the region from about 7 000 A down into the u.v. was recorded on type 103a-F plates. Kodak 35 mm spectroscopic films were used with the Bausch and Lomb grating spectrograph. The u.v. region was covered by Spectrum Analysis No. 1 film and the visible region to about 7 000 A was studied with type 103-F film. All of the films and plates were developed with Kodak D-19 high contrast developer for 3·5 to 5 min and fixed with Kodak F-5 fixing solution for 15 to 20 min. The somewhat reduced developing time of 3·5 min instead of the recommended 4 to 5 min was used to prevent undesirably high negative background density in the 'prefogged' astronomical plates. Filters were used with the Bausch and Lomb grating spectrograph to eliminate confusion due to the overlapping of the first and second order spectra.

The distance from the slit of the spectrograph to the flame was generally about 10 to 20 cm. Exposure times varied from a few seconds on the prism spectrograph to a few hours on the grating spectrograph. Mercury comparison spectra were obtained with a mercury lamp.

Burners

Two types of burners were used to produce the flames studied. The simpler burner consisted of two glass nozzles which directed the issuing gas jets together. This type of burner was used in the early studies with hydrogen.

Burners consisting of two or three concentric tubes were used in later studies. A typical concentric burner might consist of an outer brass tube of about 1·9 cm o.d. around two concentric glass tubes of 1·2 and 0·6 cm o.d. as shown in *Figure 1*. The outer annular space would carry nitrogen and the inner spaces fuel and oxidant. When all-brass burners were used it was found that brass tube surfaces exposed to perchloryl fluoride corroded very rapidly to a distance of several millimetres below the lip in contact with the flame. Pyrex glass tubes also corroded on the area in contact with the flame, but the destruction was not as rapid as that of the brass tubes.

Materials

The perchloryl fluoride was obtained from the Pennsylvania Salt Manufacturing Co. No analysis was carried out. Previous samples have been found to contain nitrogen and carbon dioxide as impurities[4].

Linde USP grade oxygen was used.

Airco hydrogen of better than 99·57 per cent purity was used.

Airco nitrogen was used. The purity is said by the supplier to exceed 99·9 per cent.

Matheson anhydrous ammonia was used. The minimum purity is said by the supplier to be 99·9 per cent.

Matheson hydrogen sulphide was used. The minimum purity is stated to be 99·5 per cent.

The natural gas had the composition: CH_4 71·7, C_2H_6 6·6, C_3H_8 4·1, C_4H_{10} 0·4, N_2 17·1, O_2 0·1 per cent.

Hydrogen–perchloryl fluoride flames

The combustion of hydrogen and perchloryl fluoride gave an intense pale-blue flame cone followed by light blue flame gases, similar to a hydrogen–oxygen diffusion flame. The central tube of the burner used here and in diffusion flames (whose visual appearances are described subsequently) carried perchloryl fluoride and the surrounding concentric tube carried the fuel gas. The gaseous mixture was not self-igniting.

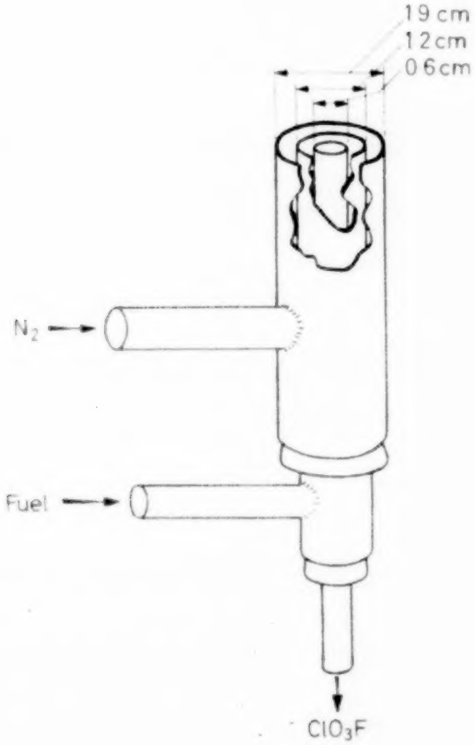

Figure 1. Concentric burner used as spectral source

The most prominent features of the spectra are the OH band systems arising from the $^2\Pi$ to $^2\Sigma^+$ transitions[5]. The principal heads of the observed OH bands are found at 2 444, 2 608, 2 811, 3 064 and 3 428 Å, corresponding to the (3,0), (2,0), (1,0), (0,0) and (0,1) vibrational transitions, respectively. These features are marked on *Figure 2*. On some hydrogen–perchloryl fluoride flame spectra taken with the Hilger prism spectrograph a series of poorly defined bands was observed between about 3 700 and 4 500 Å. These structures could not be located on any of the hydrogen–oxygen flame spectra taken under similar conditions or published in the literature. These diffuse bands are almost indiscernible on spectra recorded by the 1·5 m grating spectrograph. Neither spectrograph records any details of the rotational structure or the position of the band heads.

A. G. Gaydon and G. Pannetier[6] have described some bands which have the same characteristics as the observed bands from observations made on hydrogen–oxygen flames into which small amounts of chlorine were injected. The resulting diffuse bands were attributed to the ClO molecule. The wavelengths of the 'band heads' (regions of highest negative density) recorded by Gaydon and Pannetier are marked on *Figure 2*. It can be seen that these 'band heads' correspond rather well with the regions of higher negative density observed in the hydrogen perchloryl fluoride flame spectra, and that the pattern of the series of bands is the same. Comparison of the observed spectra with the published plates of Pannetier and Gaydon shows the close similarity of the spectral features. The ClO molecule is thus tentatively identified in the flame gases.

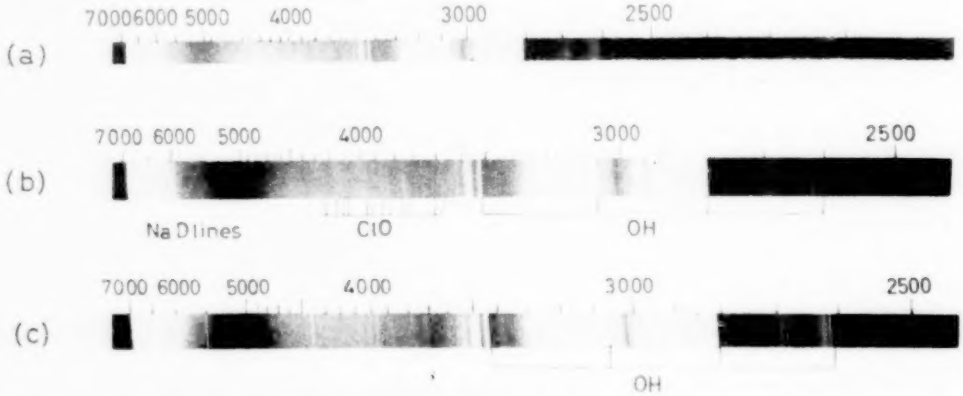

Figure 2. Hydrogen perchloryl fluoride flame at (a) and (b); (c) hydrogen oxygen flame

Methane–perchloryl fluoride flames

Three distinct regions were observed in premixed methane perchloryl fluoride flames. The innermost cone was an intense pale-blue colour, the outer margins were luminous yellow, and the intermediate region was relatively colourless. The gaseous mixture was not self-igniting.

The observed spectra of the methane–perchloryl fluoride flame are similar to those observed for the methane–oxygen flame. The OH bands at 2 608, 2 811, 3 064 and 3 428 A are again prominent. The CH band systems at about 3 900 Å [$^2\Sigma \rightarrow {}^2\Pi$] and 4 300 Å [$^2\Delta \rightarrow {}^2\Pi$] are strongly emitted[3]. The CH band at 3 143 A was not observed. The strong band systems at 4 700, 5 100 and 5 600 A have been identified as the C_2 Swan bands. The 6 000 A (0,2) C_2 band system appeared faintly on some plates at the edge of a continuum which extended down from the red. An interesting plate obtained using a brass burner also showed band systems of CuCl, CuF and CuO and atomic lines of Cu. *Figure 3* shows the details of the methane–perchloryl fluoride flame spectra.

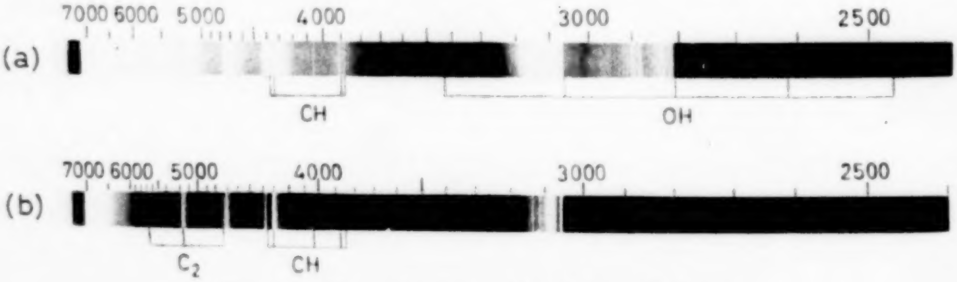

Figure 3. Natural gas–perchloryl fluoride flame

Ammonia–perchloryl fluoride flames

Ammonia–perchloryl fluoride diffusion flames possess three distinct zones: the first zone is the pale-blue flame front cone; just above the flame cone is a deep yellow zone; beyond the deep-yellow zone is a yellow to yellow-white zone. The flame is not self-igniting.

The emission spectra of some ammonia–perchloryl fluoride flames are shown in *Figure 4* and are similar to the spectra of ammonia–oxygen flames. The OH bands are again a principal feature. The NH [$^3\Pi \rightarrow {}^3\Sigma$] bands at 3 360 and 3 370 Å are prominent and account for the bright yellow colour of the flame. The extensive NH_2 α bands appear diffuse under the low dispersion of the prism spectrograph, but are resolved into a pattern of many rotational lines with no apparent band heads by the 1·5 m grating spectrograph.

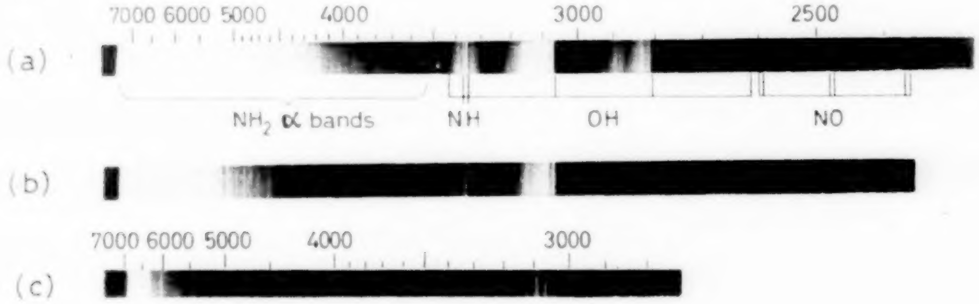

Figure 4. Ammonia–perchloryl fluoride flame

The identification of these features as the NH_2 α bands was accomplished by a comparison of the wavelengths of the more intense lines of the observed spectra with the values recorded by W. B. RIMMER[7]. Visual comparison of the observed spectra with the plates published by W. B. RIMMER and by A. FOWLER and J. S. BADAMI[8] confirmed their identity. On one plate (ML–11) the γ bands of NO were observed at 2 260, 2 360 and 2 470 Å corresponding to the (0,0), (0,1) and (0,2) vibration–rotation bands of the [$^2\Sigma^+ \rightarrow {}^2\Pi$] electronic transition as determined by comparison of band head measurements with the values reported by Fowler and Badami[8] and visual comparison of the published plates with the observed spectra. On some plates (e.g. ML–11) bands coinciding with the tentatively identified ClO bands could be seen, and the presence of ClO in the ammonia–perchloryl fluoride flame gases is thus indicated.

Hydrogen sulphide–perchloryl fluoride flames

The hydrogen sulphide–perchloryl fluoride diffusion flames gave a blue flame cone, followed by a somewhat lighter blue zone in which a pale yellow to pink colour could be detected (possibly due to small amounts of sodium from the burner); this zone was in turn followed by a blue-white zone. The gas mixture was not self-igniting.

The spectra of the hydrogen sulphide–perchloryl fluoride flames are similar to those of the hydrogen sulphide–oxygen flames. The predominant features of both spectra are the strong S_2 bands[5, 9] extending almost over the entire region covered by the spectrographs. Superimposed upon the S_2 bands are OH bands at 2 811 and 3 064 A and the SO_2 system[7] at 2 500 A. These features may be seen in *Figure 5*.

Results of spectral studies

A comparison of the emission spectra of flames involving perchloryl fluoride with flames supported by more conventional oxidizing agents such as oxygen or nitrous oxide indicates few important differences between them. The presence of bands attributable to ClO in the spectra of hydrogen–perchloryl fluoride and ammonia–perchloryl fluoride flames is the only unusual result obtained. The presence of ClO in the flame gases is not unlikely, since the spectra of this molecule were first obtained by Gaydon and Pannetier[6] by the introduction of a small amount of chlorine gas into a hydrogen–oxygen flame. There is no evidence for new spectra of ClF, OF, HF or O_2 of high intensity, although these molecules may yield some of the less intense background bands.

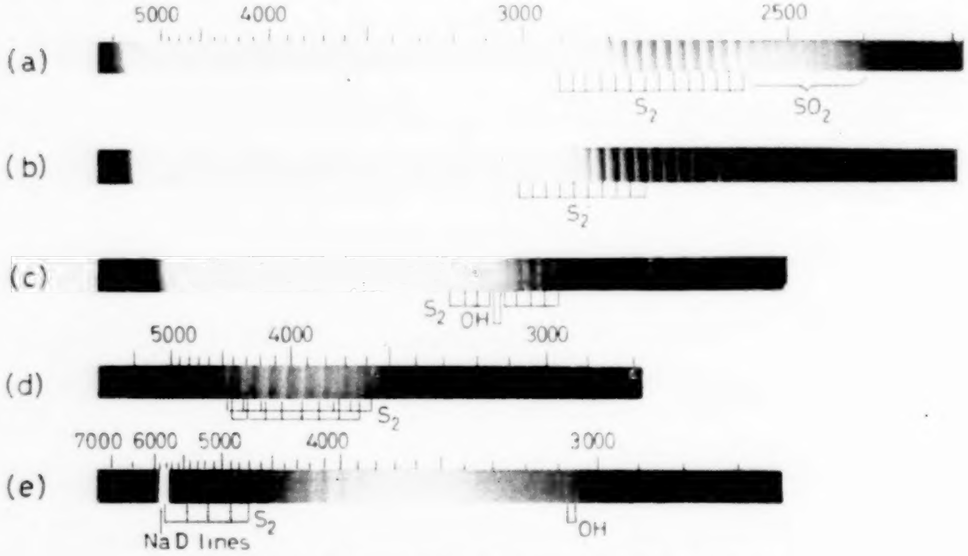

Figure 5. Hydrogen sulphide perchloryl fluoride flame

INFLAMMABILITY LIMITS OF PERCHLORYL FLUORIDE–NATURAL GAS–NITROGEN MIXTURES

The inflammability limits of the perchloryl fluoride–natural gas–nitrogen system were determined in connection with flame velocity trials by the tube method. The tubes were placed horizontally and were enclosed in an explosion screen. Most of the data were taken with Pyrex tubes 22 mm in internal diameter and about 120 cm in length. For mixtures containing 30 per cent nitrogen diluent or less, the tube length of the 22 cm internal diameter tubes was shortened to about 60 cm to prevent the destruction of the tube with every trial. Ignition was usually accomplished by a Tesla coil spark across a gap near the open end of the tube. However, in mixtures containing 30 per cent nitrogen diluent or less, the spark failed to ignite the mixture, and a burning splint applied to the open end of the tube served as the ignition source. In either case the ignition source was applied immediately after carefully opening one end of the tube with a minimum disturbance of the gaseous mixture within the tube. The gas-filled tubes were allowed to stand a few minutes before ignition in order to allow the gas mixture to become quiescent.

The data obtained are plotted in *Figure 6*. The corresponding flammability limits of the nitrogen–methane–oxygen system are also shown on the graph[10, 11]. The principal sources of error in these measurements are the errors in measuring the mixture composition, the quenching effect of the walls of the tube, and the determination of the distance travelled by the flames. The third-mentioned error, essentially the decision as to whether or not the flame would continue to propagate itself indefinitely through the given mixture in the given tube, is occasionally a source of difficulty, especially for flames of low velocity.

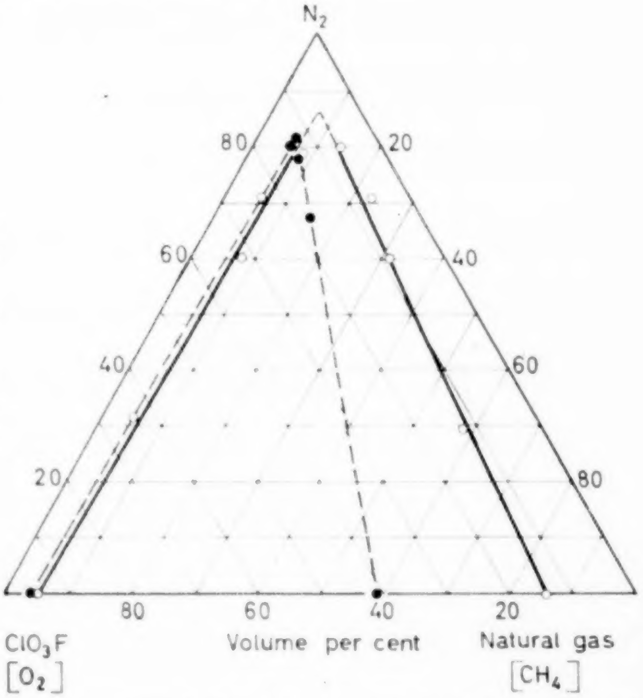

Figure 6. Inflammability limits for natural gas perchloryl fluoride–nitrogen and methane oxygen nitrogen mixtures

In the perchloryl fluoride-supported flames, however, the region of mixture compositions which will propagate a flame only a short distance seems to be quite small. Furthermore the detonation limits appear to lie rather close to the flammability limits, and a flame front which accelerates rapidly almost invariably detonates instead of dying out, as often occurs in less easily detonatable mixtures. Thus the use of shortened tubes in this investigation to prevent the destruction of the tubes by the frequent detonations would not seem to introduce appreciable errors into the data.

The quenching effect of the tube walls might have some influence on the results presented here. The data were accumulated during attempts to measure the flame velocity by the tube method, and the tubes used were 22 mm in internal diameter. The accepted standard tube diameter for combustion limit determinations is 2 inches (5·1 cm)[11]. It is expected, however, that the effect on the lower limit is not significant, while the effect on the upper limit would be small. Furthermore, the extreme breadth of the inflammability limits of the perchloryl fluoride–natural gas–nitrogen systems makes it likely that the curve for percentage fuel versus limiting tube diameter is rising steeply at the upper limit as well as at the lower limit, minimizing the errors due to quenching of chain carriers on the tube walls.

BURNING VELOCITIES OF SOME METHANE–PERCHLORYL FLUORIDE MIXTURES

The experimental methods employed for the determination of fundamental flame velocities may be classified into five general groups[12]: (*1*) bunsen burner methods, (*2*) cylindrical tube methods, (*3*) soap bubble methods, (*4*) spherical vessel methods, and (*5*) flat flame methods.

Bunsen burner methods fall into two general categories: (*1*) those utilizing the flame cone area[13], and (*2*) those utilizing the linear unburnt gas velocity at a point on the flame cone and the angle made by a tangent to the flame cone at that point and the axis of the flame cone[11]. Burner methods have the advantages of simplicity of apparatus, convenience and rapidity of measurements, and a relative wealth of literature for the comparison of the burning velocity values obtained.

In the Gouy method[13], the flow rate of the gas mixture is divided by the flame front area, and a cone is used as an approximation to the flame front surface. Photography may be used for the determination of the flame front area. Most workers attempt to correct for the errors due to the use of flame front areas near the tip and base of the flame cone, and it has been pointed out by Lewis and von Elbe[11] that methods arbitrarily eliminating regions of the flame cone near the tip and base have no sound theoretical justification.

Even with refinement, the burner method is primarily designed for mixtures with rather low burning velocities. The validity of these methods when applied to fast burning mixtures, such as methane and oxygen, has been questioned because of the high gas velocities and small orifices required to prevent flashback[12].

Apparatus and procedure

Figure 7 gives a schematic diagram of the burner apparatus. Two Greiner G-9144B predictability flowmeters were used. The flow rates were calculated from the flowmeter readings according to the method given by the Greiner Co. The manometer fluid was dibutyl phthalate. The mixing chamber and burner details are also shown in *Figure 7*. The mixing chamber was filled with glass beads of about 4 mm diameter which were held in their proper place by copper screening. An aluminium foil cover was held tightly over the top of the mixing chamber by a rubber band and formed a satisfactory rupture disc. A similar rupture disc protected the apparatus, especially the flowmeters, from damage when the flame flashed back into the burner tube and mixing chamber. The leakage around both rupture discs was immeasurable on the flowmeters.

The burner itself consisted of a tube cooled by a brass water jacket.

It was made from a $\frac{3}{8}$ in. diameter stainless steel rod 2 cm in length through which a hole of 1·51 mm diameter was drilled and polished. A similar burner of 2·06 mm diameter was found to be too large to permit measurements of the faster flames. At least approximate laminar flow was achieved in all of the results reported. The burner was attached to a $\frac{3}{8}$ in. brass tube about 30 cm long. A tight-fitting brass collar was placed around the top of the burner.

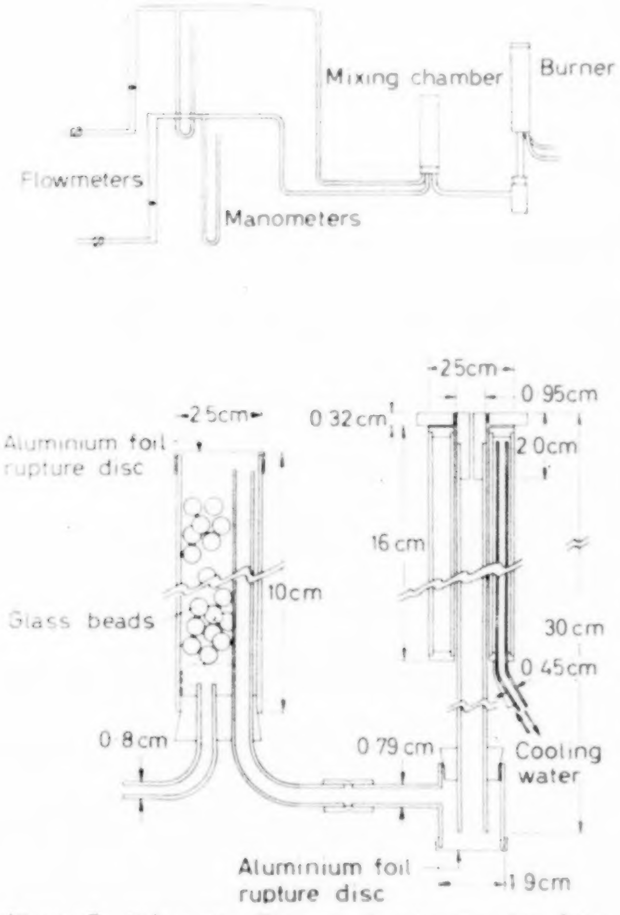
Mixing chamber
Burner
Flowmeters
Manometers
2·5cm
Aluminium foil rupture disc
Glass beads
10cm
0·8 cm
2·5cm
0·95cm
0·32 cm
2·0cm
16 cm
30 cm
0·45cm
0·79 cm
Cooling water
Aluminium foil rupture disc
1·9cm

Figure 7. Schematic diagram of apparatus for determining flame velocities by burner method

The flame was photographed by a camera which remained fixed in position throughout a series of runs. Kodak Linagraphic film was used to record the flame cone dimensions. The scale of the photographs was established by photographing a piece of centimetre graph paper placed in the position of the flame cone both before and after a series of flame pictures.

Burning velocities were calculated by a total area method. The photograph included in *Figure 8* shows a typical flame cone shape, and the drawing indicates the line elements by which the theoretical flame is outlined. The construction lines on the photograph show that a right circular cone is a good approximation for the flame shape. The burning velocities may be calculated from the expression

$$U_f = \text{volume rate of flow}/\text{flame cone area}$$

The results of all the measurements by the burner method are shown in *Figure 9*.

CONCLUSIONS

The burning velocities presented here are compared with the methane–oxygen flame, which has a burning velocity of about 330 cm/s[15], because of

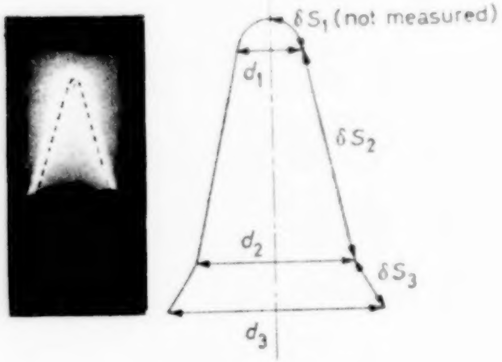

Figure 8. Method for determining flame area from photograph of flame

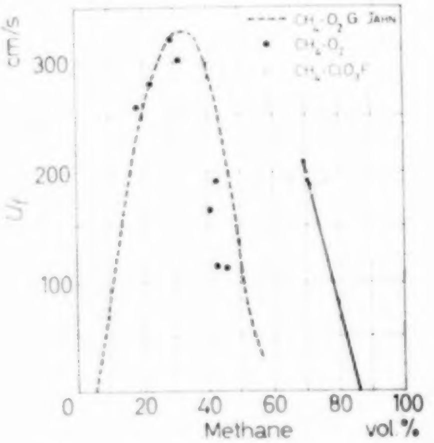

Figure 9. Burning velocities of methane–perchloryl fluoride and methane–oxygen mixtures

the similarity in the method of measurement. The somewhat low U_f values obtained in the high-methane mixtures probably arise from errors in locating the inner flame cone. The photographic negatives of these methane-rich flames showed a high density due to the luminosity of the flames, and the inner cone was not always clearly distinguishable.

The position of the U_f versus composition line, extrapolated to $U_f=0$ at the inflammability limit, *Figure 9*, suggests that the maximum methane–perchloryl fluoride burning velocity will be considerably higher than that of the methane–oxygen flame. Because of the wide difference in upper inflammability limits it is difficult to estimate accurately the maximum burning velocity from these data, even on the basis of a ratio between the burning velocities observed for methane–perchloryl fluoride mixtures and those of methane–oxygen mixtures.

Department of Chemistry,
University of Wisconsin,
Madison, Wisconsin

(*Received July 1958*)

REFERENCES

[1] Engelbrecht, A. and Atzwanger, H. *Mh. Chem.* 1952, **83**, 1087
[2] Engelbrecht, A. and Atzwanger, H. *J. inorg. nucl. Chem.* 1956, **2**, 348
[3] Barth-Wehrenalp, G. *J. inorg. nucl. Chem.* 1956, **2**, 266
[4] Neugebauer, C. A. and Margrave, J. L. *J. Amer. chem. Soc.* 1957, **79**, 1338
[5] Pearse, R. W. B. and Gaydon, A. G. *The Identification of Molecular Spectra*, 2nd ed. Wiley: New York, 1950
[6] Gaydon, A. G. and Pannetier, G. *Nature, Lond.* 1948, **161**, 242
[7] Rimmer, W. B. *Proc. Roy. Soc. A*, 1923, **103**, 696
[8] Fowler, A. and Badami, J. S. *Proc. Roy. Soc. A*, 1931, **133**, 325
[9] Fowler, A. and Vaidya, W. M. *Proc. Roy. Soc. A*, 1931, **132**, 310
[10] White, A. G. *J. chem. Soc.* 1924, **125**, 2387
[11] Lewis, B. and von Elbe, G. *Combustion, Flames and Explosions of Gases*. Academic Press: New York, 1951
[12] Linnett, J. W. *Fourth Symposium (International) on Combustion*, p 20. Williams and Wilkins: Baltimore, 1952
[13] Gouy, M. *Ann. chim. Phys.* 1879, **18**, 27
[14] Jost, W. and Croft, H. O. *Explosion and Combustion Processes in Gases*. McGraw-Hill: New York, 1946
[15] Jahn, G. See Lewis, B. and von Elbe, G. *loc. cit.* pp 460–466

Detonation Overpressures in Saturated Knallgas[*]*–Steam Mixtures*

L. B. ADLER[†] and J. A. LUKER

Reflected pressures corresponding to the development of detonation in saturated mixtures of knallgas and steam at 100° C were measured. The maximum pressure observed was about three times that predicted for theoretical reflected detonation by solution of the Chapman–Jouguet detonation equations and equations for normal shock reflection. Composition limits defining non-reactive and detonatable regions for the particular experimental system employed were also determined. Some considerations applicable to the study of detonation in gaseous mixtures having long detonation stabilization distances are noted, and pressure/time records of different stages of the transition from flame to detonation are shown.

A NUMBER of investigators[1–7] have noted the existence of pressures during the development of detonation in a gaseous explosive which exceed those normally associated with the fully developed, stable detonation wave. Clearly, such 'overpressures' are of important practical as well as fundamental significance, particularly in situations where physical systems must be designed to contain a detonation. Gas mixtures having long detonation stabilization distances, i.e. mixtures in which the formation of detonation is a relatively slow process, are of specific interest because the unstable overpressure region preceding the formation of stable detonation in such cases generally exists for a longer period of time and may thus be more effective in causing physical damage. The slower development of detonation in these mixtures also makes them more amenable to experimental study.

As is well known, stable detonation parameters are readily, and in most cases, ably predicted by theoretical calculation. Unfortunately, properties exhibited during the development of detonation cannot be predicted with the relative ease that stable detonation parameters can. The transition from flame to detonation is a much more complex picture than that of the plane, stable detonation front which is the basis of the well known Chapman–Jouguet theory[8, 9]; it has not yet become practicable to obtain quantitative estimates of unstable detonation pressures from theoretical calculations, even though this phase of the detonation process has received theoretical treatment[10]. Such information must be obtained experimentally.

The purpose of this work was to study the development of detonation and determine representative detonation overpressures in saturated mixtures of knallgas and steam at 100° C. It was necessary to obtain pressure records of the reaction in knallgas–steam mixtures at various stages of the development of detonation. This was done by mounting a pressure indicator in the end of a reaction tube at a fixed distance from the source of ignition;

---

[*] Stoichiometric mixture of hydrogen and oxygen ($2H_2 + O_2$).

[†] Present address: Brookhaven National Laboratory, Upton, New York.

this indicator measured 'reflected' reaction pressures due to its 'head-on' orientation with respect to an approaching combustion or detonation wave. Mixtures of knallgas and steam were then prepared and fired, a pressure record being obtained for each shot. The strength of each of these experimental mixtures was changed by varying the ratio of knallgas/steam. Since the distance which a flame front must propagate before detonation is formed varies with the strength of the explosive mixture, the pressure record obtained at the end of the tube for each shot corresponded to a different stage of the transition to detonation, provided the mixture was detonatable. The success of this method of attack depends upon the detonation stabilization distances of weak knallgas–steam mixtures being longer than the effective length of the reaction tube; otherwise, only stable detonation would be observed at the tube end in mixtures above the detonation limit. A suitable reactor length was indicated by preliminary data obtained at this laboratory.

The experimental results are best compared with values predicted by theory. Calculations were made to define constant-volume explosion and incident and reflected stable detonation parameters for the knallgas–steam system. The explosion and reflected detonation parameters are employed in an analysis of the data. Incident and reflected detonation wave calculations were also made for dry knallgas, used to 'dynamically' calibrate the experimental pressure transducer.

APPARATUS

Details of the experimental apparatus and the physical layout of the detonation laboratory are shown in *Figure 1*.

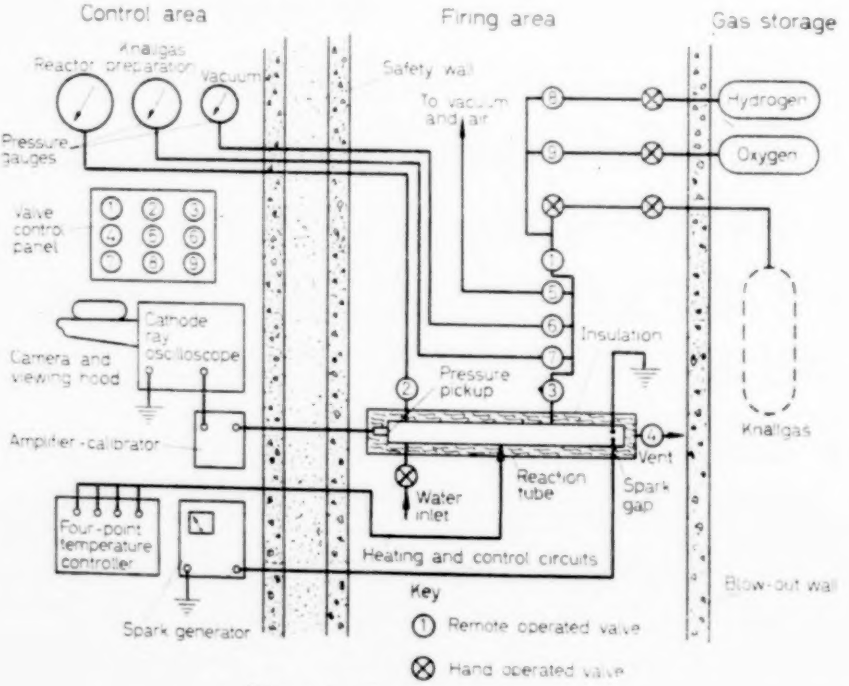
Control area
Firing area
Gas storage
Knallgas preparation
Reactor
Vacuum
Pressure gauges
Safety wall
To vacuum and air
Hydrogen
Oxygen
Valve control panel
1 2 3
4 5 6
7 8 9
Cathode ray oscilloscope
Camera and viewing hood
Insulation
Pressure pickup
Knallgas
Amplifier-calibrator
Vent
Reaction tube
Water inlet
Spark gap
Four-point temperature controller
Heating and control circuits
Blow-out wall
Spark generator
Key
Remote operated valve
Hand operated valve

Figure 1. Experimental system

The reaction tube, 2·43 cm in inner diameter, was constructed of type 304 stainless steel. A spark gap was located 7·6 cm from one tube end; a pressure pickup was contained in the opposite tube end. The distance between the spark gap and the pressure pickup was 2·35 m. The ignition spark was produced by the discharge of a 0·01 microfarad capacitor maintained at a firing potential of 6 kV. A high-voltage thyratron was employed as a firing switch to minimize switching losses. The spark energy was 180 millijoules.

The pressure pickup was a SLM PZ–14 quartz pressure transducer. Its electrical output was monitored by a Kistler PC–14H amplifier-calibrator and displayed as a pressure/time signal on the screen of a DuMont type 324 cathode ray oscillograph. The pressure/time signal was recorded with a DuMont type 302 Polaroid land camera utilizing type 44 Polaroid land film.

The reaction tube was wrapped and heated with four sections of Nichrome resistance wire. Asbestos tape and Fibreglas were employed as insulation. The temperature of the tube was controlled to ±1°C by a Celectray four-point indicating temperature controller employing iron–constantan thermocouples silver-soldered to the tube wall as control elements.

All pressure lines, gauge lines and valves for the control of gas flows were Aminco high-pressure stainless steel fittings rated for pressures up to 2,000 atm. The remote-operated valves were controlled from the valve panel by means of valve extenders. Measurements of the experimental mixture pressure prior to firing were made with a Heise precision bourdon tube gauge which could be read to ±0·1 lb/in^2. Due to the presence of steam in the experimental mixture, the lead lines and bourdon tube of the reactor gauge were filled with water to eliminate condensation and ensure a correct pressure reading.

CALIBRATION OF EQUIPMENT

The reaction tube and temperature controller were calibrated for operation at 100°C with saturated steam. The tube was charged with a proper amount of distilled water when cold. It was then heated and maintained at a series of temperature settings. The setting at which the saturation pressure of the steam was read to be 1 atm absolute (within ordinary control fluctuation) was fixed as the 100°C control point.

The manufacturer's calibration was accepted for the Heise reactor gauge. It was accurate to within the precision with which a pressure reading could be made.

Two different methods of calibration were employed to determine the relationship between electrical output and pressure for the PZ–14 pressure transducer. In one case, a 'static' calibration was obtained by applying a series of known hydrostatic pressures to the transducer with a Crosby Style CD–210 dead-weight tester. A 'dynamic' calibration was then obtained by applying a series of known transient pressures to the pickup. This was done by recording the output of the transducer in response to stable detonation waves of varying strength in dry knallgas at room temperature (20 to 25°C). Calculated reflected detonation pressures were assumed valid for the dry knallgas calibrating waves. The conditions for which each of these calibrations are valid are discussed later in the text.

KNALLGAS PREPARATION

The knallgas was prepared by premixing and storing the proper amounts of hydrogen and oxygen. The storage tank was filled with the partial pressure of each component predicted by assuming Dalton's law for the mixture and representing the *P–V–T* data for hydrogen and oxygen with the aid of compressibility charts. The electrolytic hydrogen employed had a rated purity of better than 99·9 mole per cent. The oxygen was U.S.P. grade of 99·6 mole per cent purity. The freshly prepared knallgas was allowed to mix for a minimum of three days before use. Successive mixtures prepared in this manner were found to deviate from the stoichiometric composition by less than 0·5 per cent. The mixture analysis, based on oxygen absorption, was made with a safety-shielded precision Orsat apparatus.

PROCEDURE

The basic procedure was the same for each run. The reaction tube was evacuated and charged with an amount of distilled water necessary for saturation at 100°C. Next, it was filled with the proper amount of knallgas to achieve a desired mixture composition. The tube was then heated to and controlled at 100°C for a total operating period of three hours. This period of time was allowed for the gases in the reactor to obtain mass equilibrium; the actual heating of the reactor from room temperature to 100°C required only half an hour. Just prior to firing, the total mixture pressure was read and the reactor gauge valve shut. A spark was passed through the mixture. The resulting reaction pressure was recorded by means of the pressure transducer, oscillograph and camera. After a suitable amount of time to allow heating effects of the reaction to dissipate, the total mixture pressure was again read in order to determine what fraction of the knallgas in the original mixture had been consumed. Preparation for the next experimental run involved venting the remainder of the reacted mixture and cooling and drying the reaction tube by sweeping it with compressed air.

THEORETICAL CALCULATIONS

The theoretical explosion and detonation parameters were calculated with the aid of an IBM 650 digital computer. With knallgas and steam, the initial mixtures were not assumed to behave ideally; saturation compositions were predicted by employing a method based on the use of Dalton's law for the mixture with the *P–V–T* data of the pure constituents. The validity of this type of method has been demonstrated for saturated steam–helium and steam–oxygen mixtures by J. A. LUKER, T. GNIEWEK and C. A. JOHNSON[12, 13].

Chapman–Jouguet considerations were employed to determine incident detonation wave properties; sound velocity was assumed 'frozen' at the composition of the Chapman–Jouguet plane. Reflected detonation parameters were calculated from equations based on the normal reflection of a shock wave from a rigid boundary (see R. H. COLE[13]). The thermodynamic data employed were in the analytical form derived by P. L. McGILL[14] from the tabular values of V. N. HUFF, S. GORDON and V. E. MORRELL[15]. Complete reaction to thermodynamic equilibrium was assumed: the reaction products, consisting of the chemical species H_2O, H_2, O_2, OH, H and O were treated as ideal gases. Equilibrium concentrations in the burnt gas were calculated by a formalized iterative procedure based on the generalized method of H. J. KANDINER and S. R. BRINKLEY, Jr[16]. The explosion and detonation equations were solved by a modified formalized iterative procedure suggested by P. L. McGILL[14] and based on the Newton–Raphson solution method for simultaneous equations (see J. B. SCARBOROUGH[17]). Convergence of the primary unknowns was obtained to approximately 1 part in 1 000.

Table 1. Calculated reaction pressures in saturated knallgas–steam mixtures at 100°C

Initial mixture pressure atm	*Mixture composition mole % knallgas*	*Explosion pressure atm*	*Incident detonation pressure atm*	*Reflected detonation pressure atm*
1	0	—	—	—
1·2	16·45	3·991	7·388	16·34
1·5	32·98	7·463	14·10	32·54
2	49·59	12·22	22·98	53·68
3	66·28	20·68	38·87	91·17
4	74·65	28·97	54·49	128·2
5	79·68	37·29	70·15	165·2

Some representative pressure values obtained from the theoretical calculations are given in *Tables 1* and *2*. The base temperature for the dry knallgas calculations, as noted, was 25°C.

Table 2. Calculated detonation pressures in dry knallgas at 25°C

Initial knallgas pressure atm	*Incident detonation pressure atm*	*Reflected detonation pressure atm*
1	18·12	43·00
2	37·24	88·65
3	56·69	135·2
4	76·36	182·3
5	96·17	229·9

RESULTS

The experimental results are shown in *Figure 2*. *Figure 2* is designed to show the variation in the reaction pressure obtained at the tube end as a result of changing the strength of the experimental mixture. This is done by plotting the ratio of the peak reaction pressure to the initial mixture pressure versus the mixture composition in mole per cent knallgas. The same relationship could have been plotted in a number of different ways; however, the use of this ratio tends to accentuate the shape of the curve and emphasize certain important differences. Semi-logarithmic coordinates were employed to expand the scale of the ordinate so that the low-region

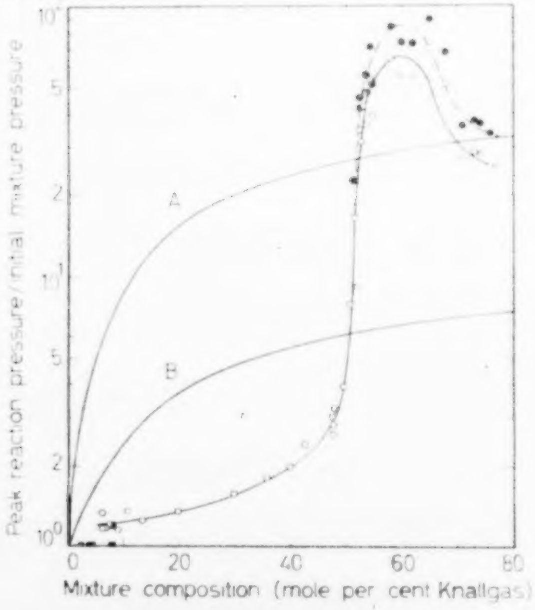

Figure 2. Effect of mixture composition on reaction pressures. A. Theoretical reflected detonation; B. Theoretical explosion; ■ *No reaction;* —●— *Dynamic pressure calibration;* ——— *Static pressure calibration*

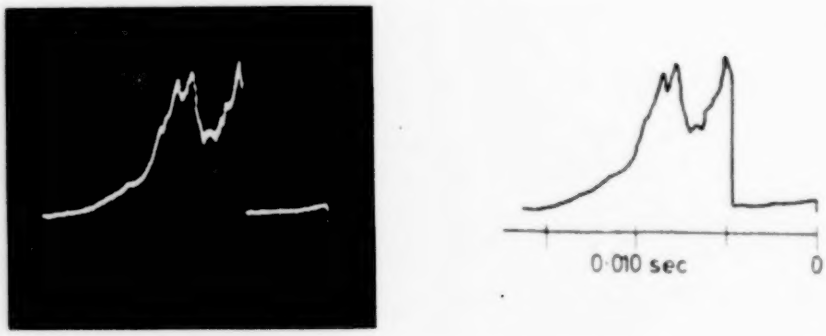

(a) *Composition = 30·0 mole per cent knallgas; peak reaction pressure = 2·27* atm; knallgas reacted = 23 per cent*

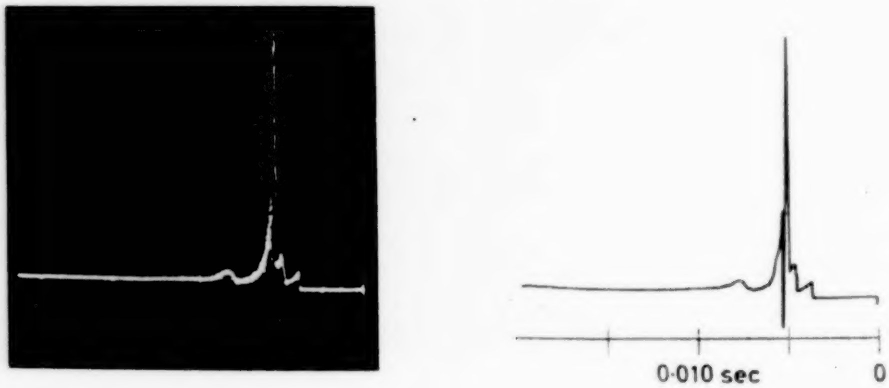

(b) *Composition = 54·5 mole per cent knallgas; peak reaction pressure = 156† atm; knallgas reacted = 88 per cent* points could be represented more effectively. The peak reaction pressures were evaluated from the experimental pressure/time records. Each reading was taken as the point of maximum pressure, regardless of the particular shape of the signal. Mixture compositions were predicted, as in the theoretical calculations, by the method of J. A. LUKER *et al.*[12, 13].

---

*Static pressure calibration.

†Dynamic pressure calibration.

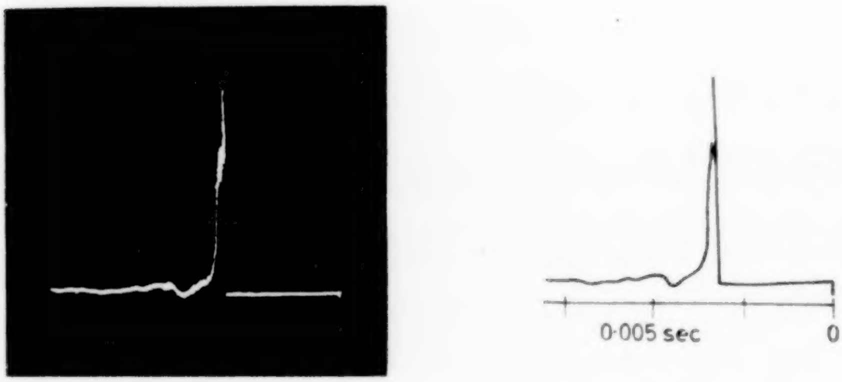

(c) *Composition = 59·9 mole per cent knallgas; peak reaction pressure = 184† atm; knallgas reacted = 87 per cent*

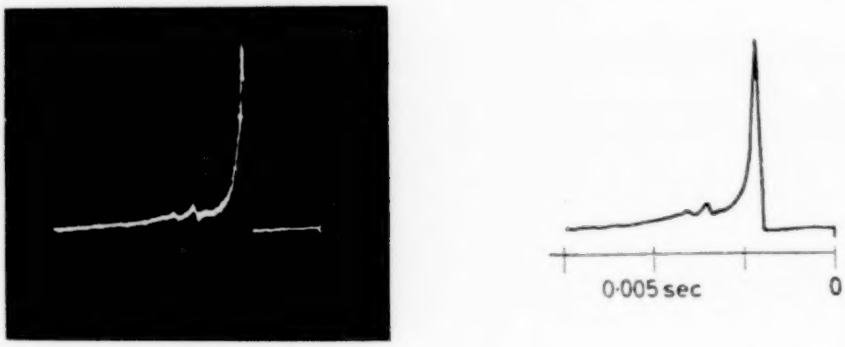

(d) *Composition = 70·6 mole per cent knallgas; peak reaction pressure = 122† atm; knallgas reacted = 93 per cent*

Figure 3. Pressure/time records of typical reactions. Vertical axis: pressure. Horizontal axis: time

Some pertinent observations can be made with reference to *Figure 2*. The first of these is that no mixture will support a reaction below a composition of about 6 mole per cent knallgas. The pressure records in this region exhibited no discernible pressure rise upon ignition. It is possible that a weak reaction could be initiated which would not propagate to the tube end; however, there was no drop in total pressure caused by passage of the spark in these mixtures, indicating negligible, if any, reaction.

---

†Dynamic pressure calibration.

The conclusion that no mixture will *support* a reaction below the 6 per cent level seems to be valid in either case.

Relatively weak combustion waves were generated in the composition range extending from 6 to 45 mole per cent knallgas. The pressures observed are much lower than those predicted for theoretical constant-volume explosion: the theoretical values represent upper limits to explosion pressures in this region. The low reaction pressures are accentuated by the fact that the total per cent of knallgas reacted in these mixtures averaged about 25 per cent, while the theoretical curve was calculated on the basis of complete chemical reaction (to equilibrium); in addition, most pressure/time traces exhibited more than one area of energy release, e.g. *Figure 3*(a), with two distinct pressure 'peaks'.

Since detonation will arise from an ordinary combustion wave in detonatable mixtures ignited by a spark, it is not possible to tell which of the mixtures in the region from 6 to 45 per cent knallgas are detonatable and which are not, i.e. the combustion wave observed at the tube end may be an ordinary combustion wave in a mixture that will not detonate, or it may be a combustion wave which is the forerunner of detonation in a mixture in which the stabilization distance to detonation is long. In the latter case, the disturbance does not have time to develop sufficiently before the tube end is reached. This consideration is obviously important. Points in this region cannot be accepted as being below the true composition limit for detonation in saturated knallgas–steam at 100° C, even though they are below the limit of detonation in the particular experimental system employed. Such an observed limit depends largely on the makeup of the experimental system and is related to a number of physical factors, among them tube diameter and length, the mode and strength of ignition employed, and the condition of the tube surface. In this system, for example, lengthening of the reaction tube only should result in the observation of detonation at weaker knallgas compositions. Considerations of this nature must be made in attempts to determine detonation limits in an experimental system where detonation stabilization distances are longer than the tube length in which the study is performed.

The detonation limit for this experimental system occurs at about 50 mole per cent knallgas, i.e. detonation cannot occur below a mixture strength of about 50 mole per cent knallgas. This is evidenced by the sharp climb in the experimental curve to pressures exceeding that corresponding to theoretical reflected detonation. As mentioned previously, the reflected parameters are used because the face of the pressure transducer was directed head-on to the approaching detonation wave in the experimental system. The pressure 'hump' between 50 and 75 mole per cent knallgas is the overpressure region corresponding to unstable detonation. Typical pressure signals in this region clearly indicate distinct stages in the development of detonation. *Figure 3*(b) shows compressional shocks preceding the overtaking detonation front; this is consistent with the picture of the development of detonation first presented by W. A. Bone, R. P. Fraser and W. H. Wheeler[18] (see also G. B. Kistiakowsky[19]). In *Figure 3*(c) the detonation front and leading shock waves have coalesced to form an unstable detonation wave. The tapering-off of the experimental curve at still richer knallgas compositions indicates that the detonation stabilization distances are close to equalling the effective tube length. A more stable detonation is shown in *Figure 3*(d). A major fraction (80 to 95 per cent) of the knallgas was consumed by reaction in all mixtures above the detonation limit.

Pressure readings for the detonation region of the curve in *Figure 2* were evaluated by both the static and the dynamic transducer calibrations, as shown. The difference in the method of calibration does not affect the shape of the experimental curve nor any conclusions that have been made; however, it is felt that the dynamic calibration does give more reliable estimates of the actual reaction pressures in this region. The measurement of true detonation pressures has not yet been reported with any conviction because of the lack of a dependable pressure-measuring system with the necessary frequency response to reproduce faithfully the extremely transient pressures associated with a detonation wave. The rated frequency response of the PZ–14 transducer system was 15 000 cycles per second with a minimum rise time of about 70 microseconds. This rise time is much greater than the rise time or the duration of the detonation pulse. Where such a system of limited frequency response is exposed to a pressure transient of extremely short duration, the resultant signal will be a function of the particular physical and/or electrical characteristics of the measuring equipment. Calibrating the measuring system with known transient pressures gives a more correct interpretation of the system output because the majority of factors which influence the overall response of the system are taken into account in the calibration.

The calculated reflected pressures for dry knallgas were taken as correct in performing the dynamic calibration of the pressure transducer. The basis for this assumption is the highly satisfactory agreement between calculation and experiment for this mixture with respect to the detonation velocity (see B. LEWIS and J. B. FRIAUF[20] or D. J. BERETS, E. F. GREENE and G. B. KISTIAKOWSKY[21]). Stability of the calibrating waves was assured because the detonation stabilization distances which have been reported for dry knallgas under conditions similar to those of the calibrating procedure[22] were considerably shorter than the 2·35 m distance between the spark gap and transducer.

Experimental signals exhibiting minimum rise time were evaluated by the dynamic as well as static transducer calibrations. The 'dynamic' pressures are higher than those determined using the static calibration; this means that the true measuring-system response to a detonation pulse should have been higher than was actually recorded. Based on the upper curve, it is seen that the maximum reflected overpressure appearing in the unstable detonation region is about 85 times the initial mixture pressure. It is not determinable whether the experimental curve should approach the theoretical curve as it descends at the higher knallgas concentrations; the validity of theoretical calculations based on Chapman–Jouguet theory has not yet been determined for the saturated knallgas–steam system. The long stabilization distances and the low percentage of gas reacted in the weaker combustible mixtures do indicate that steam possibly acts as a reaction inhibitor as well as a diluent. Significant deviation from theory may very well be noted for stable detonation waves in this system.

Figure 4 is an alternate representation of the experimental data. The ratio of the peak reaction pressure to the theoretical reflected detonation pressure is plotted versus the mixture composition. This particular graph serves to accentuate the detonation limit for the experimental system and the extent of the detonation overpressures. The maximum overpressure, occurring at about 61 mole per cent knallgas, is about three times the reflected detonation pressure that would be expected at this composition. The maximum overpressure ratio may vary with the strength of the mixture at which the overpressure occurs, but it is felt that the observed value is representative of the ratios that will be obtained for the majority of saturated knallgas–steam mixtures at 100 °C.

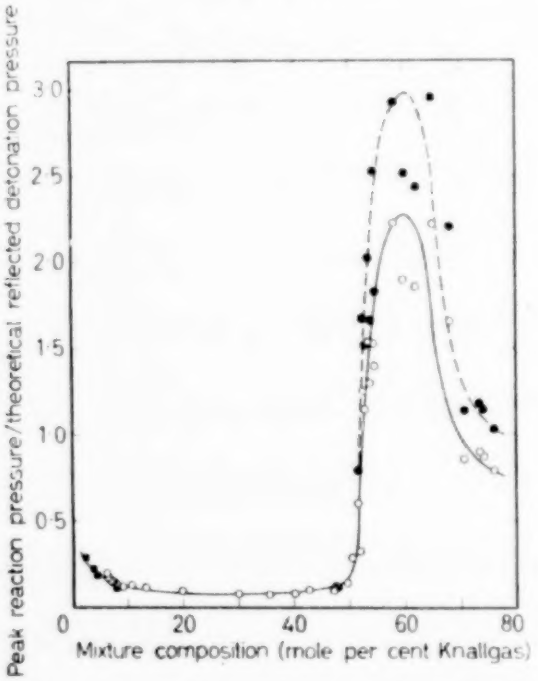

Figure 4. Detonation 'overpressures. ■ *No reaction;* ——●—— *Dynamic pressure calibration;* ——○—— *Static pressure calibration*

ERRORS

The error involved in applying the method of J. A. Luker *et al.*[12, 13] to predict saturation compositions in this system is estimated to be within ±2 per cent of the correct value. This would cause a maximum possible error of about ±1·5 mole per cent knallgas at the upper limit of the composition range investigated. An error in predicting mixture compositions is also attributable to the temperature fluctuations of the reaction tube. This error is a maximum at the low mixture compositions. A temperature variation of ±1 °C is equivalent to ±0·5 lb/in^2 variation in steam pressure. This would cause a possible error of ±3·5 mole per cent knallgas in the value of the no-reaction limit, which is at 6 mole per cent knallgas. At the detonation limit (50 mole per cent knallgas), the possible error due to temperature control is ±0·8 mole per cent knallgas.

It is not easy to estimate the errors associated with the pressure values presented. It is felt that the possible error associated with pressures evaluated by the static transducer calibration only is governed by the precision with which the experimental photographs can be read. A general value is ±5 per cent. The difficulty of measuring the detonation pressures has been emphasized, and no estimate of error will be made; however, those pressures evaluated by the dynamic calibration are probably the best representation of the actual pressures that can be made with this measuring system. Calculated reaction pressures are estimated to be correct to within 0·25 per cent.

The authors wish to express their grateful acknowledgment to Oak Ridge National Laboratory and the Union Carbide Nuclear Company, under whose auspices this work was performed. The aid of Mr Edward C. Hobaica and of Dr Bruce Gilchrist, Director of the Syracuse University Computing Center, is also gratefully acknowledged.

Syracuse University Research Institute,
Syracuse 10, New York

(*Received July 1958*)

REFERENCES

[1] Campbell, C., Littler, W. B. and Whitworth, C. *Proc. Roy. Soc. A*, 1932, **137**, 380

[2] Rimarski, W. and Konschak, M. *Autogene Metallbearb.* 1934, **27**, 209

[3] Henderson, E. *Proc. Pacif. Cst Gas Ass.* 1941, **32**, 98

[4] Smith, J. B. 'Explosion pressures in industrial piping systems.' Paper presented before the International Acetylene Convention, 1949

[5] Turin, J. J. and Huebler, J. *Rep. Comm. Industr. Commer. Gas Res., Project I. G. R.–59.* American Gas Association, 1951

[6] White, D. R. *J. fluid Mech.* 1957, **2**, 513

[7] Mooradian, A. J. and Gordon, W. E. *J. chem. Phys.* 1951, **19**, 1166

[8] Chapman, D. L. *Phil. Mag.* Ser. 5, 1899, **47**, 90

[9] Jouguet, E. *J. Math. pures appl.* 6 sér., 1905, **1**, 347; 1906, **2**, 6

[10] Oppenheim, A. K. *J. appl. Mech.* 1952, **19**, 63

[11] Cole, R. H. *Underwater Explosions*, pp 55–57. Princeton University Press: Princeton, 1948

[12] Luker, J. A., Gniewek, T. and Johnson, C. A. *Industr. Engng Chem., Chem. and Engng Data Ser.* 1958, **3**, 3

[13] Luker, J. A., Gniewek, T. and Johnson, C. A. *Industr. Engng Chem., Chem. and Engng Data Ser.* 1958, **3**, 8

[14] McGill, P. L. *Ph.D. Dissertation.* Syracuse University, 1957

[15] Huff, V. N., Gordon, S. and Morrell, V. E. *Nat. Adv. Comm. Aero. Rep. No. 1037* (1951)

[16] Kandiner, H. J. and Brinkley, S. R. Jr. *Industr. Engng Chem.* (*Industr.*), 1950, **42**, 850

[17] Scarborough, J. B. *Numerical Mathematical Analysis*, pp 187–190. Johns Hopkins Press: Baltimore, 1930

[18] Bone, W. A., Fraser, R. P. and Wheeler, W. H. *Phil. Trans. A*, 1936, **235**, 29

[19] Kistiakowsky, G. B. *Industr. Engng Chem.* (*Industr.*), 1951, **43**, 2794

[20] Lewis, B. and Friauf, J. B. *J. Amer. chem. Soc.* 1930, **52**, 3905

[21] Berets, D. J., Greene, E. F. and Kistiakowsky, G. B. *J. Amer. chem. Soc.* 1950, **72**, 1080

[22] Laffitte, P. and Dumanois, P. *C. R. Acad. Sci., Paris*, 1926, **183**, 284

Radiation from Explosion Flames of Carbon Monoxide

A. SMEETON LEAH and H. WATSON

It has long been known that chemiluminescence occurs in flame gases, but little information regarding its magnitude or importance has hitherto been available. The two principal contributions appeared to give conflicting views on the subject. That both sets of authors were justified in their conclusions is now elucidated, and the present work shows that chemiluminescence occurs almost entirely before maximum pressure is developed. Details of the elaborate techniques evolved are given; the new spherical explosion vessel is described, and the necessary computational procedures indicated. The nature of the latter render progress slow.

IN a previous paper[1] an attempt was made to carry out a quantitative study of the radiation emitted by explosion flame gases and to measure the separate contributions which could be ascribed to purely thermal radiation and to radiation of chemiluminescent origin. Chemiluminescent radiation was here defined as the radiation emitted by gases not in thermal and chemical equilibrium in excess of that which would be emitted were the gases in perfect equilibrium. Although quite impracticable, the ideal experiment would have been to isolate a quantity of gaseous mixture in space, ignite the whole volume instantaneously and follow the changes of temperature, volume and composition while simultaneously measuring the thermal and chemiluminescent radiation being emitted. As an approximation to this ideal a tubular explosion vessel was used, ignition occurring at one end while the other end was open to atmosphere. The measurements were then confined to the early stages of the explosion while the flame front was still almost spherical in shape. The results proved beyond doubt that the greater part of the radiation emitted during the early stages of combustion is of chemiluminescent origin and confirmed the discovery of W. E. GARNER and F. H. POLLARD[2,3] that water vapour or hydrogen additions to carbon monoxide mixtures greatly reduce the amount of chemiluminescent radiation emitted. Unfortunately, the experiments failed in their main objective of obtaining quantitative estimates of the thermal and chemiluminescent radiation emitted during the whole combustion process. This failure was due to the fact that in carbon monoxide–air and carbon monoxide–oxygen mixtures the reaction zone behind the flame front was found to be at least two inches in depth and consequently, chemiluminescent radiation continued to be emitted after the flame front had lost its sphericity and begun to extend preferentially in the direction of the open end of the explosion tube. At this stage it was decided to abandon the tubular explosion vessel and use a spherical vessel with central ignition instead. This inevitably introduced a complication, namely the rise of pressure during explosion, which had been avoided in the tubular vessel by having the distant end open to atmosphere. On the other hand, no matter how deep the reaction zone may be, it enables quantitative measurements of the thermal and chemiluminescent radiation to be made at all stages of the explosion down to the final cooling period after combustion is complete. The present work gives the results so far obtained with the new spherical explosion vessel.

Actual physical separation of the chemiluminescent radiation from the purely thermal radiation is, of course, impossible since both have their origin in the vibrational excitation of the molecules formed during combustion. It was therefore necessary to calculate from the temperature distribution in the flame gases the rate of normal thermal radiation for each instant from which, by integration, the total thermal radiation which should have been emitted up to any instant could be found. Accurate information on the emissivity of carbon dioxide gas was therefore required to perform the computations. Although H. C. HOTTEL and R. B. EGBERT[1] have published an exhaustive review of extant data on the emissivity of carbon dioxide the values they give for high temperatures are obtained by extrapolation and possibly no great accuracy would be claimed for them. Furthermore, data on the radiation for total pressures exceeding one atmosphere are almost non-existent. Hence, at the outset, a large number of explosions of a carbon monoxide–oxygen mixture containing carbon dioxide as a diluent were carried out over a range of initial pressures and the total radiation emitted together with the pressure variation was found in each case. As the products consist almost entirely of carbon dioxide, it was possible to deduce the emissive power, or the emissivity, and the overall absorption coefficient for carbon dioxide over a sufficiently wide range of temperature and pressure for use in the estimation of the thermal radiation.

Two mixtures were then chosen for the main investigation, namely, (*1*) 25% CO + 0·5% H_2 + 74·5% air and (*2*) a very carefully dried mixture of 25% CO + 75% air.

APPARATUS

A spherical steel explosion vessel of 4 in. internal diameter was built up out of three sections as shown in *Figure 1*. The upper section was fitted with a sensitive diaphragm type optical indicator recording on a rotating drum camera. The middle section was equipped with a slit window of Perspex fitted across a diameter of the sphere and through which the flame movement could be recorded by means of a lens system and the rotating drum camera. In addition, this section had three plug holes to contain the sparking plug giving central ignition, a filling cock for evacuation and filling and an adjustable wire holder. The bottom section was fitted with a fluorite window $1\frac{11}{16}$ in. in diameter and $\frac{11}{32}$ in. in thickness behind which a bolometer was placed for recording the total radiation emitted. The whole vessel could be rotated through 90° so that records of flame movement could be taken across vertical and horizontal diameters in order to allow for the convective rise of the flame in the subsequent calculations.

Ignition of the mixtures was usually effected by a high tension induction coil connected to the spark plug and suitably wired through its primary winding to a contact breaker on the camera drive shaft. This system would not ignite the hydrogen-free mixtures and the discharge from a 4 microfarad condenser charged to about 2 kV had to be used.

The wire holder was for supporting the resistance thermometer elements for deducing the flame gas temperature at any instant and at any radius from the centre of the vessel. The resistance elements consisted of quartz-coated platinum rhodium wires, the quartz covering effectively inhibiting surface catalysis during reaction. The double wire technique described by C. ROUNTHWAITE[2] was used, the overall diameters of the two wires being approximately 0·0005 and 0·001 in. The changes of resistance of the wires during the explosions were recorded by use of an a.c. bridge fed with a 2 kc/s input and recording on one beam of a cathode ray oscilloscope after suitable amplification of the output.

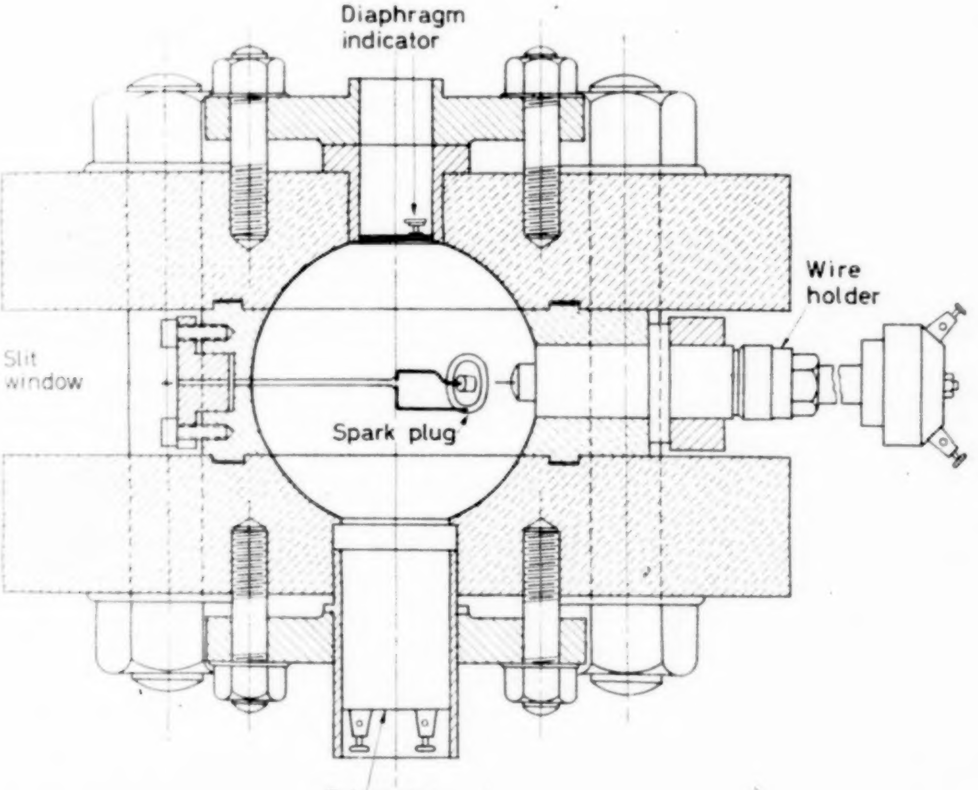

Figure 1. Explosion vessel

The bolometer was of the same general construction as that used in the earlier work[1]. It consisted of about 9 ft of 0·001 in. diameter enamelled copper wire wound non-inductively in the form of a hollow 60° cone and bound together with a minutely thin coating of collodion on its outside surface. The bolometer was mounted in an ebonite holder which fitted behind the fluorite window. Its change of resistance on receiving radiation from flame gases was recorded through a second a.c. bridge and associated amplifiers feeding the second beam of the cathode ray oscilloscope.

The inside surface of the bolometer cone was given a thin film of camphor smoke to reduce reflection of the incident radiation.

CALIBRATIONS

The calibrations of the various instruments used in the work were somewhat involved and space will only permit a brief reference to the methods used. The flame movement was calibrated by photographing an illuminated scale placed across the centre of the vessel in the plane of the slit window. The pressure indicator was calibrated by the dynamic application of known pressures at different temperatures and with different rates of rise of pressure. The resistance coefficient of the quartz-coated wires was found by direct insertion of the wires into a tubular electric furnace giving temperatures up to 1 400°C. The resistance/temperature curve was continued to the fusing point value obtained by observing the resistance as the wire was about to fuse in a trial explosion.

The fluorite window was in fact the same as was used in the earlier experiments[1] when its transmissibility to the carbon dioxide radiation was taken to be 0·94. This value was verified by a further series of tests viewing the radiation from an open flame of carbon monoxide–air with and without the interposition of the fluorite window.

The temperature coefficient of resistance of the bolometer copper wire was determined by winding a sample length non-inductively round the bulb of a very accurate mercury in glass thermometer and immersing this in paraffin contained in a Dewar flask. Measurement of the wire resistance at different paraffin temperatures yielded a resistance coefficient of 0·00427 ohm per ohm °C.

The heat capacity of the bolometer could be estimated from the known weights of copper, enamel and collodion comprising the bolometer but this was not felt to be sufficiently accurate for the present work and direct measurement was undertaken. Briefly, the method adopted was to heat the bolometer electrically by a known d.c. current fed to a d.c. bridge in which the bolometer acted as one arm. A d.c. cathode ray oscilloscope was used in conjunction with the bridge to record the resistance change of the bolometer during heating. At a given instant during the heating, a relay switched the bolometer from the d.c. heating bridge into the a.c. resistance recording bridge which thereafter recorded the change of resistance, and hence temperature, during the cooling. A series of such experiments in which the bolometer was heated to different temperatures made it possible to deduce the law of cooling (this involves the deduction of the ambient air temperature around the bolometer which increases slightly as the bolometer is being heated and cooled) and hence to find the heat capacity of the bolometer. This varied from 0·00171 cal/°C at 28°C to 0·00181 cal/°C at 76°C.

Unfortunately, the law of cooling of the bolometer after electrical heating does not apply exactly during actual irradiation from the explosion flames. This is because the thin film of air between the fluorite window and the ebonite bolometer holder becomes heated during irradiation, the heat flowing from the ebonite surface to the air by conduction, and the expansion of the air then causes a forced convective cooling of the bolometer. The law of cooling applicable during the explosions had therefore to be found by heating the bolometer by radiation through the fluorite window. Full details of the procedure are available[6].

RESULTS

(1) *Explosions of the carbon dioxide diluent mixtures*

A series of explosions of a mixture consisting of 34·64% $CO + 0{\cdot}49\%\ H_2 + 21{\cdot}55\%\ O_2 + 43{\cdot}32\%\ CO_2$ was carried out at initial pressures of 0·2, 0·4, 0·6, 0·8, 1·0 and 1·2 atmosphere and all at approximately 20°C initial temperature. Records of pressure variation and total radiation emitted were taken during each explosion. Assuming that only normal dissociation occurs during the cooling period after reaction is complete and neglecting temperature gradients within the vessel it is now possible to calculate the mean flame gas temperature from the measured pressure at any instant. The dissociation equilibria actually considered were:

$$2CO + O_2 = 2CO_2$$

$$CO + H_2O = CO_2 + H_2$$

$$2OH + H_2 = 2H_2O$$

$$2O = O_2$$

The mean temperatures so obtained together with the corresponding temperature rise of the bolometer corrected for the cooling loss are shown for each pressure in *Figure 2*. From this set of curves it is quite simple to

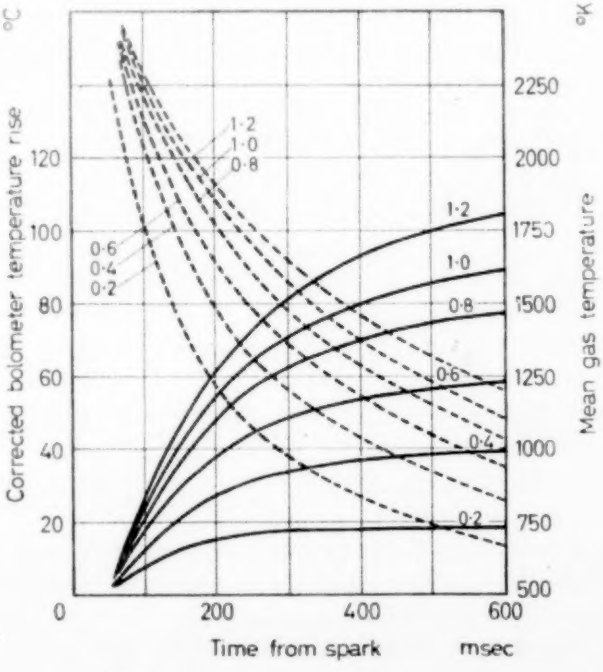

Figure 2. Mean gas temperatures (broken curves) and corresponding corrected bolometer temperature rise (full curves) as functions of time from spark

find the rate of rise of bolometer temperature, $\mathrm{d}T_b/\mathrm{d}t$, for any mean gas temperature at each of the different pressures. From the rates of bolometer temperature rise the rate of heat reception by the bolometer, $\mathrm{d}R_b/\mathrm{d}t$, can be found using the appropriate heat capacity.

It is now necessary to deduce what we have defined as the emissive power of the radiating gas, namely, the rate of radiation from a small element of gas measured per unit mass of gas. The radiation emitted during the cooling period after maximum pressure, when reaction has largely ceased, may be assumed to be of purely thermal origin and to emanate from carbon dioxide alone since the amount of water vapour present is so small. The concentration of the carbon dioxide plus water vapour present is already known from the dissociation analysis. Furthermore, it is required to find the mean absorption coefficient for the radiation emitted in all three wavebands. A somewhat roundabout procedure has to be adopted to effect these deductions. It is first assumed that the flame gases are perfectly transparent to their own radiation. A simple calculation taking into account the geometry of the sphere and the disposition of the fluorite window and bolometer then yields the following relation

$$\mathrm{d}R_b/\mathrm{d}t = 0{\cdot}4692\,\eta A\,\mathrm{d}R_v/\mathrm{d}t$$

where $\mathrm{d}R_b/\mathrm{d}t$ is the rate of radiant heat reception by the bolometer, η is the transmissibility of the fluorite window, A is the projected area of the bolometer and $\mathrm{d}R_v/\mathrm{d}t$ is the emissive power of the gas per unit volume. The values of $\mathrm{d}R_v/\mathrm{d}t$ at different temperatures and pressures can now be found and these may readily be converted into emissive powers per unit mass of gas, $\mathrm{d}R_m/\mathrm{d}t$. Because the amount of carbon dioxide plus water vapour varies with temperature and pressure due to dissociation, a small correction has here been applied to bring the values to a standard concentration of 0·7845 mol per 1 mol of initial mixture, which is the concentration when combustion is complete. Values of $\log \mathrm{d}R_m/\mathrm{d}t$ plotted against $\log T$ [°K] for a range of gas pressures are shown in *Figure 3*. For convenience only, the unit of mass has been taken to be the weight of 1 in³ of the final products of combustion at a standard temperature of 1 700°K and pressure of 3 000 mm of mercury.

It will be immediately apparent that the assumption that the gases are perfectly transparent, or that the absorption coefficient is zero, must be incorrect since the emissive power appears to vary widely with total pressure. A small extrapolation of the values of $\mathrm{d}R_m/\mathrm{d}t$ when plotted against pressure for different temperatures yields the values of $\mathrm{d}R_m/\mathrm{d}t$, subsequently denoted by the symbol q_0, at zero total pressure, and hence, at zero partial pressure of the carbon dioxide. If, however, the emissive power at any fixed partial pressure depends upon the total pressure, q_0 will have different values at other total pressures. Neglecting this possibility for the moment, the mean absorption coefficients may now be found.

The procedure is to revert again to the geometry of the sphere and calculate, for a range of assumed mean absorption coefficients, the rate of radiation received by the bolometer when the gas has an emissive power

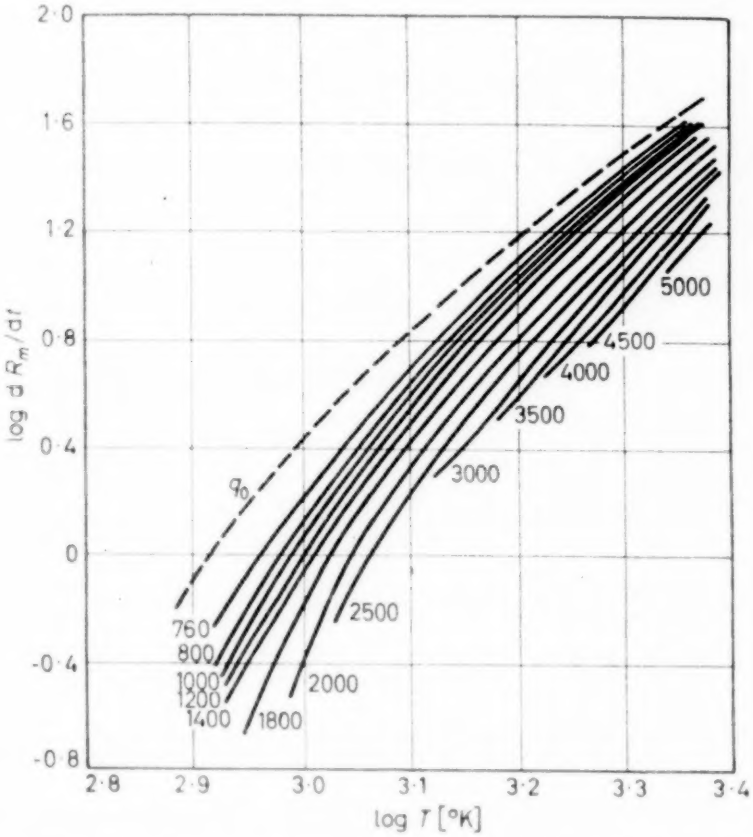

Figure 3. Values of log dR_m/dt *versus* log T *for a range of gas pressures*

$\mathrm{d}R_{\rm c}/\mathrm{d}t$. The calculation involves some rather awkward exponential integrals which, however, finally yield the simple expression

$$\mathrm{d}R_{\rm b}/\mathrm{d}t = C\eta A\,\mathrm{d}R_{\rm c}/\mathrm{d}t$$

where C is the constant calculated for each assumed absorption coefficient. The ratio of C with absorption to the previously determined value of $C = 0{\cdot}4692$ without absorption can therefore be obtained. This ratio must also be the ratio of the emissive power at any pressure p, as given by the curves of ***Figure 3***, to the emissive power at zero pressure q_0, as shown by the broken line in ***Figure 3***. Hence, denoting the ratio as ρ and the emissive power at pressure p by the symbol q, we obtain the relation

$$\log q - \log q_0 = \log \rho$$

The values of q and q_0 from ***Figure 3*** together with the values of ρ then yield the mean absorption coefficients α ft^{-1}, which are shown plotted against total pressure in ***Figure 4***.

The experimental points will be seen nearly to coincide with the straight lines drawn and this would not have been so had the emissive power varied widely with total pressure. It must be admitted, however, that some small increase with total pressure may occur but our data are not sufficiently comprehensive to detect the change. Fortunately, this uncertainty is of little consequence in the later work because the use of the observed emissive powers and mean absorption coefficients in the later explosions tends to cancel out any errors.

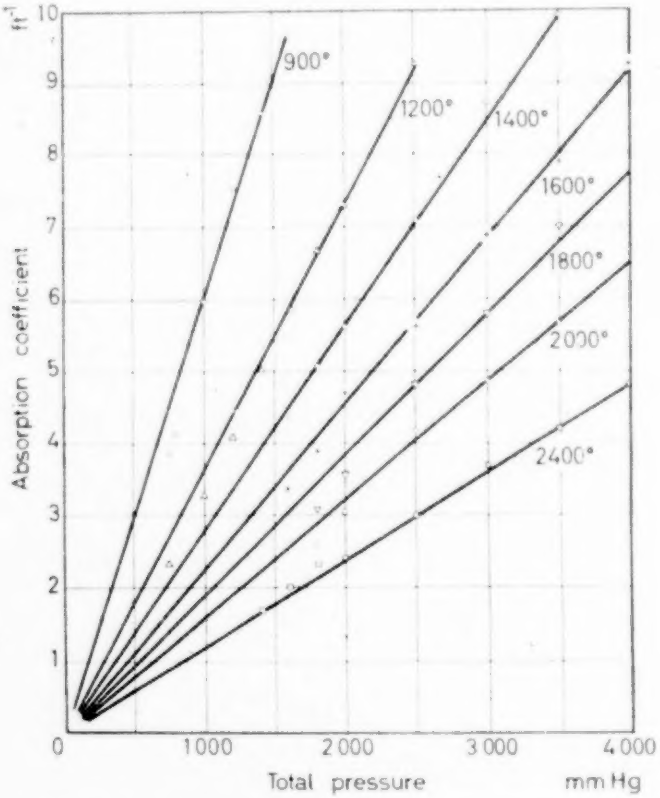

Figure 4. Mean absorption coefficients versus total pressure (temperatures in °K)

The data may be readily expressed in the alternative form of gas emissivities and a few typical values are shown plotted in *Figure 5* which, for comparison, also shows as broken lines the values given by Hottel and Egbert[1]. The product *PL* is the partial pressure of the carbon dioxide times the beam length expressed in ft.atm. The mean value of *PL* with which we are concerned is about 0·9 ft.atm at which value our results agree very closely with those of Hottel and Egbert.

(2) *Explosions of the carbon monoxide–air mixture containing hydrogen*
Series of explosions were now carried out using a mixture of 24·94% CO + 0·52% H_2 + 74·54% air all at an initial pressure of 1 atm and an initial temperature of about 20°C. Measurements of pressure variation, flame spread across both a vertical and a horizontal diameter, bolometer temperature rise and resistance thermometer temperature rise were obtained. With this relatively rapid burning mixture the flame spread was found to be the same in all directions showing that the flame front remained concentric with the vessel and spherical. The average results of a large number of explosions

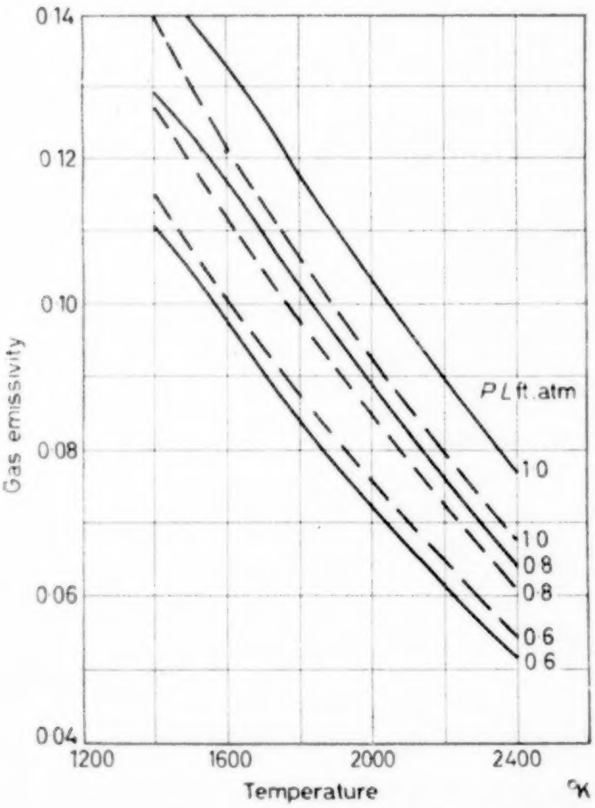

Figure 5. Gas emissivity as a function of temperature

are shown in *Figure 6* and *Figure 7*. In *Figure 6* are given the flame diameter, bolometer temperature rise and pressure rise, this latter being corrected to an initial temperature of exactly 20°C. *Figure 7* shows the flame gas temperature variation, derived from the wire records, for different radii from the centre of the vessel. From these gas temperature curves the temperature gradient curves of *Figure 8* were then constructed. The platinum–rhodium resistance wires, of course, fuse at a temperature of about 1 850°C which corresponds to a rather higher gas temperature. Hence, the temperature gradient curves had to be extended into the high temperature region by assuming the flame gases behind the flame front to be adiabatically compressed through the observed pressure ratios. An interesting check on the accuracy of the temperature gradient curve given for the instant of maximum pressure can be made here. The mean gas temperature from the gradient curve is given by the expression

$$T_{mb} = r^3/3 \int_0^r (x^2/T_b)\,\mathrm{d}x$$

where r is the radius of the vessel and T_b the gas temperature at radius x. This yields a value of $T_{mb} = 2\,456$°K, whereas the value calculated from the observed maximum pressure is 2 450°K.

The data given in *Figures 6* and *8* combined with the emissive powers and mean absorption coefficients given in the previous section now enable the estimation of the normal thermal radiation rates from the flame gases to be

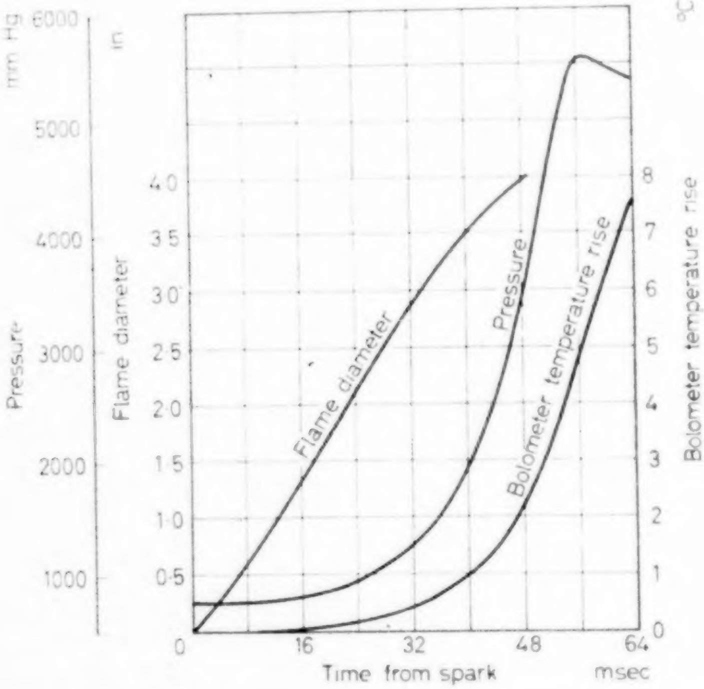

Figure 6. Flame diameter, bolometer temperature rise and pressure rise versus time from spark

made. A difficulty presents itself here, however, because it will be clear that the unburnt gas ahead of the flame contains carbon monoxide which itself can absorb, or emit, radiation and also it is apparent that the flame gases behind the flame front do not contain the final equilibrium concentrations of carbon dioxide and must, therefore, contain some unburnt carbon monoxide. Although some data on the emissivity of carbon monoxide are known, the interaction effects with carbon monoxide are not easy to forecast. Hence, it was decided to carry out the computations on the basis of three different assumptions, namely, (*a*) that the carbon monoxide did not radiate or absorb at all, (*b*) that it radiates and absorbs exactly the same as one

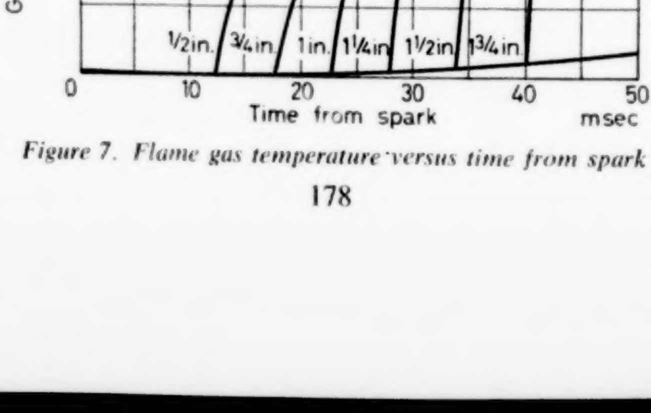

Figure 7. Flame gas temperature versus time from spark

half of its concentration of carbon dioxide and (*c*) that it may be assumed to be carbon dioxide. The concentration of carbon monoxide behind the flame front was estimated by making the assumption that the proportion of carbon dioxide formed at any instant was directly proportional to the temperature rise in the flame at that instant. The actual computations are very laborious involving some hundreds of graphical integrations for each of the eight flame radii considered. Details of the method may be found in the thesis previously mentioned[6]. No temperature gradients could be actually measured with the resistance thermometers after the instant of maximum pressure as the wires have then fused. The radiation computations for times after maximum pressure were, therefore, made assuming a uniform temperature equal to the mean value derived from the observed pressure. The thermal radiation values calculated on the basis of the three assumptions curiously enough gave much the same results and the values using assumption (*b*) have been taken as most nearly representing the truth.

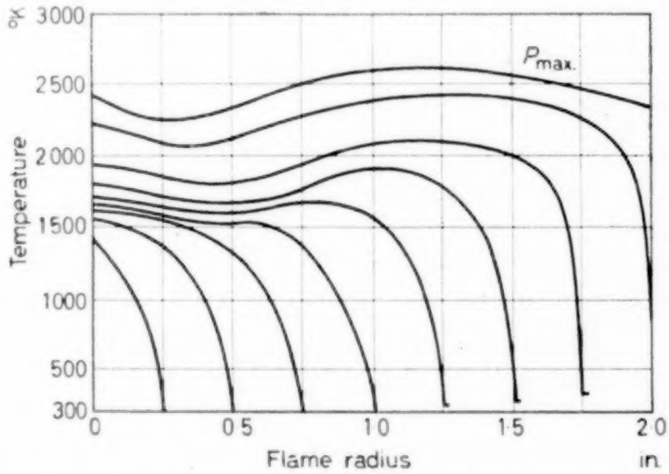

Figure 8. Temperature gradient related to flame radius

The total radiation emitted during the early stages of the flame movement was found with high accuracy by greatly increasing the amplification in the bolometer circuit. As the bolometer could 'see' the whole contents of the explosion vessel it was only necessary to multiply the values of $\mathrm{d}R_b/\mathrm{d}t$ by the ratio of the solid angle of a sphere to that subtended by the bolometer. Here it should be pointed out that internal reflection from the inside surface of the sphere was assumed to be negligible as the surface had been very carefully coated with lampblack prior to the explosions. The measured total radiation, R_t cal, is given in the third column of *Table 1* and in the next column the computed thermal radiation, R_{th} cal, is given for each of a number of time intervals after ignition. The final column shows the difference, $R_t - R_{th}$, which must be ascribed to chemiluminescence. Inspection of *Table 1* shows that in the early stages of the explosion chemiluminescence is the predominant radiation whereas after maximum pressure it becomes an ever smaller proportion of the total for, after maximum pressure, reaction is becoming completed and no further chemically excited molecular vibrations can be expected within the products. The values in *Table 1* also provide an excellent check on the internal accuracy of the radiation computations. Consider the final values at a time of 120 msec; the computed thermal radiation is some 6 per cent less than the measured total radiation. It it be assumed that this defect is due to errors in the emissive power and absorption data then all the values for the computed thermal radiation given in the column should be increased by approximately 6 per cent. But this would still leave about 1·5 cal unaccounted for at maximum pressure and would have no noticeable influence at the small flame radii.

Table 1

Time from spark msec	*Flame radius in.*	*Total radiation R_t cal*	*Thermal radiation R_{th} cal*	*Chemiluminescent radiation R_c cal*
12·48	0·5	0·054	0·00021	0·05379
17·8	0·75	0·153	0·00245	0·15055
22·8	1·0	0·2345	0·00947	0·22503
28·0	1·25	0·455	0·03737	0·4176
33·9	1·50	0·7865	0·14163	0·6449
40·4	1·75	1·581	0·52477	1·0562
49·3	2·0	3·862	2·3821	1·4799
57·4	*Max. press.*	8·160	6·2866	1·8734
60		9·480	8·0541	1·4259
70		14·620	13·1841	1·4359
80		19·175	17·684	1·491
100		27·02	25·374	1·646
120		33·88	31·824	2·056

The radiation values in *Table 1* can be expressed as percentages of the total heat of combustion of the initial mixture and the heat balance drawn up as shown in *Table 2*. Smoothed values of the thermal and chemiluminescent radiations are given in this case. The column headed E_p per cent gives the internal energy rise of the products of combustion, the next column headed E_{ub} per cent gives the internal energy rise of the unburnt gas; the Q_{ub} per cent values are the heats of combustion of the uninflamed gas, while the column headed ME per cent gives the balance by difference and represents the missing energy. The next column gives the amount of energy accounted for by normal dissociation, D per cent, and the final column gives the unaccounted energy, UE per cent. Part of this unaccounted energy is due to the conduction and convection heat loss to the vessel walls which at maximum pressure is probably of the order of 3 per cent. This would leave a final unaccounted energy of about 5 per cent.

(3) *Explosions of the dry carbon monoxide–air mixture*

The experiments described in the previous section were next repeated using a very carefully dried mixture consisting of 25% CO + 75% air. The averaged values of pressure, bolometer temperature rise and flame spread in

Table 2. Heat account: 24·94% $CO + 0{\cdot}52\%\ H_2 + 74{\cdot}54\%$ air explosion, 1 atm initial pressure

Time from spark msec	Flame diameter in.	Based on total heat of combustion								
		R_t %	R_{th} %	R_c %	E_p %	E_{ub} %	Q_{ub} %	ME %	D %	UE %
12·48	1·0	0·01385	0·00005	0·0138	0·093	0·116	99·26	0·5172		
17·8	1·5	0·03912	0·00062	0·0385	0·419	0·261	97·88	1·4009		
22·8	2·0	0·0651	0·0024	0·0627	1·243	0·421	95·03	3·241		
28·0	2·5	0·1164	0·0095	0·1069	2·165	0·950	90·52	6·249		
33·9	3·0	0·2013	0·0362	0·1651	7·32	1·445	82·63	8·404		
40·4	3·5	0·4049	0·1344	0·2705	17·80	1·919	65·43	14·446		
49·3	4·0	0·9889	0·6312	0·3577	67·30	0	0	31·711		
57·4	*Max. press.*	2·079	1·708	0·3710	83·63	0	0	14·291	6·46	7·83
60		2·427	2·054	0·3731	81·75	0	0	15·823	4·67	11·15
70		3·744	3·366	0·3777	75·31	0	0	20·946	2·71	18·24
80		4·910	4·531	0·3791	72·08	0	0	23·010	1·75	21·26
100		6·920	6·540	0·3000	65·43	0	0	27·65	0·76	26·89
120		8·677	8·297	0·3800	59·60	0	0	31·723	0·40	31·32

the vertical and horizontal planes are shown in *Figure 9*. It will be apparent from the curves that the time of explosion is vastly greater than in the previous case. In consequence the convective rise of the flame becomes established long before maximum pressure as is shown by the flame spread in the vertical plane. Indeed, the flame front has not reached the bottom of the vessel at the moment of maximum pressure. The derived temperature distribution curves across a horizontal diameter are shown in

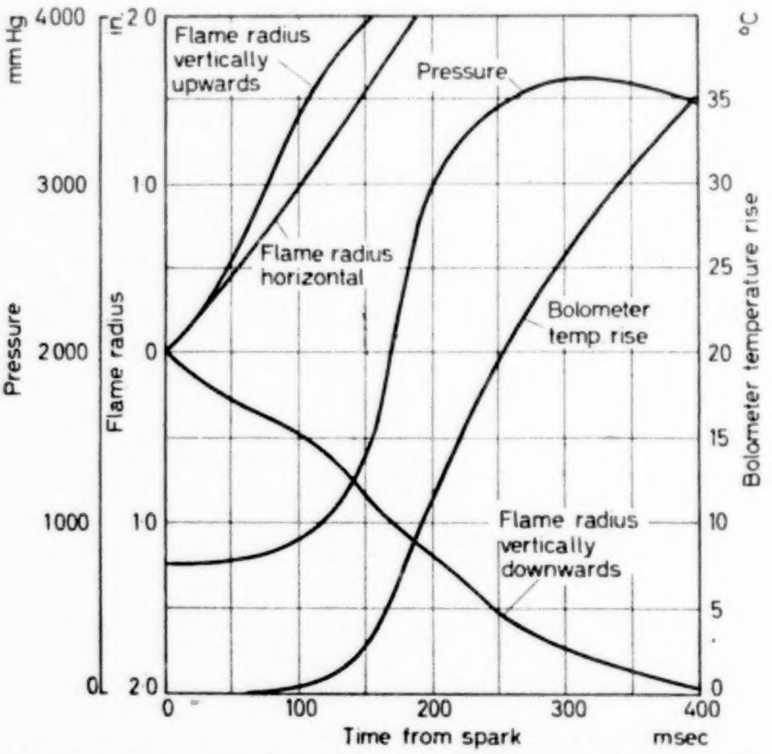

Figure 9. Averaged values of pressure, bolometer temperature rise and flame spread in vertical and horizontal planes versus time from spark

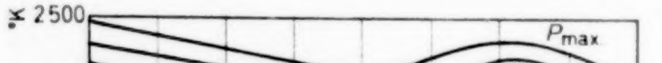

Figure 10. Derived temperature distribution curves across a horizontal diameter as a function of flame radius

Figure 10. Unfortunately, time did not permit the taking of temperature traverses across a vertical diameter but the vertical gradients have been derived by assuming that temperature gradient from the flame front inwards is much the same in all radial directions. The calculation of the mean gas temperature from the gradient curves is somewhat more complex than in the previous experiments but at the instant of maximum pressure the result is found to be 1 613°K. The actual mean temperature deduced from the maximum pressure is 1 595°K which appears to be close enough agreement to justify the gradients assumed.

Table 3

Time from spark msec	*Flame radius in.*	*Total radiation R_t cal*	*Thermal radiation R_{th} cal*	*Chemiluminescent radiation R_c cal*
55·0	0·5	0·1466	0·00248	0·1441
81·0	0·75	0·270	0·02616	0·244
104·5	1·0	0·671	0·0922	0·579
126·5	1·25	1·690	0·2488	1·441
146·0	1·5	3·517	0·6012	2·916
166·5	1·75	7·820	2·0236	5·796
189	2·0	14·580	6·6696	7·910
316	*Max. press.*	46·17	37·055	9·12
325		48·05	38·58	9·47
350		52·70	43·20	9·50
375		56·79	47·43	9·36
400		60·67	51·24	9·43
425		64·15	55·12	9·03
450		67·37	57·78	9·04

The computation of the normal thermal radiation, which now has to take into account the asymmetry of the flame, and the bolometer records yield the values for total, thermal and chemiluminescent radiation given in *Table 3*. The heat account is shown in *Table 4*. It will be at once apparent that the chemiluminescent radiation is much greater than with the hydrogen-containing mixture. Actually, the chemiluminescent radiation appears to decrease slightly after maximum pressure which is, of course, impossible and merely indicates that a relatively small error has occurred in the thermal radiation computations. The percentage values of thermal and chemiluminescent radiation given in *Table 4* are again smoothed values.

The total chemiluminescent radiation emitted from the dry mixture explosion was 2·48 per cent of the heat of combustion whereas the corresponding total from the hydrogen-containing mixture was 0·38 per cent. Thus the dry mixture emitted about 6·5 times as much chemiluminescent radiation as was emitted by the hydrogen-containing mixture, a conclusion which completely confirms the semi-quantitative work of Garner and Pollard[2, 3]. In the early stages of explosion the chemiluminescent radiation emitted per 1 in^3 of mixture inflamed is about 1 cal for the dry mixture and 0·2 cal for the other mixture. The rate per 1 in^3 gradually

Table 4. ***Heat account:*** *dry 25% CO + 75% air explosion, 1 atm initial pressure*

Time from spark msec	*Flame diameter in.*	*Based on total heat of combustion*						
		R_t %	R_{th} %	R_c %	E_p %	E_{ub} %	Q_{ub} %	*ME* %
55	1·0	0·0383	0·0008	0·0375	0·123	0·021	99·452	0·388
81	1·5	0·0703	0·0068	0·0635	0·428	0·189	98·26	0·420
104·5	2·0	0·175	0·024	0·151	1·350	0·426	95·85	2·199
126·5	2·5	0·440	0·065	0·375	3·224	0·81	91·38	4·146
146	3·0	0·916	0·157	0·759	6·505	1·248	84·74	6·591
166·5	3·5	2·04	0·53	1·51	14·45	1·850	71·22	10·34
189	4·0	3·80	1·74	2·06	26·60	2·11	56·03	11·47
200		4·65	2·52	2·13	30·82	2·11	51·52	10·89
225		6·50	4·16	2·34	37·60	1·99	44·20	9·71
250		8·19	5·79	2·40	41·88	1·86	39·22	8·85
275		9·78	7·32	2·46	44·77	1·72	35·25	8·68
300		11·14	8·74	2·40	46·30	1·54	31·37	9·65
316	*Max. press.*	12·03	9·56	2·47	46·56	1·40	28·43	11·59
325		12·52	10·05	2·47	46·47	1·29	26·70	13·02
350		13·73	11·25	2·48	46·88	0·996	20·76	17·73
375		14·29	12·36	2·43	46·55	0·66	13·50	24·50
400		15·81	13·35	2·46	45·88	0·31	6·30	31·70
425		16·71	14·25	2·46	44·27	0	0	39·02
450		17·55	15·05	2·50	42·13	0	0	41·32

diminishes as the flame grows in size until the final averages of 0·28 cal and 0·044 cal are reached. This diminution is no doubt due to the rising pressure increasing the chance of de-activation of the excited molecules by collision.

DISCUSSION

Although it has long been known that chemiluminescence occurs in flame gases, very little information regarding its magnitude or importance has been obtainable. Indeed, the two chief contributions to the study of radiation from explosion flames, namely, those of W. T. **DAVID**[7] and W. E. **GARNER** and F. H. **POLLARD**[2, 3] appear to give conflicting views on the subject. David, using a large cylindrical explosion vessel, concluded that the radiation emitted from the flame gases was almost entirely of thermal origin whereas Garner and Pollard, using a narrow tube in which they claimed that cooling would be so rapid behind the flame front as largely to eliminate thermal radiation, detected chemiluminescence and discovered the remarkable influence of hydrogen and water vapour in carbon monoxide flames. In a previous paper[1] it was shown that Garner and Pollard were certainly correct in their views and now, from the present work, it is clear that David, who could only consider the state of affairs after maximum pressure due to the low frequency response of his recording instruments, was also right in his conclusion.

The present work shows that chemiluminescence occurs almost entirely before maximum pressure and for this reason it is not surprising that H. D. **BAKER** and G. L. **LASERSON**[8] from their radiation experiments on an internal combustion engine cylinder should conclude that: 'evidence of occurrence of chemiluminescent radiation is thus herein lacking' since the bulk of the radiation they measured was of thermal origin and was emitted during the expansion stroke. In other words, looking at the overall picture they had come to the same conclusion as David.

The elaborate techniques involved and the laborious computations needed in this type of work make progress rather slow and it is not surprising that many problems still remain, not least of which is the problem of flames of hydrogen and of hydrogen-bearing compounds.

Department of Mechanical Engineering,
University of Leeds

(*Received October 1958*)

REFERENCES

[1] **LEAH**, A. S., **GODRICH**, J. and **JACK**, H. R. S. 'Radiation and chemiluminescence from explosion flames of carbon monoxide.' *Fuel, Lond.* 1955, **34**, 133

[2] **GARNER**, W. E. 'Radiant energy from flames.' *Industr. Engng Chem.* (*Industr.*), 1928, **20**, 1008

[3] **GARNER**, W. E. and **POLLARD**, F. H. 'The catalytic effect of hydrogen on the carbon monoxide flame.' *J. chem. Soc.* **1935**, 144

[4] **HOTTEL**, H. C. and **EGBERT**, R. B. 'The radiation of furnace gases.' *Trans. Amer. Soc. mech. Engrs*, 1941, **63**, 297

[5] **ROUNTHWAITE**, C. 'Double wire method of resistance thermometry in gaseous explosions.' *Fuel, Lond.* 1955, **34**, 59

[6] WATSON, H. 'A study of the energy liberated in gaseous explosions with particular reference to the thermal and chemiluminescent radiations.' *Ph.D. Thesis*. University of Leeds, 1957

[7] DAVID, W. T. 'Radiation in explosions of coal gas and air.' *Proc. Roy. Soc. A*, 1911, **211**, 375

[8] BAKER, H. D. and LASERSON, G. L. 'An investigation into the importance of chemiluminescent radiation in internal combustion engines.' *Proceedings of the General Discussion on Heat Transfer*. Institution of Mechanical Engineers: London, 1951

Comparative Study of Flame Propagation in Compounds containing Nitrogen Oxides

S. DE JAEGERE and A. VAN TIGGELEN

Flame propagation velocities and temperatures have been measured in methyl nitrite, nitromethane and methane–nitrogen dioxide mixtures with oxygen. Mixtures of methyl nitrite or methane plus nitrogen dioxide with sufficient oxygen behave like more classical fuel–oxidant mixtures. Activation energies and reaction orders with respect to fuel and oxidant have been derived. Very rich methyl nitrite–oxygen flames are to be compared with pure methyl nitrite decomposition flames: their burning velocities are abnormally low. Nitromethane–oxygen flames are characterized by a low activation, but are much slower than what might be expected from the theory.

FLAME propagation in compounds containing oxides of nitrogen and in flammable mixtures of nitric oxide or nitrogen dioxide offers considerable interest not only from a practical point of view but also because some of these flames are characterized by an abnormally low burning velocity although their temperatures are comparatively high. Furthermore, double reaction zones have often been observed which are explained by a two-stage burning of the fuel, the first giving almost exclusively nitric oxide which is further reduced only in the second stage.

Much attention has already been paid to the subject and an abundant literature has been published on nitric oxide or nitrogen dioxide flames[1–10] and on decomposition flames of nitrite and nitrate esters[11–15]. More information on the detailed reaction kinetics in the flame front is still needed before some attempt can be made to correlate all these observations.

The purpose of this paper is to investigate the burning velocities in three kinds of mixtures which can obviously be compared:

(*1*) Methyl nitrite (CH_3ONO): burning velocities on decomposition flames are already available[13]; our measurements concern $CH_3ONO–O_2–N_2$ mixtures.

(*2*) Nitromethane (CH_3NO_2): decomposition flames have not been observed[12]; our experiments were made on $CH_3NO_2–O_2–N_2$ mixtures.

(*3*) Methane–nitrogen dioxide mixtures: the ratio CH_4/NO_2 was kept equal to one whilst varying amounts of oxygen and nitrogen were added to the mixture.

EXPERIMENTAL PART

The experimental procedure will only be mentioned briefly here since most of the techniques have been described in detail in previous publications.

(a) *Measurement of burning velocities and temperatures*

Flame propagation velocities were measured by the classical burner method applied to the schlieren image as described previously[16]. Determination of flame temperatures was made by the sodium line reversal method. In some cases we measured the distance between the schlieren and the visual cone; for multistage flames this distance was taken from the schlieren cone to the last (external) visual cone.

When we had to measure flame temperatures for flames burning in very rich mixtures, a flow of inert gas around and along the flame prevented any afterburning due to the diffusion of air into the primary flame gases. This was done in order to avoid the increase in temperature which would occur from the combustion of primary products in a later stage.

For the mixtures

$$[CH_4 + NO_2]/[CH_4 + NO_2 + O_2] = 0{\cdot}709$$

and

$$[CH_3ONO]/[CH_3ONO + O_2] = 0{\cdot}7$$

this method could not be applied, because the flames in these mixtures were not stable enough to be shielded by an inert gas stream.

(b) *Flow measurements*

Gas flows for methane, nitrogen, oxygen and methyl nitrite were measured by means of rotameters which were calibrated against a standard gas meter. Because of the corrosive properties of nitrogen dioxide the flow of this gas was read on a capillary flowmeter: its calibration was achieved by potassium permanganate titration of the total amount of gas delivered during different times.

In the case of the vapour of nitromethane above 105°C we used the same technique as described previously for hydrazine flames[17].

(c) *Gas supplies*

Nitrogen, oxygen and methane were commercial gases (purity 99 per cent), nitrogen dioxide and nitric oxide were supplied by the Matheson Co. Methyl nitrite was prepared as described by J. A. GRAY and P. W. G. STYLE[18]. Nitromethane: purity 95 per cent (99 per cent nitroparaffin).

EXPERIMENTAL RESULTS

All our results are given in tables where the following data are reported:

Ratio fuel/fuel plus oxygen
Per cent nitrogen
Flame propagation velocity: V_0 cm/s
Flame temperature: T_f °K
Distance between schlieren and visual cone: *s* cm
Burner mouth diameter in cm.

From the burning velocities in mixtures with constant ratio fuel/oxidant but varying dilution, a global apparent activation energy *E* can be derived[19] according to the relation

$$\log V_0 + \tfrac{1}{2}\log T - \tfrac{1}{2}i \log Y = K - 0{\cdot}4343\,E/2RT$$

where *T* represents the mean temperature of the flame front and is given[20] by

$$T = T_0 + 0{\cdot}74\,(T_f - T_0)$$

Y is equal to the concentration of the yet undiluted flammable mixture, viz.

$$Y = \{100 - \%\,[N_2]\}\,/\,100$$

and i is the apparent order minus one of the branching processes[21]; by analogy with most mixtures investigated so far, i will be taken as unity.

(a) *Methyl nitrite flames*

All results are reported in *Table 1*.

Table 1

$\frac{CH_3ONO}{CH_3ONO + O_2}$	% N_2	V_0 *cm/s*	T_f °*K*	T_0 °*K*	*s cm*	*Burner mouth diameter (cm)*
0·289	26·85	101·0	—	292	—	0·3
	28·85	—	2355			
	30·40	91·5	—			
	32·01	87·5	2325			
	33·25	84·7	2307			
	34·80	81·0	2289			
0·328	28·08	107·5	2421	292	0·0200	0·3
	29·12	105·7	—		—	
	32·00	99·0	2399		0·0219	
	35·00	92·6	2375		—	
	36·00	90·0	2365		0·0243	
	37·73	86·4	—		0·0252	
	40·99	76·5	—		0·0271	
0·439	44·80	74·3	2448	292	0·0163	0·5
	48·18	66·5	2416		0·0183	
	50·00	—	2387		—	
	51·50	58·8	2363		0·0201	
	54·50	52·2	—		0·0219	
0·480	45·75	69·5	—	292	0·0124	0·5
	47·00	66·5			0·0132	
	50·50	57·5			0·0152	
	52·10	54·6			0·0180	
0·695	12·32	22·0	2555	292	—	0·5
	18·70	19·8	2520			
	20·60	19·6	2510			
	26·50	18·8	2468			
	35·00	16·6	—			
1·000	00·00	3·20	1373	288	—	2·56
		4·45	1406	321		
		4·60	1418	333		
		4·90	1450	365		
		5·10	1468	378		
		5·40	1488	398		
		6·00	1518	428		
		6·10	1535	445		
		7·00	1573	483		

The following remarks concern the data given on methyl nitrite flames:

(*1*) The visual cone was often so diffuse that measurement of flame front thickness (*s*) became impossible.

(*2*) The nine lowest lines in *Table 1* concern burning velocities of decomposition flames of pure methyl nitrite measured by P. GRAY and M. W. T. PRATT[13]: their measurements were made at different initial temperatures. The flame temperatures for these decomposition flames are estimated from the calculated flame temperature when $T_0 = 20°C$, by simply adding to this last temperature the increase of T_0 with respect to 20°C. This approximation is quite acceptable, since the dissociation of reaction products is unimportant at the low flame temperatures considered here.

For all series of mixtures where the ratio ($CH_3ONO/CH_3ONO + O_2$) is smaller than 0·5 we have plotted ($\log V_0 + \frac{1}{2}\log T - \frac{1}{2}i \log Y$) against $1/T$ (*Figure 1*). The value of the activation energy was found to be 37·5 kcal.

Table 2

$\frac{CH_3NO_2}{CH_3NO_2 + O_2}$	% N_2	V_0 *cm/s*	T_f °K	*s cm*
0·25	10	164·8	2432	0·0098
	15	155·0	2378	0·0103
	20	145·5	2308	0·0108
	25	135·5	2215	0·0113
	30	126·0	—	0·0137
	35	116·0	—	0·0158
	40	107·0	—	0·0177
0·36	20	161·5	2509	0·0050
	25	151·5	2455	0·0082
	30	142·3	2383	0·0112
	35	131·5	2300	0·0136
	40	121·4	2210	0·0157
0·43	20	156·6	2600	0·0080
	25	146·7	2560	0·0101
	30	136·9	2502	0·0122
	35	127·0	2440	0·0146
	40	117·2	2365	0·0168
0·55	20	109·6	2610	0·0152
	25	104·6	2564	0·0168
	30	99·7	2509	0·0183
	35	94·8	2455	0·0197
	40	89·8	2386	0·0208
	45	85·0	2325	0·0216
0·58	20	85·8	2552	0·0191
	25	82·7	2502	0·0204
	30	79·5	2445	0·0220
	35	76·3	2380	0·0250
	40	72·8	2300	0·0268

$T_0 = 292°K$; burner mouth diameter 0·2 cm.

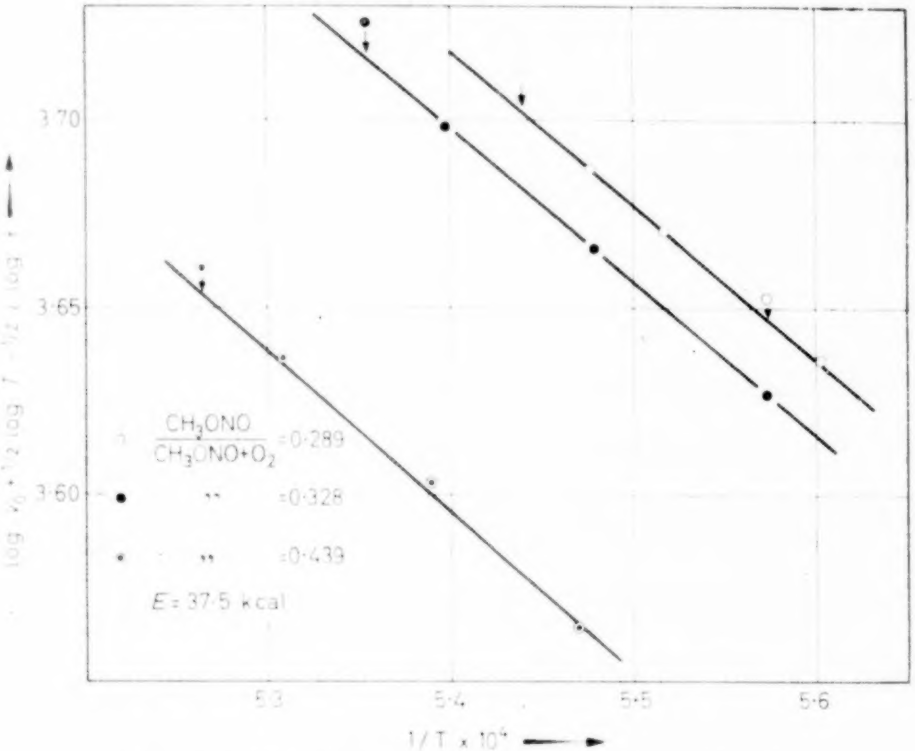

Figure 1. Methyl nitrite–oxygen–nitrogen flames with $i = 1$

When the data obtained for $(CH_3ONO/CH_3ONO + O_2) = 0{\cdot}7$ are plotted on the same graph a smaller value is obtained for the activation energy. It should be mentioned that only for these fuel-rich flames is a double stage flame observed: first a yellow-grey cone followed later by an intense blue zone[22]. The change in flame properties for very rich fuel mixtures will be discussed later.

(b) *Nitromethane flames*

Table 2 contains all results concerning nitromethane–oxygen flames.

In all the flames investigated here a single stage was observed. *Figure 2* represents the plots of $(\log V_0 + \frac{1}{2} \log T - \frac{1}{2} i \log Y)$ against $1/T$; one plot for each ratio of fuel/oxidant. The activation energy derived from these graphs is equal to 15·5 kcal: a slightly smaller value (10 kcal) is obtained for the richest mixtures $(CH_3NO_2/CH_3NO_2 + O_2) > 0{\cdot}5$.

The change in colour[12] from pale red to blue occurs at the same time that the value of E changes from 10 to 15·5 kcal.

(c) *Methane–nitrogen dioxide flames*

Since our experiments were intended for comparison with nitromethane and methyl nitrite, we have only investigated methane–nitrogen dioxide mixtures with a molar ratio equal to unity. The experimental data are given in *Table 3*.

The flame velocities are calculated as usual with regard to cold gases supposing that N_2O_4 would be completely dissociated into NO_2 at ordinary temperatures[1].

Table 3

$\frac{CH_4 + NO_2}{CH_4 + NO_2 + O_2}$	% N_2	V_0 *cm/s*	T_f °*K*	*s cm*	*Burner mouth diameter (cm)*
0·709	35	25·6	2390	—	0·5
	40	23·8	2340		
	45	21·2	2264		
	50	17·5	2180		
	55	13·3	2080		
0·660	44	40·5	2379	0·0475	0·5
	46	37·0	2354	0·0521	
	48	33·8	2321	0·0578	
	50	30·5	2280	0·0650	
	52	27·5	2234	0·0735	
	54	25·0	2192	0·0855	
0·569	48	86·0	2272	—	0·3
	50	78·6	2232		
	52	72·0	2193		
	54	63·5	2143		
	56	56·0	2094		
0·473	50	84·6	2358	—	0·3
	52	74·7	2303		
	54	64·6	2249		
	56	54·5	2193		
	58	44·2	2140		

$T_0 = 292°K$.

The plots of ($\log V_0 + \frac{1}{2} \log T - \frac{1}{2}i \log Y$) against $1/T$ are given in *Figure 3*. The activation energy derived in this manner is equal to 41kcal.

Two zones are observed in these flames on the rich side, for $(CH_4 + NO_2)/(CH_4 + NO_2 + O_2) > 0{\cdot}57$; in this case an orange cone appears below the blue cone which is observed in the leaner mixtures.

INTERPRETATION OF RESULTS

(a) *Normal flames*

Considering the results given in this paper it seems that two groups of mixtures behave like the more classical fuel–oxygen mixtures: the activation energies, 41 kcal for the methane–nitrogen dioxide–oxygen mixtures and 37·5 kcal for the lean methyl nitrite–oxygen mixtures, are such that the observed values of the burning velocities may be compared with the values observed in conventional fuel–oxygen mixtures. This normal behaviour can be shown readily by the extrapolated intercept of the

$$(\log V_0 + \tfrac{1}{2} \log T - \tfrac{1}{2}i \log Y)$$

curve at $(1/T) = 0$ in *Figures 1* and *3*: values of ~5·8 (methyl nitrite) and

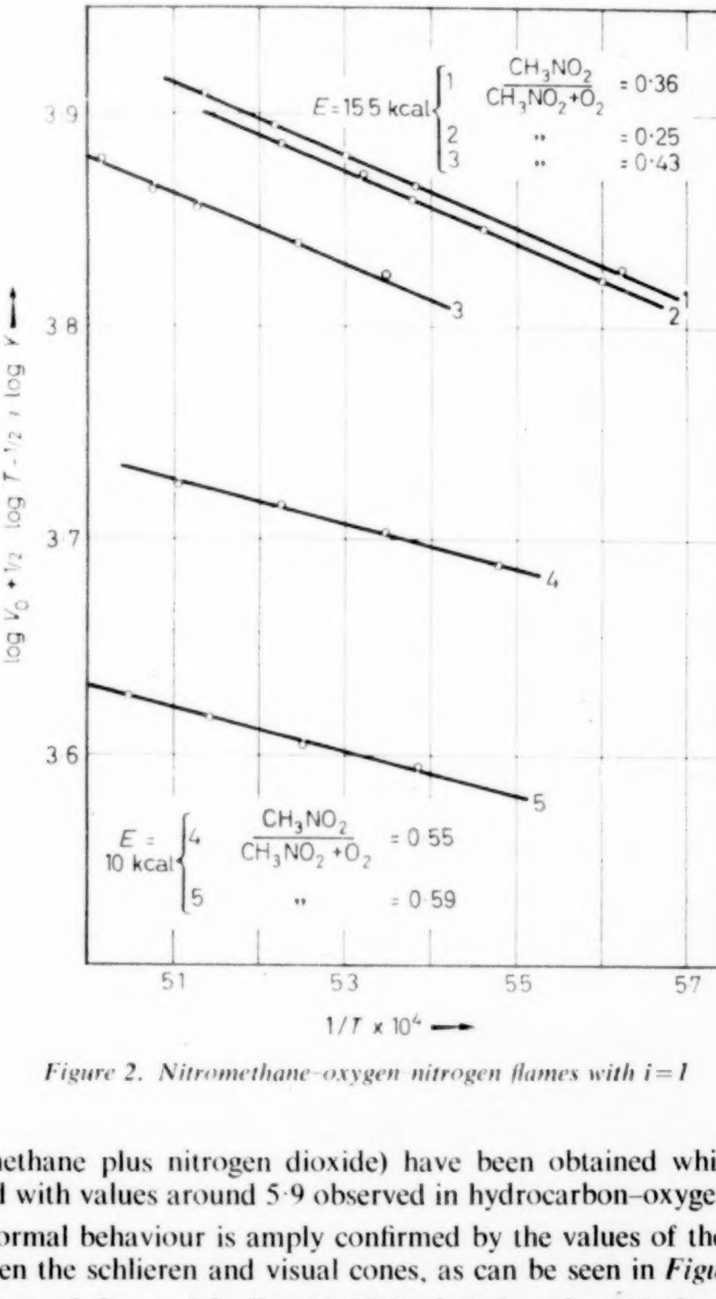

Figure 2. Nitromethane–oxygen–nitrogen flames with i = 1

~ 5·9 (methane plus nitrogen dioxide) have been obtained which can be compared with values around 5·9 observed in hydrocarbon–oxygen flames[19].

This normal behaviour is amply confirmed by the values of the distances (s) between the schlieren and visual cones, as can be seen in ***Figure 4***.

The slope of the straight line $V_0/T^{1/2}$ plotted against $1/s$ has the usual value found for the more conventional flames[16, 23]: it corresponds to a mean molecular weight M of the chain carriers equal to 17.

Considering the fact that the reduction of nitric oxide in flames is a rather difficult process[1–10] it seems quite probable that, in the mixtures discussed here, we are dealing with a normal reaction of the fuel with oxygen (initially present and given by the dissociation of $NO_2 \rightarrow NO + \frac{1}{2}O_2$); most of the nitric oxide acts probably as an inert diluent and does not take part in the reaction.

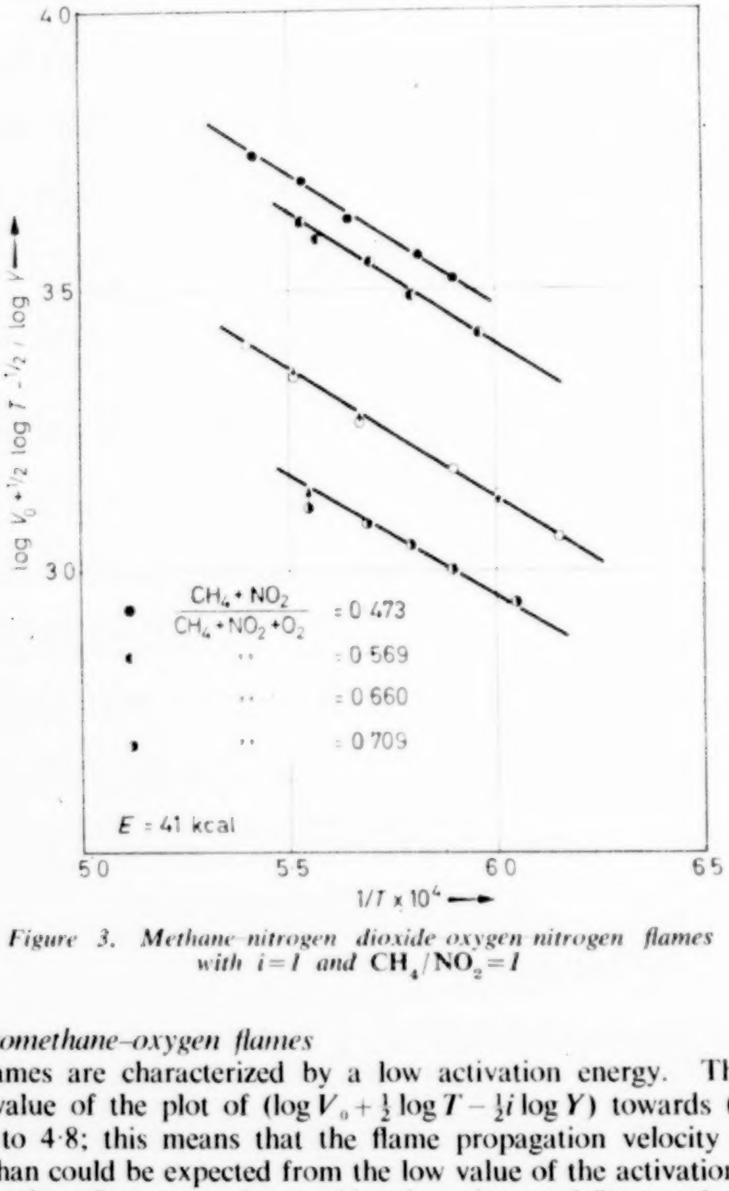

Figure 3. Methane–nitrogen dioxide–oxygen–nitrogen flames with $i=1$ and $CH_4/NO_2=1$

(b) *Nitromethane–oxygen flames*

These flames are characterized by a low activation energy. The extrapolated value of the plot of $(\log V_0 + \frac{1}{2}\log T - \frac{1}{2}i\log Y)$ towards $(1/T)=0$ is equal to 4·8; this means that the flame propagation velocity is much smaller than could be expected from the low value of the activation energy. Therefore these flames may be considered as abnormal flames; the reaction kinetics and the nature of chain carriers are probably very different from those occurring in classical flames. This point of view is further supported by the fact that a different value is also obtained, from the distances between luminous and schlieren images (*Figure 4*), for the mean molecular weight of the chain carriers. Furthermore the temperatures of the nitromethane–oxygen flames differ notably from the temperatures of the corresponding methyl nitrite–oxygen flames at the same dilution. The differences are too large to be explained by the difference between the heats of formation of the two fuel molecules (16·5 kcal for methyl nitrite and 25 kcal for nitromethane). This means of course that the reaction products from the combustion of nitromethane are not the same as those from the combustion of methyl nitrite.

As a consequence the reaction sequences need to be quite different; a possible explanation would be that the nitrogen dioxide molecules, given by the splitting of the C—N bond, have a certain chance to react before their decomposition into the relatively inert nitric oxide molecule. In that case the branching probablity δ of the chains must be a function of the partial pressure of the undissociated nitrogen dioxide in the flame front: this partial pressure being lower than the partial pressures of the initial components, the value of δ becomes smaller than in the usual cases where the branching process occurs through a reaction with one of the initial components.

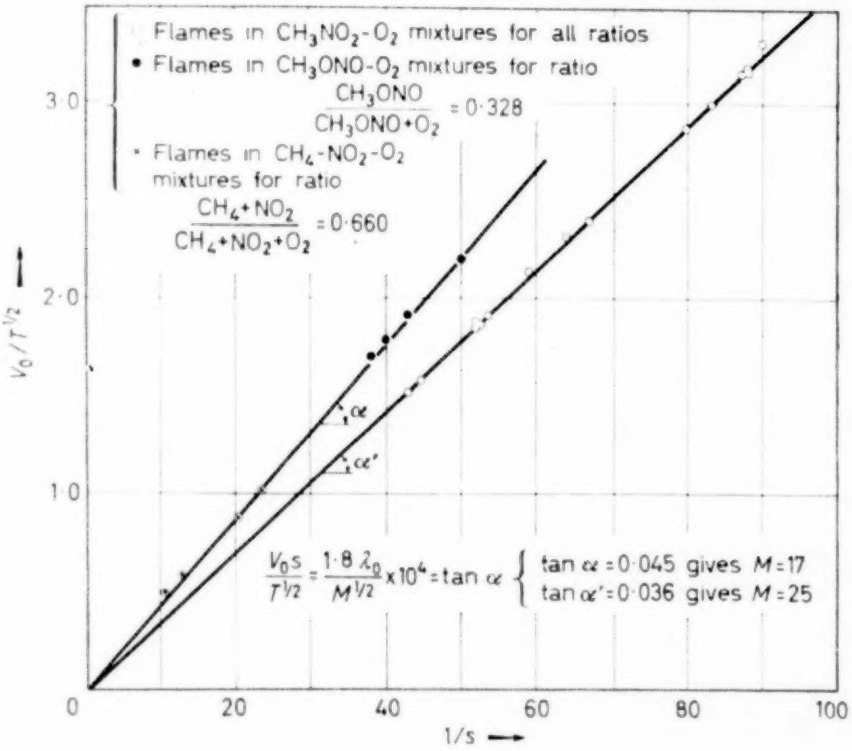

Figure 4. Normal behaviour of all mixtures tested

Any decrease in the value of δ means a decrease of the burning velocity for which the following basic equation has been proposed[21]

$$V_0 = (4T_0/\pi)(2R/3)^{1/2}([\delta-\beta]/MT)^{1/2}$$

where R is the gas constant in ergs, M is the mean molecular weight of the chain carriers, and β = probability of chain termination which may be neglected when the mixture is not too near to the flammability limits.

More knowledge about the reaction is needed in order to give more precision about the value of δ in the above equation. However, sufficient data are available to apply the method described elsewhere[24] for the determination of the apparent partial orders of the branching reaction with respect to nitromethane and oxygen; doing so, the following equation is obtained

$$V_0 = k\,\{([CH_3NO_2]^{0\cdot 36}\,[O_2]^{0\cdot 64}/P)\exp(-15\,500/RT)\}^{1/2}$$

where P = total pressure, and $[CH_3NO_2]$ and $[O_2]$ = the respective partial pressures of the constituents.

It should be mentioned that with the results obtained for the methyl nitrite–oxygen flames, we found only limiting values for the orders: $[CH_3ONO]^{<0\cdot 3}$ and $[O_2]^{>0\cdot 7}$.

(c) *Methyl nitrite decomposition flames*

The data about the decomposition flame of methyl nitrite obtained by Gray and Pratt[13] may be used directly to calculate the activation energy from the plot of $(\log V_0 + \frac{1}{2}\log T - \frac{1}{2}i\log Y)$ against $1/T$. In this case of course $\log Y = 0$ since we are dealing with pure methyl nitrite without addition of any diluent; the points obtained in this manner give the lower part of the straight line in *Figure 5*.

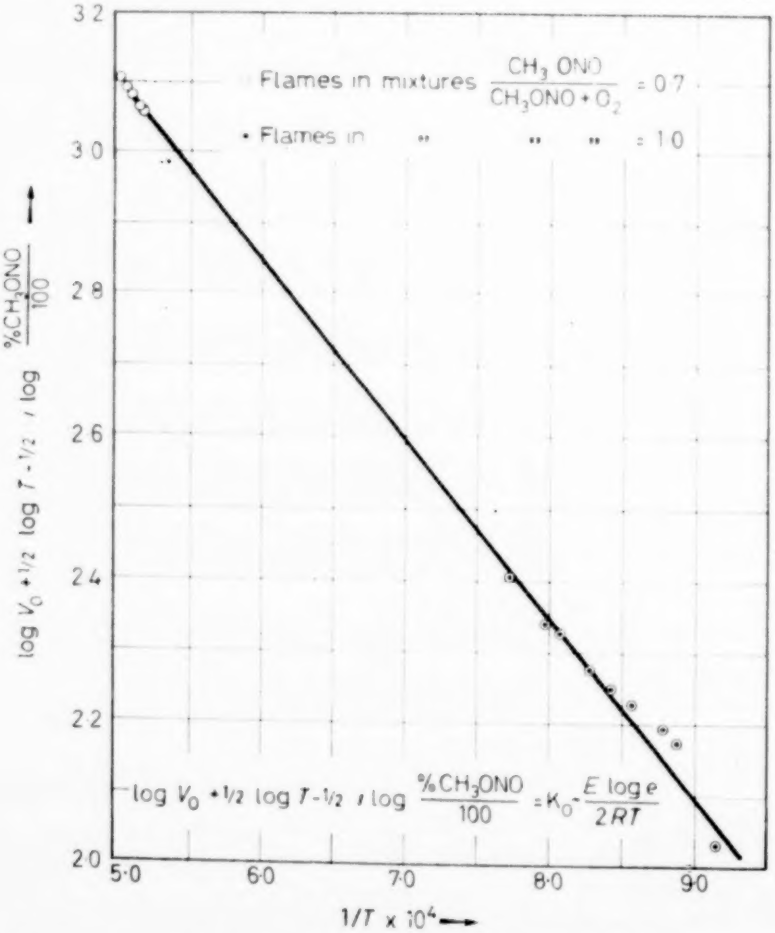

Figure 5. Methyl nitrite decomposition flames with E = 22·6 kcal and i = 1

The activation energy is equal to 22·6 kcal. The same technique was also applied in the study of the hydrazine decomposition flame[17]. There is, however, an important difference between the two cases; for the hydrazine flames the extrapolation (to $1/T=0$) of the straight line gave us a value of 5·8 which agrees well with the theoretical value

$$\log(4T_0/\pi)(2R/3M)=5{\cdot}9\ (\text{with } M=17)$$

With the data on methyl nitrite flames the much smaller value 4·4 is obtained by the same extrapolation.

Most surprisingly we found that our data obtained with very fuel-rich mixtures $(CH_3ONO/CH_3ONO+O_2)=0{\cdot}7$ could be placed on the same graph (upper part of the plot in *Figure 5*) provided they are corrected for the amount of dilution as follows

$$\log V_0+\tfrac{1}{2}\log T-\tfrac{1}{2}i\log(\%\ CH_3ONO/100)$$

This means of course that for very fuel-rich mixtures we are dealing with decomposition flames where the presence of oxygen only increases the flame temperature but does not play an important part in the reaction kinetics. The situation was exactly the same in the combustion flames of hydrazine burning with different oxidizers[17].

A very unexpected observation supports the view that the presence of oxygen in rich methyl nitrite flames does not play an important role in the kinetics: the temperature of the flame in the mixture with composition 25 per cent nitrogen and $(CH_3ONO/CH_3ONO+O_2)=0{\cdot}7$ is higher than in the mixture 25 per cent nitrogen and $(CH_3ONO/CH_3ONO+O_2)=0{\cdot}55$; thereafter the temperature increases again with increasing oxygen content, it reaches a maximum when $(CH_3ONO/CH_3ONO+O_2)=0{\cdot}45$ as can be seen in *Figure 6*. In the upper part of this graph the full curve corresponds to the normal flames discussed under paragraph (a) above; the broken curve concerns the decomposition flames of methyl nitrite. In the lower part of the graph, the burning velocities are plotted against the ratio (CH_3ONO/CH_3ONO+O_2); it can be seen that at the ratio value 0·7, the flame velocity falls rapidly although the temperature has slightly increased. The only explanation of these anomalies is to be found in a profound change of reaction kinetics.

It should also be remembered that a methane–oxygen mixture, with ratio $(CH_4/CH_4+O_2)=0{\cdot}7$, corresponds to a composition which is not between the flammability limits; part of the oxygen, from the oxygen-containing group present in the CH_3ONO molecule, must therefore be used up in the very rich methyl nitrite–oxygen flames discussed here.

The abnormal value of the extrapolated intercept on the ordinate axis (value 4·4) is difficult to explain; it means of course that the burning velocity in methyl nitrite decomposition flames or in very rich methyl nitrite–oxygen flames is given by

$$V_0=\{4T_0/\pi\}\,\{2R/3M\}^{1/2}\,\{([CH_3ONO]/P)\,(\exp[-22\,500/RT]/T)\,(1/100)\}^{1/2}$$

This equation is only empirical and poses the question: why has the branching probability δ to be divided by a factor of one hundred in order to make it agree with the experimental data? We might suggest here again that the branching only occurs in a collision of a chain carrier with some species A which is present only in very small concentration in the flame front: in this case the partial pressure of this species should be equal to about $1/100 = [A]/P$.

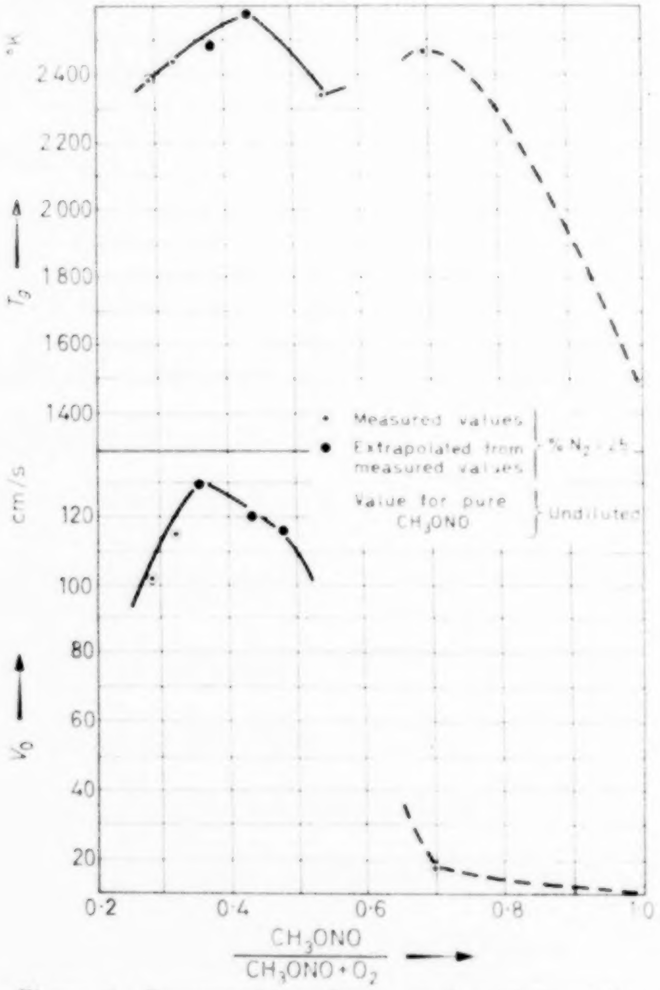

Figure 6. Decomposition flames and methyl nitrite–oxygen–nitrogen flames

CONCLUSIONS

No definite conclusions can be derived from the observations reported here; still more data on the kinetics of the flame reaction are needed. However, a few facts can be pointed out.

It is certain that in the presence of sufficient supplementary oxygen there is nothing out-of-the-way with fuels containing oxides of nitrogen or with nitrogen oxide–fuel mixtures. No inhibition seems to occur and, probably, most of the nitrogen oxide is not reduced and remains amongst the reaction products as an inert component.

When no oxygen is present, or with only small amounts of oxygen, some reactions occur which are completely different (a different activation energy and a different branching process are observed). Comparable fuels like methyl nitrite and nitromethane behave in a completely different manner. Since the primary attack of the fuel molecule must differ because of the differences in binding energies, it can be expected that the chain carriers are also different in these flame reactions: the importance of the nature of chain carriers is therefore shown very pertinently. Most probably the formation of nitric oxide or nitrogen dioxide in some elementary process would not be equivalent even in the presence of oxygen when the equilibrium $2NO + O_2 \rightleftharpoons NO_2$ cannot be established before NO (or NO_2) reacts with some transient species. In order to gain more information concerning this problem, we intend to extend our observations to fuel–nitric oxide and fuel–nitric oxide–oxygen mixtures.

The authors express their thanks to the European Office of the Air Research and Development Command [Contract No. AF61(514)–1245] which has partly sponsored this research and to the Fonds National de la Recherche Scientifique for financial support to the laboratory. One of them (S.D.J.) is also indebted to the I.R.S.I.A. for a postgraduate fellowship.

Laboratory for Inorganic Chemistry,
University of Louvain

(*Received November 1958*)

REFERENCES

[1] PARKER, W. G. and WOLFHARD, H. G. *Fourth Symposium (International) on Combustion*, p 420. Williams and Wilkins: Baltimore, 1953
[2] PARKER, W. G. and WOLFHARD, H. G. *Fifth Symposium (International) on Combustion*, p 718. Reinhold: New York, 1955
[3] ADAMS, G. K., PARKER, W. G. and WOLFHARD, H. G. *Disc. Faraday Soc.* 1953, **14**, 97
[4] ADAMS, G. K. and STOCKS, G. W. *Combustion des Mélanges Gazeux*, p 483. Technip: Paris, 1958
[5] WOLFHARD, H. G. and STRASSER, A. *J. chem. Phys.* 1958, **28**, 172
[6] MYERSON, A. L., TAYLOR, F. R. and FAUNCE, B. G. *Sixth Symposium (International) on Combustion*, p 154. Reinhold: New York, 1957
[7] MILLER, E. and SETZER, H. J. *Sixth Symposium (International) on Combustion*, p 164. Reinhold: New York, 1957
[8] WHARTON, W. W., VIOLETT, T. D. and MILLER, E. *Sixth Symposium (International) on Combustion*, p 173. Reinhold: New York, 1957
[9] WHARTON, W. W. and MILLER, E. *Combustion des Mélanges Gazeux*, p 474. Technip: Paris, 1958
[10] MAKOVKY, A. *Combustion des Mélanges Gazeux*, p 497. Technip: Paris, 1958
[11] ADAMS, G. K. and SCHRIVENER, J. *Fifth Symposium (International) on Combustion*, p 656. Reinhold: New York, 1955
[12] HALL, A. R. and WOLFHARD, H. G. *Sixth Symposium (International) on Combustion*, p 190. Reinhold: New York, 1957
[13] GRAY, P. and PRATT, M. W. T. *Sixth Symposium (International) on Combustion*, p 183. Reinhold: New York, 1957
[14] ARDEN, E. A. and POWLING, J. *Sixth Symposium (International) on Combustion*, p 177. Reinhold: New York, 1957
ARDEN, E. A. and POWLING, J. *Combustion & Flame*, 1958, **2**, 55
[15] POWLING, J. and SMITH, W. A. W. *Combustion & Flame*, 1957, **1**, 308; 1958, **2**, 157
[16] VAN WONTERGHEM, J. and VAN TIGGELEN, A. *Bull. Soc. chim. Belg.* 1954, **63**, 235
[17] DE JAEGERE, S. and VAN TIGGELEN, A. *Combustion des Mélanges Gazeux*, p 451. Technip: Paris, 1958
[18] GRAY, J. A. and STYLE, P. W. G. *Trans. Faraday Soc.* 1952, **48**, 1137

[19] VAN WONTERGHEM, J. and VAN TIGGELEN, A. *Bull. Soc. chim. Belg.* 1955, **64**, 99
[20] VAN TIGGELEN, A. *Mém. Acad. R. Belg. Cl. Sci.* 1952, **27**, 1
[21] VAN TIGGELEN, A. and DECKERS, J. *Sixth Symposium (International) on Combustion*, p 61. Reinhold: New York, 1957
[22] GRAY, P., HALL, A. R. and WOLFHARD, H. G. *Proc. Roy. Soc. A*, 1955, **232**, 389
[23] VAN WONTERGHEM, J., SLOOTMAEKERS, P. J. and VAN TIGGELEN, A. *Bull. Soc. chim. Belg.* 1956, **65**, 899
[24] SLOOTMAEKERS, P. J., DE JAEGERE, S. and VAN TIGGELEN, A. *XXXIme Congrès de Chimie Industrielle, Bruxelles, September 1958*. In press

A Modified Analysis for the Determination of the Burning Velocity of a Gas Mixture in a Spherical Constant Volume Combustion Vessel[*]

K. H. O'DONOVAN and C. J. RALLIS

An analysis, based on that of Lewis and von Elbe, is developed to provide a more accurate means of determining the burning velocity of a gas mixture in a spherical constant volume vessel with central ignition. Th approach is that of deriving an exact equation for the mass fraction burnt at any instant during combustion, valid throughout the combustion period. This involves a consideration of the temperature distribution in the vessel at any instant. The results given require that experimental records of pressure/time and flame radius/time be taken. The development avoids the possibility of magnification of errors of observation. The analysis proposed permits full use to be made of the chief advantage of the constant volume method, viz. that the burning velocity may be found over a large range of pressures in a single explosion. An approximate version of the analysis is also given to allow the burning velocity to be determined over the whole combustion range within reasonably close limits, using either a pressure/time or a radius/time record of combustion only.

THE burning velocity of a particular gas mixture is a constant under given conditions of temperature and pressure. Any experimental method used for its determination should give the same result, provided that the method is reliable. Due to the difficulty of obtaining accurate experimental conditions, and lack of agreement in the precise definition of the position of the flame front, not many results can be accepted without reservation. The data given by different investigators are often at variance and the reason for the discrepancies not explained. J. W. LINNETT and co-workers have made a valuable contribution to the clarification of the position by a critical examination of two methods used to determine burning velocity, viz. the soap bubble (constant pressure) method, and the burner (stationary flame) method, using both direct and schlieren photography[1–4].

Such a systematic comparison does not appear to have been made between the constant volume method and other methods. The reason for this is perhaps due to the limited results available for this case, but it is more likely to be due to a tendency to suspect the method of being inaccurate. The analysis involved is inevitably more complicated than in other methods because of the variation in pressure during the explosion. This necessitates the introduction of simplifying assumptions, and the value of the method rests on the validity of these assumptions and the extent of their influence on the results.

---

[*] University of the Witwatersrand Report No. 1/58. Dewey decimal classification: 536.461.

CONSTANT VOLUME METHOD

Before the constant volume method can be established as suitable for determining burning velocity, it is important first to examine how the analysis may best be effected to ensure sufficient accuracy. The ideal approach is to make such necessary assumptions as can be accepted as reasonable or verifiable by experiment, and to develop the analysis in such a way that the effect of errors, either in observation or interpretation, is reduced to an acceptable minimum.

A method of determining burning velocity from constant volume explosions in a spherical vessel was developed by E. F. FIOCK *et al.*[5]. The equation developed is unwieldy in application and magnifies observational errors. B. LEWIS and G. VON ELBE[6] introduced additional assumptions to give a result more readily applicable and which was not subject to the disadvantage of magnification of errors. However, the range was then limited to the early stages of combustion where the pressure was low, besides being admittedly approximate even within the range utilized.

The analysis developed by these investigators has been included here (in a concise but slightly different form), mainly for purposes of reference, and logical presentation. The limitations of this analysis are discussed, and a modified version is proposed which avoids many of the drawbacks inherent in the original.

ANALYSIS

The combustion process in a spherical combustion vessel involves compression of the unburnt gas ahead of the flame front, expansion within the flame front, and compression of the burnt gas behind it, at any stage of the combustion.

Notation

Suffix b denotes state of burnt gas
Suffix i denotes initial condition of gas before ignition
Suffix u denotes state of unburnt gas
m_b = mass of gas burnt at any instant
m_i = initial mass of unburnt gas
n = mass fraction of gas burnt at any instant
P = pressure at any instant during combustion
P' = pressure when flame is at any given radius
P_a = pressure at end of combustion
P_c = calculated pressure at end of combustion
P_i = initial pressure of unburnt gas
R_b = specific gas constant for burnt gas
R_u = specific gas constant for unburnt gas
r_a = radius of vessel
r_b = radius of flame at any instant during combustion
r_i = radius of burnt gas at any instant under initial conditions
S_u = burning velocity
$\bar{T}_a$ = mean temperature of burnt gas at end of combustion
$\bar{T}_b$ = mean temperature of burnt gas at any instant
T_b = temperature of flame at initial pressure
T'_b = temperature of flame at given radius

$T_{b,p}$ = temperature at centre of vessel at any instant
$T'_{b,p}$ = temperature at given radius at any instant
T'_{u} = temperature rise due to combustion at given radius
T_i = initial temperature of unburnt gas
T_u = temperature of unburnt gas at any instant
T'_u = temperature of unburnt gas at given radius
t = interval of time after ignition for any instant during combustion
v = volume of vessel
v_b = volume of gas burnt at any instant
v_i = volume occupied by burnt gas at any instant under initial conditions
v_u = volume of unburnt gas at any instant
γ_u = ratio of heat capacities of unburnt gas
γ_b = ratio of heat capacities of burnt gas

Assumptions made

Fiock *et al.*[5] listed the assumptions which they made and justified them by the statement that they were consistent with physical observations of the behaviour of the gas mixture during combustion. Lewis and von Elbe[6] made the same assumptions, being satisfied that the error involved in making them was negligible. These assumptions are:

(*1*) The pressure at any instant during combustion is equalized throughout the vessel

(*2*) No heat is lost to the walls of the container during combustion

(*3*) The temperature and pressure of the unburnt gas rise during combustion in accordance with the law of adiabatic compression for perfect gases

(*4*) The flame front remains spherical throughout combustion

(*5*) The flame front is a surface of discontinuity across which the change from the unburnt to the burnt state takes place

(*6*) The ratio of the gaseous specific heats for the unburnt gas remains constant

(*7*) The total mass of gas and the change in the number of molecules remain constant during combustion.

In addition to the above, B. LEWIS and G. VON ELBE[7] made the following assumptions:

(*8*) The temperature and pressure of the burnt gas rise during combustion according to the law of adiabatic compression for perfect gases

(*9*) The ratio of the gaseous specific heats for the burnt gas is constant and equal to the mean value between beginning and end of combustion.

Condition before ignition

The instant of ignition is considered to be the starting point of combustion, i.e. the instant of zero time. The initial unburnt state of the gas mixture is the condition immediately prior to ignition as denoted by the suffix *i*. The initial pressure, temperature and mass of unburnt gas are given by P_i, T_i and m_i respectively. Also

$$\text{initial volume of unburnt gas} = \text{volume of vessel } v = 4\pi r_a^3/3$$
$$= m_i R_u T_i / P_i$$

Condition at time t after ignition

Here the flame front is at radius r_b.

Pressure throughout vessel $= P$

Mass of burnt gas $= m_b$

Mass fraction of total gas burnt $= m_b/m_i = n$

∴ Mass fraction of unburnt gas $= 1 - n$

Mass of unburnt gas, m_u $= m_i(1-n)$

Temperature of unburnt gas, T_u $= T_i(P_i/P)^{(1-\gamma_u)/\gamma_u}$

Volume of unburnt gas, v_u $= 4\pi(r_a^3 - r_b^3)/3$

$= m_i(1-n)R_uT_u/P$

$= v(1-n)(P_i/P)^{1/\gamma_u}$

Volume of burnt gas, v_b $= 4\pi r_b^3/3$

$= v\{1-(1-n)(P_i/P)^{1/\gamma_u}\}$

Therefore flame front radius

$$= r_b = r_a\{1-(1-n)(P_i/P)^{1/\gamma_u}\}^{1/3} \qquad \ldots.[1]$$

Alternatively

$$n = 1 - (1 - r_b^3/r_a^3)(P_i/P)^{1/\gamma_u} \qquad \ldots.[2]$$

Volume occupied by burnt gas under conditions obtaining before ignition

$$v_i = 4\pi r_i^3/3 = m_bR_uT_i/P_i = nv$$

Hence initial radius of burnt gas

$$r_i = r_a n^{1/3} \qquad \ldots.[3]$$

$$\text{i.e.} \quad r_i = r_a\{1-(1-r_b^3/r_a^3)(P/P_i)^{1/\gamma_u}\}^{1/3} \qquad \ldots.[4]$$

Condition at time $(t + \mathrm{d}t)$ after ignition

During the element of time dt, the flame front advances from radius r_b to radius $(r_b + \mathrm{d}r_b)$ with burning velocity S_u. The flame advance may be considered to be made up of two parts, viz. that due to burning of the gas at constant pressure P and that due to mass movement of the flame caused by expansion of the gas at the flame front and adiabatic compression of the unburnt gas ahead of the front.

Increase in volume enclosed by the flame front, $\mathrm{d}v_b$ $= 4\pi r_b^2\,\mathrm{d}r_b$

Also advance of front due to combustion during time dt $= S_u\,\mathrm{d}t$

Therefore volume consumed by flame in time dt $= 4\pi r_b^2 S_u\,\mathrm{d}t$

Volume increase due to compression of unburnt gas $= \mathrm{d}v_u = \mathrm{d}v_b - 4\pi r_b^2 S_u\,\mathrm{d}t$

$= 4\pi r_b^2(\mathrm{d}r_b - S_u\,\mathrm{d}t)$

Now for adiabatic compression of unburnt gas

$$\frac{\mathrm{d}P}{P} = -\gamma_u\frac{\mathrm{d}v_u}{v_u} = -\gamma_u\left\{\frac{-4\pi r_b^2(\mathrm{d}r_b - S_u\,\mathrm{d}t)}{4\pi(r_a^3 - r_b^3)/3}\right\}$$

From which

$$S_u = \left[1 - \left(\frac{r_a^3 - r_b^3}{3r_b^2P\gamma_u}\right)\frac{\mathrm{d}P}{\mathrm{d}r_b}\right]\frac{\mathrm{d}t}{\mathrm{d}r_b} \qquad \ldots.[5]$$

This equation, due to Fiock *et al.*[5], gives the burning velocity of the gas mixture at any stage in the combustion.

Limitations of burning velocity equation

In order to find the value of the burning velocity of a gas mixture using equation 5, the quantities $\mathrm{d}r_b/\mathrm{d}t$, $\mathrm{d}P/\mathrm{d}r_b$, r_b, P, γ_u and r_a must be known.

The value $\mathrm{d}r_b/\mathrm{d}t$ is the rate of change of flame radius with time at any instant during combustion, i.e. the flame speed. It can be found directly from a photographic trace of the flame movement.

The radius r_b is derived from the width of the flame trace at the instant considered. Here an error of observation is possible due to the fact that the precise position of the flame front is not necessarily coincident with the edge of the luminous zone.

The pressure P at any instant is observed from a pressure/time record. This pressure is most conveniently measured at the radius of the vessel and is considered uniform throughout the vessel at the instant.

The value of $\mathrm{d}P/\mathrm{d}r_b$ is derived from the radius/time and pressure/time records and involves the same error of observation as the term r_b.

The chief drawback in using the equation is the fact that the second term in the square brackets is very nearly equal to unity in the early stages of the process. Thus a small error in measuring r_b or P leads to a greatly magnified error in the value deduced for S_u.

Alternative burning velocity equations

To avoid the difficulty of magnification of errors, the burning velocity equation can be rendered in a different form by the following consideration[6].

During the time interval $\mathrm{d}t$ at time t, an elementary mass of gas mixture $\mathrm{d}m$ is burnt. This mass of gas is at a temperature T_u and a pressure P immediately prior to burning, and occupies a volume $\mathrm{d}v_u$ given by

$$\mathrm{d}v_u = \mathrm{d}m\, R_u T_u / P$$

In terms of the initial temperature T_i and pressure P_i the volume would be $\mathrm{d}v_i$ as given by

$$\mathrm{d}v_i = \mathrm{d}m\, R_u T_i / P_i$$

Therefore
$$\mathrm{d}v_u = (P_i/P)\,(T_u/T_i)\,\mathrm{d}v_i$$
$$= (P_i/P)\,(T_u/T_i)\,4\pi r_i^2\,\mathrm{d}r_i$$

Also
$$\mathrm{d}v_u = 4\pi r_b^2 S_u\,\mathrm{d}t$$

Therefore
$$S_u = (\mathrm{d}r_i/\mathrm{d}t)\,(r_i^2/r_b^2)\,(P_i/P)^{1/\gamma_u} \qquad \ldots.[6]$$

This equation is not immediately applied, as the values $\mathrm{d}r_i/\mathrm{d}t$ and r_i must first be determined.

Equation 3 gives the values of r_i in terms of the radius of the vessel and the mass fraction burnt at the time t after ignition. Using this relationship, equation 6 may then be written

$$S_u = \tfrac{1}{3}\,(\mathrm{d}n/\mathrm{d}t)\,(r_a^3/r_b^2)(P_i/P)^{1/\gamma_u} \qquad \ldots.[7]$$

If the value of n as given in equation 2 is differentiated with respect to t and the result inserted in the above equation, the original burning velocity equation 5 is obtained. This process serves no purpose other than to verify equation 7.

The value r_b can be expressed in terms of n, P_i and P, using equation 1, giving

$$S_u = \frac{\frac{1}{3}(\mathrm{d}n/\mathrm{d}t)\, r_a (P_i/P)^{1/\gamma_u}}{\{1-(1-n)(P_i/P)^{1/\gamma_u}\}^{2/3}} \qquad \ldots . [8]$$

The pressures P_i and P are given by the pressure record. The mass fraction n remains to be evaluated in order to solve for burning velocity from equation 8.

DISCUSSION ON EVALUATION OF MASS FRACTION

It is clear that n is a function of the radius r_b and the pressure P at time t, as evidenced by equation 2.

Lewis and von Elbe[6] give the following approximate relation between n and P

$$n = (P - P_i)/(P_e - P_i) \qquad \ldots . [9]$$

Using this relationship, the burning velocity can be computed for a gas mixture from a pressure record of the combustion only. The relationship is approximate because it assumes a linear proportionality between r_b and P. The error involved in this assumption is not large in the early stages of combustion, so that the application of equation 9 must be confined to small values of n.

Since constant pressure is assumed to exist throughout the vessel at any instant, the radius of the flame front, as deduced from the pressure record, does not indicate a particular edge in the flame front, but it gives rather some kind of mean value over the whole reaction zone.

The pressure P_e in equation 9 is taken to be the final pressure at the end of combustion as computed from thermodynamic data, assuming that thermodynamic equilibrium is established in the flame. Consequently the evaluation of P_e is based on the assumption that the temperature distribution in the burnt region is uniform.

It is claimed[8] that the values of n computed from equation 9 are precise for small values of n. This is justified by using the values of n so obtained to derive the values of r_b at different instants during combustion, and comparing these with the corresponding experimental values of r_b. The results given show that in every case the difference was small, being at worst about one per cent of the radius r_b. However, it can be shown that a large variation in the value taken for P_e will not affect the resulting value of r_b to any great extent. For example, even for a five per cent variation of the value of P_e, the resulting calculated radius r_b is, in most cases, still within one per cent of the observed radius in the cases tested. The actual final pressure obtained from the pressure/time trace is well within five per cent of the fictitious pressure P_e, so that it would appear far more convenient to employ the actual pressure, since the final result is within the same limits of accuracy.

The suitability of equation 9 for use in finding burning velocity is somewhat doubtful because, although the error involved may be small in the early stages of combustion in the cases where it has been used, there is no guarantee that this would be so for other gas mixtures, particularly when the rate of combustion is high. If attention is confined to the early stages of combustion, as it must be using this equation, the constant volume method loses its greatest advantage, viz. that the burning velocity of a gas mixture can be found over a large range of pressures in a single explosion. Other methods, particularly the soap bubble method, can then give as much information with far less experimental and analytical difficulty.

It has been shown that equation 7 makes it possible to achieve greater accuracy in the determination of the burning velocity of a flame than can be obtained by using equation 5 in the early stages of combustion, even when employing what is in effect an assumed value of n. Thus, if the fraction n can be evaluated accurately over the whole combustion range, valuable results for burning velocity would be obtained. Experimental records of the variation of pressure, temperature or flame front radius with time are obtainable, so that the fraction n would need to be found in terms of one or more of these parameters. At the same time the original disadvantage of magnification of error must be avoided, which precludes the use of equation 2 for the purpose.

DERIVATION OF MASS FRACTION

The following analysis has for its object a more rigorous derivation of the mass fraction n. The assumptions quoted above are retained, as all of these have been shown by earlier experimenters to be valid. One additional assumption is made here; namely, that the temperature of the burnt gas at any instant is given by the mean temperature throughout the burnt gas volume at that instant. The validity of this assumption is investigated below.

Temperature distribution

An element of gas at the centre of the spherical combustion vessel will be at a pressure P_i and temperature T_i immediately before ignition. This element will be the first to burn after ignition. Therefore the combustion of the element will take place at constant pressure P_i and its temperature will rise to T_b, equal to the flame temperature, during combustion (if the external effect of ignition on the element is negligible). Subsequently, its temperature will be further increased due to adiabatic compression as the flame progresses beyond it, until at time t after ignition it reaches a value T_{bP} corresponding to the pressure P at that instant. A second element of gas remote from the centre is first compressed adiabatically. This element then burns at a constant pressure, higher than P_i, and is subsequently compressed adiabatically until at time t after ignition it reaches a temperature T'_{bP} less than T_{bP}. The process can be illustrated by means of *Figure 1*.

The curves (γ_b) and (γ_u) indicate adiabatic compression of burnt and unburnt gas respectively. The rise in temperature with time during adiabatic compression as the flame progresses is greater for burnt than for unburnt gas. An element at radius r_0 burns to temperature T_b and its temperature is then raised by compression to T_{bP} after time t, giving point A. Elements at radii r_1 and r_2 are compressed as unburnt gas, then burned, and then compressed further as burnt gas during the time interval t, giving the curves 0MNB and 0PQC respectively. An element at r_3 burns at time t after being compressed as unburnt gas, giving the curve 0RD. The temperature rise during burning decreases slightly with increase of combustion pressure, so that $RD < PQ < MN < L0$ and the curve joining LNQD has a slightly smaller slope than curve 0MPR at corresponding points.

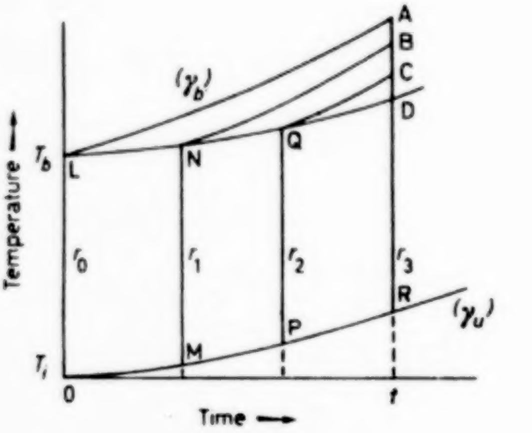

Figure 1

A family of curves of temperature versus radius at time t can thus be plotted using such points as A, B, C and D, for radii r_0, r_1, r_2 and r_3 respectively. In this case t represents the interval of time that has elapsed from the instant of ignition to the instant when the flame front reaches the radius considered. For example, when the flame front reaches the radius r_2, a time t_2 has elapsed since ignition and the temperature gradient throughout the vessel is given by the curve EFGH in *Figure 2*.

The temperature of the burnt gas at the instant t_2 varies from radius r_0 to radius r_2 according to the curve EF. In particular, the curve ABCD gives the temperature gradient in the whole vessel at the instant the flame front reaches the wall (radius r_a).

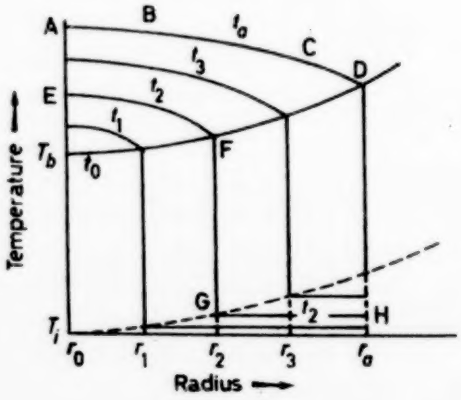

Figure 2

If, in general, curves such as EF are expressed as $T=T(r_b)$, then the mean temperature of the burnt gases at time t is given by

$$\bar{T}_b=(1/r_b)\int_0^{r_b} T(r_b)\,\mathrm{d}r_b \qquad \ldots.[10]$$

At the end of combustion, the mean temperature is

$$\bar{T}_a=(1/r_a)\int_0^{r_a} T(r_b)\,\mathrm{d}r_b$$

A general expression for the temperature gradient in the burnt region at any instant is obtained as follows:

In *Figure 1* the points A, B, C, D, for time t are points on the required curve. Such points are in general arrived at in three stages, viz. (*a*) adiabatic compression of unburnt gas, (*b*) constant pressure temperature rise due to burning, and (*c*) adiabatic compression of burnt gases.

Thus temperature rise, stage (*a*) $=T'_u-T_i$

temperature rise, stage (*b*) $=T'_b-T'_u$

temperature rise, stage (*c*) $=T'_{bP}-T'_b$

where $T'_b=$ temperature at beginning of adiabatic compression of burnt gases (pressure P'), and $T'_{bP}=$ temperature after adiabatic compression of burnt gases to pressure P from pressure P'.

$$\begin{aligned}\text{Total temperature rise} &=(T'_u-T_i)+(T'_b-T'_u)+(T'_{bP}-T'_b)\\ &=T'_{bP}-T_i\\ &=[(P'/P)^{(1-\gamma_b)/\gamma_b}]\,T'_b-T_i\end{aligned}$$

Let $T'_b-T'_u=T'_H$

$=$ temperature rise due to combustion from temperature T'_u

Therefore

$$\text{temperature rise}=(P'/P)^{(1-\gamma_b)/\gamma_b}[T'_H+T_i(P_i/P')^{(1-\gamma_u)/\gamma_u}]-T_i$$

Therefore the temperature at any point on the curve EF (*Figure 2*) is

$$T=(P'/P)^{(1-\gamma_b)/\gamma_b}[T'_H+T_i(P_i/P')^{(1-\gamma_u)/\gamma_u}] \qquad \ldots.[11]$$

The pressure P' is a function of r_b, since it is the pressure at which burning takes place at any particular radius r_b. Hence equation 11 is an expression for the temperature gradient in the burnt region at time t in terms of the radius of the flame front at that instant. T'_H is the temperature rise of the gas when burnt at pressure P'.

Mass equations

The mass of the system as a whole is the same at the end as at the beginning of combustion. Hence

$$m_i=m_a$$

i.e.

$$P_i v/R_u T_i=P_a v_a/R_b\bar{T}_a$$

Also, the volume v at the beginning is the same as the volume v_a at the end of combustion. Therefore

$$T_i/\overline{T}_a = P_i R_b / P_a R_u$$

or

$$(T_i/\overline{T}_b)(\overline{T}_b/\overline{T}_a) = P_i R_b / P_a R_u \qquad \ldots.[12]$$

The ratio n is given by m_b/m_i, i.e.

$$n = (P v_b / R_b \overline{T}_b)/(P_i v / R_u T_i)$$

Therefore

$$n = P\overline{T}_a r_b^3 / P_a \overline{T}_b r_a^3 \qquad \ldots.[13]$$

Now

$$m_i = m_b + m_u$$

i.e.

$$P_i v / R_u T_i = P v_b / R_b \overline{T}_b + P v_u / R_u T_u$$

or

$$P_i r_a^3 / R_u T_i = P r_b^3 / R_b \overline{T}_b + P (r_a^3 - r_b^3) / R_u T_u$$

Hence

$$r_b^3 / r_a^3 = (P_i/PT_i - 1/T_u)/(R_u/R_b\overline{T}_b - 1/T_u) \qquad \ldots.[14]$$

where

$$T_u = (P/P_i)^{(\gamma_u - 1)/\gamma_u} . T_i$$

Substituting equation 14 in 13 gives

$$n = \frac{\overline{T}_a}{\overline{T}_b}\left\{\frac{P - P_i(P/P_i)^{(\gamma_u-1)/\gamma_u}}{P_a - (T_i R_u P_a / R_b \overline{T}_b)(P/P_i)^{(\gamma_u-1)/\gamma_u}}\right\}$$

and when using equation 12

$$n = \frac{\overline{T}_a}{\overline{T}_b}\left\{\frac{P - P_i(P/P_i)^{(\gamma_u-1)/\gamma_u}}{P_a - (\overline{T}_a/\overline{T}_b) P_i (P/P_i)^{(\gamma_u-1)/\gamma_u}}\right\} \qquad \ldots.[15]$$

Comparing equations 15 and 9, it is noted that two additional terms, $\overline{T}_a$ and $\overline{T}_b$, must be evaluated in order to solve for n. Equation 15 has the considerable advantage of being valid for all values of n, as well as being subject to fewer assumptions, thus rendering it more exact.

PROCEDURE FOR DETERMINING BURNING VELOCITY

The solution of the burning velocity of a gas mixture using a constant volume explosion in a spherical vessel is obtained by the application of equations 8, 10, 11 and 15. For convenience, these equations are rewritten below, in the order in which they are to be applied.

$$T = (P'/P)^{(1-\gamma_b)/\gamma_b}[T'_u + T_i(P_i/P')^{(1-\gamma_u)/\gamma_u}] \qquad \ldots.[11]$$

$$\overline{T}_b = 1/r_b \int_0^{r_b} T(r_b)\,\mathrm{d}r_b \qquad \ldots.[10]$$

$$n = \frac{\overline{T}_a}{\overline{T}_b}\left\{\frac{P - P_i(P/P_i)^{(\gamma_u-1)/\gamma_u}}{P_a - (\overline{T}_a/\overline{T}_b)P_i(P/P_i)^{(\gamma_u-1)/\gamma_u}}\right\} \qquad \ldots.[15]$$

$$S_u = \frac{\frac{1}{3}(\mathrm{d}n/\mathrm{d}t)\,r_a\,(P_i/P)^{1/\gamma_u}}{\{1-(1-n)(P_i/P)^{1/\gamma_u}\}^{2/3}} \qquad \ldots.[8]$$

Consider a series of radii r_b taken at equal intervals. The pressure obtaining in the vessel when the flame reaches radius r_b is P' and is given by a correlation of the pressure/time and radius/time traces.

At a particular time t after ignition, the pressure is P throughout the vessel. The temperature at the radii taken are given by equation 11.

The curves of temperature versus radius are plotted for various time intervals between the beginning and end of combustion. The mean temperatures obtaining at these time intervals are most easily found by graphical integration of these curves, the result being a solution of equation 10.

The mass fraction n is evaluated using equation 15 for various pressures corresponding to the time intervals chosen, and plotted against time.

Finally, the burning velocity is computed from equation 8, inserting the corresponding values of $\mathrm{d}n/\mathrm{d}t$, n, P and t as found above.

Observations required

To carry out the procedure outlined above it is necessary to have available sufficient experimental results. The following information is required:

(*a*) Constituents and proportion of gas mixture
(*b*) Initial temperature T_i and pressure P_i immediately before ignition
(*c*) Record of pressure P versus time t throughout combustion
(*d*) Record of flame radius r_b versus time t throughout combustion
(*e*) Radius of spherical vessel.

Thermodynamic constants

In addition to the experimental values enumerated above, it is necessary that γ_u, γ_b, and T'_u be evaluated for each mixture at the particular condition of temperature and pressure.

For a mixture of perfect gases, the mean value of γ is defined by:

$$\gamma = \frac{\Sigma\, x_q C_{pq}}{\Sigma\, x_q C_{vq}} = \frac{\Sigma\, m_q \Delta H_q}{\Sigma\, m_q \Delta E_q} \qquad \ldots.[16]$$

where the suffix q refers to each constituent present, x_q = mole fraction, C_{pq} and C_{vq} = mean molal heat capacities at constant pressure and constant volume respectively, ΔH_q and ΔE_q = change in specific enthalpy and internal energy respectively, and m_q = mass of constituent q present in the mixture. The determination of γ_u presents no difficulties, since the mole fractions of the various constituents are not significantly affected by temperature. Also, the use of a mean value for γ is justifiable, since the temperature changes are relatively small.

For the evaluation of γ_b, it is first necessary to determine $T'_b(=T'_H+T'_u)$. This is done by the simultaneous solution of the two equations—the dissociation and energy equations—for the layer of mass dm, from the given initial conditions of temperature T'_u and pressure P'. From this the composition of the equilibrium mixture at temperature T'_b may be found. During subsequent adiabatic compression of these combustion products, the equilibrium shifts, and alters the mole fraction distribution in a determinable manner. Thus, since all the x_qs are known, and the ΔH_qs and ΔE_qs over the temperature range are available from tables, the mean value of γ_b can be calculated.

SIMPLIFICATION

It is possible to reduce the computational and experimental labour involved in the above analysis by making certain simplifying approximations. These would inevitably lead to somewhat less accurate results. However, this may often be acceptable as a check or, if the differences are insignificant, such approximation may be utilized directly. The only really satisfactory way of validating such approximation is by a sufficient number of experimental comparisons.

General approximation

It seems reasonable to assume that the temperature rise due to combustion (T'_H) is constant, since the actual variation of this quantity is relatively small. This renders equation 11 and hence 10 fairly easily soluble.

Burning velocity using pressure/time records only

The value of the burning velocity at any instant during combustion can be obtained using only equations 15 and 8, if a satisfactory average value for the mean temperature $\bar{T}_b$ is used. The advantage of doing this is that the burning velocity can then be obtained using only a pressure/time record of the combustion. If the ratio of $\bar{T}_a$ to $\bar{T}_b$ in equation 15 is assumed equal to unity, then results of the same order of accuracy as those obtained by Lewis and von Elbe[6] using equation 9 can be expected. This approximate form of equation 15 is equivalent to equation 9 except that it is valid throughout the full range of combustion.

It is possible to improve on this by noting that the ratio $\bar{T}_a/\bar{T}_b$ varies from $\bar{T}_a/T_b$ at the beginning, to unity at the end, of combustion. The values of $\bar{T}_a$ and T_b can be determined by taking a temperature/time record at the centre of the spherical vessel during combustion. The manner in which the ratio varies between $\overline{T}_a/T_b$ and unity can be assumed or further points on the curve plotted by using temperature/time records at various radii in the vessel.

Burning velocity using radius/time records only

Consider the combustion process at any instant when the flame has propagated to a radius r_b. Here

$$m_b+m_u=m_i$$

i.e.

$$\frac{Pr_b^3}{R_bT_b} + \frac{P(r_a^3 - r_b^3)}{R_uT_u} = \frac{P_ir_a^3}{R_uT_i}$$

Substituting for $T_u = T_i(P/P_i)^{(\gamma-1)/\gamma_u}$ and rearranging gives

$$P^{1/\gamma_u} + \left[\frac{r_b^3}{(r_a^3 - r_b^3)} \cdot \frac{R_uT_i}{R_bT_b} \cdot P_i^{(1-\gamma_u)/\gamma_u}\right]P = \frac{r_a^3}{(r_a^3 - r_b^3)} P_i^{1/\gamma_u}$$

i.e.

$$P^{1/\gamma_u} + C_1P = C_2 \qquad \ldots.[17]$$

Here it is apparent that for any set of initial conditions and observed flame radius r_b, C_1 and C_2 can be evaluated provided $\bar{T}_b$ can be determined or estimated.

Values for P at different radii r_b then follow. Use of these results in equation 2 leads to values for n and thus $\mathrm{d}n/\mathrm{d}t$. Substituting in equation 7 then yields the burning velocity.

Alternatively, of course, if both r_b and P are measured, equation 17 can be used to solve for $\bar{T}_b$. The burning velocity can then be determined by using equations 15 and 8.

CONCLUSION

The general analyses outlined above are intended to provide a method of solving for the burning velocity of a gas mixture that is at once accurate and relatively simple. The accuracy is, of course, dependent on the validity of the assumptions made. These assumptions are, in general, the same as those made in the references quoted[5, 6]. The accuracy obtainable by this method is not implicitly greater than that of the previous methods, but the possibility of obtaining satisfactory results is increased by avoiding any magnification of incidental small errors of observation and calibration. The usefulness of the constant volume method of obtaining burning velocities of gas mixtures is in this way extended.

Department of Mechanical Engineering,
University of the Witwatersrand,
Johannesburg, S. Africa

(*Received September 1958*)

REFERENCES

[1] LINNETT, J. W. and HOARE, M. F. 'Burning velocity determinations, Part III. Burning velocities of ethylene–air–carbon dioxide mixtures.' *Trans. Faraday Soc.* 1951, **47,** 179

[2] LINNETT, J. W., PICKERING, H. S. and WHEATLEY, P. J. 'Burning velocity determinations, Part IV. The soap bubble method of determining burning velocities.' *Trans. Faraday Soc.* 1951, **47,** 981

[3] CONAN, H. R. and LINNETT, J. W. 'Burning velocity determinations, Part V. The use of schlieren photography in determining burning velocities by the burner method.' *Trans. Faraday Soc.* 1951, **47,** 981

[4] PICKERING, H. S. and LINNETT, J. W. 'Burning velocity determinations, Part VI. The use of schlieren photography in determining burning velocities by the soap bubble method.' *Trans. Faraday Soc.* 1951, **47,** 989

[5] Fiock, E. F., Marvin, C. F., Caldwell, F. R. and Roeder, C. H. 'Flame speeds and energy considerations for explosions in a spherical bomb.' *Nat. Adv. Comm. Aero., Wash., Rep. No. 682* (1940)

[6] Lewis, B. and von Elbe, G. *Combustion, Flames and Explosions of Gases*, p 448 ff. Academic Press: New York, 1951

[7] Lewis, B. and von Elbe, G. *Combustion, Flames and Explosions of Gases*, p 651 ff. Academic Press: New York, 1951

[8] Manton, J., von Elbe, G. and Lewis, B. 'Burning velocity measurements in a spherical vessel with central ignition.' *Fourth Symposium (International) on Combustion*, p 358. Williams and Wilkins: Baltimore, 1953

Spray Combustion Theory

F. A. WILLIAMS*

The coupled steady-state equations of motion of a statistical ensemble of spherical droplets and a coexisting multicomponent reacting gaseous continuum are derived under the assumption that the induced random fluctuations in the properties of the fluid are negligible. These equations are reduced to a form appropriate for describing the one-dimensional flow of a fluid containing a spray which is stationary with respect to the gas. The burning-rate eigenvalue problem for one-dimensional heterogeneous combustion processes of the type $A \rightarrow nB$ *is formulated, and an analysis for sprays composed of uniform droplets illustrates the properties of the eigenvalue. An approximate analytical solution for the burning velocity is shown to be in numerical agreement with experiments on tetralin.*

THE statistical description of an ensemble of droplets composing a spray has previously been developed and applied to situations in which the spray produces a negligible effect upon the gaseous medium in which it is embedded[1]. Since the interaction of the spray with the encompassing fluid is often of primary importance in practical spray combustion problems, it is of interest to develop theoretical methods for treating the coupled equations of motion of the fluid and the spray. We first present the steady-state form of these coupled equations for the limiting case of dilute sprays. Since it is often important to include droplets of different chemical compositions (e.g. fuel and oxidizer droplets in rocket chambers), the equations are presented in a form which allows for an arbitrary number of sprays. The special form of these governing equations which applies to one-dimensional flow processes is analysed in detail for the case in which the relative motion of droplets and fluid is negligible.

It has been demonstrated experimentally[2] that, for sprays composed of sufficiently large droplets ($\sim 20\,\mu$), the value of the one-dimensional laminar burning velocity changes, presumably because a heterogeneous burning mechanism replaces the homogeneous chemical reaction as the rate-controlling process. In an effort to determine theoretically this heterogeneous burning velocity, the one-dimensional flame problem is formulated for the case of a single heterogeneous reaction of the type $A \rightarrow nB$ by employing the spray equations derived below. It is demonstrated that the burning velocity appears as an eigenvalue in the solution of an integro-differential equation. For the case in which the droplets in the spray are initially uniform in size, the integro-differential equation is reduced to an ordinary differential equation, and an approximate analytical solution for the eigenvalue is obtained. The theoretical burning velocity is shown to agree in many respects with the experimentally observed[2] burning rate of tetralin sprays.

LIST OF SYMBOLS

A	Stream tube cross sectional area
a	A parameter defined in equation 61

---

*Present address: Harvard University, Cambridge, Massachusetts.

b	A parameter defined in equation 62
c_p	Specific heat capacity at constant pressure for the gas
$c_{p,l}$	Specific heat capacity at constant pressure for the liquid
$\mathbf{F}$	Droplet acceleration vector (force per unit mass)
F	The x component of $\mathbf{F}$
f	Number of droplets per unit range of radius, velocity and volume
G	Number of droplets per unit range of radius and volume
g	A function defined in equation 45
$\mathscr{H}$	A constant defined in equation 38
H	A constant of integration in the energy equation [see equation 26]
h	Specific enthalpy of the gas
h_j	Enthalpy added to the gas per unit mass of vaporizing material
h_l	Specific enthalpy of the liquid
L	Latent heat of vaporization per unit mass
$\mathscr{M}$	Mass flow rate per unit area [see equation 27]
M	Total number of different kinds of droplets
m	Total mass flow rate [see equation 14]
N	Total number of chemical components in the gas
n	Number of droplets per unit volume
$\mathfrak{P}$	Pressure tensor
p	Hydrostatic pressure
Q	Standard heat of reaction [see equation 35]
Q'	Effective heat of reaction defined in equation 37
$\mathbf{q}$	Heat flux vector
q	The x component of $\mathbf{q}$
R	Time rate of increase of the radius of a droplet
R^0	Universal gas constant
R'	Gas constant per unit mass
r	Droplet radius
T	Gas temperature
T_l	Liquid temperature
$\mathfrak{U}$	Unit tensor
$\mathbf{U}$	Diffusion velocity
U	The x component of $\mathbf{U}$
$\mathbf{u}$	The (mass-average) gas velocity
u	The x component of $\mathbf{u}$
$\mathbf{v}$	Velocity of a droplet
v	The x component of $\mathbf{v}$
W	Molecular weight
X	Size-independent factor in the droplet evaporation rate [see equation 41]
$\mathbf{x}$	Spatial position vector
x	Coordinate in the flow direction
Y	Mass fraction of a component of the gas
Z	Mass fraction of the gas
Z_j	Mass fraction of droplets of type j
α	A parameter defined in equation 58
β	A parameter defined in equation 59
γ	A parameter defined in equation 60
δ	Width of the reaction zone
ε_{kj}	Mass of species k added to the gas per unit mass of vaporizing material
ζ	Normalized reaction progress variable defined in equation 47

Λ	Dimensionless burning velocity eigenvalue [see equation 64]
λ	Thermal conductivity of the gas
μ	A variable defined in equation 44
ρ	Density
τ	Shear stress tensor
τ	Dimensionless temperature defined in equation 46
τ_{xx}	The x—x component of τ
ϕ	A function defined in equation 69
Ψ	A function defined in equation 67
ψ	A function defined in equation 68
ω	Mass rate of production of a gaseous constituent by homogeneous reactions

Subscripts

f	Gaseous fluid
g	Gas
j	A type of droplet
k	A chemical species
l	Liquid
n	An order of approximation
0	At the cold boundary ($x=-\infty$)
s	Spray
∞	At the hot boundary ($x=+\infty$)

DERIVATION OF GOVERNING EQUATIONS

In the absence of droplet collisions and sources of droplets, the steady-state equation of motion of a statistical ensemble of particles of type j in a gaseous medium has been shown to be[1]

$$\frac{\partial}{\partial r}(R_j f_j)+\nabla_x\cdot(\mathbf{v}f_j)+\nabla_v\cdot(\mathbf{F}_j f_j)=0 \qquad j=1,\ldots,M \qquad \ldots.[1]$$

where the subscript j identifies the chemical composition of the droplet and the other symbols are defined in ref. 1 and in the list of symbols. Equation 1 is coupled with the hydrodynamical equations of motion of the gas through the variables R_j and F_j which depend upon the local properties of the fluid. If the spray is sufficiently dilute, then the statistical fluctuations in the gas properties induced by the spray are negligible and accurate average fluid flow variables can be defined. The motion of the gas is then governed by the ordinary fluid mechanical equations with boundary conditions determined by average spray properties.

If ρ_f is the density of the fluid and $\mathbf{u}$ is the (mass-average) gas velocity, the overall continuity equation for the fluid becomes

$$\nabla_x\cdot(\rho_f\mathbf{u})=-\sum_{j=1}^{M}\int\int\rho_{l,j}\,4\pi r^2 R_j f_j\,\mathrm{d}r\,\mathrm{d}\mathbf{v} \qquad \ldots.[2]$$

where $\rho_{l,j}$ represents the specific gravity of the liquid in the droplets of the j^{th} type. The source term on the RHS of equation 2, which accounts for the mass added to the gas by the evaporating droplets, is an expression of the appropriate boundary conditions on the continuity equation at the surfaces of the droplets. Since the density ρ_f is related to the actual mass of fluid per unit volume of space available to the gas ρ_g through the equation

$$\rho_f/\rho_g = 1 - \sum_{j=1}^{M} \int\int \tfrac{4}{3}\pi r^3 f_j \, \mathrm{d}r \, \mathrm{d}\mathbf{v}$$

the assumption of a dilate spray enables us to use the relation $\rho_g \approx \rho_f$.

The conservation of mass of chemical species k is expressed by the relation

$$\nabla_x \cdot [\rho_f (\mathbf{u} + \mathbf{U}_k) Y_k] = \omega_k - \sum_{j=1}^{M} \int\int \rho_{L,j} 4\pi r^2 R_j \varepsilon_{kj} f_j \, \mathrm{d}r \, \mathrm{d}\mathbf{v} \qquad k = 1, \ldots, N \quad \ldots . [3]$$

where Y_k represents the mass fraction of species k in the gas, $\mathbf{U}_k$ equals the diffusion velocity of species k, and ω_k is the mass rate of production of component k by homogeneous gaseous chemical reactions. Here ε_{kj} is the (radial) mass flux fraction of component k flowing to the gas from the edge of the surface layer of droplets of type j. If heterogeneous chemical reactions occur in the neighbourhood of droplets of type j, then ε_{kj} may not be equal to the flux fraction of component k evaporating from the droplet surface. In such cases ε_{kj} is determined by the overall stoichiometry of the reaction in the surface layer surrounding each droplet and by the chemical composition of the liquid in the droplet.

If the force exerted upon the fluid by the spray is taken into account, then the equation for the conservation of momentum of the gas is found to be

$$\rho_f \mathbf{u} \cdot \nabla_x \mathbf{u} = -\nabla_x \cdot \mathfrak{P} - \sum_{j=1}^{M} \int\int \rho_{L,j} \tfrac{4}{3}\pi r^3 \mathbf{F}_j f_j \, \mathrm{d}r \, \mathrm{d}\mathbf{v} \quad \ldots . [4]$$

Here the pressure tensor $\mathfrak{P}$ is related to the hydrostatic pressure p and the viscous stress tensor τ through the expression[3]

$$\mathfrak{P} = p\mathbb{U} + \tau$$

where $\mathbb{U}$ is the unit tensor.

The equation for the conservation of energy of the gas can be written in the form

$$\nabla_x \cdot [\rho_f \mathbf{u} (h + \tfrac{1}{2}u^2)] = -\nabla_x \cdot \mathbf{q} - \nabla_x \cdot (\tau \cdot \mathbf{u})$$
$$- \sum_{j=1}^{M} \int\int \rho_{L,j} \tfrac{4}{3}\pi r^3 \mathbf{F}_j \cdot \mathbf{v} f_j \, \mathrm{d}r \, \mathrm{d}\mathbf{v} - \sum_{j=1}^{M} \int\int \rho_{L,j} 4\pi r^2 R_j (h_j + \tfrac{1}{2}u^2) f_j \, \mathrm{d}r \, \mathrm{d}\mathbf{v} \quad \ldots . [5]$$

where $\mathbf{q}$ is the heat flux vector[3], h is the total specific enthalpy of the fluid and h_j represents the total enthalpy added to the gas by a droplet of type j during the evaporation of a unit mass of liquid. The last two terms in equation 5 account for the work done on the fluid by the spray and the energy added to the fluid by the spray. The value of h_j is determined by the processes occurring in the droplet surface layer.

The governing conservation equations [1 to 5 inclusive] must be supplemented by the ideal gas equation of state

$$p = \rho_f R^0 T \sum_{k=1}^{N} (Y_k / W_k) \quad \ldots . [6]$$

where R^0 is the universal gas constant, T signifies the gas temperature, and W_k is the molecular weight of species k. A set of $M+N+4$ integro-differential equations are thus obtained for the $M+N+4$ unknowns f_j, Y_k, ρ_f, **u**, h and p. Although the precise solution of many practical problems will require the simultaneous consideration of all of these equations employing methods previously described[1], many essential features of the results can be obtained from analysis of the simplified set given in the following section.

SIMPLIFIED ONE-DIMENSIONAL FLOW EQUATIONS

Let us consider the one-dimensional form of equations 1 to 5 for the case of small droplets and fluid velocity gradients. For these systems the droplet acceleration is rapid enough to allow the velocity difference $v-u$ to be neglected. Elementary estimates of the corresponding maximum permissible droplet size indicate that this assumption will often be valid throughout much of the chamber of high-performance rocket combustors, for example. By letting the relation

$$f_j = G_j\delta(\mathbf{v}-\mathbf{u}) \qquad j=1,\ldots,M \qquad \ldots.[7]$$

define the size distribution functions $G_j(r,\mathbf{x})$, equation 1 can be integrated over all velocity coordinates and the spatial coordinates y and z to obtain

$$\frac{\partial}{\partial r}(R_jG_j)+\frac{1}{A}\frac{\partial}{\partial x}(uG_jA)=0 \qquad j=1,\ldots,M \qquad \ldots.[8]$$

in the one-dimensional case. Here $\delta(\mathbf{v}-\mathbf{u})$ is the (three-dimensional) Dirac delta function, A equals the local cross sectional area of the stream tube and u is the x component of the velocity **u**, of which the other two components vanish.

The integral over **v** in equation 2 can now be performed with the result that

$$\frac{1}{A}\frac{\mathrm{d}}{\mathrm{d}x}(\rho_f uA)=-\sum_{j=1}^{M}\int_0^{\infty}\rho_{l,j}4\pi r^2R_jG_j\,\mathrm{d}r \qquad \ldots.[9]$$

and equation 3 similarly becomes

$$\frac{1}{A}\frac{\mathrm{d}}{\mathrm{d}x}[\rho_f(u+U_k)Y_kA]=\omega_k-\sum_{j=1}^{M}\int_0^{\infty}\rho_{l,j}4\pi r^2R_j\varepsilon_{kj}G_j\,\mathrm{d}r \qquad k=1,\ldots,N\ \ldots[10]$$

If the mass density of the spray is defined as

$$\rho_s=\sum_{j=1}^{M}\int_0^{\infty}\rho_{l,j}\tfrac{4}{3}\pi r^3G_j\,\mathrm{d}r \qquad \ldots.[11]$$

then by multiplying equation 8 by $(\rho_{l,j}\frac{4}{3}\pi r^3)$, integrating over r, and summing over j it is found that

$$\frac{1}{A}\frac{\mathrm{d}}{\mathrm{d}x}(\rho_s uA)=\sum_{j=1}^{M}\int_0^{\infty}\rho_{l,j}4\pi r^2R_jG_j\,\mathrm{d}r \qquad \ldots.[12]$$

From equations 9 and 12 it is seen that the total mass per unit volume

$$\rho=\rho_f+\rho_s \qquad \ldots.[13]$$

obeys the continuity equation

$$\left.\begin{aligned} \frac{\mathrm{d}}{\mathrm{d}x}(\rho u A) &= 0 \\ \rho u A = m &= \text{constant} \end{aligned}\right\} \qquad \ldots [14]$$

Upon defining the mass fraction of fluid as

$$Z \equiv \rho_l/\rho = 1 - (\rho_s/\rho) \qquad \ldots [15]$$

and the mass fraction of droplets of type j as

$$Z_j \equiv \frac{1}{\rho} \int_0^\infty \rho_{l,j} \tfrac{4}{3}\pi r^3 G_j \,\mathrm{d}r \qquad j = 1, \ldots, M \qquad \ldots [16]$$

it is found from equations 8, 9 and 14 that the relation

$$\frac{\mathrm{d}Z}{\mathrm{d}x} = -\frac{A}{m} \sum_{j=1}^{M} \int_0^\infty \rho_{l,j} 4\pi r^2 R_j G_j \,\mathrm{d}r = -\sum_{j=1}^{M} \frac{\mathrm{d}Z_j}{\mathrm{d}x} \qquad \ldots [17]$$

determines the overall spray evaporation rate, where

$$\frac{\mathrm{d}Z_j}{\mathrm{d}x} = \frac{A}{m} \int_0^\infty \rho_{l,j} 4\pi r^2 R_j G_j \,\mathrm{d}r \qquad j = 1, \ldots, M \qquad \ldots [18]$$

When ε_{kj} is independent of r, equations 10, 14, 15 and 18 imply that the rate of production of gaseous species k is given by the expression

$$\frac{\mathrm{d}}{\mathrm{d}x}\left[Z\left(1 + \frac{U_k}{u}\right) Y_k\right] = \frac{A\omega_k}{m} - \sum_{j=1}^{M} \varepsilon_{kj} \frac{\mathrm{d}Z_j}{\mathrm{d}x} \qquad k = 1, \ldots, N \qquad \ldots [19]$$

Here the first term on the right represents homogeneous chemical reactions and the second term accounts for heterogeneous processes.

The simplified form of the momentum equation can be deduced by multiplying equation 1 by $(\rho_{l,j} \frac{4}{3}\pi r^3 \mathbf{v})$, integrating over r and $\mathbf{v}$, and summing over j. After integrations by parts it is found that in the one-dimensional case

$$\sum_{j=1}^{M} \int\int \rho_{l,j} \tfrac{4}{3}\pi r^3 F_j f_j \,\mathrm{d}r \,\mathrm{d}\mathbf{v} = \frac{1}{A}\frac{\mathrm{d}}{\mathrm{d}x}\left(A \sum_{j=1}^{M} \int\int \rho_{l,j} \tfrac{4}{3}\pi r^3 v^2 f_j \,\mathrm{d}r \,\mathrm{d}\mathbf{v}\right)$$
$$- \sum_{j=1}^{M} \int\int \rho_{l,j} 4\pi r^2 R_j v f_j \,\mathrm{d}r \,\mathrm{d}\mathbf{v}$$

By substituting equation 7 into this relation and using equations 11 and 12, it is seen that

$$\sum_{j=1}^{M} \int\int \rho_{l,j} \tfrac{4}{3}\pi r^3 F_j f_j \,\mathrm{d}r \,\mathrm{d}\mathbf{v} = \rho_s u \frac{\mathrm{d}u}{\mathrm{d}x} \qquad \ldots [20]$$

When equation 20 is substituted into the one-dimensional form of equation 4, then the momentum equation is found to be

$$\rho u \frac{\mathrm{d}u}{\mathrm{d}x} = -\frac{\mathrm{d}p}{\mathrm{d}x} - \frac{\mathrm{d}\tau_{xx}}{\mathrm{d}x} \qquad \ldots .[21]$$

where the subscripts on τ identify the x—x component of the shear stress tensor.

If equation 1 is multiplied by $(\rho_{l,j}\frac{4}{3}\pi r^3 v^2)$ and a procedure analogous to that used in deriving equation 20 is completed, then the relation

$$\sum_{j=1}^{M} \int\int \rho_{l,j}\tfrac{4}{3}\pi r^3 \mathbf{F}_j \cdot \mathbf{v} f_j \,\mathrm{d}r\,\mathrm{d}\mathbf{v} = \rho_s u \frac{\mathrm{d}}{\mathrm{d}x}(\tfrac{1}{2}u^2) \qquad \ldots .[22]$$

is obtained for one-dimensional flow. By using equations 12, 14, 15, 18 and 22 in the one-dimensional form of equation 5, it is seen that the energy equation becomes

$$\frac{\mathrm{d}}{\mathrm{d}x}(Zh + \tfrac{1}{2}u^2) = -\frac{1}{m}\frac{\mathrm{d}}{\mathrm{d}x}(Aq) - \frac{1}{m}\frac{\mathrm{d}}{\mathrm{d}x}(A\tau_{xx}u) - \sum_{j=1}^{M} h_j \frac{\mathrm{d}Z_j}{\mathrm{d}x} \qquad \ldots .[23]$$

where q is the x component of $\mathbf{q}$ and h_j has been assumed to be independent of r. Equations 8, 14, 19, 21 and 23 constitute the required simplified one-dimensional conservation equations.

Actually a first integral of equation 23 can be obtained for the common cases in which there is no production of total (thermal plus chemical) enthalpy in the droplet surface layers. For such systems, if the total specific enthalpies of the liquid in the droplets $h_{l,j}$ are assumed to be independent of r, then the rate of increase of total enthalpy of a droplet of type j and radius r is given by

$$\begin{aligned} \rho_{l,j} 4\pi r^2 R_j h_j &= \frac{\mathrm{d}}{\mathrm{d}t}(\rho_{l,j}\tfrac{4}{3}\pi r^3 h_{l,j}) \\ &= \rho_{l,j}\tfrac{4}{3}\pi r^3 u \frac{\mathrm{d}h_{l,j}}{\mathrm{d}x} + \rho_{l,j} 4\pi r^2 R_j h_{l,j} \qquad \ldots .[24] \end{aligned}$$

where the identity $\mathrm{d}/\mathrm{d}t = u\partial/\partial x + R_j\partial/\partial r$ has been employed. When equation 24 is multiplied by G_j, integrated over all values of r, and summed over j, it is found that

$$\sum_{j=1}^{M} h_j \frac{\mathrm{d}Z_j}{\mathrm{d}x} = \sum_{j=1}^{M} Z_j \frac{\mathrm{d}h_{l,j}}{\mathrm{d}x} + \sum_{j=1}^{M} h_{l,j}\frac{\mathrm{d}Z_j}{\mathrm{d}x} = \sum_{j=1}^{M} \frac{\mathrm{d}}{\mathrm{d}x}(Z_j h_{l,j}) \qquad \ldots .[25]$$

where use has been made of equations 16 and 18. By substituting equation 25 into equation 23 and integrating, we obtain the desired form of the energy equation, viz.

$$Zh + \sum_{j=1}^{M} Z_j h_{l,j} + \tfrac{1}{2}u^2 + \frac{Aq}{m} + \frac{A\tau_{xx}u}{m} = H = \text{constant} \qquad \ldots .[26]$$

A similar reduction can be effected in equation 19 when there are no chemical reactions in the droplet surface layer (ε_{kj} = constant throughout the surface layer); however, heterogeneous reactions are of primary interest in the following sections.

FORMULATION OF THE HETEROGENEOUS BURNING-VELOCITY EIGENVALUE PROBLEM

As an application of the equations derived above we shall consider the heterogeneous burning-velocity eigenvalue problem for a reaction of the type A $\rightarrow$ nB (i.e. $M=1$, $N=1$ and the gas is of uniform composition). In this case the stream-tube area A is assumed to be constant, viscous stresses are neglected ($\tau_{xx}=0$), the Mach number is assumed to be small ($\frac{1}{2}u^2 \ll h$ and $p=$ constant), and no homogeneous gas-phase reactions occur ($\omega_k=0$). In view of the approximation $\mathbf{v}=\mathbf{u}$, we are constructing the analogue of a thermal laminar flame theory.

From equations 14, 26 and 6, it is seen that the governing equations now become

$$\rho u = m/A \equiv \mathcal{M} = \text{constant} \qquad \ldots.[27]$$

$$(q/\mathcal{M}) + Zh + (1-Z)\,h_l = H = \text{constant} \qquad \ldots.[28]$$

and

$$p = Z\rho R'T = \text{constant} \qquad \ldots.[29]$$

where according to equations 17 and 8, Z is determined by the relation

$$\mathrm{d}Z/\mathrm{d}x = -\int_0^\infty \rho_l\, 4\pi r^2 RG\,\mathrm{d}r/\mathcal{M} \qquad \ldots.[30]$$

in which G is obtained from the expression

$$\frac{\partial}{\partial r}(RG) + \frac{\partial}{\partial x}(uG) = 0 \qquad \ldots.[31]$$

Since the droplets are all of the same type ($M=1$), summations over j do not appear in these equations. The identity $Z_1 = 1 - Z$, which follows from equations 11, 15 and 16 when $M=1$, has been used in equation 28. The subscripts j are unnecessary here and have been omitted from equations 27 to 31 inclusive. Since $N=1$, equation 19 is trivially satisfied and need not be included in the governing set of equations. In equation 29 the specific gas constant R' has been defined as $R' = R^0/W_1$ and use has been made of equation 15. The momentum equation does not appear in these governing relations because of the assumption of low Mach number.

If the dependence of R upon r and the fluid properties, the values of ρ_l and h_l, and the thermodynamic coefficients for the gas are given, then, since h is a function of T and the gas composition, the five unknown variables in the equations 27 to 31 are ρ, u, T, Z and G. The cold boundary values at $x=-\infty$, viz. ρ_0, u_0, T_0, Z_0 and $G_0(r)$, are all specified. In addition, the adiabatic requirements that $q=0$ at $x=\pm\infty$ and the chemical equilibrium condition $Z=1$ at $x=\infty$ must be imposed. This leads us mathematically to suspect that solutions may exist only for certain characteristic values of a parameter, which according to physical considerations is the burning rate eigenvalue $\mathcal{M}$.

In equation 28 the heat flux q is given by[3]

$$q = -\lambda\,\mathrm{d}T/\mathrm{d}x \qquad \ldots.[32]$$

where λ is the thermal conductivity of the gas, which we shall assume to be constant. The specific enthalpy of the fluid h is related to the temperature through the equation

$$h = h^0 + c_p(T - T^0) \qquad \ldots.[33]$$

in which h^0 is the standard specific enthalpy of formation of the gas at temperature T^0 and c_p equals the (constant) specific heat at constant pressure for the fluid. The enthalpy of the liquid is similarly given by the expression

$$h_l = h_l^0 + c_{p,l}(T_l - T^0) \qquad \ldots.[34]$$

where h_l^0 is the standard enthalpy of formation of the liquid and $c_{p,l}$ represents the (constant) specific heat of the liquid which is at a temperature T_l. After a flame has developed in the surface layer of the droplet, T_l remains very nearly constant and within a few degrees of the boiling temperature of the liquid. We shall therefore assume that T_l is constant everywhere, recognizing that this is not an acceptable approximation when the initial liquid temperature is excessively low. It will also be assumed that $T_0 = T_l$, a condition which is necessary if a quasi-equilibrium state is to exist at the cold boundary. The standard (gaseous) heat of reaction is defined as

$$Q = h_l^0 - h^0 + L \qquad \ldots.[35]$$

where L is the heat of vaporization of the liquid. In view of equations 32 to 35 inclusive, the energy equation [equation 28] may be written in the form

$$Zc_pT - ZQ' - \frac{\lambda}{\mathscr{M}}\frac{\mathrm{d}T}{\mathrm{d}x} = \mathscr{H} = \text{constant} \qquad \ldots.[36]$$

where the effective (constant) heat of heterogeneous reaction is

$$Q' \equiv Q - L + c_{p,l}T_l + (c_p - c_{p,l})\,T^0 \qquad \ldots.[37]$$

and

$$\mathscr{H} \equiv H - h_l^0 - c_{p,l}(T_l - T^0) \qquad \ldots.[38]$$

The cold boundary condition $\mathrm{d}T/\mathrm{d}x = 0$ at $T = T_l$ and $Z = Z_0$ implies that

$$\mathscr{H} = Z_0(c_pT_l - Q') \qquad \ldots.[39]$$

while the requirement that $\mathrm{d}T/\mathrm{d}x = 0$ and $Z = 1$ at $x = +\infty$ shows that the temperature at the hot boundary, which equals the adiabatic flame temperature for the heterogeneous system, is

$$T_\infty = (\mathscr{H} + Q')/c_p \qquad \ldots.[40]$$

For most evaporation and heterogeneous combustion processes, the dependence of the rate R upon r is determined by the relation

$$R = -X/r \qquad \ldots.[41]$$

where the function X is independent of droplet size. For the heterogeneous reaction $A \rightarrow nB$, in which the liquid constituent A evaporates from the droplet and reacts in the gaseous phase to form the product B, an accurate theoretical expression for X, which agrees with single-droplet experiments at large activation energies, is[4]

$$X = \frac{4\lambda}{\rho_l c_p}\left[\frac{T-T_l}{T-T_l+(L/c_p)}\right] \qquad \ldots.[42]$$

Since $X = 0$ at $x = -\infty$ according to equation 42, the familiar cold-boundary difficulty of laminar flame theories, which may be accentuated in the heterogeneous case because of the relatively weak dependence of X upon T, is avoided in the present problem*.

From equation 41, the solution to equation 31 with the boundary condition $G = G_0(r)$ at $x = -\infty$ is easily seen to be[1]

$$G = \frac{u_0}{u}\frac{r}{\mu}G_0(\mu) \qquad \ldots.[43]$$

where

$$\mu \equiv \left(r^2 + 2\int_{-\infty}^{x}\frac{X}{u}\,\mathrm{d}x\right)^{1/2} \qquad \ldots.[44]$$

Equation 30 may therefore be written as

$$\frac{\mathrm{d}Z}{\mathrm{d}x} = \frac{4\pi\rho_l u_0}{\mathscr{M}}\frac{X}{u}\int_0^{\infty}\frac{r^2}{\mu}G_0(\mu)\,\mathrm{d}r = \frac{4\pi\rho_l u_0}{\mathscr{M}}\frac{X}{u}\,g\left(\int_{-\infty}^{x}\frac{X}{u}\,\mathrm{d}x\right) \qquad \ldots.[45]$$

where the function $g[\int_{-\infty}^{x}(X/u)\,\mathrm{d}x]$ is determined by the droplet size distribution at the cold boundary. Equation 31 is thus eliminated from the governing set of relations at the expense of complicating the form of the integro-differential expression, equation 30.

Since equations 27 and 29 are algebraic, the problem has now been reduced to that of finding the solution of one differential equation and one integro-differential equation. It is useful to introduce the normalized dimensionless variables

$$\tau \equiv (T-T_l)/(T_\infty - T_l) \qquad \ldots.[46]$$

and

$$\zeta \equiv (Z-Z_0)/(1-Z_0) \qquad \ldots.[47]$$

From equations 27, 29, 36 and 45 it is seen that after we obtain the solution to the equations

$$\frac{\mathrm{d}\zeta}{\mathrm{d}x} = \left[\frac{4\pi\rho_l p}{\rho_0 R'\mathscr{M}(1-Z_0)}\right]\frac{Xg}{[Z_0+(1-Z_0)\zeta][T_l+(T_\infty-T_l)\tau]} \qquad \ldots.[48]$$

and

$$\frac{\mathrm{d}\tau}{\mathrm{d}x} = \frac{\mathscr{M}}{\lambda(T_\infty - T_l)}\{[Z_0+(1-Z_0)\zeta][c_p T_l - Q' + c_p(T_\infty - T_l)\tau] - \mathscr{H}\} \qquad \ldots.[49]$$

---

*In view of the processes occurring in spray combustion, it is reasonable to remedy the cold-boundary difficulty by an ignition temperature concept as in the corresponding homogeneous laminar flame problem.

with the boundary conditions $\tau=\zeta=0$ at $x=-\infty$ and $\tau=\zeta=1$ at $x=+\infty$, ρ and u are determined by the equation

$$u=\frac{\mathscr{M}}{\rho}=\frac{\mathscr{M}R'}{p}\left[Z_0+(1-Z_0)\zeta\right]\left[T_l+(T_\infty-T_l)\tau\right] \quad \ldots.[50]$$

The method of solution of equations 48 and 49 will clearly depend upon the nature of the function g. In the following section we obtain a solution for the case in which the droplets are initially of uniform size.

DETERMINATION OF THE BURNING VELOCITY FOR UNIFORM SPRAYS

For monodisperse sprays the droplet size distribution at the cold boundary is given by

$$G_0(r)=n_0\delta(r-r_0) \quad \ldots.[51]$$

where $\delta(r-r_0)$ is the Dirac delta function, r_0 is the initial droplet radius and the initial number density of droplets is

$$n_0=\frac{\rho_0}{\rho_l}\,\frac{(1-Z_0)}{\frac{4}{3}\pi r_0^3} \quad \ldots.[52]$$

in which use has been made of equations 11 and 15. By substituting equations 44 and 51 into equation 45 and evaluating the integral, we find that

$$g=\begin{cases} n_0\left(r_0^2-2\int\limits_{-\infty}^{x}\frac{X}{u}\,\mathrm{d}x\right)^{1/2} & \text{for } 2\int\limits_{-\infty}^{x}\frac{X}{u}\,\mathrm{d}x\leqslant r_0^2 \\ 0 & \text{for } 2\int\limits_{-\infty}^{x}\frac{X}{u}\,\mathrm{d}x> r_0^2 \end{cases} \quad \ldots.[53]$$

For uniform sprays the RHS of equation 53 can be expressed in terms of Z by utilizing equations 11, 15 and 43 which imply that

$$1-Z=\frac{u_0}{\rho u}\,\tfrac{4}{3}\pi\rho_l\int\limits_0^\infty\frac{r^4}{\mu}\,G_0(\mu)\,\mathrm{d}r \quad \ldots.[54]$$

If equations 51 and 52 are substituted into equation 54, the integration is performed, and use is made of equation 27, then the identity

$$1-Z=\begin{cases} \left(\frac{1-Z_0}{r_0^3}\right)\left(r_0^2-2\int\limits_{-\infty}^{x}\frac{X}{u}\,\mathrm{d}x\right)^{3/2} & \text{for } 2\int\limits_{-\infty}^{x}\frac{X}{u}\,\mathrm{d}x\leqslant r_0^2 \\ 0 & \text{for } 2\int\limits_{-\infty}^{x}\frac{X}{u}\,\mathrm{d}x> r_0^2 \end{cases} \quad \ldots.[55]$$

is obtained. By substituting equation 55 into equation 53 it is found that the simplified expression for g becomes

$$g=n_0r_0\left[(1-Z)/(1-Z_0)\right]^{1/3} \quad \ldots..[56]$$

which enables us to reduce equation 48 from an integro-differential equation to an ordinary differential equation.

By substituting equations 56, 52 and 42 into equation 48 and using equations 46 and 47, the expression

$$\frac{\mathrm{d}\zeta}{\mathrm{d}x}=\frac{a\tau(1-\zeta)^{1/3}}{(\tau+\alpha)(\tau+\beta)(\zeta+\gamma)} \qquad \ldots.[57]$$

is obtained, where the definitions

$$\alpha=L/c_p(T_\infty-T_l) \qquad \ldots.[58]$$

$$\beta=T_l/(T_\infty-T_l) \qquad \ldots.[59]$$

$$\gamma=Z_0/(1-Z_0) \qquad \ldots.[60]$$

and

$$a=12\lambda p/[\mathcal{M}r_0^2c_p\rho_lR'(T_\infty-T_l)(1-Z_0)] \qquad \ldots.[61]$$

have been employed. If the further definition

$$b=\mathcal{M}(1-Z_0)c_p/\lambda \qquad \ldots.[62]$$

is used with equations 39 and 40 in equation 49, then we find

$$\mathrm{d}\tau/\mathrm{d}x=b[\zeta\tau+\gamma\tau-(1+\gamma)\zeta] \qquad \ldots.[63]$$

By dividing equation 63 by equation 57 we eliminate the independent spatial variable x and reduce the heterogeneous burning velocity problem to that of obtaining the eigenvalue

$$\Lambda\equiv\frac{b}{a}=\frac{\mathcal{M}^2r_0^2(1-Z_0)^2c_p^2\rho_lR'(T_\infty-T_l)}{12\lambda^2p} \qquad \ldots.[64]$$

from the differential equation

$$\frac{\mathrm{d}\tau}{\mathrm{d}\zeta}=\Lambda\frac{(\tau+\alpha)(\tau+\beta)}{\tau}\frac{(\zeta+\gamma)}{(1-\zeta)^{1/3}}[\zeta\tau+\gamma\tau-(1+\gamma)\zeta] \qquad \ldots.[65]$$

with the boundary conditions $\tau=0$ at $\zeta=0$ and $\tau=1$ at $\zeta=1$.

Actually some properties of the mass burning velocity $\mathcal{M}$ can be deduced from the dimensionless form of the equations without completing the solution. Thus, since equation 65 implies that Λ can be a function of α, β and γ only, equation 64 implies that for given values of Z_0, T_l, T_∞ and L/c_p, the dependence of $\mathcal{M}$ upon the initial droplet size, pressure, specific gravity of the liquid, thermal conductivity and specific heat is given by

$$\mathcal{M}\sim\frac{1}{r_0}\frac{1}{\rho_l^{1/2}}p^{1/2}\left(\frac{\lambda}{c_p}\right) \qquad \ldots.[66]$$

The dependence of $\mathcal{M}$ upon p, λ and c_p shown in equation 66 is the same as that found for a homogeneous laminar flame. The variation $\mathcal{M}\sim 1/r_0$ states that, as the droplet size is decreased and the number of droplets increased in order to keep Z_0 constant, the burning rate increases. If it is remembered that these results apply only in the limit of negligible homogeneous reaction (viz. for droplet diameters larger than about 25 μ in the data of J. H. BURGOYNE and L. COHEN[2]), this prediction appears to agree with the observations reported in ref. 2 for oxidation reactions.

The non-separable term in equation 65, which is an essential feature of problems of this type, prevents us from obtaining an exact solution for $\tau(\zeta)$. An iterative method for obtaining an approximate solution to equation 65 may be started by choosing a reasonable 0^{th} approximation $\tau_0(\zeta)$. If equation 65 is multiplied by $\tau/(\tau+\alpha)(\tau+\beta)$ and integrated from 0 to ζ, then it is found that

$$\psi(\tau) = \Lambda \left[\int_0^\zeta \tau \frac{(\zeta+\gamma)^2}{(1-\zeta)^{1/3}} \mathrm{d}\zeta - \phi(\zeta) \right] \equiv \Lambda \Psi(\zeta) \qquad \ldots.[67]$$

where

$$\psi(\tau) \equiv \int_0^\tau \frac{\tau}{(\tau+\alpha)(\tau+\beta)} \mathrm{d}\tau = \ln\left[\left(1+\frac{\tau}{\alpha}\right)^{\alpha/(\alpha-\beta)} \left(1+\frac{\tau}{\beta}\right)^{-\beta/(\alpha-\beta)}\right] \ldots.[68]$$

and

$$\phi(\zeta) \equiv (1+\gamma) \int_0^\zeta \frac{\zeta(\zeta+\gamma)}{(1-\zeta)^{1/3}} \mathrm{d}\zeta = (1+\gamma) \left\{ \left(\frac{27}{40} + \frac{9}{10}\gamma\right) - (1-\zeta)^{2/3} \left[\frac{3}{8}\zeta^2 + \left(\frac{9}{20} + \frac{3}{5}\gamma\right)\zeta + \left(\frac{27}{40} + \frac{9}{10}\gamma\right)\right]\right\} \qquad \ldots.[69]$$

The requirement that $\tau = 1$ at $\zeta = 1$ implies that $\Lambda = \psi(1)/\Psi(1)$ ….[70]

By substituting the 0^{th} approximation $\tau_0(\zeta)$ into the integral in equation 67, the 0^{th} approximation $\Psi_0(\zeta)$ is obtained. The first approximation for the eigenvalue is $\Lambda_1 = \psi(1)/\Psi_0(1)$, and the first approximation $\tau_1(\zeta)$ is obtained from equation 67, viz. $\psi(\tau_1) = \Lambda_1 \Psi_0(\zeta)$. In general, the n^{th} approximation to the solution is given by the equations

$$\Lambda_n = \psi(1)/\Psi_{n-1}(1) \quad \ldots.[71] \qquad \text{and} \qquad \psi(\tau_n) = \Lambda_n \Psi_{n-1}(\zeta) \quad \ldots.[72]$$

The first approximation for the eigenvalue has been computed by assuming

$$\tau_0(\zeta) = 1 - (1-\zeta)^{5/3} \qquad \ldots.[73]$$

an expression which, in addition to having the required limiting values at $\zeta = 0$ and $\zeta = 1$, has the correct asymptotic behaviour at the hot boundary as is easily verified by expanding equation 65 about the point $\zeta = 1$. By substituting equation 73 into the RHS of equation 67 and performing the integration, it is found that

$$\Psi_0(1) + \phi(1) = \frac{15}{14}(1+\gamma)^2 - \frac{3}{5}(1+\gamma) + \frac{15}{104} \qquad \ldots.[74]$$

which, in view of equations 68, 69 and 71, implies that

$$\Lambda_1 = \frac{\dfrac{1}{\alpha-\beta} \ln\left[\left(\dfrac{1+\alpha}{\alpha}\right)^\alpha \left(\dfrac{\beta}{1+\beta}\right)^\beta\right]}{\dfrac{6}{35}(1+\gamma)^2 - \dfrac{3}{8}(1+\gamma) + \dfrac{15}{104}} \qquad \ldots.[75]$$

The expression for the burning velocity $u_0 = \mathcal{M}/\rho_0$ in physical units may be obtained by substituting equations 58, 59, 60 and 64 into equation 75.

COMPARISON WITH EXPERIMENT

Although this theory has been constructed for the reaction $A \rightarrow nB$, the magnitude of X and its dependence upon τ and ζ is roughly the same for monopropellant and bipropellant (diffusion flame) heterogeneous reactions. Hence it is of interest to compare the burning velocity computed from equation 75 with available experiments on the oxidation of monodisperse fuel sprays in which homogeneous chemical reactions are negligible. The experiments reported in ref. 2, which deal with tetralin sprays in air, correspond to the conditions $p = 1$ atm, $T_l = 300$°K, $c_p = 0{\cdot}3$ cal/g°K, $\lambda = 5 \times 10^{-4}$ cal/cm sec °K, $\rho_l = 0{\cdot}971$ g/cm^3, $L = 75$ cal/g and $Q' = 10\,350$ cal/g. A test condition for which we expect the present theory to be nearly valid is $r_0 = 19\,\mu$, $1 - Z_0 = 0{\cdot}039$ and $\rho_0 = 1{\cdot}233 \times 10^{-3}$ g/cm^3, for which the theoretical burning velocity, $u_0 = 34$ cm/sec, is to be compared with the experimental value $u_0 = 58$ cm/sec. The difference between these theoretical and experimental results is within the accuracy of the theoretical computations, in which the principal sources of error are the uncertainties in the values of the average thermal conductivity λ and the specific heat c_p. For the experimental conditions of ref. 2, the theory also predicts a slight increase in u_0 with increasing Z_0 at constant r_0 as was observed experimentally. It will be noted that the constants appearing in this theory are much more accurately known than the activation energies and frequency factors which appear in the corresponding homogeneous laminar burning velocity problem. This is probably the reason for the better agreement between theory and experiment in the present case.

Equation 63 implies that a rough estimate for the thickness of the reaction zone δ for a one-dimensional heterogeneous flame is

$$\delta \sim 1/b = \lambda/[c_p\, \mathcal{M}(1 - Z_0)] \qquad \ldots .[76]$$

For the experimental conditions of ref. 2 this estimate yields $\delta \sim 1{\cdot}2$ cm, which is roughly 10 times the thickness of the corresponding homogeneous laminar flame. The estimate given in equation 76 is in approximate agreement with the experiments reported in ref. 2.

This work was supported by the Office of Ordnance Research, U.S. Army, under Contract No. DA-04-495-Ord-46 with the California Institute of Technology. The author is indebted to Dr S. S. Penner for proposing this investigation and for helpful suggestions.

Daniel and Florence Guggenheim Jet Propulsion Center,
California Institute of Technology,
Pasadena, California

(Received September 1958)

REFERENCES

[1] WILLIAMS, F. A. *Physics of Fluids*, 1958, **1**, 541
[2] BURGOYNE, J. H. and COHEN, L. *Proc. Roy. Soc. A*, 1954, **225**, 375
[3] HIRSCHFELDER, J. O., CURTISS, C. F. and BIRD, R. B. *Molecular Theory of Gases and Liquids*, pp 698–700. Wiley: New York, 1954
[4] WILLIAMS, F. A. 'The theory of monopropellant droplet burning.' *Tech. Rep. No. 21*, Office of Ordnance Research, U.S. Army, Contract DA-04-495-Ord-446, California Institute of Technology, Pasadena (1958); also to appear in *Combustion and Flame*

Optical Flame Structure Studies: Examination of Reaction Rate Laws in Lean Ethylene–Air Flames

A. LEVY and F. J. WEINBERG

Several flat ethylene air flames have been studied by the 'inclined slit' method under conditions of varying initial temperature and composition. Temperature profiles so deduced together with burning velocities determined by a particle track technique have been used to derive distributions of heat release rate and other relevant parameters. These results are evaluated for their kinetic significance. It is concluded, inter alia, *that profiles of effective orders and activation energies indicate a varying reaction scheme such that an overall reaction model, whilst entirely untenable at lower temperatures, may be of use for the zones near the maximum heat release rate. These zones appear to characterize the behaviour of the flame as a whole and their rate laws approach those determining blow-out under highly mixed conditions. Temperature disequilibrium effects are shown to be unimportant for the flames considered.*

THE work presented here forms part of an investigation of laminar flame structure designed to study *in situ* the mechanism and chemical kinetics of flame propagation. As in previous work[1-3], the approach is based on the mapping of ray deflections across a flat premixed flame, at atmospheric pressure, by recording the distorted images of inclined slits through which is passed a beam of parallel light. The use of reactant compositions near the lower limit of inflammability ensures that the variation in physical properties across the flame due to temperature changes is much greater than that occasioned by composition variations. The temperature profiles deduced from the recorded refractive index distributions are used, together with measured burning velocities, to calculate the profiles of volumetric heat release rate as a first step in the analysis of flame processes. The more detailed aim of the work presented here, however, differs from that of the earlier communications referred to and this has necessitated certain changes in approach and refinements in the method of interpretation.

The exploitation of the advances made in recent years in predictive mathematical theories of combustion phenomena has been retarded by lack of relevant detailed and quantitative kinetic information. Even where results of 'slow' kinetic studies are available, their application to the extreme conditions prevailing in combustion zones seems an unreasonable extrapolation. The combustion engineer is therefore forced to base his theoretical models upon the concept of an 'overall' reaction mechanism. The justifications offered include that of simplicity and, occasionally, have been based on the supposition of one rate-controlling step of a sequence (in which case it still remains to be demonstrated that the concentrations in the pre-exponential term of the rate law ought really to be those of the reactants). No justification in fact appears necessary in the present state of knowledge, since the postponement of predictive calculations to await detailed kinetics would be undesirable. Certain theories based on 'global' kinetics, in particular in laminar flame propagation and in the case of the 'fully stirred reactor'[4], have indeed enjoyed considerable practical success.

The question therefore arises as to whether, and if so under what conditions, it is valid to assume a rate of heat release everywhere proportional to the local concentrations of the primary reactants raised to appropriate 'order' powers and to the Arrhenius factor, in a system which is presumably a complex and currently irresolvable assembly of consecutive and/or parallel reaction steps. The main aim of the present work has been the examination of the validity of the 'overall reaction' concept within the flames studied.

This aim suggested the need for analysing several flames connected by some simple variable, so that the observable consequences such as, for instance, variation in burning velocity could be connected through the measured changes in flame structure. Deductions from the analysis of a single flame, being tied to a particular composition/temperature relationship, afford no means of cross-checking. (The effective 'rate laws' of one flame could be a property of the structure of the flame, as much as of the reactants). Variation of the initial gas temperature was chosen as the simplest parameter.

The structure of the flames examined and its dependence on the initial variables are of relevance to such a variety of aspects of combustion and flame propagation that some subdivision of the discussion proved necessary. Those aspects dealing with the mechanism of flame propagation and its theory have been the subject of a previous publication[5]. Its topics included the aerodynamics of the flat flame as stabilized on the Egerton–Powling[6, 7] burner with particular reference to the use of the burner for accurate burning velocity measurement; the dependence of such burning velocities on initial temperature and composition for lean ethylene–air flames and the use of the measured heat-release rate profiles for the testing of individual steps in 'comprehensive' theories of flame propagation. The latter was concerned primarily with the examination of the validity of the concept of 'unit Lewis number' and the mathematical methods of arriving at a burning velocity from given heat-release profiles, both divorced from any assumed kinetic laws. Repetition of these earlier conclusions will be avoided here except for brief summaries of those aspects which are essential to the arguments developed.

APPARATUS

The burner

The flames were stabilized upon a modified version (*Figure 1*) of the Egerton–Powling burner, in which the flow of reactant gas is randomized by a bed of glass beads and then rendered uniform by a streamlining 'matrix' spirally wound from alternate layers of plane and corrugated cupronickel tape (*Figure 2*). The burner and its operation have been discussed previously[6, 7], as have certain modifications necessary for optical work[2]. Only those innovations demanded by the present approach will be summarized here.

It was necessary to control the temperature of the approach stream both in magnitude and uniformity of distribution. This was achieved by means of two coaxial tubular electric heaters of independently variable power inputs. The inner, a winding of Eureka strip, was hermetically sealed with refractory cement to avoid contact between hot metal and reactants and was embedded in the glass beads as shown in *Figure 1*. The outer heater was wound upon asbestos paper on the outside of the burner tube and externally sealed and lagged.

The matching of the heater inputs was, in each case, such as to minimize the radial temperature distribution across the gas stream in the presence of a flame and at the particular preheat temperature. It has previously been shown[2] that at the flow rates employed the temperature of the gas approaching the flame is indistinguishably close to that of the top surface of the matrix and further that, in the absence of heaters, a considerable radial temperature distribution exists. To record the initial temperature and its distribution, eight thermocouples were disposed spirally between centre and periphery of the matrix top surface. The matrix itself and a strip of matrix material formed one component of the junction, common to all the couples, the other consisting of glass-fibre sheathed Nichrome wire, spot-welded to the top surface and passed through the narrow channels (*Figure 2*) to the base of the burner and hence to a switchboard.

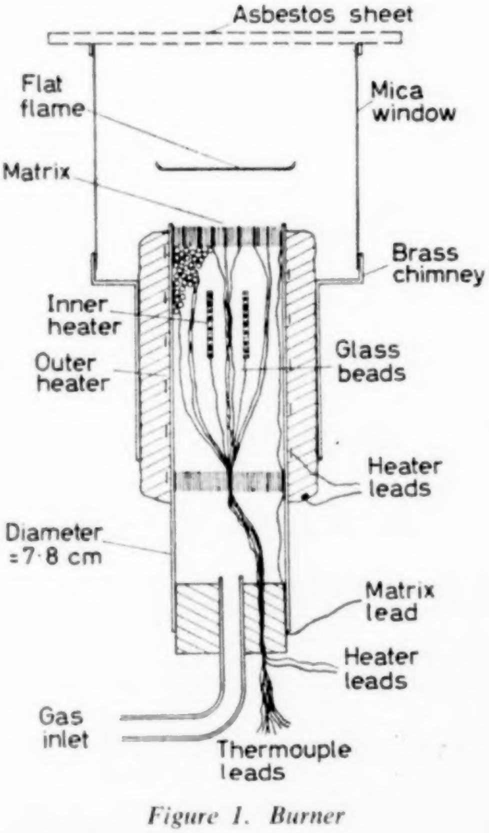
Asbestos sheet
Flat flame
Mica window
Matrix
Brass chimney
Inner heater
Outer heater
Glass beads
Heater leads
Diameter =7·8 cm
Matrix lead
Heater leads
Gas inlet
Thermouple leads

Figure 1. Burner

In practice it was found that by suitable matching of heater inputs the deviation from temperature uniformity could always be maintained to better than ±3° C of the mean value.

The lower limit of the useful initial temperature range, at about 130° C, was set by the self-preheating effect of the burner. The detailed mechanism of this effect has been investigated and discussed in the first part of this work. The upper limit was dictated by the danger of pre-reaction. Evidence of the onset of reaction in the burner became detectable at temperatures in excess of 400° C and an upper limit was therefore chosen at 350° C.

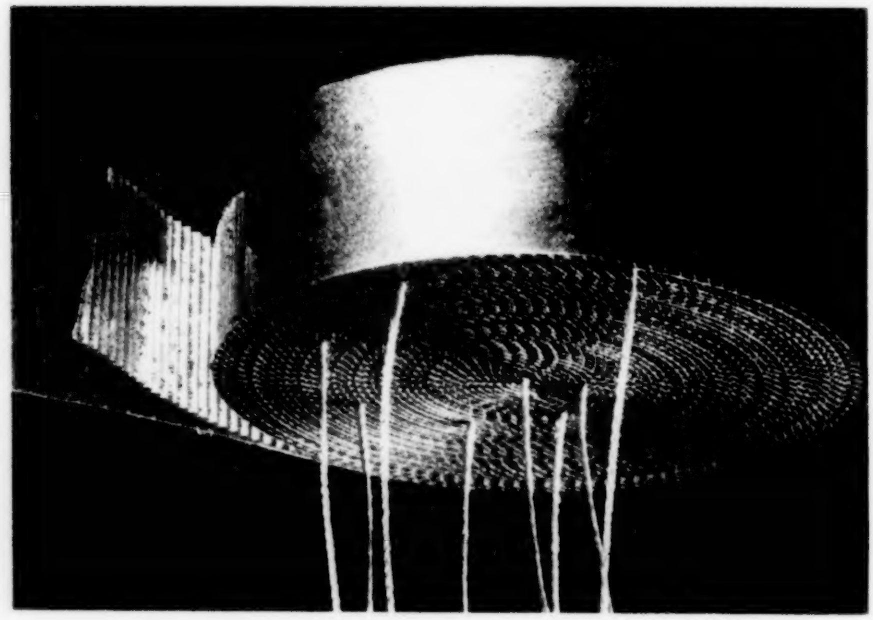

Figure 2. 'Matrix' with thermocouples

The flow system

Ethylene from a cylinder and air pumped from the laboratory, suitably filtered and dried, were thoroughly mixed in a series of packed towers before entering the burner. (It had been found that, due to the steep dependence of burning velocity on fuel content in this range, small fluctuations in composition were more likely to affect the flame's stability adversely than corresponding fluctuations in flow velocity.)

Initial flow velocity and mixture composition were determined by capillary flow metering. The relatively small useful composition range of the flat flame burner made the accuracy of this measurement of particular importance. By the use of fine capillaries, sensitive manometers and cross-calibrations at various total line pressures and temperatures, the aggregate error in the ethylene concentration was reduced to a minimum.

The purposes of the analysis similarly demand accurate knowledge of burning velocity. A critical comparison of values based on dividing volumetric flow rates by flame areas, with streamline velocities at the flame centre as determined by particle track measurement, was carried out. The detailed conclusions have been reported previously. They have led to the adoption, for present purposes, of the particle track technique, largely because of the uncertainty in the definition of the flame boundaries involved in the 'area' method. A simple device for injecting a burst of particles (of colloidal clay, mean diameter 4μ) was attached to the base of the burner. Continuous flow of particles was avoided so as to ensure that the temperature traverses obtained by the optical method could not be affected by the presence of foreign bodies in the flame. The particles were illuminated by an intense, convergent and interrupted light beam passing horizontally above the matrix centre. The light source, a high pressure mercury arc, was a.c.-operated so that the interruption frequency of the photographically recorded tracks was twice that of the supply. A typical record is shown in *Figure 3*. The computed error in burning velocity determined at the flame centre by this method, allowing for the free fall velocities of the particles, was within ±0·01 cm/sec. for burning velocities between 4 and 10 cm/sec.

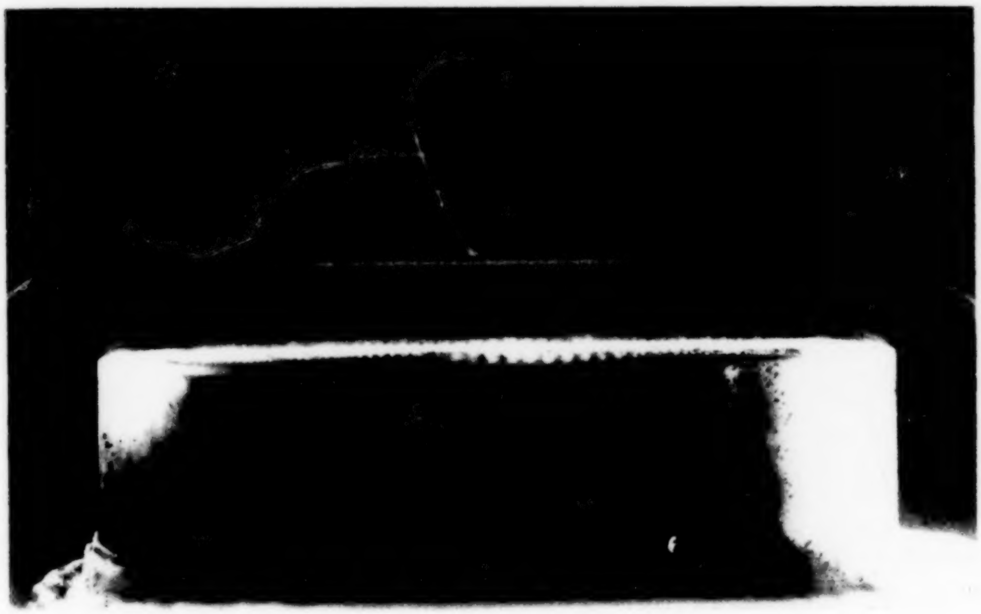

Figure 3. Typical particle track record

The number of initial variables, each with its effect on burning velocity, demands that the total flow rate be variable at any set fuel/air ratio without readjustment of the reactant supply rates. This facility was provided by the use, immediately after the mixing towers, of a rotating float flowmeter as a bleed to the atmosphere, followed by a throttle controlling the burner flow. At each setting of the latter, the former acted as a constant pressure, self-adjusting and recording leak, whose effect could not feed back to the fuel and oxidant valves.

The optical system

Measurement of the temperature profile through the flame front was based on the light ray deflection method mentioned previously[1-3]. The distribution of deflection so recorded is, in effect, a graph of some calculable function of the refractive index profile. In practice a screen of slits is used to provide data also for edge corrections. For the purposes of the present work this method of temperature distribution measurement has been refined in respect of both experimental technique and interpretation of the photographic record.

Refinements in experimental method were devoted to improving the accuracy of ray deflection measurement. The optical system is illustrated in *Figure 4* and differs from that previously employed principally in that a lens has been interposed between the flame and photographic plate. In the absence of this additional lens, an angle of deflection, θ, gives rise to a displacement of the point of ray incidence in the receptor of $z\theta$ where z is the distance between the flame and photographic plate. Contrary to this purely geometric relationship, however, the sensitivity of the method is not simply proportional to z, since the distorted shadow-image is in fact the diffraction pattern produced by the slit. The uncertainty in locating

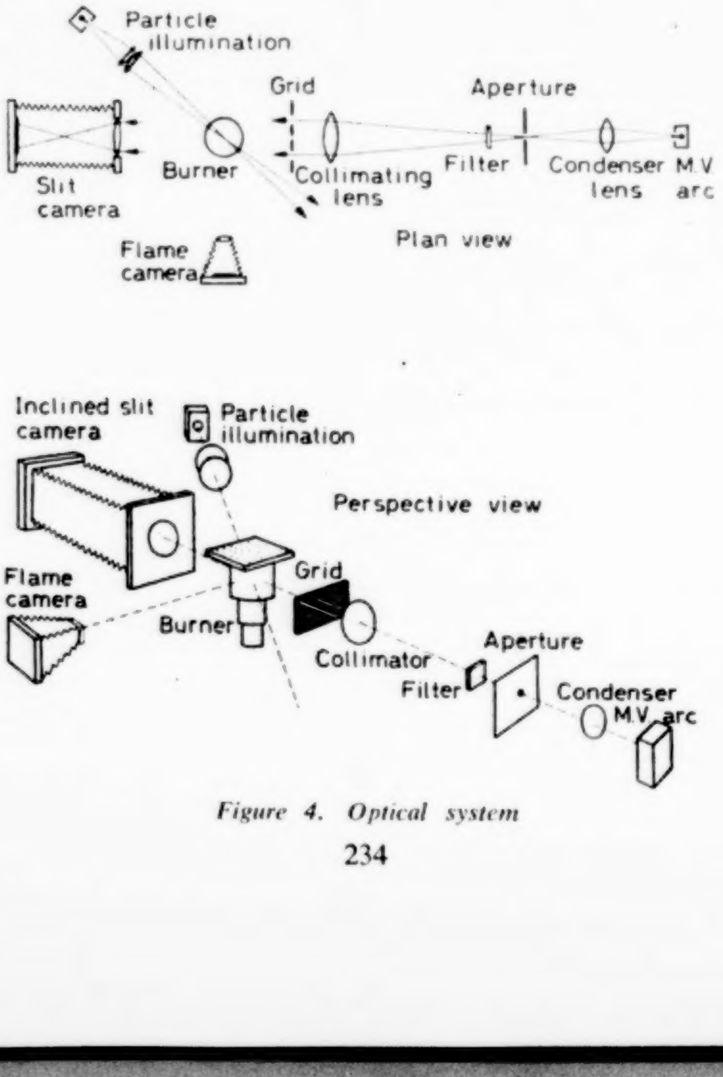
Particle illumination
Grid
Aperture
Slit camera
Burner
Collimating lens
Filter
Condenser lens
M.V arc
Flame camera
Plan view
Inclined slit camera
Particle illumination
Perspective view
Flame camera
Grid
Burner
Collimator
Aperture
Filter
Condenser
M.V. arc

Figure 4. Optical system

any part of the image is thus dependent on the spread of the pattern and hence also proportional to z. The method is therefore subject to a finite 'resolving power'; beyond a certain value of z no improvement in sensitivity is to be expected from further increases in this distance. This limitation can be reduced by introducing an additional lens, provided the grid is at some distance from the flame. If the lens images the grid on the photographic plate, for instance, diffraction is minimized without destroying the deflection. (As mentioned below, however, this does not usually represent the optimum disposition of the optical elements.)

The green line of mercury was employed by use of a combination of two filters (Kodak Wratten Nos. 58 and 77) with a mercury arc; all refractive indices refer to that wavelength. The light was condensed on an aperture of 0·014 cm diameter accurately positioned at the focus of a telescope objective of 142 cm focal length, acting as a collimator. This combination resulted in a beam whose calculated parallelism lay within 24 seconds of arc, the maximum measured deviation within the region of interest being less than 30 seconds of arc.

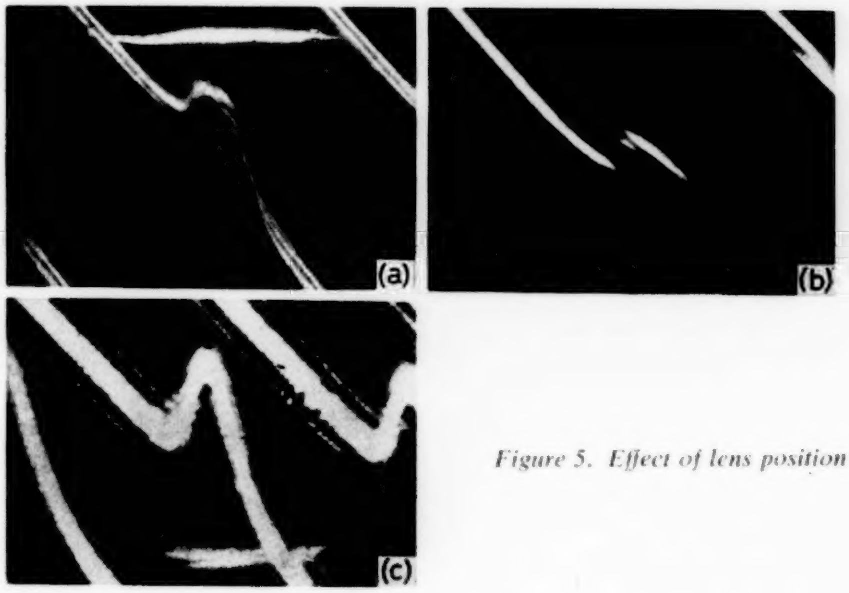

Figure 5. Effect of lens position

The effect of flame-induced deflections on the sharp monochromatic diffraction pattern inclined to the flame, in general, is to cause the fringes to cross, thereby introducing inaccuracies in displacement measurements [*Figure 5*(a)]. Although focusing the 'camera' on the slits recombines the diffraction pattern in undeflected regions, it does not do so in the important zones because of the optical properties of the flame. Such properties, moreover, vary from flame to flame so that the optimum position of the lens is a parameter of the reactant composition and temperature. Accordingly it was found most convenient to determine the setting producing the clearest image empirically in each case. *Figure 5* illustrates the differences due to lens position—*Figure 5*(b) is due to faulty setting and *Figure 5*(c) one regarded as suitable.

The introduction of the second lens results in a linear displacement changed both in magnitude and in direction (downward deflections producing upward displacements) and the theory relating s, the linear displacement, to θ, the angular deviation from the parallel introduced by the flame, had to be established for the general, non-conjugate case. It can be shown that

$$\theta = fs/\{fd + e(f-d)\} \qquad \ldots.[1]$$

where d = distance between flame centre and the forward principal point of the lens, f = focal length of lens, e = distance between screen or photographic plate and rear principal point of lens.

As $f \rightarrow \infty$ (i.e. as the lens tends to a slab of glass), $\theta \rightarrow s/(d+e) = s/z$ which is the relationship applying in the absence of the lens.

The positions of the principal points and the focal length of the lens employed were determined by Newton's method. The maximum aggregate error due to uncertainties in s, f, d and e in the above equation was estimated at 0·5 per cent. In addition, an experimental test was carried out by substituting a slit for the flame. The resulting diffraction pattern was compared with that predicted by diffraction theory for the wavelength employed and also with that measured in the absence of the lens. As predicted, all errors lay within 0·5 per cent.

The screen of slits used in all subsequent flame work consisted of a grid produced photographically on a high contrast (Kodak B4) emulsion supported on selected plate glass to avoid secondary distortions.

METHOD OF INTERPRETATION

Experimental procedure

Each flame analysis was based on the following set of records:

(*i*) Barometric pressure; (*ii*) Flow rates of fuel, air and bleed to atmosphere; (*iii*) Eight thermocouple readings portraying the radial temperature distribution across the gas stream; (*iv*) Photograph of flame (luminous zone); (*v*) Photograph of interrupted tracks of particles introduced into gas stream; (*vi*) Photograph of distorted slit images; and (*vii*) Distances between optical components.

As mentioned previously, any possibility of interference by particles was removed by not exposing (*v*) simultaneously with (*iv*) and (*vi*). Where any possibility of variation with time existed in the case of non-simultaneous measurements, readings were taken immediately before and after the main exposures. If any difference could be detected the whole set of measurements was rejected. The quantities immediately derived from these measurements were the initial reactant parameters (temperature, mixture composition and volumetric flow rate) and the consequent flame characteristics (burning velocity, flame shape and ray deflection profile). Corrections (e.g. of direct flame photographs for non-parallelism of light and hence distance distortion) were carried out at this stage. The effect of errors in measurement upon the accuracy of the subsequent analysis has been discussed elsewhere[2, 8].

The treatment of the distorted slit images and their interpretation is further discussed below.

Deflection profile

The shapes of the central maxima of the inclined slits were read under a two-coordinate travelling microscope nominally to within $\pm 0{\cdot}0005$ cm and the readings re-plotted at a magnification of 100 ×. The interpolated straight line between the undeflected extremities was constructed for each slit and regarded as the reference line for displacement measurements. It has previously been shown[2] that this procedure renders negligible any errors due to refraction at the boundaries between hot flame gases and cold laboratory air, including the 'cylindrical lens effect', in a horizontal plane, of a column of hot gas.

In terms of the optics of the second lens (see above) these records lead directly to the distribution of θ, the total angle of deflection induced by the flame.

Refractive index profile

For a perfectly unidimensional refractive index profile, $n = \mathrm{f}(x)$, with discontinuous boundaries, giving rise to deflections small enough to cause no appreciable deviation of rays from the parallel with surfaces of equal n, the total deflection can be assumed[2] to be

$$\theta = -(\mathrm{d}n/\mathrm{d}x)\,D \qquad \ldots.[2]$$

where D is the length of the ray path perpendicular to x. In its application to flames, two types of correction to the above relationship arise. The first is due to the ray deflection which already in the flame causes the ray to deviate from its horizontal path and thus to traverse regions of varying $\mathrm{d}n/\mathrm{d}x$. The second is a consequence of the deviations of the flame from the unidimensional model—effects of slow curvature over appreciable distances, of rapid curvature over small distances at the edges and of diffusivity effects at boundaries.

The former correction is very small in the systems under examination. It can be derived, in the form of a series, by successive approximations and all but the first two terms of the series are quite insignificant. These lead to a correction, used previously[2], of

$$\mathrm{d}n/\mathrm{d}x = (\mathrm{d}n/\mathrm{d}x)_{\mathrm{uncorrected}}\,[1 + (D^2/6)(\mathrm{d}^2n/\mathrm{d}x^2)] \qquad \ldots..[3]$$

which, though small, has been applied to all readings.

Errors due to any deviation of a flame from unidimensionality had formerly[2] been corrected by a method of extrapolation of the multiple slit records to the flame centre. In view of the conclusions concerning flames as stabilized on the flat flame burner[5], it was considered more accurate to make, if possible, no assumptions concerning the flame shape (this is in accord with the determination of burning velocities at the flame centres). The present method is based solely on two assumptions—that the system is axially symmetrical and that the detailed structure perpendicular to the flame surface is invariant. The latter assumption must be correct for all but the extreme edges where diffusive effects may enter and for which a small empirical correction was incorporated, based on linearity of spreading loci of constant composition.

On these assumptions, given the shape of the axial section of any one isotherm, the shape of all other isotherms may easily, if laboriously, be constructed geometrically, their separation alone remaining as the unknown profile. The basic isotherm used was the lower edge (shown free from optical error[9]) of a photograph of the luminous zone, taken in its plane and corrected for the finite camera–flame separation.

Such isotherms were constructed on a diagram at a magnification of about 40× (equivalent to a flame thickness of approximately 20 cm), their separation being chosen small enough to justify the assumption of constant refractive index gradient within each interval. In practice the maximum zone thickness was 0·03 cm (actual) and this was halved in the region of maximum refractive index gradient. The deflection equation may be written as

$$\theta = -\Sigma_j (\mathrm{d}n/\mathrm{d}p)_j D_j \cos\psi_j \qquad \ldots . [4]$$

where $(\mathrm{d}n/\mathrm{d}p)_j$ is the refractive index gradient perpendicular to the flame in the j^{th} zone (—a constant for that zone), D_j the length of the ray path in the zone, ψ_j the angle between the ray and j^{th} zone and the summation extends over the path of each ray. Since the total deflections are known, the profile may now be derived numerically. Starting from the side from which isotherms appear convex, $(\mathrm{d}n/\mathrm{d}p)_1$ is obtained for the first zone which gives rise to a measurable deflection, no other zones being involved. The second ray, chosen to traverse the first two zones, yields $(\mathrm{d}n/\mathrm{d}p)_2$ by subtraction of the now calculable effect of the first zone from the measured deflection, and so forth. It transpires, in fact, that by far the largest part of the path of each ray lies within, and parallel to, the central zone; but this consequence of the flatness of the flames is no longer basic to the interpretation.

The resulting curve of refractive index gradient against distance perpendicular to the flame front is integrated graphically from the 'cold' boundary where the temperature, composition and hence refractive index are accurately known. The result is equivalent to the distribution in x perpendicular to an idealized flat flame.

Temperature profile

The measured refractive index profile is due to changes in both the distance between, and the nature of, the constituent molecules. Both are caused, in the general case, by a combination of temperature and composition variations occasioned by the reaction.

If temperatures are too low for appreciable dissociation, mole number is unaffected by temperature, while if reaction proceeds without change in the number of molecules, the overall composition change does not affect intermolecular distance. Finally, if the reactants are diluted by great excess of one component, composition effects generally become very small.

All these extenuating circumstances apply here and the thermal effect is by far the larger. Moreover, δ in

$$n = 1 + \delta$$

at its maximum is of the order 3×10^{-4}, so that the relationships of Gladstone and Dale and of Lorenz and Lorentz become indistinguishable and all second-order effects become negligible. Thus δ may be regarded as additive by volume and inversely proportional to temperature.

For complete reaction, in the mixtures here considered, there is no change in the number of molecules and the change in $\delta \times T$ is 1·03 per cent in a typical case. The smallness of this effect is largely due to the great excess of air in the reactants. Thus, although reaction to any intermediates is likely to involve some change in the number of molecules, the effect cannot be large.

The correction applied for composition changes was based on an overall reaction commencing at 700°K, reaching completion at the final flame temperature, conversion being proportional to temperature in the interval. Although hardly rigorous (a much better approximation could have been based on the results obtained for each flame) this approach was considered adequate for a 1 per cent correction and since it can be incorporated in the variation of δ with T, yields a 'corrected' temperature profile without recourse to successive approximations.

The maximum temperatures so obtained were compared with calculated final flame temperatures. In spite of the large error magnification entailed in integration from the cold boundary[8], the differences were relatively small (mean 2·7 per cent) and without trend. The temperature profiles were 'adjusted' to coincide with the calculated final temperature by using a scaling factor at the deflections stage. The mean deviation from unity of these factors was less than 1·8 per cent and the main purpose of the manoeuvre was to avoid the consequences of any experimental error in the subsequent analysis.

Profile of volumetric heat release rate

The steady state heat conservation equation for the unidimensional flame can be written as

$$\frac{\mathrm{d}}{\mathrm{d}x}\left[M \int_{T_0}^{T} c_p \, \mathrm{d}T - k\frac{\mathrm{d}T}{\mathrm{d}x}\right] - \dot{q}''' = 0 \qquad \ldots.[5]$$

Here M = mass burning rate, c_p = specific heat at constant pressure, k = thermal conductivity of gases at x, $\dot{q}'''$ = heat release per unit volume per unit time, and radiation flux has been neglected because of the transparency of gases consisting largely of air. The bracketed terms, the convective and conductive enthalpy fluxes, are calculable from the measured burning velocity and temperature profile if the enthalpy and thermal conductivity of the gas at any x are known. As with refractive index, the variation of these properties with x is largely determined by the temperature profile in the mixtures employed. The values were calculated for the mixtures from those of their constituents using published temperature dependence data[10, 11], but the small variations due to *changes* in composition were adequately dealt with by the unsophisticated method mentioned in connection with refractive index calculations.

In this manner the volumetric heat release rate profiles were deduced as a measure of the distribution of reaction rate.

'Concentration profiles'

Up to this point the analysis is considered rigorous (apart from experimental error). Extension to calculating 'species distributions', however, implies an assumed relationship between the rates per unit volume of heat release and generation (or destruction) of the species concerned. In the present context such calculations are used *to test the validity of the implied assumptions* (in particular that of 'global' reaction). In spite of conclusions of sampling studies that the deviations for reactants are not large, no absolute significance is here attributed to the 'concentration profiles'. This statement applies throughout the subsequent argument and the quotation marks will henceforth be omitted.

The steady state conservation equation for the j^{th} species, equivalent to that for heat content stated above, is

$$\mathrm{d}\,(\boldsymbol{M}m_j+\mu_j)/\mathrm{d}x-\dot{m}'''=0 \qquad \ldots.[6]$$

where m_j is the local fractional density of the species, μ_j its diffusion flow rate per unit area, $\dot{m}'''$ the rate of formation per unit volume (i.e. change of sign if species j is a reactant) and other symbols are as previously defined. It can be shown that

$$\mu_j=\frac{\boldsymbol{D}_j\rho}{1-m_j(1-\overline{\boldsymbol{W}}/\boldsymbol{W}_j)}\,\frac{\mathrm{d}m_j}{\mathrm{d}x} \qquad \ldots.[7]$$

where $\boldsymbol{D}$ = diffusion coefficient and $\boldsymbol{W}$ = molecular weight, the bar denoting the local mean value. The benefits derived from the use of a lean mixture here again are seen to be considerable. Diffusion coefficients were obtained by calculation[12] and, where available, from experimental data[13] also. In testing the 'global' concept, $\dot{m}_j'''$ for the major species is proportional to $\dot{q}'''$ and the constant of proportionality follows from the stoichiometry and heat of reaction.

The distribution of m_j is then calculable by stepwise integration from the hot boundary.

Thermal equilibrium

Much has been said about disequilibrium between degrees of freedom and the meaning of 'temperature' in flames. The temperature here used as index of reaction progress being translational, a comparison of the extent of possible disequilibrium with the error in temperature measurement was carried out. The measured flame structure lends itself readily to the calculation of the distributions both of $\mathrm{d}T/\mathrm{d}t$ (the rate of temperature rise) and of the time required for one molecule to execute any particular number of collisions. On choosing this number of collisions to be that required for any initial disequilibrium to be dissipated, the product of the two distributions gives the 'disequilibrium temperature uncertainty' as a profile through the flame. This test was carried out as part of the interpretation.

RESULTS

Flames burnt

The approximate range of burning velocities for adequately flat flames was 4 to 10 cm/sec, for the burner used. This, together with the temperature range (130° to 350°C) mentioned above, confined the useful composition range to approximately 1·8 to 2·4 volume per cent of ethylene. Within these limits, many flames were stabilized in several series sharing some common parameter (such as one fuel/air ratio), all the readings described in the previous section being recorded. Such data were used in burning velocity and limits of inflammability correlations but, because of the labour and time involved in the complete interpretation, only four of the flames were fully analysed. Selection of these four was such that three were close to the lean limit of propagation and two were of equal initial fuel/air ratio (differing only in initial temperature, the lower temperature being at the limit of inflammability). At the same time, the four flames utilized virtually the full range of the burner in terms of mixture strength, initial temperature and burning velocity.

Burning velocities

The details and full conclusions of the investigation into 'flat-flame burning velocities' having been presented elsewhere[5], only those results used in the present work are summarized below.

Burning velocity, S cm/sec, is given corrected to s.t.p. irrespective of T_0, the initial temperature; i.e.

$$S = M/\rho_{\text{s.t.p.}} \qquad \ldots\ldots [8]$$

Over the range investigated, its dependence on both initial temperature and initial composition (C per cent by volume of ethylene) was sensibly linear and could be represented by

$$\left.\begin{aligned} S &= 0{\cdot}0473\,T_0 - 2{\cdot}97 \text{ (at constant } C) \\ \text{and} \quad S &= 12{\cdot}30\,C - 26{\cdot}73 \text{ (at constant } T_0) \end{aligned}\right\} \qquad \ldots\ldots [9]$$

The 'chemical energy equivalent' for unit preheat of reactants at constant burning velocity

$$(\partial C/\partial T_0)_s = -0{\cdot}00290 \text{ per cent ethylene per degree centigrade} \qquad \ldots\ldots [10]$$

as compared with the classical value of $-0{\cdot}0027$ due to A. G. WHITE[14].

Thermal disequilibrium

The calculation of the 'temperature uncertainty' profile, due to possible disequilibrium between degrees of freedom has been discussed above. *Figure 6* shows the result for an assumed 'relaxation time' of 500 collisions for nitrogen. The maximum 'temperature uncertainty' is seen to be less than 3×10^{-2} °C. Alternatively, if comparison with experimental accuracy allows an uncertainty of ±1°K, the permissible number of collisions within which any disequilibrium must be dissipated, becomes as high as 17 500. These results are based on the fastest of the flames burnt in the present investigation (corresponding to a maximum rate of temperature rise of less than 200 000°C/sec). Disequilibrium effects will accordingly be neglected. This conclusion has obviously no general validity and the situation rapidly deteriorates at increasing fuel/air ratios.

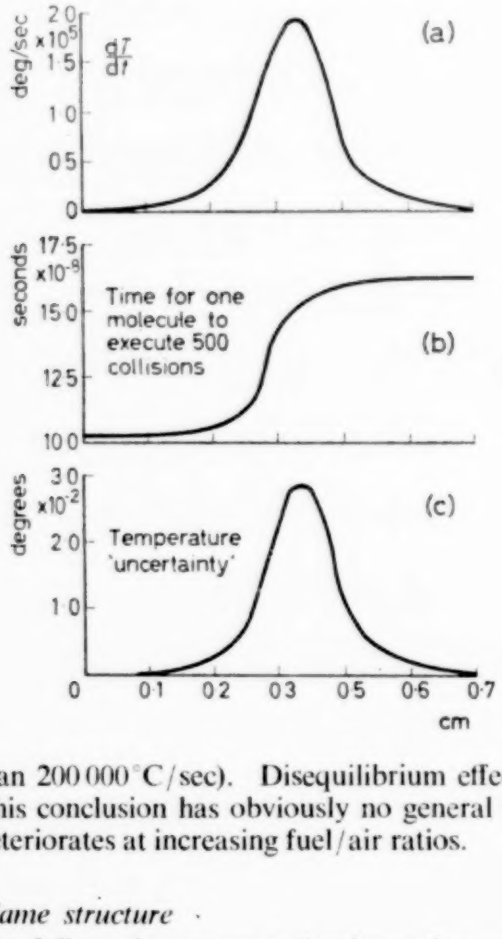

Figure 6. Extent of disequilibrium

Flame structure

The full results are too voluminous for presentation here and are therefore illustrated by *Figure 7* which portrays the distance structure of the fastest flame and *Figure 8* showing volumetric heat release rates as functions of temperature for four flames.

Figure 7 shows some evidence of the 'tail'[15, 16]—a zone of after-burning attributed, in hydrocarbon combustion, to the slower oxidation of carbon monoxide, but nevertheless present in flames in which carbon monoxide is the sole fuel[17]. It is seen that even at atmospheric pressure the last 10 per cent of the temperature rise occupies 0·2 cm, i.e. about 45 per cent of the distance over which changes are detectable. Similarly, whilst the heat release rate falls to 10 per cent of its maximum value within 0·11 cm, in going from the maximum towards the burnt boundary, the remaining 10 per cent occupies 0·15 cm. The apparent extent of the 'tail' depends, of course, on the sensitivity of detection and, unlike probe and thermocouple measurements which are deemed to be particularly suited to the

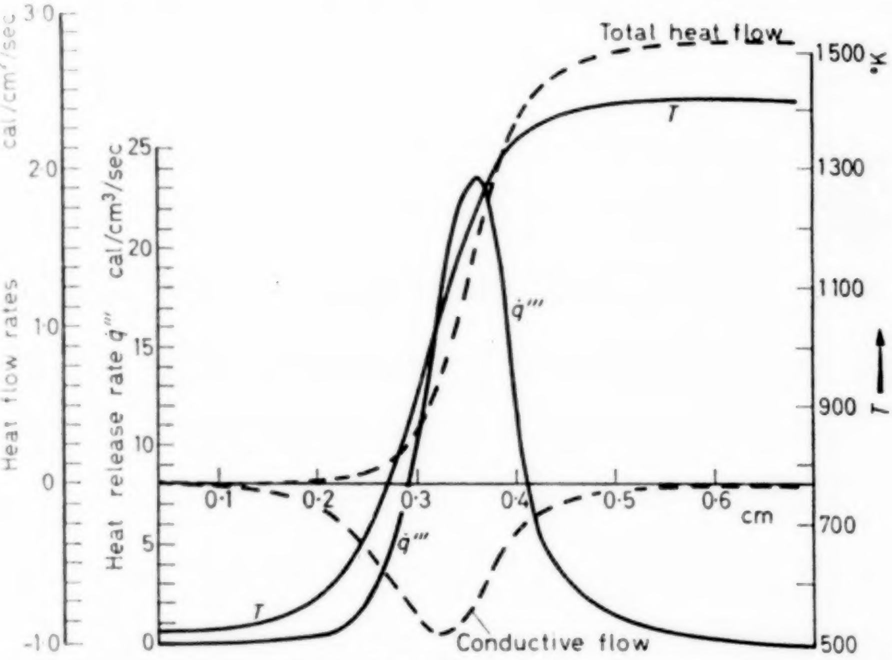

Figure 7. Profiles for Flame 6

recording of profiles beyond the zone of steep gradients[17], optical methods decrease in accuracy towards higher temperatures. Nevertheless, an appreciable shortening of this zone was observed in moving even nearer towards the limit of inflammability.

Another concept for which the profiles were examined was that of an 'ignition temperature'. Whether ignition was deemed to occur when some fixed small fraction of either the maximum heat release rate or of the total

Figure 8. Rate of heat release

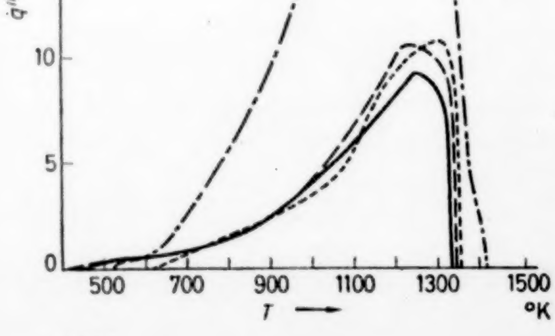

conversion was attained (the need for some such definition is dictated by the asymptotic approach of all curves to the distance axis) no correlation became apparent. All such 'ignition temperatures' varied with initial temperature both at constant fuel/air ratio and at constant burning velocity.

Mechanism of flame propagation

Since the aspects of the analysis relating to the mechanism of propagation of flat flames have been discussed previously, only a summary of those involved in the subsequent discussion is again necessary. Two conclusions emerged from independent tests of the individual steps constituting a theory of flame propagation.

First, substitution of the experimental heat release profiles into burning velocity equations and comparison of the result with measured burning velocities was used as a direct test of the procedure for solving the final equations, without involving any assumptions concerning kinetics, composition/temperature relationship etc. It transpired that, whilst D. B. SPALDING's refinements[18] resulted in considerable improvement over the original Semenov–Frank-Kamenetski approach[19], the latter was a good first approximation. It accounted for trends correctly and was found to be in error, in individual predictions, by generally less than one third. This qualified success is here significant because the theory is based on the concept that most of the reaction may be considered to occur at the final temperature.

The second point emerged from an examination of the frequently employed assumption that the diffusion coefficient of various species may be equated to the thermal diffusivity of the mixture (i.e. 'Lewis number' = 1). It was concluded that, for the lean flames examined and for the species involved in an 'overall' reaction scheme, this again was a reasonable working assumption (the biggest discrepancy occurring in the case of water) and was much superior to the neglect of diffusion. The present relevance of this result is that it can be shown on this assumption that the distribution (in terms of mass fraction) in one flame of all species whose rate of disappearance is proportional to rate of heat release is the same.

KINETICS

Method

The main aim of the part of the work here reported has been to assess the validity of the concept of an 'overall' kinetic scheme. The variety of intermediates detected in sampling studies (see e.g. ref. 15) already suggests that any such scheme is likely to be effective rather than real. Various approaches based on the heat release profile suggest themselves[20], the least deductive being the testing of proposed mechanisms. Perhaps the most obvious is the solution of four simultaneous equations representing four experimental points for constants K_1 to K_4 in

$$\dot{q}''' = K_1 [C_2H_4]^{K_2} [O_2]^{K_3} e^{-K_4/T} \qquad \ldots . [11]$$

The solutions based on, say, four points within one flame could then be compared with those derived from other flames.

The common failing of all such schemes is that if no correlation materializes the effort has largely been wasted, the one conclusion being the rather negative one that the usually linear relationship obtained by plotting the logarithm of one quantity against the reciprocal of another is not quite so insensitive to underlying physical relationships as may have been hoped. Such an outcome seemed sufficiently probable to justify the use of methods more laborious but more analytical and informative in conclusion. An example is the calculation of the profiles of collision frequency and of numbers of collisions resulting in reaction (from heat release), leading to the distribution of the fraction of successful collisions and hence the effective activation energy. If an 'overall' mechanism applies, this quantity should be constant throughout each flame and from one flame to another. If it is not, the fact that for unit 'Lewis number' any reactant would manifest the same partial density distribution, lends significance to the 'local' values of activation energy.

This form of approach is particularly desirable since it is beginning to appear almost as appropriate to test the 'overall' kinetics to carbon monoxide and water as that to complete combustion products. One reason for not attempting this in the present instance is that both the existence of a 'tail' in carbon monoxide flames[17] and its apparent shrinkage at lower burning velocities observed here suggest that the phenomenon is at least as likely to be fundamental to flame propagation as to hydrocarbon oxidation. The main reason is, however, that the overall reaction to carbon dioxide is the one assumed in practice and hence that to be tested.

'Activation energy' effective in propagation

The measured variation of burning velocity with initial temperature, at constant initial composition, can be used to deduce an 'activation energy'. This magnitude is characteristic of the behaviour of the flame as a whole and depends to some extent on the particular theory used to express burning velocity as a function of reaction rate.

The theory[19] here employed for this purpose is that of Zeldovich and Frank-Kamenetski, for the following reasons. As discussed above, it had been shown[5] to account reasonably well for observed burning velocities in terms of measured heat release profiles. Though a 'comprehensive' theory, it expresses burning velocity explicitly in terms of integrated heat release rate and assumes most of the reaction to occur close to the final temperature, T_f. It is therefore both easy to use for the present purpose and clear as to the significance of the result obtained. Such activation energies are values that would be required to account for the effect of initial temperature on the propagation of flames whose simple reaction mechanisms release all their heat close to the final state.

According to this theory applied to a bimolecular reaction whose overall stoichiometry involves no change in mole number

$$V_0^2 = A\,\frac{T_0^2 T_f^4}{(T_f - T_0)^3}\exp\left(-\frac{E_p}{RT_f}\right) \qquad \ldots\ldots[12]$$

conversion was attained (the need for some such definition is dictated by the asymptotic approach of all curves to the distance axis) no correlation became apparent. All such 'ignition temperatures' varied with initial temperature both at constant fuel/air ratio and at constant burning velocity.

Mechanism of flame propagation

Since the aspects of the analysis relating to the mechanism of propagation of flat flames have been discussed previously[3], only a summary of those involved in the subsequent discussion is again necessary. Two conclusions emerged from independent tests of the individual steps constituting a theory of flame propagation.

First, substitution of the experimental heat release profiles into burning velocity equations and comparison of the result with measured burning velocities was used as a direct test of the procedure for solving the final equations, without involving any assumptions concerning kinetics, composition/temperature relationship etc. It transpired that, whilst D. B. SPALDING's refinements[18] resulted in considerable improvement over the original Semenov–Frank-Kamenetski approach[19], the latter was a good first approximation. It accounted for trends correctly and was found to be in error, in individual predictions, by generally less than one third. This qualified success is here significant because the theory is based on the concept that most of the reaction may be considered to occur at the final temperature.

The second point emerged from an examination of the frequently employed assumption that the diffusion coefficient of various species may be equated to the thermal diffusivity of the mixture (i.e. 'Lewis number' = 1). It was concluded that, for the lean flames examined and for the species involved in an 'overall' reaction scheme, this again was a reasonable working assumption (the biggest discrepancy occurring in the case of water) and was much superior to the neglect of diffusion. The present relevance of this result is that it can be shown on this assumption that the distribution (in terms of mass fraction) in one flame of all species whose rate of disappearance is proportional to rate of heat release is the same.

KINETICS

Method

The main aim of the part of the work here reported has been to assess the validity of the concept of an 'overall' kinetic scheme. The variety of intermediates detected in sampling studies (see e.g. ref. 15) already suggests that any such scheme is likely to be effective rather than real. Various approaches based on the heat release profile suggest themselves[20], the least deductive being the testing of proposed mechanisms. Perhaps the most obvious is the solution of four simultaneous equations representing four experimental points for constants $\boldsymbol{K}_1$ to $\boldsymbol{K}_4$ in

$$\dot{q}''' = \boldsymbol{K}_1 [C_2H_4]^{K_2} [O_2]^{K_3} e^{-K_4/T} \qquad \ldots.[11]$$

The solutions based on, say, four points within one flame could then be compared with those derived from other flames.

The common failing of all such schemes is that if no correlation materializes the effort has largely been wasted, the one conclusion being the rather negative one that the usually linear relationship obtained by plotting the logarithm of one quantity against the reciprocal of another is not quite so insensitive to underlying physical relationships as may have been hoped. Such an outcome seemed sufficiently probable to justify the use of methods more laborious but more analytical and informative in conclusion. An example is the calculation of the profiles of collision frequency and of numbers of collisions resulting in reaction (from heat release), leading to the distribution of the fraction of successful collisions and hence the effective activation energy. If an 'overall' mechanism applies, this quantity should be constant throughout each flame and from one flame to another. If it is not, the fact that for unit 'Lewis number' any reactant would manifest the same partial density distribution, lends significance to the 'local' values of activation energy.

This form of approach is particularly desirable since it is beginning to appear almost as appropriate to test the 'overall' kinetics to carbon monoxide and water as that to complete combustion products. One reason for not attempting this in the present instance is that both the existence of a 'tail' in carbon monoxide flames[17] and its apparent shrinkage at lower burning velocities observed here suggest that the phenomenon is at least as likely to be fundamental to flame propagation as to hydrocarbon oxidation. The main reason is, however, that the overall reaction to carbon dioxide is the one assumed in practice and hence that to be tested.

'Activation energy' effective in propagation

The measured variation of burning velocity with initial temperature, at constant initial composition, can be used to deduce an 'activation energy'. This magnitude is characteristic of the behaviour of the flame as a whole and depends to some extent on the particular theory used to express burning velocity as a function of reaction rate.

The theory[19] here employed for this purpose is that of Zeldovich and Frank-Kamenetski, for the following reasons. As discussed above, it had been shown[5] to account reasonably well for observed burning velocities in terms of measured heat release profiles. Though a 'comprehensive' theory, it expresses burning velocity explicitly in terms of integrated heat release rate and assumes most of the reaction to occur close to the final temperature, T_f. It is therefore both easy to use for the present purpose and clear as to the significance of the result obtained. Such activation energies are values that would be required to account for the effect of initial temperature on the propagation of flames whose simple reaction mechanisms release all their heat close to the final state.

According to this theory applied to a bimolecular reaction whose overall stoichiometry involves no change in mole number

$$V_0^2 = A\frac{T_0^2 T_f^4}{(T_f - T_0)^3}\exp\left(-\frac{E_p}{RT_f}\right) \qquad \ldots.[12]$$

where V_0 is the initial flow velocity $(= S\rho_{u,T_0}/\rho_0)$, A is a constant for a given initial composition, E_p the 'propagation' activation energy under discussion and the relationship is based on the assumption that the thermal conductivity is proportional to the initial temperature. For a temperature-independent thermal conductivity the power of T_0 in the numerator rises from 2 to 3.

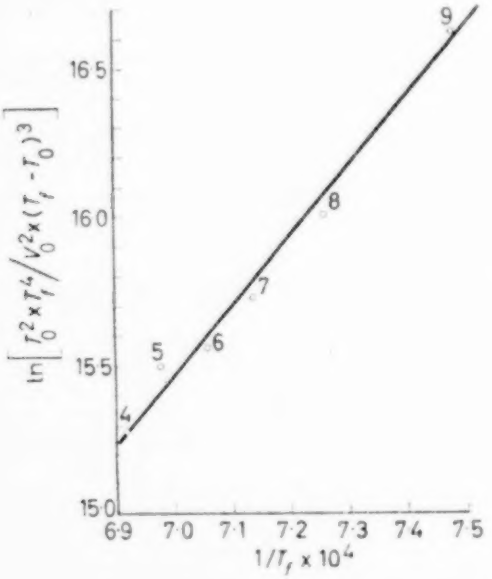

Figure 9. Activation energy from burning velocity

These relationships were examined, using a series of six flames of constant initial composition (2·31 per cent ethylene—two of these have been analysed in detail), and varying initial temperatures utilizing the whole of the available range. On the assumptions underlying the above equation, a graph of $\ln[T_0^2 T_f^4 / V_0^2 (T_f - T_0)^3]$ against $1/T_f$ should be a straight line of slope E_p/R. *Figure 9* illustrates how closely the experimental results approach the ideal. The form of the correlation is not very sensitive to a small change in the exponent of T_0 and the constant conductivity case can equally well be represented by a straight line. In making this transition, however, E_p falls by about 17 per cent.

The 'propagation activation energy' deduced from the slope is 48·8 kcal for a thermal conductivity proportional to T_0 and 41 kcal for a constant conductivity. The assumptions of the Zeldovich–Frank-Kamenetski theory make a much closer approach between these limits rather unprofitable. These values compare well with that (42 kcal) obtained by blow-off in a 'fully stirred reactor'[4] and, somewhat surprisingly, also with that (42 kcal) deduced[21] in closed vessel kinetic studies. They are further compared below with values deduced from flame structures.

Effective reaction order

If the reaction rate could truly be represented by an overall kinetics then values of a and b in the equation

$$\dot{q}''' \propto [O_2]^a [C_2H_4]^b f(T) \qquad \ldots.[13]$$

determined from distributions of $[O_2]$ and $[C_2H_4]$, calculated on the basis of such a model, would remain constant throughout each flame and from one flame to another. In order that the results should yield some information even if a and b are not constant, as discussed above, the following procedure was adopted.

Since the concept to be examined can be expressed as

$$\frac{\dot{q}_1'''}{\dot{q}_2'''} = \frac{[O_2]_1^a\,[C_2H_4]_1^b}{[O_2]_2^a\,[C_2H_4]_2^b} \qquad \ldots.[14]$$

where suffixes 1 and 2 represent two sets of results at one temperature, the relationship can be represented as the straight line

$$ax + by = 1 \qquad \ldots.[15]$$

by using logarithms. The coordinates are

$$x = \frac{\log([O_2]_1/[O_2]_2)}{\log(\dot{q}_1'''/\dot{q}_2''')} \quad \text{and} \quad y = \frac{\log([C_2H_4]_1/[C_2H_4]_2)}{\log(\dot{q}_1'''/\dot{q}_2''')}$$

Thus, by using concentrations calculated on the overall reaction model to be tested, for points in several flames but at one particular temperature and by plotting these as indicated, the effective orders become the two intercepts of the graph. The merit of the approach is that it yields values at each temperature throughout the profile, independently of other parts of the flame. Moreover, if a and b are indeed constants for the reaction then all points from all flames should lie on the same straight line.

The results showed that not only did all points eminently not lie on a single line but the 'orders' manifested a systematic trend from exceedingly high values in the low-temperature regions to reasonable ones near the zone of maximum heat release rate. At temperatures below 900°K, values of b exceeded 10 but this decreased steadily, reaching 1·6 at 1 250°K in the region of high reaction rate. Values of a were both always smaller than those of b and much more erratic. The latter is due to errors magnified by the smallness of reaction-induced changes in $[O_2]$, in the very lean mixtures employed. This can be confirmed by ignoring the oxygen-dependence altogether, whereupon the b profile changes only very little. Within these limitations, the form of the trend is much the same a exceeding 4 below 800°K and reaching 0·1 at 1 250°K.

The following conclusions emerge. At low temperatures it is necessary, in order to account for the observed changes in reaction rate in terms of those in reactant concentrations, to postulate enormous 'orders' with respect to ethylene and oxygen. These values are so large that it is obvious that the rate must, in fact, be determined by species whose concentrations vary (from flame to flame, at constant temperature) much more rapidly than do those of the main reactants. Results discussed subsequently indicate that these are likely to be radicals. The same mechanism, however, does not appear to hold throughout the flame and as the final state is approached the values attained make explanations based on overall kinetics at least possible. Indeed the sum of the 'orders' near maximum reaction rate is seen to be 1·7 as compared with the 'total order' of 1·8 determined at blow-out (and hence maximum reaction rate) by the 'stirred reactor' technique[1]. Thus, although an overall kinetics manifestly does not apply, it may well appear to do so in measurements based on blow-out burning velocities and, in general, those dominated by the maximum reaction rate. It also appears, in accordance with other measurements, that the rate is much more fuel- than oxygen-dependent.

Activation energies from flame structure

Two forms of approach, based respectively on the statistical theory and on the Arrhenius factor, seem particularly relevant.

From measured temperature profiles and composition profiles based, initially, on the assumption of an overall reaction to be tested, the distribution of collision frequency between fuel and oxygen molecules is calculable. Thus, ${}_1Z_2$, the volumetric collision rate between species 1 and 2 is given[22] by

$${}_1Z_2 = (A^2/4)(\sigma_1+\sigma_2)^2 c_1c_2[8\pi RT(1/M_1+1/M_2)]^{1/2} \qquad \ldots.[16]$$

where σ, M and c represent respectively the collision diameters, molecular weights and concentrations (mole/cm^3) of the species concerned, A is Avogadro's number and other symbols have been defined previously. The distribution of the frequency of successful collisions (i.e. those resulting in heat release) is readily obtainable from the heat release rate profile, its local value being $A\dot{q}'''/H$, where H is the molar heat of reaction. A profile of the fraction of successful collisions can therefore be derived which, on the statistical theory, is the distribution of $Pe^{-E_c/RT}$, where P is a steric factor and E_c an 'effective collision activation energy'. On assuming a value of P, the profile of E_c can then be plotted.

Before examining experimental values of E_c, an alternative approach will be considered. The relationship can be written in the form

$$E/RT = \ln c_1c_2T^{1/2}/\dot{q}''' + \ln(PK) \qquad \ldots.[17]$$

where K is a constant for one pair of species. If the temperature dependence of P is negligible then the gradient of a graph of the first term on the RHS, plotted against $1/T$, is E/R. It may appear at first sight that the two approaches are equivalent, the second procedure being merely based on the differential of the first. In fact, however, the second is based on nothing more than the assumption of a rate/temperature dependence of

$$\dot{q}''' \propto T^{1/2}\exp(-E/RT) \qquad \ldots.[18]$$

(at constant concentration). The value of this 'activation energy', which will be denoted by E_A, unlike E_c, is independent of any errors in, say, collision diameters. Furthermore, whilst E_c involves an assumed value of P, E_A is based only on effective constancy of P. (It has been shown[23], by a more detailed analysis of the results presented, that variation of P cannot appreciably influence the results obtained.)

Perhaps the most striking and desirable property of the second approach, however, is that it is not rigorously tied to the reaction model under test.

As stated above, the profile of reduced concentration (i.e. deviation from initial value as fraction of maximum change) is the same for all species whose disappearance is proportional to the release of heat and whose 'Lewis number' is equal to unity. This similarity of distributions may be taken even beyond 'reactants', as defined above, in the early zones of the flame. Concentrations of all species vary due to reaction, diffusion and changes in temperature. In zones where reaction is slow and temperature is low, the latter effect becomes dominant. Thus the product of two concentrations falls by 75 per cent due to temperature changes alone in going from 300° to 600°K. With the exception of species whose concentrations vary rapidly due to local reactions very different from the main heat-releasing reaction or whose presence is entirely due to diffusion (see section below), all concentration profiles tend to become geometrically similar as temperature tends to its initial value.

Now any constants in c_1 and c_2 in the expression $\ln(c_1c_2T^{1/2}/\dot{q}''')$ may, of course, be transferred to the constant 'intercept' term without affecting the value of E_A. This is the reason why, although the present argument is based on profiles of $[C_2H_4]$ and $[O_2]$ calculated on the overall model under examination, the E_A deduced *may equally be due to bimolecular collisions between other species, particularly at the lower temperatures.*

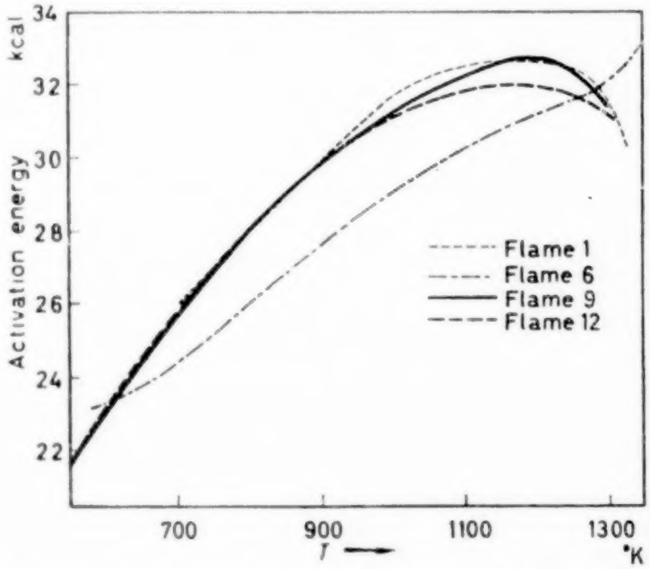

Figure 10. Calculation of E based upon an overall reaction with unit steric factor

Against this merit, it will be appreciated that the derivation of a quantity by measuring slopes on a logarithmic versus reciprocal temperature graph is a most inaccurate procedure (even though frequently used in chemical kinetics) and in terms of accuracy alone, E_c is more reliable than E_A.

Figure 10 shows graphs of E_c calculated for unit steric factor plotted against temperature. It is seen that E_c varies throughout each flame. The three flames close to the limit of inflammability give rise to almost identical graphs, but even that giving rise to more than twice the volumetric heat release rates (see *Figure 8*) differs by only about 6 per cent. All start at low values (about 20 kcal in the low temperature regions) and rise to exceed 32 kcal in approaching the zone of maximum heat release.

No particular importance is attributed to the apparent falling off, for 3 flames, of E_c close to the maximum temperature attained. Although this could be some consequence of an 'after-burning' mechanism, the small heat release rate in this zone is obtained by subtracting two large quantities one of which is determined by a measurement whose accuracy falls with increasing temperature. It therefore seems advisable to leave investigations of the 'tail' mechanism to methods claimed to be particularly suited to this region of slow reaction and to be capable of coping with its inherent difficulties.

Before considering the implications of the observed trends, it is of interest to compare them with those derived by the E_A approach. The four graphs of $\ln([O_2][C_2H_4]T^{1/2}/q''')$ against $1/T$ again lie close together, but since the measurement of the tangent of the angle of inclination is so sensitive to small changes in inclination at large slopes, it seemed advisable to average these results over all the flames at constant temperatures. The mean values of E_A at 850° K and 1 250° K were, respectively, 12·7 kcal and 36 kcal, the latter increasing further at higher temperatures, thus showing the same trend as those of E_c over an even wider range. (A somewhat similar trend has been observed in stationary manometric studies[24].)

The conclusions reinforce those arrived at in the preceding section. All 'effective activation energies' vary across each flame zone. The *detailed* reaction mechanism does not even approximately resemble an overall model. Towards the cold boundary these 'activation energies' have values characteristic of radical rather than whole molecule reactions. (It is recognized, of course, that these values of E may not correspond to any actual reaction, if the local rate-controlling step occurs between species, which, for one of the reasons mentioned, is not accommodated by the approach. In that case, however, in virtue of these reasons, the species is equally likely to be a radical.)

As the zone of maximum heat release and the hot boundary is approached, the 'activation energies' rise to more familiar values. Once again it seems quite conceivable that measurements based on the fast reaction zone alone give every appearance of obeying a 'global' mechanism of activation energies in the neighbourhood of 40 kcal.

Alternative single reaction

It now becomes of interest to invert the argument to the point of *defining* a single rate-controlling process as one whose activation energy remains constant throughout the flame and inquiring into the form of the relevant species distribution required to produce the observed heat release profile. A reaction between an unknown species and one of the reactants (say the attack of one particular intermediate upon the fuel, as a trigger rate-controlling the heat release) seems the only possibility profitable enough to justify the test of a postulated mechanism. This can again be carried out in a very general manner.

The method amounts to a reversal of the E_A calculation. If E_A is constant and the c_1 profile is that of the generalized reactant (closely similar to that of ethylene) the shape of the c_2 profile may be deduced in arbitrary but self-consistent units. The shape depends entirely on the value of activation energy chosen. *Figure 11* illustrates the profiles for 40 kcal and 5 kcal—values regarded as close to reasonable limits of possibilities. The most relevant aspect of the results, however, is that intermediate values of activation energy lead to profiles manifesting a *minimum* at intermediate temperatures.

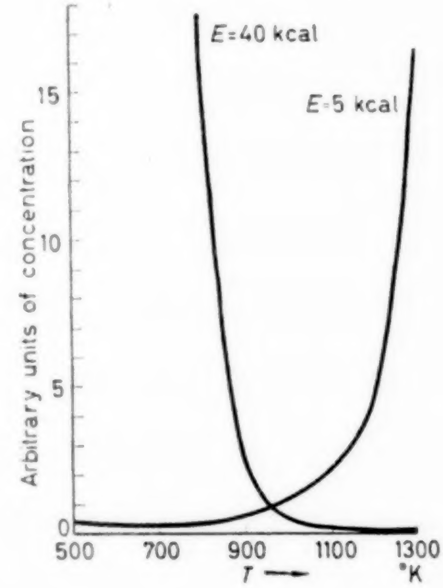

Figure 11. Relative concentration profiles

The shape of these curves is regarded as implausible. The high activation energy one is likely to describe only a reactant and this type of mechanism is proved unsound in the previous sections.

It is true that the low activation energy curve is not incompatible (on inspection—no calculations have been carried out) with the Tanford and Pease flame model of a radical distribution characterized by diffusion from its source at the burnt boundary. Current opinion, however, tends to regard a maximum in radical concentration at intermediate temperatures more probable than one at the final equilibrium state. Moreover, neither curve tends to flatten out at the flame boundaries.

The conclusions of this section are advisedly cautious. The above does not constitute proof that flame reactions cannot be accounted for by *some* single mechanism step common throughout the thickness of the flame. Even within the scheme tested in this section, a low activation energy 'triggering' by one of the products remains a marginal possibility. The type of scheme that had, *a priori*, been regarded as most likely has, however, not materialized (the profile manifesting a central minimum for most plausible *E*s) and what remains seems less probable than a scheme whose rate-controlling step varies from point to point.

CONCLUSIONS

The burning velocities of, and the refractive index distributions perpendicular to, flat flame fronts have been measured for a number of lean ethylene–air flames. The controlled variables were the initial (uniform) temperature and composition. The results have been used to deduce the distributions of volumetric heat release rate and other parameters as functions of the initial conditions. Interpretation was attempted in terms of both the mechanism of flame propagation and the relevant rate laws—in particular the concept of 'overall kinetics'. Conclusions concerning the former have been reported elsewhere[3]; those concerning the latter may be summarized as follows:

(*i*) The lack of precision in defining temperatures due to disequilibria is negligible throughout the flames studied.

(*ii*) It has been shown[3] that a theory of the form developed by Semenov, Zeldovich and Frank-Kamenetski predicts burning velocities, from measured heat release rates, which are reasonably close to measured burning velocities. It is concluded that the theory may be used to yield activation energies from initial temperature/burning velocity data (at constant fuel/air ratio) characteristic of the behaviour of the flame as a whole. The values obtained approximate to those used to account for blow-out in stirred reactors.

(*iii*) The flame structure cannot be accounted for by an overall mechanism based on reactant concentrations. No simple alternative scheme based on other species but common to all the flame zones, suggests itself.

(*iv*) Examination of the profiles of 'effective orders' and of 'activation energies' suggests, on the contrary, that in the low temperature zones heat release is controlled by reactions between species whose concentration profiles differ greatly from those of the reactants—probably low activation energy radical reactions.

(*v*) However, as the high temperature, high heat release flame zones are approached (excluding any after-burning 'tail') the reaction begins to resemble an overall mechanism. Both 'activation energy' and 'orders' based on reactants approach values obtained by blow-out studies and by flame propagation characteristics.

(*vi*) This appears to be the explanation of the paradox of the success the unlikely overall mechanisms have enjoyed when applied to processes determined by the zone of maximum heat release rate.

The conclusion may be considered rather fortunate as it tends to justify both the chemists' contempt for, and the engineers' use of, the 'global reaction' concept, each within their respective fields of application.

The authors are indebted to Professor D. M. Newitt for his interest and encouragement throughout the progress of the work and to Sir Alfred Egerton and Dr J. H. Burgoyne for many stimulating discussions.

Department of Chemical Engineering,
Imperial College of Science and Technology,
London, S.W.7

(*Received April 1959*)

REFERENCES

[1] Burgoyne, J. H. and Weinberg, F. J. *Fourth Symposium (International) on Combustion*, p 294. Williams and Wilkins: Baltimore, 1953

[2] Burgoyne, J. H. and Weinberg, F. J. *Proc. Roy. Soc. A*, 1954, **224,** 286

[3] Weinberg, F. J. *Sixth Symposium (International) on Combustion*, p 765. Reinhold: New York, 1956

[4] Longwell, J. P. and Weiss, M. A. *Industr. Engng Chem. (Industr.)*, 1955, **47,** 1634

[5] Levy, A. and Weinberg, F. J. *Seventh Symposium (International) on Combustion*, p 296. Butterworths: London, 1959

[6] Powling, J. A. *Fuel, Lond.* 1949, **28,** 25

[7] Egerton, Sir A. and Thabet, S. K. *Proc. Roy. Soc. A*, 1952, **211,** 445

[8] Reck, J., Sumi, K. and Weinberg, F. J. *Fuel, Lond.* 1956, **35,** 364

[9] Weinberg, F. J. *Proc. Roy. Soc. A*, 1957, **243,** 107

[10] Rossini, F. D. *et al. Selected Values of the Properties of Hydrocarbons.* American Petroleum Institute: New York, 1956

[11] Stops, D. W. *Nature, Lond.* 1949, **164,** 966

[12] Hirschfelder, J. O., Curtiss, C. F. and Bird, R. B. *Molecular Theory of Gases and Liquids.* Wiley: New York, 1954

[13] Klibanov, T. M., Pomerantsev, V. V. and Frank-Kamenetski, P. A. *J. tekh. Phys., U.S.S.R.* 1942, **12,** 14

[14] White, A. G. *J. chem. Soc.* 1925, **127,** 672

[15] Fristrom, R. M. and Westenberg, A. A. *Combustion & Flame*, 1957, **1,** 217

[16] Friedman, R. and Burke, E. *J. chem. Phys.* 1954, **22,** 824

[17] Friedman, R. and Nugent, R. G. *Seventh Symposium (International) on Combustion*, p 311. Butterworths: London, 1959

[18] Spalding, D. B. *Combustion & Flame*, 1957, **1,** 287

[19] Evans, M. W. *Chem. Rev.* 1952, **51,** 363

[20] Weinberg, F. J. *Aeronaut. Res. Coun. Rep. No. 19*, 1957, C.F. 401

[21] Trotsenko, M. A. and Polyakov, M. V. *Dokl. Akad. Nauk S.S.S.R.* 1954, **96,** 115

[22] Jeans, J. *Dynamical Theory of Gases.* Cambridge University Press: London, 1925

[23] Levy, A. *Ph.D. Thesis.* University of London, 1958

[24] Harding, A. J. and Norrish, R. G. W. *Proc. Roy. Soc. A*, 1952, **212,** 291

Recent Developments and Notes

FUEL CONSUMPTION TESTER

A NEW fuel consumption test equipment has been developed by Farnell Instruments Ltd to facilitate research in the design of motor fuel systems. It is difficult to measure accurately the increased or decreased efficiency of fuel systems when minor modifications have been made, but with the new equipment the result of a minor modification can be measured with an accuracy of 1 per cent.

The new equipment not only achieves greater accuracy in test-bed work, but reduces the number of personnel required for a particular test, releasing operators for other research work.

The electronic equipment incorporates a burette with two level marks and a series of photoelectric cells. When the fuel reaches the first level of the burette at the start of the test, the first photocell brings into circuit a time interval meter and a revolution counter, thus ensuring that the exact engine revolutions are counted and are not an assumed average. These continue operating until the fuel level reaches the second mark on the burette, when the second photocell automatically brings the test to an end.

To prevent unnecessary stops of the engine when fuel tests are carried out, the fuel consumption tester has been designed to allow the incoming fuel to fill the burette and to feed the engine under test at any time. When the fuel test is required, an electrically operated valve in the fuel input line closes. Before the fuel has been completely run out of the burette the photocell operates and opens the incoming fuel supply line thus preventing any break in fuel supply to the engine. The time taken for a test varies according to the speed of the engine and the size of burette used, but is about one or two minutes on the average.

FLAME-DRIVEN OSCILLATIONS

In two further papers in a series on the analysis of heat-driven oscillations of gas flows, H. J. MERK has derived a characteristic equation for flame-driven oscillations of the organ-pipe type and has discussed the theoretical results [*Appl. sci. Res., Hague, A*, 1958, **7**, 2/3, 175–191, 192–204]. The results published in previous papers in the series [*Appl. sci. Res., Hague, A*, 1957, **6**, 317–335, 402–420] have been used for the derivation of the equation. Transfer functions for the oscillations in pressure and velocity before and behind the flame front are derived. These are found to depend on fluctuations in the normal combustion velocity for which, in turn, transfer functions are defined relating to fluctuations in temperature and pressure in the flame front. By matching conditions for acoustic fluctuations on either side of the flame region, the characteristic equation is obtained. For low frequencies, an equivalent electric network may be used to investigate the flame stability.

On applying the results to actual flames, it appears that, in most cases, only the fluctuations in flame area are responsible for fluctuations in heat release. On this basis, the characteristic equation can be used to derive a condition of instability which, in effect, represents a mathematical statement of Rayleigh's criteria. The theory has been applied to the rocket-shaped burner described by A. A. PUTNAM and W. R. DENNIS [*Trans. Amer. Soc. mech. Engrs*, 1953, **75**, 15] and qualitative agreement is found with the experimental results. This would suggest that analysis of the acoustic behaviour of the flow system may be successful in explaining peculiar features of unstable combustion [M. A. MAYERS, *Appl. mech. Rev.* 1958, **11**, 703].

FLUE GAS CORROSION

Two papers were read before a meeting of the Institute of Fuel in February on methods for assessing the corrosion of surfaces by flue gases. D. ANSON, of 'Shell' Research Ltd, Thornton Research Centre, Chester, described the design and use of a radioactive corrosion probe, and R. W. KEAR, of the Oil Products Development Department, Shell Petroleum Co. Ltd, described a constant temperature corrosion probe.

The method of most practical value in investigating low temperature corrosion, as may occur especially in modern high efficiency steam boilers, is to expose an internally cooled steel probe to the gas stream for one or two hours, remove the corrosion products and analyse them. The objective in the development of a radioactive probe was primarily to reduce the time needed to complete a measurement by using short exposure times and a rapid or even continuous method of analysis.

The principle of the method is that of estimating the metal lost from an air-cooled probe during a test by a count of the radioactivity of the probe washings. Accurate results were shown to be possible using probe exposure times as short as ten minutes, and counting times of two minutes with conventional counting equipment. It may be possible to develop such a probe to give a continuous indication of corrosivity. With the design of probe described health hazards due to radioactivity are very slight if elementary precautions are taken.

It would be an obvious advantage to be able to vary, within limits, the area, size and material of the test surface which is the essential feature of a corrosion probe. It is found by experience, however, that close control of the temperature of the test surface, particularly if fairly large, is difficult if air cooling is used. Consequently in the design of the constant temperature corrosion probe, described in the second paper, water is used for lowering the temperature. This probe has been designed for long test periods with a minimum of service or attention. Various models have been in use at a number of C.E.G.B. stations and the probes have been found to function satisfactorily.

FIRE PROTECTION

The Fire Offices' Committee Fire Protection Association (Garrard House, 31–45 Gresham Street, London, E.C.2) established in 1946, is an authoritative, non-profit making organization, offering technical and general advice on fire protection. Since 1954 the Association has issued about four times a year a *Fire Protection Bulletin* designed as a propaganda leaflet devoted to a single fire hazard and made available free of charge to the public generally. This *Bulletin* has now been issued in a new style [*New Series No. 1, Spring 1959*; Quarterly, 1*s* 6*d*]. It has been enlarged in scope and will cover a variety of subjects, dealing entirely with industrial hazards and precautions. The present issue deals with dust hazards, railway-side fires, notes on some industrial fires, and automatic fire alarm systems.

METHANE OXIDATION

An investigation has recently been described by E. M. MAGEE, of the Humble Oil and Refining Company, Texas, dealing with the kinetics of methane oxidation, especially as regards the dependence of certain variables on the oxygen concentration [*J. Amer. chem. Soc.* 1959, **81**, 278]. As is well known, the mechanism of methane oxidation is obscure in many respects and more experimental data are required to show detailed relationships between variables of kinetic importance.

These experimental studies of the methane–oxygen reaction were carried out in a quartz, flow-type reactor at 815°C. The relationship between the maximum concentration of the intermediate formation of formaldehyde and the concentration of reactants is important, and this has been particularly studied, as this relationship will enter into any expression for the maximum rate of reaction.

The results obtained show that the maximum concentration of formaldehyde is proportional to the concentration of oxygen, which is of great theoretical importance. The rate of disappearance of methane at the formaldehyde maximum is proportional to the concentration of oxygen raised to the power 2·8 and the concentration of oxygen at the formaldehyde maximum is 0·70 times the initial concentration. The time at which the maximum concentration of formaldehyde appears is a linear function of the reciprocal oxygen concentration. The author suggests that these results indicate the need for revision of previously proposed mechanisms for the slow oxidation of methane.

WRINKLED FLAMES

A paper presenting important evidence for the wrinkled continuous laminar wave concept of turbulent burning has been published by J. K. RICHMOND, W. F. DONALDSON, D. S. BURGESS and J. GRUMER [*Jet Propulsion*, 1958, **28**, 393]. They describe how piloted burner flames of natural gas–air mixtures were investigated by means of flame radiation photometer measurements. Emission from the CH and C—C radicals and the continuum from the combustion of carbon monoxide were studied for time-average values and transient fluctuations of light intensity. Flow conditions ranged from Reynolds number 4 000 to 160 000 and from 1 to 2 per cent pipe-flow turbulence to 3 to 6 per cent grid-induced turbulence. For well-piloted flames, a continuously connected flame front was indicated; for inadequately piloted flames 'holes' or breaks in the flame were evident. Experiments using an electronic probe and smoke photography corroborated the existence of a wrinkled continuous laminar combustion wave in turbulent flames under restricted conditions.

Whilst with these experimental conditions it appears possible to distinguish between wrinkled continuous laminar flame, distributed reaction zone, and disconnected flamelets, gaps in the flame wave of less than 0·002 in. would probably remain undetected because of instrumentation limitation [J. M. SINGER, *Appl. mech. Rev.* 1959, **12,** 56].

JAPANESE RESEARCH ON ATOMIZATION AND COMBUSTION OF OIL

Y. TANASAWA and his colleagues have carried out a considerable number of researches on the atomization and combustion of oil droplets since about 1936 and a paper summarizing the investigations on the atomization of a liquid jet issuing from a cylindrical nozzle was published by Y. TANASAWA and S. TOYODA about four years ago [*Technol. Rep. Tôhoku Univ.*, 1955, **19,** 2, 135–156]. The behaviour of a liquid jet was studied by means of spark illumination of very short duration, at increasing pressures. The successive phases of dripping, a lengthening stream breaking into drops at the end, roughening of the stream surface with stripping of liquid filaments from it, and finally the stream breaking up into droplets forming a spray, were investigated. The effect of injection pressure on mean drop size was also shown. As a result of a theoretical analysis a dimensionless number termed 'Jet Number' was introduced as a characteristic quantity for the mode of atomization.

Subsequent work on atomization has been reported in a series of papers during the past three years by Y. TANASAWA *et al.*, which have recently become available in Western countries [*Technol. Rep. Tôhoku Univ.*, 1955, **20,** 1, 27–58; 1956, **21,** 1, 117–145; 1957, **22,** 1, 73–95; 1958, **22,** 2, 153–172]. The first two of these reports cover work carried out for several years on the principles of atomization by the swirl type of atomizer and on the atomizing characteristics of injection for diesel engines.

In the more recent reports investigations are described on the atomization of liquids by means of impingement nozzles and the possible application of these in some form for use in diesel engines. With flat impingement nozzles atomization is found to occur by film formation.

With regard to the combustion of liquid fuels, Y. TANASAWA and Z. TAMURA have discussed the theory of combustion of a single fuel droplet, taking into consideration the variation of the physical properties of the surrounding gas with temperature [*Science of Machines*, 1957, **9,** 671–677 (in Japanese)]. Assuming that the thermal properties of the surrounding gas, namely, the thermal conductivity, the coefficient of diffusion, and the specific heat, are linear functions of the temperature, expressions are obtained for the temperature distribution and for the concentration of fuel vapour around a single drop during combustion. The effects of the surrounding pressure on the coefficient of combustion velocity are also discussed.

The rate of combustion of a fuel spray is difficult to determine owing to the variety of drop sizes and their distribution. The problem has been examined in a paper by Y. TANASAWA and T. TESIMA [*Bull. J.S.M.E.* 1958,

1, 1, 36–41]. A simplified theory is put forward and the authors derive, partly by mathematical and partly by graphical methods, a formula giving the unburnt amount at a given instant after the beginning of combustion. Charts are given for the change of weight distribution during combustion for various initial size distributions of droplets in the spray. The results apply only to an initial distribution of the Rosin–Rammler type and consequently the expressions derived by the authors are only of relative value as they do not correspond to actual conditions [from abstracts by K. J. DeJuhasz, *Appl. mech. Rev.* 1959, **12**, 66, 134].

The most recent of these papers is one by Z. Tamura and Y. Tanasawa on the evaporation and combustion of a drop contacting with a hot surface [*Seventh Symposium (International) on Combustion, London and Oxford, 1958*, p 509. Butterworths: London, 1959].

MECHANISM OF HYDROCARBON OXIDATION

Several reaction schemes have been put forward to account for the main features of the slow oxidation of hydrocarbons on the basis of a degenerately branching free-radical chain mechanism. There is, however, considerable uncertainty as to the nature of the basic chain-propagating steps and of the intermediate product responsible for branching. The chain-propagating mechanism has recently been investigated by J. H. Knox, R. F. Smith and A. F. Trotman-Dickenson, at the Chemistry Department, The University of Edinburgh [*Trans. Faraday Soc.* 1958, **54**, 1509]. The basic chain being mainly responsible for the disappearance of hydrocarbon in an oxidation process, the relative rates of the main propagating reactions in a mixed oxidation may be found by measurement of the relative rates of disappearance of the two hydrocarbons. In this investigation this measurement was made for ethane and propane mixtures by analysing the reaction products using gas chromatography.

The relative rate of disappearance of ethane and propane in mixtures of the two gases reacting with oxygen was found to be $0{\cdot}44 \pm 0{\cdot}03 : 1$. This value is almost independent of temperature, composition and total pressure between 274° and 495° C. The chain propagation reactions in the competitive oxidation of these two hydrocarbons therefore have equal activation energies and the radicals formed in the two propagation reactions attack a given hydrocarbon, ethane or propane, at equal rates.

It is concluded that the oxidation of both ethane and propane is probably propagated either by the same radical over the whole temperature range or, if different radicals operate at different temperatures, by radicals having very similar properties. The radical involved would appear to react with low activation energy with both hydrocarbons. If the heat of formation of HO_2 is 102 kcal/mole as given by M. G. Evans, N. S. Hush and N. Uri [*Quart. Rev. chem. Soc., Lond.*, 1952, **6**, 189], the results of this research point strongly to the conclusion that the HO_2 radical is the main chain propagator in the temperature range considered.

ROYAL SOCIETY OF ARTS PRIZES

The Royal Society of Arts, as trustees for certain endowments, offers two prizes during the year 1959. The Howard Trust was established in 1868 for the purpose of making awards periodically to the authors of treatises on steam or other motive agents, and a prize of £50 will be awarded to the author of a treatise on some aspect of the subject of motive agents. Under the Fothergill Trust, established in 1821, a prize of £20 is offered for a descriptive essay or model embodying some new idea for the prevention or suppression of fire.

Entries for the above prizes must be received by the Secretary of the Royal Society of Arts, 6–8 John Adam Street, Adelphi, London, W.C.2, not later than 31 July 1959, and must be clearly marked with the entrant's name and address and the prize for which they are submitted. Essays must be typewritten. Further particulars may be obtained from the Secretary at the above address.

EXPLOSION HAZARDS OF KEROSINE

In a paper presented to the American Petroleum Institute, M. G. **Zabetakis** reported an investigation on the explosion hazards associated with the handling of kerosine [*Proc. Amer. Petrol. Inst.* 1957, **37,** 296; abstract in *Chem. Abstr.* 1958, **52,** 9601]. The roles of combustible and oxidant in the explosion of kerosine vapour, mist and foam in air and in vitiated air were examined. The hazards at temperatures below the flash point of kerosine are related to the formation of mists and foam in the vapour space above the liquid surface. It is suggested that oxygen concentrations in the atmosphere should be decreased when there is a possibility of explosive vapour–mist–air mixtures being formed, since it is extremely difficult to eliminate all potential ignition sources. Kerosine foams are flammable in air and also in air which is vitiated with nitrogen or carbon dioxide. Flame propagation through such foams appears to involve combustion of the mist produced by the collapse of the foam. The use of antifoam agents to control foam formation was investigated but so far the result has not been satisfactory.

EFFECT OF SURFACES IN COMBUSTION OF METHANE

D. E. **Cheaney**, D. A. **Davies**, A. **Davis**, D. E. **Hoare**, J. **Protheroe** and A. D. **Walsh** presented a paper to the *Seventh Symposium (International) on Combustion, London and Oxford, 1958*, p 183, on the effects of surfaces on the combustion of methane and the mode of action of anti-knocks containing metals.

A classification of surfaces with regard to their effects on slow oxidation is made by these authors, first of all, by accepting that the basic mechanism of hydrogen–oxygen reaction at the second explosion limit means that the particular fate of HO_2 radicals depends on which one of two types of surfaces adsorbs these radicals. A further feature of the classification is the recognition of the varying ability of surfaces to destroy H_2O_2.

Three categories of surfaces are proposed:

Category I: silicic acid, boric acid, phosphoric acid and germanium dioxide

Category II: metallic oxides, probably hydroxides, and salts in general

Category III: metallic surfaces, such as silver, which are known to be extremely effective heterogeneous catalysts for the decomposition of H_2O_2.

These three categories of surfaces yield different kinetic laws governing the slow oxidation of methane which are discussed in the paper. The following reactions are considered as being involved for the fate of HO_2 and H_2O_2, according to the three different types of surface:

HO_2: I. *Either* preserved *or* $HO_2 \rightarrow (HO_2)_{ads.} \xrightarrow{H^+} \frac{1}{2}H_2O_2 + \frac{1}{2}O_2$

II. $HO_2 \rightarrow (HO_2)_{ads.} \xrightarrow{e} \frac{1}{2}H_2O + \frac{3}{4}O_2$: diffusion-controlled

III. $HO_2 \rightarrow (HO_2)_{ads.} \xrightarrow{e} \frac{1}{2}H_2O + \frac{3}{4}O_2$: diffusion-controlled

H_2O_2: I. Preserved

II. $H_2O_2 \rightarrow (H_2O_2)_{ads.} \xrightarrow{e} H_2O + \frac{1}{2}O_2$: not diffusion-controlled

III. $H_2O_2 \rightarrow (H_2O_2)_{ads.} \xrightarrow{e} H_2O + \frac{1}{2}O_2$: diffusion-controlled

A portion of this paper is occupied with a discussion of the mode of action of anti-knocks containing metals. As a result of their considerable investigations of this subject previously carried out, these authors conclude that lead tetraethyl produces fog in an engine cylinder and, in view of the known acute inhibition by PbO surfaces, there can be little doubt that it is the surfaces of the fog particles that cause the anti-knock action. The common feature of metallic derivatives that act as anti-knocks is that they are known, or strongly expected, to produce on oxidation fogs of solid particles. The characteristic effects of these anti-knocks are likely to be associated with Category II surfaces.

SOLID PROPELLANT BURNING

An important investigation on the resonant burning of a solid propellant with cross flow has been made by L. GREEN, Jr [*Jet Propulsion*, 1958, **6,** 386]. The author uses a model in which a coupling of two processes is assumed: (*i*) heat flux from the burnt gases to a reaction zone across a film whose thickness is governed by aerodynamic rather than by chemical factors, and (*ii*) exponential dependence of reaction rate on the temperature of the reaction zone which is determined by a heat balance. After making some simplifying assumptions steady-state equations are solved and the variables are shown to be reasonably related to one another. The model is then used for a study of non-steady state burning by a perturbation treatment of the steady-state equations. The variation of burning rate is assumed to follow the variation of reaction zone temperature with a time lag. When the frequency of parallel velocity fluctuations resulting from acoustical oscillations has an appropriate relation to the thermal and ballistic properties of the propellant, the model predicts a resonant condition which would give rise to large fluctuations of reaction temperature. If the reaction rate increases faster than linearly with temperature, as is presumed, this fluctuating temperature would cause an increase in mean effective burning rate [R. FRIEDMAN, *Appl. mech. Rev.* 1959, **12,** 204].

IGNITION OF FIREDAMP BY HOT GASES

It has been noted by H. G. **Wolfhard** in his researches on the ignition of explosive mixtures by jets of hot gases that the observed ignition temperatures do not correlate with other known flame characteristics. The differences are specially marked when the values are compared with 'spontaneous ignition temperatures' measured in furnaces. For example, hydrogen and carbon monoxide have high 'spontaneous ignition temperatures', whereas their relative 'gas ignition temperatures' are low.

The earlier work on this subject has been extended to conditions that may be expected to prevail in the ignition of firedamp by hot spent detonation gases, as may occur in mining conditions. This work was described in a paper by H. G. **Wolfhard** and M. M. **Vanpee** read to the *Seventh Symposium (International) on Combustion, London and Oxford, 1958*, p 446. In this investigation hot jets which were running continuously were used whereas firedamp ignition underground is by a short burst of hot gas. The time factor involved is of considerable importance and some of the conclusions reached may need modification in view of this difference in conditions.

The influence of the velocity of the hot jet on ignition temperature, the ignition temperatures of fuel mixtures, the influence of the oxygen index on ignition, and ignition temperatures with a hot jet containing a fuel or an oxidizer, were investigated. It was found that under ideal conditions in the method used and for laminar hot jets, the ignition process is highly reproducible. This contrasts with the results obtained in the testing of explosives which have to be expressed in a statistical manner. The turbulence of the hot jet emerging from a shot-hole introduces an element of uncertainty and the breakup of the jet into eddies under such conditions is not reproducible in the laboratory. The presence of 9 per cent ethane in a mixture with methane, representing the approximate composition of firedamp, reduces the ignition temperatures by about 30°C.

The most important conclusion arrived at is that the concept of a 'most ignitable mixture', as exemplified by the use of an 8 per cent natural gas–air mixture for testing purposes, is useful only if the hot jet is inert, consisting only of carbon dioxide, water vapour or nitrogen. If oxygen is present in the hot jet the most ignitable mixture may be close to the rich limit. When small amounts of hydrogen and/or carbon monoxide are present in the products of a detonated explosive, this may reduce the ignition temperatures of fuel–air mixtures by as much as 500°C. It also makes fuel–air mixtures near the lean limit, which are more likely in a mine, the most ignitable. Large amounts of hydrogen and carbon monoxide in the products also decrease their temperature, consequently the most dangerous explosives may be those that liberate small amounts of hydrogen and carbon monoxide.

IONIZATION IN FLAMES

Several papers were read at the *Seventh Symposium (International)* on *Combustion, London and Oxford, 1958* on different aspects of ionization in flames and combustion gases. Two of these were by S. **Basu** and J. A. **Fay** (p 277), on ionization in detonation waves, and by H. **Williams** (p 269), on the predominant process of electron decay in the mantle of an acetylene–air flame.

In the first of these papers measurements were made by a d.c. probe technique of the electrical conductances of stoichiometric oxy-hydrogen detonation waves at varying initial pressures up to 1 atm. and of oxy-acetylene detonation waves at 1 atm initial pressure, with mixture composition varying from 30 to 80 per cent of acetylene. Since the electrical properties of ionized gases depend partly upon the electron density, it is of considerable interest to determine whether or not thermodynamic equilibrium with respect to ion formation is established behind the wave.

It is concluded that equilibrium ionization is achieved in these mixtures. The formation of NO^+ ions dominates the ionization in oxy-hydrogen detonation and it is suggested that OH^- are probably not formed due to lack of time. In oxy-acetylene detonation agreement between theory and experimental results was not so good and with 66 per cent acetylene in the mixture there is found to be homogeneous rather than total equilibrium. In very rich mixtures, with more than 70 per cent acetylene, the measured conductivity is as much as ten times the value computed from equilibrium considerations. This may be due, according to the authors, to the formation and ionization of polymers of lower ionization potential than that of acetylene, such as benzene.

In the second paper an investigation is described to determine the relative roles of recombination and attachment in the decay of ionization in hot flame gases. An acetylene–air flame, with its exceedingly high concentration of electrons, was studied by determining the decay of ionization with distance, and consequently with time, above the reaction zone. The decay of ionization was detected by its damping effect on a self-resonant electrical circuit. The preliminary results obtained strongly indicate that the process of attachment, whereby an electron attaches to a neutral molecule to form a negative ion, is predominant at distances greater than 6 cm above the reaction zone.

At the XVIme Congrès International de l'Union Internationale de Chimie Pure et Appliquée, held in Paris in April 1957, M. Sasiadek, Ecole polytechnique, Wroclaw, presented a paper describing his work on the relation between the ionization and the luminosity of gases during the explosion of solid explosives [*Rev. Inst. Franç. Pétrole*, 1958, **13**, 697]. A relationship is shown between the variation in intensity of the luminosity and in the amount of ionization with time, such as has been previously observed in gaseous explosions (W. A. Kirkby, *J. chem. Soc.* 1935, **137**, 160, 165).

THE INITIATION OF DETONATION IN GASES

Several papers were presented to the *Seventh Symposium (International) on Combustion, London and Oxford, 1958*, on the subject of the mechanism of initiation of detonation in gases. The main conclusions of these are noted here.

A. K. Oppenheim and R. A. Stern (p 837) described a method of analysis for the evaluation of the effects produced by wave propagation and interaction phenomena which are observed during the transition from deflagration to detonation in a constant area duct. The analysis is built up from experimental records of shock front and flame traces in the time–distance domain. By this means a complete description is said to be given of the thermodynamic and dynamic aspects of the initiation of detonation and it is concluded that the development of detonation does not involve anomalous chemical kinetics and the process is controlled principally by gas-dynamic wave-phenomena.

G. K. Adams and D. C. Pack (p 812) presented some observations on the problem of transition from deflagration to steady detonation. They reject the idea put forward by Oppenheim that changes occur in passing through the Chapman–Jouguet states such that the flame catches up its accompanying shock wave. They believe that a deflagration wave can at best achieve the speed of its accompanying shock wave, and when this happens the detonation wave is set up.

These authors discuss the problem as to the state of flow set up by a wave of chemical reaction moving with a given velocity down a tube. They conclude that deflagration and detonation states which in conventional treatments are represented in terms of Hugoniot curves as widely separated states reached by compression or expansion from a common initial state, are related by a continuous set of solutions of the flow problem corresponding to experimentally realizable situations. In this way it is possible to see how transition from deflagration to detonation will take place, given some mechanism for increasing the flame speed to the required value. Two mechanisms for the increase in flame speed are discussed, an increase in area of the flame surface and an increase in the transport properties within the reaction zone. Under suitable conditions turbulence plays a part in bringing about these increases.

S. R. Brinkley, Jr and B. Lewis (p 807) in their paper on this subject emphasize the importance of the intermittent generation of pressure pulses during the propagation of highly turbulent flames. These pressure pulses are due to the almost instantaneous reaction of the unburnt gas contained in the turbulent flame brush and there is recent experimental evidence to indicate the part played by these pulses in the acceleration mechanism of the deflagration wave during the final stages of the run. This evidence is particularly due to B. Karlovitz [*Selected Combustion Problems*, p 176. Butterworths: London, 1954; and a paper on 'The growth and burnout of flame surface in a turbulent stream', *Seventh Symposium (International) on Combustion, London and Oxford, 1958*, p 604].

M. A. Cook, D. H. Pack and W. A. Gey (p 820) described experimental researches on the transition from deflagration to detonation in gaseous, liquid and solid explosives. Their results indicate that the transition involves essentially the same phenomena in all three types. They obtained direct evidence in the detonation of nitromethane of a *heat pulse* or *flash-across* which is a new phenomenon that they consider may constitute a major advance for the formulation of a theory of detonation. The speed of the flash-across phenomenon was found to have the remarkable value of 35 mm/μsec. This is regarded by the authors as the heat pulse predicted by M. A. Cook, R. J. Keyes and A. S. Filler [*Trans. Faraday Soc.* 1955, **52**, 369; *J. chem. Phys.* 1955, **23**, 409]. It is believed that there is a non-adiabatic explanation of this phenomenon and there appears to be considerable evidence that heat transfer is not a negligible factor in detonation.

SPECTROSCOPIC STUDY OF FLAMES IN HIGH SPEED FLOW

S. Barrère and M. Barrère, O.N.E.R.A., Châtillon-sous-Bagneux, Seine, read a paper at the XVIme Congrès International de l'Union Internationale de Chimie Pure et Appliquée, held in Paris in April 1957, on a spectrographic study of combustion in high speed flow [*Rev. Inst. Franç. Pétrole*, 1958, **13**, 649]. The point of view from which this work was undertaken is that molecules detected by the spectrograph, although arising from secondary reactions, act as indicators of the fluctuations in the medium in which they exist. Consequently variations in their concentration which can be found by measurements of the intensity of molecular bands, are indicative of the state of combustion at any given instant at a given position in the flame. The emitting radicals define by their intensity the zone of active combustion and a study of their distribution allows, at least in some cases, an insight into the precise mechanism of the combustion process. The authors state that a previous investigation of a turbulent flame has shown that it is not necessary to consider the zone of combustion as consisting of superposed laminar flame fronts, but as a zone of progressive combustion [R. R. John and M. Summerfield, *Jet Propulsion*, 1957, **27**, 2, 1, 169].

Two experimental methods are described using either the head of the emitting band or the band itself, simultaneous measurements being made at a given point of the flame, of the intensity variation of CH, C_2 and OH bands. These methods are applied to the study of two types of flames stabilized in high speed flow, either by a bluff body or by a pilot flame. The intensity ratio of the CH and C_2 bands is found to be a parameter particularly related to the local mixing process of fresh and burnt gases, and the values found for these intensity ratios show an identical distribution for the two types of flames. This emphasizes the importance of the mixing process in the stabilization of flames by a bluff body.

SALTERS' INSTITUTE OF INDUSTRIAL CHEMISTRY

Professor A. R. J. P. Ubbelohde, M.A., D.Sc., F.R.S., Professor of Thermodynamics at The Imperial College of Science and Technology, London, has been appointed Director of the Salters' Institute of Industrial Chemistry on the retirement of Sir Alfred Egerton, F.R.S., on 30 June 1959.

FUEL

The following *Notes* appeared in the April issue of *Fuel* and may be of interest to readers of *Combustion and Flame*:

The efficient use of fuel
New motor fuel
Reactivity of coke

Combustion Institute Interests

EIGHTH INTERNATIONAL SYMPOSIUM ON COMBUSTION, 1960

Preliminary planning of functions in connection with the Eighth International Symposium on Combustion, 1960, is being made under the direction of W. J. BENNET, Chairman of the Arrangements Committee for the Eighth Symposium. Technical sessions are tentatively proposed for 5 to 9 September 1960.

WESTERN STATES SECTION (U.S.A.) OF THE COMBUSTION INSTITUTE

Present members of the Executive Committee of the Western States Section of the Combustion Institute were elected on 24 March 1959 and are: W. J. BENNET, Marquardt Aircraft Co., Chairman; E. S. STARKMAN, University of California, Vice-Chairman; G. S. BAHN, Marquardt Aircraft Co., Secretary; M. W. RIGG, Office of Naval Research, Treasurer; R. S. LEVINE, Rocketdyne, Arrangements Committee Chairman; G. A. AGOSTON, Stanford Research Institute, Finance Committee Chairman; H. B. ELLIS, Aerojet-General Corp., Membership Committee Chairman; E. E. ZUKOSKI, California Institute of Technology, Papers Review Committee Chairman; A. L. BERLAD, Convair Scientific Research Laboratory, Programme Committee Chairman.

SPRING MEETING OF THE WESTERN STATES SECTION

The spring meeting of the Western States Section of the Combustion Institute took place at San Diego, Calif., on 23 to 24 March. The following are brief abstracts of papers presented and readers are referred to G. S. BAHN, Secretary, Marquardt Aircraft Co., 16555 Saticoy Street, P.O. Box 2013—South Annex, Van Nuys, California, for fuller information.

Study of combustion processes affecting self-sustenance of reaction in monopropellant gas generators

By J. W. BJERKLIE

A model of combustion in an ethylene oxide monopropellant gas generator has been chosen and analysed. Those factors contributing to the ability of a combustion device to sustain its operation after removal of initial ignition source have been lumped together and termed the self-sustenance process. It includes fuel injection, spray formation, droplet ignition, droplet burning, and gas entrainment by propellant spray. A suitable model of a spray was found to be gaseous fluid jet of the same geometry, mass flow, and momentum as the liquid spray.

Non-adiabatic flame theory

By A. L. BERLAD and C. H. YANG

This paper treats a non-adiabatic laminar flame in a homogeneously premixed gaseous medium which is contained in an infinitely long cylinder, Numerical examples are calculated for various stoichiometric propane–oxygen–nitrogen flames. Close agreement between calculated values and experimental data for flame extinction limits are obtained.

Effect of physical and chemical mechanisms on combustor performance optimization

By R. J. Brazil and A. Feder

Optimization of a ramjet or rocket combustor thrust to weight ratio consistent with very high combustor performance is at the present time a trial and error procedure. However, by combining empirical correlations, engineering experience and basic fundamental analysis, thinking can be directed toward a rational approach to combustor optimization. Quantitative descriptions of three important physical and chemical mechanisms of the combustion process are considered: (*a*) fuel and/or oxidizer vaporization; (*b*) flamespreading—the propagation of the flame through the unburnt fuel–oxidizer mixture; and (*c*) turbulent fuel diffusion—the preparation of the fuel–oxidizer mixture. Unique methods will be presented which evaluate the above mechanisms quantitatively to permit combustor optimization. These methods are: (*1*) extension of experimental fuel vaporization data to a wide range of combustor operating conditions; (*2*) correlation of the flame propagation angle with operating conditions; (*3*) optimization of parameters in the fuel distribution equation to yield minimum temperature stratification at the combustor exit.

Study of partially premixed flames of butane–oxygen

By S. R. Smith and A. S. Gordon

Studies of the mechanism of burning in hydrocarbon diffusion flames indicate that the fuel first pyrolyses and the resultant hydrogen and carbonaceous particles are burnt. On the other hand, the pyrolysis of oxygenated hydrocarbon fuels results in oxygenated intermediates and ultimately carbon monoxide is formed in addition to hydrogen and carbonaceous particles. Studies of premixed hydrocarbon flames have not clearly indicated whether oxygenated compounds (e.g. formaldehyde) are formed in the reaction zone. The temperature becomes so high in fully premixed flames that probing at atmospheric pressure is unsatisfactory. We have premixed small amounts of oxygen to spread out the reaction zone and keep the temperature low enough to permit use of probing techniques. The butane–oxygen flame was studied.

Application of surface decomposition kinetics to detonation of ammonium nitrate and *Detonatability of solid composite propellants*

By W. H. Andersen and R. F. Chaiken

Kinetic rate data for the linear surface gasification (pyrolysis) of ammonium nitrate are used in conjunction with the Eyring grain-burning theory to calculate the detonation reaction time for ammonium nitrate. A new grain-burning mechanism is postulated which results in a reaction time for detonating ammonium nitrate which is consistent with that calculated by means of the nozzle and curved-front diameter theories. The possible implications of the new model with respect to low velocity detonation in mixtures of granular explosives are discussed. Discussion of the ammonium nitrate detonation reaction strongly suggests that the rate-controlling step of grain burning is an endothermic surface gasification process.

A fundamental investigation of the factors involved in the detonation and abnormal (accelerating) deflagration of solid composite propellants is described. A theoretical model of propagation of detonation in propellants is presented. This model is based on the hypothesis that detonation is propagated by the same rate-controlling chemical reactions that occur during normal burning of the oxidizer. In particular, it is assumed that a grain-burning process occurs and that the linear-surface decomposition (pyrolysis) rate of the oxidizer is the rate-controlling chemical reaction. Preliminary data on the surface decomposition of ammonium perchlorate, which were obtained by the linear-pyrolysis technique, suggest that sublimation of ammonium perchlorate (with an apparent activation energy of ~ 20 kcal/mole) is the rate-controlling step in the surface-decomposition reaction. These rate data are used in conjunction with the detonation model to calculate critical diameters for cylindrical charges of detonating propellant. The calculated critical diameters for pure ammonium perchlorate (1 to 5 in.) are consistent with those observed experimentally. Utilizing the assumption that the binder in a detonating propellant acts only as an inert heat sink in the detonation reaction zone, the calculated critical diameters for essentially non-porous solid composite propellants are found to be several feet. The role of ignition processes in the detonation and rapid deflagration of solid composite propellants is discussed. The concepts of the grain-burning detonation model are re-evaluated in terms of the possible effects of porosity on detonation ignition. A preliminary theoretical approach to accelerating burning in a porous propellant is also presented. This approach indicates that porous burning in rocket motors containing a solid composite propellant can lead to very rapid chamber-pressure build-up so that an explosion could occur within 0·01 second after porous burning begins.

Experimental research in combustion instability of solid propellants

By E. W. Price

An extensive programme of research conducted under laboratory conditions during the last two years has revealed some aspects of unstable combustion which could not be established conclusively by tests in rocket motors. It has been shown that the combustion is capable of exciting gas oscillations over a wide range of frequencies with no intermediate 'forbidden frequencies' suggested by some theories of combustion instability. It has been shown that the excitation of gas oscillations occurs under an environment of oscillating pressure, density, and temperature rather than one of tangential gas oscillations at the burning surface. It has been shown that the gross changes in propellant burning rate associated with combustion instability occur primarily in an environment of tangential gas oscillations at the burning surface, that these rate changes are usually increases, and that they may or may not be associated with macroscopic disruption of the propellant surface (depending on the propellant and the severity and frequency of the gas oscillation). The burning rate changes are roughly proportional to amplitude of the pressure oscillations, differ conspicuously for various propellants, and are not critically sensitive to frequency of the gas oscillation as suggested by theory.

Questionable heats of formation of boron compounds

By J. Perrine, G. N. Tyson, Jr and I. Shapiro

If the mechanism for the vaporization of liquid boric oxide is considered, then the variation in the vapour pressure with temperature cannot be used to determine the heat of formation of gaseous boric oxide. Further, the mechanism of vaporization indicates that the equation of state of gaseous boric oxide will be very different from that for ordinary gases. The reported heats of formation for BN (g) and B_2 (g) are not in conformance with boron chemistry and it is very probable that neither has ever been seen spectroscopically in the ground state. Spectroscopic identification of B_2 (g) is based on an incorrect nuclear spin assignment for the ^{11}B nucleus, i.e. 5/2 instead of 3/2.

A simplified method of predicting combustion temperatures and specific impulses using the energy parameter

By J. R. Perrin, C. J. O'Brien and A. Kuestner

A direct method for predicting combustion temperatures resulting from the reactions of fuels and oxidizers is presented. This method uses an energy parameter which had been developed previously for the prediction of laminar flame velocities. The correlation of specific impulses with the energy parameter shows considerable promise. A method is presented for predicting stoichiometric flame or combustion temperatures based on the correlation of flame temperatures with the energy parameter. Thirty different fuels were used with eight different oxidizers.

High speed camera studies of high explosive phenomena

By J. K. Crosby and C. H. Bagley

The study of high explosive phenomena by the use of high speed cameras is described and examples of the results obtained are shown. The Beckman and Whitley Framing Camera, which records at rates up to 2·5 million frames per second, is described. This camera may be used for: studies of the movement, interaction, and shaping of detonation fronts; shock front interaction with free surfaces and other shocks; fragmentation processes; and the ignition of a monopropellant by an electric discharge. A framing disc camera, designed to operate at a rate of up to 15 000 frames per second is described. Examples of its work include studies of the breakup of liquid drops and events taking place when an elastic material is stretched until it breaks.

Investigation of droplet combustion in the shock tube

By K. Sato

A shock tube has been employed to investigate the interaction between liquid-fuel droplets and a transverse shock wave in an oxidizing atmosphere, A high speed motion picture camera was employed to follow the course of droplet breakup. The results obtained in this investigation show that the breakup of liquid droplets is due primarily to the gas flow following the shock front. Extremely rapid dispersion of droplets was observed with the shock strengths employed in this investigation.

Shattering of burning and non-burning propellant droplets by shock waves

By E. Rabin

Studies have been conducted in a 1 in. square shock tube to determine the effect of shock waves in the breakup of burning and non-burning liquid fuel droplets. Experimental data show the existence of two main classes of breakup, a bag type and a shear type occurring for both burning and non-burning drops. Type of breakup and critical velocity required to cause breakup are found to be significantly influenced by the duration of the flow plateau following the shock front; however, as yet no generalized correlation has been established. The critical velocity for burning drops was found to be slightly lower than for non-burning drops of RP-1, probably due to differences in surface tension. The effect of test section pressure was examined briefly and it appears that the ratio of critical velocity varies inversely as the 3/4 power of the pressure ratio.

Combustion of a fuel spray in the channel of a shock tube

By W. T. Webber

The experimental technique employed was to burn sprays of liquid fuel in an oxygen atmosphere in the channel of a shock tube through which a pressure pulse was passed. The pressure, velocity, and temperature perturbations of the wave affect the combustion rate at the location of and in the wake of the wave, and thus can act to sustain or augment the wave to the point where it resembles a detonation. Some experiments were conducted to determine which combinations of droplet size, initiating pulse amplitude, pulse duration, extent of combustion completed before introduction of the pulse, etc., cause the wave to grow to detonation strength, and which allow it to decay. Other experiments were conducted to infer combustion rates quantitatively as functions of wave strength, by measuring pressure histories at several positions along the tube. In these experiments, Reynolds numbers (based on an assumed mean droplet diameter of 1 000μ) ranged from about 15 000 to 150 000. Combustion rates do not disagree with the classical correlations for heat and mass transfer up to Reynolds numbers of about 45 000. Beyond this point there is a sudden increase in rate which may be associated with droplet breakup.

Scaling of fuel distribution in air-fuel combustors

By D. A. Moberg

Rules are presented for fuel injector scaling requirements for (*a*) low, and (*b*) high, speed combustion mechanisms. To realize fully the reduction in combustor development cost that exact scaling implies, these rules must be subjected to experimental verification and modification. The rough analysis given here hopefully provides at least a starting point for future analytical and experimental investigation.

Exploratory wedge rocket motor tests (motion picture)

By H. B. ELLIS

This picture shows high speed filmed records of the combustion of several different liquid propellants in a transparent sector of a research thrust chamber. Different combustion characteristics are indicated by variations in the distribution of the combustion in the thrust chamber. The differences in flame propagation are noted in addition to the observable areas of intense mixing, recirculation and non-burning pockets.

FALL MEETING OF WESTERN STATES SECTION OF COMBUSTION INSTITUTE

Based upon an earlier inquiry and its responses, the Western States Section of the Combustion Institute has chosen as the subject of its fall meeting, at Los Angeles in November 1959, 'Kinetics, Equilibria, and Performance of High Temperature Systems'. A classified session is planned. Attention will be paid to: (*1*) identity of chemical species in high temperature systems; (*2*) thermochemistry and kinetics of their formation; (*3*) calculation of equilibrium concentrations and equilibrium thermodynamic properties; (*4*) establishment of deviations from equilibrium in actual systems; (*5*) jet engine performance calculations.

Publications

AIRCRAFT AND MISSILE PROPULSION

Volume II. The Gas Turbine Power Plant, Turboprop, Turbojet, Ramjet and Rocket Engines

M. J. Zucrow. New York: Wiley; London: Chapman and Hall, 1958. *xiv* + 636 *pp.*
(illus.) $13.00 or 104*s*

Books on jet propulsion proliferated since 1945 and Professor Zucrow's well known volume *Principles of Jet Propulsion and Gas Turbines* was one of the first authoritative texts. His new treatise, Volume I of which covered thermodynamics of fluid flow while Volume II is the subject of the present review, covers a rather wider field and in much greater detail. The present volume deals very thoroughly with the performance characteristics of turbine engines, ramjets and chemical rockets; the author approaches the subject historically with a review of the early ventures in gas turbines and jet propulsion but his main treatment is thermodynamic, covering the performance of various engine cycles, the effects of design factors, component efficiencies and operating conditions. The argument is set forth with admirable clarity, copiously illustrated with diagrams and examples. But in spite of the thoroughness which characterizes this work a number of omissions must be noted: there is little or no discussion of bypass and ducted fan engines, of intakes and intake matching problems, of turbine cooling and its effect on engine performance or of turbojet propulsion at speeds above Mach 2·4.

Combustion problems are treated in accordance with this general pattern; the effects of pressure and heat losses in combustion on cycle performance is indicated and the choice of fuels, oxidizers and propellants is examined but combustion processes as such are not treated in detail. There is, however, a useful section on the instabilities manifested by liquid and solid fuelled rockets.

In general this book can be recommended as a competent and very detailed treatment of the thermodynamics of engine cycles, but it does not go outside this field for the aerodynamic, mechanical and functional problems are not examined; the scope of the book is therefore rather narrower than the title might suggest.

P. Lloyd

GAS CHROMATOGRAPHY 1958

Edited by D. H. Desty. London: Butterworths Scientific Publications; New York:
Academic Press, 1958. *xiii* + 383 *pp.* (illus.) 70*s* or $12.00

Like its predecessor in 1956, this volume includes both the scientific papers presented at a symposium organized by the G. C. Discussion Group (this time in Amsterdam, in collaboration with the Koninklijke Nederlandse Chemische Vereniging, in May 1958), and the discussions which followed. The format and style of presentation are similar to those of the 1956 volume, but there are two innovations which deserve special mention. The first is the use of 'Reporters', responsible for writing up the discussion of particular topics. This gives unity to what can otherwise be a series of somewhat disjointed remarks, and leads to the crystallization of trends. The other welcome addition is a name index, which was not available in the earlier volume, and which described briefly the points which speakers were making. This is particularly useful since in lively discussions, some of the participants make comments on a variety of topics. The absence of a subject index, however, is to be regretted.

The contents illustrate the trends in the last two years. Theory has been used, by Purnell and by Scott, to produce long packed columns of high efficiency, while

Golay has deduced an approach to high efficiencies based on coated capillary columns. Such improvements have required greater sensitivity in the detecting systems, and these have been described by Lovelock, McWilliam, and others. The very simple katharometer devised by Stuve also deserves mention, since it is based on the filaments of small light bulbs. Preparative applications, including automatic sampling, have also been discussed.

Finally, the obvious usefulness of this volume, both in the preprint and final forms, receives a substantial contribution from the abstracts at the beginning of each paper. It is regrettable that some symposium proceedings are still published without including this valuable feature.

G. J. Minkoff

FUNDAMENTALS OF ADVANCED MISSILES

R. B. Dow. New York: Wiley; London: Chapman and Hall, 1958. *xvi* + 567 *pp.* (illus). $11.75 or 94s

The author of this volume aims to give a comprehensive treatment of the sciences which are fundamental to the design and operation of complete missile systems. These sciences are so various, and the specialization of most workers in the field is so narrow, that such a book is certainly needed. The chapter headings will indicate the ground covered: kinematics of flight, application of fluid mechanics to aerodynamics and propulsion, dynamics, some applications of probability and statistics, properties of micro-waves, application of infra-red radiation, radar, guidance, and guided-missile systems.

The reviewer has learned much, and expects to learn more, from perusal of the chapters outside his own field. It ought, however, to be recorded that a number of errors or misleading statements have been found in the other chapters. For example: on page 41, the Bernoulli and Steady-Flow Energy equations are confused; on page 53, it is stated that a Perfect Gas has zero viscosity; on page 57, efficiency is defined as work output divided by work input, and the fluid in a constant-pressure combustor is said to perform a cycle; on page 59 a very curious '*p V*' cycle' is said to apply to rocket motors; and on page 69 a formula is given for the thickness of a shock wave which does not contain the pressure.

Elsewhere, the author's acquaintance with his subject matter appears to be more profound; the reviewer hopes that the above examples are not typical of the whole. The book is extremely well produced.

D. B. Spalding

Letter to the Editors

Letters to the Editors on points of scientific interest related to combustion and flames are invited. The Editors do not hold themselves responsible for opinions expressed in correspondence. Anonymous contributions cannot be accepted.

Deviation from Chemical Equilibrium in Gas Flow

IN A recent note[1] the authors have shown that estimates of the temperature deviation due to vibrational energy lag in gas flow made from

$$\Delta T = \tau \mathrm{D}T/\mathrm{D}t \qquad \text{....[1]}$$

where $\mathrm{D}T/\mathrm{D}t$ is the usual cooling rate and τ is the usual vibrational relaxation time, are conservative, i.e. predict too large a ΔT. If, however, one includes a factor on the RHS to correct for the fact that vibrational energy need not account for the entire rate of temperature change, one obtains a more realistic result. For a diatomic molecule this factor approaches 2/7 at high temperatures ($T > \theta$, where θ is the vibrational temperature) and falls several orders of magnitude at lower temperatures[1]. In this communication the analogous predictions for a recombination reaction will be examined and compared with the more exacting treatment of one of the authors.

For a diatomic recombination process the approximate treatment[2] gives the relations

$$|\Delta T| = |z\mathrm{D}T/\mathrm{D}t| \qquad \text{....[2a]}$$

where

$$z = \{k\,(pK_p/R_0^2T^2)\,[2\,(1+4p/K_p)^{1/2}-1]\}^{-1} \qquad \text{....[2b]}$$

Here p is the pressure, R_0 is the absolute gas constant, k is the specific recombination reaction rate, and K_p is the usual equilibrium constant expressed in partial pressures.

The more exact result may be derived from equations (2c) and (8) of reference 3, wherein the notation is also defined. Substitution of the former into the latter and the use of $\mathrm{d}/\mathrm{d}l = (1/V)\,\mathrm{D}/\mathrm{D}t$ leads to

$$|\mathrm{D}T/\mathrm{D}t| \leqslant VT\,|E_1F_3/(F_2+E_1F_1)|_{\,|\Delta T/T|=Q\%} \qquad \text{....[3]}$$

As interpreted in reference 3, this equation states that if the cooling rate is less than or equal to the value predicted by the RHS (when evaluated at $|\Delta T/T| = Q\,\%$), then the condition $|\Delta T/T| = Q\,\%$ at the p, v and T in question is a stable condition; i.e. the value of $|\Delta T/T|$ will either become smaller or get no larger. If the inequality is not satisfied, $|\Delta T/T|$ will grow until both sides of equation 3 are equal. Therefore, the flow always endeavours to achieve the value of $|\Delta T/T|$ for which both sides of equation 3 are equal. The value of ΔT predicted from this *equality* should be considered a value characteristic of the flow with reaction. No more definite ΔT may be derived without considering the particular initial conditions and history.

To derive equation 4 given below from equation 3, use is made of the expressions for F_1, F_2 and F_3 given in section VI of reference 3 as well as an expression for E_1 easily obtained from the prescription in section I of that paper. Also, we have made the following assumptions in these equations to agree with those made in deriving equation 2: first, that the efficiencies as a third body of an atom and a diatomic molecule in the recombination process are equal ($k_1 = k_2$); and, secondly, that there are no spontaneous dissociation reactions from a high vibrational–rotational state ($k_3 = 0$). Noting also that $k_1 = k_2 = kK_p/RT$ and $K = RT/K_p$, one obtains

$$\Delta T = |f_1/f_2|\, R_0^2 T^2/(K_p k p)\cdot \mathrm{D}T/\mathrm{D}t \equiv z'\mathrm{D}T/\mathrm{D}t \qquad \ldots.[4]$$

where

$$f_1 = \Upsilon(\delta - z)(1 - \Phi z)^{-1} + B(\delta - 1) - \delta$$

$$f_2 = [\delta - W(\delta - 1)]\left\{\frac{Z^2 - 3Z - 2}{2Z(1 - Z)}\left(\frac{2B + \delta}{2W + \delta}\right) - \left(\frac{2 - Z}{Z}\right)\left[\frac{1}{2} + \frac{2(\Upsilon - 1)}{(Z - 1)(Z - 2)}\right]\right\}$$

These equations may be expressed as functions of $K_p(T)$, p, T and V by use of

$$z^{-1} = \left\{\Phi + \frac{\Upsilon[(1 - \Phi)W - 1]}{(\Upsilon - 1)W + B}\right\}, \qquad \Upsilon = 1 - \frac{(Z - 1)(Z - 2)}{2}\,\frac{\mathrm{d}\ln K_p}{\mathrm{d}\ln T},$$

$$W = 3/2 - G + D/RT, \qquad G = (\theta/T)/(\mathrm{e}^{\theta/T} - 1),$$

$$B = 3/2 + 2/Z + G^2\mathrm{e}^{\theta/T}(2 - Z)/Z, \qquad \delta = V^2/RZT,$$

$$\Phi = 1 + 2p(Z - 1)^3/ZK_p, \qquad Z = 1 + [K_p/(K_p + 4p)]^{1/2}.$$

Here, D is dissociation energy and R is gas constant, both per unit mass of a diatomic molecule.

Using values of $K_p(T)$ obtained from tables[4], the ratio z'/z was computed for hydrogen recombination at pressures of 1, 10 and 100 atmospheres and flow velocities of 10^3, 3×10^4 and 5×10^4 feet per second. In the range of practical interest (1 500 to 3 000° K) it may be seen from the curves that the use of the more approximate expression leads to results too large by a factor varying from about three to several orders of magnitude—depending on the pressure/velocity conditions. These results are similar to those for vibrational relaxation[1] except that the latter were pressure independent. It will be noticed that at the higher temperatures relative minima occur in the curves. These minima have no physical significance and are induced by taking the ratio of two expressions derived from different considerations. Both z and z' have no points of inflection when plotted separately in the same range (*Figure 1*).

At still higher temperatures than shown, z'/z approaches zero. The reason for this and for the approach to zero at very low temperatures is that the derivation of equation 2 tacitly assumes that the *entire* rate of

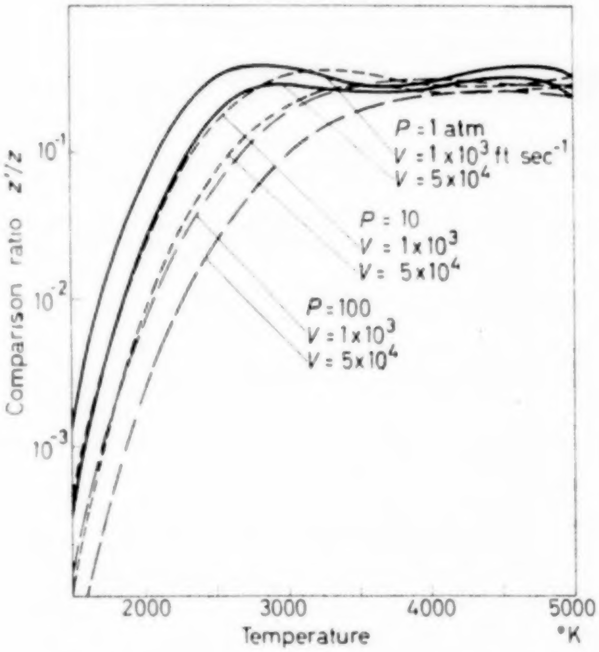

Figure 1. The comparison ration z'/z as a function of temperature for various pressures and velocities

temperature change must be accounted for by the recombination process, when actually there are other forms of energy present. This assumption becomes increasingly inappropriate at both very high and very low temperatures, because the amount of recombination possible becomes negligible at both limits.

M. Rudin and H. Aroeste

Lockheed Missile Systems Division,
Research Laboratory,
Palo Alto, California

(*Received April 1959*)

REFERENCES

[1] Aroeste, H. and Rudin, M. *Jet Propulsion*, 1958, **28**, 690
[2] Penner, S. S. *Chemistry Problems in Jet Propulsion*, pp 298–303. Pergamon: London, 1957 or *Chemical Reactions in Flow Systems*, pp 44–50. Butterworths: London, 1955
[3] Rudin, M. *Physics of Fluids*, 1958, **1**, 384
[4] Huff, V. N., Gordon, S. and Morrell, V. E. 'General methods and thermodynamic tables for computation of equilibrium composition and temperature of chemical reactions.' *Nat. Adv. Comm. Aero., Wash., Rep. No. 1037*, 1951

ERRATA

TRANSITION PROBABILITIES OF MOLECULAR SPECTRA ARISING FROM COMBUSTION PROCESSES

OWING to a combination of unfortunate circumstances, the authors' corrections to the above paper (March, pp 13 to 38) did not arrive in time for inclusion and Professor R. W. NICHOLLS, P. A. FRASER and W. R. JARMAIN have sent the following notes to clarify obscurities.

Page 16. Final paragraph, third sentence should read:
No data are included for band systems of CH and NH in all but one of which the change in internuclear separation is very small (thus q_{00}, q_{11}, … are all very nearly unity and all others are negligible); for which there is doubt as to the applicability of the Morse oscillator model; and further for which in view of the $\omega_e x_e$ values of the states the method of Fraser and Jarmain[14-16] is not appropriate (if one were to assume a Morse model).

Page 17. Table 1
The upper state of the NO γ system should be labelled as $A^2\Sigma^+$. The upper state of the Schumann–Runge system should be labelled $B^3\Sigma_u^-$. The data given for the OH violet system are those for the isotopic molecule OH^2. The correct data (which were used in the calculation of *Table 18*) are:

State	ω_e	$\omega_e x_e$	r_e
$A^2\Sigma^+$	3180·56	94·93	1·0121
$X^2\Pi$	3735·21	82·81	0·9706

The bracketed values in the r_e column are r_0 values.

Pages 30–31. Tables 15, 16
NO β and γ systems contain some $p_{v'v''}$ obtained by extrapolating the empirical $R_e(r)$ curves outside the range of r over which $R_e(r)$ was determined. The upper state of the NO γ system should be labelled $A^2\Sigma^+$.

Pages 32–33. Tables 17(a, b). O_2 : *Schumann–Runge system*
The upper state should read $B^3\Sigma_u^-$. The notation *G.F.* in certain band locations in *Table 17*(a) refers to the work of Garton and Feast[36].

Effect of the Electric Field upon the Spectra of the Hydrocarbon Diffusion Flame

J. NAKAMURA

The supposition that there is a relationship between the mechanism of ion production and CH *formation or* C_2 *extinction has been examined using the propane flame, a rectangular burner and a longitudinal electric field. Rotational temperatures of* CH, C_2 *and* OH *were measured by microphotometric tracing of the spectra, and the results of measurements of relative radiational intensities are shown graphically. It is concluded that the ions in a flame are produced in the carbon formation stage.*

IN a previous paper[1], it was shown that there were always plenty of ions in hydrocarbon diffusion flames and their concentration was a maximum at the premixed-gas combustion zone (green-blue coloured zone). The spectral intensity of C_2 radicals was strongest at the lower part of the *P* zone (premixed-gas combustion zone) and was very weak at the middle and upper parts of this *P* zone, while the spectral intensity of CH was strongest at the middle part of the *P* zone. By considering these facts, it may be supposed that there is a relationship between the mechanism of ion production and CH formation or C_2 extinction[2].

Now, if a longitudinal electric field is applied to the flame, the *P* zone assumes a light blue colour with violet shade, and the flame is slightly lengthened, but when the field is reversed, the colour of the *P* zone turns to deep green and the flame itself is slightly diminished. Qualitatively all hydrocarbon diffusion flames show similar effects in an applied electric field. The question is whether the mechanism of emission or the ion concentration is influenced by the applied electric field. Investigation of this question should help to clarify the mechanism of ionization in flames, and this communication deals with the effect of the longitudinal electric field upon the spectroscopic characteristics of the *P* zone in hydrocarbon diffusion flames.

The following experiment is relevant to the question. As shown in *Figure 1*, alcohol is dropped from a burette and ignited by a torch. When there is no electric field between the plane parallel electrodes P_1 and P_2, the alcohol droplets fall burning; but if the field is applied to the gap P_1P_2, the droplet flame is extinguished at the instant of entering into this gap and the fuel can be collected in the catchpot.

From this experiment, it had been thought that the mechanism of combustion might have been changed by applying the electric field. Undoubtedly ions are always present at the time of ignition or combustion, and perhaps they play an important role in the mechanism of combustion. But it is shown in the investigation which follows that neither the numbers of ions nor the extent of excitation of radicals in a flame is affected by the

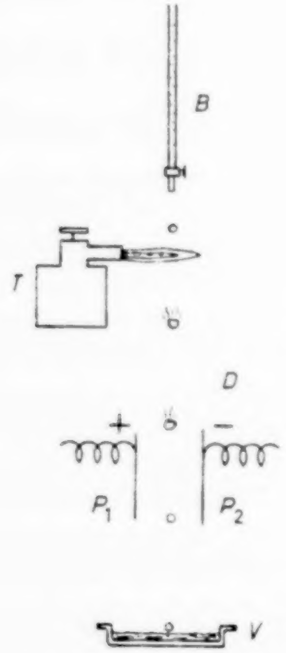

Figure 1. *Extinction of alcohol droplet flame by means of electric field. B: burette. T: torch. D: alcohol droplet. P_1, P_2: plane parallel electrodes. V: catchpot*

applied field; only the distribution of the radicals seems to be displaced by a kind of Chattock electric wind or pressure. There is no evidence that there is an effect of the external electric field upon the mechanism of combustion.

EXPERIMENTAL

98 per cent commercial propane gas was used as fuel. The burner used was the rectangular type as shown in *Figure 2*(a). With this burner, a two-dimensional flame as shown in *Figure 2*(b) could be formed. In *Figure 2*(b) the wall thickness of the burner is 2 mm.

With this burner the *P* zone of the flame is nearly vertical. Otherwise the *P* zone is inclined and curved, which makes measurement along the *P* zone very troublesome. As shown in *Figure 3*, the flame, quartz lens and

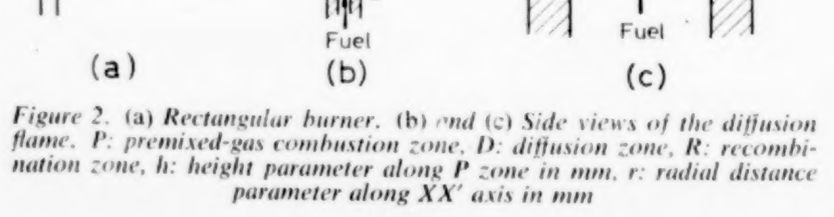

Figure 2. *(a) Rectangular burner. (b) and (c) Side views of the diffusion flame. P: premixed-gas combustion zone, D: diffusion zone, R: recombination zone, h: height parameter along P zone in mm, r: radial distance parameter along XX′ axis in mm*

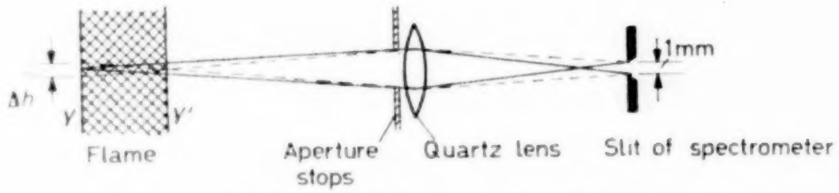

Figure 3. Schematic imaging system

quartz spectrograph are arranged in series along the YY' axis. By stopping down the lens aperture and making the distance between flame and lens a considerable length (*ca.* 1 200 mm), the contamination of the radiation from regions of different height (h) will become small and the single spectrum will correspond to the radiation from the small portion of Δh about 1 mm in the P zone. This enables determination of the intensity curves of CH, C_2 and OH along h with precision.

The rotational temperature of radicals was measured by microphotometric tracing of the spectra. However, since we used a medium spectrograph, only the relative rotational temperature of the CH (0, 0) band in the 4315Å system was obtained.

Wire gauze was placed 7 cm above the top of the burner: it was charged negatively or positively by the rectified high voltage source through the smoothing condenser circuit and voltage was read by the current through a standard high resistance (100 MΩ).

It was desirable to measure an ion distribution in the flame, but this was difficult because the potential difference between two probes was largely disturbed by the applied field. So only the electric potential in the flame was measured by the probe method.

The electric potential was measured by the Langmuir probe method, as shown in *Figure 4*(a). In this case, one point probe is needed. It is found that the platinum point probe covered with double insulating tubes of fused silica and alundum is most suitable [*Figure 4*(b)]. Alundum plays the role of thermal insulator and fused silica that of electrical insulator. To determine the plasma potential V_p, the current/voltage characteristic should be traced. As a point-type rather than plane-type probe was used, the

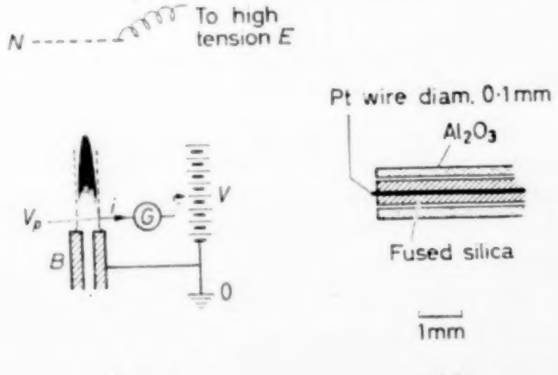

Figure 4. Schematic view of probe method. (a) *Measurement of electric potential in a flame: G: galvanometer, N: wire gauze, B: burner, V_p: plasma potential, i: current through probe, V: probe potential:* (b) *construction of point probe*

discontinuity in the characteristic was not clear. Alternatively, it may be considered that a flame is a semiconductor. In the region at which the field gradient was small, the following method was adopted. The positive ion concentration is assumed to be the same as the negative one and the temperature of positive ions equal to the electron temperature; then the plasma potential V_p is obtained by

$$V_p = V - (kT/2e)\log(M/m)$$

where V is the probe potential at which the probe current $i = 0$, M is the positive ion mass and m is the electron mass[2]. The flame temperature T was measured by a Pt/Pt–Rh thermocouple. The electron temperature T_e may be higher than T, but in the P zone, except for the cathode fall region, their difference may not exceed 30 per cent which affects V_p by several per cent only. It is also assumed that M is of the order of $20 \sim 40$ times the proton mass. The value of M does not much affect the inclination of the V_p/h curve and it is sufficient to use a rough value of M in the present deduction.

RESULTS

Results of the measurements of relative radiational intensities are shown in *Figure 5*. With no electric field, C_2 radiation is strong at low values of h and is extinct at about $h = 4$. With a negative charge on the gauze, C_2 radiation can be discerned all over the P zone; on the other hand, with a positive charge, it is limited to the range from $h = 0{\cdot}5$ to $h = 2$. In respect to CH and OH radiation intensity, their distribution has a similar trend to that of the C_2 intensity curve: that is, they have a tendency to extend a little to the region of large h with negative charge and to contract to the region of small h with positive charge. Thus the flame colour, or the relative strength of the radical intensities, changes considerably. The total intensity of C_2 radicals in the P zone, however, seems to be unchanged. It is concluded from *Figure 5* that the total intensities of other radicals are also invariable.

Figure 6 shows results of the photometry of the relative intensity of the CH (0, 0) band in the 4 315 A system. It is seen that the region from $\nu = 19$ to $\nu = 22$ is best suited for the calculation of the rotational temperature.

Figure 7 shows the distribution of the rotational temperature in the P zone. Generally, rotational temperature is high in the lower part of the P zone and low in the upper part. It is apparent that the maximum and minimum rotational temperatures are the same whether or not a field is applied. From these facts, it seems that the mechanism of excitation is not affected by the applied field, but only its distribution is shifted.

The results using the probe are shown in *Figure 8*. On account of a large number of ions in the flame the field gradient in the flame is very small, except in the region of cathode fall. In the region $h = 0{\cdot}5 \sim 2$ with $E = +2$ kV, the field gradient is largely disturbed by the applied field. And it is there supposed that neither the concentration nor the temperature of the ions is uniform. Hence, in these regions, the plasma voltage was determined from current/voltage characteristics as stated above. It is shown that even in these regions the field gradient is much less than the applied mean field

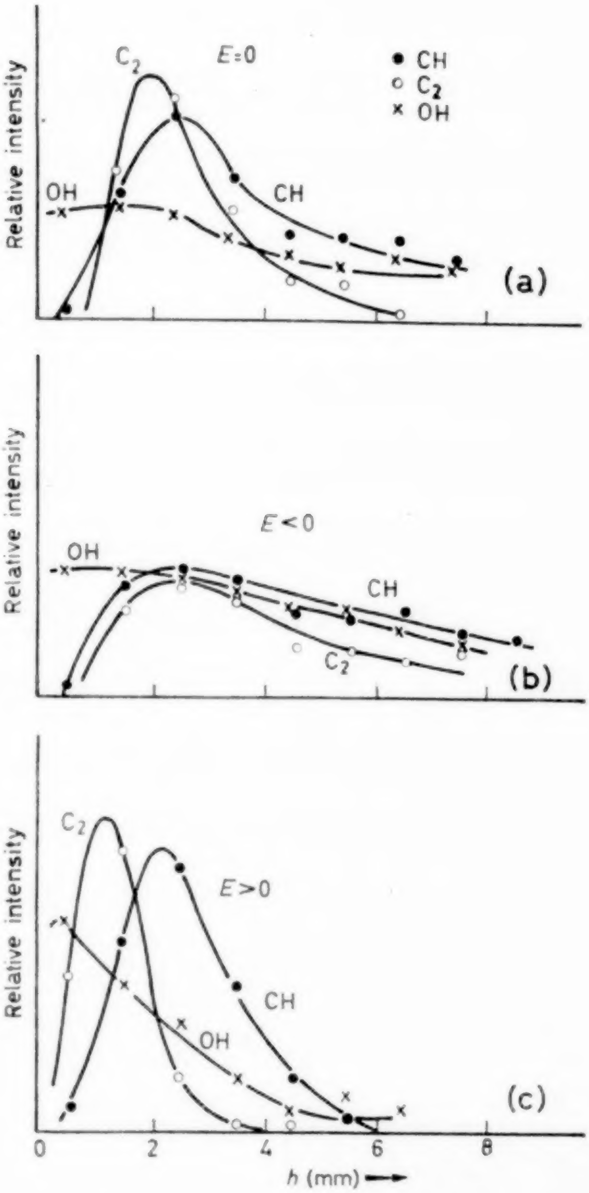

Figure 5. Relative intensity of radical radiation in P zone of C_3H_8 *diffusion flames:* (a) *with no field, E=0;* (b) *applying a negative field, E=−7kV;* (c) *applying a positive field, E=+2kV*

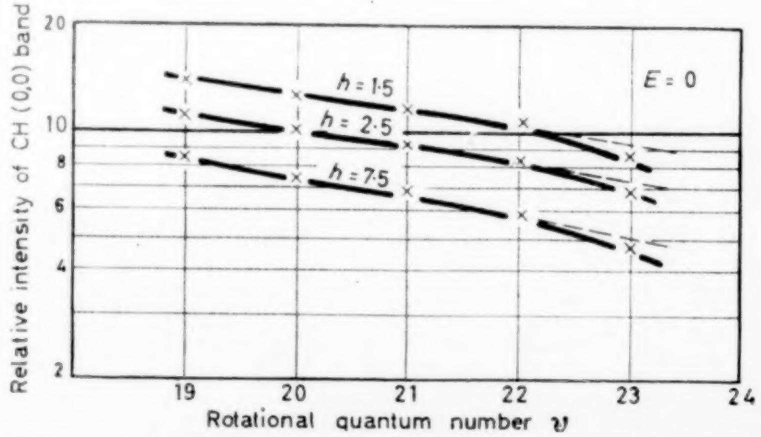

Figure 6. Examples of observed relative intensity of CH (0, 0) *band in 4 315Å system*

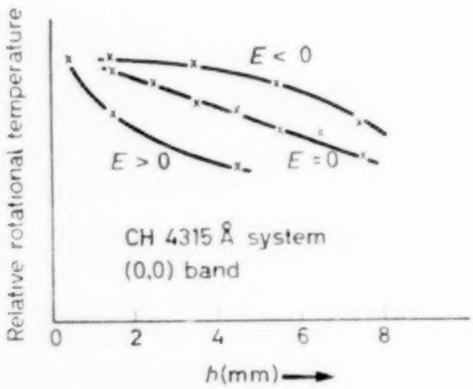

Figure 7. Relative rotational temperature in P zone

gradient. Thus it seems that the mechanism of radiation is not influenced by an external electric field of this order. If a stronger field is applied, flames oscillate or are extinguished as stated below. This case is beyond the scope of this paper. The minimum and maximum voltages used in our experiments were −7 kV and +2 kV.

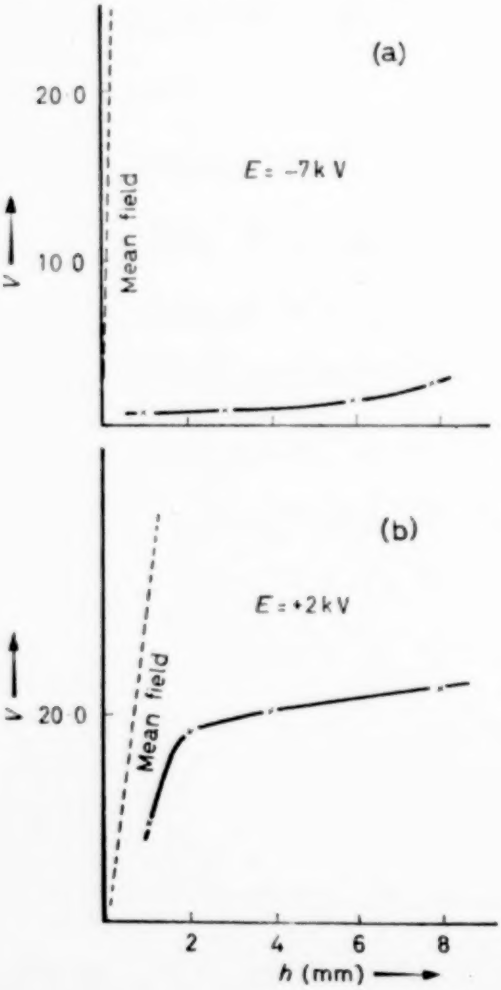

Figure 8. Electric potential in P zone under longitudinal electric field. E: electric potential of wire gauze

DISCUSSION

These conclusions are supported also by the following facts. E. M. GUENAULT and R. V. WHEELER[4] found that, when the flame front progresses in coaxial tubes, and the inner tube is charged positively, the flame front is deflected towards the negative electrode (outer tube) and the burning velocity seems to be increased. This is interpreted as follows. The electric pressure drives the front towards the negative electrode and as a result of the increase in the front area, the fuel volume consumed per unit time will increase; and the overall velocity seems to be increased.

H. F. CALCOTE[5] applied a transverse electric field to a flame and recognized that the flame inclined towards the negative electrode. The electric field accelerates the electric double layer of an outer shell of the flame and does not accelerate the ions in the flame uniformly, as he explained. In any case, deformation of the flame is explained by the positive ion movement.

We found[6] that when the longitudinal electric field is applied to a flame burning at a wick fed by a liquid fuel, the flame lengthened and became thin. This caused a reduction of brightness and so decreased the quantity of evaporation of fuel gas from the wick. Then the flame became small, causing further reduction of emission, and finally it was extinguished. The above experiment with alcohol droplets is also explained by this effect, that is, flames become smaller and smaller and are extinguished due both to the decrease of the rate of evaporation and to the electric wind.

The electric field gradient in a flame is small in the region where the ion concentration is high, as shown in *Figure 8*. Accordingly it is not strange that the mechanism of combustion is not affected by the applied field. From *Figure 5*(c) and *Figure 8*(b), it seems that the layer accelerated by the electric field is the one above the C_2 radiation, for the Swan band is confined to a very limited region in *Figure 5*(c). Therefore when the field gradient is small, that is with a negative charge, radical distributions in the *P* zone are not greatly different from the case of no field.

R. E. FERGUSON[7] proved that the formation of C_2 occurs in a rather later stage of combustion. Again, K. HONDA[8] ascertained that, in a soot-producing flame, the soot had an electric charge. Moreover, we verified[6] that in hydrocarbon diffusion flames, there is a close relation between ion concentration and carbon formation both of which increase with the carbon number of the hydrocarbon molecules. From these facts it may be concluded that the ions in a flame are formed in the stage of carbon formation. Concerning the ion itself, however, further investigation is needed.

College of General Education,
University of Tokyo

(*Received October 1956*)

REFERENCES

[1] KINBARA, T. and NAKAMURA, J. *Fifth Symposium (International) on Combustion*, p 285. Reinhold: New York, 1955

[2] BROIDA, H. P. and GAYDON, A. G. *Proc. Roy. Soc. A*, 1953, **218**, 60

[3] LOEB, L. B. *Fundamental Processes of Electrical Discharge in Gases*, p 232. Wiley: New York, 1939

[4] GUENAULT, E. M. and WHEELER, R. V. *J. chem. Soc.* **1931**, 195; **1932**, 2788

[5] CALCOTE, H. F. *Third Symposium on Combustion, Flame and Explosion Phenomena*, p 245. Williams and Wilkins: Baltimore, 1949

[6] KINBARA, T. and NAKAMURA, J. *Sci. Pap. Coll. Gen. Educ., Univ. Tokyo*, 1954, **4**, 21

[7] FERGUSON, R. E. *J. chem. Phys.* 1955, **23**, 2085

[8] HONDA, K. *Bull. Inst. phys. chem. Res. Japan*, 1927, **6**, 921

A Thermal Layer Mechanism of Combustion of Solid Composite Propellants: Application to Ammonium Nitrate Propellants

R. F. Chaiken

A mechanism for the combustion of ammonium nitrate solid composite propellants is presented, utilizing the recent 'two-temperature' theory of propellant burning. According to the theory, the rate-controlling reactions associated with the gasification (pyrolysis) of the solid oxidizer and of the solid binder in a composite propellant are essentially independent of each other. A model of steady-state combustion is set up which considers the pyrolysis of oxidizer separately from the binder. It is assumed that the surface pyrolysis is the result of the transfer of heat from a flame zone surrounding the oxidizer particle, and that this flame zone is the result of the gas-phase redox reactions between the oxidizer pyrolysis products. It is assumed that a thermal layer exists about an oxidizer particle; the thickness of this layer (distance between the oxidizer surface and the flame zone) is related to the velocity at which gas expands away from the surface, and the rate of the gas-phase reaction. From heat transfer considerations, an analytical expression for the thickness of the thermal layer is obtained in terms of the pressure, oxidizer particle size, and the kinetics of the solid and gas-phase reactions. The agreement between the theory and the available data on ammonium nitrate propellants is reasonable.

In 1950, R. E. Wilfong, S. S. Penner and F. Daniels[1] first advanced the hypothesis that in the combustion of a double-base solid propellant the rate-controlling reaction occurs in the monomolecular surface layer exposed to the flame. This concept was applied to the combustion of solid composite propellants by R. D. Schultz and A. O. Dekker[2] in the form of a 'two-temperature' theory which suggested that the gasification of oxidizer and binder at the surface proceed essentially independently of each other, and that these surface reactions are rate-controlling. Thus, the linear rate of regression of the propellant surface during steady state burning must be determined by conditions which make the linear rate of regression of the oxidizer equal to the linear rate of regression of the binder.

In a recent paper by W. H. Andersen *et al.*[3] is described a model for the combustion of ammonium nitrate (AN) composite propellants which is based upon the 'two-temperature' theory and kinetic data on the pyrolysis (gasification) of propellant oxidizer and binder (fuel). It is postulated that in an AN (oxidizer) propellant, the oxidizer gasifies first at about 600°K by an endothermic reaction to form ammonia and nitric acid. These gaseous products then undergo an exothermic redox reaction (or reactions) near the surface to establish an adiabatic flame at a temperature of about 1 250°K which governs the pyrolysis of the propellant binder. The gaseous products from the pyrolysis of the binder then react with gaseous products from pyrolysis of the oxidizer to form a hot flame zone (~2 400 K) at some distance from the propellant surface. It is thought that for many oxidizer–binder systems the heat from the final oxidizer–binder gas reactions contributes very little to establishing the effective surface temperature. This is suggested by the observation that, in general, changes in the chemical structure of the binder (or even complete absence of binder) have only a minor influence on the burning characteristics.

The author makes use of the concept of the independence of regression rates of oxidizer and binder, and the boundary conditions imposed by the model described by Andersen *et al.* to delineate the important energy flow processes involved in the combustion of AN solid composite propellants. Expressions are derived which describe the dependence of the propellant burning rate on the pressure, and the possible effects on the burning rate of variations in oxidizer particle size and of the presence of chemical additives. This is accomplished by considering the heat transfer processes and the gas-phase reactions associated with the decomposition of the oxidizer alone. The reactions involving the binder are considered not to have a significant influence on the processes occurring at the oxidizer surface, as suggested by Andersen *et al.* It is shown that this mechanism leads to results which are in reasonable agreement with the available burning rate data on AN composite propellants.

THE 'THERMAL LAYER' MODEL OF A BURNING PROPELLANT

The chemical changes which are thought[3] to occur during the burning of an AN composite propellant are symbolically described as follows:

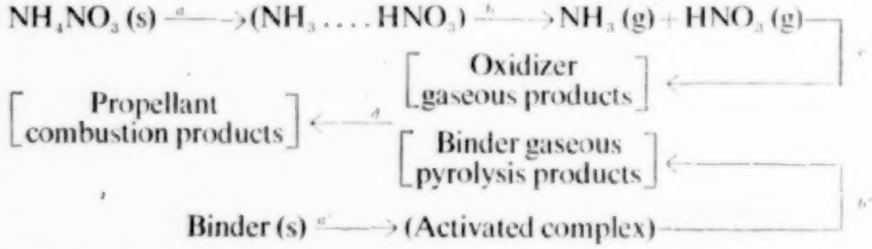

Here *a*, *b* represent the pyrolysis of solid AN which involves the formation of an activated complex on the surface of the solid followed by dissociation into NH_3 (g) and HNO_3 (g). The rate-controlling step is believed to be the desorption of nitric acid from the surface (with measured activation energy of 7·1 kcal/mole). The overall reaction forming NH_3 (g) and HNO_3 (g) is endothermic to the extent of ~40 kcal/mole.

c is an exothermic redox reaction between NH_3 (g) and HNO_3 (g) to establish a 1 250°K flame near the oxidizer surface.

a', *b'* represent the pyrolysis of the binder in the flame zone established by the reaction *c*.

d is the exothermic reaction between the gaseous products from the decomposition of the oxidizer and of the binder to establish a hot flame zone (~2 400°K) at a distance from the propellant surface.

The burning surface of an AN propellant is pictured as consisting of protrusions and depressions, with the protrusions being the slower pyrolysing constituent. For the purposes of the following discussion, it is required to treat only the region above the oxidizer particles, and a microscopic scale zonal model will be set up and treated in a manner somewhat similar to the 'Fizz-Flame' model of O. K. RICE and R. GINELL[4]. However, the above reaction scheme permits several important simplifications to be made.

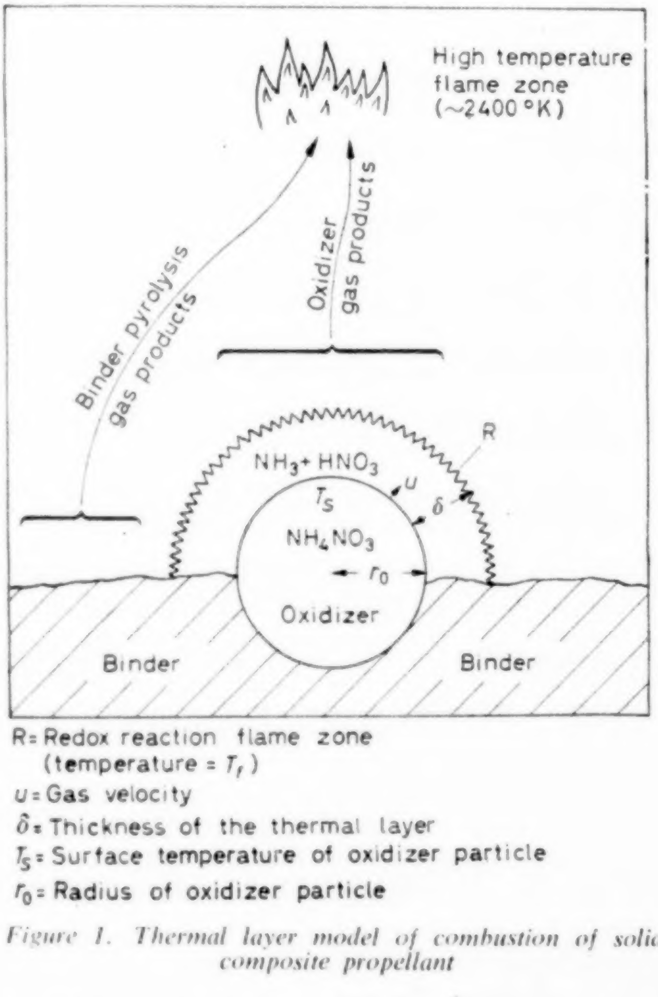

R = Redox reaction flame zone (temperature = T_f)

u = Gas velocity

δ = Thickness of the thermal layer

T_s = Surface temperature of oxidizer particle

r_0 = Radius of oxidizer particle

Figure 1. Thermal layer model of combustion of solid composite propellant

Consider a solid-composite propellant where spherical particles of oxidizer are imbedded in a binder matrix. At the burning surface, which is an irregular contour, the oxidizer spheres expose a certain fraction of their surface area to a hot gaseous medium. Looking at a single particle (see *Figure 1*), heat flows into the oxidizer sphere causing the surface layer to gasify (reactions *a, b*). The gas which is generated expands away from the surface and undergoes an exothermic reaction (reaction *c*). The completion or near completion of the redox reaction occurs near the surface of the particle and results in a flame zone (~ 1 250°K) which envelops the exposed oxidizer surface area. The distance between the flame zone and the surface can be designated as a thermal layer having a certain thickness. The heat from this flame envelope, which is transferred across the thermal layer to the surface, sustains the surface dissociation reaction. Therefore, the self-propagating combustion process is essentially a feed-back type of system. If the second flame zone (reaction *d*) is established far away from the oxidizer surface, little heat will be transferred from that zone to the oxidizer. In any case, the first flame zone (reaction *c*) will act as a buffer zone with respect to heat transfer to the oxidizer from regions beyond the flame envelope.

Assuming that the heat transfer mechanism is predominantly that of thermal conduction (neglecting thermal radiation from the low temperature flame envelope), the rate of heat input into the oxidizer particle ($\dot{q}_{in}$ cal/sec) can be written, in general, as

$$\dot{q}_{in} = 4\pi n r_0^2 \sigma \left(\frac{\partial T}{\partial r}\right)_{r_0} = 4\pi n r_0^2 \sigma \left(\frac{T_f - T_s}{\delta}\right) \qquad \ldots.[1]$$

where n is the fraction of particle surface area exposed, σ is the coefficient of heat conduction of the gaseous medium (cal/cm.sec. °C), $(\partial T/\partial r)_{r_0}$ denotes the temperature gradient in the gaseous medium at the particle surface (°C/cm), r is the radial distance from the centre of the sphere (cm), r_0 is the radius of the particle (cm), T_f is the temperature of the flame envelope (°K), T_s is the temperature of the particle surface (°K), and δ is the thickness of the thermal layer (cm).

The introduction of the concept of the thermal layer thickness, δ, is a convenient device which will be used to linearize the temperature profile in the gas phase as an approximation to the heat transfer equation. It will be shown later that, for the model under consideration, δ is related to the motion of gas in a normal direction away from the surface, and to the rate at which the gas phase reactions (reaction *c*) take place.

Now the rate of heat flow into the particle surface during burning is equal to the sum of: (*1*) the rate of heat flow required to maintain the endothermic surface gasification (reactions *a, b*) at a given rate; and (*2*) the rate of heat flow by conduction into the interior of the particle. Since most composite propellants exhibit only a small temperature sensitivity (change in burning rate with ambient temperature), it is a reasonable first-order approximation to assume that the rate of heat flow into the interior is small compared to that required for dissociation. Therefore, neglecting the heat flow to the interior,

$$\dot{q}_{in} = \dot{m}\,\Delta H = 4\pi n r_0^2 \rho_s \Delta H\, v \qquad \ldots.[2]$$

where $\dot{m}$ is the rate of gasification of solid (g/sec), ΔH is the endothermicity of the surface gasification reaction (cal/g), n is the fraction of particle surface area which is burning (exposed), ρ_s is the density of the oxidizer particle (g/cm³), and v is the linear rate of regression of oxidizer surface (cm/sec).

Equating 1 and 2 yields the following expression for the energy balance.

$$(T_f - T_s)/\delta = \rho_s \Delta H\, v \qquad \ldots.[3]$$

It is now necessary to relate δ and $\dot{r}$ in terms of the physicochemical parameters of the combustion process.

W. H. ANDERSEN *et al.*[3, 5] and R. D. SCHULTZ and A. O. DEKKER[6, 7] have shown that the linear rate of regression of a solid surface which is undergoing gasification can be expressed by an Arrhenius-type equation

$$\dot{r} = A_s \exp(-E_s/RT_s) \qquad \ldots.[4]$$

where T_s is the surface temperature of the solid (°K), E_s is the activation energy for the surface gasification reaction (cal/mole), A_s is the pre-exponential constant factor (cm/sec), and R is the gas constant (cal/mole. °C).

For the pyrolysis of AN (both CP grade and AN containing 3 wt % ammonium dichromate) the reported values of E_s and A_s are 7 100 cal/mole and $1{\cdot}2 \times 10^2$ cm/sec respectively[3, 5].

Thermal layer thickness

The solution of equation 3 for T_s is complicated by heat generation and motion of gases in the thermal layer. Indeed, an exact treatment of the heat transfer processes at the oxidizer surface would be a formidable if not impossible task. To accomplish the goal of relating δ to measurable parameters, a heuristic-type solution will be presented which depends upon several reasonable assumptions concerning the combustion process. First, it will be shown that δ can be considered to be proportional to the product of the average gas velocity away from the oxidizer surface and the time required for these gases to react at temperatures near T_i. This concept is then utilized to extend a solution of a heat transfer problem involving a stagnant gaseous medium to a problem involving a moving gaseous medium. A simple analytical expression for δ is obtained by this method.

It is assumed that the temperature profile in the gaseous medium near the oxidizer surface (across the thermal layer thickness, δ) is linear. It should be noted that if only the adiabatic redox gas-phase reactions were considered, it might be expected that the temperature profile would be exponential. However, it is reasonable to expect that the heat feed-back to the oxidizer surface would tend to alter such a temperature profile so that a linear approximation may in fact be more realistic. Gases which stream away from the surface will see an increasingly higher temperature environment as they move farther away from the surface. Since the reaction rate constant (k_g) can be expressed by an Arrhenius rate equation ($k_g = A_g \exp E_g/RT$, where for many gas reactions A_g is of the order of the molecular collision frequency and E_g is of the order of 25 or more kcal/mole), it follows that little reaction will occur until a certain temperature, T_g, is reached. Above that temperature the reaction will proceed rapidly. For practical purposes it is possible to consider the thermal layer, δ, as being composed of two regions (see *Figure 2*); region 1 has a length $\Delta r' = r_1 - r_0$, where little reaction occurs, and region 2 has a length $\Delta r = \delta - \Delta r'$, where essentially complete reaction occurs.

For steady state burning, the rate of flow of gases from region 1 into region 2 must equal the rate at which these gases react. In this manner region 2 is considered to be a volume of reaction, and the mass continuity at r_1 can be expressed as

$$4\pi r_1^2 \rho_1 u_1 = \dot{m}' \qquad \ldots. [5]$$

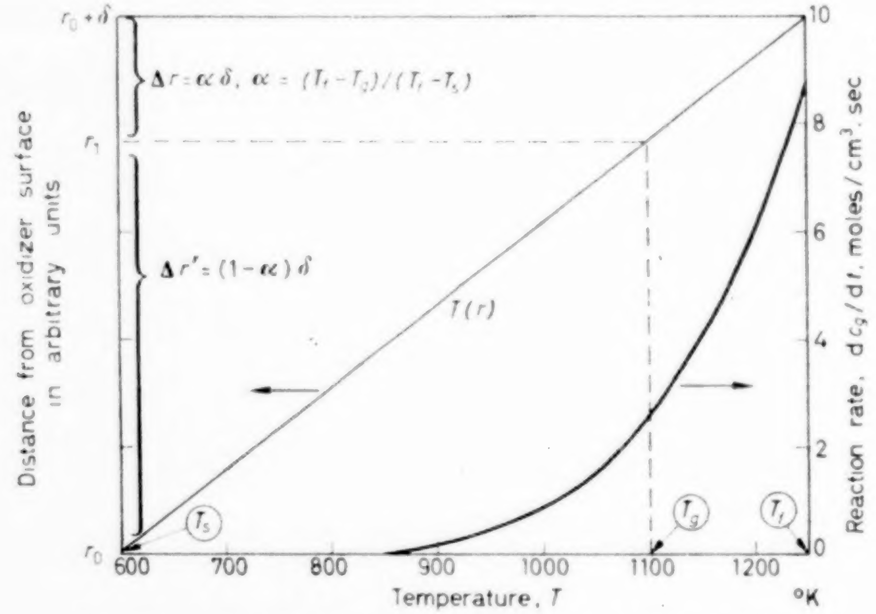

Figure 2. Temperature and reaction rate profile in the thermal layer

where $\dot{m}'$ is the mass rate of reaction between the gaseous reactants in the entire volume of region 2, and ρ_1 and u_1 are the average gas density and velocity respectively in region 1. For a second-order gas phase reaction with equal molar concentration of reactants, the rate equation is

$$-\mathrm{d}c_g/\mathrm{d}t = k_g c_g^2 = c_g/t_{1/2} \qquad \ldots. [6]$$

where c_g is the concentration of one of the gas reactants (mole/cm³), k_g is the reaction rate constant (cm³/mole.sec), and $t_{1/2}$ is the half-life of the gas phase reaction (sec).

Since c_g is proportional to the gas density (ρ_g) in region 2, the mass rate of reaction in the reaction volume is

$$\dot{m}' \simeq 4\pi r_1^2\, \Delta r\, (\rho_g/t_{1/2}) \qquad \ldots. [7]$$

where $t_{1/2}$ now refers to the half-life of the reaction at a temperature T_g near T_f.

Equating 5 and 7, and solving for the mass velocity in region 1, yields

$$u_1 = (\Delta r/t_{1/2})(\rho_g/\rho_1) \qquad \ldots. [8]$$

Now the temperature (T_g) at the interface between regions 1 and 2 should be a constant parameter which depends upon the particular reactions involved in establishing T_f. By virtue of the assumption of a constant temperature gradient across δ, Δr will be proportional to δ, i.e. $\Delta r = \alpha\delta$, where the proportionality factor $\alpha = (T_f - T_a)/(T_f - T_s)$. The expression for u_1 thus becomes

$$u_1 = (\alpha\delta / t_{1/2})(\rho_g / \rho_1) \qquad \ldots.[9]$$

The mass velocity in region 1 can also be expressed in terms of the thermal layer thickness and a gas transport time, τ'.

$$u_1 = \Delta r' / \tau' = \delta(1 - \alpha)/\tau' \qquad \ldots.[10]$$

Substituting for u_1 in equation 9, and solving for τ', yields

$$\tau' = t_{1/2}\{(1 - \alpha)/\alpha\}(\rho_1/\rho_g) \text{ sec} \qquad \ldots.[11]$$

Since ρ_1/ρ_g and α will be relatively constant, in equation 11, we have explicitly related the transport time for the gases moving from the oxidizer surface to the flame zone to the half-life of the gas phase reaction at a temperature T_a near T_f.

Expressions 10 and 11 for the gas transport velocity and time can be utilized in determining an analytical expression for δ in terms of the half-life of the gas phase reactions. To do this we first obtain the solution to a hypothetical problem in which heat is transferred to a body immersed at zero time in a stagnant hot gaseous medium. The solution to this problem for both planar and spherical bodies yields an expression for the thermal layer thickness as a function of time, $\delta_h(t)$. Under steady-state conditions, heat transfer from the stagnant gaseous medium results in a thermal layer of constant thickness, $\delta_h(\tau)$, defined by a characteristic time constant, τ. We then obtain a solution to the problem of heat transfer to a semi-infinite plane which is moving at constant velocity past a heat source. The solution to this problem yields an expression for the thermal layer thickness which is a function only of the velocity and thermal diffusivity of the medium. A comparison of the two heat transfer solutions for the semi-infinite plane indicates that the value for the characteristic time, τ, which defines a steady-state thermal layer for the case of a gaseous medium moving radially from the surface of a sphere, is related to the gas transport time. The latter conditions are almost identical to those which exist at the oxidizer surface during steady-state propellant combustion.

Consider then the heat transfer problem when a sphere of radius r_0 and constant temperature, T_s, is suddenly immersed into an infinite environment of constant thermal diffusivity, K (cm^2/sec), and initially uniform temperature, T_f. Assuming radial symmetry, the heat equation describing this case can be written as

$$\frac{\partial U}{\partial t} = K\left[\frac{\partial^2 U}{\partial r^2} + \frac{2}{r}\frac{\partial U}{\partial r}\right] \qquad \ldots.[12]$$

with the following conditions: (*1*) $r > r_0$; (2) $U(r, t) = T_f - T(r, t)$; (*3*) $U(r_0, t) = T_f - T_s$, a constant, and (*4*) $U(r, 0) = 0$.

The solution to equation 12 with the stated boundary conditions can be found in ref. 8.

$$T_f = T(r, t) = \frac{r_0(T_f - T_s)}{r} \operatorname{erfc} \frac{r - r_0}{2K^{1/2}t^{1/2}} \qquad \ldots.[13]$$

where $$\operatorname{erfc} x = 1 - \frac{2}{\pi^{1/2}} \int_0^x e^{-y^2}\,dy$$

Differentiation of T with respect to r and taking the limit $r \to r_0$ yields

$$\left.\frac{\partial T}{\partial r}\right|_{r=r_0} = \frac{(T_f - T_s)}{r_0}\left[1 + \frac{r_0}{(\pi K t)^{1/2}}\right] \qquad \ldots .[14]$$

Thus, for the hypothetical case of a sphere at constant surface temperature in an environment at initial uniform temperature, the time-dependent thermal layer thickness, δ_{th}, is (see equation 1)

$$\delta_{th}(t) = r_0 / \{1 + r_0/(\pi K t)^{1/2}\} \qquad \ldots .[15]$$

Note that for the case of a semi-infinite plane geometry ($r_0 \to \infty$)

$$\delta_{th}(t) = (\pi K t)^{1/2} \qquad \ldots .[16]$$

Examination of equations 15 and 16 reveals that increasing time has the effect of moving the outer boundary of the thermal layer away from the surface of the sphere. Under steady-state conditions, i.e. T_f and δ_{th} are constant, the time variable can be replaced by a time constant. It is now easily seen that the conditions of the steady-state hypothetical case are almost identical to those prevailing at the surface of an oxidizer particle during steady-state combustion except for the assumption of a stagnant gaseous medium. However, it should be possible to choose a value (τ) for the time constant such that the following identity holds:

$$\underset{\text{Steady-state burning}}{\left.\frac{\partial T}{\partial r}\right|_{r=r_0}} \equiv \frac{(T_f - T_s)}{\delta_{th}(\tau)} = \frac{(T_f - T_s)}{r_0}\left[1 + \frac{r_0}{(\pi K \tau)^{1/2}}\right] \qquad \ldots .[17]$$

Thus it can be considered that $\delta_{th}(t)$ reaches the steady-state value required to describe propellant combustion after a certain characteristic time period has elapsed. From the physical description of the burning process, it is reasonable to suppose that the characteristic time period is the gas transport time (which is proportional to the half-life). This can be shown more explicitly by the following application of D. ROSENTHAL's work with moving sources of heat[9].

Consider, now the problem of a semi-infinite medium of initial temperature T_s moving past a plane (at $x = 0$) which is a heat source ($\dot{q}'$). When the temperature of the source (T_f) and the velocity of the medium (u) are constant, the steady-state temperature of any part of the medium at a distance x away from the source is

$$T(x) - T_s = (T_f - T_s)\exp(-ux/K) \qquad \ldots .[18]$$

The moving heat source problem describes the problem of the 'thermal layer' mechanism in one dimension when the heat source is the redox flame zone, and a distance, δ, from the plane $x = 0$ is considered such that $T(\delta) \simeq T_s$ and $\dot{q}' \simeq (T_f - T_s)/\delta$.

This leads to the approximation

$$T(\delta) - T_s = (T_f - T_s)\exp(-u\delta/K) \simeq 0 \qquad \ldots.[19]$$

Expanding the exponential term of equation 19 and neglecting high order terms yields

$$(T_f - T_s)(1 - u\delta/K) \simeq 0 \qquad \ldots.[20]$$

or

$$u\delta/K \simeq 1 \qquad \ldots.[21]$$

The velocity of the medium within the thermal layer can be equated to the average gas transport velocity (u_1). Therefore, from equations 10, 11 and 21

$$\delta \simeq \{(Kt_{1/2}/\alpha)(\rho_1/\rho_g)\}^{1/2} \qquad \ldots.[22]$$

We now note that equation 22 is nearly identical in form to equation 16 for the thickness of the planar stagnant thermal layer, δ_p, particularly since it will be shown that for the nitric acid–ammonia gas reaction $\rho_1/\alpha\rho_g$ is approximately three. It seems reasonable therefore to associate the characteristic time constant, τ, of equation 17 with the half-life $t_{1/2}$ for the gas phase reactions, or more generally

$$\pi\tau = t_{1/2}\rho_1/\alpha\rho_g \qquad \ldots.[23]$$

Thus the expression for the thermal layer thickness of a burning spherical oxidizer particle becomes

$$\delta = r_0/\{1 + r_0/(Kt_{1/2}\rho_1/\alpha\rho_g)^{1/2}\} \qquad \ldots.[24]$$

The surface temperature expression

It is now possible to express the surface temperature of the oxidizer particles in a burning propellant in terms of the solid and gas-phase chemical reactions. By substituting equations 4 and 24 into the energy balance equation (equation 3) and solving for T_s, the following expression for the surface temperature is obtained.

$$T_s = [-E_s/R]/\ln[\sigma(T_f - T_s)(1 + r_0/\{Kt_{1/2}\rho_1/\alpha\rho_g\}^{1/2})/r_0\rho_s\Delta H\,A_s] \qquad \ldots.[25]$$

Inspection of equation 25 reveals that certain approximations can be made. Because logarithms of functions vary much more slowly that the functions themselves, it should be possible to treat the quantity $(T_f - T_s)$ as an averaged constant. This should be valid as long as the chosen value of $(T_f - T_s)$ is not different from the true value by several factors. For the present case $(T_f - T_s)$ in the logarithmic quantity will be taken equal to $\frac{1}{2}T_f$ (this will be certaintly valid for ammonium nitrate since $T_f = 1\,250$°K and, from experiment[5], $T_s \simeq 600$°K).

In general, T_s will be relatively insensitive to small variations in any of the parameters appearing in the logarithmic quantity of equation 25.

The dependence of the surface temperature on pressure

The relationship between the oxidizer surface temperature and pressure can be derived by considering the kinetics of the gas-phase reactions and the thermal diffusivity. As before, it is assumed that the oxidizer gas-phase redox reactions which establish T_s are controlled by second-order kinetics, and the half-life at temperature T_g can be expressed as

$$t_{1/2} = 1/c_g k_g \qquad \ldots.[26]$$

Since $2c_g = \rho_g/M$ (where M denotes average molecular weight of the gaseous reactants in g/mole), the half-life expression becomes

$$t_{1/2} = 2M/\rho_g k_g \qquad \ldots.[27]$$

Now the average thermal diffusivity as used in equation 24 is independent of the gas flow in region 1 and therefore has the usual definition

$$K = M\sigma/C_p\rho_1 \text{ cm}^2/\text{sec} \qquad \ldots.[28]$$

where C_p is the average molar heat capacity of the gases at constant pressure in cal/mole.°C. It should be noted that over the pressure and temperature range of interest, C_p and σ can be considered as constants.

Combining equations 25, 27 and 28 yields the following expression for the surface temperature.

$$T_s = [-E_s/R]/\ln[\sigma(T_f - T_s)(1 + \{r_0\rho_g/M\}\{\alpha C_p k_g/2\sigma\}^{1/2}/r_0\rho_s \Delta H A_s] \qquad \ldots.[29]$$

If it is assumed that the gases obey the perfect gas law, then

$$\rho_g = MP/R_g T_g \qquad \ldots.[30]$$

where R_g, the gas constant, is expressed in units of atm.cm^3/mole.°C.

Also, if an Arrhenius form of rate equation is assumed for k_g, then

$$k_g = A_g \exp(-E_g/RT_g) \qquad \ldots.[31]$$

where A_g is the pre-exponential constant (cm^3/mole.sec), E_g is the activation energy of the gas-phase reaction (cal/mole), and R is the gas constant (cal/mole.°C).

Utilizing equations 29, 30 and 31 and the approximation that $(T_f - T_s) \simeq \frac{1}{2}T_f$, in the logarithmic term of equation 29, the surface temperature/pressure relation becomes

$$T_s \simeq [-E_s/R]/\ln[\theta(1 + \varphi P)] \qquad \ldots.[32]$$

where $\theta = \sigma T_f/2r_0\rho_s \Delta H A_s$

and $\varphi = [r_0 \exp(-E_g/2RT_g)/R_g T_g][\alpha C_p A_g/2\sigma]^{1/2}$

As can be observed from equation 32, θ and φ can be considered as constants for any given propellant system (namely A_g, E_g, r_0, T_g, ΔH and A_s are considered constant).

DISCUSSION

It is now possible to calculate the oxidizer surface temperature in a burning propellant provided that thermodynamic and kinetic data are available for the solid and gas phase reactions.

For the case of ammonium nitrate propellants, adequate data exist for the solid-phase reactions, but little is known by direct experiment concerning the gas-phase reactions. However, on the basis of the experimental work done by W. A. ROSSER and H. WISE[10] on the nitrogen dioxide–ammonia reaction, the rate-controlling process of the gas phase reaction between ammonia and nitric acid evolved from the oxidizer is assumed to be

$$NH_3 + NO_2 \underset{}{\overset{k_g}{\rightleftarrows}} NH_2 + HNO_2 \longrightarrow \text{Products} \qquad \ldots .[33a]$$

The nitrogen dioxide is believed to be the result of the relatively rapid decomposition

$$HNO_3 \rightleftarrows NO_2 + OH \qquad \ldots .[33b]$$

The work of Rosser and Wise[10] suggests that it is unlikely that the OH radicals would set up reaction chains which would interfere with the bimolecular second-order reaction 33a.

The nitrogen dioxide–ammonia reaction was studied in the temperature range of 600° to 800° K and the rate constant is given by the Arrhenius equation

$$k_g = 5 \times 10^{12} \exp(-27\,500/RT) \text{ cm}^3/\text{mole.sec} \qquad \ldots .[34]$$

The value of α can be obtained by plotting the reaction rate (equation 6) versus temperature. From *Figure 2*, it is seen that rapid reaction does not occur until a temperature of approximately 1 100° K is reached.

Table 1. List of values for calculation of θ and ϕ for ammonium nitrate-based propellants

$\lambda = 10^{-4}$ cal/cm. sec. °C
$T_f = 1\,250$° K
$\rho_s = 1{\cdot}7$ g/cm^3
$\Delta H = 521$ cal/g (ref. 11)
$E_s = -7\,100$ cal/mole
$A_s = 120$ cm/sec
$r_0 = 10^{-3}$ cm
$R = 1{\cdot}99$ cal/mole. °C

$E_g = 27\,500$ cal/mole
$A_g = 5 \times 10^{12}$ cm^3/mole. sec
$R_g = 82{\cdot}05$ atm. cm^3/°C. mole
$T_g = 1\,100$° K
$M = 30$ g/mole
$C_p = 12$ cal/mole. °C (0·4 cal/g. °C)
$\alpha = (T_f - T_g)/(T_f - T_s) = 0{\cdot}23$

Using the values listed in *Table 1*, θ and ϕ were calculated to be $5{\cdot}9 \times 10^{-4}$ and $5{\cdot}5 \times 10^{-3}$ atm^{-1}, respectively.

It should be noted that the value of ϕ is relatively insensitive to the particular value of T_g which is chosen for the start of the rapid phase of the gas reactions. This is easily shown by evaluating ϕ for different reasonable values of α or T_g. *Table 2* shows the variation in ϕ with T_g when the approximation $\alpha = (T_f - T_g)/(T_f - T_s) \simeq 2(T_f - T_g)/T_f$ is used.

Table 2. Values of ϕ for different values of T_g and α

ϕ (*atm*$^{-1}$)	T_g (°*K*)	$\alpha \simeq 2(T_f - T_g)/T_f$
$1{\cdot}26 \times 10^{-3}$	800	0·72
$2{\cdot}60 \times 10^{-3}$	900	0·56
$4{\cdot}11 \times 10^{-3}$	1 000	0·40
$5{\cdot}60 \times 10^{-3}$	1 100	0·24
$4{\cdot}84 \times 10^{-3}$	1 200	0·08
$3{\cdot}86 \times 10^{-3}$	1 225	0·04

It is interesting to compare equation 32 with the surface temperature/pressure relation which is derived from the conventional empirical burning rate equation

$$v = a + bP \qquad \ldots . [35]$$

where a and b are constants.

Equation 35 can be rearranged to give

$$v = a[1 + (b/a)P] \qquad \ldots . [36]$$

which can be equated to the Arrhenius form of the burning rate (equation 4)*

$$a[1 + (b/a)P] = A_s \exp(-E_s/RT_s) \qquad \ldots . [37]$$

Solving for the surface temperature results in

$$T_s = [-E_s/R]/\ln[(a/A_s)\{1 + (b/a)P\}] \qquad \ldots . [38]$$

The similarity of the above expression to equation 32 is obvious and suggests that $\theta = a/A_s$ and $\phi = b/a$.

Now the Crawford bomb burning rates of several ammonium nitrate–polystyrene propellants containing three weight per cent ammonium dichromate as catalyst, and with the molecular weights of the polystyrene ranging from $1{\cdot}4 \times 10^5$ to 5×10^5 g/mole, have been reported by Andersen *et al.*[5]. From their averaged data the burning rate equation can be written as

$$v = a_1 - bP_0 + bP = a + bP \qquad \ldots . [39]$$

where $a_1 = 0{\cdot}178$ cm/sec, $b = 2{\cdot}05 \times 10^{-3}$ cm/atm.sec, and $P_0 = 41{\cdot}85$ atm.

Table 3. Comparison of experimental and theoretical burning rate and surface temperature parameters

Quantity	*Experimental*	*Theoretical* ($E_a = 27{\cdot}5$ *kcal/mole*)	*Theoretical* ($E_a = 22{\cdot}5$ *kcal/mole*)
a, *cm/sec*	0·092	0·071	0·071
b, *cm/sec. atm*	0·0020	0·0004	0·0012
θ	$7{\cdot}66 \times 10^{-4}$	$5{\cdot}9 \times 10^{-4}$	$5{\cdot}9 \times 10^{-4}$
ϕ, atm^{-1}	$2{\cdot}23 \times 10^{-2}$	$5{\cdot}5 \times 10^{-3}$	$1{\cdot}7 \times 10^{-2}$
v, *cm/sec*†	0·232	0·099	0·155
T_s, °*K*†	572	500	536
$\partial T_s/\partial P$, °*K/atm*†	0·80	0·28	0·62

†$P = 70$ atm.

The first three columns of *Table 3* show a direct comparison of the values of the theoretical and experimental burning rate and surface temperature parameters. The agreement between the theoretical and experimental

---

*The linear burning rate (v_p) of a solid composite propellant can be expressed in terms of the rate at which layers of oxidizer particles (assuming a stacked packing arrangement) are being decomposed: $v_p = r_0/t_1$, where t_1 is the lifetime of a single oxidizer particle. Since t_1 is approximately r_0/v, we have $v_p \simeq v$. It should be pointed out that about 90 per cent of the mass of a spherical particle is contained in the outer one-half shell thickness. In keeping with the previous approximations, it is reasonable to assume that the oxidizer particle size remains essentially constant during the greater portion of its lifetime. Alternatively, due to the variation of T_s with particle size (see *Figure 3*), the same conclusion can be reached if one considers v to vary with particle size.

values is reasonable in view of the approximations that were necessary in order to make the calculations, and the possible errors in the Crawford bomb data. The uncertainties involved in the *a priori* estimates of many of the parameters in *Table 1* could easily account for the factor of five discrepancy between the experimental and theoretical values of b. Another explanation for the discrepancy is suggested in the subsequent discussion in connection with the effect of chemical additives on the burning rate.

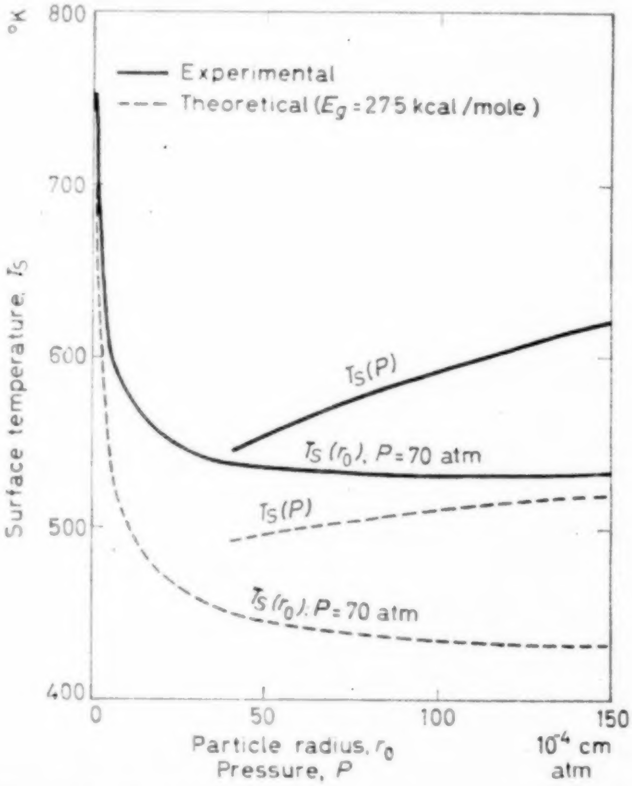

Figure 3. Oxidizer surface temperature versus pressure and particle radius

Figure 3 shows a plot of T_s/P and T_s/r_0 (for $P = 70$ atm) using the values listed in *Table 3*. It is seen that the surface temperature is relatively insensitive to pressure changes. Also, the particle size effect on the surface temperature is relatively small for oxidizer particles greater than about 25 microns.

It is known that the burning rates of composite solid propellants can sometimes be altered by the incorporation of small quantities of certain chemical additives to the propellant–binder system. In terms of the 'two-temperature' theory and the 'thermal layer' mechanism, the effectiveness of chemical additives can be attributed to a partial catalysis of the gas-phase redox reaction. In other words, chemical additives can act as heterogeneous catalysts which speed up the gas-phase reactions (thereby increasing T_s) without altering the mechanism of the solid decomposition reaction. The magnitude of the change in burning rate will depend upon the effectiveness of the catalyst, and the particular value of $r_0/\{Kt_{1/2}\rho_s/\alpha\rho_g\}^{1/2}$ which characterizes the non-catalysed oxidizer (see equations 24 and 25). If $r_0/\{Kt_{1/2}\rho_s/\alpha\rho_g\}^{1/2} < 1$, then the propellant will be relatively insensitive to chemical additives; however, if $r_0/\{Kt_{1/2}\rho_s/\alpha\rho_g\}^{1/2} > 1$, then the propellant will be sensitive to chemical additives. The effect of catalytic chemical additives on the burning rate can be described in terms of a change in the activation energy, E_g, of the gas-phase reactions.

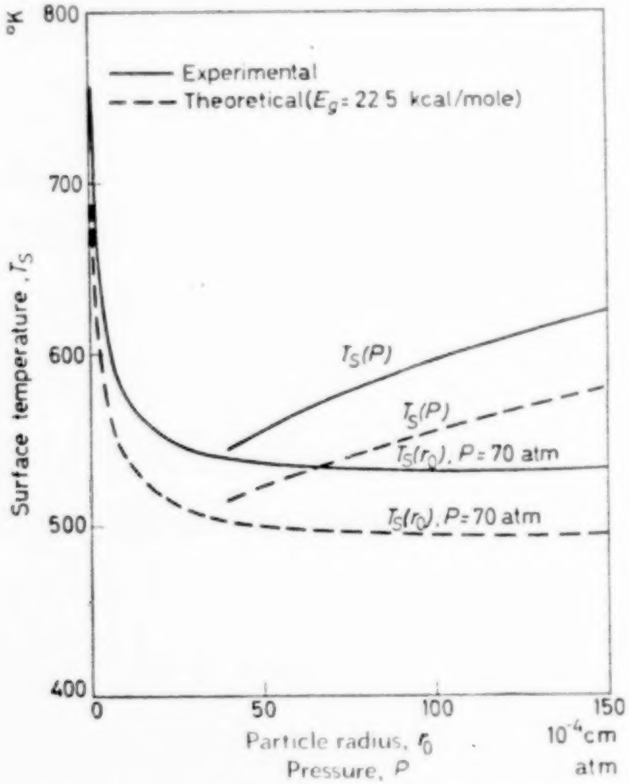

Figure 4. Oxidizer surface temperature versus pressure and particle radius

The possible catalytic effect suggests an explanation for the discrepancy between the empirical and theoretical values listed in *Table 3* for the constant coefficient of the pressure term of equation 32. The given value for φ was calculated using an activation energy (27·5 kcal/mole) which was measured for the uncatalysed reaction between nitrogen dioxide and ammonia, while the value of b/a was taken from propellant burning-rate data using propellants with ammonium nitrate oxidizer catalysed by three weight per cent ammonium dichromate. It is then possible that φ was derived from an E_g which was too large. If it is considered that the ammonium dichromate speeds up the rate-controlling reaction step (equation 33a) then the correct value of E_g, which is used for comparing φ with b/a, should be somewhat less than 27·5 kcal/mole.

It is interesting to calculate the increase in φ due to a 5 kcal decrease in E_g. From equation 32, it is seen that the value of φ given in *Table 3* would be altered by a factor of $\exp(5\,000/2RT_0)$ or $e^{1\cdot14}$. This results in an increase in ϕ by a factor of 3·13 or $\phi = 1\cdot7 \times 10^{-2}$ atm^{-1}, which compares more favourably with the experimental results. This is shown by the last column of *Table 3* and the T_f/P curves of *Figure 4*.

CONCLUSIONS

The 'two-temperature' theory of solid composite propellant combustion has suggested the formulation of a 'thermal layer' mechanism of propellant burning based on the decomposition of the oxidizer component alone. By considering the chemical reactions and energy transfer processes at the surface of individual oxidizer particles, it is possible to relate propellant burning-rate parameters to the kinetics of the solid- and gas-phase oxidizer reactions. Although the treatment presented here has been applied only to ammonium nitrate propellants, it might be applicable to some ammonium perchlorate propellants. It is interesting to note that in a recent paper by R. FRIEDMAN, G. G. NUGENT, K. E. RUMBEL and A. C. SCURLOCK[12], it was suggested that the rate-controlling process in the burning of some ammonium perchlorate–organic binder mixtures occurs at the solid surface where the temperature might be similar to that which exists when pure ammonium perchlorate burns. This suggestion is consistent with the mechanism described here for ammonium nitrate propellants.

It should be noted that the present model of propellant burning is not based upon a thermal layer which arises from diffusion of oxidizer and binder gas products. Instead, it is assumed that the thermal layer involves a process which can be considered to be the expansive movement of premixed gases from the oxidizer surface which react in a flame zone at their adiabatic flame temperature. Diffusion processes involving the binder cannot be precluded completely from the propellant burning mechanism, however, since it is probable that the gaseous products from the pyrolysis of solid binder diffuse into the secondary gaseous products from the ammonia–nitric acid reaction prior to further reaction which results in the high rocket chamber temperature. However, if this diffusion flame occurs at a relatively large distance from the oxidizer surface, it should contribute little heat to the oxidizer decomposition reaction. It is also possible for the binder gas products to diffuse through the oxidizer flame zone, thereby diluting the ammonia–nitric acid flame and decreasing T_f. It is believed that these binder effects do not occur in any significant degree in many of the ammonium nitrate cases studied[3].

Although there are many assumptions in the derivation and evaluation of the steady-state thermal layer thickness, they all appear to be reasonable, and the agreement encountered with experimental data lends support to the validity of the simple approach used. However, additional work on a more rigorous treatment of the energy transfer at the oxidizer surface is warranted.

The author wishes to express his appreciation of the time given to him by several personnel of the Aerojet-General Corporation. The many discussions held with Drs W. H. Andersen and R. D. Schultz were of great *help in the formulation and presentation of this paper. The help of Dr G. Moe in editing the final draft is also acknowledged.*

Chemical Division,
Aerojet-General Corpn,
Azusa, Calif.

(*Received July 1958*)

REFERENCES

[1] WILFONG, R. E., PENNER, S. S. and DANIELS, F. *J. phys. Chem.* 1950, **54**, 836
[2] SCHULTZ, R. D. and DEKKER, A. O. Unpublished work (1952). Reviewed in a paper by R. D. SCHULTZ, L. GREEN, Jr, and S. S. PENNER, *Combustion and Propulsion*, pp 367–420. Pergamon: New York, 1958
[3] ANDERSEN, W. H., BILLS, K. W., MISHUCK, E., MOE, G. and SCHULTZ, R. D. 'A model describing combustion of solid composite propellants containing ammonium nitrate'. *Combustion & Flame*, 1959, **3**, 301
[4] RICE, O. K. and GINELL, R. *J. phys. Chem.* 1950, **54**, 885
[5] ANDERSEN, W. H., BILLS, K. W., MISHUCK, E., MOE, G. and SCHULTZ, R. D. *Jet Propulsion*, 1958, **28**, 831
[6] SCHULTZ, R. D. and DEKKER, A. O. *Fifth Symposium (International) on Combustion*, p 260. Reinhold: New York, 1955
[7] SCHULTZ, R. D. and DEKKER, A. O. *J. chem. Phys.* 1955, **23**, 2133
[8] CARSLAW, H. S. and JAEGER, J. C. *Conduction of Heat in Solids*, p 209. Oxford University Press: London, 1947
[9] ROSENTHAL, D. *Trans. Amer. Soc. mech. Engrs*, 1946, **68**, 849
[10] ROSSER, W. A. and WISE, H. *Progr. Rep. Jet Prop. Lab. No. 20 273*. California Institute of Technology (15 September 1955)
[11] TAYLOR, J. and SILLITTO, G. P. *Third Symposium on Combustion, Flame and Explosion Phenomena*, p 572. Williams and Wilkins: Baltimore, 1949
[12] FRIEDMAN, R., NUGENT, G. G., RUMBEL, K. E. and SCURLOCK, A. C. 'Deflagration of ammonium perchlorate'. *Sixth Symposium (International) on Combustion*, p 612. Reinhold: New York, 1957

A Model Describing Combustion of Solid Composite Propellants Containing Ammonium Nitrate

W. H. ANDERSEN, K. W. BILLS, E. MISHUCK, G. MOE and
R. D. SCHULTZ

A 'two-temperature' model describing the burning of ammonium nitrate, AN, composite propellants is presented. This theory postulates that in an AN propellant, the oxidizer gasifies first at about 300° to 350°C by a highly endothermic surface process to give premixed ammonia and nitric acid. The oxidation–reduction reactions of these two gases establish a flame with a maximum temperature of about 1 000°C. Burning catalysts influence burning characteristics of AN propellants mainly through a heterogeneous catalysis of these gas-phase reactions. Particles of binder protrude from the burning oxidizer surface and pyrolyse in this hot flame-zone. Since the pyrolysis of solid oxidizer and of solid binder are independent processes it is possible with this theory to estimate average surface temperatures of both the oxidizer and binder in the burning propellant by means of linear pyrolysis-rate data. Unique experiments demonstrate that the binder–oxidizer gas reactions often take place at a relatively large distance from the surface in a region of relatively high temperature. The heat produced by these exothermic binder–oxidizer gas reactions (diffusion flame) must therefore contribute very little to the determination of the effective temperature at the surface with many typical AN propellants. The theory predicts a lower limit of about 0·04 cm/sec to the burning rate of AN propellants.

THIS paper summarizes an investigation directed toward elucidating the physical and chemical processes involved in the burning of composite propellants employing ammonium nitrate, AN, as the oxidizer. The burning rates of AN propellants as a class are low, and most of them will not burn unless they contain a few per cent of a suitable combustion accelerator ('catalyst'). Various chromate and dichromate salts have been found to be particularly effective for this purpose[1].

It was first suggested by R. WILFONG, S. S. PENNER and F. DANIELS[2] that the rate-controlling reaction in the thermal decomposition of a solid occurs in the monomolecular surface layer exposed to the flame zone and not below this surface layer. According to this view, the possibility of partial decomposition in the sub-surface layers during the burning process is not ruled out completely; however, this partial decomposition is not considered to be rate-controlling. In a recent publication[3] a study of the surface decomposition kinetics of pure AN is reported. It was demonstrated that there are important differences between the surface decomposition and the conventional liquid-phase (bulk) decomposition for this compound. In particular, it was shown that at a given temperature the surface gasifies at a rate which is greater than that predicted on the basis of the bulk decomposition reaction. This rate of gasification proceeds by a mechanism which involves a small activation energy (about 7 kcal/mole), has a high endothermicity of reaction, and initially produces essentially only nitric acid vapour and ammonia. This surface decomposition is accomplished by a high-rate, surface heating technique, and appears to involve the same phenomena of solid super-heating as reported by R. D. SCHULTZ and A. O. DEKKER for ammonium chloride[1]. The bulk decomposition of AN, on the other hand, is essentially a liquid-phase reaction which is exothermic, and produces mostly nitrous oxide and water. It is rate-controlled by a high activation energy.

The experimental approach which was adopted in this investigation was to measure first the linear pyrolysis rate of catalysed AN, and a series of binders of various chemical structures. Changes in pyrolysis rates of the oxidizer on addition of small amounts of binder, and vice versa, were then measured. The Crawford bomb burning rates of strands of stoichiometrically loaded composite propellant made from these binders and catalysed AN were then determined, and the ignition temperatures of molten catalysed AN with the binders measured. Studies were also made of the flames produced by propellants of simple geometry. Finally a correlation between the pyrolysis rates of the oxidizer and binder with the burning rate of the corresponding composite propellant was established.

THE INDIVIDUAL LINEAR PYROLYSIS RATES OF OXIDIZER AND BINDERS

Linear pyrolysis rate of catalysed ammonium nitrate

The linear pyrolysis rates of AN containing various conventional burning accelerators were measured in the same manner as for pure AN[3]. Briefly, the measurements were made by pressing highly compressed samples of a homogeneous mixture of C.P. AN and the burning catalyst (average particle sizes about 10 microns) against a heated surface, and measuring the linear rates of regression of the surface of the samples as a function of surface temperature. The surface temperature was measured by means of a flattened thermocouple (24 B. and S. gauge wires of Pt and Pt + 20% Rh) interposed between the sample surface and a thin sheet of mica covering the hot element. The pyrolysis rates were determined by means of a potentiometer mounted on a sample feeding device which provided for automatic recording of the position of the sample surface as a function of time. The apparatus used for many of the measurements is shown in *Figure 1*. It is a prototype of the hot-plate pyrolysis apparatus which is described in detail elsewhere[5].

Figure 2 shows the results of the experimental linear pyrolysis rates of AN containing three weight per cent of ammonium dichromate. The experimental pyrolysis rate data for pure AN are included for comparative purposes. It is seen that the presence of ammonium dichromate has no visible effect on the pyrolysis rate of AN. This was also found to be true when other typical burning catalysts were employed in small amounts, *ca.* 3 per cent (or less). Larger concentrations of these additives produced a solid residue which interfered with accurate measurement of the temperature of the reaction interface. However, from the results with small percentages it was concluded that the linear pyrolysis rate of AN is not significantly influenced by the addition of a few weight per cent of these typical burning accelerators. This result indicates that ordinary burning

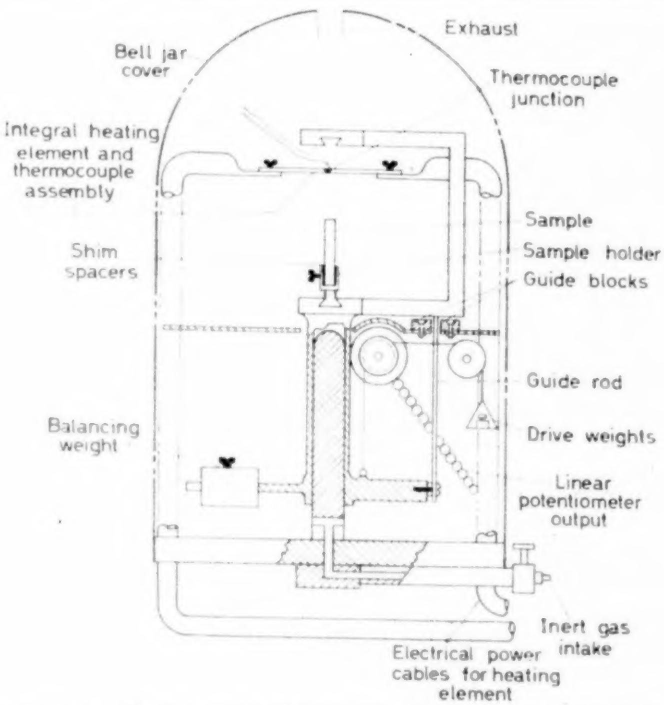
Exhaust
Bell jar cover
Thermocouple junction
Integral heating element and thermocouple assembly
Sample
Sample holder
Shim spacers
Guide blocks
Guide rod
Balancing weight
Drive weights
Linear potentiometer output
Inert gas intake
Electrical power cables for heating element

Figure 1. Linear pyrolysis apparatus—schematic diagram

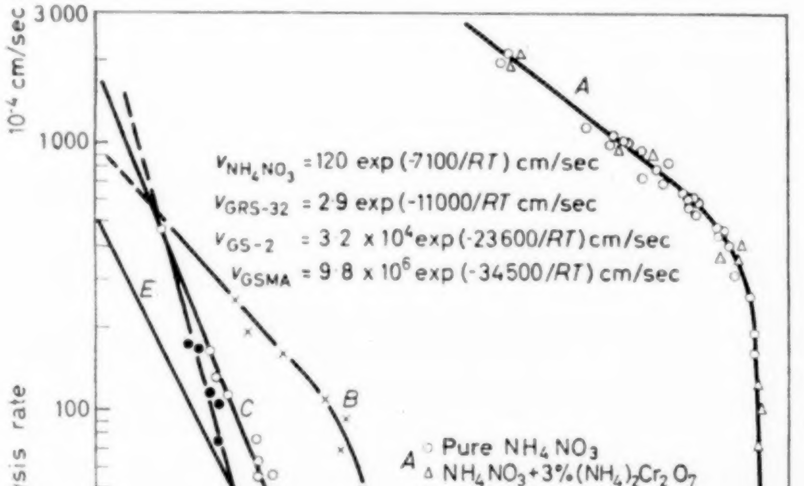

Figure 2. Linear pyrolysis rates of polymeric binders and AN

catalysts do not promote the direct transformation of solid AN into either liquid or gas; i.e. they do not affect the gasification rate of AN *per se*, but must act in a different capacity in increasing burning rates of AN propellants.

Experiments, which will not be described here, have shown that the decomposition rate of molten AN is increased several hundredfold when a few per cent of these catalysts is added. However, the same quantity of these catalysts only approximately doubles the burning rate of a given AN propellant. These results, together with those described above, suggest that the principal mechanisms by which ordinary burning catalysts increase burning rates of AN propellants are by heterogeneous catalysis of the gaseous decomposition products of the oxidizer near the surface, and possibly by flameholder effects, thereby establishing a higher average surface temperature. This is further confirmed by the fact that hot, freshly prepared chromic oxide (from the thermal decomposition of ammonium dichromate) is capable of catalysing decomposition of the vapour from subliming AN. (Nitrogen dioxide gas is one of the products of this catalysed decomposition. Hot chromic oxide ash also induces nitrogen dioxide formation from nitric acid but is not effective in producing it from ammonia or nitrous oxide.)

From the discussion above it is seen that the linear decomposition rate of catalysed AN is the same at any given surface temperature as that of pure AN. The rate as a function of surface temperature may therefore be expressed by the equation[3]

$$v = 120 \exp(-7\,100/RT_s) \text{ cm/sec} \qquad \ldots.[1]$$

where T_s is the absolute surface temperature, °K, and R is the gas constant 1·99 cal/g.mole/°K. The activation energy and the pre-exponential factor for the pyrolysis of AN are both small, and hence high surface temperatures are necessary to achieve rapid pyrolysis and high burning rates for this substance. High oxidizer surface temperatures are difficult to establish in AN propellants because of the large endothermicity of the surface reactions.

Linear pyrolysis rate of polymeric binders

The linear pyrolysis rates of a variety of polymeric binders were measured as a function of surface temperature. The linear pyrolysis rates of most ordinary propellant binders are much lower than that of AN over the entire range of temperatures studied. *Figure 2* shows the experimental pyrolysis rates as a function of surface temperature for three polymeric binders, GRS-32, GS-2, and GSMA, which have been employed in actual propellant systems. GRS-32 is a modified butadiene–styrene copolymer, GS-2 is a polyester–styrene based copolymer, and GSMA is a polyester–styrene–acrylate based copolymer. All of these binders are highly crosslinked. The pyrolysis rate data were obtained using small sticks of the binder (about ¼ in. × ⅛ in. cross section) and a hot-plate pyrolysis apparatus similar to that shown in *Figure 1*. The samples were fed upward to the bottom surface of the heating element with a constant loading force of about 850 g/cm². The pyrolysis measurements were conducted in a nitrogen atmosphere at atmospheric pressure. The pyrolysis data for the above binders give the following rate expressions over the indicated temperature ranges.

$$v_{GBS-32} = 2{\cdot}9 \exp(-11\,000/RT) \text{ cm/sec } (382° \text{ to } 502°\text{C})$$

$$v_{GS-2} = 3{\cdot}2 \times 10^{4} \exp(-23\,600/RT) \text{ cm/sec } (440° \text{ to } 545°\text{C})$$

$$v_{GSMA} = 9{\cdot}8 \times 10^{6} \exp(-34\,500/RT) \text{ cm/sec } (413° \text{ to } 552°\text{C})$$

The linear pyrolysis rates as a function of surface temperature were also determined for a series of five cast linear polystyrenes of different molecular weights (varying degrees of polymerization). The interesting discovery was made that the pyrolysis rate decreases as the degree of polymerization is increased over the range studied. The activation energy appears to remain the same, however, and it is only the pre-exponential factor which increases as the degree of polymerization is reduced. The results are shown in *Figure 3* and summarized in *Table 1*. Much of the experimental scatter was due to the tendency of the polystyrene to soften and spread on the heating element before vaporizing. In spite of these

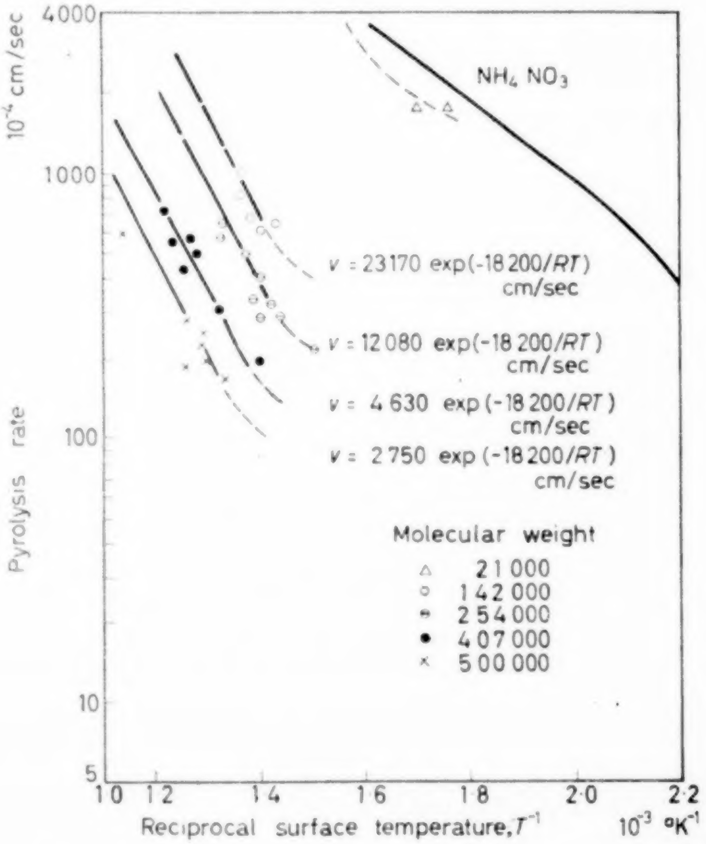

Figure 3. Linear pyrolysis rate of polystyrene of various molecular weights

limitations, the errors have been too small to cause a shift in the order of the curves.

The linear pyrolysis rates of linear polymethylmethacrylate (PMM) and PMM crosslinked with 2 per cent and 5 per cent, respectively, of ethylene glycol diacrylate (EGDA) were also determined. It was found that, over the temperature range studied, the effect of increasing the extent of crosslinking is to decrease the pyrolysis rate at a given temperature. Again the activation energy appears to remain unchanged. The results are shown in *Figure 4* and summarized in *Table 2*.

Table 1

Mol. wt	*Pyrolysis rate (450° to 550° C) cm/sec*
142 000	23 170 exp $(-18\,200/RT)$
254 000	12 080 exp $(-18\,200/RT)$
407 000	4 630 exp $(-18\,200/RT)$
500 000	2 750 exp $(-18\,200/RT)$

The pyrolysis results of both polystyrene and PMM are thus in agreement in that pyrolysis rates decrease with increase in molecular size. External gas pressure up to 10^3 lb/in² gauge had no visible influence on the linear

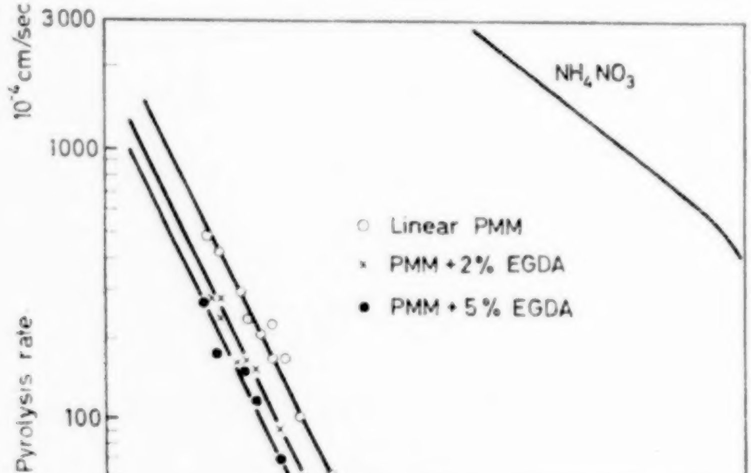

Figure 4. Linear pyrolysis rate of PMM of various degrees of crosslinking

pyrolysis rates of pure PMM, and it may be surmised that gas pressure does not significantly influence the linear pyrolysis rate of other conventional polymeric binders.

The linear (surface) pyrolysis rates at the high temperatures encountered during propellant burning possess a lower activation energy than that reported for the bulk degradation[6] at lower temperatures where the depolymerization process is usually rate-determining. This suggests that some sort of desorption process may possibly be rate-determining during the high temperature surface pyrolysis, but the exact mechanism is as yet unknown.

Table 2

Binder	*Pyrolysis rate (440° to 575°C) cm/sec*
Polymethylmethacrylate	$3\,800 \exp(-18\,640/RT)$
PMM, crosslinked with 2% EGDA	$2\,248 \exp(-18\,640/RT)$
PMM, crosslinked with 5% EGDA	$1\,593 \exp(-18\,640/RT)$

From the data reported above it is seen that below about 300°C, the linear pyrolysis rates of the binders are negligible in comparison with that of AN. Extrapolating the pyrolysis rate data of both the oxidizer and binders shows that at surface temperatures around 700°C the linear pyrolysis rate of AN is still many times greater than that of the binders.

'TWO-TEMPERATURE' THEORY OF PROPELLANT BURNING

The above results show that there is usually a large difference in the pyrolysis rate of AN compared with those of a number of polymeric binders (at constant surface temperature). It has been found that the presence of small amounts of various binders does not influence the pyrolysis rate of AN, and vice versa. The latter experiments were conducted in the same manner as those for the catalysed AN. Also, many of these ground fuels are relatively inert when added to molten catalysed AN, and have little or no effect on the decomposition rate of the latter. Window-bomb observations during the combustion of a sandwich composed of alternate solid blocks of fuel and catalysed AN show that the catalysed oxidizer burns completely, without noticeable melting, and apparently independently of the fuel with which it is in contact. These observations suggest the following picture for the burning process. During the ignition and burning of many types of AN composite propellants, the oxidizer, because of its lower pyrolysis temperature, pyrolyses first and in a manner which is essentially independent of the binder. Exothermic reactions involving the initial pyrolysis products of AN (i.e. nitric acid and ammonia) are assumed to take place in the gas phase. Particles of binder, because of their slower pyrolysis rate, then protrude from the surface and pyrolyse in this hot-flame zone. This indicates that during burning of the propellant it is possible to speak of different average surface temperatures for both the oxidizer and binder, the individual values being a true statistical average over both space and time. The average surface temperatures for the oxidizer and binder in a burning propellant can be estimated in the following manner, which is based on the fact that, under steady-state burning conditions, the linear rate of regression of the fuel in a propellant is equal to that of the oxidizer, which in turn is equal to the burning rate of the propellant. A graph showing the individual pyrolysis rates of the catalysed oxidizer and binder as a function of surface temperature is used. A horizontal line is then drawn intersecting the curves for the separate pyrolysis rates of catalysed oxidizer and binder at the rate corresponding to the observed burning rate of the propellant containing the binder and catalysed AN (see *Figure 5*). From the points of intersection of this horizontal line with the pyrolysis curves of the binder and the catalysed AN the average surface temperatures for the binder and for the oxidizer in the burning propellant are determined. The estimated average surface temperatures obtained in this manner for the oxidizer and binder for several propellants are summarized in *Table 3*.

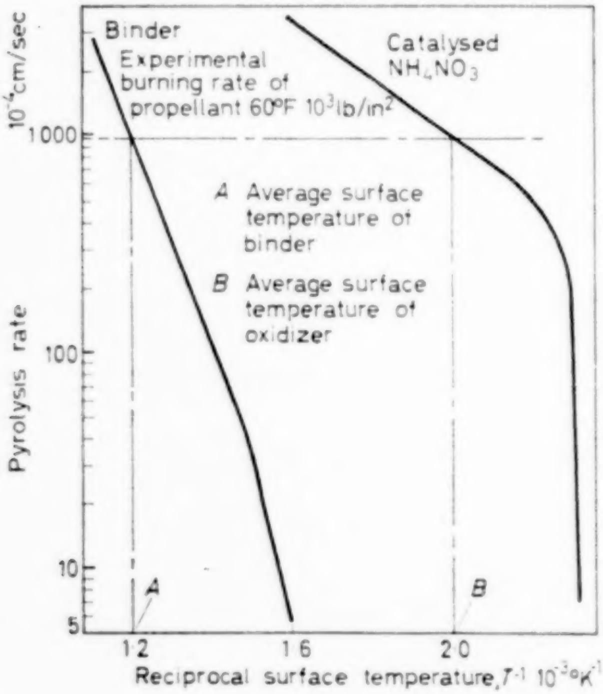

Figure 5. Determination of average temperature of oxidizer and binder in a propellant from individual linear pyrolysis rate data

It appears that the mean surface temperature of the binder in each stoichiometric propellant is greater than that of the catalysed AN. The high surface temperatures of the fuels can be explained if a large portion of the fuel decomposition takes place in a hotter region of the flame zone. That is, the oxidizer gasification process must take place first, allowing the unburnt fuel segments to project from the propellant surface into a hotter region of the flame. It is to be noted that, because of the complex geometry of the fuel–oxidizer mixture in a propellant, actual local temperatures at specific points in the burning surface can be vastly different from the average temperature. Indeed, high speed motion pictures of the burning of catalysed AN composite propellants in a window bomb show a non-uniformity in the flame structure which is distributed in both space and time. The gas motion near the surface varies in space and time and exhibits both laminar and turbulent behaviour.

The above studies suggest that any direct microscopic experimental measurement of the 'surface' temperature of a composite AN propellant (i.e. by thermocouple or optical techniques) must give a temperature which is some intermediate between the temperature at which the oxidizer pyrolyses and the temperature at which the binder pyrolyses.

Table 3. 'Two-temperature' theory estimates of binder, oxidizer, mean surface temperatures during burning of some composite propellants

*Propellant composition**	*Burning rate‡ in nitrogen in a Crawford bomb at 60°F cm/sec*	*Mean surface temperature, °K*	
		Binder	*Oxidizer*
NH_4NO_3 *alone*	0·26	—	588
NH_4NO_3 + *polystyrene (MW 21 000)*	0·30	(610)	599
NH_4NO_3 + *polystyrene (MW 142 000)*	0·24	796	577
NH_4NO_3 + *polystyrene (MW 254 000)*	0·23	840	573
NH_4NO_3 + *polystyrene (MW 407 000)*	0·24	928	578
NH_4NO_3 + *polystyrene (MW 500 000)*	0·23	979	576
NH_4NO_3 + *PMM*	0·21	950	562
NH_4NO_3 + *PMM crosslinked with 5% EGDA*	0·21	1030	562
NH_4NO_3 + *GS-2 polymer*	0·25	1020	582
NH_4NO_3 + *GSMA polymer*	0·26	976	588
NH_4NO_3 + *GRS-32 polymer*	0·36	1373†	615
NH_4ClO_4 *alone*	0·97	—	(1266)
NH_4ClO_4 (75 *wt %*) + *GS-2 polymer*	0·64	947	(1177)

*The propellant samples used for study consisted of highly compressed strands, made from stoichiometric mixtures of ground fuel (80 mesh) and the oxidizer (average particle size about 10 microns). The AN in each case contained 3 wt % ammonium dichromate.

†The estimated surface temperature for GRS-32 polymer may be too high by 100° to 200°K because of the fact that this material leaves a residue during linear pyrolysis measurements which interferes with the accurate estimation of surface temperatures.

‡The burning rates were obtained at 10^3 lb/in² gauge.

( ) The temperatures in parentheses are based on preliminary linear pyrolysis rate data.

The above studies also indicate that the burning surface of a propellant is not planar but rather consists of protrusions and depressions. The depressions represent sites where vaporization of AN to ammonia and nitric acid is occurring at an average temperature of about 600°K. The protrusions represent fuel filaments which project from the propellant into a flame zone whose maximum temperature is about 1 250°K (i.e. the flame temperature of the ammonia–nitric acid oxidation–reduction reaction). Since the fuel pyrolysis in this zone is an endothermic process the average surface temperature of a fuel filament will in general be lower than 1 250°K. The general structure of the burning surface is necessarily time-dependent. However, when attempting to formulate a mathematical model of the burning process it is convenient to use a steady-state approximation. The 'two-temperature' concept described above makes possible, for this steady-state approximation, the assignment of definite temperature boundary-conditions in space near the propellant surface (after the time is averaged out), and hence should be of considerable value for any future detailed quantitative theory of the steady-state burning process.

It is interesting to compare the estimated burning surface temperatures of the components of an AN propellant with those for an ammonium perchlorate propellant employing the same binder. The data for propellants employing GS-2 plastic as the fuel are summarized in *Table 3*. The pyrolysis data used for estimation of the surface temperatures of ammonium perchlorate are those given in *Figure 2*. It is seen that in the ammonium perchlorate propellant, the oxidizer has a higher estimated surface temperature than the binder, in contrast to the AN propellant. This indicates that for ammonium perchlorate propellants it is the oxidizer rather than the fuel particles that protrude into the hot flame region*. It is also seen that the addition of binder to either oxidizer decreases the burning rate. It is concluded that the incorporation of the binder in the strands interferes in some manner with the heat-transfer process to the burning surface.

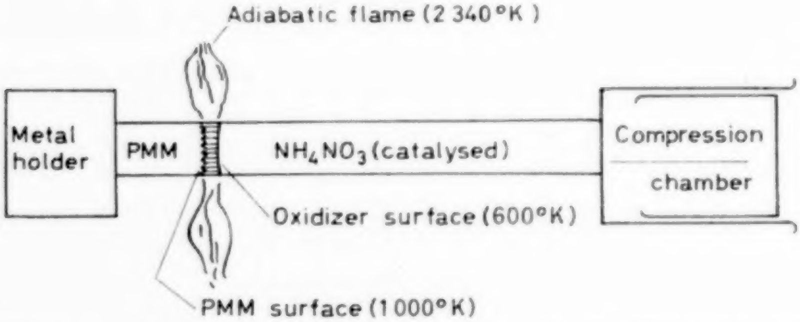

Figure 6. End-to-end combustion of blocks of AN (catalysed) and PMM in a window bomb

Semi-quantitative substantiation of the 'two-temperature' theory for the burning of AN propellants has been obtained from a study of the nature of the flames produced by end-to-end burning of blocks of catalysed AN with blocks of typical binders. Sticks of compressed AN containing three weight per cent ammonium dichromate were lightly pressed against weighed strands of typical binders and ignited at the common interface. The samples were held in a pulley device which provided a constant contact pressure (about 700 g/cm^2) between the oxidizer and binder during the burning process. The experiments were conducted and photographed in a window bomb under a 10^3 lb/in^2 gauge nitrogen atmosphere. The surface of the oxidizer was coated with an inhibitor to restrict burning to the end in contact with the binder. The rate of consumption of the oxidizer was determined by measuring the linear rate of travel of the sample, whereas the rate of consumption of the binder was determined by measuring the weight of binder consumed in a given time. *Figure 6* shows a schematic picture of the end-to-end burning process.

---

*Unpublished work at Aerojet-General has shown that extinguished ammonium perchlorate-based propellants indeed show this pattern.

During end-to-end burning of PMM (both linear and crosslinked) with catalysed AN, the consumption of oxidizer and binder proceeds in a nearly stoichiometric ratio. The rates of consumption were 0·0127 g/sec for the binder, and 0·1755 g/sec (0·311 cm/sec) for the oxidizer. This corresponds to 93·3 per cent by weight of oxidizer as compared to 88·2 per cent required for stoichiometric loading. Because of these stoichiometric considerations, the rate of weight loss of the binder in the end-to-end burning experiment is not equal to the rate of weight loss of the oxidizer. On the other hand, in a composite propellant which is stoichiometrically loaded, the linear pyrolysis rates of the oxidizer and binder must be equal to the burning rate. Thus in a propellant which burns at the rate of 0·311 cm/sec, the oxidizer and binder both pyrolyse at that rate. This requires a pyrolysis temperature of 992°K for the PMM, and 600°K for the AN. Measurements were made of the surface temperature of the binders by interposing a flattened 20-gauge thermocouple between the oxidizer and binder surfaces in an end-to-end burning experiment. Although the surface temperatures which were recorded by the thermocouple fluctuated over a considerable range, the maximum temperature recorded was 970°K, which is in very good agreement with the calculated value of 992°K. The fluctuations resulting in temperatures below 970°K were attributed to temperature readings closer to the oxidizer surface. Indeed, these readings were at times as low as 470°K. End-to-end burning rate measurements employing 5 per cent crosslinked PMM gave maximum thermocouple readings of about 1 000°K for the binder surface temperature. This compares to 1 040°K which is predicted from the pyrolysis curves by the 'two-temperature' theory. The agreement between experimental average binder surface temperatures and those estimated from consideration of the pyrolysis curves is striking and provides strong evidence that burning in the propellant does follow the simple postulated 'two-temperature' model. It is particularly interesting that the maximum surface temperature (experimental) for the 5 per cent crosslinked binder is higher than that of the linear polymer. This is exactly what is predicted by the 'two-temperature' theory, in view of the fact that the burning rate of the propellant with the linear binder is the same as that with the crosslinked binder at 10^3 lb/in^2 gauge.

The end-to-end burning experiments described above demonstrate that both burning of composite AN propellants and end-to-end burning of oxidizer and binder proceed according to the simple 'two-temperature' model given previously. The experimental and predicted binder surface temperatures are both around 1 000°K. This is considerably lower than the adiabatic flame temperature of the propellant, which is about 2 340°K (see *Figure 6*).

It must be concluded, therefore, that very little of the heat produced by binder–oxidizer gas-phase reactions contributes to the effective surface temperature of the binder in PMM and presumably in many other types of AN propellants as well. These reactions must therefore take place at a considerable distance from the surface, and the limiting pyrolysis temperature of the binder will be near the adiabatic flame temperature of decomposed ammonium nitrate (*ca.* 1 250 K) when conventional-type burning catalysts are employed. In most actual cases the temperature will be lower due to dilution of the flame by the binder pyrolysis gases, as well as to incomplete reaction of the pyrolysis products of AN. Estimation of the surface temperatures of all binders for which linear pyrolysis measurements have been made reveal that all are below or near the adiabatic flame temperature of AN. This temperature thus appears to be an important limiting constant in AN propellants. The inability of most fuels substantially to increase the burning rate of AN over that at which it burns itself (plus catalyst) is thus explained. Fuels which increase the burning rates do so by virtue of the fact that they can react exothermally with the decomposition products of AN at the relatively low temperatures near the propellant 'surface' and hence contribute to the surface temperature. This belief is substantiated by the fact that only a small percentage of a large number of typical polymer and non-polymeric binders (fuels) was found to influence significantly the burning rate (in the conventional pressure range) of AN propellants employing these binders. Moreover, those binders which are most effective in lowering the temperature for ignition and decomposition of molten catalysed AN also induce faster burning in the corresponding propellants.

The above conclusion that heat from the exothermic oxidizer–binder gas reactions does not contribute substantially to surface temperature may often be reached from other considerations. The burning rate data given in *Table 3* and the linear pyrolysis rate data given in *Figure 3* for polystyrenes of varying molecular weight show that large changes in the pyrolysis rate of the binder have little influence on the burning rate of the corresponding AN-based propellant. A relatively large change in the burning rate would be expected if the oxidizer–binder gas reactions markedly influenced surface temperature, since the binder pyrolysis rate should influence the structure of the oxidizer–binder gas diffusion flame. Thus the flame from the oxidizer–binder gas reactions must frequently have little influence on the burning characteristics of AN-based propellants.

CORRELATION OF BURNING PARAMETERS OF AMMONIUM NITRATE PROPELLANTS WITH LINEAR PYROLYSIS RATES

The discussion in this section represents an attempt partially to interpret the experimental burning characteristics of AN composite propellants with the aid of the 'two-temperature' theory and a modification of a burning rate equation first suggested by R. B. PARLIN and H. EYRING[7] for single and double base propellants. The original Parlin–Eyring equation is

$$v = A \exp - E/R(T_0 + \alpha P) \qquad \ldots. [2]$$

In order to adapt this equation to the present discussion, however, the terms must be re-defined.

The velocity of burning of a propellant can be considered as the rate at which material leaves the propellant surface. According to the 'two-temperature' theory, the propellant surface reactions involve only the surface reactions of the individual oxidizer and binder. Furthermore, the linear rate of regression of the propellant surface during steady-state burning is equal to the linear rate of regression of the oxidizer, which rate is in turn equal to the linear rate of regression of the binder. This suggests that separate equations similar to equation 2 can be written for both the oxidizer and binder during burning, i.e.

$$A_b \exp - E_b/R(T_{0,b} + \alpha_b \Delta P) = A_{ox} \exp - E_{ox}/R(T_{0,ox} + \alpha_{ox} \Delta P) \quad \ldots . [3]$$

where the various terms are now defined: v is the velocity of burning the propellant, cm/sec; E_b, E_{ox} are the experimental activation energies for the linear pyrolysis of the pure binder and oxidizer, respectively, cal/g.mole); A_b, A_{ox} are the experimental pre-exponential factors for the linear pyrolysis of the pure binder and oxidizer, respectively, cm/sec; R is the gas constant, 1·99 cal/g.mole/°K; $T_{0,b}$, $T_{0,ox}$ are the temperatures of the binder and oxidizer surfaces, respectively, when the propellant is burning at the minimum pressure required to sustain burning. (This will be designated hereafter as the minimum burning pressure, MBP); ΔP is the difference between the actual chamber pressure and the minimum burning pressure; α_b, α_{ox} are approximately constant parameters which when multiplied by ΔP give the increase over $T_{0,b}$ and $T_{0,ox}$, respectively, of the surface temperature. (These parameters are closely related to the kinetics and the thermal conductivity in the gas phase.); $(T_{0,b} + \alpha_b \Delta P)$, $(T_{0,ox} + \alpha_{ox} \Delta P)$ are the total binder and oxidizer surface temperature (°K) respectively, at the existing chamber pressure.

The values of T_0 will depend upon the type and concentration of the burning catalyst employed. However, for a given catalyst concentration, T_0 to a good first approximation may be treated as a constant. Equation 3 may be expanded to give expressions of the form

$$v = A \exp(-E/RT_0) + A \exp(-E/RT_0) \times (\alpha E/RT_0^2) \Delta P + \quad \ldots . [4]$$

where only terms to the first power of the pressure have been retained. Equation 4 is of the conventional type

$$v = a + b\Delta P \quad \ldots . [5]$$

for the burning of a propellant, where ΔP is now the difference in pressure between the MBP and the actual chamber pressure. The coefficients a and b in the burning rate expression 5 are thus given more explicitly in terms of parameters which have physical interpretations. If an independent method could be devised for determination of the values of $T_{0,b}$, $T_{0,ox}$, α_b, and α_{ox}, the burning characteristics of a given propellant formulation could be calculated. However, the theory can be used in an inverted sense to calculate the values of these terms from the experimental burning characteristics of the propellant, together with the pyrolysis rate data of the individual oxidizer and binder. The values obtained serve to give information about the structure of the reaction zone, and the nature of the burning processes.

The various parameters of equation 3 have been evaluated for the series of pressed AN–polystyrene propellants given in *Table 3*, and are shown in *Table 4*. The propellant strands were identical except that the molecular weights of the ground polystyrene employed in the formulation were varied. The experimentally measured burning parameters of this series, the experimental linear pyrolysis rates of the propellant components and the calculated values of the parameters of equation 3 are given below. The minimum burning pressure was determined experimentally and found to be approximately 600 lb/in² gauge. The ΔP contributions to the surface temperature are evaluated for a chamber pressure of 10^3 lb/in² gauge.

The above calculated burning parameters suggest several interesting features about the burning process. It is very noteworthy that $\alpha\Delta P$ is relatively small compared to the total surface temperature of either binder

Table 4. Experimental and calculated burning equation parameters

POLYSTYRENE

Mol. wt of binder	a	b	*Pyrolysis rate*	$(T_{0,b}+\alpha_b\Delta P)$	$\alpha_b\Delta P$
	(cm/sec)	10^{-4} $\left(\frac{cm.\,in^2}{lb.\,sec}\right)$	exp $(-18\,200/RT)$ *cm/sec*	°*K*	°*K*
21 000	0·253	1·150	—	—	—
142 000	0·182	1·380	23 170	796	19·9
254 000	0·168	1·445	12 080	840	24·8
407 000	0·184	1·440	4 630	928	27·7
500 000	0·179	1·320	2 750	979	29·0

AMMONIUM NITRATE

Mol. wt of binder	a	b	*Pyrolysis rate cm/sec*	$(T_{0,ox.}+\alpha_{ox.}\Delta P)$	$\alpha_{ox.}\Delta P$
	(cm/sec)	10^{-4} $\left(\frac{cm.\,in^2}{lb.\,sec}\right)$		°*K*	°*K*
21 000	0·253	1·150	120 exp $(-7\,100/RT)$	599	16·9
142 000	0·182	1·380		578	26·0
254 000	0·168	1·445		573	28·4
407 000	0·184	1·440		582	27·0
500 000	0·179	1·320		579	27·6

or oxidizer. However, although $\alpha\Delta P$ is small it has a significant effect on the burning rate. For example, although an increase of 400 lb/in² in the chamber pressure results in an $\alpha\Delta P$ contribution of only about 30°K, the burning rate is increased about 7 per cent. The result that $\alpha\Delta P$ is approximately the same for oxidizer and binder suggests that both of these components are receiving heat from the same flame zone (i.e. the ammonia–nitric acid reaction zone). It should further be noted that the value of $T_{0,b}$ increases with molecular weight. Thus it appears that during the burning of the propellant, the slower pyrolysing binder merely decomposes at a higher temperature, and results in a burning rate which is nearly independent of molecular weight.

These results suggest an interesting semi-quantitative picture of the temperature profile in the gas phase near the burning surface as illustrated in *Figure 7*. There appear to be at least three distinct reaction zones which determine the temperature distribution in the gas phase. The reaction occurring in the gas phase near the surface (i.e. in the zone from the origin to x, x') is believed to be primarily the redox reaction between ammonia and nitric acid. In the vicinity of x, x' the ammonia–nitric acid redox reactions are substantially complete, resulting in a reaction temperature of about 1 250°K. Organic vapours from the pyrolysis of the polymeric binder diffuse into the product gases from these redox reactions, and lower the temperature gradient for a relatively long distance (to y, y'). The organic vapours now react more rapidly with the oxidizing gases (i.e. in the zone y, y' to z, z') resulting in a steeper rise of temperature. At z, z' the organic vapours have been completely oxidized and the adiabatic flame temperature of the propellant has been attained.

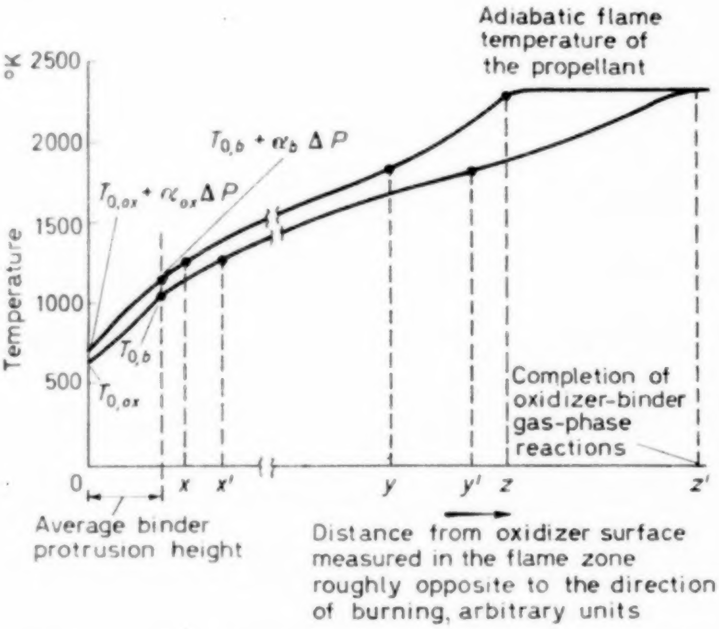

Figure 7. Temperature profile near the burning surface of AN propellants

One of the temperature profiles depicted in *Figure 7* is for burning at the MBP. An explanation of the MBP results from the following considerations.

Examination of the available data on AN propellant burning indicates that the MBP values in a Crawford bomb for many propellants are in the vicinity of 500 to 600 lb/in² gauge, corresponding to minimum burning rates of about 0·07 cm/sec. Much lower burning rates have never been obtained in this laboratory. From the model according to the 'two-temperature' theory, together with the linear pyrolysis curve of AN, it is found that a surface regression rate of 0·07 cm/sec corresponds to an oxidizer surface temperature during steady state burning at the MBP of only about 20°C higher than the melting point at AN (170°C, 443°K).

Thus it appears that ignition and sustained burning at any given pressure can occur only if the rate of heat transfer from the oxidizer gas phase redox reactions permits the oxidizer surface temperature slightly to exceed the melting point of AN. The theoretical minimum burning rate is thus about 0·04 cm/sec, and would occur with a surface temperature equal to the melting point of AN.

When the chamber pressure is increased from the MBP value to 10^3 lb/in² gauge, the temperature profile in the gas phase is altered so that:

(1) The surface temperature of the binder is increased by an increment $\alpha_b \Delta P = 20°$ to $29°$ K.

(2) The surface temperature of the oxidizer is increased by an increment $\alpha_{ox}\Delta P = 17°$ to $28°$ K.

Although the increased pressure probably increases the temperature gradient in the y–z region where oxidizer–binder gas phase reactions are occurring, this apparently does not greatly affect the greater temperature gradient in the 0–x zone where the ammonia–nitric acid redox reactions are occurring. In other words, $\alpha\Delta P$, the pressure-dependent contribution to the surface temperature is relatively small. It is noted from the data in the above table that an eightfold increase in the linear pyrolysis rate of the polymeric binder results in very little change in the propellant burning rate. It is therefore concluded that faster pyrolysing binders do not necessarily produce significantly faster burning propellants. Instead, the pressure-independent surface temperature of the binder, $T_{0,b}$, is decreased, thereby lowering the total binder surface temperature so that the burning rate remains approximately constant. The decrease in $T_{0,b}$ indicates that the faster pyrolysing binder particles do not project into the ammonia–nitric acid reaction zone as far as the slower burning binder particles. This is further substantiated by the fact that the $\alpha\Delta P$ contribution to the binder surface temperature is slightly lower for faster pyrolysing binders. This argument suggests that the type of polymeric binder required to produce a faster burning ammonium nitrate propellant must not only have a faster pyrolysis rate but must also produce gaseous pyrolysis products which will react very rapidly with the vapours from AN, thereby completely altering the shape of the gas phase temperature profile to produce a steeper temperature gradient near the surface and consequently increased surface temperatures of both solid oxidizer and solid binder.

It should be mentioned that many binders do not initially pyrolyse cleanly. Some decompose initially into both gaseous products and unknown carbonaceous-type materials. Typical binders in this group include various rubbers. For binders of this type the pyrolysis rate constants, A and E, which apply in equation 3, are those describing the gasification process. The non-volatile carbonaceous material probably acts as a flameholder and helps result in an increase in the value of T_0.

This paper is based on work performed at Aerojet-General Corporation under Contract AF33(616)–2551 with the Aeronautical Research Laboratory, Wright Air Development Center, United States Air Force.

The authors wish to express their appreciation to Dr A. O. Dekker of Aerojet-General Corporation for advice and encouragement during various phases of this work. In particular Dr Dekker contributed to the formulation of an early version of the 'two-temperature' theory discussed in the paper. The techniques described for measurement of the linear pyrolysis rates of propellant components were developed with the help of Drs Dekker and M. K. Barsh under the sponsorship of the U.S. Air Force through the Office of Scientific Research under Contracts AF18(600)–1026 and AF18(603)–74. The 'end-to-end' burning experiment was first suggested by Dr R. W. Lawrence of Aerojet-General. Mr G. M. Therneau and Mr C. L. Hayner assisted in various aspects of the experimental work. The encouragement given to this research by Mr R. D. Geckler and Dr D. L. Armstrong of Aerojet-General is also gratefully acknowledged.

Chemical Division,
Aerojet-General Corpn,
Azusa, Calif.

(Received July 1958)

REFERENCES

[1] Taylor, J. and Sillitto, G. P. *Third Symposium on Combustion, Flame and Explosion Phenomena*, p 572. Williams and Wilkins: Baltimore, 1949
[2] Wilfong, R., Penner, S. S. and Daniels, F. *J. phys. Chem.* 1950, **54**, 863
[3] Andersen, W. H., Bills, K. W., Dekker, A. O., Mishuck, E., Moe, G. and Schultz, R. D. 'Kinetics of the surface decomposition of ammonium nitrate', *Aerojet-General tech. Memor. No. 295*, January 1958; also, 'The gasification of solid ammonium nitrate', *Jet Propulsion*, 1958, **28**, 831
[4] Schultz, R. D. and Dekker, A. O. *Fifth Symposium (International) on Combustion*, p 260. Reinhold: New York, 1955
[5] Barsh, M. K., Andersen, W. H., Bills, K. W., Moe, G. and Schultz, R. D. *Rev. sci. Instrum.* 1958, **29**, 392
[6] Jellinek, H. H. G. *Degradation of Vinyl Polymers*, p 176. Academic Press: New York, 1955
[7] Parlin, R. B. and Eyring, H. An unpublished work concerning the burning rates of some single and double base propellants, Princeton University *ca.* 1945

Bluff-Body Flame Stabilization: Blockage Effects

F. H. WRIGHT

Experiments have been performed to define the influence of blockage on flame stabilization by bluff bodies in ducted flow. Flameholders of a particularly simple geometry were studied over a wide range of blockage ratios. The studies were made while combustion was taking place and showed that flow speeds and flame geometry depend strongly on blockage. However, the experiments demonstrated convincingly that, at flame blowoff, the particular combination of these variables known as the characteristic mechanical time is independent of blockage as well as of other gross fluid dynamic parameters. Further experiments explored the influence of Mach number on the flows and showed quantitatively the changes in flow speeds and flame geometry to be expected at high Mach numbers. The experiments showed that the value of the mechanical time at blowoff remains unchanged at high Mach numbers despite large changes in the flow speeds and lengths that constitute this mechanical time. As a guide for the experiments, a free-streamline theory was developed. This purely fluid dynamic theory, supplemented by a few simple experimental results, suffices to predict most of the features of bluff-body flameholding. A result of practical importance, predicted by the theory and confirmed by experiment, is that maximum blowoff speed occurs at a relatively low blockage ratio.

EXPERIMENTAL studies by E. E. ZUKOSKI and F. E. MARBLE[1] of bluff-body flameholders have demonstrated that flameholding ability depends directly on the length L of the recirculation zone, the sheltered region just downstream from the bluff body (*Figure 1*). Flameholding limits also depend on the nature of the combustible mixture. Fortunately, experiments[1] have shown that the influence of mixture properties may be expressed by a single parameter, the chemical time τ. As a result, the blowoff speed from a bluff-body flameholder may be written very simply as $(V_2)_{BO} = (L/\tau)$ where V_2 is the flow speed past the flame.

This equation is a powerful tool in the correlation and prediction of flameholder blowoff, since the chemical time depends only on the pressure and temperature of the combustible mixture and on fuel type and fuel/air ratio; chemical time is independent of the gross fluid dynamic variables such as flow speed and flameholder geometry. For a given combustible mixture the chemical time is the same for all flameholders. On the other hand, the recirculation-zone length depends essentially only on the fluid dynamic variables.

The blowoff equation shows how the blowoff flow speed V_2 past the wake varies with recirculation-zone length and chemical time at blowoff. Of greater practical interest, however, is the speed V_1 far upstream. In terms of this speed the blowoff relation becomes $(V_1)_{BO} = (V_1/V_2)(L/\tau)$. The velocity ratio V_2/V_1 depends on flameholder geometry and is strongly influenced by the proximity of duct walls or other flameholders: it depends on blockage. Blockage also affects the length of the recirculation zone.

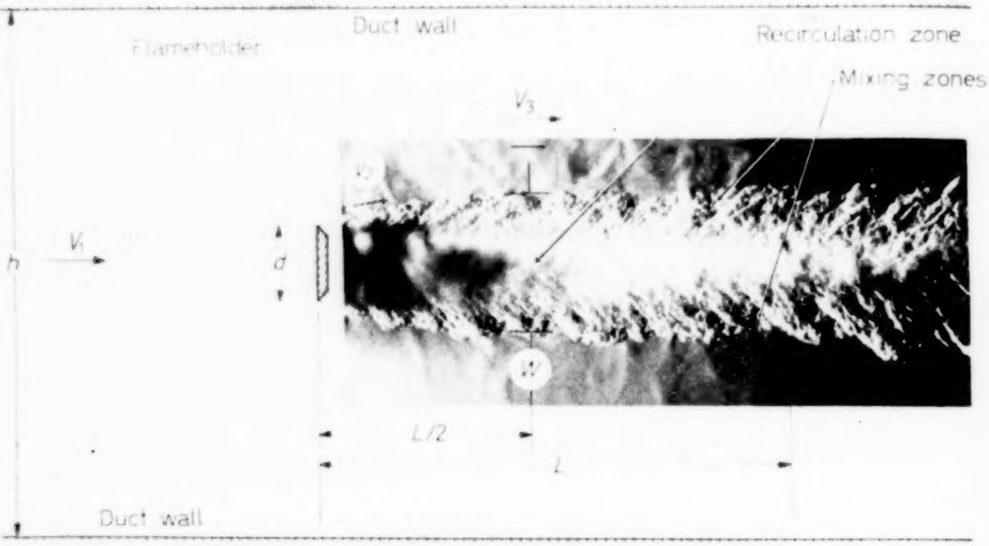

Figure 1. Flame held on flat-plate flameholder

In fact, experiments[2-3] indicated that recirculation-zone length varies inversely as the square root of the blockage and that flow speed past the wake increases almost linearly with blockage. However, further study was required to elucidate the effects of blockage and other fluid dynamic variables. Hence an experimental and theoretical investigation of the influence of blockage on the performance of flameholders of a particularly simple geometry was initiated. The flow about flat plates oriented normal to the stream was studied; this paper presents the results of the study.

EXPERIMENTAL STUDIES

Equipment

The experiments were run in a 1 in. × 4 in. duct with the flameholder set across the narrow dimension and completely spanning the duct. The duct extended 6 in. downstream from the flameholder; for comparison purposes a few experiments were carried out with a 9 in. duct length. Duct side walls were of Vycor glass.

Flameholders were thin flat plates with bevelled edges, oriented so that the flat sides faced upstream. Except for a few comparison runs, the flameholders were water-cooled.

Fuel was Standard Oil Co. thinner No. 200, a gasoline-like hydrocarbon which was injected into heated air far upstream from the flameholder, forming a homogeneous gaseous combustible mixture. Normal mixture temperature was 339° K.

Flame shapes and widths were obtained from spark schlieren photographs.

Recirculation-zone lengths were measured by injecting salt water into the flame. Salt injected into the recirculation zone colours the whole region; salt injected downstream from the end of the recirculation zone leaves the recirculation region uncoloured.

Recirculation-zone length

The recirculation zone is the sheltered region just downstream from a bluff-body flameholder in which hot gas recirculates, and the length L of this region plays an extremely important role in Zukoski and Marble's view of flame stabilization[1]. Hence one of the first experiments to be performed was the study of the influence of various fluid dynamic and chemical parameters on the length L.

Several variables were found to have little effect on the recirculation-zone length. For example, changing flameholder temperature made no measurable difference in the length, nor did changing flameholder aspect ratio by running a flameholder in ducts of different widths.

On the other hand, the flow speed is a fluid dynamic variable that might be expected to influence the recirculation-zone length. Experiments were performed to test this influence, and some of the results are shown in *Figure 2*. The dimensionless length L/d of the recirculation zone is plotted versus the upstream Mach number M_1 for various blockage ratios (BR). The length does indeed depend upon M_1 and hence upon the upstream speed, but only weakly. Variation of length with speed is always less rapid than speed raised to the one-quarter power. The length changes shown in *Figure 2* are small but complex. For very low Reynolds numbers the flames are laminar[1] and their recirculation zones are long. As shown in *Figure 2*, this is so for BR = 1 : 32 and 1 : 16 at very low Mach numbers. As the speed (and Reynolds number) increases, the flame becomes turbulent and the recirculation zone shortens. This behaviour is easily explained by consideration of the mixing zones (*Figure 1*). Recirculation-zone length depends on the spreading rate of the mixing zones. When the mixing zones spread rapidly, as they do with turbulent flames, the recirculation zone is short, whereas when the zones spread slowly, as they do when the mixture is laminar, the recirculation zone is long.

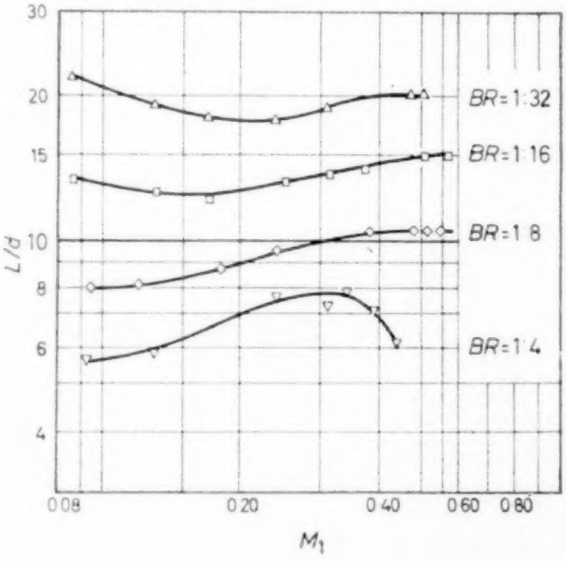

Figure 2. Recirculation-zone lengths versus Mach number: φ = 1·0

At low Reynolds numbers, the upper two curves of *Figure 2* decrease with increasing speed; then they pass through a minimum, and thereafter increase until a plateau is reached. Recirculation-zone length then remains constant as the speed increases. Only when the flow past the flame becomes supersonic does the recirculation-zone length again change. If the blockage is high, this change may occur at a relatively low value of the upstream Mach number, as the BR = 1 : 4 curve in *Figure 2* shows. However, for moderate blockage ratios and flameholder sizes, blowoff occurs in the plateau region where length does not change with speed, and flow past the flame is never supersonic.

Recirculation-zone length changes slowly with such variables as flameholder temperature, aspect ratio, and flow speed. Length does, however, vary rapidly and consistently with flameholder blockage, as *Figure 3* shows. The dimensionless length L/d varies inversely with the square root of the blockage ratio (the actual slope is $-0{\cdot}46$). This is the variation found[2, 3] for circular cylinders but, as shown in *Figure 3*, the flat-plate lengths are 17 per cent greater. The data for the upper curve of *Figure 3* were obtained by running flat plates of different sizes in the 1 in. × 4 in. duct. Hence both blockage and aspect ratios varied as the plates were changed; but the entire effect was ascribed to blockage, since previous experiments had shown that aspect ratio had negligible influence. The blockage effect is fluid dynamic and may be computed with the aid of the free-streamline theory (see Appendix).

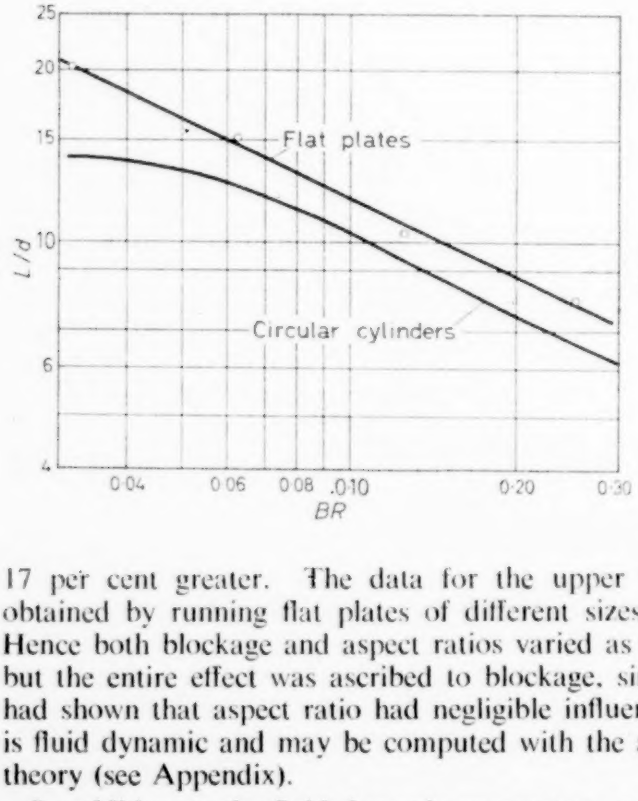

Figure 3. Recirculation-zone length versus blockage ratio

In addition to the fluid dynamic parameters, a chemical parameter—the mixture strength—was studied, and its influence on recirculation-zone length was explored. Lengths were measured holding flameholder geometry and flow speed constant. *Figure 4* shows typical results of such measurements for a blockage ratio of 1 : 32. The flames at $M_1 = 0{\cdot}24$ and $M_1 = 0{\cdot}47$ are turbulent, or nearly so, and the two curves are similar in that recirculation-zone length is a minimum close to stoichiometric and increases appreciably as the mixture ratio departs from stoichiometric. A possible explanation for this behaviour is that the spreading rate of the mixing zones is greatest close to stoichiometric, where the temperature is highest, and that recirculation-zone length is a minimum for the highest spreading rate.

The third curve of *Figure 4* ($M_1 = 0{\cdot}13$) corresponds to a set of laminar flames and is different from the curves for turbulent flames. In general, the recirculation zones are longer than the zones that would be expected for turbulent flames at this speed, and the length increases monotonically with fuel/air ratio. Again, this curve may be explained by the spreading rates of the mixing zones. Rich laminar flames are very smooth and mixing is slow (if the fuel has a molecular weight greater than that of air). On the other hand, lean flames are frequently distorted by large-scale waves which increase the mixing rates; recirculation-zone lengths may be even shorter than at stoichiometric.

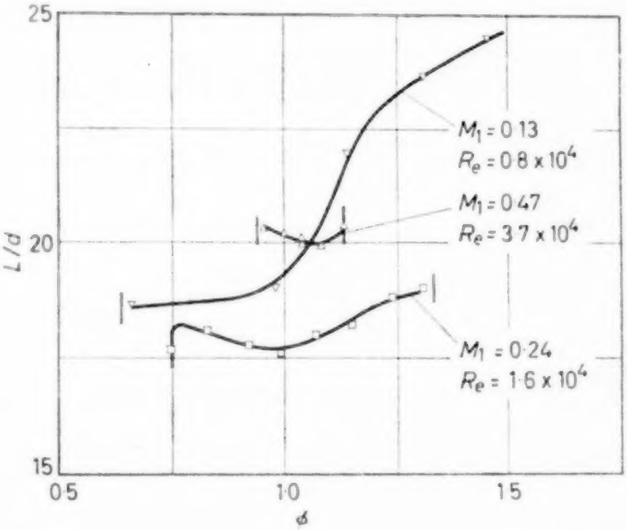

Figure 4. Recirculation-zone length versus fuel/air ratio; BR = 1:32

In *Figure 4*, the situation approaching blowoff (indicated by short vertical lines) is interesting. The propagating flame, downstream from the recirculation zone (*Figure 1*), becomes more and more tenuous until finally it disappears altogether, an event which has been defined to be blowoff. However a residual flame frequently remains beyond this point if flow conditions are very stable. The residual flame occupies just the recirculation-zone region, and the recirculation-zone length remains unchanged. As conditions become slightly more stringent, cold air enters the downstream end of the recirculation zone and the zone shortens. A point is plotted on the lean end of the $M_1 = 0{\cdot}24$ curve in *Figure 4* to show the decrease in length that may be observed under these circumstances, even though this point is beyond the normally defined blowoff. The curves of *Figure 4* show that a chemical parameter, the mixture strength, does not greatly affect recirculation-zone length, nor do most of the fluid dynamic parameters that have been studied. Only the blockage has been shown to have a strong influence on recirculation-zone length. Hence it will be especially interesting to study the influence of blockage on other flame characteristics.

Wake width

Closely related to the recirculation-zone length is the flame or wake width. This width may readily be measured on a schlieren photograph (see *Figure 1*). Unfortunately, the outer edges of the wake are not smooth and regular, and in measuring the width it is necessary to pick an average width and also to average several pictures. When this is done, the results are remarkably consistent. For a given blockage ratio, the width is virtually constant, independent of mixture ratio, and independent of speed (*Figure 5*) except when the Mach number of the flow past the flame approaches unity, at which time the wake width decreases.

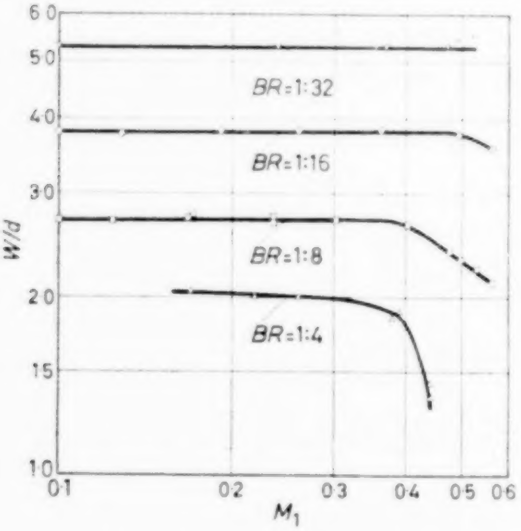

Figure 5. Wake width versus Mach number: $\varphi = 1{\cdot}0$

The width plotted in *Figure 5* was measured at the middle of the recirculation zone. Actually, for all blockage ratios except the smallest, this width applies to the entire downstream half of the recirculation zone; in this region, width does not change with distance from the flameholder.

The data of *Figure 5* yield another interesting result: the ratio of wake width to flameholder diameter W/d varies inversely with the square root of the blockage, which is exactly the variation previously found for L/d. Hence the ratio of recirculation-zone length to wake width may be expected to be independent of blockage ratio. This supposition is confirmed experimentally for turbulent flames at high speeds (*Figure 6*): the L/W ratio is independent of flameholder size and blockage ratio and varies only slightly with speed, approaching a constant value at very high speeds. (Measurements for M_2 close to unity are not reliable and should be disregarded.)

The observations show, then, that the L/W ratio is independent of blockage and nearly independent of speed, at least for speeds close to blowoff. Also, the L/W ratio is nearly the same as that found for other bluff-body flameholders[2].

These results have several interesting applications. They show that the wake width multiplied by a constant factor may be used in the blowoff

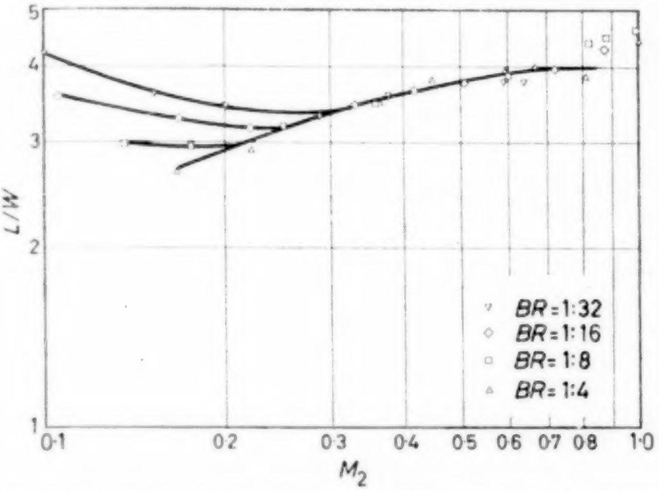

Figure 6. Ratio of recirculation-zone length to width versus Mach number; $\phi = 1{\cdot}0$

formula in place of the recirculation-zone length. (G. MATTON[5] and others have used this method.) The recirculation-zone length may be determined from the wake width by means of the relation $L=(L/W)W$. This procedure is convenient experimentally, since the wake width is more easily measured than the recirculation-zone length. Conceptually, however, it seems appropriate to regard the length L as the primary parameter.

The L/W ratio has another interesting application. It gives an approximate measure of the rate of spreading of the mixing zones. The mixing zones start at the flameholder and spread until, at the downstream end of the recirculation zone, they completely fill the wake. The width of the wake at the end of the recirculation zone is approximately W, and the distance along the flame from flameholder to the end of the recirculation zone is only slightly greater than L. Hence the spreading rate for one mixing zone is approximately $W/2L$, or about one in eight for turbulent flames. The mixing-zone spreading angle is roughly 7°, or about one-half the spreading angle observed in some isothermal mixing zones. (This difference may be partly a matter of definition.) Mixing-zone spreading rate may also be measured directly from some of the schlieren photographs. The measured spreading angle of the thermal mixing zones is about 7°.

Pressure and velocity distributions

Static and total pressures were measured at many points in the duct, and velocities were calculated from the pressures; from these measurements several interesting conclusions can be drawn. In the free stream outside the flame, the total pressure is constant. On the other hand, in the immediate neighbourhood of the flameholder the static pressure varies rapidly in all directions. For example, *Figure 7* shows the variation of velocity and hence of static pressure in the streamwise direction along a line close to the duct wall (blockage ratio 1 : 4). Speed starts to increase about two flameholder widths ahead of the flameholder; it increases rapidly over a distance of four flameholder widths and then remains practically constant for the rest of the travel past the recirculation zone. The velocity-distribution curve is shown for stoichiometric but is the same for all fuel/air ratios, at least to the end of the recirculation zone.

Static pressure and speed also vary in the direction normal to the duct axis. This variation is shown in *Figure 8* for three different stations along the duct. Upstream from the flameholder, the speed is nearly constant across the duct. Opposite the flameholder, however, speed changes rapidly from a moderately low value at the duct wall to a maximum at the flameholder edge. Downstream, at the middle of the recirculation zone, speed is again constant outside the flame and equal to the speed near the flame at the flameholder. In fact, flow speed along the flame surface is nearly constant throughout this entire region. At low blockages, the velocity distribution is not flat opposite the middle of the recirculation zone but peaks at the flame surface. Nevertheless, the velocity along the flame is constant, and the static pressure inside the recirculation zone is practically constant.

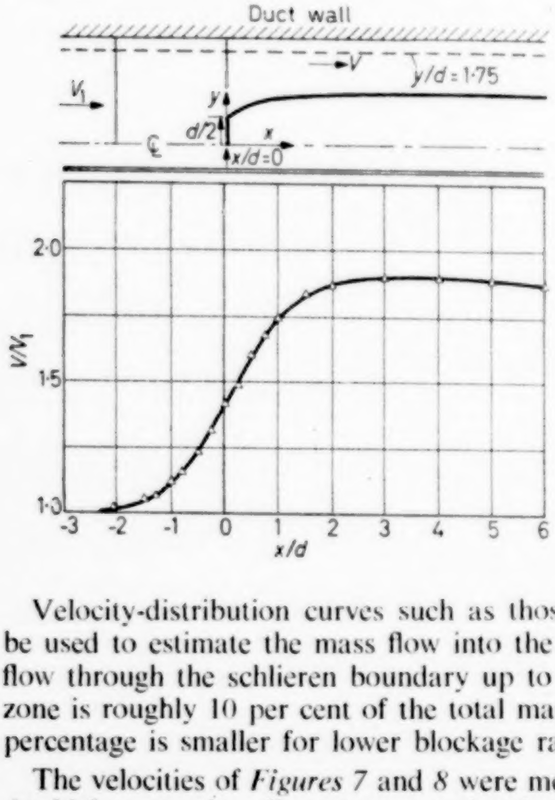

Figure 7. Velocity variation in streamwise direction along a line close to duct wall; BR = 1:4

Velocity-distribution curves such as those of *Figures 7* and *8* can also be used to estimate the mass flow into the wake. For example, the mass flow through the schlieren boundary up to the middle of the recirculation zone is roughly 10 per cent of the total mass flow for 1 : 4 blockage. The percentage is smaller for lower blockage ratios.

The velocities of *Figures 7* and *8* were measured at relatively low speeds. At higher speeds, all pressures and velocities vary with Mach number. For example, *Figure 9* shows the variation with Mach number of the static pressure on the downstream face of the flameholder. Measurements made at different temperatures have clearly demonstrated that the pressure variation does indeed depend on Mach number and not on another variable such as Reynolds number. For low and moderate Mach numbers the pressure coefficient varies as M_1^2, while at very high Mach numbers the variation is faster. Models can be devised that will predict the pressure variation with Mach number, but for reasonable accuracy at very high Mach numbers the models are complex and will not be discussed.

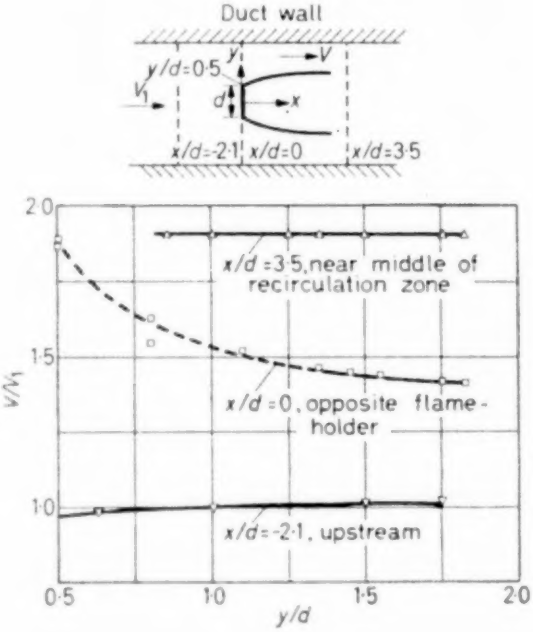

Figure 8. Velocity variation in direction normal to flow; BR = 1:4

The variation of velocity ratio V_2/V_1 with Mach number strongly influences blowoff speed $(V_1)_{BO}$. The effect is especially marked at high blockage ratios and is also influenced by the actual size of the flameholder, since blowoff speed increases with flameholder size and Mach-number influence is more severe for higher speeds. This is an important result that

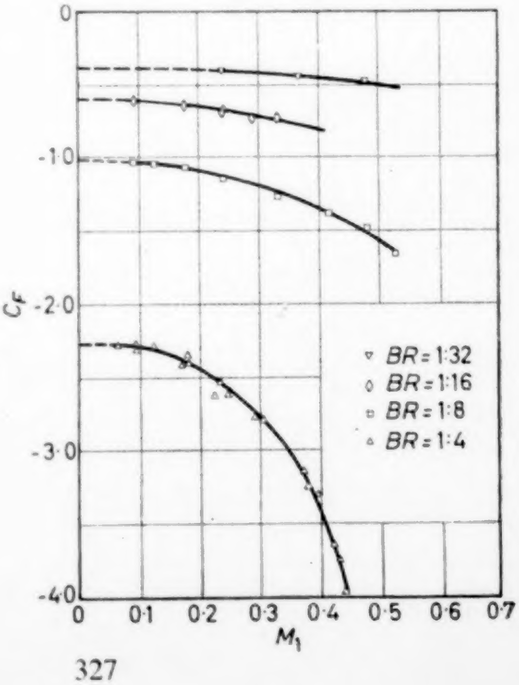

Figure 9. Flameholder static pressure coefficient versus Mach number for several blockage ratios

has been obtained from the velocity measurements. The measurements have revealed several other striking features of the flow about flat-plate flameholders. The recirculation zone lies largely in a region of constant pressure; inside the recirculation zone, the pressure actually increases slightly going upstream along the centre line, and the flow direction is contrary to that of the main stream: gas recirculates. The mixing zones bordering the recirculation zone are regions of almost constant pressure, and flow speed along the flame edge is nearly constant. Hence the mixing may be studied as a constant-pressure process.

COMPARISON OF EXPERIMENT WITH FREE-STREAMLINE THEORY

The fact that the wake of a bluff-body flameholder is a region of almost constant pressure suggests that a free-streamline model may accurately simulate flow conditions about the flameholder. In order to check this supposition, flow conditions about the flat-plate flameholders have been compared with flows computed on the basis of a free-streamline theory (see Appendix). This theory was developed to represent the flow about a bluff body in a channel, and includes both the Betz–Petersohn[6] and Roshko[7] theories as special cases.

The free-streamline theory yields all flow quantities in terms of two parameters, which may be chosen to be the blockage ratio BR and the velocity ratio V_2/V_1. If a relation between V_2/V_1 and blockage ratio can be found from experiment, then all flow quantities can be expressed in terms of the blockage ratio alone. Wake width, wake spreading length (the distance required for the theoretical wake to reach its maximum width), free-streamline shape, and velocity at every point in the duct will be predicted by the theory as functions of the blockage ratio for the particular experimental arrangement, and the predictions may be compared with measured values.

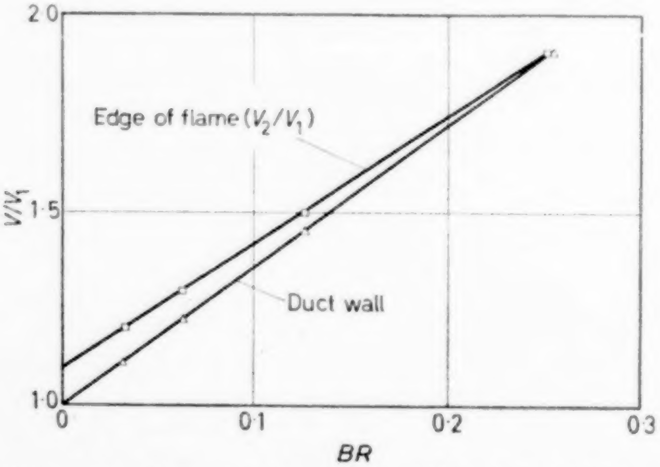

Figure 10. Flow speed opposite middle of recirculation zone versus blockage ratio

The flat-plate flameholder experiments yield the V_2/V_1 versus BR curve shown in *Figure 10*. From this curve, the wake width and wake spreading length were computed and are shown in *Figure 11* for blockage ratios up to 1 : 4. *Figure 11* shows that experimental values of the wake width agree well with the predicted curve. The experimental values are the separations between the mass flow boundaries, and the resulting wake widths are slightly smaller than the widths between schlieren boundaries (*Figure 5*).

The upper curve of *Figure 11* may also be compared with an experimental quantity. The experiments showed that the wake reaches a maximum width at approximately the middle of the recirculation zone, and that downstream from this point the wake width is practically constant. As a result, the recirculation-zone half-length may be compared with the wake spreading length. Downstream from this point the theoretical wake has constant width.

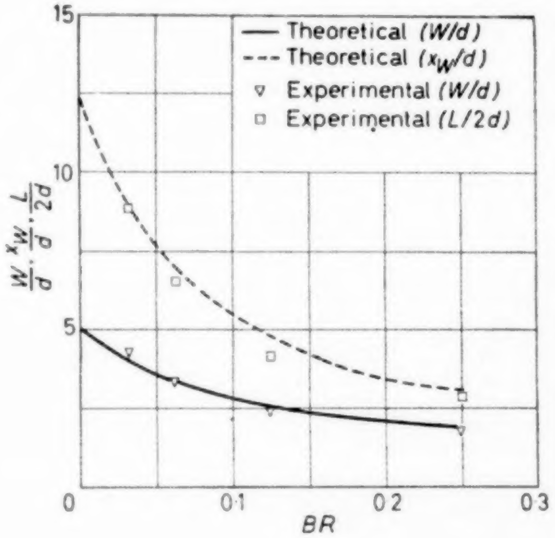

Figure 11. Wake width and recirculation-zone half-length versus blockage ratio

Agreement between recirculation-zone half-lengths and theoretical wake spreading lengths is surprisingly good. In fact, considering the idealizations of the model, the agreement is better than might be expected. The model has sharp boundaries between wake and outer flow, while in reality inner and outer flows are separated by moderately thick shear zones. Downstream from the recirculation zone the model has little resemblance to reality, yet it accurately simulates the flow over the important forward part of the recirculation zone and serves as a useful guide for prediction of the influence of blockage on the flow. For small blockage ratios, this model is appreciably better than the Betz–Petersohn model[6, 8], which assumes that the flow speed far downstream is equal to the free-streamline speed. Experimentally, this assumption is found to be good for blockage ratios larger than 1 : 4 but is not justified for smaller blockages.

For small blockages the free-streamline speed is not equal to the speed far downstream; nor is the speed far downstream equal to the free-stream speed as would be required in Roshko's theory[7] for zero blockage. Proper choice of the velocity ratio leads to better agreement with experiment than is possible with either of the limiting theories (*Figure 12*).

Figure 12 shows that use of the zero blockage curve to predict wake widths is misleading. On the other hand, drag calculations based on the zero blockage model may be fairly good if the proper value of V_2/V_1 is used. The zero blockage theory predicts approximately the same value for the pressure-drag coefficient, $C_D = 0{\cdot}89\,(V_2/V_1)^2$, as does the theory that takes blockage into account. However, the zero blockage theory does not predict the variation of V_2/V_1 with blockage; the present theory provides this information and leads to an expression for C_D for flat plates at low speeds

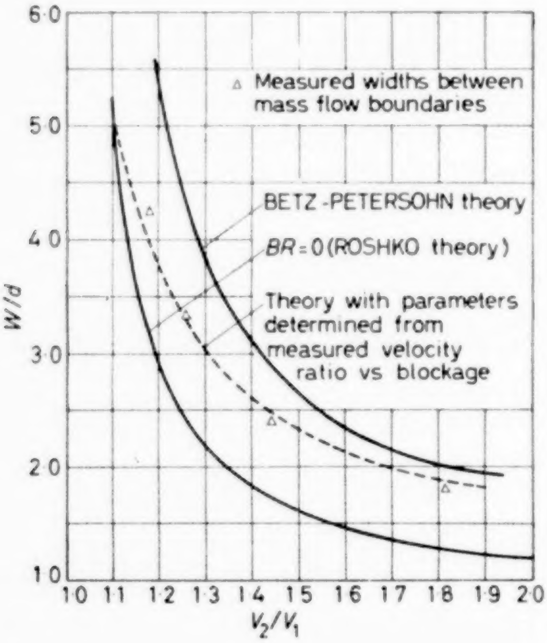

Figure 12. Wake width versus V_2/V_1, experimental and theoretical

$$C_D \simeq 1{\cdot}1 + 6{\cdot}2\,(\text{BR}) + 9{\cdot}1\,(\text{BR})^2 \qquad \ldots .[1]$$

(At high speeds, C_D increases more rapidly with blockage than this equation indicates.) The theory provides an easy calculation of the flameholder pressure drag, an important quantity that is difficult to measure. The calculation may be presumed to be accurate, since theoretical and measured pressures agree well in the neighbourhood of the flameholder.

A final plot (*Figure 13*) further demonstrates the utility of the theory as an aid to experiment. The entire flow field close to the flat plate is shown for blockage 1 : 4. Although the plot is based on theory, it almost perfectly represents the experimentally measured flow field. It is useful in that it gives a consistent picture of the variations of velocity throughout the entire field. The theoretical plot supplies other information that is of value in an experimental study of the flow. For example, it shows proper locations for static-pressure reference taps, proper orientations for static-pressure tubes, velocity gradients to be expected, etc.

Thus the free-streamline theory, although calculated for a perfect fluid, does agree surprisingly well with experimental results for flat-plate flameholders held normal to the stream in a duct. The theory leads to reasonably accurate predictions of flameholder characteristics for varying blockage ratios. If one quantity such as the coefficient of static pressure behind the flameholder is known, then the theory exhibits the entire flow field.

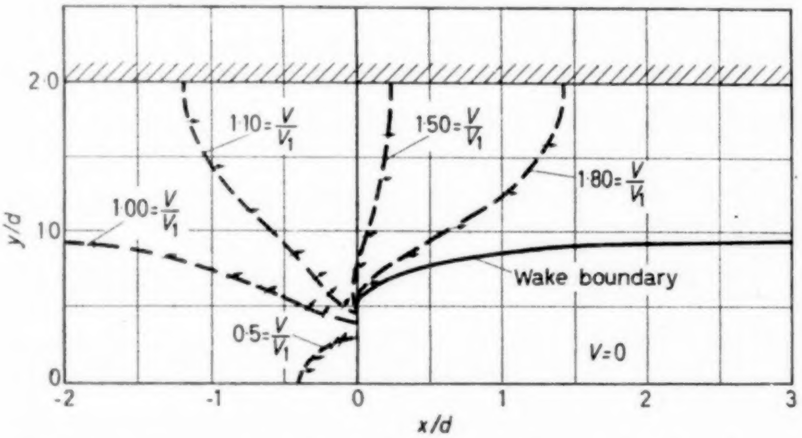

Figure 13. Theoretical velocity distribution about a flat-plate flameholder; $BR = 0{\cdot}2507$

FLAME BLOWOFF

An important aim of the flat-plate-flameholder experiments was to find whether or not the flat plates followed the blowoff rule valid for other bluff-body flameholders. This rule states that if the blowoff parameter, $K_{BO} = (V_2\tau/L)$, is greater than unity, the flame will blow off. The rule further says that the chemical time τ does not depend upon the flameholder; hence a plot of τ versus ϕ (the fuel/air ratio, fraction of stoichiometric) will be a unique curve for all flameholders that satisfy this rule. Inversely, from the τ/ϕ curve the blowoff speed can be obtained for any flameholder for which L and V_2/V_1 are known. *Figure 14* shows the τ/ϕ curve for the flat-plate flameholders. All the flat-plate results fall close to this curve. Further, the curve is identical with that found[2] for other flameholders, such as circular cylinders, in the same duct.

The chemical times found in the 1 in. × 4 in. duct are slightly longer than those observed in a duct twice as wide, possibly because of greater heat transfer to the walls in the narrow duct. Measurements indicate that recirculation-zone temperatures are lower in the narrower duct, thus supporting the view that heat lost to the walls may be important. Also, blowoff speeds and recirculation-zone temperatures are lower with metal duct walls than with glass. The change in blowoff speed may be due to change in chemical time with recirculation-zone temperature. However, if wall heat transfer is important, then the agreement in the τ/ϕ curves for different blockage ratios in the same duct is surprising, since the aspect ratio and the relative importance of end effects change with blockage. The discrepancy in τ between different ducts requires further study.

The blowoff parameter does, then, apply to flat-plate flameholders. Blowoff speeds may be predicted if the behaviour of three variables, V_2,

L and τ, is known close to blowoff. Fortunately, V_2 and L depend in simple fashion on factors such as flameholder size and blockage ratio, and their values may be found from fluid dynamic experiments or from free-streamline theory. In addition, the chemical time τ is known from previous experiments. Hence, for the flat-plate flameholders, the blowoff speed may be written

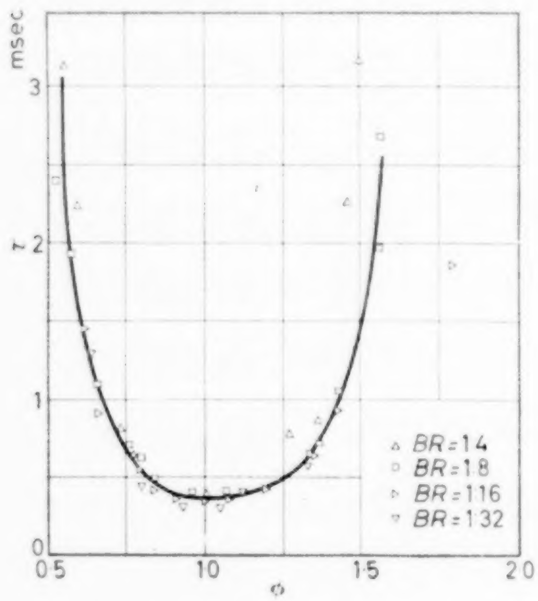

Figure 14. Chemical time τ *versus* mixture ratio ϕ

$$(V_1)_{\mathrm{BO}} = \left(\frac{V_1}{V_2}\right)\left(\frac{L}{d}\right)\left(\frac{d}{h}\right)\left(\frac{h}{\tau}\right) \simeq \left[\frac{(\mathrm{BR})^{1/2}}{C_1 + C_2(\mathrm{BR})}\right]\left(\frac{h}{\tau}\right) \qquad \ldots [2]$$

where h is the duct height, d is the flameholder size, L is the length of the recirculation zone, BR is the blockage ratio d/h, and C_1 and C_2 are constants. The last part of the formula is approximate and applies only for moderate blockage ratios and at low speeds. The formula predicts that maximum blowoff speed will be found for blockage ratio C_1/C_2. This blockage turns out to be roughly 0·35 for flat plates and roughly 0·56 for circular cylinders.

Blockage for peak blowoff speed is even less than the preceding values when the Mach number of the flow past the flame is high. Indeed, the entire blowoff formula is subject to correction when this Mach number is high: blowoff speeds are lower than those predicted by the low-speed formula. The correction increases with blockage ratio, and the peak of the blowoff versus blockage curve is shifted toward low values of the blockage. This shift is apparent in an experimental curve presented in *Figure 15*. Peak blowoff occurs at a blockage less than 1 : 10. However, the top of the curve is flat and blowoff speeds at the higher blockage ratios are only slightly lower than the peak velocity.

Corrections to be applied to the blowoff formula depend upon flameholder shape and size as well as upon blockage ratio. The corrections are larger for flat plates than for other shapes such as wedges or cylinders. The corrections are large for large flameholders whose normal blowoff speed is high and hence, for a given blockage ratio, the corrections are greater in a large duct than in a small one. Further, since lean blowoff speeds are lower, the Mach number has less influence on lean blowoffs than on blowoffs close to stoichiometric.

For several reasons, the very low value of blockage for maximum blowoff shown in *Figure 15* probably does not have great significance for practical applications. Factors such as flow oscillations, turbulence, interference effects, Reynolds number, and mixture inhomogeneities, which were carefully avoided in these experiments, may have less influence upon blowoff speeds from large flameholders than upon blowoffs from small flameholders operating at low blockage ratios.

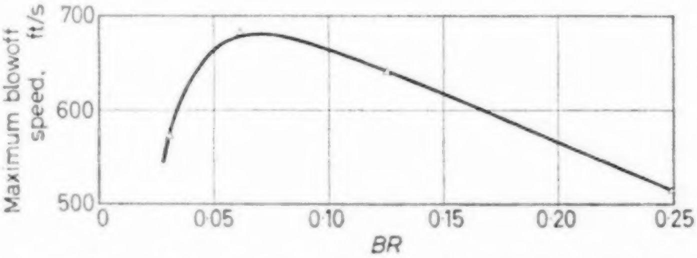

Figure 15. Maximum blowoff speeds for flat-plate flameholders in 1 in.×4 in. duct

CONCLUSIONS

Previous work[1] had shown that the problem of bluff-body flameholding can be divided into two parts: the chemistry of the combustion reaction and the fluid dynamics of the flow. Even more convincingly than past work, the experiments reported here demonstrated that the two parts of the problem may be studied separately. The flat-plate experiments were particularly significant in showing that the flow patterns about bluff-body flameholders are nearly independent of the combustion chemistry and depend only on fluid dynamic variables. In fact, the flow patterns can be predicted by a purely fluid dynamic theory developed in this paper as a guide for the experiments.

Flame blowoff depends on the flow patterns and hence depends directly on fluid dynamic parameters. An interesting example of an essentially fluid dynamic variable that influences blowoff is furnished by the blockage. The free-streamline theory predicts the principal effects of blockage on flame stabilization, thus emphasizing the essentially fluid dynamic character of one part of the flameholding problem. Theory and experiment both show that both the flow speed V_2 past the flame and the recirculation-zone length L depend upon flameholder blockage. Hence the value of the blowoff parameter $(\tau V_2/L)$ depends directly on the blockage. If the explicit variations of speed and recirculation-zone length are taken into account, the blowoff speed may be written as a function of the blockage as follows

$$(V_1)_{\mathrm{BO}} \simeq \left[\frac{(\mathrm{BR})^{1/2}}{C_1 + C_2(\mathrm{BR})}\right]\left(\frac{h}{\tau}\right) \qquad \ldots . [2]$$

where V_1 is the upstream speed, BR is the blockage ratio, h is the duct height, τ is the chemical-time parameter, and C_1 and C_2 are constants. The formula predicts that maximum blowoff speed will occur at $\mathrm{BR} \simeq C_1/C_2$; for flat-plate flameholders this blockage turns out to be 0·35, a surprisingly low value.

When the Mach number of the flow past the flame is very high, compressibility affects the flow patterns and it is necessary to apply a correction to the preceding blowoff formula. Fortunately, the correction may be made by straightforward application of fluid dynamic principles; the validity of this procedure is a further demonstration of the essentially fluid dynamic character of one portion of the blowoff problem.

The experiments and the analysis showed the manner in which various fluid dynamic parameters influence flame blowoff as well as demonstrating the fact that the influence is nearly independent of chemical parameters. On the other hand, experiments demonstrated that the combustion chemistry is also an important factor governing blowoff and that the chemistry is not influenced by gross fluid dynamic variables such as flow Reynolds number, Mach number, or blockage. An impressive example of the independence of the chemistry is afforded by *Figure 14*, in which the chemical-time parameter is plotted versus fuel/air ratio. The chemical time at a given mixture strength is identical for different-sized flameholders and is indeed the same as the chemical time found for other types of flameholders[1].

The experiments with flat-plate flameholders and the associated fluid dynamic theory furnished convincing proof that the complex flame-stabilization problem may be split into two simple and nearly independent parts, one fluid dynamic and the other chemical.

NOMENCLATURE

BR = blockage ratio = d/h
C_D = pressure drag coefficient
C_P = (flameholder static pressure minus upstream static pressure)/upstream dynamic pressure
d = flameholder width or diameter (in y direction)
h = duct height (in y direction)
K_{BO} = $V_2\tau/L$ = blowoff parameter, reciprocal of Damkohler's parameter I
L = recirculation-zone length
M = Mach number
M_1 = Mach number far upstream
M_2 = Mach number at edge of flame
Q = source strength
R_e = Reynolds number, based on flameholder width and flow speed far upstream
$\bar{v}$ = conjugate of complex velocity
V = flow speed
V_1 = flow speed far upstream
V_2 = flow speed at edge of flame
V_3 = flow speed far downstream
W = wake width opposite middle of recirculation zone, $x = \frac{1}{2}L$

x = axial coordinate measured from front face of flameholder
x_W = distance from flameholder to beginning of constant wake width (theoretical)
y = transverse coordinate measured from duct centre line
$z = x + iy$
θ = angular coordinate in hodograph plane
τ = chemical-time parameter
φ = fuel/air ratio, fraction of stoichiometric
Φ = complex potential of flow in z plane

Subscripts:

1 = conditions far upstream
2 = conditions at outer edge of flame
3 = conditions far downstream
BO = blowoff
F = flameholder
W = initial point of constant width wake

APPENDIX

FREE-STREAMLINE FLOW ABOUT FLAT PLATES ORIENTED NORMAL TO THE FLOW IN A CHANNEL

A new free-streamline theory for the flow about a flat plate in a duct (*Figure 16*) has been developed. This theory does not require the speed V_3 far downstream to equal the speed V_2 along the free streamline, and thus is more general than the theory of A. Betz and E. Petersohn[6].

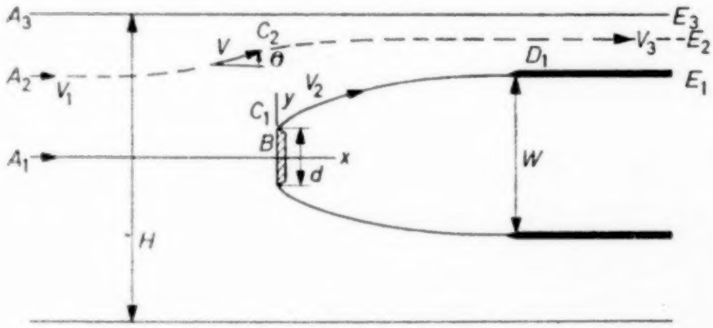

Figure 16. Free-streamline flow pattern

The flow may be obtained by considering the hodograph, *Figure 17*. The hodograph is drawn for the conjugate v of the complex velocity. That is,

$$v = V \exp(-i\theta) \qquad \ldots.[3]$$

where V is the magnitude of the velocity at any point in the physical plane and the angle θ specifies its direction. The complex potential Φ of the flow in the physical or z plane is easily found from a distribution of sources and sinks in the hodograph plane (*Figure 18*).

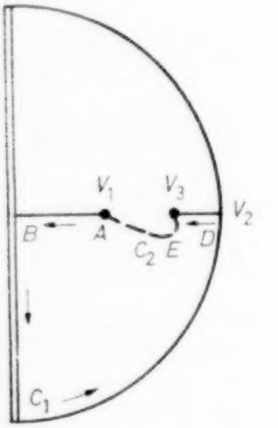

Figure 17. Hodograph for free-streamline pattern

$$\Phi = \left(\frac{h}{2\pi}\right)\left(\frac{V_1}{V_2}\right)\ln\left[\frac{\left(\frac{v^2}{V_2^2} - \frac{V_1^2}{V_2^2}\right)\left(\frac{v^2}{V_2^2} - \frac{V_2^2}{V_1^2}\right)}{\left(\frac{v^2}{V_2^2} - \frac{V_3^2}{V_2^2}\right)\left(\frac{v^2}{V_2^2} - \frac{V_2^2}{V_3^2}\right)}\right] \qquad \ldots.[4]$$

Then, since

$$v = \mathrm{d}\Phi/\mathrm{d}z \qquad \ldots.[5]$$

the coordinate $z(=x+iy)$ of any point in the physical plane is given in terms of (v/V_2), (V_1/V_2), and (V_3/V_2) by

$$z = \int \frac{1}{v}\frac{\mathrm{d}\Phi}{\mathrm{d}v}\,\mathrm{d}v \qquad \ldots.[6]$$

The explicit formula for z is lengthy and will be omitted. A few special cases are:

Blockage ratio:

$$\mathrm{BR} = \frac{d}{h} = \left(1 - \frac{V_1}{V_3}\right) - \frac{2}{\pi}\left[\left(1 - \frac{V_1^2}{V_2^2}\right)\tan^{-1}\left(\frac{V_1}{V_2}\right) + \left(\frac{V_1V_3}{V_2^2} - \frac{V_1}{V_3}\right)\tan^{-1}\left(\frac{V_3}{V_2}\right)\right] \qquad \ldots.[7]$$

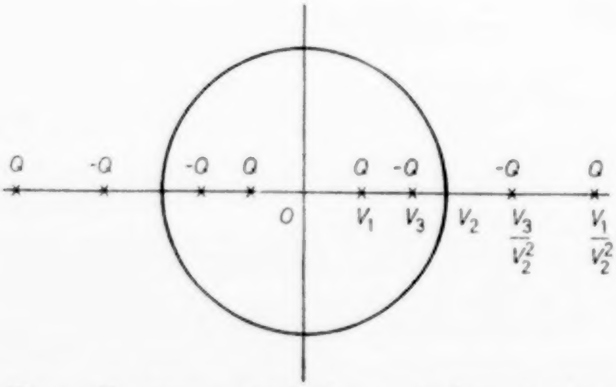

Figure 18. Source distribution in hodograph plane

Wake spreading length:

$$\frac{l_w}{h} = \frac{1}{\pi}\left(\frac{V_1}{V_2}\right)\left[\left(\frac{V_1}{V_2}+\frac{V_2}{V_1}\right)\tan h^{-1}\left(\frac{V_2}{V_1}\right)-\left(\frac{V_3}{V_2}+\frac{V_2}{V_3}\right)\tan h^{-1}\left(\frac{V_3}{V_2}\right)\right] \quad ..[8]$$

Wake width:

$$\frac{W}{h} = \left(1-\frac{V_1}{V_3}\right) \quad ....[9]$$

Applying formula 7, the velocity ratio V_2/V_1 may be plotted versus blockage ratio with V_3/V_2 as parameter. For comparison with experimental reality the appropriate value of V_3/V_2 must be chosen for each blockage ratio. Then all other quantities may be expressed in terms of the blockage ratio alone. (It is, of course, unnecessary to start with the blockage ratio. In some cases the wake width or the free-streamline shape may prove to be convenient starting points.)

This free-streamline theory includes both the zero blockage[7] and the $V_3 = V_2$ theories[6, 8] as special cases but involves an additional parameter. The theory has been developed for flat plates only but can easily be extended to other bluff bodies, such as wedges, by a suitable arrangement of sources and sinks in the hodograph plane.

This paper presents the results of one phase of research carried out at the Jet Propulsion Laboratory, California Institute of Technology under Contract No. DA-04-495-Ord 18, sponsored by the Department of the Army, Ordnance Corps.

Jet Propulsion Laboratory,
California Institute of Technology

(*Received September 1958*)

REFERENCES

[1] ZUKOSKI, E. E. and MARBLE, F. E. Paper in *Proceedings of the Gas Dynamics Symposium on Thermochemistry* (held at Northwestern University, Evanston, Illinois, 22–24 August 1955), pp 205–210. Northwestern University Press

[2] FOSTER, J. R. 'The effects of combustion chamber blockage on bluff body flame stabilization.' *Thesis* in Aeronautical Engineering, California Institute of Technology, June 1956

[3] ZUKOSKI, E. E. *Sixth Symposium (International) on Combustion*, pp 942–943. Reinhold: New York, 1956

[4] ZUKOSKI, E. E. and MARBLE, F. E. Paper No. 14 in AGARDograph No. 9, *Combustion Researches and Reviews 1955*. Butterworths: London, 1955

[5] MATTON, G. *Rech. Aéro.* 1957, **57**, 11

[6] BETZ, A. and PETERSOHN, E. *Tech. Note Nat. Adv. Comm. Aero., Wash., No. 667* (1932)

[7] ROSHKO, A. *Tech. Note Nat. Adv. Comm. Aero., Wash., No. 3168* (1954)

[8] CORNELL, W. G. *Trans. Amer. Soc. mech. Engrs*, 1956, **78**, 573

Effect of Combustor Length on Afterburner Combustion

James W. Useller

The effect of combustion-chamber length on afterburner combustion performance has been experimentally determined with two full-scale turbojet-engine afterburners. Combuster lengths from 2·5 to 6·5 ft have been investigated. The influence of combustor-inlet velocity, equivalence ratio, and pressure level is discussed, as well as a consideration of the structural-cooling requirements.

The time available to the combustion process in a turbojet-engine afterburner has a significant influence on the completeness of the reaction that is attainable. Because the afterburner diameter is usually determined by the space limitation of the airframe installation, the available combustion time is primarily controlled by the combustion-chamber inlet velocity and the length of the combustion zone.

The time required for ideal combustion is a function of: (*1*) the afterburner approach conditions of temperature and pressure, because these factors affect the combustion reaction rate; (*2*) the fuel employed, because the flame velocity depends on the chemical composition of the combustible mixture; and (*3*) the turbulence introduced into the gas stream by the flameholder and by the combustion process itself.

To date, there has been a paucity of experimental data, especially with large-scale combustors, concerning the effect of combustion-chamber length on the combustion process. The data presented herein are the results of several full-scale turbojet-engine afterburner investigations that have been conducted by the NASA at the Lewis Research Center in Cleveland.

The afterburners were designed to operate at a high performance level and were constructed in such a manner that the combustion-chamber length could be varied from about 2·5 to 6·5 ft in progressive increments. The combustion efficiency has been used as a criterion of the afterburner performance.

The effects of inlet velocity (425 to 600 ft/sec), equivalence ratio (0·7 and 1·0), and pressure level (1 600 and 1 050 lb/ft^2) have been investigated with the various combustor lengths. The effect of combustion length on the stability of combustion as characterized by the lean combustion-blowout limit has been determined. A consideration of how the combustor length affects the afterburner structural-cooling requirements because of flame spreading has been included because this may require a compromise in a practical application.

APPARATUS

The full-scale afterburners used to obtain the data presented herein were similar to that shown schematically in *Figure 1*(a). The primary components included a conical annular diffuser, a two-ring V-gutter flameholder with a fixed-area exhaust nozzle, and an external-manifold fuel system. The fuel was introduced through a series of radial spray bars that were equally spaced around the circumference of the afterburner. The diameter and spacing of the orifices in the fuel spray bars were arranged to provide a uniform fuel-air profile across the afterburner diameter; see below.

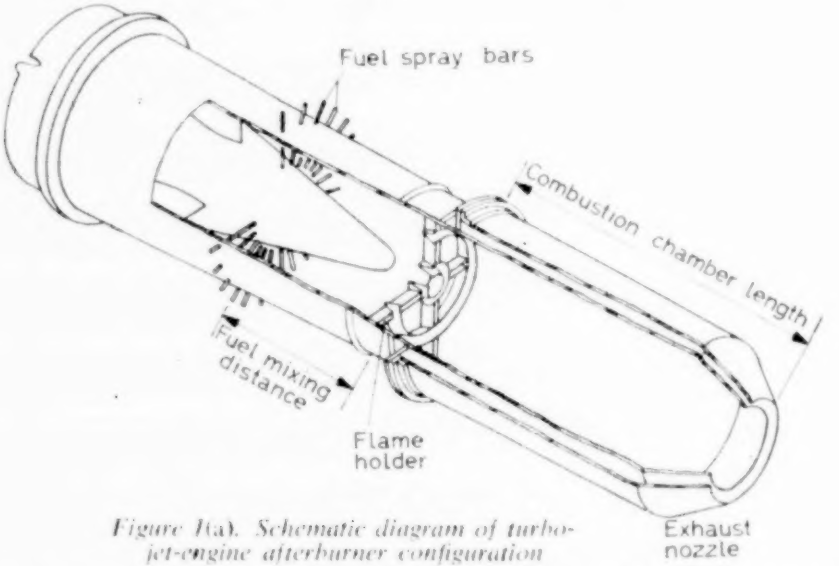
Fuel spray bars
Combustion chamber length
Fuel mixing distance
Flame holder
Exhaust nozzle

Figure 1(a). Schematic diagram of turbojet-engine afterburner configuration

The detailed dimensions of the two afterburner configurations are shown in *Figure 1*(b). The combustion-chamber length (distance *h*), defined as the distance from the flameholder to the exhaust-nozzle exit, was varied in progressive increments by inserting different lengths of the cylindrical section between the flameholder and the exhaust nozzle.

The combustion-chamber lengths investigated were as follows:

Configuration I		Configuration II	
Nominal length, ft	Actual length, in.	Nominal length, ft	Actual length, in.
6·5	78·6	5·5	66·0
5·0	60·6	4·5	54·0
4·0	48·6	3·5	42·0
3·0	36·6	2·5	30·0

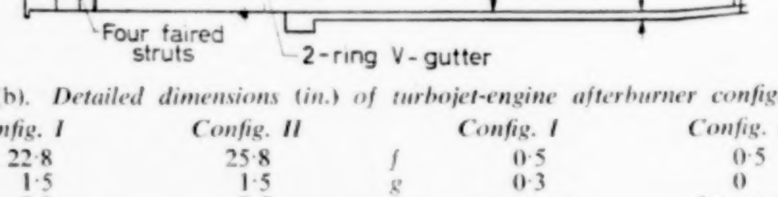
j
i
h
Spray bar location
Cooling air chamber
Cooling air shroud
g
b
e
c
d
a
f
Four faired struts
2-ring V-gutter

Figure 1(b). Detailed dimensions (in.) of turbojet-engine afterburner configuration

	Config. I	*Config. II*		*Config. I*	*Config. II*
a	22·8	25·8	*f*	0·5	0·5
b	1·5	1·5	*g*	0·3	0
c	9·0	9·5	*h*	*(see text)*	*(see text)*
d	15·8	18·5	*i*	25·0	31·5
e	13·0	—	*j*	35·7	63·8

The afterburner instrumentation included a survey of 48 thermocouples, 20 total-pressure and 4 static-pressure probes at the inlet, and 13 total-pressure and 8 static-pressure probes at the exhaust nozzle. The total mass flow was determined from the airflow and fuel flow entering the afterburner. The afterburner fuel flow was measured by a calibrated rotameter.

As a part of the structural-cooling phase of the study, four skin thermocouples were spot-welded 90° apart on the afterburner wall at five longitudinal stations along the afterburner. The afterburner structure was air-cooled by means of a separate liner that extended from the flameholder to the exhaust-nozzle exit. Afterburner cooling air was supplied at room temperature from an outside source.

When the afterburner was designed to achieve maximum performance with stoichiometric operation, extremely good mixing of the fuel and air entering the combustion zone was required. To establish a uniform fuel–air distribution, the mass-flow profile entering the combustion zone was determined by a survey of temperature and pressure profiles at the fuel-injection plane. A typical mass-flow profile is shown in *Figure 2*. The fuel spray bars were then designed to provide fuel-flow rates matched to the airflow pattern for stoichiometric operation. The resultant fuel–air-ratio pattern is shown in *Figure 3*. The fuel–air ratio was surveyed by means of an NASA combustible-gas-mixture analyser. The fuel–air ratio was decreased slightly near the walls to reduce the maximum wall temperature and thus preclude serious structural-overheating problems.

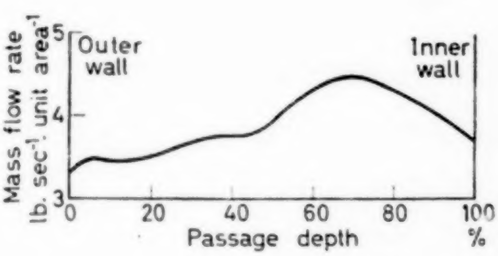

Figure 2. Typical mass flow distribution in plane of fuel injection in afterburner

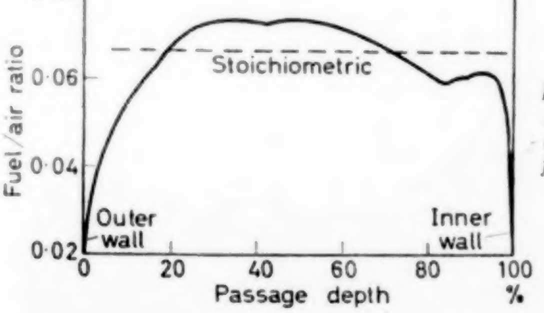

Figure 3. Fuel–air distribution across afterburner annular diffuser. Designed for stoichiometric mixture operation

Afterburner ignition was accomplished by providing a short burst of additional fuel through the turbine that produced a local 'hotstreak' of flame sufficient for ignition. The fuel used was MIL–F–5624a grade of JP–4 fuel.

DISCUSSION

The full-scale afterburner performance obtained with four combustion-chamber lengths from 2·5 to 6·5 ft with configuration II is shown in *Figure 4*. Each combustor length was operated at four inlet velocities from 425 to 600 ft/sec. As the inlet velocity was increased, the combustion process became less efficient. The combustion efficiency improved significantly as the combustion-chamber length was increased to 5·5 ft for any particular inlet velocity, but the deleterious effect of increasing the inlet velocity on the combustion performance also increased as the longer combustors were investigated. For example, increasing the inlet velocity from 425 to 600 ft/sec with the 2·5 ft combustor produced a 16 per cent decrease in combustion efficiency, while a similar increase in the inlet velocity with the 5·5 ft combustor caused a 22·5 per cent decrease in combustion efficiency. The combustion efficiency data have an estimated random deviation of ±2 to 5 per cent.

The afterburner inlet velocity was varied by changing the velocity in the diffuser upstream of the plane of fuel introduction. Thus the velocity of the gas in the fuel mixing zone between the fuel spray bars and the flameholder was also varied as the afterburner inlet velocity was changed. The degree of fuel vaporization and the droplet characteristics of the atomized fuel could not be held constant as the inlet velocity was varied. Poor fuel vaporization due to the decreased time available and less desirable atomization due to the decreased penetration of the fuel into the airstream with an increase in inlet velocity would tend to decrease the combustion efficiency. As the inlet velocity is increased, the turbulence issuing from the flameholder would also increase and result in better fuel–air mixing. From the data of *Figure 4*, the improvements at the flameholder apparently are not enough to counter the deleterious effects of the increased velocity in the fuel mixing zone.

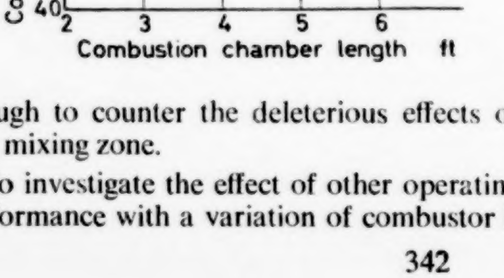

Figure 4. Influence of afterburner inlet velocity on combustion efficiency for several combustion-chamber lengths. Pressure level, 1 270 lb/ft^2; inlet temperature, 1 660° R; equivalence ratio, 0·82; configuration II

To investigate the effect of other operating conditions on the combustion performance with a variation of combustor length, the remaining data were collected by using afterburner configuration I in which the combustor inlet velocity was maintained constant at 550 ft/sec. Thus, the influence of velocity in the fuel mixing zone and changes in the level of turbulence were held relatively constant.

Increasing the combustion-chamber length produced correspondingly better combustion performance until a length of between 5 and 5·5 ft was reached (*Figure 5*). The afterburner was operated with an inlet temperature of 1 460 R and at a pressure level of 1 600 lb/ft². A peak combustion efficiency of 82 per cent was attained with an equivalence ratio of 1·0, while operation with an equivalence ratio of 0·7 approached a maximum efficiency of only 75 per cent with the longest combustor length investigated. Because the fuel–air distribution was designed for stoichiometric operation, off-design operation at an equivalence ratio of 0·7 provided a poor distribution of the fuel and air that resulted in a lower efficiency of combustion.

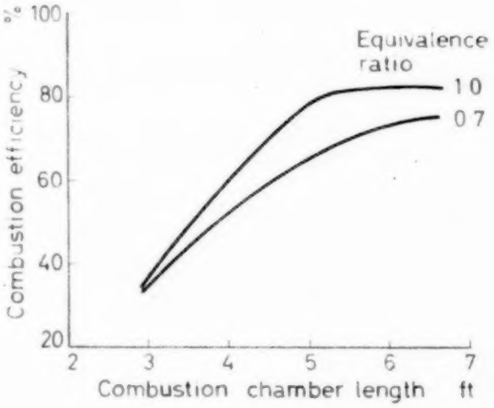

Figure 5. Influence of equivalence ratio on afterburner combustion efficiency. Pressure level, 1 600 lb/ft²; equivalence ratio, 1·0; inlet temperature, 1 460° R; configuration I

Reducing the pressure level in the afterburner from 1 600 to 1 060 lb/ft² during operation with a stoichiometric mixture reduced the level of efficiency obtained; this is shown in *Figure 6*. The maximum efficiency was reduced approximately 8 per cent with a pressure reduction of approximately 34 per cent. In spite of this reduction in the maximum efficiency attainable, the

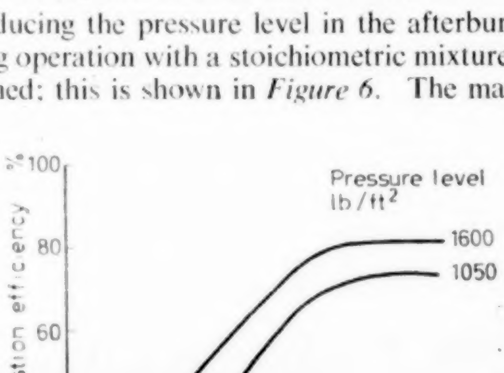

Figure 6. Variation of combustion efficiency with combustion-chamber length at pressure levels of 1 600 and 1 050 lb/ft²; equivalence ratio, 1·0; inlet temperature, 1 460° R; configuration I

efficiency curves are quite similar. Increasing the combustor length beyond 5 ft produced negligible improvement in the efficiency at either pressure level.

An indication of the stability of an afterburner is the lean combustion-blowout limit. If the lean combustion limit is primarily a function of the conditions in the plane of the flameholder, it would be expected that varying the combustion-chamber length would have no effect on the lean limit of operation. However, the results of this investigation indicate that the lean limit is somewhat dependent on combustor length. *Figure 7* shows the minimum equivalence ratio at which combustion could be sustained with each combustion-chamber length. Combustion was not possible in the shaded portion of the figure. The data points indicate equivalence ratios at which combustion blowout was experienced.

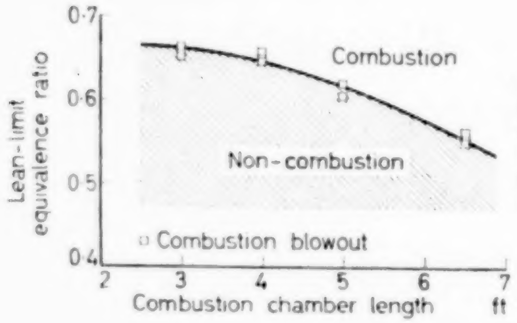

Figure 7. Effect of combustion-chamber length on lean combustion limit of afterburner designed for stoichiometric operation. Pressure level, 1 600 lb/ft²; configuration I

The 6·5 ft combustor was operable at equivalence ratios down to 0·56, while the 3 ft combustor was limited to lean operation at 0·66. Although this decrease in the lean-limit equivalence ratio is small, it could be quite significant in the design of an afterburner intended for sustained operation at relatively low combustion temperatures. An example of this would be the use of an afterburner in a supersonic airplane, where maximum thrust (hence, high equivalence ratios) would be required of the afterburner for takeoff, acceleration and climb, and where reduced thrust (lean operation in the afterburner) would be desired for economy reasons during extended high-speed cruise.

Although the structural-cooling requirements of an afterburner are only remotely related to the combustion performance, in a particular application serious consideration must be given to how lengthening the combustor will affect the formation of regions of structural overheating. The average wall temperature is important from a consideration of the installation, but local regions of high temperature will determine structural failure due to overheating. The maximum individual afterburner wall temperatures measured during this investigation are shown in *Figure 8* for cooling airflows from 0 to 29 per cent of the afterburner gas flow. A maximum local temperature of 2 000°R was used as the limit of safe operation.

Combustion-chamber lengths of less than 4 ft do not require auxiliary cooling air to maintain temperatures below 1 550°R. This is a result of the provision in this particular fuel-system design for lean fuel–air ratios adjacent to the afterburner walls. Combustion chambers greater than 4 ft in length require sizable quantities of cooling air to maintain safe maximum structure temperatures. For example, a 5 ft-long combustor would require a cooling airflow of 10 per cent of the afterburner gas flow for a maximum structure temperature of 1 750 R, and proportionately larger quantities of cooling airflow to maintain lower structure temperatures. Further increases in combustion-chamber length would require even greater quantities of cooling airflow to maintain a given structure temperature.

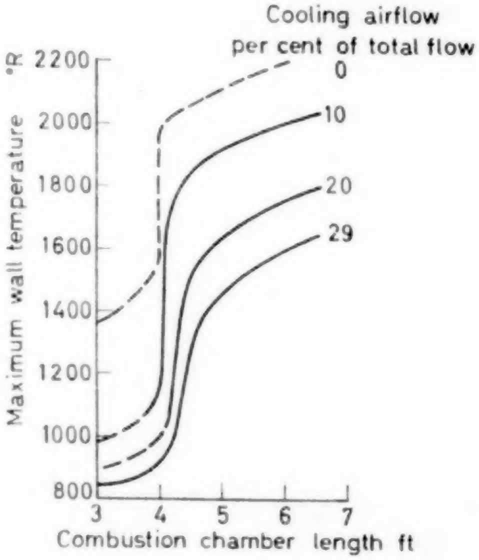

Figure 8. Afterburner cooling requirements with various combustion-chamber lengths. Equivalence ratio, 1·0; pressure level 1 600 lb/ft²; inlet temperature, 1 460° R; configuration I

ATTEMPT AT GENERALIZATION OF DATA

The goal of those engaged in the application of combustion research to full-scale models has been to derive analytical equations for flameholder and combustion-chamber design that would involve simple, measurable quantities. These quantities would probably be functions of the fuel burned, the fuel–air ratio, the velocity across the combustor, the turbulent flame velocity, and the heat loading capacity per unit volume. J. JENNISSEN* has derived such a relation based on the concept of flame velocity. From this theory, it should be possible to generalize afterburner combustion performance as a function of residence time, where this term is defined as the combustor length divided by the mean velocity through the afterburner.

Figure 9 shows the same data as *Figure 4* for configuration II, where four combustor lengths were operated at four inlet velocities each, plotted as a function of residence time. Data for similar combustor lengths have been connected with dashed curves. There is a distinct separation of these data into a family of curves that is a function of inlet velocity. These data do not refute the predicted relation, but rather point out that other factors are involved in applying the theory to full-scale afterburners. It is believed that the separation with inlet velocity results from the influence of the changes in the afterburner approach velocity on the fuel vaporization and

---

*JENNISSEN, J. 'A theory of space requirements for combustion behind grids in a close duct.' *Fifth Symposium (International) on Combustion.* Reinbold: New York, 1955.

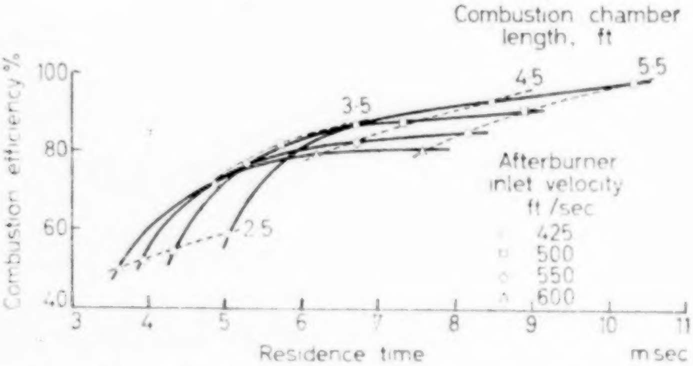

Figure 9. Full-scale afterburner combustion performance. Inlet temperature, 1 660 R; pressure level, 1 270 lb/ft²; equivalence ratio, 0·82; configuration II

atomization, as well as the change in the degree of turbulence created by the flameholder as the velocity is increased. Unfortunately, it was not possible to hold these factors constant during our investigations. It is suggested that the Jennissen theory shows promise for the afterburner designer, but that additional functions are required to generalize the performance data in a practical application. This area certainly deserves more study and experimentation.

CONCLUDING REMARKS

The effect of combustion-chamber length on combustion efficiency, lean-operational limits, and cooling requirements was investigated on several afterburners designed for high performance operation. The combustion performance increased appreciably with increasing combustor length up to between 5 and 5·5 ft. Further increases in length produced only small performance increases.

Increasing the inlet velocity and decreasing the pressure level each lowered the combustion performance of the afterburner. Off-design operation, lower equivalence ratio than design, produced a decrease in combustion performance and indicated that a combustor longer than that required for design operation would be necessary to achieve maximum efficiency. Although lengthening the combustion chamber had only a minor effect on the afterburner stability as characterized by the lean limit of operation, it was possible to operate the longer combustors to lower lean limits that might prove advantageous for certain applications.

Lengthening the afterburner combustor beyond 4 ft necessitated substantial increases in the quantity of cooling air required for safe structural operation. A compromise between the cooling requirements and the combustion performance must be made when an afterburner combustion-chamber length is chosen for a particular application.

The author gratefully acknowledges the contribution of Mr Charles R. King who was responsible for the data shown for configuration II.

Lewis Research Center,
National Aeronautics and Space Administration,
Cleveland, Ohio

(Received May 1958)

Flame Propagation through Kerosine Foams

A. BARTKOWIAK, S. LAMBIRIS and M. G. ZABETAKIS

Under certain conditions, liquid fuels such as kerosine may form foams flammable at temperatures below the flash point of the fuel. Thomas found that at one atmosphere pressure kerosine foam would not burn in air but would burn in oxygen-enriched air. Since it appeared possible to produce flammable foams with certain combustible liquids in air, an investigation was undertaken to determine the conditions under which these foams would be formed. It was found that flammable foams could be produced quite readily with kerosine and other light oils in air and in nitrogen- and carbon dioxide-enriched air. Because these foams constitute a potential gas explosion hazard, a series of experiments was conducted in various enclosures to determine the maximum pressures developed when these foams were ignited. Tests were conducted in containers ranging from ca. *$0{\cdot}1$ to 10^3 ft^3. The maximum pressure was found to be a function of the amount of foam, free space above the liquid surface and number of points of ignition. Maximum pressures of 35 lb/in^2 gauge were encountered in small containers. The rates of pressure rise were considerably smaller than those encountered with explosions through combustible vapour-air mixtures. Photographs of the flame propagating through kerosine foam in air show that the foam collapses and forms droplets as the flame approaches. The vapour around these droplets is then ignited and in turn acts as an ignition source to continue the propagation.*

AT temperatures below the flash point of a fuel, flammable vapour–air mixtures are not formed at one atmosphere pressure, although they may be formed at reduced pressures. However, fuel mists and sprays are known to be flammable in air at atmospheric pressure at temperatures below the flash points of the fuels[1–3]. In addition, Thomas found that kerosine foam is flammable under certain conditions at such temperatures[4]. He found that this foam propagated flame in oxygen-enriched air at one atmosphere pressure. However, since foam is produced in many of the operations involved in the transportation, storage and use of kerosine while in contact with air, the present investigation was undertaken to determine the conditions under which this foam presents an explosion hazard[5].

EXPERIMENTAL DETAILS AND DISCUSSION

To simulate various operations involved in transporting, storage and use of kerosine, foams were produced by stirring, mechanical agitation, pumping and bubbling air through this liquid*. Test vessels ranging in volume from 2 quarts to $10^3 ft^3$ were used in this work.

Preliminary experiments were conducted in an open glass container, 12 in. high and 6 in. by 15 in. in cross section. Foam layers two to three

---

*The kerosine used in this study had an initial boiling point of 342°F and end point of 485°F; an API gravity of $44{\cdot}2$, a flash point (*ASTM D56–52*) of 120°F; and a viscosity of $1{\cdot}44$cS at 100°F inches thick were readily produced by stirring kerosine in this container. The foam was ignited readily by a spark discharge, and the resultant flame propagated throughout the foam. *Figure 1* shows the initiation and propagation of flame through such a foam; the propagation of flame appears to involve combustion of the mist produced by the collapse of foam at the flame front.

Since the above experiments indicated that flame propagated with ease through kerosine foam in air at room temperature and one atmosphere pressure, additional experiments were conducted in vitiated air in a 12 in. cube. The foam was formed in these atmospheres by stirring the kerosine through a rotary seal in the top face of the steel cube. These experiments were conducted primarily to determine the minimum oxygen requirement for flame propagation through this foam. The limiting condition for flame propagation was attained with an atmosphere containing 15 vol. per cent carbon dioxide and 85 vol. per cent air (18 vol. per cent oxygen). The rate of flame propagation through the foam decreased as carbon dioxide was added to the atmosphere in which the foam was formed. Flammability experiments conducted with kerosine vapour–air–carbon dioxide mixtures at 150° C and one atmosphere pressure gave a corresponding limiting condition for flame propagation with 38 vol. per cent carbon dioxide and 62 vol. per cent air (13 vol. per cent oxygen).

The pressure rise that resulted from the combustion of kerosine foam in air was determined in closed containers of various sizes. Preliminary experiments were conducted in a 2-quart, 6-in.-diameter, cylindrical container equipped with a lid which released at a pressure of about 20 lb/in^2 gauge. A foam was produced by agitation of one quart of kerosine which was placed in this container. Upon ignition of this foam, the pressure in the closed container rose to *ca.* 20 lb/in^2 gauge, at which time the lid flew off. *Figure 2* shows four successive frames from a motion-picture sequence (128 frames per second) of photographs taken during one of these experiments. The maximum pressure and rate of pressure rise resulting from the ignition of foam were found to be much less than those for flammable vapour–air mixtures. For example, a maximum pressure of 20 lb/in^2 gauge was obtained in 1 sec after ignition of foam formed on the surface of 1 gal of kerosine contained in a closed, 1·0 ft^3, cubical test bomb. A maximum pressure of 120 lb/in^2 gauge was obtained in 0·1 sec upon ignition of a near-stoichiometric gasoline–vapour–air mixture in the same bomb.

Preliminary experiments indicated that the maximum pressure produced in a closed vessel upon ignition of a layer of foam depended on the amount of foam burnt and on the free air space above the liquid. Accordingly, tests were conducted in 2- and 4-in.-diameter cylindrical glass pipes 36 and 42 in. long, respectively. These were closed at both ends and equipped with a maximum-pressure-indicating gauge and a spark gap that could be positioned vertically along each tube axis. For any one series of tests with these pipes they were first filled with kerosine to a predetermined level, and the spark gap was positioned approximately $\frac{1}{2}$ to $\frac{3}{4}$ in. above the liquid surface. The desired thickness of foam was next produced by rocking each pipe. They were then placed in vertical position, and the foam was ignited

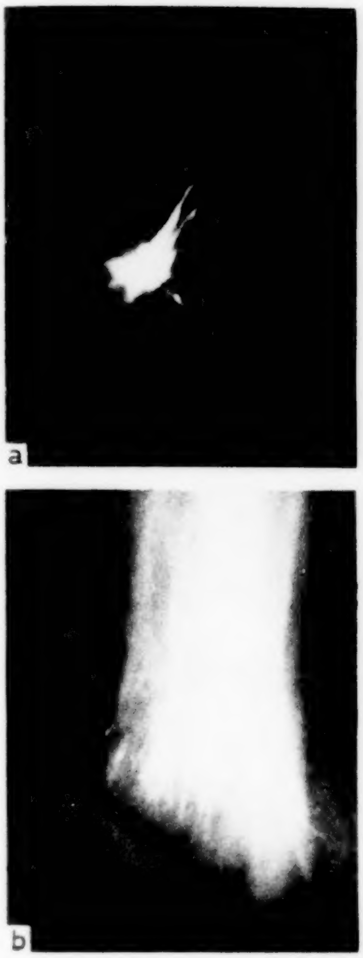

Figure 1

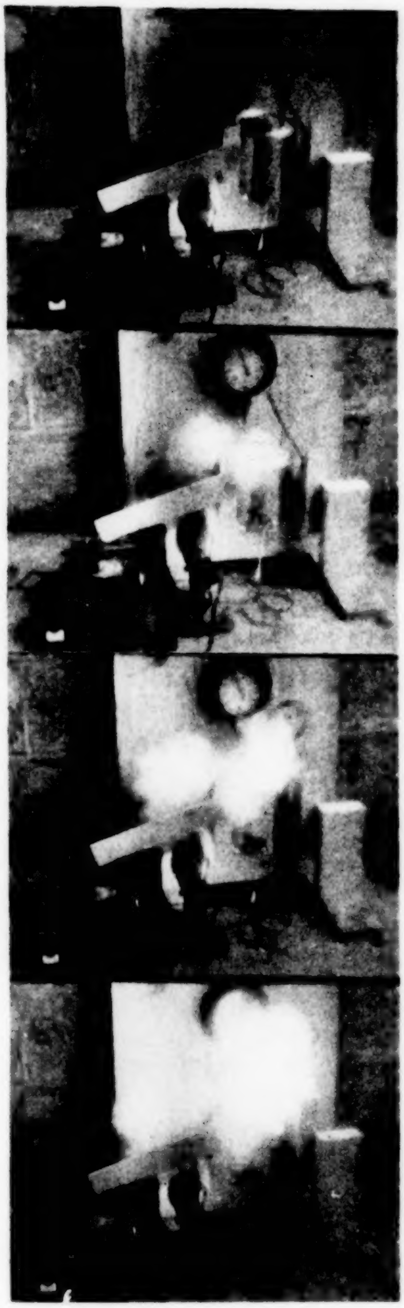

Figure 2

Figure 1. Initial stages in (a) *initiation, and* (b) *propagation, of flame through kerosine foam in air at 70°F*

Figure 2. Four successive frames from motion picture sequence (128 frames per second) of spark-initiated kerosine foam-air explosion in 2-quart container

by a spark discharge at the instant the desired foam thickness was attained. This procedure was repeated for several thicknesses of foam ranging from 0·5 to 3 in. After one such series of tests in which the only variable was the

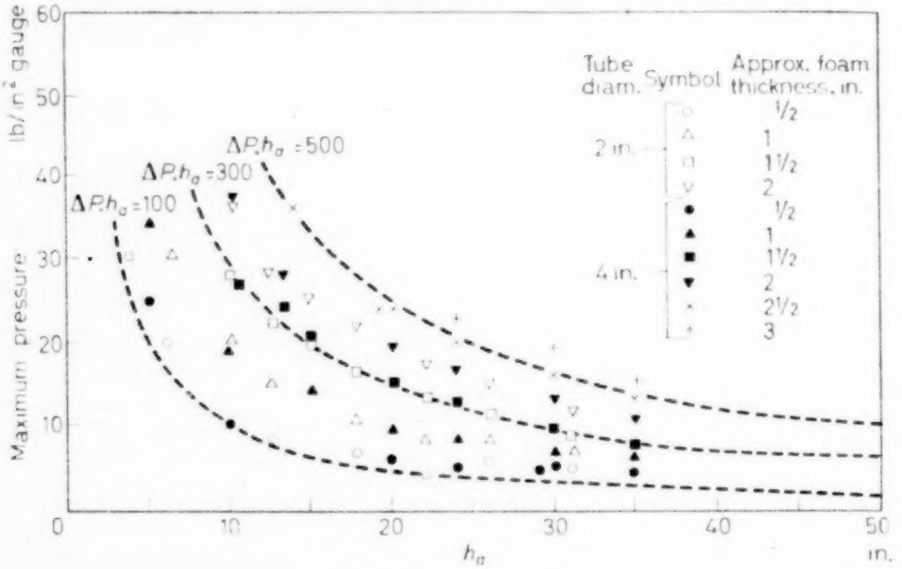

Figure 3. Variation in maximum pressure obtained in closed 2 in. and 4 in. diameter vertical cylinders following the burning of kerosine foam in air at 60° F as a function of the height of the air space (h_a) above the kerosine

foam thickness, the kerosine level was changed and the entire procedure repeated at this new level. Data were thus obtained to show the effect of both foam thickness and air space above the kerosine upon the maximum pressure rise produced under these conditions; all the foam was burnt in each of these tests. The results of these tests at 60° F are presented graphically in ***Figure 3*** (tests conducted at 30° F gave essentially the same results), in which the pressure rise is plotted as a function of the height of air space above the kerosine. The results show that the pressure rise developed when a layer of kerosine foam is burnt is independent of the diameter of the bomb; that is, the maximum pressure rise is a function only of the volume of kerosine foam burnt per unit volume of air space above the liquid level.

Similar experiments were conducted in a closed 10^3 ft^3, cubical steel test tank. Foam was produced in this tank by pumping kerosine into it at various rates up to *ca.* 2 000 gal/min. The kerosine was permitted to fall approximately 40 in. from a 6 in. filling pipe. This drop produced a blanket of foam between 1 and 1·5 in. thick. However, because of rapid collapse of the foam and motion of the liquid, it was difficult to burn more than a few square feet of foam by igniting it with a single point source. This resulted in an insignificant pressure rise. Accordingly, additional experiments were conducted with multiple ignition sources. The data obtained under these conditions are presented graphically in ***Figure 4***. As noted in this figure, two heights of air space (85 and 100 in.) and up to 16 spark gaps were used in these tests. The foam was not all burnt, even in these experiments, so that the maximum pressure rise was only 0·45 lb/in^2 gauge. It is interesting to note that an extrapolation of the data presented in ***Figure 3*** indicates that, with an air space height of 100 in., a pressure rise

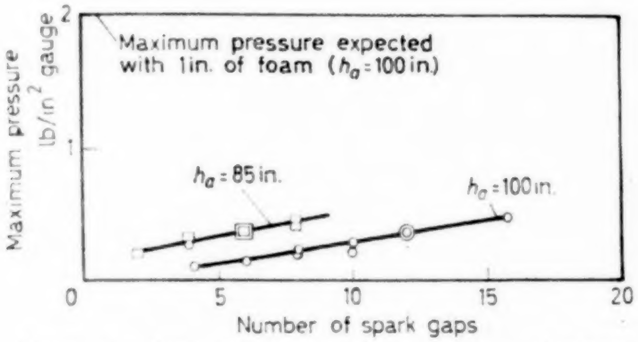

Figure 4. Variation in maximum pressure obtained in closed 10^3 ft^3 test tank following ignition of kerosine foam as a function of number of ignition sources (spark gaps) and height of air space (h_a) above kerosine

of approximately 2 lb/in^2 gauge could be expected if 1 in. of foam was burnt in this tank.

The data in *Figure 3* indicate that the pressure rise that results after combustion of a given thickness of foam in a closed container is inversely proportional to the height of air space above the kerosine level. This is to be expected if negligible heat losses are encountered during combustion of a layer of foam.

Let K_f = heat of combustion of a unit volume of foam, A_f = surface area of burnt foam, h_f = average thickness of burnt foam, V_a = volume of air above the kerosine level, E_2 = energy content per unit volume of air after combustion, and E_1 = energy content per unit volume of air before combustion; then

$$K_f A_f h_f = (E_2 - E_1) V_a \qquad \dots.[1]$$

but

$$E = C_v T \rho_a \propto P$$

so

$$K_f A_f h_f \propto \Delta P \times V_a \qquad \dots.[2]$$

and

$$\Delta P \propto (A_f / V_a) \times h_f \qquad \dots.[3]$$

For a vessel of constant cross section,

$$V_a = A_a h_a$$

where A_a = cross sectional area and h_a = height of air space above kerosine level, so that equation 3 becomes

$$\Delta P \propto A_f h_f / A_a h_a \qquad \dots.[4]$$

If the ratio A_f/A_a is taken to be unity (i.e. the area of foam that burns is equal to the cross sectional area of the vessel) then

$$\Delta P \propto (1/h_a) \times h_f \qquad \dots.[5]$$

Equation 5 indicates that the pressure increase following combustion of a layer of foam is proportional to the thickness of foam burnt and inversely proportional to the height of the air column above the kerosine, so that a plot of the pressure increase against air-column height should give a series of hyperbolas dependent on the foam thickness burnt.

The experimental data plotted in *Figure 3* indicate the approximate validity of equation 5. Several curves of constant $\Delta P \times h_a$ have been drawn in *Figure 3* to show how nearly the experimental points fall along such hyperbolic curves. There is considerable deviation in the region of small h_a, which may be attributed to the small amount of available space in this region, making the formation and ignition of foam rather difficult. Therefore, for small values of h_a equation 5 is not applicable in practice; however, for values of h_a greater than approximately 10 in., the correlation is satisfactory for extrapolation to free space values encountered in the 10^3 ft^3 test tank. As noted above, extrapolation to a height of 100 in. of air column and for a foam thickness of 1 in., which was typical of conditions encountered in the large-scale tests, shows that a maximum pressure rise of 2 lb/in^2 gauge could be expected if the entire foam area were burnt quickly. Such a condition could conceivably be obtained if a sheet discharge of static electricity occurred across the surface of kerosine through a layer of foam of appropriate thickness.

It is interesting to note that the $\Delta P \times h_a$ values obtained from *Figure 3* are approximately the same as those that would be obtained by burning a stoichiometric kerosine vapour–air mixture in the volume occupied by the foam (that is, the heat of combustion of a unit volume of kerosine foam in air was the same as that of a unit volume of a stoichiometric kerosine vapour–air mixture).

CONCLUSIONS

Kerosine and other combustible foams are readily produced in many industrial and other processes. When ignited, the foams can propagate flame in an air atmosphere. Such flames propagate through kerosine foam in vitiated air containing up to 15 vol. per cent carbon dioxide. Propagation of flame appears to involve the combustion of the mist produced by the collapse of foam at the flame front.

The pressure rise produced by the ignition of kerosine foam in air in closed containers was found to be a function of the thickness of the foam that burned and the height of the space above the liquid surface. The maximum pressure rise obtained by burning up to 2 in. of foam in small containers was *ca.* 35 lb/in^2 gauge. The rates of pressure rise resulting from the burning of the foam were considerably smaller than those encountered in explosions of combustible vapour–air mixtures.

The heat released by burning a unit volume of kerosine foam in air was found to be the same as that which would be released by burning a unit volume of a stoichiometric kerosine vapour–air mixture.

This research is a part of the work carried out at the Bureau of Mines under a cooperative agreement with the Cities Service Research and Development Co. Work on this manuscript was completed 28 March 1958.

The authors gratefully acknowledge the contributions to this work of the following members of the Branch of Gas Explosions, Division of Explosives Technology: Allan F. Smith, Irving Spolan, Robert E. Kennedy, and Walter H. Mason.

U.S. Department of the Interior,

Bureau of Mines, Pittsburgh, Pa

(*Received August 1958*)

REFERENCES

BURGOYNE, J. H. and COHEN, L. *Proc. Roy. Soc. A*, 1954, **225**, 375

BROWNING, J. A., TYLER, T. L. and KRALL, G. W. *Industr. Engng Chem. (Industr.)*, 1957, **49**, 142

ANSON, D. *Fuel, Lond.* 1953, **32**, 39

THOMAS, A. *Sixth Symposium (International) on Combustion*, p 701. Reinhold: New York, 1957

ZABETAKIS, M. G. and ROSEN, B. H. *Proc. Amer. Petrol. Inst.*, Sect. III, 1957, **37**, 296

Heterogeneous Burning in a Diverging Reactor[*]

F. A. WILLIAMS[†], S. S. PENNER[‡], G. GILL and E. F. ECKEL

Experimentally determined pressure profiles in a diverging reactor have been used to estimate effective mean drop diameters and size distributions at the injector end. The available results may be correlated in terms of two simplified models using (a) *a uniform mean drop size for the spray and* (b) *a generalized size distribution of the Rosin Rammler type. Mean drop sizes of the order of 5 to 10 microns, and effective overall reaction orders between* $\frac{1}{2}$ *and 2 are obtained if the phenomenological burning rate law familiar from single droplet studies is used for heterogeneous burning in bipropellant LOX–RP1 mixtures.*

IN a previous publication[1] we have described experimentally determined pressure profiles obtained in a diverging reactor with LOX–RP1 propellants. We have also presented a summary of theoretical studies involving chemical reactions for premixed gases in a diverging reactor[1]. Although the measured pressure profiles could be correlated in terms of the formulae derived from the theoretical studies on premixed gaseous reactants, it appears highly desirable to use the experimental data for the determination of effective combustion parameters in spray burning. It is the purpose of the present investigations to outline a simplified analytical approach and interpretation of available experimental results relating to heterogeneous burning in diverging reactors.

A useful method for correlating data on steady, heterogeneous burning in one-dimensional flow systems is described below. The resulting profiles for the rate of change of mass fraction of gas with distance from the injector are used in the following two sections in order to determine the effective injector parameters for the diverging reactor. The analysis in the first of these refers to sprays with uniform drop size whereas the discussion in the other is concerned with spray-size distributions of a generalized Rosin–Rammler type. Concluding remarks relate to the use of diverging reactors for the determination of kinetic parameters.

CORRELATIONS OF EXPERIMENTALLY DETERMINED PRESSURE PROFILES IN TERMS OF OVERALL CONSERVATION EQUATIONS FOR ONE-DIMENSIONAL STEADY FLOW

We assume that the droplets move with the same velocity as the gas mixture and ignore droplet collisions and droplet sources downstream of the injector end.

---

[*] The experimental studies described in this paper were carried out at Rocketdyne. The theoretical investigations were performed at the Gruen Applied Science Laboratories and were sponsored by Rocketdyne. The work was supported by the United States Air Force.

[†] Consultant; formerly with the Daniel and Florence Guggenheim Jet Propulsion Center, California Institute of Technology, Pasadena, Calif. Present address: Harvard University, Cambridge, Mass.

[‡] Consultant; permanent address: Daniel and Florence Guggenheim Jet Propulsion Center, California Institute of Technology, Pasadena, Calif.

(a) *Conservation of mass*

The overall equation for conservation of mass is

$$\rho_t v A = m = \text{constant} \qquad \ldots .[1]$$

Here

$$\rho_t = \rho_g + \rho_d \qquad \ldots .[2]$$

identifies the (mass of mixture)/(cm^3 of mixture), ρ_g is the (mass of gas)/(cm^3 of mixture) and ρ_d is the (droplet mass)/(cm^3 of mixture); also v represents the flow velocity, A denotes the cross sectional area, and m is the total mass flow rate. The quantities ρ_t, ρ_g, ρ_d, m and A are functions of the distance x measured downstream from the injector end. If gaseous and liquid propellants are injected, then the mass fraction of gas

$$Y = \rho_g / \rho_t \qquad \ldots .[3]$$

increases from a specified value at the injector end toward unity for the completely burnt mixture.

(b) *Conservation of momentum*

The overall momentum equation is

$$\rho_t v \, \mathrm{d}v/\mathrm{d}x = -\mathrm{d}p/\mathrm{d}x \qquad \ldots .[4]$$

since the pressure gradients must accelerate the gas–liquid mixture*.

(c) *Conservation of energy*

We shall consider two functional forms for the energy equation which apply, respectively, for (*1*) injection of liquid propellants, and (*2*) injection of liquid fuel with gaseous oxidizer or of gaseous fuel with liquid oxidizer.

(1) *Injection of liquid propellants*—The equation for conservation of energy may be written as

$$Y h_g + (1 - Y) h_l + \tfrac{1}{2} v^2 = h_0 = \text{constant} \qquad \ldots .[5]$$

where

$$h_g = h_g^0 + c_p (T - T^0) \qquad \ldots .[6]$$

is the specific enthalpy (i.e. the enthalpy per unit mass) of gas with constant specific heat c_p at the temperature T if the superscript ^{0} to h_g and T identifies corresponding standard reference conditions; similarly

$$h_d = h_d^0 + c_{p,l} (T_l - T^0) \qquad \ldots .[7]$$

stands for the specific enthalpy of the liquid droplets at the temperature T_l if the constant specific heat is $c_{p,l}$. From equations 5 to 7 it follows that

$$\tfrac{1}{2} v^2 + Y c_p T - Y q' = H$$

where

$$q' = h_d^0 - h_g^0 + c_{p,l} T_l + (c_p - c_{p,l}) T^0$$

and

$$H = h_0 - h_d^0 - c_{p,l} (T_l - T^0)$$

---

*We use the one-dimensional momentum equation, which is easily shown to represent a very good approximation for the small divergence angle used in our diverging reactor.

For effectively constant values of T_l, both q' and H are constants. Furthermore, for $v = Y = 0$ at the injector end (i.e. liquid droplet injection with negligibly small velocities), $H = 0$; we may regard q' as an effective (constant) heat of reaction for heterogeneous systems. Thus the energy equation is given by the following approximate expression

$$\tfrac{1}{2}v^2 + Y(c_pT - q') = 0, \quad 0 \leqslant Y \leqslant 1 \qquad \ldots .[8]$$

(2) *Injection of gaseous and of liquid propellant mixtures*—We assume that the initial combustible mixture is described by the mass fraction Y_R of gaseous reactant and $1 - Y_R$ of liquid reactant. Let Y_P represent the mass fraction of gaseous reaction products formed during flow. Then

$$Y = Y_R + Y_P \qquad \ldots .[9]$$

and equation 5 is replaced by the expression

$$Y_Rh_R + Y_Ph_P + (1 - Y)\,h_d + \tfrac{1}{2}v^2 = h_0 = \text{constant} \qquad \ldots .[10]$$

where

$$h_R = h_R{}^0 + c_p(T - T^0) \qquad \ldots .[11]$$

$$h_P = h_P{}^0 + c_p(T - T^0) \qquad \ldots .[12]$$

h_d is again given by equation 7, the specific heats of the gaseous components have been assumed to be constant and equal to c_p, and $h_R{}^0$ and $h_P{}^0$ denote standard specific enthalpies of formation for the gaseous reactants and products, respectively. If $Y_R{}^\bigstar$ denotes the mass of gaseous reactant consumed per gramme of reactant mixture, then

$$-(1/Y_R{}^\bigstar)\,\mathrm{d}Y_R = \mathrm{d}Y_P \qquad \ldots .[13]$$

represents the increase in product mass fraction in the gas phase. The integral of equation 13 is

$$Y_P = (Y_{R,0} - Y_R)/Y_R{}^\bigstar \qquad \ldots .[14]$$

since $Y_P = 0$ at $x = 0$ where $Y_R = Y_{R,0}$. From equations 9 and 14 we now find that

$$Y_R = (Y_{R,0} - YY_R{}^\bigstar)/(1 - Y_R{}^\bigstar) \qquad \ldots .[15]$$

and

$$Y_P = (Y - Y_{R,0})/(1 - Y_R{}^\bigstar) \qquad \ldots .[16]$$

Introduction of equations 7, 11, 12, 15 and 16 into equation 10 yields the expression

$$\begin{aligned}\tfrac{1}{2}v^2 + Yc_pT - Y\,[c_{p,l}(T_l - T^0) + c_pT^0 + h_d{}^0 + Y_R{}^\bigstar h_R{}^0/(1 - Y_R{}^\bigstar) - h_P{}^0/(1 - Y_R{}^\bigstar)]\\ + c_{p,l}(T_l - T^0) + h_d{}^0 + Y_{R,0}h_R{}^0/(1 - Y_R{}^\bigstar) - Y_{R,0}h_P{}^0/(1 - Y_R{}^\bigstar) = h_0\end{aligned}$$

or

$$\tfrac{1}{2}v^2 + Y(c_pT - q'') = H'' = \text{constant} \qquad \ldots .[17]$$

where

$$q'' = c_{p,l}(T_l - T^0) + c_pT^0 + h_d{}^0 + Y_R{}^\bigstar h_R{}^0/(1 - Y_R{}^\bigstar) - h_P{}^0/(1 - Y_R{}^\bigstar) \qquad \ldots .[18]$$

and

$$H'' = h_0 - h_d{}^0 - Y_{R,0}h_R{}^0/(1 - Y_R{}^\bigstar) + Y_{R,0}h_P{}^0/(1 - Y_R{}^\bigstar) - c_{p,l}(T_l - T^0) \qquad ..[19]$$

Comparison of equations 8 and 17 shows that the energy equation has the same functional form, to the order of approximation used, for the injection of either pure liquid propellants or liquid–gas mixtures. A reasonable approximation to H'' may be obtained by using the injection conditions. Thus

$$H'' = \tfrac{1}{2}v_0^2 + Y_{R,0}(c_pT_0 - q'') \simeq -Y_{R,0}q''$$

(d) *Equations of state*

For constant values of T_l the equation of state for the liquid may be ignored whereas the equation of state for the gas becomes

$$p \simeq (Y\rho_l)R'T \qquad \ldots.[20]$$

since the mass of gas per (cm³ of mixture), viz. $Y\rho_l = \rho_g$, is practically equal to the mass of gas per (cm³ of fluid which is not occupied by the liquid), i.e. at some distance from the injector end the gas volume makes up practically all of the fluid volume*. The quantity R' denotes the specific gas constant.

(e) *Interpretation of measured pressure profiles*

Proceeding as in our earlier publication[1], we obtain from equations 1, 4, 8 or 17 and 20 the results

$$\left.\begin{array}{l}
\dfrac{\mathrm{d}v}{\mathrm{d}x} = -\dfrac{A}{m}\dfrac{\mathrm{d}p}{\mathrm{d}x} \\[2ex]
\rho_l = -m/Av \\[2ex]
Y = \dfrac{1}{q'}\left(\dfrac{v^2}{2} + \dfrac{pc_p}{\rho_l R'}\right) \text{ for liquid-propellant injection} \\[2ex]
\text{or} \\[1ex]
Y = \dfrac{1}{q''}\left(\dfrac{v^2}{2} + \dfrac{pc_p}{\rho_l R'} - H''\right) \text{ for injection of gas–liquid mixtures,} \\[2ex]
\text{and} \\[1ex]
T = p/Y\rho_l R'
\end{array}\right\} \quad \ldots.[\mathrm{I}]$$

For known values of $A(x)$ and m, we may use measured values of $p(x)$ to obtain successively $\mathrm{d}p/\mathrm{d}x$, $\mathrm{d}v/\mathrm{d}x$, $v(x)$ if $v(x=0)$ is negligibly small or else specified, $\rho_l(x)$, $Y(x)$, $\mathrm{d}Y/\mathrm{d}x$ and $T(x)$. Because of the dependence of the energy equation on the specified injection conditions, we must distinguish between injection of liquid propellants, of liquid fuel with gaseous oxidizer and of liquid oxidizer with gaseous fuel.

(1) *Injection of liquid propellants*—The use of representative numerical values (e.g. $c_p = 0{\cdot}40$ cal/g.°K, $R' = 0{\cdot}08$ cal/g.°K, $q' = 2\,400$ cal/g) in the system of equations I shows that the effective gas temperature $T(x)$ assumes a very high value throughout most of the divergent reactor. This result is not unexpected since we have assumed implicitly that the reaction products are at the adiabatic flame temperature which is reached without allowing for dissociation of reaction products. We may correct roughly for this effect by introducing the parameter $\delta = q'/2\,400$ where δ is expected to lie between 0·5 and 0·8.

---

*It is important to observe that the conservation equations are really applicable only at some distance downstream from the injector end even though we use [compare equation 8] boundary conditions referring to the injector end.

Representative data deduced from the experimentally determined pressure profiles are shown in *Figure 1* for $\delta\,[\mathrm{d}Y(x)/\mathrm{d}x]$. It is interesting to observe that the apparent rate of change of $\mathrm{d}Y/\mathrm{d}x$ with distance is very large near the injector end but decreases rapidly as x increases.

(2) *Injection of liquid fuel and of gaseous oxidizer**—For the injection of liquid fuel and of gaseous oxidizer, the subscript R identifies the oxidizer and $Y_R^\star = 0{\cdot}78$ for LOX–RP1 mixtures. Also $q'' \simeq 10\,900$ cal/g and $H'' = 10\,900\,Y_{R,0}$ cal/g. Using the known value of $Y_{R,0}$, the same estimates for c_p and R' as before, and the appropriate relations from equations I, we may again compute $Y(x)$, $T(x)$ and $\mathrm{d}Y/\mathrm{d}x$ from the measured pressure profiles. The results obtained for the engine test used in the derivation of the data shown in *Figure 1* are shown in *Figure 2* for the assumed model of liquid fuel and gaseous oxidizer injection.

It is found that the mass fraction of gas now increases only very slowly from the initial mass fraction of oxidizer $Y_{R,0} \simeq \frac{2}{3}$. The gas temperatures are greatly reduced because of the relatively large volume of gas present at all times; the numerical values of T are, in fact, intermediate between those computed for gaseous reactants[1] and for bipropellant droplets. The $\mathrm{d}Y/\mathrm{d}x$ versus x curve has the same shape as before (see *Figure 1*) but the absolute value of the reaction rate is reduced, approximately, by the factor $(1 - Y_R^\star)$ for the same mass fraction of gas at the injector.

(3) *Injection of gaseous fuel and of liquid oxidizer†*—The quantity Y_R now refers to the fuel and $Y_R^\star = 0{\cdot}22$. Also $q'' \simeq 3\,100$ cal/g and $H'' = 3\,100\,Y_{R,0}$. For experimental results used for construction of the curves shown in *Figures 1* and *2* we now find that the mass fraction of gas increases slowly from its initial value of 0·38, that the temperature profile

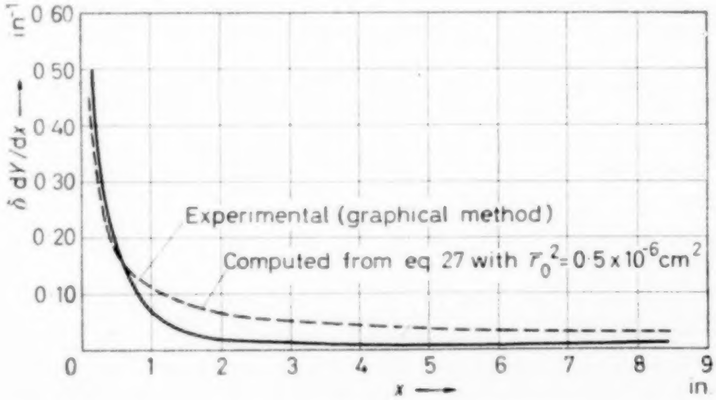

Figure 1. Comparison of the reaction rates $\mathrm{d}Y/\mathrm{d}x$ *computed graphically and from equation 27 for a representative motor test*

is somewhat above the result deduced for the liquid fuel–gaseous oxidizer model, and that the dY/dx versus x curve corresponds to the results shown in *Figure 1* except that the reaction rate is reduced, approximately, by the factor $(1 - Y_{0}^{\star})$ for the same injection conditions.

---

*To the extent that a particular liquid bipropellant mixture involves a very volatile oxidizer, the present analysis may be applied in adequate approximation since the heat of evaporation of the more volatile component is generally very small compared with q''.

†For bipropellant mixtures containing a very volatile fuel the present analysis may be applied in first approximation.

We now turn to the interpretation of the profiles $dY(x)/dx$ versus x in terms of simplified theoretical models for spray combustion.

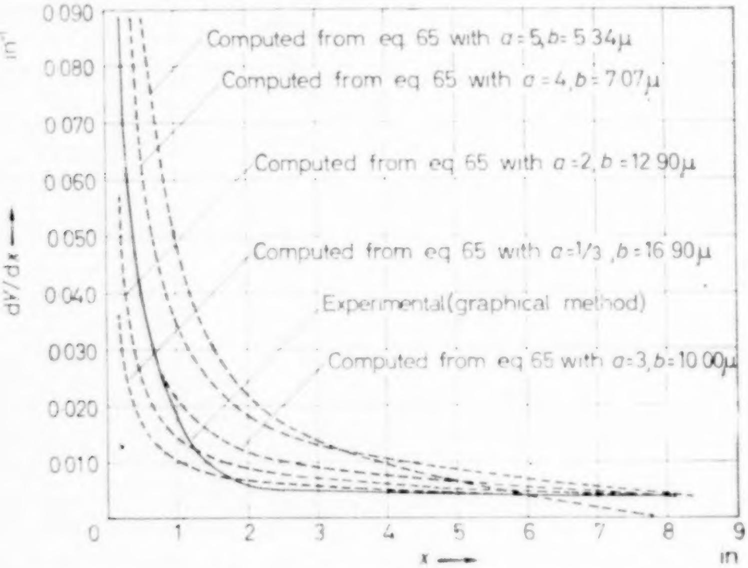

Figure 2. Comparison of the reaction rates dY/dx computed graphically and from equation 65 for various values of the injector parameters a and b for a representative motor test, assuming burning of liquid fuel droplets in gaseous oxidizer

SPRAY COMBUSTION IN ONE-DIMENSIONAL STEADY FLOW FOR HETEROGENEOUS SYSTEMS WITH UNIFORM DROP RADII AND INJECTION OF LIQUID REACTANTS

The theoretical analysis of one-dimensional steady flow for heterogeneous mixtures containing drops with uniform radii can be carried out quite simply if we assume that the droplet burning law established for either fuel droplets in an infinite stagnant oxidizing medium or for oxidizer droplets in an infinite stagnant fuel atmosphere may be applied to the diverging reactor. This assumption, as well as the neglect of droplet collisions and relative motion between liquid and gas, will tend to reduce the overall burning rate, i.e. the resulting identification of required initial drop radii $\bar{r}_0$ will correspond to an effective lower limit for this parameter.

(a) *Reaction-rate equation*

If $n(x)$ denotes the total number of droplets in unit volume, then the following droplet conservation equation applies since we make an implicit distinction even between very small liquid droplets and gas molecules:

$$Avn = A_0 v_0 n_0 = \text{number of droplets passing any station in unit time} \quad \ldots [21]$$

Here the subscript $_0$ identifies conditions at the injector. Furthermore, the mass flow rate (g/sec) of the droplets with radius $\bar{r}$ is

$$\tfrac{4}{3}\pi\bar{r}^3\rho_l n v A = (1-Y)\,m = (1-Y)\tfrac{4}{3}\pi\bar{r}_0^{\,3}\rho_l n_0 v_0 A_0 \qquad \ldots.[22]$$

In view of equation 21, equation 22 leads to the relations:

$$\bar{r} = \bar{r}_0\,(1-Y)^{1/3} \qquad \ldots.[23]$$

$$Y = 1-(\bar{r}/\bar{r}_0)^3 \qquad \ldots.[24]$$

and

$$\frac{\mathrm{d}Y}{\mathrm{d}x} = -\frac{3}{2}\frac{1}{\bar{r}_0^{\,2}}\left(\frac{\bar{r}}{\bar{r}_0}\right)\frac{\mathrm{d}\,(\bar{r}^2)}{\mathrm{d}x} = -\frac{3}{2}\frac{1}{\bar{r}_0^{\,2}}\left(\frac{\bar{r}}{\bar{r}_0}\right)\frac{1}{v}\,\frac{\mathrm{d}\,(\bar{r}^2)}{\mathrm{d}t} \qquad \ldots.[25]$$

where we have used the steady-flow approximation. For the rate of change of droplet radius with time we use the result obtained for single droplets in the special case that the Lewis number is unity[2–4], viz.

$$-\frac{\mathrm{d}\,(\bar{r}^2)}{\mathrm{d}t} = 2\,\frac{\lambda}{c_p\rho_l}\ln\left(1+\frac{T_R-T_l}{\Delta l/c_p}+\frac{q}{\Delta l}\,\frac{Y_R}{Y_R{}^{\star}}\right) \qquad \ldots.[26]$$

where λ is an average thermal conductivity for the gas, Δl is the specific heat of evaporation of the burning liquid (fuel or oxidizer) droplet, $T_R = T$ is the temperature of the gaseous reactant far from the droplet, Y_R is the mass fraction of gaseous reactant far from the droplet, $Y_R{}^{\star}$ is the value of Y_R in a stoichiometric fuel–oxidizer mixture, and q represents, approximately, the standard heat of combustion for one gramme of liquid fuel. It is apparent from equation 26 that $\mathrm{d}\,(\bar{r}^2)/\mathrm{d}t$ depends on x [through $T(x)$] and on the properties of the fuel–oxidizer mixture. Equations 26 and 25 yield the following phenomenological law for the rate of change of Y with distance

$$\frac{\mathrm{d}Y}{\mathrm{d}x} = -\frac{3}{2}\frac{1}{\bar{r}_0^{\,2}}\left[\frac{\mathrm{d}\,(\bar{r}^2)}{\mathrm{d}t}\right](1-Y)^{1/3} \qquad \ldots.[27]$$

i.e. the apparent reaction order with respect to the mass fraction of liquid is one third since $\mathrm{d}\,(\bar{r}^2)/\mathrm{d}t$ is a weak function of $(1-Y)$.

(b) *Comparison between calculated reaction rates and reaction rates derived from measured pressure profiles*

Since $\mathrm{d}\,(\bar{r}^2)/\mathrm{d}t$ is known, equation 27 may be compared with the curves relating $\mathrm{d}Y/\mathrm{d}x$ to x which were deduced in the previous section. In this manner it is possible to estimate the effective average drop radius at the injector end $\bar{r}_0$.

In *Figure 1* we have indicated the results computed from equation 27 for $\lambda = 0{\cdot}4\times10^{-4}$ cal/cm.sec.°K, $c_p = 0{\cdot}4$ cal/g.°K, $\rho_l = 1$ g/cm^3, $\Delta l = 66$ cal/g, $T_l = 200$°K, $Y_R{}^{\star} = 0{\cdot}5$, $q = 2\,400$ cal/g, and $\bar{r}_0^{\,2} = 0{\cdot}5\times10^{-6}$ cm^2. Reference to *Figure 1* shows fair accord between the mass fraction profiles deduced from the measured pressure profiles, on the one hand, and calculated from equation 27, on the other hand. The estimated average initial drop radius $\bar{r}_0 \simeq 7$ microns is representative of results derived from measured pressure profiles by using the specified procedure. The surprisingly small value for r_0 may indicate either that our assumptions lead to relatively small estimates for the mean drop radius or, more plausibly, that the injector used in the diverging reactor is exceedingly efficient and produces very fine sprays. This last supposition is borne out also by the analysis described below.

SPRAY COMBUSTION IN ONE-DIMENSIONAL STEADY FLOW FOR HETEROGENEOUS SYSTEMS WITH GENERALIZED ROSIN–RAMMLER TYPE SIZE DISTRIBUTIONS

Equations 21 to 27 must now be replaced by expressions obtained for specified initial drop-size distribution functions. From the basic equation[1] for the (single) drop-size distribution function

$$\frac{\partial f}{\partial t} = -\frac{\partial}{\partial r}(Rf) - \nabla_x \cdot (\mathbf{v}f) - \nabla_v \cdot (\mathbf{F}f) + Q + \Gamma$$

we find for one-dimensional steady flow ($\partial f/\partial t = 0$), in the absence of droplet source terms ($Q = 0$), and without droplet collisions ($\Gamma = 0$), that

$$\frac{\partial}{\partial r}(Rf) + \nabla_x \cdot (vf) + \nabla_v \cdot (Ff) = 0 \qquad \ldots . [28]$$

Here $R = \mathrm{d}r/\mathrm{d}t$ is the rate of change of droplet radius with time, $F = \mathrm{d}v/\mathrm{d}t$ is the droplet acceleration and $f(r, x, v)\,\mathrm{d}r\,\mathrm{d}x\,\mathrm{d}v$ measures the probable number of droplets with radius between r and $r + \mathrm{d}r$, at the position between x and $x + \mathrm{d}x$, in the velocity range between v and $v + \mathrm{d}v$. In view of equation 26, R is of the form*

$$R = -X/r \qquad \ldots . [29]$$

where X depends on x and on the physicochemical properties of the reactants. When all droplets are travelling at the same velocity, integration of equation 28 over the velocity and the area A normal to the flow direction shows that

$$\frac{\partial}{\partial r}(Rg) + \frac{1}{A}\frac{\partial}{\partial x}(Avg) = 0 \qquad \ldots . [30]$$

if the divergence theorem is used to eliminate the third term. Here we define $g(r, x) = \int_0^\infty f(r, x, v)\,\mathrm{d}v$. From equations 29 and 30 it follows that

$$-\frac{1}{r}\frac{\partial}{\partial r}\left(\frac{Avg}{r}\right) + \frac{v}{X}\frac{\partial}{\partial x}\left(\frac{Avg}{r}\right) = 0 \qquad \ldots . [31]$$

---

*The discussion presented in this section has been generalized and extended by F. A. WILLIAMS[3] for burning rate functions of the form $R = -X/rk$.

Introduction into equation 31 of the independent variables

$$\xi = \frac{r^2}{2} - \int_0^x \frac{X}{v}\,\mathrm{d}x \qquad \ldots.[32]$$

and

$$\eta = \frac{r^2}{2} + \int_0^x \frac{X}{v}\,\mathrm{d}x \qquad \ldots.[33]$$

and of the dependent variable

$$\psi = Avg/r \qquad \ldots.[34]$$

shows that

$$\partial\psi/\partial\xi = 0 \qquad \ldots.[35]$$

and

$$\psi = \psi(\eta) \qquad \ldots.[36]$$

The use of equation 36 permits evaluation of $g(r)$ in terms of the size distribution at the injector end $g_0(r)$. Since $r = (2\eta)^{1/2}$ at the injector end according to equation 33, it follows from equations 36 and 34 that

$$\psi = \psi_0(\eta) = A_0 v_0 g_0\{(2\eta)^{1/2}\}/(2\eta)^{1/2} \qquad \ldots.[37]$$

Hence we find from equations 34 and 37 that

$$g(r, x) = g_0\{(2\eta)^{1/2}\}\,(A_0 v_0/Av)\,[r/(2\eta)^{1/2}] \qquad \ldots.[38]$$

at any position in the motor.

The mass flow rate of droplets at any cross section is

$$\int_0^\infty \tfrac{4}{3}\pi r^3 \rho_l g(r, x)\, vA\,\mathrm{d}r = (1 - Y)\,m \qquad \ldots.[39]$$

whence

$$\frac{\mathrm{d}Y}{\mathrm{d}x} = -\frac{1}{m}\frac{\mathrm{d}}{\mathrm{d}x}\int_0^\infty \tfrac{4}{3}\pi r^3 \rho_l g(r, x)\, vA\,\mathrm{d}r$$

However, multiplication of equation 30 with $\frac{4}{3}\pi r^3 \rho_l$, followed by integration over r, shows that

$$\frac{\mathrm{d}}{\mathrm{d}x}\int_0^\infty Avg(r, x)\tfrac{4}{3}\pi r^3 \rho_l\,\mathrm{d}r = \tfrac{4}{3}\pi A\rho_l \int_0^\infty r^3 \frac{\partial}{\partial r}(Rg)\,\mathrm{d}r = -4\pi A\rho_l X \int_0^\infty rg\,\mathrm{d}r$$

where the integral on the RHS of the equation has been evaluated by partial integration using the relations $g(r = \infty, x) = 0$ and equation 29. Hence

$$\frac{\mathrm{d}Y}{\mathrm{d}x} = \frac{4\pi\rho_l AX}{m}\int_0^\infty rg(r, x)\,\mathrm{d}r = \frac{4\pi\rho_l A_0 v_0}{m}\,\frac{X}{v}\int_0^\infty \frac{r^2}{(2\eta)^{1/2}}[g_0\{(2\eta)^{1/2}\}]\,\mathrm{d}r. \;[40]$$

The theoretical evaluation of the rate of change of Y with distance has now been reduced to the evaluation of the integral appearing in equation 40 for specified drop-size distribution functions at the injector.

Before proceeding with the explicit determination of dY/dx, we consider briefly the meaning of reaction order for heterogeneous systems[2]. It is apparent from equations 38, 39 and 40 that the liquid mass fraction and its rate of change with distance are given by the following expressions:

$$1-Y=\frac{4\pi\rho_l A_0 v_0}{m}\,\frac{1}{3}\int\limits_0^\infty \frac{r^4}{(2\eta)^{1/2}}\left[g_0\{(2\eta)^{1/2}\}\right]\mathrm{d}r$$

and

$$-\frac{\mathrm{d}(1-Y)}{\mathrm{d}x}=\frac{\mathrm{d}Y}{\mathrm{d}x}=\frac{4\pi\rho_l A_0 v_0}{m}\,\frac{X}{v}\int\limits_0^\infty \frac{r^2}{(2\eta)^{1/2}}\left[g_0\{(2\eta)^{1/2}\}\right]\mathrm{d}r$$

Since the functional relation between η and r involves x, we cannot expect that dY/dx varies as a constant power of $(1-Y)$ for all values of x even if X is independent of $(1-Y)$, i.e. the effective reaction order with respect to the liquid mass fraction will usually be a function of position. However, for small values of x, the reaction order may be estimated without difficulty by expanding $[g_0\{(2\eta)^{1/2}\}]/(2\eta)^{1/2}$ about $x=0$ where $\eta=\frac{1}{2}r^2$ and evaluating the resulting integrals over r. Details concerning these calculations are given elsewhere[2] from a general point of view and below for the more restricted case which is of interest for the present analysis.

(a) *Spray size-distribution parameters*[1]

The generalized Rosin–Rammler size-distribution function will be assumed to describe the spray at the injector end. Thus

$$g_0(r)=Nr^t\exp(-\alpha r)^s \qquad \ldots.[41]$$

where

$$\alpha=\frac{1}{\bar{r}_0}\,\frac{\Gamma\{(t+2)/s\}}{\Gamma\{(t+1)/s\}} \qquad \ldots.[42]$$

$$N=\frac{n_0 s}{\Gamma\{(t+1)/s\}}\,\alpha^{t+1} \qquad \ldots.[43]$$

t and s are empirically determined constants, n_0 represents the initial number of drops per unit volume, $\Gamma(z)$ is the gamma function of the argument z, and

$$\bar{r}_0=\int\limits_0^\infty r g_0(r)\,\mathrm{d}r/n_0 \qquad \ldots.[44]$$

is the number-weighted average initial drop radius.

(b) *Reaction-rate equation*

In terms of the reduced variables

$$\hat{r}=r/\bar{r}_0 \qquad \ldots.[45]$$

and

$$\hat{x}=\frac{2}{\bar{r}_0^{\,2}}\int\limits_0^x \frac{X}{v}\,\mathrm{d}x \qquad \ldots.[46]$$

the parameter $(2\eta)^{1/2}$ becomes, according to equation 33,

$$(2\eta)^{1/2} = \bar{r}_0 (\hat{r}^2 + \hat{x})^{1/2} \qquad \ldots . [47]$$

whereas

$$g_0 \{(2\eta)^{1/2}\} = \frac{A_0 v_0}{A v} \frac{n_0 s [\Gamma\{(t+2)/s\}]^{t+1}}{\bar{r}_0 [\Gamma\{(t+1)/s\}]^{t+2}} \hat{r} (\hat{r}^2 + \hat{x})^{(t-1)/2}$$
$$\left\{ \exp - (\hat{r}^2 + \hat{x})^{s/2} \left[\frac{\Gamma\{(t+2)/s\}}{\Gamma\{(t+1)/s\}} \right]^s \right\} \qquad \ldots . [48]$$

The introduction of equation 48 into equation 40 now yields an explicit expression for $\mathrm{d}Y/\mathrm{d}x$. However, the required integration cannot be performed in terms of tabulated functions. It is apparent from equation 46 that $\hat{x} \ll 1$ near the injector end and, furthermore, an *a posteriori* calculation shows that $x \leq \frac{1}{4}$ throughout the entire motor. Since $r \simeq 1$, a two-term expansion of equation 48 in powers of x constitutes an adequate approximation for $g_0 \{(2\eta)^{1/2}\}$. Thus

$$g_0 \{(2\eta)^{1/2}\} = \frac{A_0 v_0}{A v} \frac{n_0 s [\Gamma\{(t+2)/s\}]^{t+1}}{\bar{r}_0 [\Gamma\{(t+1)/s\}]^{t+2}} \hat{r}^t \left[1 + \frac{\hat{x}}{\hat{r}^2} \left\{ \frac{t-1}{2} - \right.\right.$$
$$\left.\left. \frac{s}{2} \left(\frac{\Gamma\{(t+2)/s\}}{\Gamma\{(t+1)/s\}} \right)^s \hat{r}^s \right\} \right] \left\{ \exp - \left[\hat{r} \frac{\Gamma\{(t+2)/s\}}{\Gamma\{(t+1)/s\}} \right]^s \right\} \qquad \ldots . [49]$$

and

$$\frac{\mathrm{d}Y}{\mathrm{d}x} = \frac{4\pi\rho_l A_0 v_0 n_0 \bar{r}_0}{m} \frac{X}{v} \left\{ 1 - \frac{\hat{x}}{2} \frac{\Gamma\{(t+2)/s\} \Gamma(t/s)}{[\Gamma\{(t+1)/s\}]^2} \right\} \qquad \ldots . [50]$$

But [compare equation 1] $m = \rho_{t,0} v_0 A_0$ whence

$$\frac{4\pi\rho_l A_0 v_0 n_0 \bar{r}_0}{m} = \frac{4\pi\rho_l n_0 r_0}{\rho_{t,0}} = \frac{\rho_{d,0}}{\rho_{t,0}} \frac{3}{\bar{r}_0^2} \frac{[\Gamma\{(t+2)/s\}]^3}{[\Gamma\{(t+1)/s\}]^2 [\Gamma\{(t+4)/s\}]} \ldots . [51]$$

since

$$\rho_{d,0} = \int_0^\infty \tfrac{4}{3}\pi r^3 \rho_l g_0(r)\,\mathrm{d}r = \rho_l n_0 \tfrac{4}{3}\pi \bar{r}_0^3 \frac{[\Gamma\{(t+1)/s\}]^2 [\Gamma\{(t+4)/s\}]}{[\Gamma\{(t+2)/s\}]^3} \; .[52]$$

Therefore equation 50 becomes

$$\frac{\mathrm{d}Y}{\mathrm{d}x} = (1 - Y_{R,0}) \frac{3X}{v\bar{r}_0^2} \frac{[\Gamma\{t+2)/s\}]^3}{[\Gamma\{(t+1)/s\}]^2 [\Gamma\{(t+4)/s\}]}$$
$$\left\{ 1 - \frac{\hat{x}}{2} \frac{\Gamma\{(t+2)/s\} \Gamma(t/s)}{[\Gamma\{(t+1)/s\}]^2} \right\} \qquad \ldots . [53]$$

where use has been made of the relation $\rho_{d,0}/\rho_{t,0} = 1 - Y_{R,0}$.

It is now desirable to replace $\hat{x}$ in terms of Y in equation 53. This may be accomplished by evaluating

$$\rho_d = \int_0^\infty \tfrac{4}{3}\pi r^3 \rho_l g\,\mathrm{d}r$$

through introduction of equations 45 and 49. The result is

$$\rho_d = \frac{A_0 \bar{v}_0}{A \bar{v}} \rho_{d,0} \left\{ 1 - \frac{3}{2} \hat{x} \frac{[\Gamma\{(t+2)/s\}]^3}{[\Gamma\{(t+1)/s\}]^2 \Gamma\{(t+4)/s\}} \right\} \qquad \ldots . [54]$$

where equation 52 has been used. But

$$\frac{A_0 \bar{v}_0}{A \bar{v}} = \frac{\rho_t}{\rho_{t,0}} \quad \text{and} \quad \frac{\rho_d}{\rho_t} = 1 - Y$$

Hence equation 54 may be solved for $\hat{x}$ with the result

$$\hat{x} = \frac{2}{3} \frac{[\Gamma\{(t+1)/s\}]^2 \Gamma\{(t+4)/s\}}{[\Gamma\{(t+2)/s\}]^3} \frac{Y - Y_{R,0}}{1 - Y_{R,0}} \qquad \ldots . [55]$$

The use of equation 55 in equation 53 finally leads to the relation

$$\frac{\mathrm{d}Y}{\mathrm{d}x} = \frac{3X(1 - Y_{R,0})}{\bar{v} b^2} \left[1 - a \frac{(Y - Y_{R,0})}{(1 - Y_{R,0})} \right] \qquad \ldots . [56]$$

where

$$a \equiv \frac{1}{3} \frac{\Gamma\{(t+4)/s\} \Gamma(t/s)}{[\Gamma\{(t+2)/s\}]^2} \qquad \ldots . [57]$$

measures the shape of the drop-size distribution function and

$$b \equiv \bar{r}_0 \left\{ \frac{[\Gamma\{(t+1)/s\}]^2 \Gamma\{(t+4)/s\}}{[\Gamma\{(t+2)/s\}]^3} \right\}^{1/2} \qquad \ldots . [58]$$

depends primarily on $\bar{r}_0$ since the factor multiplying $\bar{r}_0$ lies between 1·0 and 2·5.

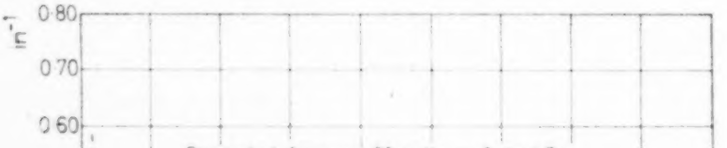

Figure 3. Comparison of the reaction rates $\mathrm{d}Y/\mathrm{d}x$ *computed graphically and from equation 68 for various values of the injector parameters a and b for a representative motor test, assuming burning of liquid oxidizer in gaseous fuel*

Fitting of the theoretical formula given in equation 56 to experimentally determined results yields estimates for the drop size and distribution parameters b and a. For the Rosin–Rammler distribution ($t=s-4$) we may relate a and $\bar{r}_0/b$ to the parameter s by referring to *Figures 4* and *5* where these quantities have been plotted according to equations 57 and 58. The mass-weighted average initial droplet radius is

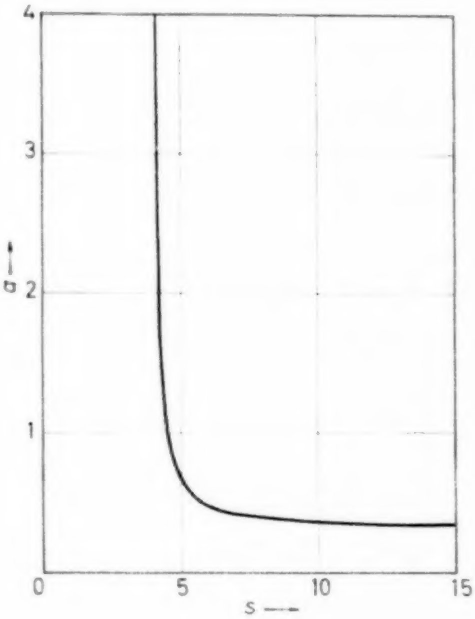

Figure 4. The shape parameter a as a function of the exponent s for the Rosin–Rammler drop-size distribution ($t=s-4$)

$$\bar{r}_0' = \int_0^\infty r\left(\tfrac{4}{3}\pi r^3 \rho_l\right) g_0(r)\,\mathrm{d}r / \rho_{d,0}$$

$$= \bar{r}_0 \frac{\Gamma\{(t+5)/s\}\,\Gamma\{(t+1)/s\}}{\Gamma\{(t+4)/s\}\,\Gamma\{(t+2)/s\}} \qquad \ldots.[59]$$

and the ratio $\bar{r}_0'/b$ is shown as a function of s for $t=s-4$ in *Figure 6*. *Figures 4* to *6* are useful for relating a and b to s and to the number-weighted average ($\bar{r}_0$) and mass-weighted average ($\bar{r}_0'$) droplet radii.

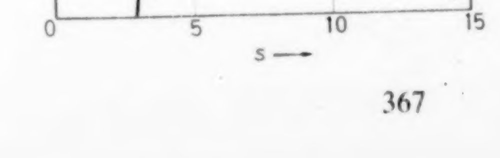

Figure 5. The ratio $\bar{r}_0'/b$ ($\bar{r}_0$ = initial mass-weighted average droplet radius) as a function of the exponent s for the Rosin–Rammler drop-size distribution

The distribution function given in equation 48 approaches a uniform distribution as $t \to \infty$. It is seen from equations 57 and 58 that in this limiting case $b = r_0$ and $a = \frac{1}{3}$. The reaction rate expression given in equation 56 is then found to be

$$\frac{dY}{dx} = \frac{3X(1-Y_{R,0})}{\pi r_0^2}\left[1 - \frac{1}{3}\left(\frac{Y-Y_{R,0}}{1-Y_{R,0}}\right)\right]$$

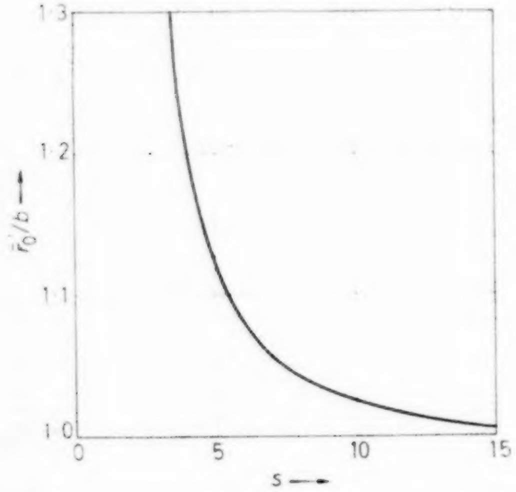

Figure 6. The ratio $\bar{r}_0'/b$ ($\bar{r}_0'$ = initial number-weighted average droplet radius) as a function of the exponent s for the Rosin Rammler drop-size distribution

Since $\hat{x}$ was assumed to be small in the derivation of equation 56, it follows that

$$\left[1 - \frac{1}{3}\left(\frac{Y-Y_{R,0}}{1-Y_{R,0}}\right)\right] \simeq \left(\frac{1-Y}{1-Y_{R,0}}\right)^{1/3}$$

to the same degree of accuracy as equation 56. Hence we find for uniform droplets the result

$$\frac{dY}{dx} = \frac{3X}{\pi \bar{r}_0^2}(1-Y_{R,0})^{2/3}(1-Y)^{1/3}$$

which is identical with equation 27 for uniform droplets with $Y_{R,0} = 0$.

For arbitrary size distributions we may similarly use the approximation

$$1 - a\left(\frac{Y-Y_{R,0}}{1-Y_{R,0}}\right) \simeq \left(\frac{1-Y}{1-Y_{R,0}}\right)^a \qquad \ldots . [60]$$

in order to obtain from equation 56 the general rate expression

$$\frac{dY}{dx} = \frac{3(1-Y_{R,0})^{1-a}}{b^2}(1-Y)^a \frac{X}{\pi} \qquad \ldots . [61]$$

Reference to equation 61 shows that the effective order of the heterogeneous reaction with respect to $1-Y$ is a. The effective order of reaction with respect to $1-Y$ therefore depends upon the shape of the droplet size distribution curve and is always greater than one third. This conclusion is, of course, valid only when $\hat{x}$ is small; for larger values of $\hat{x}$ it is, in general, impossible to define a constant order for the overall reaction rate.

(c) *Comparison between calculated reaction rates and reaction rates derived from measured pressure profiles*

In fitting equation 56 to the reaction-rate profiles derived from pressure measurements, we must again consider three separate cases, namely, injection of liquid bipropellants, injection of liquid fuel and gaseous oxidizer, and injection of gaseous fuel with liquid oxidizer.

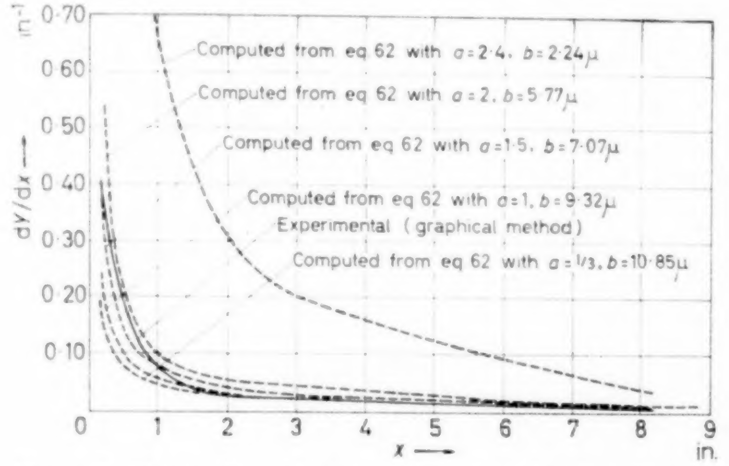

Figure 7. Comparison of the reaction rates dY/dx *computed graphically and from equation 62 for various values of the injector parameters a and b for a representative motor test, assuming burning of liquid fuel droplets with liquid oxidizer droplets*

(1) *Injection of liquid propellants*—The dY/dx versus x curve derived from the experimental pressure profiles has been replotted from *Figure 1* in *Figure 7*. For $Y_{R,0} = 0$, equation 56 becomes

$$\frac{\mathrm{d}Y}{\mathrm{d}x} = 3 \times 10^{-3} \frac{(1 - aY)}{vb^2} \ln\left(1 + \frac{(11\,800 + T - 12\,000\,Y)}{165}\right) \quad \ldots . [62]$$

where equation 26 has been used with appropriate numerical values. Data calculated from equation 62 for selected values of a and b are also shown in *Figure 7*. It is apparent from *Figure 7* that the values $a = 1{\cdot}8$ and $b = 6$ microns constitute acceptable choices for these parameters. Hence it follows, in particular, that the diverging reactor data are consistent with $s = 4{\cdot}3$, $\bar{r}_0 = 4{\cdot}3$ microns and $\bar{r}_0' = 7{\cdot}0$ microns for the Rosin–Rammler drop-size distribution function. It is interesting to observe that this 'best' estimate for $\bar{r}_0$ is only slightly smaller than the 'best' value deduced for the spray composed of uniform droplets (compare *Figure 1*). The exponent $s \simeq 4$ lies in the centre of the range of exponents (3 to 5) observed in impingement atomization experiments[1]. The use of two adjustable parameters (see *Figure 7*) allows a better fit than the use of a single adjustable parameter (see *Figure 1*). Results similar to those shown in *Figures 1* and *7* have been obtained for experimental data other than those described in the present report.

(2) *Injection of liquid fuel and gaseous oxidizer*—Representative results derived from pressure measurements on the assumption that the injected oxidizer vaporizes instantaneously have been plotted in *Figure 2*. In order to carry out the corresponding theoretical reaction-rate calculation, we note that for fuel droplets the boiling temperature is approximately $T_l = 400$ °K. Since $\rho_l = 0{\cdot}8\ \mathrm{g/cm^3}$ and $\lambda = 0{\cdot}64 \times 10^{-4}$ cal/cm.sec. °K, we find in the present case that

$$X\,(\mathrm{cm^2/sec}) = 2 \times 10^{-4} \ln\left[1 + (T - 400 + 7\,700\,Y_R)/200\right] \qquad \ldots .[63]$$

where, according to equation 15,

$$Y_R = (1/0{\cdot}22)\,(Y_{R,o} - 0{\cdot}78\,Y) \qquad \ldots .[64]$$

Equation 56 becomes now

$$\frac{\mathrm{d}Y}{\mathrm{d}x} = 6 \times 10^{-4}\,\frac{(1 - Y_{R,o}) - a\,(Y - Y_{R,o})}{\pi b^2}\ln\left(1 + \frac{T - 400 + 7\,700\,Y_R}{200}\right) \qquad \ldots .[65]$$

Results calculated from equations 64 and 65 are shown in *Figure 2* for selected values of a and b. Acceptable results are $a = 3$ and $b = 10$ microns, i.e. the apparent size distribution is less uniform than for liquid injection and the apparent average droplet radius has been increased by a factor of about two relative to the data obtained for liquid bipropellant injection.

(3) *Injection of gaseous fuel and liquid oxidizer*—A typical $\mathrm{d}Y/\mathrm{d}x$ versus x curve obtained from the measured pressure profiles for instantaneous evaporation of the fuel droplets has been shown in *Figure 3*. Assuming $T_l = 90$ °K, $\rho_l = 1{\cdot}14\ \mathrm{g/cm^3}$, and $\lambda = 0{\cdot}68 \times 10^{-4}$ cal/cm.sec. °K, it is now found that

$$X = 1{\cdot}5 \times 10^{-4} \ln\left[1 + (T - 90 + 27\,000\,Y_R)/127\right] \qquad \ldots .[66]$$

where

$$Y_R = (1/0{\cdot}78)\,(Y_{R,o} - 0{\cdot}22\,Y) \qquad \ldots .[67]$$

Also equation 56 reduces to

$$\frac{\mathrm{d}Y}{\mathrm{d}x} = 4{\cdot}5 \times 10^{-4}\,\frac{[(1 - Y_{R,o}) - a\,(Y - Y_{R,o})]}{\pi b^2}\ln\left(1 + \frac{T - 90 + 27\,000\,Y_R}{127}\right) \quad \ldots [68]$$

in the present case. The use of representative values of a and b in equation 68 shows that equation 68 correlates the results derived from pressure-profile determinations for $a = 1{\cdot}5$ and $b = 6{\cdot}3$ microns, i.e. the apparent drop-size distribution is more uniform and the droplets are smaller than for the model based on rapid evaporation of the oxidizer droplets.

CONCLUDING REMARKS

The correlations of measured pressure profiles obtained for the diabatic motor by using calculations appropriate for either premixed gaseous reactants[1] or for heterogeneous burning have not led to conclusive evidence concerning the nature of the combustion reactions. In general, the number of adjustable parameters is sufficiently large to permit a reasonably successful fit of pressure profiles for all of the assumed models. Significant progress on the determination of reaction rates from diverging reactor data clearly requires supplementary experimental information. Furthermore, the interpretative job can be greatly simplified by performing experimental studies on any of the following systems: premixed gaseous reactants, liquid fuel droplets injected with a gaseous oxidizer, or liquid oxidizer droplets injected with a gaseous fuel. For each of these types of propellants we presumably understand at least the important qualitative features of the combustion reactions, a statement which is unfortunately not true for bipropellant liquid reactants.

Gruen Applied Science Laboratories Inc.,
Western Division, Pasadena, Calif.

Rocketdyne, North American Aviation Corpn,
Canoga Park, Calif.

(*Received October 1958*)

REFERENCES

GILL, G., ECKEL, E. F., WILLIAMS, F. A. and PENNER, S. S. 'Determination of rocket motor combustion parameters by means of a diverging reactor', *Seventh Symposium (International) on Combustion*, p 712. Butterworths: London, 1959

PENNER, S. S. and WILLIAMS, F. A. *Tech. Rep. No. 19, Contract* DA 04-495-Ord 446. Calfornia Institute of Technology, Pasadena, Calif., May 1957

PENNER, S. S. *Chemistry Problems in Jet Propulsion*, p 295. Pergamon: London, 1957

WILLIAMS, F. A. *Ph.D. Thesis*, California Institute of Technology, Pasadena, Calif., June 1958

WILLIAMS, F. A. *J. chem. Phys.* 1959, **30**, 1017

Similarity Criteria for the Study of Furnace Flames by Means of Cold Models

G. G. THURLOW

The use of cold, isothermal models to study the behaviour of industrial furnace flames is increasing. There is no doubt about the value of this technique but there is a danger that it may be applied without due consideration being given to its limitations. The conditions necessary to get similarity between a model and a furnace have, therefore, been considered in detail. The criteria developed are similar to those derived more inductively by earlier workers but the more formal approach illuminates the conditions under which these can be applied. Criteria are derived for two cases dependent on whether the momentum of the secondary air is appreciable or not. The first case is thought not to have been treated before.

Tests are reported on a small gas-fired furnace and a cold model of similar overall dimensions. Conditions in the small furnace exaggerate some of the difficulties in the use of model techniques, and the problems of buoyancy are particularly discussed. Errors due to the incorrect estimation of the mean flame temperatures are also investigated. It is concluded that reasonable agreement between the mixing of fuel and air in a hot and a cold furnace can often—though not always—be obtained though it is emphasized that this is unlikely to be better than of the order of ±20 per cent.

INCREASING use is being made of various forms of cold models in order to study the behaviour of industrial furnace flames. These experiments are based on the assumption that, in most such flames, the mixed air and fuel combine so fast chemically that their rate of combustion is determined by the rate at which they mix. Hence, if the rate of mixing can be measured in suitably scaled cold models, the rate of combustion can be predicted.

It is, of course, most important to determine the necessary criteria for designing the models.

M. W. THRING and M. P. NEWBY[1] derive similarity conditions for a turbulent free jet assumed to have conical form and constant density. They apply these similarity conditions to enclosed jets by analogy with the free jet claiming that the amounts of recirculation may be made similar. The first part of the present paper aims at redeveloping these results by providing a generalized theory of similarity between hot and cold furnace models. The second part of the paper compares mixing in a simple furnace and in a cold model as a check of the use of these criteria.

THEORY OF SIMILARITY BETWEEN HOT AND COLD SYSTEMS

Approach

The true velocity pattern in the enclosed jet is considered, in the following treatment, to be made up of the averaged velocity pattern on which is imposed a turbulence field with no general flow direction. A hypothetical non-turbulent jet is first considered and the flow pattern and mixing due to the averaged velocity field alone determined. The influence of the turbulence field on this is then assessed and the necessary conditions for relating mixing to turbulence determined without actually determining the form of this influence.

This leads to conditions that obviously cannot be maintained throughout a flame. It is shown that similarity can only be considered in that region—called the 'body'—of a flame in which the temperature can be assumed constant. The conditions in a cold model for which the velocity and concentration patterns on the boundary between the body of the flame and the region nearer the nozzle will be proportional to their counterparts in the furnace are then determined assuming that the momentum of the flame up to this region is conserved. From these, the necessary similarity criteria can be found.

The non-turbulent jet

The concentration C of the nozzle fluid at any point P (x, y, z) in the furnace, is given by

$$C_{(x,\,y,\,z)} \equiv \frac{(\text{Mass density of fuel at P})}{(\text{Total mass density at P})}$$

Here x is defined as the longitudinal coordinate as measured from the fuel nozzle and y, z as the transverse coordinates.

It is assumed that the prototype and model are geometrically similar and, hence, for corresponding points,

$y/x\,(\equiv\theta)$ and $z/x\,(\equiv\varphi)$ are equal in full scale and model.

If $\lambda \equiv$ (size of model)/(size of original) and if subscripts c and h denote the properties of the cold model or hot furnace respectively, there is by definition similarity between a cold model and hot furnace if and only if

$$C_{(x,\,\theta,\,\varphi)_h} = C_{(\lambda x,\,\theta,\,\varphi)_c} \qquad \ldots.[1]$$

at all points in the body of the flame. It is convenient to describe the turbulent velocity field $V_{(x,\,\theta,\,\varphi)}$ in terms of an averaged velocity field $U_{(x,\,\theta,\,\varphi)}$ and a turbulence field $W_{(x,\,\theta,\,\varphi)}$, i.e.

$$V_{(x,\,\theta,\,\varphi)} = U_{(x,\,\theta,\,\varphi)} + W_{(x,\,\theta,\,\varphi)} \qquad \ldots.[2]$$

where $$U_{(x,\,\theta,\,\varphi)} = \int_r V_{(x',\,\theta',\,\varphi')}\,\mathrm{d}r' \Big/ \int_r r\,\mathrm{d}r'$$

The centre of the volume r is (x, θ, φ) and the volume is assumed just sufficiently large so that any small increase will not substantially change the direction or magnitude of V. W is then, according to equation 2, the difference between V and U and is a completely turbulent field with no general flow direction. The hypothetical case $W = 0$ may be studied exactly by applying the law of conservation of matter, both to the 'air' and to the 'fuel jet' streams, the density being a function of position. It is found that the concentration gradient is always perpendicular to the velocity field.

In fact, for these particular conditions, the concentration of any small fluid volume dv will always remain the same and mixing between adjacent streams of fluid does not occur. Thus, if the concentration distributions of two systems are equal on some cross section $x=x_1$ of the furnace, the pattern of concentration will be equal throughout the whole body of the furnace if the velocity patterns are equal.

Effects of turbulence

The prime effect of turbulence (and, in so far as it is important, of molecular diffusion) is to blur the concentration field. Hence, the actual concentration on any cross section $x=x_1+\delta x_1$ is that which would have been transported from $x=x_1$ in the absence of turbulence but for a blurring of the concentration gradients. One may thus approximate to the actual concentration by a series of small transport steps each followed by the appropriate small blurring. The result of this step process is, of course, a very different concentration field from that derived in the non-turbulent case.

It is clear that to obtain similarity between a hot furnace and a cold model both the blurring and the direct transfer of concentration must be the same at all points. It can be shown that one of the necessary requirements is similarity of Reynolds number and hence

$$\frac{\rho_{(\lambda x,\,\theta,\,\varphi)_c}}{\eta_{(\lambda x,\,\theta,\,\varphi)_c}}=\frac{\rho_{(x,\,\theta,\,\varphi)_h}}{\eta_{(x,\,\theta,\,\varphi)_h}}\,\frac{1}{\lambda k} \qquad \ldots .[3]$$

where ρ and η are respectively density and absolute viscosity and k is the ratio of the velocity U in the cold model to that in the hot furnace. The other requirement follows from the fact that, in the absence of net matter transport by the W field, the velocity and density fields can be related by the expression

$$\operatorname{div} \rho \boldsymbol{U}=0 \qquad \ldots .[4]$$

By expanding and applying the above expression to the hot and cold cases and equating, it can be shown that

$$\rho_{(\lambda x,\,\theta,\,\varphi)_c}/\rho_{(x,\,\theta,\,\varphi)_h}=A \qquad \ldots .[5]$$

where A is a constant. Hence, from equation 3,

$$\frac{\eta_{(\lambda x,\,\theta,\,\varphi)_c}}{\eta_{(x,\,\theta,\,\varphi)_h}}\,\frac{1}{\lambda k}=A \qquad \ldots .[6]$$

This condition is too severe to be applied throughout any furnace owing to the density change on combustion. However, a compromise may be reached by relaxing the similarity condition (equation 1) somewhat, and restricting the region in which similarity is attempted.

Relaxation of similarity conditions

In a furnace, the gas expands very rapidly as its temperature rises on combustion and the density alters considerably as a result of both this and chemical combination. However, it is often possible to restrict the region in which we try to simulate the hot furnace by the cold model to regions where the density of hot gas is reasonably constant. It has been shown[2] that much of the change of density in furnaces occurs close to the jet nozzle, and if this zone is neglected it is possible to attempt to attain similarity to a tolerable approximation over the remaining region (body) where the ratio of the hot and cold densities is reasonably constant. The changing density region is termed the 'nozzle region' and the surface dividing the two regions the 'body boundary'.

It is assumed that the aerodynamic characteristics of the jet within the nozzle region in the furnace are similar to the isothermal case and are not affected by the walls. In other words the jet profile in the nozzle region is taken as that of a free jet. This is not necessarily true in practice; and recent large scale trials on an open hearth furnace[3] have suggested that the angle of the hot jet is less than the isothermal case. However, this assumption must be made at this stage since use is made of the fact that, except close to the nozzle (less than six nozzle diameters), the profiles of velocity, etc. across all free jets are similar as long as the flow rates are fully turbulent[1]. Consideration of the case where the above assumption cannot be accepted is given below.

It can be shown from dimensional considerations that, if the shapes of the velocity, density, viscosity and concentration profiles on the body boundary are equal in two cases, then the assumption of similarity of Reynolds number in the body of the flame implies that the velocity and concentration fields throughout this volume are similar. From equations 3 and 6, the Reynolds numbers throughout the body will be similar if they are similar on the body boundary. Since it is necessary that the velocity profiles on the boundary be made similar, it follows that the total mass flow in the model

$$M_c = \lambda\,(\eta_c/\eta_h)\,M_h$$

Conditions in jet nozzles

One must next ensure that the necessary profiles at the body boundary are similar. It will be assumed that, as the jets do not hit the walls within the nozzle region, momentum will be conserved. Thus, not only the mass flow rates but also the momentum flow rates on the body boundary will be equal to those at the jet. Owing to the random directions of the turbulent field W it can be assumed that this leads to no net mass or momentum transfer and hence, as before, U can be treated as the complete velocity field as far as momentum conservation is concerned.

Let ρ_{jf} be the fuel density at the jet nozzle; ρ_{ja}, the (secondary) air density at the air entry; ρ_b, the density of the gases in the body of the flame; r_f, the fuel-jet radius; and r_a, the overall radius of air jet (assumed concentric with fuel jet). From the conservation of matter, the total mass flow rate from the jet is equal to that at the body boundary.

$$\int_0^{r_f} 2\rho_{jf} U r\,\mathrm{d}r + \int_{r_f}^{r_a} 2\rho_{ja} U r\,\mathrm{d}r = \frac{M}{\pi}$$

or, defining $\overline{U_f}$ and $\overline{U_a}$,

$$\rho_{jf} r_f^2 \overline{U_f} + \rho_{ja} (r_a^2 - r_f^2) \overline{U_a} = M/\pi \qquad \ldots.[7]$$

Similarly, for the momentum flow rates we obtain, defining $\overline{U_f^2}$ and $\overline{U_a^2}$,

$$\rho_{jf} r_f^2 \overline{U_f^2} + \rho_{ja} (r_a^2 - r_f^2) \overline{U_a^2} = \frac{1}{\pi} \iint\limits_{\text{body boundary}} \rho_b U_b^2 \, \mathrm{d}S \qquad \ldots.[8]$$

Since, as discussed above, similarity between both the densities and velocity distributions on the body boundary of the cold and hot models is assumed, it is possible to put

$$\frac{\iint \rho_{bc} U_{bc}^2 \, \mathrm{d}S_c}{\iint \rho_{bh} U_{bh}^2 \, \mathrm{d}S_h} = \left(\frac{M_c}{M_h}\right)^2 \frac{\rho_{bh}}{\rho_{bc}} \lambda^{-2}$$

Hence from equation 8

$$\frac{\rho_{jfc} r_{fc}^2 \overline{U_{fc}^2} + \rho_{jac} (r_{ac}^2 - r_{fc}^2) \overline{U_{ac}^2}}{\rho_{jfh} r_{fh}^2 \overline{U_{fh}^2} + \rho_{jah} (r_{ah}^2 - r_{fh}^2) \overline{U_{ah}^2}} = \lambda^{-2} \frac{M_c^2 \rho_{bh}}{M_h^2 \rho_{bc}} \qquad \ldots.[9]$$

Similarly from equation 7

$$\frac{\rho_{jfc} r_{fc}^2 \overline{U_{fc}} + \rho_{jac} (r_{ac}^2 - r_{fc}^2) \overline{U_{ac}}}{\rho_{jfh} r_{fh}^2 \overline{U_{fh}} + \rho_{jah} (r_{ah}^2 - r_{fh}^2) \overline{U_{ah}}} = \frac{M_c}{M_h} \qquad \ldots.[10]$$

It is obvious that the limiting concentrations after complete mixing must be the same on both model and full size and hence the air/fuel ratios must be the same in both hot and cold cases, so that from equation 10

$$\frac{M_c}{M_h} = \frac{\rho_{jfc} r_{fc}^2 \overline{U_{fc}}}{\rho_{jfh} r_{fh}^2 \overline{U_{fh}}} \qquad \ldots.[11]$$

The general case given by equations 9 and 11 is discussed in Appendix I. The common and more simple case where the air momentum may be neglected is now considered.

By neglecting the momentum carried by the secondary air, equation 9 becomes

$$\frac{\rho_{jfc} r_{fc}^2 \overline{U_{fc}^2}}{\rho_{jfh} r_{fh}^2 \overline{U_{fh}^2}} = \left(\frac{M_c}{M_h}\right)^2 \frac{\rho_{bh}}{\rho_{bc}} \lambda^{-2} \qquad \ldots.[12]$$

It is assumed that the velocity profiles across the jet are similar in both the model and the full scale and hence that

$$\overline{U_{fc}^2} / \overline{U_{fh}^2} = (\overline{U_{fc}})^2 / (\overline{U_{fh}})^2$$

Hence equations 11 and 12 can be solved for r_{fc}/r_{fh} giving

$$\left(\frac{r_{fc}}{r_{fh}}\right)^{-2} = \frac{\rho_{jfc}}{\rho_{jfh}} \frac{\rho_{bh}}{\rho_{bc}} \lambda^{-2}$$

i.e.

$$r_{fc} = \lambda r_{fh}\left(\frac{\rho_{bc}\rho_{fh}}{\rho_{bh}\rho_{fc}}\right)^{1/2} \qquad \ldots . [13]$$

If the same gas at the same nozzle temperature is used in the cold model as in the hot

$$\rho_{fh} = \rho_{fc}$$

and

$$r_{fc} = \lambda r_{fh}(\rho_{bc}/\rho_{bh})^{1/2} \qquad \ldots . [14]$$

which is the result quoted by Thring and Newby.

If the secondary air is also supplied at the same density to the hot and cold model, then, as shown in the Appendix, similarity can be obtained, even if its momentum cannot be neglected, by enlarging the cold air nozzle radius by the same factor, that is to say

$$r_{ac} = \lambda r_{ah}(\rho_{bc}/\rho_{bh})^{1/2} \qquad \ldots . [15]$$

Effect of differing jet angles between hot and cold cases

It is necessary to rely on experimental data on the similarity of turbulent free jets to confirm or otherwise that, at similar momentum rates, the velocity and concentration fields will be in fact proportional within the nozzle region. This is, of course, in spite of the fact that the flow may be either isothermal or with a continuously changing density and as mentioned earlier, there is some evidence that, in fact, this assumption is not justified.

It is not the purpose here to discuss the validity or otherwise of the available experimental evidence on the rate of spread of turbulent jets, but it is relevant to consider what can be done in such cases as that found in recent work on the open hearth furnace[3] where the jet angle in the furnace was measured at 16° compared with 25° in the model. While observations of this nature must throw doubt on the general validity of the arguments given in the previous section, it is possible that a compromise can be reached which will be sufficiently reliable for the accuracy anticipated in model work. It seems logical to ensure at least that the spread of the jet at the body boundary on the model is the same as in the furnace even though the actual distributions may no longer be completely similar. To do this, it is necessary to reduce the linear scale on the model in the direction of flow over the length of the nozzle region in proportion to the ratio of the tangents of the half-angles of the cold and hot jets.

Some justification for this suggestion can be found by considering the results obtained on the open hearth furnace[3]. A comparison of the axial mixing in model and furnace gives the results as shown in *Table 1*. The

Table 1. Comparison of axial mixing in model and open hearth furnace (using data of A. Hogg *et al.*[3]*)*

Distance from burner tip (ft)	15	20	30	40	50
Air/fuel ratio (lb/lb) on furnace	7·5	8·8	11·0	14·0	16·5
On model (15% excess air)	9	10·5	13·5	15·5	16·0
On model (corrected as above for jet angle)	7·6	9·2	12·2	15·0	16·0

lower line shows the effect of correcting the results on the model in accordance with the above suggestion though, of course, the model itself was not foreshortened.

Similarity criteria

It is now possible to collect the necessary conditions for similarity within the body of a flame.

(*1*) If it is assumed that the jet in the nozzle region in the hot furnace can be represented by the isothermal case, conditions at the body boundary are simulated if: (*a*) where the air and the fuel have the same *initial* densities in the cold case as they do in the hot, the jet-nozzle radii of both fuel and air are reduced such that

$$r_c = \lambda r_h (\rho_{bc}/\rho_{bh})^{1/2} = \lambda r_h (\rho_{jh}/\rho_{bh})^{1/2}$$

That is, they should be increased by the square root of the ratio of the density of the fluids at the jet to the density of the hot flame; (*b*) when the air-jet momentum is negligible, this condition need only be applied to the fuel jet; (*c*) in the general case, the radii of the fuel and air nozzles are reduced such that

$$r_{fc} = \lambda r_{fh} [(\rho_{bc}/\rho_{bh})(\rho_{jfh}/\rho_{jfc})]^{1/2}$$

$$r_{ac} = \lambda r_{ah} \left\{ \frac{\rho_{bc}}{\rho_{bh}} \left(\frac{\rho_{jah}}{\rho_{jac}} \left[\frac{r_{ah}^2}{r_{fh}^2} - 1 \right] + \frac{\rho_{jfh}}{\rho_{jfc}} \right) \right\}^{1/2}$$

(*2*) Should the jet angles in the hot and cold cases be different, some compromise is possible by reducing the linear scale on the model in the direction of flow over the length of the nozzle region in proportion to the ratio of the tangents of the half-angles of the cold and hot jets.

(*3*) Conditions are then simulated with the body of the flame if: (*a*) the densities are proportional throughout this region, (*b*) the viscosities are proportional throughout this region, (*c*) the air/fuel ratio by mass is the same, and (*d*) the ratio of the mass flow is similar to the ratio of viscosities. This last requirement follows from the need for Reynolds number similarity.

It should be mentioned that it has been shown by M. W. THRING[1, 4] and others that, if the gases are very turbulent, the effect of changes in Reynolds number is very small and this criterion can be neglected.

EXPERIMENTAL COMPARISON BETWEEN HOT AND COLD MODELS OF SIMILAR OVERALL SIZE

The criteria derived above were used in a comparison between a small gas-fired furnace and a cold model of the same overall dimensions; the object of the tests was to confirm experimentally the amount of similarity that can be attained.

It should be pointed out immediately that a small furnace poses problems rather different to those of a large industrial plant. In particular, the degree of turbulence is less and the Reynolds numbers involved are much smaller.

To some extent, therefore, the problems met with in this comparison may be rather specialized, though, at the same time, it should not be assumed that they can be neglected in larger furnaces without further confirmation.

Tests on the hot furnace

The furnace consisted of a cylinder 40 in. long and 5 in. in internal diameter. The original unit, cast in refractory with walls 3½ in. thick, formed the combustion chamber of the Evaluator furnace used to study flame characteristics on a small scale and described elsewhere[1]. Most of the experimental work described here, however, was carried out on a second furnace, similar inside, but 9 in. square on the outside and built from refractory bricks. The fuel jet, which was a plain refractory tube, was on the axis of the cylinder, the burner tip being located 5½ in. beyond the air entry in the chamber. The air was delivered through a pipe 2 in. in diameter, concentric with the burner and finishing flush with the base of the furnace. It was found necessary to fill the bottom of the chamber with a 2 in. layer of ball bearings in order to give an even flow of air across the whole width of the furnace. A note on the effect of removing the layer of ball bearings, so giving a significant momentum to the secondary air, is given in Appendix II.

Town's gas was used as fuel, and the air/fuel ratio was 6·5 : 1 by volume (30 per cent excess air). Tests were carried out using internal nozzle diameters of $\frac{3}{8}$ and $\frac{3}{16}$ in. with gas rates of between 1·2 and 1·54 ft^3/min. Tests in free air showed that all these flames were turbulent, the lowest Reynolds number at the nozzle being 3 100 (with the $\frac{3}{8}$ in. nozzle at a gas rate of 1·2 ft^3/min).

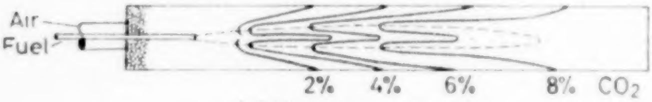

(a) Mounted vertically

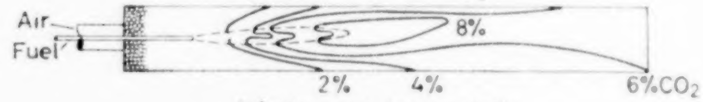

(b) Mounted horizontally

Figure 1. Comparison of flames in furnace when mounted (a) *vertically, and* (b) *horizontally. Gas rate, 1·54* ft^3*/min; air/fuel ratio, 6·5 : 1; nozzle diameter,* $\frac{3}{16}$ *in.*

The progress of combustion of the flame was studied by means of traverses of carbon dioxide and oxygen concentration at different positions above the flame. The oxygen concentrations were measured by a Cambridge magnetic oxygen meter and recorder. The carbon dioxide concentration was measured using a Fyrite apparatus, this being checked against an Orsat gas analyser.

Tests were carried out initially with the cylinder mounted vertically but, for the reasons discussed below, these were repeated with the furnace horizontal. *Figure 1* shows the carbon dioxide concentration curves for the $\frac{3}{16}$ in. diameter nozzle, mounted both horizontally and vertically.

Table 2 summarizes the operating conditions and the observed flame length (as defined in the next section) for all the tests carried out.

Tests upon the cold furnace

The cold model was constructed of Perspex and mounted vertically. Nitrogen was used to represent the nozzle fluid and the rate of mixing was determined from traverses of oxygen concentration across the flame.

In order to calculate the flow rates and equivalent nozzle diameters in the nozzle using the similarity criteria, it was first necessary to assume an average flame temperature. The tests on the Evaluator, reported in ref. 5, suggested that a value of 850°C be used. However, subsequent measurements of the gas temperature (using suction pyrometers) carried out in the course of the tests on the hot furnace just described showed that, due to the increased insulation of the walls in the brick furnace compared with that of the original Evaluator made of solid refractory, a more realistic temperature would have been of the order of 1 100 to 1 200°C. In fact, for the purpose of this comparison, measured average flame temperatures were used in calculating the equivalent characteristics of the cold model even though, in an actual application of the technique, the value would have to be little more than a judicial guess. Two tests with an assumed mean flame temperature of 850°C are included for comparison.

The Reynolds number of the gases in the combustion chamber in the hot furnace can be calculated, using the estimated mean flame temperature and assuming that it can be represented by the normal 'flow in pipes' equation. Hence, the total volume flow of the cold gases in the model which would give a similar Reynolds number can be found and, thus, the nozzle fluid rate to be used in the cold model. The Reynolds number and equivalent fluid rates are given in *Table 2*.

The equivalent nozzle diameters were calculated from equation 13, allowance having to be made of course for the difference in density between nitrogen and air. The diameters used on the cold model are also given in *Table 2*.

It will be seen that five tests are reported. With equivalents to $\frac{3}{8}$ in. nozzle on the hot furnace, two runs were carried out which were similar except for the assumed mean flame temperature—in one case, 850°C and in the other 1 200°C. This latter run, together with the third test equivalent to the $\frac{3}{8}$ in. nozzle should simulate two runs on the hot furnace at gas rates of 1·54 and 1·2 ft^3/min respectively.

A similar comparison at a gas rate of 1·2 ft^3/min has been carried out between furnace and model with a hot furnace nozzle diameter of $\frac{3}{16}$ in. Finally, a run is reported which is equivalent—except for a small deviation in gas rate—to the run reported above with an assumed mean flame temperature of 850°C but with the smaller nozzle diameter.

ESTIMATION OF FLAME LENGTH

As the fuel moves from the jet, it meets oxygen and begins to burn. Close to the burner, the fuel is in excess and the rate of combustion is limited by the availability of oxygen. Eventually, however, a point is reached at

Table 2. Summary of tests carried out

	$\frac{3}{8}$ in. diameter nozzle					*$\frac{3}{16}$ in. diameter nozzle*			
	Hot model		*Cold model*			*Hot model*		*Cold model*	
Direction of mounting	*Vert.*	*Horl*	*Vert.*	*Vert.*	*Vert.*	*Vert.*	*Horl*	*Vert.*	*Vert.*
Actual or equivalent gas rate, ft³/min	1·54	1·2	1·54	1·54	1·2	1·3	1·2	1·5	1·2
Measured or estimated average flame temperature, °C	1 200	1 100	850	1 200	1 100	1 100	1 100	850	1 100
r_e/r_h			1·33	1·5	1·45			1·33	1·45
Equiv. nozzle diameter, in.			0·5	0·56	0·54			0·25	0·27
Nozzle fluid rate, ft³/min			0·4	0·34	0·28			0·4	0·28
R_e *(nozzle)*	4 000	3 100	1 360	1 030	880	6 650	6 150	2 700	1 750
R_e *(furnace)**	1 250	970	1 010	860	710	1 050	970	1 010	710
Measured flame length, in.	27	23	26	18	19 *to* 20	27	12	14	12

*Assuming complete combustion.

which the fuel has met with sufficient oxygen for combustion to be complete. At this point, the fuel and air which have mixed will be in the stoichiometric proportions and the carbon dioxide content of the mixture will be the maximum theoretical value.

This argument ignores the effect of local turbulence. Due to this, the position at which the instantaneous fuel/air ratio is stoichiometric will fluctuate. The average fuel/air ratio over a reasonably long time interval will, however, be stoichiometric at one particular point. The argument is not invalidated by the presence of recirculation which, in effect, brings back into the flame sufficient air to compensate for the carbon dioxide it contains.

The oxygen content of the gas mixture within the curve made by joining the points of stoichiometric mixing will be zero (except for that brought in by local turbulence close to the boundary as just discussed). The carbon dioxide within the envelope cannot be precisely evaluated unless the combustion processes are known. Near to the outside, however, it is reasonable to assume that the carbon in the fuel is burnt to carbon dioxide rather than carbon monoxide and that there is no selective combustion. If the changes of volume due to combustion are small the carbon dioxide content can then be taken as $p(1-C)/(1-C_s)$ per cent by volume, where C is the proportion of fuel which has mixed, C_s is the proportion of fuel to give stoichiometric mixing, and p is the carbon dioxide content of the waste gases resulting from the combustion of fuel and air in stoichiometric proportions.

Outside the envelope, where there is excess air the oxygen content is given by $20(1-C/C_s)$ per cent by volume and the carbon dioxide content by $p\,C/C_s$ per cent by volume.

It is obvious that, in any mixture with an excess of oxygen, the carbon dioxide content of the gases at any point will be directly proportional to the amount of fuel which has combined with the air to form the mixture at that point. This fuel may have mixed with the air during the passage of the constituents outwards from the burner or may have formed part of the product recirculated back to the point under consideration from the tail of the flame. In fact, the above equations do give the relationships between the mixing of nozzle fluid and air (as given by the cold model tests) and the carbon dioxide content that would have resulted from combustion.

The flame length has been taken as the distance from the burner to the point at which the carbon dioxide content of the gas on the flame axis reaches a maximum, i.e. the point where the envelope of maximum carbon dioxide (on the hot furnace) or stoichiometric mixing (on the cold model) crosses the axis. The values obtained are shown in *Table 2*.

DISCUSSION

Buoyancy

It has been appreciated by most workers who have used model techniques to study furnace design that simulation of the buoyancy effect due to the difference in density between the flame and the surrounding gas is not achieved. This effect is, naturally, most marked in a flame fired vertically and it is apparent from the results given in *Table 2*, that, due to buoyancy, there is no significant agreement between the vertically mounted hot furnace and the equivalent cold model.

The effect of buoyancy on flames fired horizontally cannot be ignored, particularly in a low velocity jet where the vertical displacement of the flame can alter radically the flow pattern predicted from an isothermal model. Various workers have studied this problem[6, 7] and shown the magnitude of the axial deflections that occur. Both papers referred to give correlations based on model data though they agree that it is difficult to derive accurate, comprehensive formulae. The effect of the momentum of the jet is well illustrated by the tests on the horizontal furnace summarized in *Table 2*. *Figure 1* shows the displacement with the 3/16 in. diameter nozzle. It will be noticed that, in this case, combustion is completed while the flame is acting effectively as a free jet and it is to be expected that the effect of buoyancy in the similarity between hot and cold model will be small.

Tests using the 3/8 in. diameter nozzle, however, showed that the flame was impinging on the roof before combustion was completed whilst the displacement of the flame resulted in sufficient segregation in the fuel and air currents to hamper the mixing. In fact it was found that appreciable differences in flame length could be obtained by depressing or raising the burner nozzle, so affecting the degree of impingement of the flame on the roof. The length of flame obtained in these trials was of the order of 30 to 40 in., appreciably longer than the equivalent cold model test and, again, no simulation can be claimed.

Estimated flame temperature

Table 2 shows that, in the one case where a direct comparison was carried out, the error in the estimated flame length due to incorrect estimation of the mean flame temperature was of the order of 10 per cent per 100°C error in estimated temperature. *Figure 2* shows the nozzle diameters and

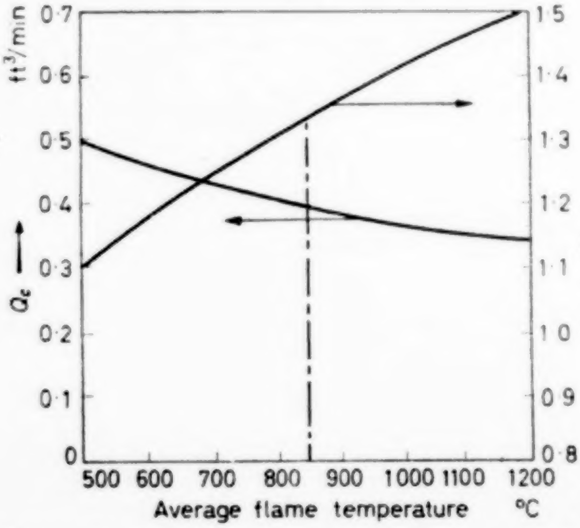

Figure 2. Flow rate and nozzle radius needed to simulate a flame by a cold model with various assumed average flame temperatures. Hot furnace burning town's gas at 1·5 ft³/min; cold furnace using nitrogen

flows to be used on the cold model to simulate various flame temperatures. It can be shown from this that the change in flame length due solely to the change in momentum from altering the nozzle diameter (at constant gas rate) is between 4 and 5 per cent per 100° C error in estimated temperature.

It would appear, therefore, that if it is desired to estimate the flame length to within 20 per cent, it is essential to estimate first the mean flame temperature to within 200° C.

The agreement between cold and hot model

In only two of the comparisons could the conditions in the hot furnace be reasonably well simulated in the cold model. These are summarized in *Table 3*.

Table 3. Agreement between hot and cold model

Gas rate ft³/min	*Nozzle diameter*	*Flame length, in.*		*% error in flame length of cold model*
		Hot flame	*Cold model*	
1·2	$\frac{1}{8}$ *in.*	23	19 *to* 20	13 *to* 17
1·2	$\frac{3}{16}$ *in.*	12	12	*Zero*

CONCLUSIONS

The mathematical treatment confirms the similarity criteria derived by Newby and Thring and emphasizes the inherent, basic assumption that the densities and viscosities in the model and the hot furnace should be proportional within the body of the flame. The fact that this is evidently not achieved in practice suggests that precise correlation between a cold model and a furnace is not possible. The effect of possible discrepancies between the behaviour of a flame and an isothermal free jet is considered and a tentative compromise solution to allow for this proposed.

The experimental work illuminates the need to estimate accurately the flame temperature. As the true temperature distributions through many industrial furnaces are not known it is probable that considerable errors may arise from this cause.

The effect of buoyancy is particularly marked in the low momentum flame tests and it is probably a fair generalization to state that the use of model techniques where combustion in the flame is not completed before it strikes the walls of the furnace is of doubtful value.

Within these limits—and it should be emphasized that this embraces many industrial furnaces—model techniques are both reliable and useful. While insufficient data have so far been obtained to enable the general level of accuracy to be assessed even for the particular case considered here, it should be borne in mind that the similarity in flow pattern between the hot furnace and cold model is unlikely to be better than of the order of, say, 20 per cent.

Mr D. Linden-Bell was responsible for the initial mathematical analysis and experimental work given in this paper. Later experimental work was carried out by Mr C. Tully.

The paper is published by permission of the Director-General of the British Coal Utilisation Research Association.

British Coal Utilisation Research Association,
Randalls Road, Leatherhead, Surrey

(Received December 1958)

APPENDIX I

Derivation of criteria for cases where the momentum of the secondary air cannot be neglected

The mass flow rates of the primary and secondary fluids, M_f and M_a, can be inserted into equation 9 using relationships of the form of equation 11.

Assuming that

$$\frac{\overline{U^2_{ac}}}{(U_{ac})^2}=\frac{\overline{U^2_{fc}}}{(U_{fc})^2}=\frac{\overline{U^2_{ah}}}{(U_{ah})^2}=\frac{\overline{U^2_{fh}}}{(U_{fh})^2}$$

this leads to the expression

$$\frac{\dfrac{1}{\rho_{jac}}\left(\dfrac{M^2_{ac}}{r^2_{ac}-r^2_{fc}}\right)+\dfrac{1}{\rho_{jfc}}\dfrac{M^2_{fc}}{r^2_{ac}}}{\dfrac{1}{\rho_{jah}}\left(\dfrac{M^2_{ah}}{r^2_{ah}-r^2_{fh}}\right)+\dfrac{1}{\rho_{jfh}}\dfrac{M^2_{fh}}{r^2_{ah}}}=\left(\frac{M_c}{M_h}\right)^2\frac{\rho_{bh}}{\rho_{bc}}\lambda^{-2}$$

As the air/fuel ratio must be the same in both hot and cold cases, this leads to

$$\frac{\dfrac{1}{1-\left(\dfrac{r_{fc}}{r_{ac}}\right)^2}+\dfrac{\rho_{jac}}{\rho_{jfc}}}{\dfrac{1}{1-\left(\dfrac{r_{fh}}{r_{ah}}\right)^2}+\dfrac{\rho_{jah}}{\rho_{jfh}}}=\frac{\rho_{bh}}{\rho_{bc}}\frac{\rho_{jac}}{\rho_{jah}}\left(\frac{r_{ac}}{r_{ah}}\right)^2\lambda^{-2} \qquad \ldots.[16]$$

Considering the system where air and fuel have the same initial densities in the cold as in the hot case

$$\rho_{jac}=\rho_{jah}, \quad \rho_{jfc}=\rho_{jfh}$$

Equation 16 is satisfied if

$$\frac{r_{fc}}{r_{fh}}=\frac{r_{ac}}{r_{ah}}=\lambda\left(\frac{\rho_{bc}}{\rho_{bh}}\right)^{1/2}$$

which is the result given in the text.

It can be shown that, for the general case,

$$\left.\begin{aligned}\frac{r_{fc}}{r_{fh}}&=\lambda\left(\frac{\rho_{bc}}{\rho_{bh}}\frac{\rho_{jfh}}{\rho_{jfc}}\right)^{1/2}\\ \frac{r_{ac}}{r_{ah}}&=\lambda\left\{\frac{\rho_{bc}}{\rho_{bh}}\left(\frac{\rho_{jah}}{\rho_{jac}}\left[\frac{r^2_{ah}}{r^2_{fh}}-1\right]+\frac{\rho_{jfh}}{\rho_{jfc}}\right)\right\}^{1/2}\end{aligned}\right\} \qquad \ldots.[17]$$

satisfy equation 16, as can be verified from that equation.

APPENDIX II

Tests with an appreciable momentum

A series of tests was carried out in the cold model without the ball-bearing layer. These tests gave a very short flame and calculations showed that the momentum of the air leaving the 2 in. diameter opening at the base of the furnace was of the same order as that of the nozzle fluid representing the fuel. It has already been stated in the theoretical part of this paper that the case of concentric jets is appreciably more complicated than when the momentum of the outer fluid flow can be neglected. In view of this, this investigation was not proceeded with at this stage. The preliminary results, however, are given for completeness and because they may have a bearing on subsequent investigations. Two nozzle sizes were studied with a wide range of flows. The change in nozzle diameter had no significant effect which may be due to the fact that the overall diameter of the two jets was not altered. It is more surprising that the range of flow rates studied also did not appear to affect the flame length; the only significant difference being due to air/fuel ratio. It was found in fact that all the results could be plotted as shown on *Figure 3* in terms of the air content of the fuel/air mixture.

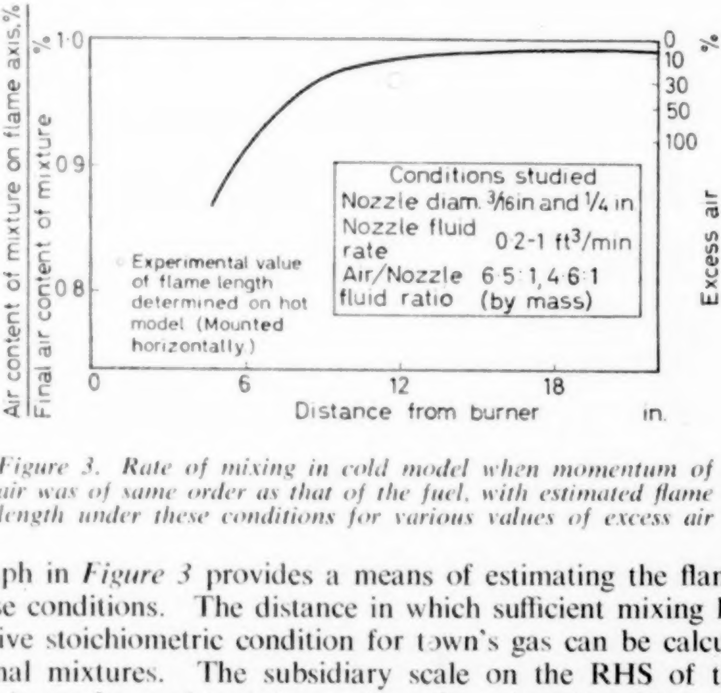

Figure 3. Rate of mixing in cold model when momentum of air was of same order as that of the fuel, with estimated flame length under these conditions for various values of excess air

The graph in *Figure 3* provides a means of estimating the flame length under these conditions. The distance in which sufficient mixing has taken place to give stoichiometric condition for town's gas can be calculated for various final mixtures. The subsidiary scale on the RHS of the graph of excess air can be used to estimate these flame lengths. Thus, at 30 per cent excess air, the estimated flame length is about 9 in. A rather rough experimental determination of flame length at this excess air value in the hot model mounted horizontally gave a value of the order of 12 inches.

REFERENCES

[1] THRING, M. W. and NEWBY, M. P. *Fourth Symposium (International) on Combustion*, p 789. Williams and Wilkins: Baltimore, 1953

[2] SUNAVALA, P. D., HULSE, C. and THRING, M. W. *Combustion & Flame*, 1957, **1**, 179

[3] Hogg, A., Holden, C. and Siddall, R. G. *Seventh Symposium (International) on Combustion*, p 639. Butterworths: London, 1959

[4] Johnstone, R. E. and Thring, M. W. *Pilot Plants, Models and Scale-up Methods in Chemical Engineering*, p 307. McGraw-Hill: New York, 1957

[5] Godridge, A. M., Thurlow, G. G. and Wallis, J. *J. Inst. Fuel*, 1958, **31,** 491

[6] Gray, F. A. and Robertson, A. D. *J. Inst. Fuel*, 1956, **29,** 424

[7] Horn, G. and Thring, M. W. *J. Inst. Fuel*, 1956, **29,** 437

The Limits of the Eigenvalue of the Laminar Flame Equation in Terms of the Reaction Rate–Temperature Centroid

J. Adler

The differential equation describing one-dimensional laminar flame propagation for temperature explicit reaction-rate functions is considered. It is shown that for a fixed centroid of the reaction-rate function, the burning velocity must lie within certain limits, which are independent of the type of reaction considered.

In a recent paper, D. B. Spalding[1] has derived a fitted equation which relates the burning velocity of a plane laminar flame to the centroid of the temperature-dependent reaction-rate function. The differential equation which defines the gradient of the dimensionless temperature, P, for a given reaction rate function $\phi(\tau)$ is

$$P\,\mathrm{d}P/\mathrm{d}\tau - P = -\lambda\phi(\tau) \qquad \ldots.[1]$$

where λ is an eigenvalue, proportional to the inverse square of the burning velocity, determined by the boundary conditions:

$$\left.\begin{array}{l} \tau=0\ :\ P=0,\quad \mathrm{d}P/\mathrm{d}\tau=1 \\ \tau=1\ :\ P=0 \end{array}\right\} \qquad \ldots.[2]$$

The dimensionless parameters occurring in equation 1 are related to physical quantities by the following relationships:

Dimensionless temperature

$$\tau=(T-T_u)/(T_b-T_u)$$

Dimensionless temperature gradient

$$P=(k/cG)(\mathrm{d}\tau/\mathrm{d}x)$$

Reaction rate function

$$\phi(\tau)=R(\tau)/\overline{R}$$

where

$$R(\tau)=(k/k_u)\,H\dot{m}_x''';\qquad \overline{R}=\int_0^1 R(\tau)\,\mathrm{d}\tau$$

Eigenvalue

$$\lambda=k_u\overline{R}/(T_b-T_u)\,c^2G^2$$

In the above x = distance in stream direction, k = local thermal conductivity, T = absolute temperature, G = mass flow rate per unit area, c = average specific heat at constant pressure, H = standard heat of reaction of main reactant A, and $\dot{m}_A$ = mass of A consumed by chemical reaction per unit volume per unit time. The suffices u and b refer to the unburnt and burnt states respectively.

The reaction rate function is so defined that

$$\int_0^1 \varphi(\tau)\,\mathrm{d}\tau = 1 \qquad \ldots.[3]$$

The function φ is always positive, has zero gradient at the origin, a single maximum and is zero again at $\tau = 1$.

By considering various families of reaction rate functions, Spalding was able to obtain the so-called centroid rule

$$\lambda = 0{\cdot}5 - 0{\cdot}6604\,(1-\tau_c) - 0{\cdot}4283\,(1-\tau_c)^2 \qquad \ldots.[4]$$

in which the centroid of the reaction rate function is given by

$$\tau_c = \int_0^1 \tau\,\varphi(\tau)\,\mathrm{d}\tau \qquad \ldots.[5]$$

Equation 4 is found to hold approximately for values of $\tau_c > 0{\cdot}6$ when $\varphi(\tau)$ represents a wide range of first and second order chemical reactions.

In attempting to find a theoretical basis for the centroid rule it seems natural to determine a domain, in the (λ, τ_c) plane, within which the relationship 4 must lie. To facilitate the derivation of one boundary of the domain, we shall obtain a simple relationship which connects the centroid of $\varphi(\tau)$ with two centroid coordinates of the temperature gradient P.

RELATIONSHIP BETWEEN CENTROIDS OF P AND $\varphi(\tau)$

On multiplication of equation 1 by τ and integration one obtains, after use of conditions 2,

$$\tau_c = \bar{x} + \bar{y} \qquad \ldots.[6]$$

where $\bar{x}$ and $\bar{y}$ are the τ and P coordinates of the centroid of area beneath the P curve shown in *Figure 1*, and defined by the integrals 7 and 8:

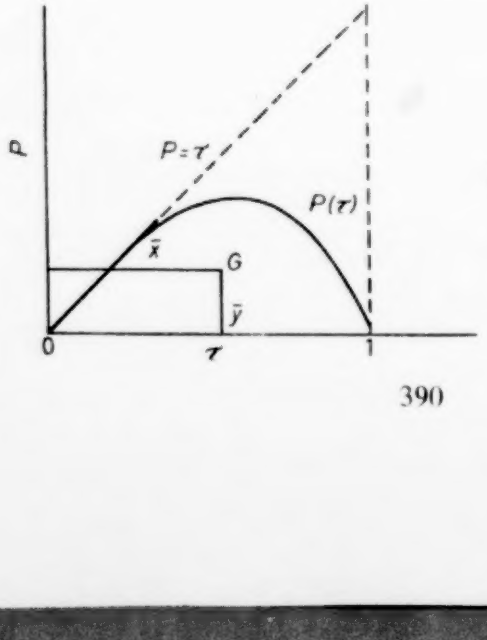

Figure 1. G denotes centroid of area under P(τ) curve

$$\bar{x} = \int_0^1 \tau P \, \mathrm{d}\tau \bigg/ \int_0^1 P \, \mathrm{d}\tau \qquad \ldots . [7]$$

and

$$\bar{y} = \tfrac{1}{2} \int_0^1 P^2 \, \mathrm{d}\tau \bigg/ \int_0^1 P \, \mathrm{d}\tau \qquad \ldots . [8]$$

On integration of equation 1 and use of the boundary conditions, it is also seen that

$$\lambda = \int_0^1 P \, \mathrm{d}\tau \qquad \ldots . [9]$$

which has been used in deriving equation 6.

DETERMINATION OF UPPER BOUND

Equation 9 shows that the eigenvalue λ is equal to the area under the P curve and from equation 6 it is seen that τ_e is the sum of the centroid coordinates of this area. For a given P curve both λ and τ_e are thus defined, although the reaction rate function $\phi(\tau)$, which determines P, has not been specified. The function P may not be chosen arbitrarily but in addition to satisfying the boundary conditions must lie within the region bounded by $P = \tau$, $P = 0$ and $\tau = 1$. This may be seen by rearrangement of equation 1.

To determine an upper bound to λ versus τ_e, we consider all P curves enclosing a constant specified area, and determine that curve for which $\bar{x} + \bar{y}$ is a minimum. Equations 6 to 9 show that this corresponds to the solution of a variational problem in which the variation is subject to the subsidiary condition $\lambda \equiv$ constant. Neglecting for the moment the requirement that P shall lie to the left of $\tau = 1$ we have as the integral which must be made stationary

$$I = \int_0^\infty P(\tau + \tfrac{1}{2}P - \mu) \, \mathrm{d}\tau \qquad \ldots . [10]$$

in which μ is a Lagrange multiplier, through which the subsidiary condition $\lambda \equiv$ constant is introduced, cf. R. COURANT and D. HILBERT[2]. From the nature of the problem it is evident that the function P for which I is sationary will produce a minimum in $\bar{x} + \bar{y}$.

Since P must satisfy the inequality $P \leqslant \tau$ we introduce the coordinate transformations

$$\left. \begin{aligned} S &= \tau - P \\ t &= \sqrt{2P} \end{aligned} \right\} \qquad \ldots . [11]$$

so that equation 10 may be written

$$I = \int_0^\infty (1/\sqrt{2}) \, t \, [S + (3/\sqrt{2}) \, t - \mu] \, \mathrm{d}S \qquad \ldots . [12]$$

with $t(S)$ an assumed function of S.

From the calculus of variation it follows that if I is to be stationary then the integrand of equation 12 must satisfy the Euler–Lagrange equation. This means that

$$S+\sqrt{2t}=u \qquad \ldots.[13]$$

are the required extremal curves. Substituting from equation 12 these become

$$P+\tau=u \qquad \ldots.[14]$$

in which u is a constant related to the area under the P curve.

For $\lambda\leq\frac{1}{4}$ the functions $P(\tau)$ which make $\bar{x}+\bar{y}$ a minimum are therefore as shown in *Figure 2* (i). A simple check to this result is provided by considering the triangles of constant area formed by $P=0$, $P=\tau$, and $P=a\tau+b$ with a and b variable and then determining a and b such that $\bar{x}+\bar{y}$ is a minimum. When $\lambda>\frac{1}{4}$ the region for which $\tau>1$ must be neglected and the extremal curves are of the form shown in *Figure 2* (ii). This follows from the fact that when the restriction $P\leq\tau$ is removed and the variational problem is applied to the quarter plane, equation 14 still represents the extremal curves. The sum of the centroids of the neglected triangular area is a minimum and hence the sum of the centroids of curve 2 (ii) is a minimum.

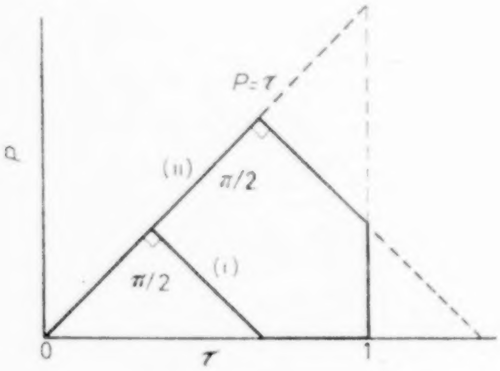

Figure 2

Using the above results the following relationships between λ and τ_c were obtained:

$$\lambda\leq\tfrac{1}{4}:\ \tau_c=\tfrac{4}{3}\lambda^{1/2} \qquad \ldots.[15]$$

$$\lambda\geq\tfrac{1}{4}:\ \tau_c=(1/\lambda)\left[\tfrac{1}{2}-\tfrac{2}{3}(\tfrac{1}{2}-\lambda)\{3-(\tfrac{1}{2}-\lambda)^{1/2}\}\right] \qquad \ldots.[16]$$

These expressions have been evaluated for various values of λ and are plotted in *Figure 4*.

DETERMINATION OF LOWER BOUND

It does not seem possible to obtain a good upper bound to τ_c for a fixed λ, from the variational principle. For $\lambda\equiv$constant it is always possible to construct a $P(\tau)$ curve for which $\bar{x}+\bar{y}=1$. Such curves are shown in *Figure 3* (i) and (ii), but comparison with *Figure 1* of Spalding shows that they are not very realistic.

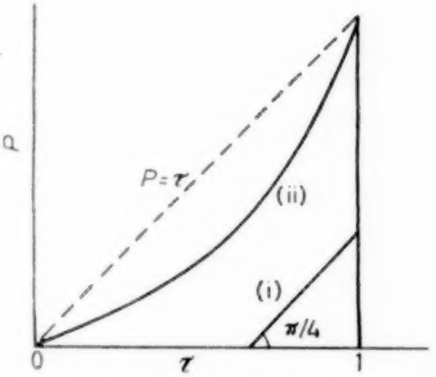

Figure 3. Curves (i) and (ii) are symmetrical about $P+\tau=1$

We use a different method of approach to find a lower bound to λ versus τ_c. On integration by parts one obtains from expression 9

$$\lambda=[P\tau]_0^1-\int_0^1\frac{\mathrm{d}P}{\mathrm{d}\tau}\tau\,\mathrm{d}\tau \qquad \ldots.[17]$$

the first term of the RHS vanishing due to the boundary conditions. Rearrangement of equation 1 and use of equation 9 gives

$$\frac{\mathrm{d}P}{\mathrm{d}\tau}=1-\frac{\phi(\tau)}{P}\int_0^1 P\,\mathrm{d}\tau \qquad \ldots.[18]$$

so that on substitution in equation 17 one has

$$\lambda=\int_0^1 P\,\mathrm{d}\tau\int_0^1\frac{\phi(\tau)}{P}\tau\,\mathrm{d}\tau-\tfrac{1}{2} \qquad \ldots.[19]$$

Integration of equation 18 and use of the boundary conditions on P also gives

$$\int_0^1 P\,\mathrm{d}\tau\int_0^1\frac{\phi(\tau)}{P}\,\mathrm{d}\tau=1 \qquad \ldots.[20]$$

Hence on substitution in equation 19 one obtains

$$\lambda=\int_0^1\frac{\phi(\tau)}{P}\tau\,\mathrm{d}\tau\Big/\int_0^1\frac{\phi(\tau)}{P}\,\mathrm{d}\tau-\tfrac{1}{2} \qquad \ldots.[21]$$

$$=\bar{\tau}-\tfrac{1}{2}\ \text{(say)}$$

To determine a lower bound for λ we shall show that one must have $\bar{\tau}\geqslant\tau_c$. We first require a result which gives the relative positions of the maxima of P and $\phi(\tau)$.

Relative positions of the maxima of P and $\phi(\tau)$

Differentiation of equation 1 gives

$$P\frac{\mathrm{d}^2P}{\mathrm{d}\tau^2}+\left(\frac{\mathrm{d}P}{\mathrm{d}\tau}\right)^2-\frac{\mathrm{d}P}{\mathrm{d}\tau}=-\lambda\phi'(\tau) \qquad \ldots.[22]$$

Let the maximum value of P be at $\tau=\tau_1$. Then

$$\tau=\tau_1: \qquad P=P_1: \qquad (\mathrm{d}P/\mathrm{d}\tau)_1=0 \qquad \ldots.[23]$$

so that from equation 22 one obtains

$$P_1\,(\mathrm{d}^2P/\mathrm{d}\tau^2)_1=-\lambda\phi'(\tau_1) \qquad \ldots.[24]$$

Similarly from equation 1 at $\tau=\tau_1$ one has

$$P_1=\lambda\phi(\tau_1) \qquad \ldots.[25]$$

Hence on division of expression 24 by 25

$$(\mathrm{d}^2P/\mathrm{d}\tau^2)_1=-\phi'(\tau_1)/\phi(\tau_1) \qquad \ldots.[26]$$

Since P has a maximum at $\tau=\tau_1$ it follows that at this point $\phi'(\tau_1)>0$. The reaction rate function is thus still an increasing function of the temperature and the bulk of the reaction occurs for values of $\tau>\tau_1$.

The inequality, $\bar{\tau}\geqslant\tau_e$

From the definitions of $\bar{\tau}$ and τ_e it is seen that the inequality is equivalent to

$$J=\int_0^1\phi(\tau)\,\mathrm{d}\tau\int_0^1\tau\frac{\phi(\tau)}{P}\,\mathrm{d}\tau-\int_0^1\tau\phi(\tau)\,\mathrm{d}\tau\int_0^1\frac{\phi(\tau)}{P}\,\mathrm{d}\tau\geqslant 0 \qquad \ldots.[27]$$

The function J may be written as

$$J=\tfrac{1}{2}\int_0^1\phi(x)\,\mathrm{d}x\int_0^1 y\frac{\phi(y)}{P(y)}\,\mathrm{d}y+\tfrac{1}{2}\int_0^1\phi(y)\,\mathrm{d}y\int_0^1 x\frac{\phi(x)}{P(x)}\,\mathrm{d}x$$

$$-\tfrac{1}{2}\int_0^1 x\phi(x)\,\mathrm{d}x\int_0^1\frac{\phi(y)}{P(y)}\,\mathrm{d}y-\tfrac{1}{2}\int_0^1 y\phi(y)\,\mathrm{d}y\int_0^1\frac{\phi(x)}{P(x)}\,\mathrm{d}x \qquad \ldots.[28]$$

which on rearrangement becomes

$$J=\tfrac{1}{2}\int_0^1\int_0^1\frac{\phi(x)}{P(x)}\frac{\phi(y)}{P(y)}(x-y)\,[P(y)-P(x)]\,\mathrm{d}x\,\mathrm{d}y \qquad \ldots.[29]$$

We have seen above that the bulk of the reaction takes place in the region beyond the maximum value of P. The dominant part of the integral J is therefore

$$J_1=\tfrac{1}{2}\int_{\tau_1}^1\int_{\tau_1}^1\frac{\phi(x)}{P(x)}\frac{\phi(y)}{P(y)}(x-y)\,[P(y)-P(x)]\,\mathrm{d}x\,\mathrm{d}y \qquad \ldots.[30]$$

Examination shows that the integrand of equation 30 is everywhere positive so that $J_1>0$. It will be seen from Spalding's results that all realistic reaction rate functions are effectively zero in a temperature range

$0 \leqslant \tau \leqslant \tau_0 < 1$ and then rise sharply to a maximum value. If one approximates to the reaction rate functions by taking $\tau_0 = \tau_1$, then $J_1 = J > 0$, so that the result $\bar{\tau} \geqslant \tau_c$ holds. Without this approximation, the contribution to J from integration over the temperature range $0 \leqslant \tau \leqslant \tau_0$ must be small compared with J_1, since τ_0 will not differ much from τ_1. It follows that in all cases one will have $\bar{\tau} \geqslant \tau_c$.

From the above arguments it is seen that a lower bound to λ, for a fixed τ_c, is

$$\lambda = \tau_c - \tfrac{1}{2} \qquad \ldots.[31]$$

This has been plotted in *Figure 4*.

DISCUSSION

Examination of the exact solutions of Spalding shows that they lie within the region defined by the upper and lower bounds of λ versus τ_c. The centroid rule has been plotted in *Figure 4* for comparison. It is seen that it lies quite close to the upper bound when $\tau_c \geqslant 0{\cdot}7$.

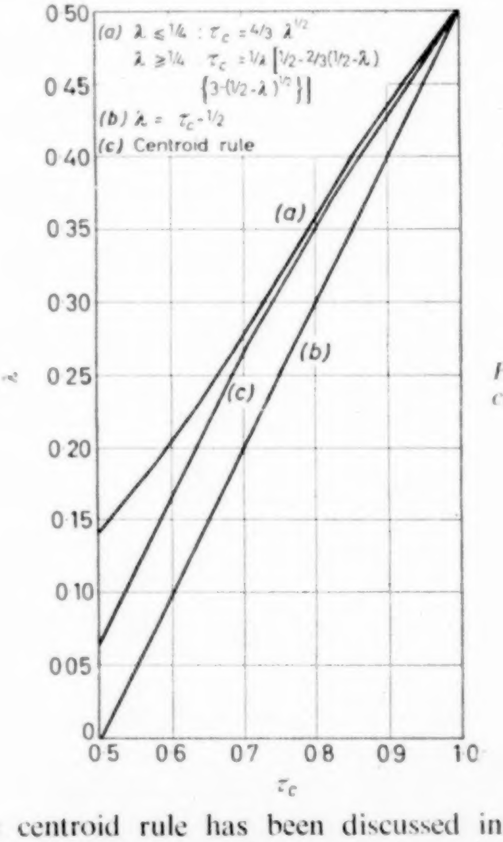

Figure 4. All λ versus τ_c curves must lie in region between (a) and (b)

The centroid rule has been discussed in a recent communication by J. MENKES[3]. He derived equation 19 and showed that $\bar{\tau} \sim \tau_c$ for $\tau_c \rightarrow 1$. From equation 21 it is seen that $\bar{\tau}$ represents the centroid of the function $(1/P)\,\varphi(\tau)$ and, since $P < 1$, this is likely to be greater than the centroid of $\varphi(\tau)$. Application of L'Hospital's theorem also shows that

$$\operatorname*{Lim}_{\tau \rightarrow 1} \frac{\varphi(\tau)}{P} = A$$

where A is a positive constant, whereas $\phi(\tau) = 0$ when $\tau = 1$. An alternative proof of the inequality $\bar{\tau} \geqslant \tau_c$ is given in the appendix.

Figure 4 shows that for a fixed centroid of the reaction rate function, the eigenvalue λ lies between upper and lower bounds $\lambda_{\text{max.}}$ and $\lambda_{\text{min.}}$ respectively, which are independent of the type of reaction considered. For the determination of these bounds it is necessary that the reaction rate functions are temperature-explicit and the conditions under which this is so have been discussed by Spalding. For reaction rates with high activation energy, the difference between $\lambda_{\text{max.}}$ and $\lambda_{\text{min.}}$ is small, enabling one to predict the burning rate with good accuracy. By rearrangement of the equation defining λ in terms of physical quantities, it is seen that the burning velocity S_u lies within limits

$$\left[\frac{k_u\overline{R}}{\lambda_{\text{max.}}(T_b - T_u)c^2\rho_u^2}\right]^{1/2} \leqslant S_u \leqslant \left[\frac{k_u\overline{R}}{\lambda_{\text{min.}}(T_b - T_u)c^2\rho_u^2}\right]^{1/2}$$

where ρ_u = density of unburnt gas.

The values of $\lambda_{\text{max.}}$ and $\lambda_{\text{min.}}$ can be found from *Figure 4* once τ_c is known, where

$$\tau_c = \frac{1}{T_b - T_u} \frac{\int_{T_u}^{T_b} (T - T_u)\, k\dot{m}_A''' \,\mathrm{d}T}{\int_{T_u}^{T_b} k\dot{m}_A''' \,\mathrm{d}T}$$

The author wishes to thank Professor D. B. Spalding for his interest in this work and for useful discussions.

Department of Mechanical Engineering,
Imperial College of Science and Technology

(Received December 1958)

APPENDIX

An alternative proof of the inequality $\bar{\tau} \geqslant \tau_c$

If one makes the substitution

$$\phi(\tau) = (P/\lambda)\,\psi(\tau) \qquad \ldots.[32]$$

the inequality 27 may be written in the form

$$K = \int_0^1 \tau\psi(\tau)\,\mathrm{d}\tau \int_0^1 P\psi(\tau)\,\mathrm{d}\tau - \int_0^1 \psi(\tau)\,\mathrm{d}\tau \int_0^1 \tau P\psi(\tau)\,\mathrm{d}\tau \geqslant 0 \qquad \ldots.[33]$$

Substitution in equation 1 shows that the function $\psi(\tau)$ is defined by

$$1 - P' = \psi(\tau) \qquad \ldots.[34]$$

We now define a new variable ζ, given by

$$\zeta = \tau - P \qquad \ldots.[35]$$

Use of equation 34 then gives

$$\mathrm{d}\zeta = (1 - P')\,\mathrm{d}\tau = \psi(\tau)\,\mathrm{d}\tau \qquad \ldots.[36]$$

and also

$$P = \tau - (\tau - P) = \tau - \zeta \qquad \ldots .[37]$$

Examination shows that for all realistic temperature gradients $P(\tau)$, ζ is monotonically increasing with τ. We may thus take τ to be a function of ζ and equation 33 becomes

$$K = \int_0^1 \tau(\zeta)\,\mathrm{d}\zeta \int_0^1 [\tau(\zeta) - \zeta]\,\mathrm{d}\zeta - \int_0^1 \tau(\zeta)[\tau(\zeta) - \zeta]\,\mathrm{d}\zeta \qquad \ldots .[38]$$

which may written in the form

$$\begin{aligned} K &= \tfrac{1}{2}\int_0^1 \tau(x)\,\mathrm{d}x \int_0^1 [\tau(y) - y]\,\mathrm{d}y + \tfrac{1}{2}\int_0^1 \tau(y)\,\mathrm{d}y \int_0^1 [\tau(x) - x]\,\mathrm{d}x \\ &\quad - \tfrac{1}{2}\int_0^1 \tau(x)[\tau(x) - x]\,\mathrm{d}x \int_0^1 \mathrm{d}y - \tfrac{1}{2}\int_0^1 \tau(y)[\tau(y) - y]\,\mathrm{d}y \int_0^1 \mathrm{d}x \\ &= \tfrac{1}{2}\int_0^1\int_0^1 [\tau(x) - \tau(y)][\{\tau(y) - y\} - \{\tau(x) - x\}]\,\mathrm{d}x\,\mathrm{d}y \qquad \ldots .[39] \end{aligned}$$

$\tau(\zeta)$ will be a monotonic function of ζ, such that when $\zeta = 0 : \tau = \tau_0$, and when $\zeta = 1 : \tau = 1$.

Further, let us select those functions which have the following properties:

$$\left.\begin{array}{ll} (i) & \tau(\zeta) \text{ monotonically increasing with } \zeta \\ (ii) & \tau(\zeta) - \zeta \text{ monotonically decreasing with } \zeta \\ (iii) & \mathrm{d}\tau/\mathrm{d}\zeta \text{ continuous except at } \zeta = 0 \\ (iv) & \text{When } \zeta = 0 : \tau = \tau_0 > 0 \\ & \qquad\;\; \zeta = 1 : \tau = 1 \end{array}\right\} \qquad \ldots .[40]$$

For the class of function defined by conditions 40, the integrand of equation 39 is positive, so that $K > 0$. Examination of these conditions shows that every realistic $\tau(\zeta)$ can be approximated sufficiently closely by a function of this type. It follows that one has $\tau \geqslant \tau_c$.

REFERENCES

[1] Spalding, D. B. *Combustion & Flame*, 1957, **1**, 296

[2] Courant, R. and Hilbert, D. *Methods of Mathematical Physics*. Interscience: New York, 1953

[3] Menkes, J. *Combustion & Flame*, 1958, **2**, 328

Recent Developments and Notes

DECOMPOSITION AND COMBUSTION OF HYDRAZINE

Considerable attention has been given recently to the décomposition and combustion properties of hydrazine. One of the reasons for this is that its vigorous combustion with oxygen, fluorine or nitric acid, provides one of the most powerful propellant systems. Further, hydrazine is an endothermic compound and in decomposition can support a flame. The properties of its decomposition flame are of considerable interest for comparison with those of hydrocarbon–oxygen combustion systems particularly for the purpose of testing theories of flame.

At the XVIme Congrès International de l'Union Internationale de Chimie Pure et Appliquée, held in Paris in April 1957, S. de Jaegere and A. van Tiggelen, of the University of Louvain, read a paper on the propagation of flame in different mixtures of hydrazine and oxygen and with different proportions of nitrogen [*Rev. Inst. Franç. Pétrole*, 1958, **13**, 451], and a paper by G. Pannetier, H. Guénebaut and R. de Hartoulari, of the University of Dijon, dealt with the analysis of the gaseous products of the decomposition of hydrazine [*Rev. Inst. Franç. Pétrole*, 1958, **13**, 457].

In the first of these papers attention is drawn to the theoretical problem posed by the combustion of a series of hydrazine–oxygen mixtures of decreasing oxygen content, when a combustion flame gradually passes into a decomposition flame, as to whether there are two distinct and well defined régimes of reaction. The method used consisted essentially of measuring the speed of flame propagation and the flame temperature for different hydrazine–oxygen mixtures which were progressively cooled by different proportions of nitrogen. The results are interpreted on the basis of branching chain reactions and it is found that the combustion flame does not differ fundamentally from the decomposition flame. In the opinion of these authors the presence of oxygen serves only to burn the initial products of decomposition and the oxidation flames are faster than the decomposition flames only because they are so much hotter.

In the second paper the results presented of the analysis of the products of hydrazine decomposition were obtained both by the use of the products of hydrazine decomposition using a stationary flame of hydrazine hydrate and by the explosive decomposition of anhydrous hydrazine by means of a high frequency electric spark or electrostatic discharge. The initial mechanism of the decomposition is represented by

$$3N_2H_4 \rightarrow 4NH_3 + N_2 + 112{\cdot}26\ \text{kcal}$$

and this reaction will be followed by the thermal decomposition of ammonia into nitrogen and hydrogen. The importance of this latter decomposition will depend on the experimental conditions and the concentration of the ammonia.

At the *Seventh Symposium (International) on Combustion, London and Oxford, 1958*, p 61, P. Gray and J. C. Lee described their recent studies on the oxidation and decomposition flames of hydrazine. In their combustion experiments the flames were supported by oxygen, by nitrous oxide and by nitric oxide. Flame speeds were determined by the schlieren method and flame temperatures and burning velocities were derived. The decomposition flame of hydrazine was also examined. Flame speed was found to be independent of pressure (corresponding to an overall kinetic order two) and dependent on final flame temperature (corresponding to an overall activation energy near to 35 kcal/mole), which is in agreement with the results of other workers. There are, however, discrepancies between the absolute values of burning velocities. The authors of this paper do not agree with van Tiggelen (see above) that in combustion flames of hydrazine prior pyrolysis is the important first stage and the oxygen only acts in a second stage to burn the decomposition products.

MODE OF IGNITION AND TYPE OF FLAME

Experiments have been described by R. Graziotti and P. Laffitte, of the Laboratoire de Chimie Générale, Faculté de Sciences, Paris, which show how different types of flames are obtained in the combustion of ethyl ether, and in some cases *n*-pentane, and air or oxygen, depending on the mode of ignition [XVIme Congrès International de l'Union Internationale de Chimie Pure et Appliquée, Paris, April 1957, *Rev. Inst. Franç. Pétrole*, 1958, **13**, 506]. The experiments were conducted in tubes of different diameters and at pressures below atmospheric.

Ignition by a train of electric sparks resulted in a normal flame being formed in a 7 to 8 per cent ether–air mixture and this was succeeded, after a vibratory period, by a cool flame which propagated throughout the tube. With oxygen instead of air, the same features were observed except that behind the cool flame a second stage flame was formed and eventually coalescence occurred.

When a normal pilot flame was used for ignition of ether–air or ether–oxygen mixtures cool flames or normal flames were formed, depending on the concentration of ether. With cool flames used for ignition, only cool flames were formed in the tubes, followed eventually by second stage flames, but never by normal flames.

With ignition by a heated filament for certain mixtures, for example, 10 per cent ether–air below 300 mm of mercury pressure, either a cool flame, or a cool flame followed by a blue second-stage flame, or a cool flame succeeded by coalescence, or a normal flame, were observed, depending on the conditions.

EFFECT OF AGED SURFACE ON SLOW HYDROGEN–OXYGEN REACTION

R. R. Baldwin and L. Mayor, Department of Chemistry, University of second limit of the hydrogen–oxygen reaction in boric acid-coated vessels. Hull, presented a paper to the *Seventh Symposium (International) on Combustion, London and Oxford, 1958*, p 8, on the slow reaction and

The paper describes some observations on a reaction between hydrogen and oxygen which was discovered accidentally during a study of the effect of withdrawal rate on the second limit in boric acid-coated vessels. In the freshly coated vessel at 500°C and 500 mm of mercury pressure, the rate of reaction of a given hydrogen–oxygen mixture is quite small, about 2 mm of mercury in 8 min. As the vessel is used, this rate increases quite slowly over a period of 10 to 14 days to a value of 6 to 8 mm in 8 min. Quite suddenly the rate then accelerates over a period of about one day, giving a pressure change of about 60 mm of mercury in 8 min. A preliminary examination of the kinetics of this reaction revealed quite unusual features, and a detailed study was undertaken. Preliminary results were reported previously [*Rev. Inst. Franç. Pétrole*, 1958, **13**, 397]. The kinetic features provide a marked contrast to those observed with potassium chloride-coated vessels and a detailed discussion is given in the paper as to the possible mechanism to account both for the slow reaction and the related second limit.

FUEL SYSTEMS FOR SUPERSONIC ENGINES

A study has recently been made within the de Havilland Engine Co. Ltd of the requirements of supersonic aircraft as regards the very wide range of fuel flow rates now involved and the considerable use to which the fuel is put for cooling purposes. These new requirements necessitate a revision of existing systems and a reconsideration of the engine control problem. An account of this study has been published by E. A. SIMONIS [*J. R. aero. Soc.* 1958, **62**, 654].

The objective in the design and development of any new supersonic fuel system is to cover altitudes up to 90 000 feet and forward speeds up to Mach 2·5. The first major problem is the large difference in fuel flow rate between high altitude flight and low level high forward speed flight. The range is about 1 : 25. The second important problem is in connection with the flow of fuel for cooling purposes. The fuel must remain liquid at the pump inlet and throughout the control system and just where temperatures are beginning to rise, fuel pressures are getting low and an adequate margin of system pressure over the fuel vapour pressure must be maintained if control is to be retained.

The vapour pressure of the three current aviation turbine fuels, AVCAT, AVTUR, and AVTAG (wide-cut), rises very sharply as the fuel temperature increases and there must be some margin allowed to ensure no vapour pressure–temperature conditions in which there can be local gas release. There is the further hazard of gum or lacquer deposition in burners, coolers, and other equipment, due to the use of fuels at high temperature in supersonic engine control systems. Considerable importance is attached to this in the U.S.A., so that a modification is being introduced to the general fuel specification and fuels will have to pass the ERDCO test which is a qualitative assessment of the tendency of the fuel to deposit gum or lacquer.

It is concluded that the uniform injection of fuel at rates varying by as much as 25 : 1 with increasing temperature as the rate drops, can be achieved with both direct injection and spill systems with adequate margin throughout, at least up to 60 000 feet and Mach 2. The margin from boiling is somewhat greater, however, for the spill system. At 85 000 feet and Mach 2 there may be some difficulties, such as distribution of fuel at the burners being affected. But the spill system has a margin even under these conditions.

IGNITION OF GAS BY ELECTRIC SPARK

A detailed quantitative investigation on the development of a steady flame from an electric spark passed through a stationary gas has been carried out in the Safety in Mines Research Establishment, Sheffield, by D. R. Lintin and E. R. Wooding [*Brit. J. appl. Phys.* 1959, **10,** 159]. The method used was to allow flashes of microsecond duration to form a shadow of the flame front on a photographic film.

The shadowgrams of incipient flames in methane–air mixtures show (*a*) a propagating kernel and (*b*) a kernel which degenerates. The first observation of flame was made 23 μs after the igniting spark had passed, no shock wave was detected, and there was no evidence of any part of the spark being more effective than another in causing ignition. The flame envelope was approximately cylindrical with slight corrugations which disappeared after between 50 and 100 μs and the flame became nearly spherical. During the next 200 μs there were the first detectable differences between propagating and degenerating flames. The critical radius, at which this difference becomes apparent, was measured for various mixtures of methane and air, and this radius and the time taken to attain it are dependent on the gas composition. It is thought that this stage coincides with the first release of energy from the gas by the combustion process. The flame kernels which failed to propagate tended to a constant radius which is dependent on the spark energy and to some extent on the gas composition, which would seem to indicate that the growth of the kernels was the result of thermal conduction only and not involving exothermic chemical reaction.

The ideal conditions for ignition are deduced from the results. The electrode separation should be twice the critical value. If less than this, energy will be removed from the gas before chemical reaction has begun; if greater, the density of energy from the spark is diminished. There should not be turbulence in the gas, so that there shall not be convolutions in the flame front to increase the flux of energy into the unburnt gas. The release of energy in the spark should be achieved in such a way that the energy density is as large as possible at the critical stage. The electrodes should be as small as possible and no solid surfaces should be present to remove energy until the flame is greater than the quenching distance.

SELF-IGNITION TEMPERATURES

D. Gross and A. F. Robertson have carried out an investigation of self-ignition temperatures of a large number of materials, including wood fibreboard, cotton linters, cork, various kinds of rubber, and various oils [*J. Res. nat. Bur. Stand.* 1958, **61,** 413]. The kinetic constants of the self-heating reactions were determined and, assuming that self-heating follows a first-order reaction, the paper illustrates the manner in which these data, obtained under conditions of negligible heat loss in an adiabatic furnace, may be used to calculate self-ignition (critical ambient) temperatures as a function of size and shape for such materials. The calculated self-ignition temperatures are in fair agreement with published experimental data for two materials, wood fibreboard and cotton linters.

The above authors have developed a special-purpose analogue computer for heat flow in building materials which may be expected at least to reduce the number of full-scale fire tests [*J. Res. nat. Bur. Stand.* 1958, **61,** 105].

ACCELERATED FLAMES

The dynamics of accelerated flames in gases, and the transition to detonation have been examined recently by H. JONES, F.R.S., Department of Mathematics, Imperial College of Science and Technology, London [*Proc. Roy. Soc. A*, 1958, **248,** 333]. The calculations show that many features of accelerated flames can be understood without detailed knowledge of the reaction rate and the structure of the flame front. The flame front is regarded as a plane of discontinuity in the gas moving with a prescribed acceleration. The disturbance preceding this plane can be calculated and a solution satisfying the necessary boundary conditions for the gas behind the plane can also be found. The conservation laws at the plane of discontinuity connect the two solutions, that before and that behind the flame. The energy which must be released at this accelerated plane in order to maintain the motion is calculated and compared with the chemical energy released in the actual process of flame propagation. The results of these calculations are compared with experimental results by H. B. DIXON, and by W. A. BONE and his colleagues.

In the pre-detonation stage of an accelerated flame there is shown to be a fall in pressure and density behind the flame front, and there the gas velocity is in the opposite direction to the motion of the flame. Increasing compression of the gas in front of the flame leads, after a time, to the development of a shock wave. It is proposed that detonation arises in this shock front which lies some distance ahead of the flame. The dynamics of the detonation wave are examined and evidence is adduced to show that complete chemical reaction does not always occur in the front of an accelerated flame.

IGNITION IN HETEROGENEOUS REACTIONS

E. WICKE and D. VORTMEYER, of the Institute of Physical Chemistry, University of Hamburg, have discussed in a recent paper the formation of ignition zones in heterogeneous reactions in gases flowing through granular beds [*Z. Elektrochem.* 1959, **63,** 145]. Attention is drawn, first of all, to the overheating of single catalyst granules or of whole 'pockets' of catalyst which may occur in exothermic reactions proceeding in gases flowing through a bed of catalyst. The origin of this overheating can be attributed to non-uniform distribution of catalytic activity, of gas flow, or of concentration of particular components in the gas phase, several of these effects generally acting together. Under certain circumstances, especially with reactions proceeding adiabatically, such regions of excess heat development can spread over the whole cross section of the bed. Consequently an *ignition zone* is formed in which there is a steeply rising temperature in the direction of the gas flow and in a short distance practically complete chemical reaction takes place. The formation of an ignition zone depends essentially on the magnitude of the enthalpy of reaction and activation energy, as well as on bed temperature. Under suitable conditions of temperature and gas flow the ignition zone migrates concurrently or countercurrently in the gas stream. This migration was investigated in activated charcoal beds with flow speeds in an empty tube between 4 and 22 cm/sec and with 5 to 11 per cent oxygen–nitrogen mixtures. By means of a special furnace which could be moved along with the migrating ignition zone, adiabatic conditions were established in the bed. A simple relation was found for the dependence of the speed of migration and the final temperature of the ignition zone on the gas flow and the concentration of the fresh gas. By the use of a model representing the conditions an explanation is given of the mechanism of the migration of the ignition zone and this shows in addition the dependence of migration on the initial temperature of the bed layer and the catalyst grain size. This dependence is confirmed by experimental results.

Using an earlier treatment of the general subject by C. WAGNER [*Chem. Techn. Neue Folge*, 1945, **18**, 28], the authors develop expressions to specify the conditions of spontaneous formation of an ignition zone in the absence of local disturbances.

NATIONAL FIRE PROTECTION CONFERENCE

The Fire Protection Association [see *Combustion & Flame*, 1959, **3**, 255] have arranged for a National Fire Protection Conference to be held in London in February 1960. The problems of fire protection in industry, commerce and the home will be discussed. The conference is being supported by the Home Office and the Ministry of Labour and National Service. The latter Government Department is responsible for legislation now being made in Parliament in the form of new clauses in the Factories Act regarding fire protection which will soon become effective. Further information regarding the conference can be obtained from the Secretary, Fire Protection Association, 31–45 Gresham Street, London, E.C.2.

FIRE RETARDANT PAINT

As a result of research for the past five years by E. I. du Pont de Nemours and Company, a new fire retardant interior paint has been devised and is now being marketed. This paint is reported as effectively slowing down the spread of fire, and it also provides durable and attractive protection for painted surfaces. This Du Pont fire retardant paint has passed tests in several categories of the Underwriters' Laboratories and the U.S. Navy [*Du Pont Magazine*, 1959, **53**, No. 2, 6].

TURBULENT COMBUSTION OF LIQUIDS

A. G. WHITTAKER, T. M. DONOVAN and H. WILLIAMS have described further work in their series of studies on burning rate [*J. phys. Chem.*

1958, **62**, 908]. They have now examined the onset of turbulent combustion of liquids contained in small tubes. In 95 different systems the transition from smooth to turbulent combustion was found to take place at some consumption rate characteristic of the system. The effects of liquid viscosity, fuel vapour pressure, combustion tube diameter and shape on the onset of turbulent combustion were studied. The results indicate that the transition is due to physical phenomena and that the entrainment of liquid droplets and a critical Reynolds number in the vapour phase may be important factors associated with the onset of turbulent combustion. It is probable that the entrainment of liquid droplets is the triggering mechanism. Some of the results are considered in the light of a theory by L. LANDAU on the transition from deflagration to detonation.

ION MOVEMENT IN FLAMES

An investigation with an interesting and novel objective concerned with the movement of ions in flames has been described recently by K. G. PAYNE and F. J. WEINBERG, Department of Chemical Engineering, Imperial College of Science and Technology, London [*Proc. Roy. Soc. A*, 1959, **250**, 316]. The best known effect due to the presence of ions in flames is the movement and deformation of flames under the influence of sufficiently strong electrostatic fields. Considerable investigations of the effect of such fields on flames were made by A. E. MALINOWSKI and his colleagues in Russia from 1924 onwards. Although considerably more quantitative measurements are required it is generally accepted that the total ion concentration in the reaction zones of flames is much in excess of that to be expected from conditions of thermodynamic equilibrium.

Earlier work indicates that gas flows comparable to the velocity of the approach stream can be induced by the drag of the moving ions. This has led the authors of the present paper to investigate the possibilities of using the movement of ions under the action of fields and the associated body forces on the gas as a means to the management of some combustion processes. Examples are the modification of volumetric heat release rates, heat transfer and carbon deposition from flame gases and the isolation of some intermediates.

Theoretical considerations are presented separately on the two phenomena of ion movement and the movement of the gas stream induced by the drag of moving ions. The velocities of the ions may be considered as not appreciably affected by the induced gas movement, so that ion movement will not differ noticeably from that in still gas. As a result of the discussion of the underlying principles preliminary experimental work was carried out on two examples of potential applications of these phenomena, namely the effect of electric fields on heat transfer from flame gases to solid bodies and on carbon deposition from diffusion flames.

For measuring the heat transfer to solid surfaces, a cylindrical water-cooled metal jacket around, and coaxial with, a vertical burner flame was used as the heat exchanger. The jacket served as a constant flow calorimeter. An axial wire in the burner flame acted as positive electrode. The i.d. of the inner tube of the calorimeter within which the flame was situated was 2·5 cm and voltages of between 4 and 5 kV were used. Appreciable increases in heat transfer rates were obtained when the field was applied and, with certain exceptions, the increase appeared to improve with increase of carbon content of the flame gases. Changes in magnitude, location and form of deposition of carbon were found to occur as a result of the electric field.

LIQUID SPRAY BEHAVIOUR

A survey of the literature on liquid spray behaviour has been published by A. E. Fuhs ['Spray formation and breakup, and spray combustion'. *AFOSR TN 58-414*. (Sundstrand Turbo, Pacoima, Calif., *TN 4*) AMF/TD No. 1199; 129 pp. +26 figs+107 refs.; Feb. 1958]. The survey is particularly concerned with liquid sprays in jet propulsion devices. Part I deals with spray formation and breakup, and Part II with spray combustion.

THE FUTURE FOR SOLID PROPELLANT ROCKETS

In the past few years there has been a considerable change of opinion as to the relative merits of liquid and solid propellants for use in rocket engines. Whereas solid propellants were earlier considered by many as capable of making only a limited contribution to rocketry, the criticisms of poor performance and lack of controllability of thrust are, to a large extent, no longer valid. In fact the improvements in performance of solid propellant rockets in the past ten years have led to their use being considered for all types of military missiles. These improvements and the outlook for the use of solid propellant rockets in the future have been discussed in a recent paper by K. W. Pearce [*J. R. aero. Soc.* 1959, **63,** 221].

Three important drawbacks originally limited the use of solid propellant rockets: (*a*) lack of cooling of the nozzle and consequent short burning time, (*b*) high inert weight of the engine due to the whole of the propellant container being subjected to the full combustion pressure and temperature, with resulting poor engine performance, and (*c*) lack of control of the magnitude and duration of the rocket thrust. The liquid propellant rocket engine, with its high overall specific impulse, does not suffer from these disadvantages, although it is a rather complicated device for which large quantities of reactive volatile liquids have to be stored. Improvements have been made in solid propellants, and the present day intimate mixtures of inorganic oxidant and organic fuel binder are sufficiently pliable to cope with the effects of temperature fluctuation so that they can be satisfactorily case-bonded. By using high-tensile alloy steels and refractory lined nozzles in conjunction with such propellants, the performance and endurance of the solid propellant engine have been increased sufficiently for it to be able to replace the liquid propellant engine as the sustainer power plant for ground-to-air missiles.

Thrust control devices are discussed by the author who considers that with their increasing use solid propellant rockets will be the most flexible rocket engines, capable of providing tailor-made thrust to meet any vehicle requirement.

In the view of E. G. D. ANDREWS and A. W. T. MOTTRAM, of Armstrong Siddeley Motors Ltd [*J. R. aero. Soc.* 1959, **63**, 265], liquid propellants may be expected to be used for the production of large thrusts for long duration and where accurate control and variability of thrust and thrust vector are required. They consider that solid propellants will be used where less stringent control of thrust is necessary. Where the increased weight of the case is offset by the saving in engine weight solid propellants would seem to be desirable.

ROAD OCTANE NUMBER OF GASOLINES

At the Fifth World Petroleum Congress held in New York, 30 May to 5 June 1959, a paper was presented by D. M. A. MASTERMAN, E. B. V. POTTER, A. SKULL and C. H. SPRAKE, of Esso Research Ltd, Abingdon, on the Road Octane Number of past, present and future gasolines. The development of laboratory test methods for the prediction of the antiknock performance of gasolines under road conditions commenced with the Motor Method in 1932. Shortly afterwards, the Research Method was also revised for general use. In recent years, many methods have been used for the prediction of Road Octane Number, the majority of which have employed a 2-variable equation involving both the Research and Motor Octane Numbers of the fuel.

These 2-variable equations have all been based on the assumption that the engine during road operation always receives fuel of the same composition as that tested in the laboratory. Such equations are not applicable when fuel segregation occurs. This happens when, during full-throttle acceleration from low engine speed, the more volatile fractions of the gasoline reach the engine cylinders in temporary excess, while the heavier fractions are subject to an appreciable time delay. Fuel segregation is transient in nature and its effect is to change the octane number of the fuel charge reaching the cylinders during a full-throttle acceleration. The extent of the change in octane number depends upon the amount of segregation which occurs and on the distribution of the octane numbers through the boiling range of the gasoline involved.

The factors in motor design and type of operation which influence fuel segregation have also been studied. The most important appear to be carburettor and manifold design, manifold heat and air velocity.

A generalized equation has been developed from theoretical considerations and verified by empirical experimental methods. This equation, which has the form indicated below, recognizes the possibility of fuel segregation occurring in the intake system of a car and closely predicts the Road Octane Number of all types of fuel in cars which exhibit segregation.

$$\text{Road O.N.} = b_1 R_T + b_2 R_a + b_3 M_T + b_4 M_a + b_0$$

where R_T, M_T = Research O.N. and Motor O.N. of total fuel, R_a, M_a = Research O.N. and Motor O.N. of the fraction a distilled overhead from the total fuel, and b_1, b_2, b_3, b_4, b_0 are constants.

Using the generalized equation as a basis, special field equations were developed for the prediction of gasoline performance in given car populations. In these, the value of the subscript a in the generalized equation varies according to the type of car involved, although it was found satisfactory to use a single best value of a for each population and to ignore the term M_a.

With cars which exhibit severe fuel segregation, poor Road Octane Numbers are obtained under low-speed accelerating conditions with gasolines blended so that their volatile components are of lower laboratory Octane Number than that of the total fuel. When compensating for this, however, the high-speed Road Octane Number provided by the gasoline is usually in excess of the requirements.

ANTIKNOCK COMPOUNDS

A paper describing the type of research and development work conducted to provide petroleum refiners with new antiknock compounds was read at the Fifth World Petroleum Congress, held in New York, 30 May to 5 June 1959, by H. J. GIBSON, W. B. LIGETT and T. W. WARREN, of Ethyl Corpn, Detroit, Michigan, U.S.A. It also describes the application work designed to help the refining industry to use antiknock compounds, both old and new, in the most economical fashion. The programme which led to the development of methyl*cyclo*pentadienyl manganese tricarbonyl (MD–CMT) as a potentially commercial antiknock is used to illustrate research and development on new antiknocks, and application work in the refinery is illustrated by studies of the economical use of both tetraethyl lead (TEL) and MD–CMT.

Among the characteristics desired in a commercial antiknock are good fuel solubility, low water solubility, reasonable freezing point, adequate volatility, stability in fluids and gasolines, and toxicity low enough for safe handling. MD–CMT fulfils these requirements and is about twice as effective as TEL as a primary antiknock. Moreover, it is remarkably effective as a supplement to maximum concentrations of TEL, particularly in certain types of fuels. The mechanism of antiknock action of MD–CMT is believed to be similar to that of TEL.

When low concentrations of MD–CMT are used as a supplement to TEL, exhaust-valve life is shortened, but this can be avoided by adding one of several phosphorus compounds as a corrective agent. Spark-plug life may be either increased or decreased by use of MD–CMT, depending on engine-operating conditions. Other engine problems are not materially affected by the presence of MD–CMT.

Efficient use of TEL in refineries requires reliable correlations of lead response, techniques for determining the cost of incremental octane numbers, linear programming, blending rules, and a cost balance with processing. Current knowledge in these areas is discussed. Data show that TEL is a very effective antiknock on the road as well as a useful tool for controlling octane number at the refinery.

Because of its cost, MD–CMT probably will not find its major use as a primary antiknock. As a supplement to TEL, however, it will affect current blending practice and will compete with increases in catalytic-reforming severity as a means of upgrading antiknock quality. The probable economic balance between TEL, MD-CMT and octane-improvement processes is described, and typical examples are presented.

ABNORMAL COMBUSTION IN ENGINES

L. S. Echols, V. E. Yust and J. L. Bame, of the Research Laboratory, Shell Oil Co., Wood River, Illinois, U.S.A., presented a paper reviewing their research on abnormal combustion phenomena in internal combustion engines, at the Fifth World Petroleum Congress held in New York, 30 May to 5 June 1959. The fundamental factors influencing autoignition and surface ignition are discussed in terms of the ignition delay theory of Semenov. These factors are then related to the practical problems of knock, hot starting noise, silent knock, preignition-induced knock, knock-induced preignition, and engine roughness, sometimes called rumble or pounding. In the absence of catalytic effects, it would appear that these phenomena are all related to the ignition delay characteristics of the fuel as determined in rapid compression machines. The controlling factor in knock appears to be autoignition irrespective of whether this is followed by rapid burning or detonation. A mechanism is given whereby apparent combustion wave velocities below detonation velocities, but well above normal turbulent flame speeds, can be formed. The effects of pressure, density and temperature on ignition delays are discussed with respect to the important reversals in the order of rating of fuels under different conditions. When ignition is catalysed by surfaces, the situation becomes more complex, it being indicated that a catalytic surface may either increase or reduce the normal surface ignition tendency of a fuel as compared with the effect of a non-catalytic surface. When the catalytic substances contain combustible solids their effect may be transient in nature and dependent on their past history both as regards operating conditions and fuels and lubricants employed. A classification of catalytic surfaces is given on this basis. The available information is employed to explain the abnormal combustion phenomena observed in current engines and to predict the future significance of these problems in motor engines.

PYROMETRY OF ROCKET EXHAUST GASES

F. S. Simmons and A. G. DeBell, of Rocketdyne, a division of North American Aviation Inc., Canoga Park, California, U.S.A., described a short time ago a photographic technique for measuring temperatures in luminous rocket exhaust flames [*J. opt. Soc. Amer.* 1958, **48**, 717]. The photographic pyrometer used for this purpose consists essentially of a camera mounted on a chassis containing four tungsten ribbon filament lamps which serve as standards; combinations of films and filters are chosen to pass light only in a narrow band centred for the present study about 6 300 Å. The apparatus is located approximately in the plane of the nozzle exit of the rocket motor and a corner-cube prism, placed behind the flame, provides the reflected radiation for application of a two-path-length technique. This technique conveniently provides for the determination of temperature and emittance from measurements of monochromatic radiation. In this way a photographic record is obtained containing an image of the rocket flame adjacent to the images of the four standard lamps whose currents have been adjusted to yield brightnesses spanning those of interest in the flame. Within the flame image is contained a brighter image of the corner-cube. The use of this prism, with its unique property of reflecting light in the direction of incidence as a reflector, obviates the need for precise alignment. The precision of the apparatus is said to be about 10° K.

More recently these authors have published another paper reviewing the above method and giving some refinements in the analysis of the film records by means of a recording microphotometer, together with values of temperatures measured at the nozzle exit of a small rocket motor [*Aircr. Engng*, 1959, **31**, 144]. At this location it is said that thermodynamic equilibrium can be assumed in the exhaust gases.

B.I.S.R.A. EXPERIMENTS ON FUEL-OIL FLAMES

In *The British Iron and Steel Research Association: Annual Report 1958* reference is made to work in the Plant Engineering and Energy Division on carbonaceous additions to fuel. Enhancing fuel-oil flames by adding carbonaceous materials improves furnace productivity and increases the fuel efficiency. There is the possibility, however, that such materials may tend to cause blockages in the feedlines and valves. Materials have therefore been sought that will form stable suspensions in fuel oil. Laboratory stability tests of suspensions of pulverized pitch and powdered graphite showed that they fulfilled these requirements; both these materials could be made available if required. The results of a series of experiments with heavy fuel-oil flames, with and without carbonaceous additions, in a small calorimeter-hearth furnace are being analysed before full-scale experiments are carried out on an open-hearth furnace.

MEASUREMENT OF GAS TEMPERATURE AND HEAT FLOW

G. G. Thurlow, of the British Coal Utilisation Research Association, has reviewed some recent developments in instruments used to study heat transfer from flames [*B.C.U.R.A. Mon. Bull.* 1959, **23**, 129]. Some of the instruments have been developed within the B.C.U.R.A. and others are due to work carried out, sometimes jointly, by the British Iron and Steel Research Association, the United Steel Companies Ltd, Land Pyrometers Ltd, the Royal Netherlands Steel Company, and the International Flame Research Foundation.

A development of the suction pyrometer has been to locate the radiation shields completely within a water-cooled probe, the top of the shield system being flush with the end of the water-cooled jacket [R. Barber, D. Meachen and W. Bateman, *J. Iron St. Inst.* 1957, **185**, 343]. It is then the heat exchange between the thermocouple and the water-cooled wall that has to be reduced rather than that between the thermocouple and the furnace walls. The heat loss to the water-cooled wall is often less than the heat that would be gained from the furnace walls, for example, in an open hearth uptake where the walls are hotter than the gas. This development has also a major practical advantage in its robustness and mechanical stability.

A new version of the B.C.U.R.A. Venturi pneumatic pyrometer, described by the author and referred to in these notes a short time ago [*Fuel, Lond.* 1958, **37**, 477], is under development at the International Flame Research Foundation. In this new instrument the entrance faces the gas stream and in order to locate the hot Venturi in this position it is necessary to reduce the throat diameter to 7 mm. Small Venturi sections which have orifice characteristics independent of Reynolds number have to be designed if the instrument is to be used as an absolute measure without having to be calibrated directly against another temperature-measuring device.

The calorimeter-type and plug-type heat flowmeters are described and the significance of the measurements obtained by their use is discussed. The method used by J. M. VAN LANGEN, of the Royal Netherlands Steel Co., in an attempt at IJmuiden to develop the heat flow technique to separate the radiation and convection components, is described and reference is made to a development by him in the form of a small heat flowmeter in which the receiving surface is both flush with and can be traversed across the surface of a model hearth. This is being used to study the heat transfer by convection to the hearth from flames striking it at different angles.

A 'spherical' or 'integrating' radiometer which is briefly described has recently been designed and is now being developed by the team of investigators at IJmuiden. This is intended to measure the radiation received by an absolute blackbody over a wide angle.

COMBUSTION OF LIQUID FUEL

J. R. JOYCE, of Shell Research Ltd, Thornton Research Centre, and B. V. POULSTON, of Shell Petroleum Co. Ltd, London, presented a paper on the atomization and combustion of liquid fuel to the 'Conference on Major Developments in Liquid Fuel Firing 1948–59', organized by The Institute of Fuel and held in Torquay, 11 to 14 May 1959. The objective of the paper was to indicate how far the knowledge gained by research in this field during the past decade has been applied to actual flames in industrial equipment.

The fundamental features of hydrocarbon combustion are first discussed and then the five major factors that influence fuel-oil combustion in a practical piece of equipment: (*i*) atomization, (*ii*) vaporization, (*iii*) fuel–oxidant mixing, (*iv*) flame stabilization, and (*v*) flame environment.

In the combustion of a practical oil spray, there are processes which partake of the features of homogeneous vapour combustion and also of the features of individual droplet combustion. From basic studies in these fields it is known that there is a beneficial effect of raising the inlet temperature of an inflammable homogeneous gas mixture. By this means the range of possible mixture velocities for successful combustion is increased, but at the same time advantage can be taken of this effect on a practical scale only by more careful control of the mixture strength since the range of possible mixture strengths at higher velocities is more restricted than at lower velocities. Reference is made to the effects of turbulence for promoting satisfactory combustion, but it is noted that there is a possibility of the setting up of pockets in a combustion system and in these the environment may be such that the chemical reactions slow down or cease, resulting in incomplete combustion and loss of efficiency. An aspect of the chemical researches of homogeneous mixture flames which is of practical importance concerns the formation of solid carbon.

With regard to atomization, the more successful techniques appear to involve spreading the fluid by aerodynamic means in a thin layer over a stationary surface, or by throwing it as a film from the edge of a rotating surface. These methods show a definite advance on those in which the fuel emerges from an orifice in a single column to meet the blast. Further improvements are required in the control of viscosity at the inlet to the burner if optimum performance is to be obtained. Viscosity indicators are being developed for this purpose and their indicating mechanisms can be used to control the heaters which raise the temperature of the oil to the required level.

The problem in the design of atomizers is that of maintaining good characteristics over a wide range of fuel flows. The range of satisfactory output can be increased by using devices which successively open ports in the atomizer, and also by using the recirculating or 'spill' principle. During recent years the latter device has been developed further, so that good atomization is obtained over a very wide range of outputs, and the change in cone angle with output is fairly small. There is great need for a combined wide-range atomizer and variable air director which will provide fully coordinated fuel and air proportioning over a reasonably wide output range.

In connection with the results of investigations on the vaporization of single droplets, there are two major difficulties in applying this knowledge to practical conditions. The first is uncertainty as to the aerodynamic conditions around the droplet, and the second is the lack of information of the effect of neighbouring droplets.

Much more work is still required before our knowledge of aerodynamic turbulence, droplet evaporation and droplet 'ballistics' can be correlated with the conditions necessary for the mixing of fuel vapour and air to produce a satisfactory fuel spray flame.

The development of techniques for flow visualization in scale models of combustion equipment has been fruitful in leading to various devices for obtaining an ordered flow pattern involving fresh mixture or burnt gases or both in some form of recirculation. The form of stabilizer, or air director, most widely used in practice is that which gives a tangential velocity component to the incoming air, creating a whirlpool effect in the combustion zone.

Reference is also made to developments: (*i*) in automatic control of oil-burning plant in the past decade, (*ii*) in high-intensity combustion chambers, and (*iii*) in the two-stage combustion process.

The authors conclude that much remains to be done to relate the basic knowledge in this field to the practice of combustion in industrial equipment. There is a lack of quantitative data on vaporization, burning of sprays, mixing, and flame stabilization.

HIGH-MOMENTUM OIL BURNERS

The design of high-momentum *steam-atomized oil* burners such as are used in an open-hearth steelmaking furnace is the subject of a paper by F. A. GRAY, G. R. MATTOCKS, S. PILKINGTON and A. D. ROBERTSON, presented to the 'Conference on Major Developments in Liquid Fuel Firing 1948–59', organized by The Institute of Fuel and held in Torquay, 11 to 14 May 1959. The paper reports the results up to date of an investigation on this subject carried out in the Research and Development Department of the United Steel Companies Ltd. The results of early work on the subject have already been published but they are included in the present paper for the sake of continuity and completeness [M. J. MCINERNEY, G. R. MATTOCKS and M. P. NEWBY, 'Oil burners for open hearth furnaces', *Proceedings of the Joint Conference on Combustion 1955*. American Society of Mechanical Engineers, New York, and Institution of Mechanical Engineers, London].

The objective of these extensive investigations is to establish a fundamental basis for the design of high-momentum oil burners and to apply the theoretical conclusions to specifications of burners for works purposes. The main function of the steam, which passes with the oil through the burner discharge nozzle, is to entrain the air required for combustion, and to control the flame length and combustion rate. In the large high-temperature furnaces under consideration, the determining factor in regard to combustion rate is the rate of mixing of the oil and combustion air. In order to obtain higher combustion and output rates in the open-hearth process, the desirable objective is to obtain the maximum thrust for a given quantity of steam and the design of the burner is intimately related to this.

The principles of burner design and performance were examined theoretically and practically by work on small- and large-scale experimental burner rigs. The characteristics of a burner are expressed in terms of momentum flux or nozzle thrust, and this is related to air entrainment and flame length.

The influence of nozzle shape and size, the pressure of the atomizing medium, and the oil/steam ratio on thrust production and nozzle efficiency were determined. Increased oil/steam ratio and decreased nozzle diameter reduce nozzle thrust efficiency. Thrust efficiency is shown to be increased by the use of convergent–divergent nozzles as compared with convergent nozzles. An internal mixing burner is considerably more efficient than an external mixing one. It was found possible to relate nozzle thrust efficiency to $(M_o/M_s)(1/d^2)$, where M_o, M_s are the mass flow rates of oil and steam respectively, and d is the nozzle throat diameter. This is of particular value in designing nozzles for works use and a series of design curves is given for this purpose.

An investigation of the partition of momentum between oil and the atomizing medium showed that the fraction of the total momentum flux carried by the liquid in a liquid–gas jet from a convergent–divergent nozzle is greater than that from a convergent nozzle. Consequently entrainment, which is chiefly due to the momentum of the gas, is reduced. With an oil–steam jet in operation, however, the gases resulting from the burning of the oil produce more efficient entrainment as they possess the momentum of the oil. Thus, apart from a lower initial rate of entrainment in the period when oil droplets are present, the greater momentum flux of flame from a convergent–divergent nozzle results in greater entrainment of combustion air.

INITIATION OF COAL DUST FLAMES

The heat transfer processes involved in the pre-reaction zone of a stationary, laminar, premixed, coal dust flame, and the conditions which are necessary for the establishment of temperature homogeneity between the dust and the surrounding air are considered and discussed in a report by V. D. Long, of the Imperial College of Science and Technology, London, and W. L. Murray, of the Safety in Mines Research Establishment [*S.M.R.E. Res. Rep. No. 145*, July 1958, 32 pp.].

It is assumed that no chemical reaction takes place in the pre-reaction zone, so that the only factor controlling rise of temperature is the transfer of heat energy. It is further assumed that there are no significant physical changes in the pre-reaction zone.

The absorption of radiation from the flame by the dust particles is postulated as the first means of heating the dust particles and air travelling towards the flame. The effects of radiation may be evident at a distance of hundreds of centimetres from the flame front, depending upon the absorptivity of the dust cloud. This results in a more gradual rise in temperature than would occur if the transfer of heat took place by conduction alone. Some of the absorbed radiation will be conducted rapidly into the interior of the particles and their temperature will rise above that of the surrounding air. At the same time the air nearest the particles will be heated by conduction and convection of heat absorbed at the surface of the dust particles.

At a distance of a few hundred microns from the reaction zone the effect of conduction from the flame will become important and will produce a sharp rise in the temperature of the air. Such a distance will be traversed, at normal burning velocities, in a few milliseconds. But the authors consider that, although the rate of heat transfer between the air and the particles will increase because of the increased relative velocity between dust and air produced by the sudden rise in velocity of the air, the temperature of the air will rise to a greater extent than that of the dust particles. Consequently a greater degree of temperature homogeneity, both in the air itself and between the dust particles and the air, may be reached. Whether the reaction, when it begins, will result primarily from the ignition of the solid material or of the inflammable vapours released from the dust, will depend on the relative temperatures attained by the dust and air.

W. A. Kirkby

THE USE OF MODELS IN FIRE RESEARCH

The Committee on Fire Research and the Fire Research Conference of the Division of Engineering and Industrial Research of the National Academy of Sciences–National Research Council is planning a two-day international symposium on the theme 'The Use of Models in Fire Research' to be held at the National Academy of Sciences in Washington, D.C., on 9 and 10 November 1959.

The meeting will be concerned with the use of models in predicting fire behaviour on a large scale. Modelling, applied with considerable success to many combustion problems, has had almost negligible application in studying fire growth and spread. Contributions have been announced from Japan, England, France, Germany and the U.S.A. A more detailed programme and names of speakers will be available later.

Attendance at the Symposium must necessarily be limited and will be by invitation. Those actively interested in basic research on fire and the spread and growth of fire should indicate their interest and request advance registration cards. Address all communications to Mr D. W. THORNHILL, Executive Secretary, Committee on Fire Research and Fire Research Conference, National Academy of Sciences, 2101 Constitution Avenue, Washington 25, D.C.

The Committee on Fire Research and the Fire Research Conference are sponsored by the Office of Civil and Defense Mobilization, the Department of Defense and the U.S. Forest Service of the Department of Agriculture.

THE INSTITUTE OF PHYSICS

At the Annual General Meeting of The Institute of Physics held in London on 7 July 1959, Sir GEORGE THOMSON (Master of Corpus Christi College, Cambridge) was re-elected President. Dr J. M. A. LENIHAN was elected a Vice-President; Dr J. TAYLOR, Honorary Treasurer, and Professor F. A. VICK, Honorary Secretary, were re-elected. The two new Ordinary Members of the Board elected were Dr V. E. COSSLETT and Mr L. ROTHERHAM.

The *Report* for 1958 which was adopted at the meeting shows that at the end of the year the total membership in all grades was 6309, an increase of 415 on the previous year. 851 applications for election or transfer to the various grades were considered (7 per cent more than 1957).

The *Report* records that at the end of the year a circular was sent to members proposing the amalgamation of the Institute and The Physical Society and that if the broad basis of intention was accepted a Joint Committee would be set up to work out all the details; it is understood that a scheme for amalgamation is about to be submitted to members of both bodies.

EIGHTH INTERNATIONAL SYMPOSIUM ON COMBUSTION, 1960

The Combustion Institute, of Union Trust Building, Pittsburgh 19, Pa. announces that it has has now been decided that the Eighth International Symposium on Combustion will be held at the California Institute of Technology, Pasadena, Calif., between 29 August and 2 September 1960, and not during the period tentatively put forward on page 265 of our June issue. Fundamental combustion problems in propulsion will be discussed including kinetics, combustion of solids, combustion of sprays, ionized gases and, possibly, radiant heat transfer.

FALL MEETING OF WESTERN STATES SECTION (U.S.A.) OF COMBUSTION INSTITUTE

The Western States Section of The Combustion Institute announces details of its forthcoming Fall Meeting on chemical equilibria and performance of high temperature combustion systems. This meeting will be held in Los Angeles on 2 to 5 November. Approximately 40 technical papers, prepared by representatives of 25 interested organizations, will be presented in the first three days. The fourth day will be devoted to a Workshop, where participants can delve into the details of the presentations. This Thursday Workshop, and the preceding Wednesday afternoon of presentations, will be Confidential sessions co-sponsored by the Air Research and Development Command.

We are investigating the publication picture, but we look upon this conference as an opportunity to learn from each other, rather than primarily as a forum for the formal presentation of papers. The Western States Section, from its inception, has striven for provision of preprints, and has tried to maximize discussion.

We are emphasizing the here-and-now picture of computer programmes, species thermodynamics, and engine performance. Where is the picture in focus? Where out of focus? What focusing can we accomplish in the first week of November? Those persons interested in helping the authors to sharpen the focus are asked to prepare, in advance, written discussions of selected papers on the programme. They are invited to communicate with the Section in this regard.

Members of The Combustion Institute should anticipate a fee of approximately \$15.00. There will be a surcharge of \$3.00 for non-members, which sum is transferred directly to Institute headquarters to pay for a current membership in The Institute. The Section has no dues, and all members of The Institute residing in the Western States are automatically made members of the Section. The meeting will be held at the IAS Building at 7660 Beverly Blvd. in Los Angeles. A volume of the proceedings of the meeting will be published by Butterworths Scientific Publications, publishers of the Combustion Symposia proceedings.

Full details and registration forms can be obtained from the office of the Secretary, Western States Section, The Combustion Institute, 16902 Bollinger Dr., Pacific Palisade, Calif.

FUEL

The July issue of *Fuel* contained *Notes*, which may be of interest to readers of *Combustion and Flame*, dealing with:

Adiabatic bomb calorimeter
American research on coal-burning gas turbine
Melchett Medal for 1959

Publications

THE KINETICS OF CHEMICAL REACTIONS IN GASES (KINETIKA KHIMICHESKIKH GAZOVYKH REAKTSII)

V. N. KONDRAT'YEV. Moscow: Soviet Academy of Sciences, 1958.
688 *pp.* 62 *tables.* 204 *figures*

BOOKS on chemical kinetics, sometimes from special points of view, appear at irregular intervals of a few years and mark limited advances towards the resolution of a subject still far from reducible to simple terms. This work by KONDRAT'YEV, except that it does not extend to reactions in solution or to heterogeneous reactions, is the most comprehensive that has yet appeared.

There is, perhaps inevitably in a straightforward account, nothing unconventional about the pattern of the book, with its chapters devoted to the general laws of kinetics and the mechanisms of chemical reactions, followed by considerations of unimolecular, dimolecular and termolecular reactions, and the interchange of energy in reactions. Much recent and new material is collected into the succeeding chapters on photochemical effects and on the influence of the electric discharge. This latter chapter includes sections on radiochemical reactions (reactions under the influence of penetrating radiation) and on activation by bombardment with fast ions and atoms.

There has been in the Russian school, on the initiative of SEMENOV, some specialization in branched chain reactions as a basic factor in combustion and explosion, and KONDRAT'YEV more than 20 years ago founded his own reputation and school on his studies of the roles of OH radicals in rarefied flames and of SO and CS radicals. It is not a matter for surprise, therefore, nor for complaint, that chapters on chain reactions and on combustion, including spontaneous combustion, and explosion and detonation, should occupy a large proportion of the book.

There are more than 1 300 references to the literature, and as rather fewer than a quarter of them are to Russian sources, they cover a fair field with no favour, which is not to be found everywhere. In addition, they come right up to 1958, the year in which the book was published. This says much for the speed with which the book was printed and marketed.

An unfortunate feature of the work is the brevity of the subject index for so vast a mass of information and examples packed into the book. A further improvement might have been the introduction of summaries at a few key points in all this detail; and some indication of the author's criticisms and preferences might have been welcomed in these summaries.

R. A. ACTON TAYLOR

ANALYTICAL CHEMISTRY—SOME NEW TECHNIQUES

A. G. JONES. London: Butterworths Scientific Publications; New York: Academic Press, 1959. *viii*+268 *pp.* (illus.) 40*s* or $7.50

THE very high rate of development of new analytical techniques is not altogether a blessing to the chemist for, while it is naturally pleasing to be able to analyse more substances in less time with less work and more precision, numerous additional problems are also posed. One of them is that of over-specialization; thus, the tremendous attention paid to partition chromatography, and particularly to gas chromatography, has necessarily resulted in the partial neglect of methods in allied fields, of which ion-exchange analysis is perhaps a good example. Another difficulty is that no sooner is a particular analytical stumbling block overcome than a flood of applications follow, of ever-increasing complexity, so that still further ingenuity is required on the part of the analyst. This monograph will help considerably in overcoming these problems and deficiencies, particularly since the author draws attention, quite fairly, to the limitations as well as the potentialities of the various techniques.

The monograph is aimed to supply non-specialist senior analysts with an introduction to the techniques developed in the years between 1950 and 1957, and the author has decided to select, from the wide choice available, those of special interest to himself (and colleagues in I.C.I. Ltd, General Chemicals Division). The result is a treatment which presents clearly the detailed procedures, the factors affecting the precision and the reproducibility, together with sufficient references for the research worker to follow up the original publications. The illustrations, print and lay-out are, as usual, excellent. Minor criticisms may include the absence of references to absorption in the chapter on Flame Photometry, although A. WALSH's papers were published *ca.* 1956; however, this is an occupational hazard, since the book might well never have appeared had the author attempted to include all the latest developments. One feature of this particular subject, which has long puzzled the reviewer, is the surprising divorce between the practice of flame photometry and the theory of flame spectra—illustrated in this case by the absence of any reference to the monographs by A. G. GAYDON. In general, however, this book can be warmly recommended both for the laboratory bench and for the desk.

G. J. MINKOFF

SEVENTH SYMPOSIUM (INTERNATIONAL) ON COMBUSTION

Published for the Combustion Institute by Butterworths Scientific Publications, London, 1959. *xlvi* + 959 *pp.* (illus.) 224s

THE Seventh International Symposium was held in Oxford in September, 1958, this being the fifth in the postwar series, but the first to be held outside the U.S.A. This volume retains the same general format as the previous four, so that they form a continuous and valuable series. The size and importance of the symposia continue to grow, and the present volume contains 124 papers; even so, many other good papers which were submitted have had to be rejected, and so this selection of papers is probably of higher standard than previously. A welcome feature is the inclusion of 21 Russian papers; this first-hand account of Russian work written in English will be most valuable.

The original plan was to restrict the symposium to 'The Physics and Chemistry of Flame', and this has largely been done, but the first main part containing 31 papers includes some interesting work on pre-flame reactions, slow combustion, etc. At the actual meeting, this part was subdivided into sections on The Hydrogen–Oxygen Reaction, the Attainment of Equilibrium in Combustion Systems, the Mechanism of Combustion Reactions of Non-hydrocarbons, the Mechanism of Combustion Reactions of Hydrocarbons, and the Inhibition of Oxidation Reactions.

The smaller Parts II and III on spectroscopy and ionization in flames include several especially good papers embodying new techniques for studying chemiluminescence, absorption spectroscopy and mass-spectrographic identification of positive ions. The 17 papers in Part IV on structure and propagation of flames deal with both new experimental results, e.g. on composition and temperature traverses through the flame front, and also with theory, e.g. on the disputed excess enthalpy hypothesis. Parts V and VI are on Ignition and Limits of Inflammability and on the Interaction of Flames and Surfaces; the latter includes some good contributions on carbon formation.

Parts VII, VIII and IX are on Turbulence in Flames, on Combustion in Practical Flowing Systems and on Detonation and its Initiation. The study of these high-intensity combustion phenomena has received considerable impetus from recent aero-engine and rocket work. The Russian contribution, with four out of seven papers in Part VII and seven out of sixteen in Part IX, is indicative of their interest and major advances in this field. Part X on Special Fuels is, however, rather thin, with only five short but interesting papers. Security considerations may have limited publication of work under the planned title 'High Temperature and High Energy

Fuels'. Part XI contains six papers on Instrumentation; other papers using new techniques are dispersed through other sections as well.

In addition to the main papers, this volume, for the first time, includes a record of the meeting discussion, this being given at the end of each part and totalling some 70 pages. It contains quite a number of valuable points of criticism and new ideas, as well as some 'stop press' results, but is, from its nature, rather difficult to disentangle. A good attempt has been made to arrange and edit this discussion. In at least one case, however, replies to criticisms are left hanging in the air, because the verbal controversial criticism itself has not been written up. The volume also includes a record of the interesting opening addresses given at the Royal Institution by Sir Cyril Hinshelwood, Dr Bernard Lewis and Sir Alfred Egerton.

To summarize, this is a very valuable collection of papers, including a good proportion of original work, to which every research worker in the combustion field must have access. Its main fault is its overpowering size, of nearly 1 000 closely written pages. Many of the papers, but by no means all, give a conclusion or summary. How much easier it would have been to handle this mass of material if only a short abstract had been included at the beginning of each paper!

A. G. Gaydon

THE EFFICIENT USE OF FUEL

Second edition. London: Her Majesty's Stationery Office, 1958. *vii* + 888 *pp.* 35*s*

This book was produced by the Education Committee of the Ministry of Power, under the chairmanship of Professor R. J. Sarjant, with the assistance of a large number of specialist authors. The chairman of the Editorial Panel was the late Dr G. E. Foxwell. The first edition was published in 1944 and is now very well known.

The new edition is 66 pages longer than the first, and several changes have been made. More space is devoted to liquid fuels and less to the properties and utilization of steam. Progress in the field of water-tube boilers is described, and the treatment of many subjects, including instruments, thermostatic control, heat transfer, fluid flow, and some auxiliary plant, has been brought up to date and in many cases expanded. The book contains a vast amount of information and deals with almost every aspect of the industrial use of fuel. Over 40 000 copies have been sold and the price is moderate, so there is no doubt of the value of the work. In addition, the authority of the book can be taken for granted in view of the list of contributors. Criticism can therefore be confined to matters of scope and presentation.

The choice of subjects must have been a difficult one, as the field is so large. For example, it is stated at the beginning of one chapter that only such numerical values are given as are necessary for explanation, and for the physical constants required in fuel technology the reader is referred to the book *Technical Data on Fuel*. But this latter work also contains much of the information on heat transfer and on the flow and measurement of fluids that is given in the text under review.

With many contributors, authority in each field is obtained, but at some cost in repetition, unevenness and lack of continuity. The size and scope of the book have led to an attempt to make each chapter more or less self-contained, and this has increased the amount of repetition. The order of presentation has sometimes contributed also, an example being that as heat transfer is considered before fluid flow, Reynolds number is defined and discussed twice.

Since the book sticks closely to a subject which depends on many branches of science and engineering it occasionally gives an impression of parochialism, as in the statement that fluid flow is a highly important branch of fuel technology. The phrasing is sometimes clumsy and there are some minor errors and misprints.

On the title page the book is said to be intended for the use of students and technical men in industry, and it is undoubtedly very useful to both, though perhaps the form of the book is rather better suited to the latter class of reader.

M. J. G. Wilson

Letter to the Editors

Letters to the Editors on points of scientific interest related to combustion and flames are invited. The Editors do not hold themselves responsible for opinions expressed in correspondence. Anonymous contributions cannot be accepted.

Mean Temperature of Burnt Gases

My attention has been drawn to the fact that equation 10 on page 209 of the June issue of this journal averages the temperature of the burnt gas along a line and therefore exaggerates the importance of the gas at the centre of the sphere. In consequence, the following re-development of this equation is put forward.

Consider an elementary spherical shell of radius r_b, and having a thickness $\mathrm{d}r_b$. Let the temperature of this shell be $T(r_b)$. Then the mass of such a shell will be $\mathrm{d}m = 4\pi r_b^2 \rho \, \mathrm{d}r_b$

$$= 4\pi \left[P / R_b T(r_b)\right] r_b^2 \, \mathrm{d}r_b$$

and its total internal energy will be $E \, \mathrm{d}m$. If it is assumed that each layer of burnt gas behaves as a perfect gas then

$$\mathrm{d}E = c_v \, \mathrm{d}T$$

Thus if it is further assumed that the heat capacity (c_v) of each elementary spherical shell is constant and equal to the mean value over the temperature range $T(r_b)$ to $\overline{T}_b$, then the change in internal energy of each such shell will be

$$\Delta E \, \mathrm{d}m = c_v \left[\overline{T}_b - T(r_b)\right] \mathrm{d}m$$

$$= \frac{4\pi P c_v}{R_b} \left[\frac{\overline{T}_b}{T(r_b)} - 1\right] r_b^2 \, \mathrm{d}r_b$$

Now since no transfer of heat or performance of work is considered to take place during the mixing process the total internal energy of the burnt gas will remain unchanged, i.e.

$$\frac{4\pi P c_v}{R_b} \int_0^{r_b} \left[\frac{\overline{T}_b}{T(r_b)} - 1\right] r_b^2 \, \mathrm{d}r_b = 0$$

and since $4\pi P c_v / R_b$ is not zero it follows that

$$\overline{T}_b \int_0^{r_b} \frac{r_b^2 \, \mathrm{d}r_b}{T(r_b)} = \int_0^{r_b} r_b^2 \, \mathrm{d}r_b$$

or

$$T_b = \tfrac{1}{3} r_b^3 \Bigg/ \int_0^{r_b} \frac{r_b^2 \, \mathrm{d}r_b}{T(r_b)}$$

This equation replaces equation 10 in the paper cited above.

C. J. Rallis

Department of Mechanical Engineering,
University of the Witwatersrand,
Johannesburg, S. Africa

(*Received September 1959*)

Studies of Autoignition and Knock with Propane as an Engine Fuel

N. P. W. MOORE and B. N. ROY

The mechanism of knock for both methane and propane is considered, with particular reference to the influence of the products of pre-flame oxidation on the knocking limit. The special problems of high temperature operation are dealt with in relation to knock-limited performance and the ability of the engine to operate using weak mixtures. Heat is added (a) by general heating of the whole charge, and (b) by local heating of part of the charge. Combustion is characterized (i) by knock-limited compression ratio in the fired engine, and (ii) by spontaneous ignition in the motored engine. It is concluded that propane is an excellent fuel for a high speed spark ignition engine, that a wide range of power output is available by quality control, and that compression ratios up to 10 : 1 can be used without knocking. Methane was less satisfactory in the engine tested.

A PREVIOUS paper[1] described comparative studies of methane and propane as fuels for high compression ratio engines. Both fuels are suitable for engines up to at least 14:1 compression ratio for methane, and 10:1 for propane for both spark ignition and dual-fuel conditions. In dual-fuel engines combustion is initiated by the compression ignition of a small quantity (usually less than ten per cent of the full load fuel supply of liquid fuel injected towards the end of the compression stroke). With both systems the ultimate power output and efficiency are limited by the onset of either 'knock' or pre-ignition. Knock involves the exceedingly rapid combustion of the last part of the charge to burn, and is associated with either spontaneous ignition ahead of the normal propagating flame front, or an abnormal and exceedingly rapid mode of flame propagation. In dual-fuel engines knock is also associated with rapid flame propagation during combustion of the gaseous fuel, and is quite distinct from combustion knock in compression ignition engines. Pre-ignition is the ignition of the charge by hot surfaces. Subsequent flame propagation involves only normal flame velocities, comparable with flame propagating in the engine cylinder from a spark ignition source[2].

The present paper considers the mechanism of knock for both methane and propane, particularly the influence of products of pre-flame oxidation on the knocking limit. Pre-flame oxidation is now universally accepted as an important precursor to knock. Further consideration is given to the special problems of high temperature operation, both with respect to the knock-limited performance, and the ability of the engine to operate with weak mixtures.

There are well established theoretical advantages in using weak mixtures, both in achieving high engine efficiencies, and also a wide range of power output by quality control of the mixture. Furthermore with weaker mixtures the knock-limited compression ratio increases, giving the possibility of even higher engine efficiencies. The ability to regulate the output of a dual-fuel engine by variation of the fuel supply only is a very important practical advantage. Restriction of the air supply can lead to difficulties in achieving satisfactory compression ignition of the pilot oil charge, and also introduces complications in governing an engine over a wide range of load and speed. The limiting mixture ratio for steady running is dependent on the inflammability limit for the fuel air mixture under engine conditions.

EXPERIMENTAL EQUIPMENT

A Ricardo E.6 engine of 3 in. bore and 4⅜ in. stroke was used throughout the present work. A detailed description of the equipment has been given[1]. The only additional equipment for the present work was a small furnace to pre-heat a portion of the inlet charge. The furnace consisted of a stainless steel tube 12 in. long and of ¾ in. bore, wound with 24 s.w.g. Nichrome wire giving a heating capacity of 1 kW. The furnace temperature could be controlled by means of a variable series resistance. The temperature of the products of reaction was measured, at the outlet of the furnace, by a chromel-alumel thermocouple, arranged for traverse along the length of the furnace. Visible reactions in the furnace were observed through a flat quartz window at one end of the furnace. The flow diagram of *Figure 1* shows how a small portion of the charge was passed through the furnace and returned to the engine manifold close to the inlet valve by means of a small (½ h.p.) rotary pump.

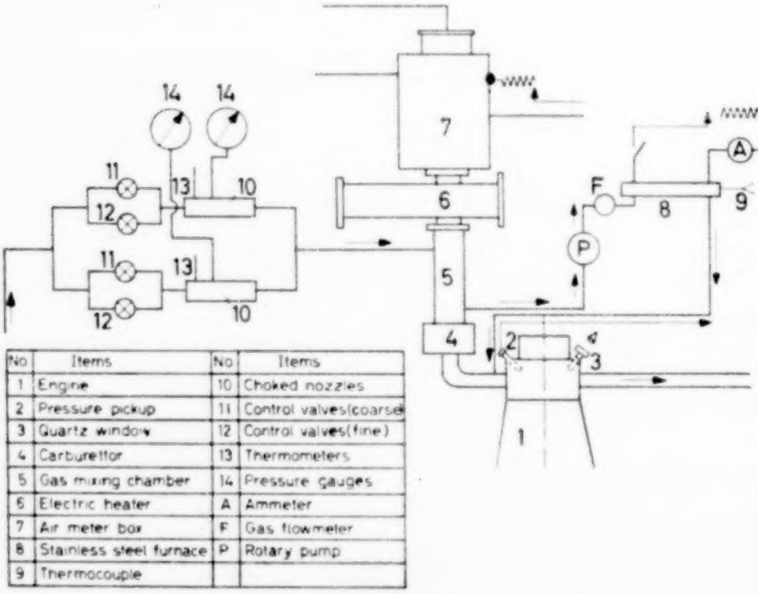

No	Items	No	Items
1	Engine	10	Choked nozzles
2	Pressure pickup	11	Control valves(coarse
3	Quartz window	12	Control valves(fine)
4	Carburettor	13	Thermometers
5	Gas mixing chamber	14	Pressure gauges
6	Electric heater	A	Ammeter
7	Air meter box	F	Gas flowmeter
8	Stainless steel furnace	P	Rotary pump
9	Thermocouple		

Figure 1. Arrangement of experimental equipment

RESULTS

The performance of the engine at various compression ratios (up to 14:1 for methane and 10:1 for propane) with spark ignition has already been presented in detail[1]. It was shown that both fuels exhibit marked temperature sensitivity, i.e. the critical compression ratio for knock is considerably reduced with increasing inlet temperature. This effect is important in limiting the knock-free power output of an engine in regions of high ambient temperature, or under highly turbo-supercharged conditions. *Figure 2* shows the knock-limited compression ratio, and the corresponding power output for both methane and propane for various mixture temperatures. The charge temperature was regulated by electrical heating. Two mixture ratios were investigated with each fuel. A weak mixture (approximately 65 per cent of the chemically correct) being representative of the mixture used in current dual-fuel engines, and a stoichiometric mixture applicable for highly rated gas engines and spark ignition engines regulated by quantity governing. High inlet temperatures may also apply under

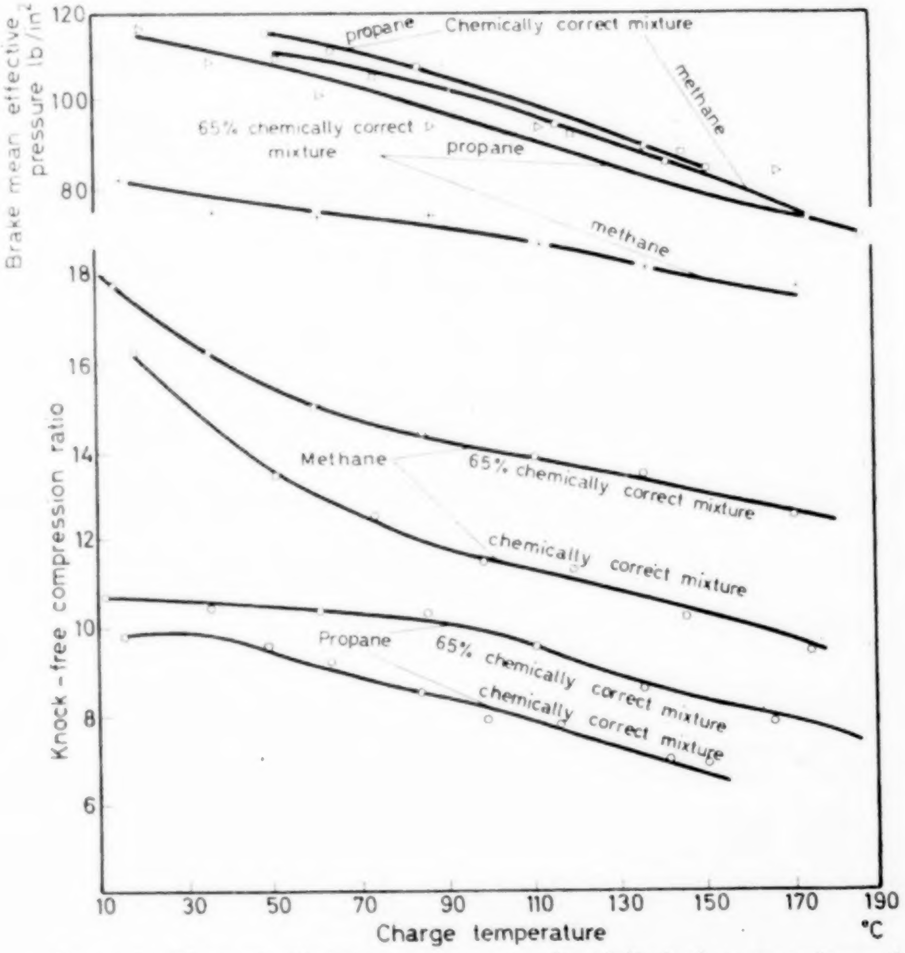

Figure 2. Effect of mixture temperature on knock-limited compression ratio of methane and propane

free-piston gas-generator conditions in which the degree of supercharging of the power cylinder exceeds that for current piston engine practice. For inlet temperatures above approximately 80° C the curves of knock-limited compression ratio exhibit a constant slope with increasing charge temperature irrespective of fuel type or mixture strength. Below this temperature, however, methane in both weak and rich mixtures shows steep knock dependence on charge temperature, whereas the knocking tendency of propane (also in weak and rich mixtures) remains almost unchanged. The corresponding engine power output, expressed as the brake mean effective pressure in lb/in^2, is given in the upper curves of *Figure 2*. The knock-limited power output will depend on opposing influences of charge density, compression ratio, and the energy content per unit volume of mixture. There is little difference between the knock-limited power output for chemically correct mixtures of the two fuels. The results for methane at weak (approximately 65 per cent of correct) mixtures, however, lie considerably below those for propane, despite the higher compression ratios possible with methane. Comparative fuel consumption loops at full throttle and at the same compression ratio indicate a greater output with propane, due to the greater energy per unit volume of charge, and also the more rapid flame propagation with this fuel. This has been reflected in corresponding values of optimum ignition advance. The knock-limited performance with methane as fuel has been determined at a mixture ratio close to the limit for steady running, and it would appear that the power output is considerably reduced by a lower cycle efficiency and by a fall in the combustion efficiency. It is in this region of mixture ratio that unburnt fuel has been detected in the engine exhaust. The results have determined, nevertheless, the true knock-limited power for a weak methane–air mixture.

Figure 3 shows the effect of passing 5 per cent of the total charge through a pre-heating furnace at temperatures up to 500° C. Results for both methane and propane for various mixture strengths are included. For methane a steady fall in knock-limited compression ratio is observed, being most marked with a weak mixture (approximately 65 per cent of chemically correct), whereas with propane for all but the richest mixtures there is initially little effect until a well defined temperature is reached at which there is a sudden drop in the knock-limited compression ratio. Beyond this point there is no further reduction even up to furnace temperatures of approximately 500° C. With all mixture ratios this sharp decrease occurs at approximately 150° to 200° C furnace temperature.

A similar experiment with a chemically correct mixture of *n*-heptane and air with only 2·5 per cent of the total mixture externally heated has been included for comparison, and indicates an effect of the same order, but at reduced compression ratio, as would be expected with a fuel of low knock resistance. A general similarity of behaviour is shown by propane and *n*-heptane; methane, however, has a quite different response to charge heating.

The results have been presented to a base of inlet temperature, since this variable can be accurately measured. The maximum compression temperature is, however, a more realistic criterion, affecting the severity of

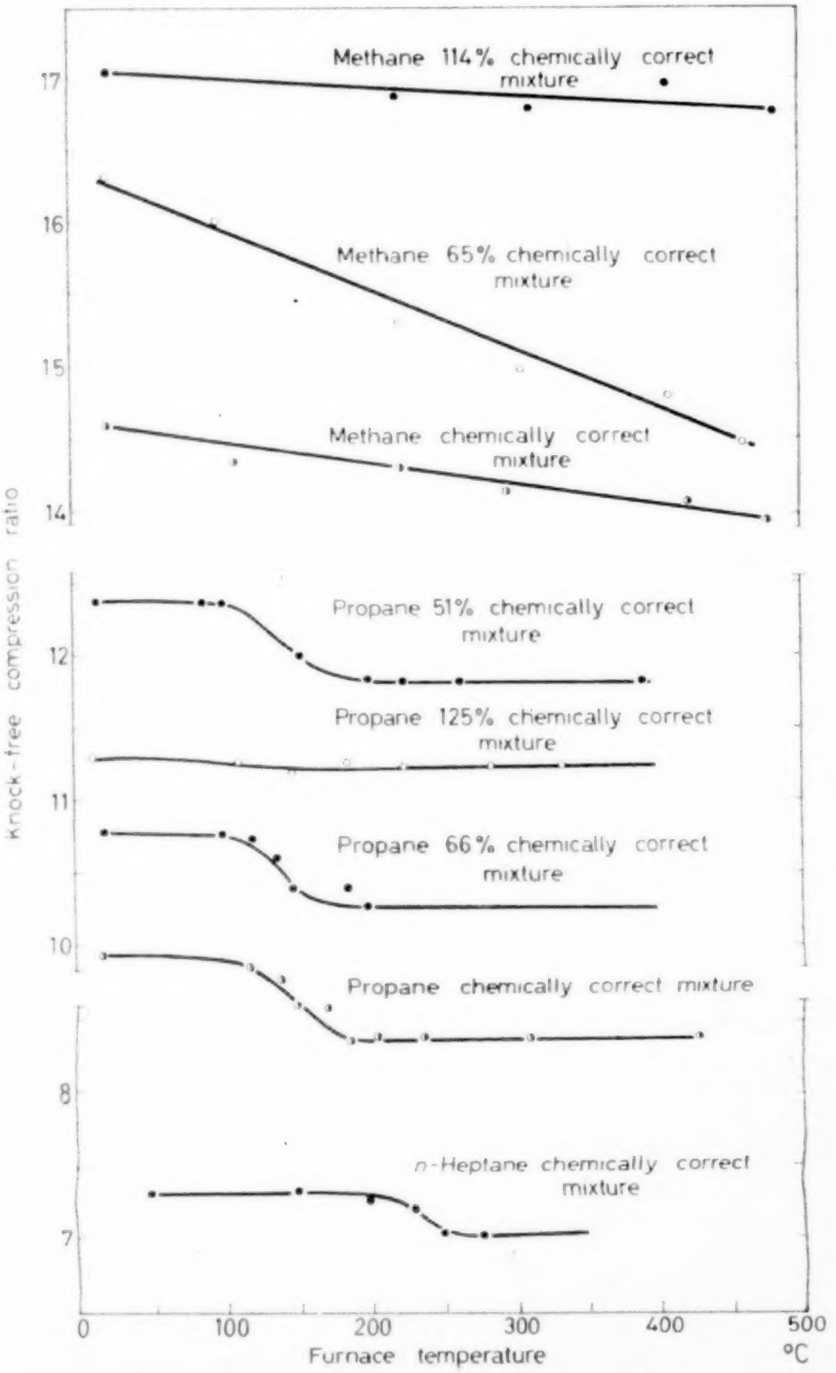

Figure 3. Effect of slow oxidation products on knock

conditions promoting pre-reaction. The data of *Figure 2* for methane and propane have been recalculated on this basis and are shown in *Figure 4*. It is seen that there is now a remarkable similarity between the results for pre-reaction promoted by the furnace and by heating the entire charge. The different behaviour of methane and propane is now even more striking.

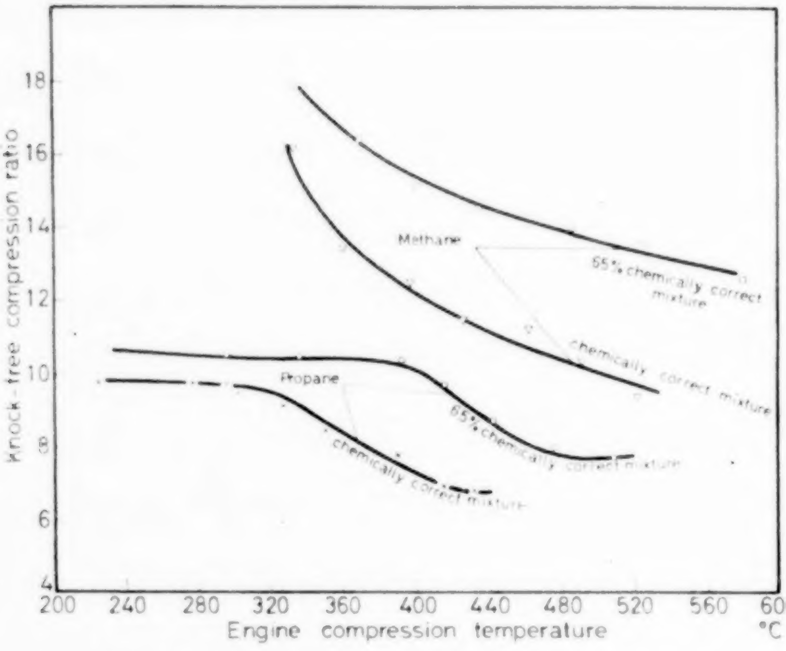

Figure 4. Variation of knock limits with engine compression temperature

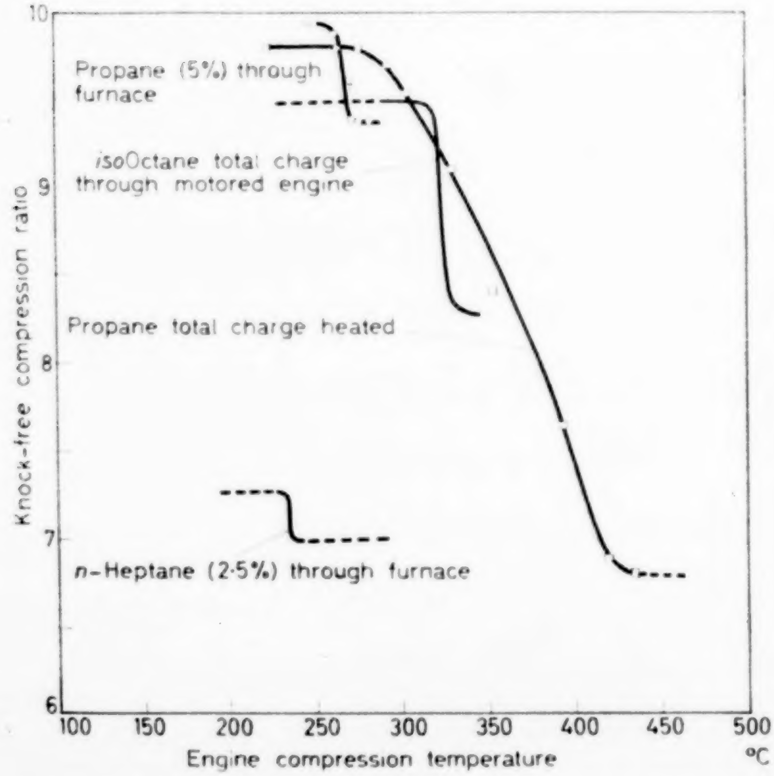

Figure 5. Effect of slow oxidation reaction on knock limit for a number of fuels

A close comparison can also be shown to work by C. WALCUTT, J. M. MASON and E. B. RIFKIN[3] in which the whole charge is pre-reacted by compression followed by expansion in a motored engine before being knock-rated in a similar firing engine, the degree of pre-reaction being controlled by varying the compression ratio of the motored engine. *Figure 5* shows a comparison between various investigations in which different techniques have been used to pre-react the charge, and for which there are corresponding measurements of knock resistance. For comparison the data have been recalculated in terms of the final compression temperature. *Figure 5* shows that propane, *n*-heptane and *iso*octane all exhibit a sharp fall in knock resistance at a compression temperature close to 325°C. The extent of the drop is far greater when the entire charge is subjected to pre-reaction, but the critical temperature at which the drop occurs is remarkably constant for the various fuels, and for the differing methods promoting pre-reaction. Methane (see *Figures 3* and *4*) behaves quite differently.

It is apparent from *Figure 3* that the furnace pre-reaction products of rich propane–air mixtures are far less effective in lowering the compression ratio for knock than corresponding weak mixtures. It is of interest to add the products of pre-reaction of a small quantity of weak mixture to an engine running on a rich mixture. This has been done by passing a separately prepared mixture to the furnace, while maintaining the furnace flow at approximately 5 per cent of the total mixture. *Figure 6* gives a typical set of results with the main charge adjusted to 125 per cent of chemically correct, and the furnace mixture ratio to 44 per cent of chemically correct. The products of this weak mixture had been shown to be effective in promoting knock in a weak mixture. *Figure 6* shows a reduction in knock resistance in the region of a critical temperature, this temperature being some 150°C greater than for the corresponding weak condition. The actual reduction in knock-limited compression ratio is well defined but somewhat less than for the data summarized in *Figure 3*. This is an important result, because it shows that pre-reaction in a small fraction of the charge can influence the entire reaction. Local regions of weak mixture arising, for instance, from maldistribution of the charge may be important in encouraging the onset of knock, despite the inherently greater knock resistance of weak mixtures.

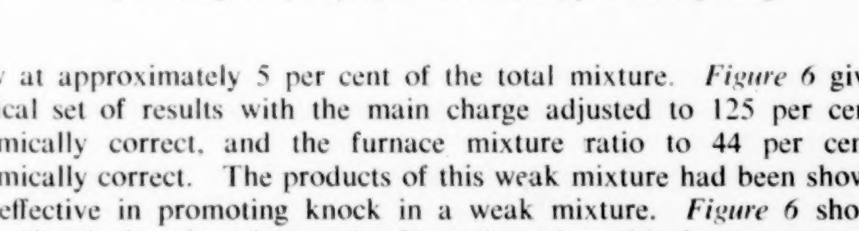

Figure 6. Effect of varying mixture ratio of pre-reacting charge

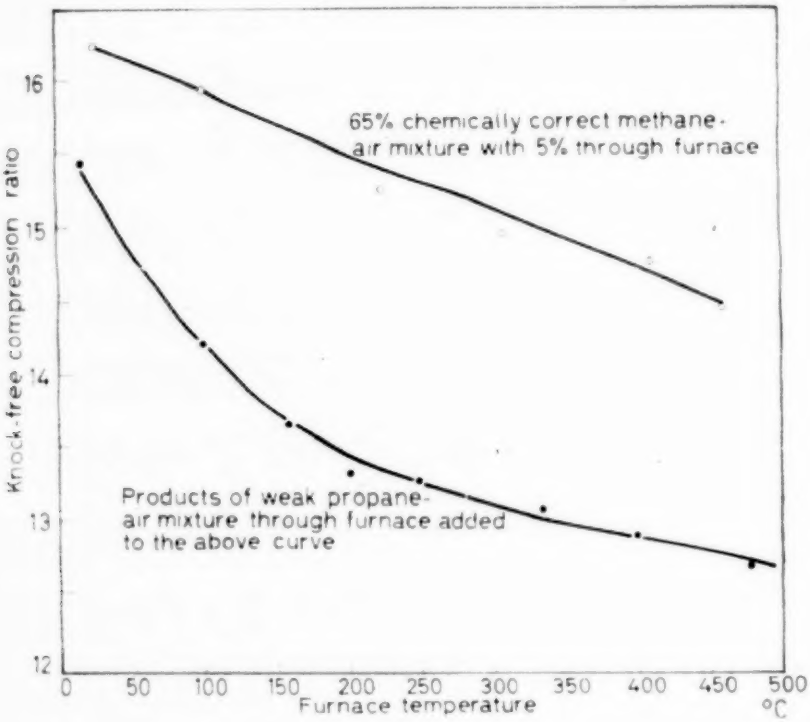

Figure 7. Effect of propane oxidation products on knock limit of methane

It has also been shown from *Figure 3* that methane does not exhibit a sudden reduction in knock resistance with increasing furnace temperature. The effect of adding the pre-reacted furnace products of propane oxidation with methane as the main fuel was therefore investigated. *Figure 7* shows a comparison for a weak methane–air mixture to which has been added the pre-reacted products, for a wide range of furnace temperatures, of a similar methane–air mixture, and also a rather greater quantity of a 90 per cent chemically correct propane–air mixture. It was shown that reduced quantities of propane–air mixture gave similar but reduced effects. It is seen that a general fall in knock resistance is encountered but that this is progressive. There is no evidence of a sudden reduction at a critical temperature, but the rate of decrease is most marked for furnace temperatures from 20° to 150° C; for higher temperatures the rate of decrease is similar for the two curves. A similar sensitivity of methane to small increases in temperature has been noted in *Figure 2* in considering the effects of pre-heating the whole charge.

EFFECT OF PRE-REACTION ON SPONTANEOUS IGNITION LIMITS

The knock reaction can be regarded as a spontaneous ignition reaction of the last part of the charge to be burnt. Special influences may condition this spontaneous ignition, giving exceedingly rapid rates of reaction. A. C. EGERTON, F. L. SMITH and A. R. UBBELOHDE[1] discussed the 'pre-sensitization' of the knocking zone by reactions leading, it was believed, to the formation of organic peroxides. This concept has been extended and supported by studies involving engine sampling and improved chemical analysis by D. DOWNS, A. D. WALSH and R. W. WHEELER[5]. The possible importance of hydrogen peroxide as an intermediate under these conditions has emerged from the later work of A. J. PAHNKE, P. M. COHEN and B. M. STURGIS[6]. The overall concept of rapid reactions, involving chain processes, remains unchanged.

The motored engine technique enables the reaction of the whole charge to be induced under 'sensitized' conditions. The severity of the conditions can be changed by varying either the compression ratio or the intake conditions. The measurements of knock-limited compression ratio have been supplemented by motored engine studies applying a furnace technique for pre-reacting the mixtures.

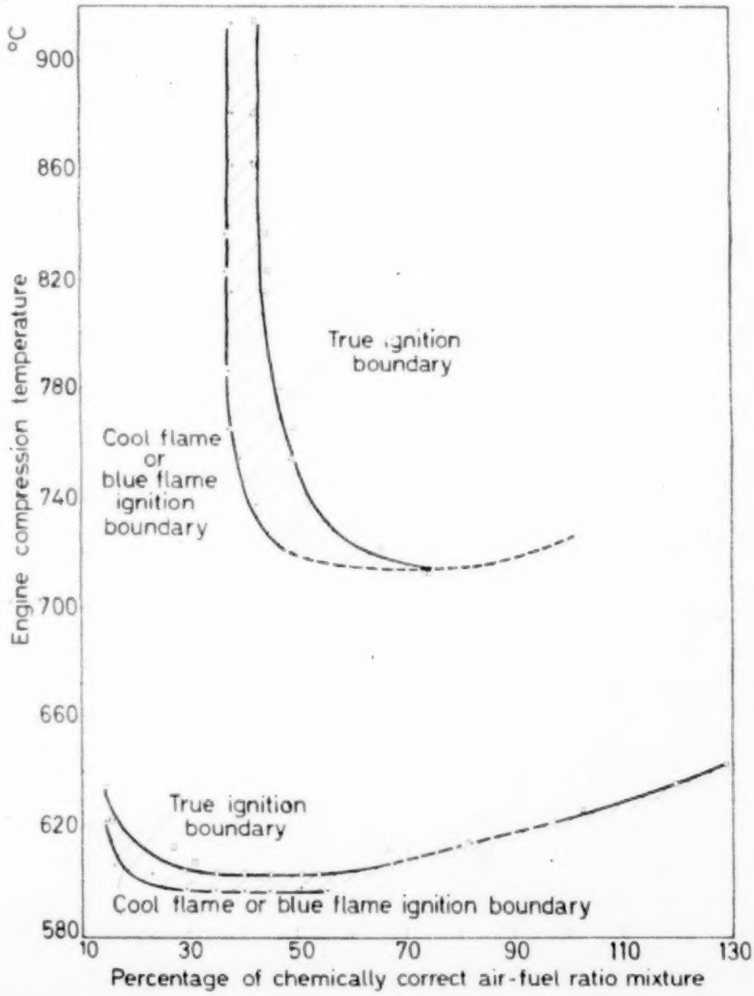

Figure 8. Effect of pre-reacted products on autoignition limits of propane

Figure 8 shows the effect of adding pre-reaction products from the furnace (adjusted so that 5 per cent of the charge is passed through the furnace) on the spontaneous ignition limits.

Considerable experimental difficulty was encountered in making these measurements. The maximum compression ratio of the engine was 20:1; with cold mixtures of propane and air this was insufficient to induce spontaneous ignition over a range of mixture strengths. Tests were consequently made at elevated intake temperatures, giving ignition well below 20:1 compression ratio. To simplify comparison of ignition boundaries, the data shown in *Figure 8* have been expressed as the calculated compression temperature necessary to give ignition in the region of top dead centre. Since it has also been necessary to vary the compression ratio, compression pressures may not always be strictly comparable. For the lower curves of *Figure 8* furnace products heated to a temperature of 200° C were added to the charge. The charge temperature was maintained constant at 135° C.

The following features are apparent. First a marked lowering of the whole diagram, including both hot and cool flame limits. A narrowing of the region in which stable cool flames were observed when pre-reacted products from the furnace were added to the charge is also evident. The diagram appears to have been displaced to regions of weaker mixtures but still exhibits weak mixture limits for cool and hot flame beyond which reaction is not observed. The spontaneous ignition reactions were particularly violent when furnace products were added to the charge; the glass observation window could not be used for mixtures richer than 60 per cent of chemically correct. In this region the hot flame boundary was defined by observation of the pressure/time record under motored engine conditions. The cool flame boundary could not be defined in this region; there appeared to be no evidence of a disturbance of the pressure record

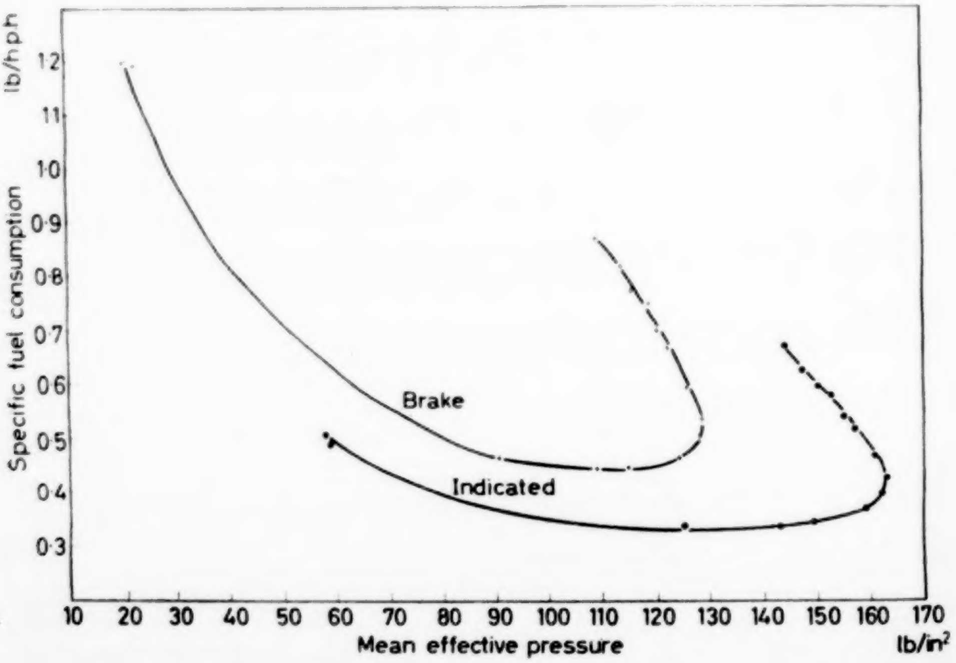

Figure 9. Fuel consumption loops for propane at 7 : 1 compression ratio

before the onset of violent hot flame ignition. The possible existence of a cool flame region below the hot flame boundary in rich mixtures cannot, however, be discounted. Cool flame limits in the weak region could not be defined without visual observation.

COMBUSTION OF WEAK MIXTURES

Earlier work has shown that a wide range of power is available at full throttle by the variation of mixture strength with propane as fuel. This is illustrated by the fuel consumption loops of *Figure 9*, for 7 : 1 compression ratio, and 1 500 r.p.m. These are shown to a base of both brake and indicated mean effective pressure. The charge is unheated and ignition timing is carefully adjusted to the optimum setting. The mixture was progressively weakened until the pressure/time diagram indicated

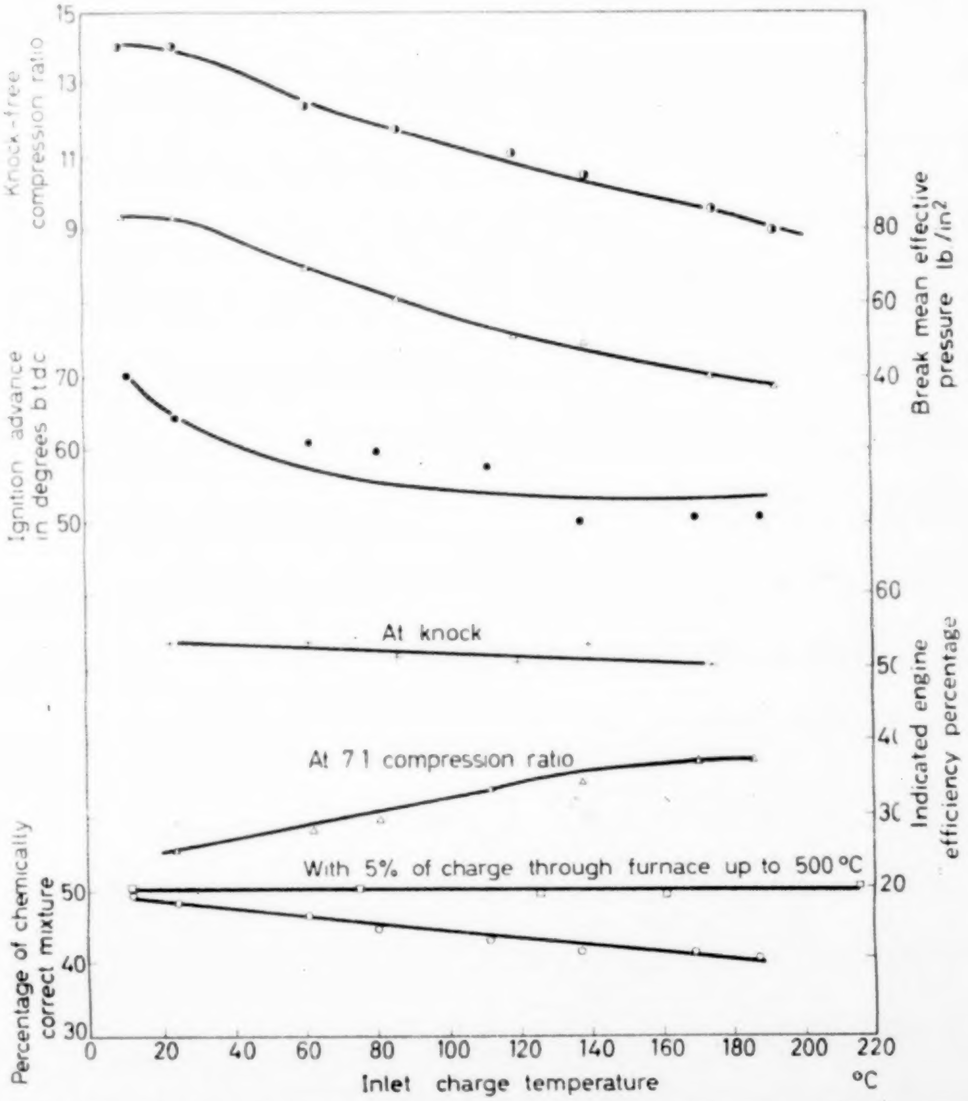

Figure 10. Effect of mixture temperature on weak mixture performance with propane

occasional misfiring. A weak limit, for a running engine, has therefore been defined. It is well known that the weak limit of inflammability of most fuels is decreased with increasing temperature, but is little affected by increasing pressure[7]. It is therefore of interest to examine the effect of increasing the charge temperature on the weak limit for stable running. *Figure 10* shows the effect of raising the charge temperature to 200° C at a fixed compression ratio of 7 : 1 and an engine speed of 1 500 r.p.m. The lowering of the limit is apparent, also the somewhat faster flame propagation reducing the optimum ignition advance. It has been shown, however, that the onset of knock is encouraged by charge heating. The knock-limited compression ratio and corresponding engine power output have therefore been determined for the range of charge temperatures, and are shown in the upper curves of *Figure 10*. The addition of the pre-reacted products (again 5 per cent of the total charge) was shown to be without effect on the limit for steady running. It is also of interest to compare the engine efficiencies under similar conditions. At the fixed compression ratio of 7 : 1 the efficiency increases with increasing charge temperature due to the operation at weaker mixtures, and also to the enhanced rates of flame propagation.

DISCUSSION

The present work has confirmed that propane is an excellent fuel for a high speed spark ignition engine, that a wide range of power output is available by quality control, and that compression ratios of up to at least 10 : 1 can be used without knocking. In the E.6 engine propane can be used more efficiently at a given compression ratio than methane, particularly at weak mixtures; this may well follow from the higher rates of flame propagation with propane, confirmed by the measured values of ignition advance. It is already accepted that the use of propane gives reduced cylinder wear and less combustion chamber deposits[8]. The comparative performance on methane and propane indicates that propane may without serious limitations be used as a fuel for development work on engines designed to operate on natural gas. The absence of readily available supplies of natural gas in the U.K. has proved a serious handicap in the development of natural gas-burning engines. Propane can be readily transported as liquefied gas, and can be evaporated and regulated to give a steady supply without the use of elaborate equipment. It is suggested that combustion chamber development can be carried out more realistically with propane as a fuel than with town gas. The latter usually contains some 40 per cent free hydrogen and is particularly prone to pre-ignition, both in the cylinder from a hot surface, and in the engine manifold from mixing with the hot residual charge. For engines of very high compression ratio it may be necessary to reduce the compression ratio for running on propane (to perhaps 10 : 1). The comparatively high knock rating of town gas (approximately 11 : 1 for a gas containing 40 per cent of hydrogen) can be misleading because the measurement can only be made under experimental conditions that deliberately prevent pre-ignition (cold jackets, zero valve overlap, etc.).

The knock-limited compression ratio has been shown to depend on mixture ratio, and the severity of engine operation. Both methane and propane exhibit a well defined minimum compression ratio for knock close to the chemically correct mixture. Both fuels show marked temperature sensitivity; this has been demonstrated for both weak, and chemically correct, mixtures. The two fuels differ in the extent of the reduction in knock resistance with moderate increases in charge temperature. It is suggested that this effect is explicable in terms of the differing effects of formaldehyde as an additive. D. Downs, J. C. Street and R. W. Wheeler[9] have shown that with methane (and benzene) formaldehyde is a pro-knock, whereas with fuels exhibiting a low temperature system formaldehyde is almost without effect. A similar trend in the position of spontaneous ignition limits in a closed vessel experiment has been recorded by G. H. H. Chamberlain and A. D. Walsh[10]. There is also a marked similarity in shape between the knock/temperature curves, and the knock/added formaldehyde curves of Downs, Walsh and Wheeler[9]. It has been well established that formaldehyde is a product of slow oxidation with both methane and propane, and it is to be expected that its concentration during the compression stroke will increase with increasing charge temperature.

If the variation in knock resistance is considered as a function of the compression temperature (*Figure 4*) the distinction between the two fuels is even more marked. Methane shows a steady reduction, while propane is little affected until a certain temperature is reached beyond which the reduction is well marked, for approximately 80° further increase in compression temperature, beyond which the pre-knock effect disappears. This is strong evidence for the production by slow oxidation, at least for propane, of active pro-knock substances, and for their formation or survival to be critically dependent on temperature. For methane it would appear that either slow oxidation is absent for the temperature/time conditions applying for the compression strokes or that the major products are not pro-knock.

It has also been shown that a steep reduction in knock resistance confined to a narrow range of temperature results from the slow oxidation of a small proportion of the charge (usually 5 per cent) in a furnace before admission to the engine. This effect has previously been observed by R. Oberdorfer[11], using *n*-heptane. It has also been possible to compare the present work with that of Walcutt, Mason and Rifkin[3] in which a motored engine was used to pre-react an *iso*octane–air mixture. A comparison of results by all methods is shown in *Figure 5*. Oberdorfer noted, and the present work has confirmed, that the products of slow oxidation active in promoting knock are formed at temperatures insufficient to give cool flames in the furnace tube. This does not rule out, however, the subsequent development of a cool flame during the engine compression stroke.

It is interesting to note that the three fuels for which a sudden drop in knock-limited compression ratio at a critical temperature has been established would all be classed as of the low temperature type. In a knocking engine it does not necessarily follow that the slow oxidation reactions lead to the passage of a cool flame before knock. Under some conditions the passage of a cool flame prior to knock appears probable, particularly judged by the two-stage nature of the peroxide curves[5] and from stroboscopic photomultiplier records[12] from a knocking region. It also leads to the conclusion that the fall in compression ratio at a critical temperature is closely linked with reactions in the low temperature region. It would seem reasonable to presume that the products formed in the furnace by slow oxidations, which lead to a sudden lowering of the knock resistance in the engine, also contribute to the development of cool flames and low temperature ignition in a spontaneous ignition experiment. A similarity in overall mechanism is also suggested. The similarity in the products formed during the compression stroke[5], during the development of spontaneous ignition in an engine[6, 13] and in a static experiment[14], is most marked.

C. N. SATTERFIELD and R. C. REID[15] have studied extensively the slow reactions of propane and oxygen over a wide range of temperatures. It has been shown that the products formed depend on the temperature. At low temperatures (below 350°C for Satterfield's experiments) hydrogen peroxide is an important product. At higher temperatures it is suggested that the concentration does not increase due to the increasing rate of decomposition. Pahnke, Cohen and Sturgis[6] have shown that hydrogen peroxide is a product of slow reaction in the engine and that it is the concentration of hydrogen peroxide that is greatly affected when knock or spontaneous ignition is suppressed by the addition of tetraethyl lead. Hydrogen peroxide has also been detected in the slow oxidation of *iso*octane and *n*-heptane by C. E. FRANK and A. U. BLACKMAN[16]. Hydrogen peroxide is now well accepted as a violent pro-knock with all fuels[5, 17]. It is suggested that it may be the formation of hydrogen peroxide by slow oxidation that is responsible for the marked lowering of knock resistance at a critical temperature with fuels of the low temperature type. Formaldehyde is well known as a major product in the slow oxidation of all hydrocarbons. Nevertheless, if hydrogen peroxide formation by slow oxidation is responsible for the sudden lowering of knock resistance it is not understood why this effect is absent when the products of propane oxidation are added to an engine running on methane. It is probable that the formation of hydrogen peroxide is not confined to reactions in the furnace but continues during the engine compression stroke. It is possible that continued reaction is inhibited by methane since methane is known to inhibit the slow oxidation of hydrogen[18].

Department of Mechanical Engineering,
Imperial College of Science and Technology

(*Received January 1957*)

REFERENCES

[1] MOORE, N. P. W. and ROY, B. N. *Chart. mech. Engr*, 1956, **3**, No. 6

[2] DOWNS, D. and PIGNÈGUY, J. H. *Proc. Auto. Div. Instn mech. Engrs*, 1950–51, Part 4, 125

[3] WALCUTT, C., MASON, J. M. and RIFKIN, E. B. *Industr. Engng Chem. (Industr.)*, 1954, **46**, No. 5, 1029

[4] EGERTON, A. C., SMITH, F. L. and UBBELOHDE, A. R. *Phil. Trans. A*, 1935, **234,** 433

[5] DOWNS, D., WALSH, A. D. and WHEELER, R. W. *Phil. Trans. A*, 1951, **243,** 463

[6] PAHNKE, A. J., COHEN, P. M. and STURGIS, B. M. *Industr. Engng Chem. (Industr.)*, 1954, **46,** No. 5, 1024

[7] JONES, G. W., KENNEDY, R. E. and SPOLAN, I. *Rep. Invest. U.S. Bur. Min. No. 4557* (1949)

[8] BROWN, A. T. *Automot. Industr., N.Y.* 1951, **104,** No. 4, 42 and 108

[9] DOWNS, D., STREET, J. C. and WHEELER, R. W. *Fuel, Lond.*, 1953, **32,** No. 3, 279

[10] CHAMBERLAIN, G. H. H. and WALSH, A. D. *Rev. Inst. franç. Pétrole*, 1949, **4,** 301

[11] OBERDORFER, R. Contribution to discussion of paper by M. W. CORZILIUS *et alii. S.A.E. quart. Trans.* 1953, **61,** 387

[12] WENTWORTH, J. T. and DANIEL, W. A. Contribution to discussion of paper by G. A. BALL. *S.A.E. Jl*, **1955,** 48

[13] MALMBERG, E. W., SMITH, M. L., BIGLER, J. E. and BABBITT, J. A. *Fifth Symposium (International) on Combustion*, p 385. Reinhold: New York, 1955

[14] NEWITT, D. M. and THORNES, L. S. *J. chem. Soc.* **1937,** 1656 and 1669

[15] SATTERFIELD, C. N. and REID, R. C. *Fifth Symposium (International) on Combustion*, p 511. Reinhold: New York, 1955

[16] FRANK, C. E. and BLACKMAN, A. U. *Industr. Engng Chem. (Industr.)*, 1954, **46,** No. 1, 212

[17] EGERTON, A. C. and MOORE, N. P. W. *Nature, Lond.*, 1949, **163,** 917

[18] BALDWIN, R. R., CORNEY, N. S. and SIMONS, R. F. *Fifth Symposium (International) on Combustion*, p 502. Reinhold: New York, 1955

Considerations Pertaining to Spherical-vessel Combustion[*]

J. GRUMER, E. B. COOK and T. A. KUBALA

Certain considerations bearing on the interpretation of measured flame speed and pressure rise rates during combustion in a spherical vessel are treated in this paper.

A. *The relation between the pressure rise and the fraction of the charge burnt as the wave traverses the vessel is involved in the evaluation of laminar burning velocity. New considerations are presented show that under the conditions of measurement the relation given by Flamm and Mache is equivalent to the equation*

$$n = (P - P_i) / P_i \gamma_u (E - 1)$$

where E is the expansion ratio for constant-pressure burning at P_i, the initial pressure, and n is the fraction burnt.

B. *An experimental technique has been developed to determine approximate empirical values of the expansion ratios for gases passing through a laminar combustion wave.*

C. *New data have been obtained over a range of sub-atmospheric and supra-atmospheric pressures to show that the pressure dependence of the burning velocity can be positive. However, a previous correlation of pressure exponents with only the burning velocity was found to be an oversimplification of the situation.*

D. *Observations were made of peak pressures and end pressures after cooling resulting from the combustion of very rich hydrogen–air mixtures at initial pressures of a half to three atmospheres. Observed values were within a few per cent of theoretical values based on assumed thermochemical equilibrium in the burnt gas.*

THE measurement of burning velocity by means of a closed spherical vessel is a procedure of long standing[1,2,3]. The spherical-vessel method has also been used to determine the pressure dependence of the burning velocity[4,5]. This paper deals mainly with recent improvements in theory and verification of the previous finding[4,5] that the pressure exponent of the burning velocity is positive for some mixtures. The ability to measure approximately expansion ratios of gases burning in a closed vessel and new tests for thermochemical equilibrium in the burnt gases and some miscellaneous considerations are also reported.

A. RELATION OF PRESSURE RISE AND FRACTION OF CHARGE BURNT

The relation between the pressure rise and the fraction of the charge burnt as the wave traverses the vessel contents is involved in the spherical-vessel method of obtaining burning velocity. L. FLAMM and H. MACHE[3,6] derived the relation as being

$$1 - n = \frac{RT_i (P_e - P)}{P_i [RT_u (\gamma_b - \gamma_u)/(\gamma_u - 1) + K (\gamma_b - 1)]} \qquad \ldots . [1]$$

In equation 1, n is the fraction burnt, R is the gas constant, K is a constant, γ is the specific heat ratio, T is temperature, P is pressure, and the subscripts

---

[*] Division of Explosives Technology Report No. 1238.

i, u, b and e indicate the initial, ambient, burnt and end states of the combustion process. Later, the assumption was made that T_i may be substituted for T_u, changing equation 1 to equation 2[5, 7].

$$n = (P - P_i)/(P_e - P_i) \qquad \ldots . [2]$$

The substitution was justified by noting that it changed the value of $1-n$ very little. However, for an error of y in $1-n$, the error in n is $(y/n)(1-n)$. When measuring burning velocities, small values of n are employed and errors in n result in about equal errors in the burning velocity. In this way, when $n \sim 0{\cdot}03$, a change in $1-n$ of 0·3 per cent will change n and the burning velocity by about 10 per cent.

Instead of the above substitution, T_u has been evaluated when $P/P_i \leqslant 1{\cdot}1$. Using this result, equation 1 has been transformed into equation 3, with an introduced error in n of less than one per cent.

$$n = (P - P_i)/P_i\gamma_u(E - 1) \qquad \ldots . [3]$$

Here, $E = (m_b T_b)/(m_i T_i)$ is the expansion ratio for constant pressure burning at $P_i T_i$; m is mols. (It is shown in Appendix I that equation 3 is an approximate simplification of equation 1 which was derived earlier by Flamm and Mache[6]. Equation 3 has been derived independently from other considerations by R. ESCHENBACH and J. T. AGNEW[8].) Since approximations are involved in reaching equations 2 and 3, it seemed best to determine experimentally whether equation 3 was more correct than equation 2. This has been done by comparing expansion ratios based on each of these two 'theoretical' equations using thermodynamically computed values with non-thermodynamically based expansion ratios based on experimental flame speed and pressure rise records. The three expansion ratios for closed vessel combustion (flame speed/burning velocity $= S/S_u$) are

$$S/S_u = 1 + [(P_e/P) - 1]/\gamma_u \qquad \text{from equation } 2^9 \qquad \ldots . [4]$$

$$S/S_u = E\,P_i/P \qquad \text{from equation 3} \qquad \ldots . [5]$$

$$S/S_u = 1\Big/\left[1 + \frac{\mathrm{d}\ln P^{1/\gamma_u}}{\mathrm{d}\ln(a^3 - r^3)}\right] \qquad \text{from experimental records} \qquad \ldots . [6]$$

The new symbols in equation 6 are a = vessel radius and r = flame radius.

Equation 3 is clearly favoured by data taken with rich hydrogen–air mixtures over a range of initial pressures of a half to three atmospheres. The data for this comparison are given in *Table 1*. The derivations for equations 3, 4, 5 and 6 are given in Appendixes I and II. The effect of asphericity of flame on equation 6 is discussed in Appendix III.

Substitution of equation 3 for equation 2 will lower the 'spherical-vessel' burning velocities reported in refs. 3, 4, 5, 9 and 10 by about the factor $\gamma_b/\gamma_u \sim 1{\cdot}1$. Burning velocities reported in this paper are based on equation 3. Except for this substiution and for modification of the procedure used to phase the records (see Appendix III), the reduction of flame growth and pressure rise records into burning velocities followed the procedure described in ref. 9.

Table 1. Comparison of experimental and theoretical expansion ratios of rich hydrogen air flames in the 30 cm i.d. spherical vessel

Per cent fuel	*Initial pressure cm* Hg	*Expansion ratios*			*Deviations, per cent*	
		1	*2*	*3*	$\frac{1-2}{1}$	$\frac{1-3}{1}$
58·3	38	4·94	5·15	4·86	−4·3	2·3
60·0*	75	6·23	4·99	4·68	20·0	24·5
60·1*	75	6·56	4·99	4·69	23·8	28·4
60·2*	153	3·90	4·99	4·68	−27·9	−20·2
60·5*	153	5·86	4·99	4·68	15·0	20·2
51·2	215	4·82	5·69	5·28	−18·0	−9·4
60·0*	216	5·13	4·97	4·66	3·2	9·1
67·7	216	4·31	4·34	4·13	−0·7	4·1
60·1*	218	4·33	4·97	4·67	−14·8	−7·9
				Average	14·2	14·0
				Sum	−4·7	51·1
Average of starred runs		5·33	4·98	4·68	6·6	12·2

Values of S/S_u when flame radius is 3 cm [from column 1—equation 6 (experimental); (2—equation 5); (3—equation 4 (theoretical)].

B. EXPANSION RATIOS

The experimental techniques employed to obtain the values in column 1 of *Table 1* are also suited for the empirical determination of the approximate expansion ratio S/S_u. This technique should be useful in instances when expansion ratios are not calculable with confidence from thermodynamic data. S/S_u is obtained entirely from experimental records by means of equation 6.

The fluctuations of values of S/S_u in column 1 of *Table 1* are attributed to experimental difficulties. It may be possible to reduce these difficulties by improving equipment. As long as the fluctuations are random, accuracy in S/S_u from equation 6 can be improved by averaging many runs. R. ESCHENBACH and J. T. AGNEW recently discussed[8] the difficulties of obtaining exact values of S_u and E from simultaneous radius and pressure measurements. Their discussion does not treat the techniques suggested in this section. Eschenbach and Agnew discuss difficuties inherent in attempting to solve for E by equating two approximate equations, each of which by itself involves the use of a thermochemically computed E. In the above section, S/S_u from equation 6 is based on a derivation which does not use a thermochemically computed E (see Appendix II).

C. NEW BURNING-VELOCITY DATA AND PRESSURE DEPENDENCE OF THE BURNING VELOCITY

The intent behind this phase of the investigation was to test* the validity of previously reported[4, 5, 10] positive pressure exponents and the dependence of these exponents on the magnitude of the burning velocity only[1, 3]. The theoretical significance of these previous findings has been indicated[1, 11].

---

*The authors had several reasons for desiring to add to previous data on the pressure dependence of burning velocity. Results with burners suffer from uncertainties discussed in ref. 12. The data on fast flames in ref. 10 are based on flame size/time measurements only and differ significantly from data in refs. 4 and 5. Due to a drum camera speed of about 300 cm/sec, the reading error (for data in refs. 4 and 5) was negligible for slow-burning mixtures but significant for fast-burning mixtures with flame speeds exceeding about 2 000 cm/sec. For the experiments reported in this paper the reading error due to the speed of the drum camera is always negligible.

Table 2 contains data on rich hydrogen–air mixtures. The burning velocities of mixtures between 43 and 51 per cent hydrogen–air are observed to increase with increasing initial pressure, confirming the reality of positive 'pressure exponents'. Those for mixtures around 60 per cent hydrogen have little pressure dependence. Around 67 per cent, a negative dependence is observed.

Table 3 contains data comparing the burning velocities of hydrogen–air and deuterium–air mixtures. The latter are slower burning, reflecting the significance of diffusional processes in propagation of these combustion waves. The data also show that the pressure dependence of the burning velocity can vary with mixture composition and the pressure range under consideration. The correlation[1, 3] of pressure exponents with the burning velocity only is an oversimplification of the situation.

Table 2. Flame speeds and burning velocities of rich hydrogen–air flames

	Flame speed, cm/sec		*Burning velocity, cm/sec*			*Per cent deviations,*
Per cent fuel	*Flame record (obs.)*	*Pressure record (calc.)*	*Flame record* $(S_u)_f$	*Pressure record* $(S_u)_p$	*Average*	$(S_u)_f - (S_u)_p / 2(S_u)_{av}$
Initial pressure: 38 cm of mercury						
43·2	1463	1507	232	239	235	−1·3
46·4	1402	1436	230	235	232	−1·2
51·1	1174	1149	204	199	201	1·0
53·8	1069	1081	192	194	193	−1·0
58·3	905	896	173	175	174	0·6
Initial pressure: 75 cm of mercury						
48·0	1414	1481	236	248	242	−2·4
49·0	1389	1451	235	245	240	−2·1
49·1	1418	1411	240	239	240	0·4
50·4	1355	1422	233	245	239	−2·4
50·5	1375	1394	237	239	238	−0·8
50·6	1385	1368	239	236	238	0·4
59·6	891	937	176	180	179	−1·2
60·0	849	868	175	179	177	−1·1
60·1	854	893	174	182	178	−2·3
66·9	538	550	121	126	124	−1·9
67·1	485	490	100	111	110	−0·5
Initial pressure: 153 cm of mercury						
48·7	1465	1545	247	261	254	2·5
60·2	832	832	168	168	168	0·0
60·5	812	840	160	166	163	−1·7
66·5	461	454	104	100	102	1·0
Initial pressure: 215 cm of mercury						
51·2	1395	1368	247	243	245	0·8
Initial pressure: 216 cm of mercury						
60·0	831	839	166	168	167	−0·6
67·7	325	330	74	76	75	−0·7
Initial pressure: 218 cm of mercury						
60·1	845	848	169	169	169	0·0

D. OVERALL THERMOCHEMICAL EQUILIBRIUM IN THE BURNT GAS

An implicit assumption in the use of flame growth/time or pressure rise/time records to obtain burning velocity data is that thermochemical equilibrium exists in the burnt gas. Although previous investigators[3] have shown this to be an acceptable assumption, their data include few experiments at elevated initial pressures and near flammability limits. Some new exploratory data are available which are presented in *Table 4*. These

Table 3. Burning velocities of hydrogen and deuterium–air flames, relative to pressure and to each other

Per cent fuel	*Initial pressure, cm* Hg	*Burning velocity*		*Pressure exponent**		$\frac{(S_u)_{H_2}}{(S_u)_{D_2}}$
		H_2–*air*	D_2–*air*	H_2–*air*	D_2–*air*	
30	38		126†		0·19	
30	75		144†			
50	38	210‡	163†	0·20	0·05	1·29
50	75	240‡	169†			1·42
60	38	163§	148†	0·12	0	1·10
60	75	177	150†			1·18
60	153	169‡		−0·11		
60	216	167		−0·06		
61·2	75	167‡	134			1·24
66·3	75	123‡	95			1·30
66·6	75	120‡	95‡			1·26
67·0	75	117‡	95			1·23
67·0	153	97§		−0·44		
67·0	216	84‡		−0·31		

* $\frac{(S_u)_{P=75\text{ cm Hg}}}{S_u} = \left(\frac{75}{P}\right)^{\text{exp.}}$

†Data obtained by J. Manton and E. B. Cook.

‡Interpolated values.

§Extrapolated values.

Table 4. Comparison of experimental (1) and theoretical (2) peak pressures and final pressures after cooling of rich hydrogen–air flames in the 12 in. i.d. spherical vessel

Per cent fuel	*Initial pressure, cm* Hg	*Peak pressures P_e cm* Hg		*Final – initial pressures cm* Hg	
		1	*2*	*1*	*2*
58·3	38			8·0	8·0
47·7	75	569	548		
59·6	75			17·0	16·6
60·0	75			16·7	16·5
60·1	75			16·5	16·4
60·3	75			15·8	16·3
50·9	153			43·6	44·0
59·8	153			37·1	36·3
59·9	153			35·6	36·2
60·2	153			35·6	36·0
60·5	153			38·2	35·7
61·7	153			33·8	34·5
66·5	153	890	855	29·9	29·9
49·8	213			63·6	65·3
50·6	216			63·2	64·6
51·2	215			65·3	64·5
60·1	218			52·5	52·7
67·7	216			40·4	41·6

data extend the range of conditions where overall thermochemical equilibrium in the burnt gas has been found. The experimental values in *Table 4* consist of observations of end pressures after cooling and peak pressures resulting from the combustion of very rich hydrogen–air mixtures at initial pressures of a half to three atmospheres.

A new spherical vessel is being constructed to extend the range of study of spherical combustion waves to elevated initial pressures (up to 20 atmospheres) and initial temperatures (up to 300° C).

This research is sponsored by Project SQUID, which is supported by the Office of Naval Research under Contract Nonr 1858(25) NR–098–038. Reproduction in full or in part is permitted for any use of the U.S. Government.

The authors are indebted to Dr D. S. Burgess and E. L. Litchfield of the Bureau of Mines, and Drs R. Eschenbach and J. T. Agnew of Purdue University for many fruitful discussions.

Flame Research Section,
Division of Explosives Technology,
U.S. Bureau of Mines,
Pittsburgh, Pa

(Received October 1958)

APPENDIX 1

Relation between fraction of charge burnt and the pressure rise

Equation 1 can be rearranged to equation 7 by cancelling out RT_i.

$$1-n=\frac{P_e-P}{P_i\left[\frac{T_u}{T_i}\left(\frac{\gamma_b-\gamma_u}{\gamma_u-1}\right)+\frac{K}{RT_i}(\gamma_b-1)\right]} \qquad \ldots.[7]$$

Let $n=0$, $T_u=T_i$ and $P=P_i$. Then equation 7 becomes 8.

$$\left(\frac{\gamma_b-\gamma_u}{\gamma_u-1}\right)+\frac{K}{RT_i}(\gamma_b-1)=\frac{P_e-P_i}{P_i} \qquad \ldots.[8]$$

This result may be substituted into equation 7 after adding and subtracting to the denominator the term $(\gamma_b-\gamma_u)/(\gamma_u-1)$. One then obtains equation 9.

$$1-n=\frac{(P_e-P)/P_i}{\frac{P_e-P_i}{P_i}+\left(\frac{T_u}{T_i}-1\right)\left(\frac{\gamma_b-\gamma_u}{\gamma_u-1}\right)} \qquad \ldots.[9]$$

Since

$$(T_u/T_i)=(P/P_i)^{(\gamma_u-1)/\gamma_u} \qquad \ldots.[10]$$

and this is approximately equal to

$$T_u/T_i=1+(\gamma_u-1)(P-P_i)/P_i\gamma_u \qquad \ldots.[11]$$

when T_u/T_i is near unity, one may write equation 9 as

$$1-n=\frac{P_e-P}{(P_e-P_i)-(\gamma_u-\gamma_b)(P-P_i)/\gamma_u} \qquad \ldots.[12]$$

The transition from equation 9 to 12 introduces an error in n of $< 0{\cdot}5$ per cent for values of $P/P_i \leqslant 1{\cdot}1$. Within this region n is usually $< 0{\cdot}02$. Equation 12 can be rearranged to give equation 13.

$$n=\frac{(\gamma_b/\gamma_u)(P-P_i)}{P_e-P_i-(\gamma_u-\gamma_b/\gamma_u)(P-P_i)} \qquad \ldots.[13]$$

For usual values of the pressures and heat capacities when $n < 0{\cdot}02$, omitting the term $(\gamma_u-\gamma_b)(P-P_i)/\gamma_u$ produces an additional error in n of $< 0{\cdot}25$ per cent. This step leads to equation 14.

$$n=\frac{\gamma_b}{\gamma_u}\frac{P-P_i}{P_e-P_i}=\frac{\gamma_b}{\gamma_u P_i}\frac{(P-P_i)}{\{(M_i/M_{b,i})(T_e/T_i)-1\}} \qquad \ldots.[14]$$

It has been assumed in equation 14 that $M_e=M_{b,i}$. J. MANTON, B. LEWIS and G. VON ELBE[9] define T_e so that

$$\frac{M_i T_e}{M_b T_i}-1=\gamma_b\left(\frac{M_i T_{b,i}}{M_b T_i}-1\right)=\gamma_b(E-1) \qquad \ldots.[15]$$

(Equation 14 in ref. 9 was inadvertently miswritten.) Substituting in equation 14, one obtains equation 3. It is significant to note that equation 3 yields good approximations of n when $P/P_i \leqslant 1{\cdot}1$. At higher pressure ratios, other more accurate considerations need to be made.

APPENDIX II

Derivation of equations 4 to 6

Equation 4—When employing equation 2, the expansion ratio (experimental flame speed/burning velocity $= S/S_u$) is given by equation 17 of ref. 9. It has been rewritten as equation 4 of this paper.

Equation 5—The same mathematical logic was employed to obtain equation 5, which differs essentially from equation 4, in that equation 5 is based on a more exact evaluation of n, the fraction of charge burnt.

Equation 16 is obtained by differentiating equation 3.

$$\frac{\mathrm{d}n}{\mathrm{d}t}=\frac{1}{\gamma_u P_i(E-1)}\frac{\mathrm{d}P}{\mathrm{d}t} \qquad \ldots.[16]$$

Equation 17 is the same as equation 11 of ref. 9.

$$\frac{\mathrm{d}n}{\mathrm{d}t}=3\left(\frac{P}{P_i}\right)^{(1/\gamma_u)}\frac{r^2}{a^3}S-\frac{1}{\gamma_u}\left(\frac{P}{P_i}\right)^{(1-\gamma_u)/\gamma_u}\left(1-\frac{r^3}{a^3}\right)\frac{1}{P_i}\frac{\mathrm{d}P}{\mathrm{d}t} \qquad \ldots.[17]$$

The expression for $\mathrm{d}P/\mathrm{d}t$ is obtained from equation 16 and substituted in equation 17, resulting in equation 18.

$$\frac{\mathrm{d}n}{\mathrm{d}t}=3\left(\frac{P}{P_i}\right)^{(1/\gamma_u)}\frac{r^2}{a^3}S-\left(\frac{P}{P_i}\right)^{(1-\gamma_u)/\gamma_u}\left(1-\frac{r^3}{a^3}\right)(E-1)\frac{\mathrm{d}n}{\mathrm{d}t} \qquad \ldots.[18]$$

Equation 9 from ref. 9 is rewritten as equation 19.

$$1 - r^3/a^3 = (1-n)(P_i/P)^{(1/\gamma_u)} \qquad \ldots . [19]$$

This is substituted into equation 18, which is then rearranged to obtain equation 20.

$$\frac{dn}{dt} = \frac{3(P/P_i)^{(1/\gamma_u)}(r^2/a^3)S}{1+(P_i/P)(1-n)(E-1)} \qquad \ldots . [20]$$

Equation 7 of ref. 9 is next employed. This is given here as equation 21.

$$S_u = \frac{1}{3}\frac{dn}{dt}\frac{a^3}{r^2}\left(\frac{P_i}{P}\right)^{(1/\gamma_u)} \qquad \ldots . [21]$$

The solution for dn/dt from equation 20 is substituted in equation 21 to yield

$$\frac{S}{S_u} = 1 + \frac{P_i}{P}(1-n)(E-1) \qquad \ldots . [22]$$

Eliminating n by means of equation 3 results in

$$\frac{S}{S_u} = 1 + \frac{P_i\gamma_u(E-1) - P + P_i}{P\gamma_u} \qquad \ldots . [23]$$

Equation 5 is a fairly exact approximation of equation 23, since $(\gamma_u - 1)(P - P_i) \ll P_i\gamma_u E$.

Equation 6—The experimental value of S/S_u can be obtained by rearranging equation 12 of ref. 9. It becomes the following equation 24.

$$\frac{S_u}{S} = 1 - \left(\frac{a^3 - r^3}{3r^2 S}\right)\left(\frac{1}{\gamma_u P}\frac{dP}{dt}\right) \qquad \ldots . [24]$$

Since $3Sr^2 = dr^3/dt$, and $d(a^3 - r^3) = -dr^3$, this is equivalent to

$$\frac{S_u}{S} = 1 + \frac{d \ln P^{(1/\gamma_u)}}{d \ln (a^3 - r^3)} \qquad \ldots . [25]$$

The reciprocal of S_u/S from equation 25 is an experimental expansion ratio based on readings of the pressure rise and flame growth as a function of time.

APPENDIX III

Miscellany

A. *Expansion ratio at the flame front*—The treatment of L. FLAMM and H. MACHE[6] resulting in equation 1 recognizes that the burnt-gas temperature in a differential element dn is T_b at the instant of burning and T_{b_r} at a later time when the wave has consumed more of the unburnt gas[3]. $T_{b_r} > T_b$ due to the adiabatic compression of the burnt gas from an early dn by the burning of subsequent differential elements of the mixture. This treatment is proper for determining the fraction of charge burnt, the burning velocity and the expansion ratio of all the burnt gas contained within the advancing flame front.

However, there may be interest in following E_r, the local expansion ratio —i.e. the expansion ratio of an element dn at the instant of its combustion.

For this purpose, cognizance may be taken of the conservation of mass during combustion and of the ambient temperature and pressure in the unburnt gas at the instant of interest.

$$\rho_u 4\pi r^2 S_u \, \mathrm{d}t = \rho_b 4\pi r^2 S \, \mathrm{d}t \qquad \ldots . [26]$$

Accordingly

$$\frac{S}{S_u} = \frac{\rho_u}{\rho_b} = \frac{\rho_i}{\rho_{b_i}} \frac{T_i}{T_u} \frac{T_b}{T_{b_i}} \frac{P}{P_i} \frac{P_i}{P} \qquad \ldots . [27]$$

Using equation 10,

$$\frac{S}{S_u} = E \frac{T_b}{T_{b_i}} \left(\frac{P_i}{P}\right)^{(\gamma_u - 1)/\gamma_u} \qquad \ldots . [28]$$

When (P_i/P) is nearly unity, T_b is not significantly larger than T_{b_i}. Later in the progress of the wave through the vessel, T_b can be calculated thermodynamically or approximated by assuming that

$$\frac{T_b}{T_i} \sim \frac{T_{b_i}}{T_i} + \left[\left(\frac{P}{P_i}\right)^{(\gamma_u - 1)/\gamma_u} - 1\right] \qquad \ldots . [29]$$

B. *Effect of asphericity of flame on equation 6*—Equation 6 is based on the assumption that the flame propagates spherically[9]. If it does not do so, the relation between the pressure-rise rate and the spread of flame along an axis of measurement ($\mathrm{d}r$) is not given accurately by equation 6. Assuming that the flame is spherical when it is aspherical introduces errors into calculations by means of this equation. (One can test for asphericity or wrinkling of the flame surface by comparing flame-growth data plus thermodynamic data with pressure-rise data plus other thermodynamic data. A better way to test for sphericity during a run is to measure flame size along cross sights. As yet this has not been done.) The spread of values in column 1 in *Table 1* is felt to be due largely to undetected asphericity of flame. The difficulty was circumvented by averaging a number of runs.

The sensitivity of equation 6 to asphericity of flame can be illustrated by assuming, in turn, that one measures flame growth along an axis of a spherical or spheroidal flame. For the sphere:

$$-\mathrm{d}(a^3 - r^3) = \mathrm{d}r^3 = a^3 \left[\left\{ 1 - n_2 \left(\frac{P_i}{P_2}\right)^{1/\gamma_u} \right\} - \left\{ 1 - n_1 \left(\frac{P_i}{P_1}\right)^{1/\gamma_u} \right\} \right]$$

$$= a^3 \, [\mathrm{f}\, P_2, P_1] \qquad \ldots . [30]$$

prolate spheroid:

Major semi-axis Apparent $\mathrm{d}r^3 = (a^3/\sigma^2) \quad [\mathrm{f}\, P_2, P_1]$

Minor $= a^3\sigma \quad [\mathrm{f}\, P_2, P_1]$

oblate spheroid:

Major semi-axis $= (a^3/\sigma) \quad [\mathrm{f}\, P_2, P_1]$

Minor $= a^3\sigma^2 \quad [\mathrm{f}\, P_2, P_1]$

where σ denotes the ratio of minor to major axis.

Assuming that S/S_u in equation 6 should equal 5, that the flame is a prolate spheroid of $e = 0{\cdot}95$ and that it is being observed along its minor axis—then equation 6 will result in an apparent value of $S/S_u = 6{\cdot}25$. This is an error of about 25 per cent. Due to this effect, it is desirable to measure the sphericity of flame as it propagates through the vessel.

It is also necessary to test for wrinkling of the flame surface. One test is that of examining the body of the schlieren flame trace, over the interval used to measure the burning velocity. If the magnification factor of the optics is near unity or greater, it is possible to see flame wrinkling as traces within the body of the flame outline. Usually such traces appear in the end of the record as the flame nears the walls of the vessel.

C. *Phasing pressure-rise and flame-growth records*—It is unnecessary to locate zero time on the records of pressure rise and flame growth when equations 5, 6 or 21 are used independently to obtain the burning velocity.

(*1*) Flame record and equation 5—equations 3 and 19 furnish values of P.

(*2*) Pressure record and equation 21—equations 3 and 19 furnish values of r and $\mathrm{d}n/\mathrm{d}t$.

(*3*) Flame record, pressure record and equation 6—A 'least squares' fit is made to values of the ratio of $(\Delta/\Delta t)\ln P^{1/\gamma_u}$ to $(\Delta/\Delta t)\ln(a^3 - r^3)$ versus r^3 to obtain equation 31.

$$\frac{\mathrm{d}\ln P^{1/\gamma_u}}{\mathrm{d}\ln(a^3 - r^3)} = B + 2cr^3 \qquad \ldots . [31]$$

This suffices for the solution of equation 6.

REFERENCES

[1] NAGEL, A. *Forschungsh. Ver. dtsch. Ing.* 1907, **54**; *Engineering, Lond.* 1908, **86**, 278

[2] WATERMEIER, L. A. *J. chem. Phys.* 1957, **27**, 1118

[3] LEWIS, B. and VON ELBE, G. *Combustion, Flames and Explosions of Gases*, pp 448–59, 473–79, 656–64. Academic Press: New York, 1951

[4] LEWIS, B. *Selected Combustion Problems*, pp 176–78. AGARD; Butterworths: London, 1954

[5] MANTON, J. and MILLIKEN, B. B. *Proceedings of the Gas Dynamics Symposium on Aerothermochemistry*, pp 151–57. Northwestern University, 1956

[6] FLAMM, L. and MACHE, H. *S. B. Akad. Wiss. Wien*, 1917, **126**, 9

[7] LEWIS, B. and VON ELBE, G. *J. chem. Phys.*, 1934, **2**, 667

[8] ESCHENBACH, R. and AGNEW, J. T. *Combustion & Flame*, 1958, **2**, 273

[9] MANTON, J., LEWIS, B. and VON ELBE, G. *Fourth Symposium (International) on Combustion*, pp 358–63. Williams and Wilkins: Baltimore, 1953

[10] SMITH, D. and AGNEW, J. T. *Sixth Symposium (International) on Combustion*, pp 83–88. Reinhold: New York, 1957

[11] GILBERT, M. *Sixth Symposium (International) on Combustion*, pp 74–83. Reinhold: New York, 1957

[12] SINGER, J. M., GRUMER, J. and COOK, E. B. *Proceedings of the Gas Dynamics Symposium on Aerothermochemistry*, pp 139–50. Northwestern University, 1956

On the Existence of Steady State Flames[*]

A. L. BERLAD and C. H. YANG

Examination of the adiabatic flame theories shows that the conditions, 'adiabatic' and 'steady state', imposed on the flame model are contradictory when a realistic reaction rate law is used. For the case of a freely propagating *flame, only a quasi-steady state can be achieved, even though the 'adiabatic' condition is removed.*

THERE have been several theoretical treatments of 'one-dimensional, adiabatic, steady state, laminar' flames[1, 2, 3]. These formulations represent attempts to describe the behaviour and structure of a flame; a dominating feature of theory and experiment is the fact that there exists a characteristic 'burning velocity'. The reasonableness of the burning velocities and flame structures resulting from the application of these theoretical treatments argues for their worth[1-3]. However, there are difficulties in the application of these theories which appear to *demand* one or the other of the following assumptions:

(*a*) there exists a flameholder at the cold boundary which serves as a small but finite heat sink;

(*b*) or, there exists a temperature, greater than the initial reactant temperature, below which chemical heat release is identically zero.

There are objections to both of these assumptions. These objections may be made on physical grounds. Assumption (*a*) is inconsistent with a general picture of a freely propagating flame, that is, a flame which does not have a 'flameholder' propagating along with it. Even more disconcerting is the fact that the model of ref. 2 lends itself to analysis even though heat losses (such as radiation and radial conduction) are neglected at all points in space except *at* the cold boundary. Neglect of the very small heat loss *at* the cold boundary prevents the existence of a solution. Assumption (*b*) represents the neglect of a very small amount of heat release on the cold side of the considered flame. Here again, small errors in the heat release throughout the flame appear to be relatively unimportant to the results. Yet, neglect of the very small amount of heat release implied by an ignition temperature prevents the existence of a solution.

It is the purpose of this paper to examine these previously treated flame models and show that the aforementioned difficulties arise from inconsistencies implicit in the models. In addition, it is shown that these difficulties need not arise when one considers an alternative model of a freely propagating flame.

---

[*] Paper presented in part at the June 1958 meeting of the Western States Section (U.S.A.) of the Combustion Institute.

THE ALLOWED SOLUTIONS ASSOCIATED WITH THE ENERGY CONSERVATION EQUATION AND ITS BOUNDARY CONDITIONS

It has been pointed out[3] that difficulties at the 'cold boundary' arise for the case of a pure thermal theory as well as for the case where diffusion processes are considered also. Actually, these difficulties arise from the incompatibility of the energy conservation equation with its associated boundary conditions. Very simply, the assumption of 'Adiabatic' and 'Steady State' are incompatible. 'Adiabatic' implies no heat loss to cold boundaries. 'Steady State' implies a positive, non-zero temperature gradient at the boundaries.

Consider the basic energy conservation equation which is common to refs. 1, 2 and 3. Essentially this equation is of the form

$$(k/\dot{m})(\mathrm{d}T/\mathrm{d}x) = (1-\varepsilon)q + (T-T_f)c_p \qquad \ldots.[1]$$

where k denotes thermal conductivity; $\dot{m}$, the mass flow rate per unit area; T, the absolute temperature; ε, the degree of reaction completeness; q, the heat of combustion; T_f, the final temperature; and c_p, the heat capacity.

Equation 1, of course, implies the existence of a steady state (the temperature structure of the flame does not change with time). Logically, if this flame is to be considered adiabatic the following boundary conditions *must be* imposed

$$(\mathrm{d}T/\mathrm{d}x) \equiv 0 \text{ at } \begin{Bmatrix} T = T_0 \\ T = T_f \end{Bmatrix} \qquad \ldots.[2]$$

Let us now examine the solutions of the system defined by equations 1 and 2. Differentiation of equation 1 in conjunction with the non-essential assumption that average k values can be used, yields

$$(k/\dot{m})(\mathrm{d}^2T/\mathrm{d}x^2) = -q(\mathrm{d}\varepsilon/\mathrm{d}x) + c_p(\mathrm{d}T/\mathrm{d}x) \qquad \ldots.[3]$$

If the problem is properly defined and has a solution, equation 3 must hold *everywhere*. Let us now consider equation 3 at the point $T = T_0$. Let us separately consider the three terms of equation 3.

$(\mathrm{d}T/\mathrm{d}x)$: This term is identically zero by the adiabatic assumption.

$(\mathrm{d}\varepsilon/\mathrm{d}x)$: This term may be written

$$(\mathrm{d}\varepsilon/\mathrm{d}x) = (\mathrm{d}\varepsilon/\mathrm{d}\theta)(\mathrm{d}\theta/\mathrm{d}x) = (\rho/\dot{m})(\mathrm{d}\varepsilon/\mathrm{d}\theta) \qquad \ldots.[4]$$

where θ is the time variable, and ρ denotes density.

On physical grounds, one demands that

(*a*) $0 \leqslant \varepsilon \leqslant 1$

(*b*) $(\mathrm{d}\varepsilon/\mathrm{d}\theta)$ is always non-zero, positive. That is, a realistic rate law is chosen, requiring that a non-zero, positive heat release rate shall exist at T_0

(*c*) ρ is always positive.

On physical grounds, $(\mathrm{d}^2T/\mathrm{d}x^2)$ cannot be negative. If it were negative, this would imply a temperature less than T_0 in the neighbourhood of T_0.

It follows, then, that equation 3 cannot be satisfied at $T = T_0$. Strictly speaking, equation 1 has no solution when considered with the imposed boundary conditions. In other words the assumptions of 'steady state' and 'adiabatic' are incompatible. It will be shown later that the primary fault in this incompatibility lies in the assumption of the steady state. Even for the case of freely propagating, *non-adiabatic* flames, it appears that only a quasi-steady state can be achieved. However, for the special case of a flame seated on a cold flameholder, the steady state can exist.

EXAMINATION OF THE 'IGNITION TEMPERATURE', 'FLAMEHOLDER', AND 'TRUNCATED KINETICS' HYPOTHESES IN ADIABATIC FLAME THEORY

The assumption of any one of three physically unacceptable hypotheses ('Ignition temperature', 'Flameholder', 'Truncated kinetics') does allow a solution of equation 1. It can be shown that these assumptions are mathematically equivalent. Let us reconsider equation 3 in the following ways:

(*a*) If $(\mathrm{d}T/\mathrm{d}x)_{T=T_0} \equiv 0$ and $(\mathrm{d}\varepsilon/\mathrm{d}x)$ is non-zero, positive, then the only way to possibly satisfy equation 3 is to have $\dot{m} \to \infty$. Thus, the infinite burning velocity that is calculated[2, 3, 6] results *directly* from the simultaneous imposition of these incompatible conditions.

(*b*) Another way of satisfying equation 3 is to compromise the strict enforcement of the condition $(\mathrm{d}T/\mathrm{d}x) \equiv 0$ at $T = T_0$. Examination of equation 3 reveals that a small positive value of $(\mathrm{d}T/\mathrm{d}x)$ at $T = T_0$ can be chosen which will allow a solution of equation 1. This approach forces us to the concept of a cold boundary heat sink (flameholder) of such a size that

$$c_p\,(\mathrm{d}T/\mathrm{d}x) \geqslant q\,(\rho/\dot{m})\,(\mathrm{d}\varepsilon/\mathrm{d}\theta) \text{ at } T = T_0$$

It then follows that

$$\mathrm{d}^2T/\mathrm{d}x^2 \geqslant 0 \text{ at } T = T_0 \qquad \ldots.[5]$$

and that solutions of equation 1 exist.

(*c*) A third way of satisfying equation 3 is again to compromise a physical fact. In this case one neglects the heat release throughout a range, $T_0 \leqslant T \leqslant T_i$. Examination of equation 3 reveals that a value of $T_i > T_0$ can be chosen which will allow a solution of equation 1. This approach forces us to the concept of an 'ignition temperature', T_i. In the range $T_0 \leqslant T \leqslant T_i$ equation 3 is then written

$$(k/\dot{m})\,(\mathrm{d}^2T/\mathrm{d}x^2) = c_p\,(\mathrm{d}T/\mathrm{d}x) \geqslant 0 \qquad \ldots.[6]$$

and at $T = T_i$

$$(k/\dot{m})\,(\mathrm{d}^2T/\mathrm{d}x^2) = -q\,(\rho/\dot{m})\,(\mathrm{d}\varepsilon/\mathrm{d}\theta) + c_p\,(\mathrm{d}T/\mathrm{d}x) > 0 \qquad \ldots.[7]$$

In view of the fact that expressions 6 and 7 can both be satisfied, it follows that a solution of equation 1 exists.

The following is another way of examining the assumption of an 'ignition temperature'. Imposing a temperature below which heat release is identically zero allows satisfaction, at negative infinity, of the condition $(\mathrm{d}T/\mathrm{d}x) \equiv 0$. To demonstrate this fact, note that in the range $T_0 \leqslant T \leqslant T_i$

$$(k/\dot{m})\,(\mathrm{d}^2T/\mathrm{d}x^2) = c_p\,(\mathrm{d}T/\mathrm{d}x) \qquad \ldots.[8]$$

where the original boundary condition, $(\mathrm{d}T/\mathrm{d}x) = 0$ at $T = T_0$, can be combined with the condition, $T = T_i$ at $x = 0$ to yield a complete description of the temperature profile within this range. Integration of equation 8 results in the expression

$$(T-T_0)/(T_i-T_0)=\exp(c_p\dot{m}x/k) \qquad \ldots . [9]$$

It is clear that $T=T_0$ occurs at negative infinity. It is interesting to note that the assumption of an ignition temperature limits the flame reaction zone to a finite region. Obviously, as $T_i \rightarrow T_0$, where T_0 exists *only* at negative infinity, the reaction zone again becomes infinitely large.

(*d*) A number of authors[7–8] have obtained solutions to equation 1 with the use of 'truncated kinetics'. The various truncated kinetic schemes used by these authors have one property in common, that is, the reaction rate goes to zero as T goes to T_0. Thus, $\mathrm{d}\varepsilon/\mathrm{d}\theta$ becomes zero at $T=T_0$ and equation 3 is, of course, satisfied. The use of such a truncated reaction rate is actually equivalent to the use of an ignition temperature, T_i, which is very close to, but not equal to, T_0. From the considerations of section (*c*), it follows that the cold boundary goes to negative infinity when T_i approaches T_0. This is the conclusion implicit in the aforementioned work[7–8]. It is also the conclusion deduced by J. B. ROSEN[1].

It is thus seen that any of these physically unreal hypotheses (the existence of a 'flameholder' or the existence of an 'ignition temperature' or the allowance of suitably 'truncated kinetics') may be invoked in order to obtain a solution of equation 1. These assumptions are mathematically equivalent even though the physical interpretations are quite different. In view of the fact that $(\mathrm{d}\varepsilon/\mathrm{d}\theta)$ is usually very small in the neighbourhood of $T=T_0$, it follows that either a very small positive value of $(\mathrm{d}T/\mathrm{d}x)$ at $T=T_0$, or a value of T_i not much larger than T_0, or the use of kinetics which permits $\mathrm{d}\varepsilon/\mathrm{d}\theta$ to equal zero at $T=T_0$ will suffice in assuring a solution of equation 1.

AN ALTERNATIVE MODEL OF A FREELY PROPAGATING FLAME

It has been shown that the concepts of 'Adiabatic' and 'Steady State' are incompatible when a realistic reaction rate law is used. In addition, it can be shown that even for a *non-adiabatic flame theory* difficulties may arise in the neighbourhood of $T=T_0$ when the steady state is assumed.

Consider the steady-state energy conservation equation associated with a non-adiabatic flame

$$(\mathrm{d}/\mathrm{d}x)\,k\,(\mathrm{d}T/\mathrm{d}x)-c_p\dot{m}(\mathrm{d}T/\mathrm{d}x)+Rq-L=0 \qquad \ldots . [10]$$

where R denotes reaction rate and L is the heat loss function. This may be rewritten

$$(k/\dot{m})(\mathrm{d}^2T/\mathrm{d}x^2)=(\mathrm{d}T/\mathrm{d}x)\,[c_p-(1/\dot{m})(\mathrm{d}k/\mathrm{d}x)]+(1/\dot{m})(L-Rq) \ldots . [11]$$

Now, consider separately the various terms of equation 11 at $T=T_0$:

$(1/\dot{m})(L-Rq)$: If $\dot{m}$ is finite, the physical facts demand that L be zero at $T=T_0$ and R be non-zero, positive (as long as $T_0>0$).

Thus, this term is non-zero, negative at $T=T_0>0$).

The arguments used in the preceding section may again be invoked to show that the other terms in equation 11 are of such a nature as to prevent a solution. Thus, the presence of heat losses does *not* guarantee the existence of a steady state. It appears that the presence of a heat sink at $T = T_0$ is necessary for the existence of a steady state, even in the non-adiabatic case.

We may, however, consider this flame to be a quasi-steady[9], non-adiabatic system. Then, a heat sink at $T = T_0$ is not necessary. Let us visualize a freely propagating non-adiabatic flame in the following manner. Suppose that the flame starts at a given time with a steady state temperature profile. Physically, we have no heat sink at $T = T_0$. Thus, we can satisfy the steady state assumption everywhere except at $T = T_0$. It follows then that the temperature profile will be changing with time. This will require that the temperature profile in the neighbourhood of T_0 increase with time. However, accompanying this temperature rise will be an increase in the conduction heat loss to walls in the neighbourhood of T_0. It is then reasonable that a quasi-steady state of the system can be reached when the magnitude of this additional heat loss becomes very close to that of the heat sink needed at $T = T_0$ to assure the steady state temperature profile. Mathematically, this quasi-steady state can be closely described by a steady-state temperature profile coupled with a moving source near the 'cold boundary' in such a way that both the temperature profile and the moving source propagate at the same velocity.

CONCLUDING REMARKS

It has been shown that the energy conservation law is violated when both adiabatic and steady-state conditions are imposed on the flame model. To preserve the conservation law one has either to change the reaction rate law or to avoid the simultaneous imposition of the 'adiabatic' and 'steady-state' conditions. Hirschfelder has chosen to relax the 'adiabatic condition' imposed on the flame model at the cold boundary by introducing the concept of a flameholder. As a consequence of this concept there are two points to be observed:

(*1*) This concept indirectly implies that the steady state does not exist in the case of a flame propagating in a long tube filled with premixed gas. For this freely propagating flame there *is no* flameholder travelling with it. The mathematical descriptions of flames that are stabilized by flameholders, therefore, throw very little light on the descriptions of flames propagating in long tubes.

(*2*) One must examine the magnitude of the heat sink that is introduced at the flameholder. In an actual experiment we may say that the magnitude of the heat sink is proportional to the difference between the higher temperature at the surface of the flameholder and the lower coolant temperature. If we fix the temperature at the surface of the flameholder but change the coolant temperature the magnitude of the heat sink will also change. Various steady states of the flame therefore will be reached at different mass flow rates. The problem is now actually different from the case of an eigenvalue problem. The *original* eigenvalue problem has a solution only when the system has a distinctive eigenvalue for the mass flow. In this problem the various characteristic values of the mass flow are determined by the equilibrium conditions established by the *interaction* of the flame with the boundaries.

Von Kármán and Penner in their treatment of a one-dimensional flame theory chose to change the reaction rate law by using the concept of an 'ignition temperature'. But to say that the chemical reaction rate is identically zero at temperatures above absolute zero is not correct. However, the mathematical use of 'ignition temperature' can be interpreted in a reasonable way if the adiabatic restriction of the cold boundary is removed. Suppose we take account of the chemical reaction at the cold boundary. But we also consider the heat loss at the cold boundary from the flame system. Assume that at T_0 the heat produced by chemical reaction and heat loss from the flame reach an equilibrium. A steady state at the cold boundary is established if the concentration of fuel changes very slowly with time and can be neglected. The heat generated at the cold boundary will be conducted away from the flame system. As far as the flame system is concerned, this is equivalent to saying that the reaction has never taken place. Only in such a sense is there an 'ignition temperature' below which no heat is released from the mixture to the flame system.

Convair Scientific Research Laboratory,
San Diego, California

(Received October 1958)

REFERENCES

[1] Boys, S. F. and Corner, J. *Proc. Roy. Soc. A*, 1949, **197**, 90
[2] Hirschfelder, J. O. and Curtiss, C. F. *Third Symposium on Combustion, Flame and Explosion Phenomena*, pp 121–127. Williams and Wilkins: Baltimore, 1949
[3] von Kármán, T. *Sixth Symposium (International) on Combustion*, pp 1–11. Reinhold: New York, 1957
[4] Hirschfelder, J. O., Curtiss, C. F. and Campbell, Dorothy. *Fourth Symposium (International) on Combustion*, pp 190–210. Williams and Wilkins: Baltimore, 1953; also comments of Rosen, J. B. pp 210–211
[5] von Kármán, T. and Penner, S. S. *Selected Combustion Problems*, pp 5–41. Butterworths: London, 1954
[6] Emmons, H. quoted in ref. 3
[7] Layzer, D. *J. chem. Phys.*, 1954, **22**, 222
[8] Spalding, D. B. *Combustion & Flame*, 1957, **1**, 287
[9] Rosenthal, D. *Trans. Amer. Soc. mech. Engrs*, 1946, **68**, 849

Quenching Diameters of Some Fast Flames at Low Pressures

EVELYN ANAGNOSTOU and A. E. POTTER, JR

Quenching diameters as a function of pressure have been presented for some fast stoichiometric hydrocarbon–oxygen and hydrogen–oxygen flames. The order of increasing ease of quenching is acetylene, ethylene, hydrogen, propane. The overall reaction orders for all flames have been found to be very close to two.

VERY few quenching diameter data are available for fast flames because of the hazards in handling such flames. Therefore quenching diameters of some of these flames were measured at pressures below half an atmosphere using an apparatus specially designed to minimize the hazards by requiring only small quantities of mixture.

Stoichiometric mixtures of propane–oxygen, ethylene–oxygen, acetylene–oxygen, propane–50% oxygen–50% nitrogen, hydrogen–oxygen and hydrogen–70% oxygen–30% nitrogen were tested.

APPARATUS AND PROCEDURE

There are four basic methods of quenching distance measurement: (*1*) Extrapolation of blowoff-flashback stability diagrams to the quenching point[1]; (*2*) the flanged-plate electrode method[2]; (*3*) determination of whether a flame stabilized on a burner will flash back or quench when flow to the burner is interrupted[3, 4]; and (*4*) determination of the critical tube diameter for the propagation of a flame in a quiescent mixture[5]. This method has been shown[6] to give the same results as method (*3*). Method (*3*) was used in this research.

The apparatus used is shown in *Figure 1*. It consists of a small brass plate 3·81 cm in diameter and 0·835 cm thick with 18 holes in it ranging in diameter from 3·18 mm to about 1 mm. This plate rested on a second plate containing thermocouples which protruded into each hole of the top plate. Both plates were contained in a holder and the whole assembly was water-cooled. Fuel–oxidant mixture was fed to the holes through grooves underneath the plate leading from a central supply tube and was ignited by a hot wire. An annular plate with a slot cut in it was used to expose any particular port desired.

To make a measurement, a small amount of mixture was allowed to flow into the burner and ignited. As the flow died down, the flame would either flash back or quench. If the flame flashed back, the thermocouple would indicate a temperature rise. The pressure was lowered until the flame quenched; the quenching pressure was then taken as the average of the pressure at which the flame flashed back and that pressure at which it quenched. These pressures usually differed by 1 to 3 mm of mercury.

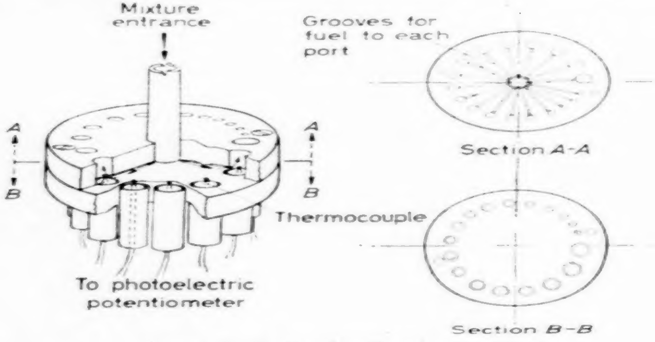
Mixture entrance
Grooves for fuel to each port
A
A
B
B
Section A-A
Thermocouple
To photoelectric potentiometer
Section B–B

Figure 1. Some details of apparatus

RESULTS AND DISCUSSION

The quenching diameters were measured in the pressure range of 0·06 to 0·35 atm. The results are shown in *Figures 2* and *3*. The slopes of the plots and the extrapolated values of the quenching diameter at 1 atm (d_0) are listed in *Table 1*. Also listed in *Table 1* are slopes and d_0 values obtained by other investigators. The data of others have been converted to quenching diameters, wherever necessary, by using the experimental relation[6] d (cylinders) $= d$ (parallel plates)/0·66.

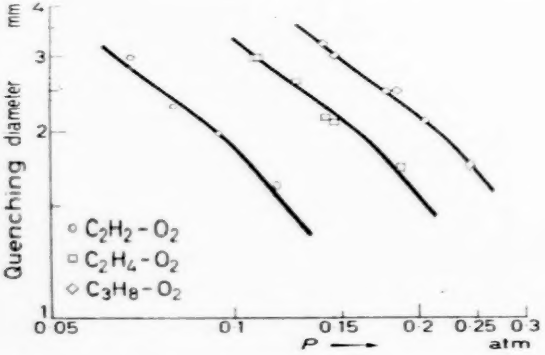

Figure 2. Quenching diameters of some stoichiometric hydrocarbon-oxidant flames as a function of pressure

It is obvious from *Table 1* that there is poor agreement between the d_0 values of Lewis and von Elbe[7, 2] (using flanged electrodes) and those of this research. In addition, the presently obtained d_0 values are in one case lower (hydrogen–oxygen) and in the other case higher (propane–oxygen) than theirs. Some of their data[8] on propane–oxygen, measured using a method similar to that of this research, do agree with our results. The agreement with the data of Gaydon and Wolfhard[1] (from stability plots) is also poor.

*Table 1. Comparison of the data of this research with previous work**

Stoichio-metric mixture	*Log-log slope, d vs P*	*Slope, others' data*	*d_0, cm*	*d_0, cm others' data*	*Burning velocity cm sec^{-1}*	*Flame temperature °K, 1 atm*
C_3H_8–O_2	1·06	0·95[2]	0·039	0·038[3]† 0·033[7]† 0·041[8]	357[9]	3 093
C_2H_4–O_2	1·06	—	0·029	—	550[1]	3 126
C_2H_2–O_2	1·06	1·07[1]	0·016	0·012[1]	800[9] 892[9] 1062[1]	3 333
H_2–O_2	1·08	1·01[2]	0·035	0·052[7]† 0·029[4]†	1067[9]	3 090
H_2–70% O_2–30% N_2	1·28	—	0·028	0·034[4]†	850[1] (69% O_2)	2 998

*Superscript numerals are references listed at end of report.

†The value written here is a quenching diameter although the original datum is a quenching distance. For direct comparison with the quenching diameter from this research, the quenching distance from the source quoted has been multiplied by the factor 1·52 to convert it to a quenching diameter[6].

The results for propane–50% oxygen–50% nitrogen agree very well with those of Berlad[3], which are shown in *Table 2*. By extrapolating his data a value of d_0 for propane–oxygen can be obtained which is in excellent agreement with our results (*Table 1*). Comparison with Friedman's data[4] (d_0s) for both hydrogen mixtures is also good. Both Berlad and Friedman used a similar technique to the one used in this research. Summarizing these comparisons, the data of this research are in good agreement with data obtained by a similar technique, but do not agree with data obtained by other techniques.

Table 2. Comparison of data for C_3H_8–50% O_2–50% N_2 with those of Berlad[3]

P atm	*d, cm This research*	*d, cm Berlad*
0·318	0·246	0·221
0·244	0·299	0·283

The overall order of a reaction is related to the slope of the log-log plot of quenching diameter versus pressure[10] and is equal to twice the slope minus a correction (not usually large) for the pressure dependence of the flame temperature. Since the slopes of the plots are all slightly greater than one, all reactions studied will have orders very close to two.

The order of increasing ease of quenching for the fuel–oxygen mixtures is acetylene, ethylene, hydrogen, propane. The relative ease of quenching of the hydrogen flame may seem anomalous in this series because of its very high burning velocity. However, this mixture has a very high thermal conductivity which presumably causes it to lose heat much more rapidly and thus be easier to quench.

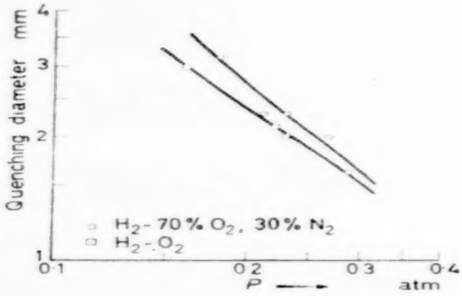

Figure 3. Quenching diameters of some stoichiometric hydrogen–oxidant flames as a function of pressure

Quenching distances can be multiplied by the appropriate values of the burning velocity and compared to the value of this product calculated using equation 4 of ref. 11. This equation relates the product to a 'thermal diffusivity' and to a term involving the chemical nature of the flame. Flame temperatures and burning velocities required for this calculation are included in *Table 1*. The flame temperatures were calculated by the method of ref. 12, except that of acetylene–oxygen, which is taken from ref. 1. The activation energy for the hydrocarbon reactions has been taken as 38 kcal/mole and, for the hydrogen reactions, as 23 kcal/mole. The order of the reaction has been assumed to be 2, and *F*, which is the fraction of the total heat of combustion which must be retained in order for the flame

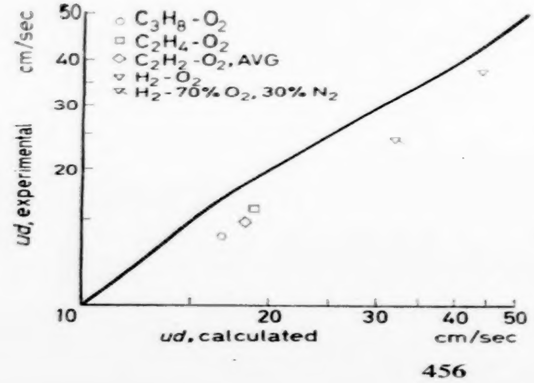

Figure 4. Comparison of experimental value of the product of burning velocity and quenching diameter with predicted values

to exist, is taken as 0·78. The results of these calculations are shown in *Figure 4*. The calculated values are consistently 20 per cent higher than the experimental ones. This may indicate that either the value of *F* chosen is too low or that the activation energies are too high or perhaps both. An increase of only 5 per cent in the value of *F* changes the calculated *Ud* product by 20 per cent while a decrease in the value of the activation energy of 10 per cent accomplishes the same effect.

National Aeronautics and Space Administration,
Lewis Research Center, Cleveland 35, Ohio

(Received September 1958)

REFERENCES

[1] GAYDON, A. G. and WOLFHARD, H. G. *Flames, their Structure, Radiation and Temperature.* Chapman and Hall: London, 1953

[2] BLANC, M. V., GUEST, P. G., VON ELBE, G. and LEWIS, B. *Third Symposium on Combustion, Flame and Explosion Phenomena*, pp 363–367. Williams and Wilkins: Baltimore, 1949

[3] BERLAD, A. L. *J. phys. chem.* 1954, **58**, 1023

[4] FRIEDMAN, R. *Third Symposium on Combustion, Flame and Explosion Phenomena*, pp 110–120. Williams and Wilkins: Baltimore, 1949

[5] SIMON, D. M., BELLES, F. E. and SPAKOWSKI, A. E. *Fourth Symposium (International) on Combustion*, pp 126–138. Williams and Wilkins: Baltimore, 1953

[6] BERLAD, A. L. and POTTER, A. E. *Fifth Symposium (International) on Combustion*, pp 728–735. Reinhold: New York, 1955

[7] LEWIS, B. and VON ELBE, G. *Combustion, Flames and Explosions of Gases*, pp 408–412. Academic Press: New York, 1951

[8] HARRIS, E., GRUMER, J., VON ELBE, G. and LEWIS, B. *Third Symposium on Combustion, Flame and Explosion Phenomena*, pp 80–89. Williams and Wilkins: Baltimore, 1949

[9] LADENBURG, R. V., LEWIS, B., PEASE, R. N. and TAYLOR, H. S. *Physical Measurements in Gas Dynamics and Combustion*, pp 431–434. Sect. K by E. F. FIOCK. Princeton University Press: New Jersey, 1954

[10] POTTER, A. E., Jr and BERLAD, A. L. *Sixth Symposium (International) on Combustion*, pp 27–36. Reinhold: New York, 1957

[11] POTTER, A. E., Jr and BERLAD, A. L. *Tech. Note Nat. Adv. Comm. Aero., Wash., No. 3882* (1956)

[12] HUFF, V. N., GORDON, S. and MORRELL, V. C. *Tech. Rep. Nat. Adv. Comm. Aero., Wash., No. 1037* (1951)

Further Measurements of Turbulence Intensity in Flame Zones

A. A. WESTENBERG and J. L. RICE

In a previous paper, a technique for measuring transverse turbulence intensity in flames by means of helium diffusion was described. The intensity is estimated from the concentration distribution of helium (determined by sampling) downstream of a 'point source' injection tube immersed in the main stream. Results were reported of the effect of various parameters on the intensity measured at a single location in highly turbulent flames stabilized on baffles in a 2 in. × 8 in. rectangular duct. The present paper contains additional results obtained at several other positions in the same duct. The data include heat release combustion efficiencies and turbulence intensities under both cold flow and burning conditions for each of two different values of approach flow turbulence intensity (approximately 5 per cent and 10 per cent). Premixed pentane air at an equivalence ratio of 0·7 and a pressure of 0·85 atm was used. The twofold increase in approach turbulence caused an approximately twofold increase in the rate of flame spreading. By comparing the absolute intensities of turbulence during burning and cold flow it is shown that in regions of actively burning gas the turbulence is higher than in cold flow, but in regions of completely burnt gas the intensity may be reduced and may even become laminar. Cold gas regions adjacent to flame zones are essentially unaffected by the presence of flame.

A TECHNIQUE for measuring transverse turbulence intensity in flames which makes use of helium diffusion has been described previously[1]. In that paper the theory and practice of the method were critically examined in considerable detail. This discussion will not be repeated here, except to say that the transverse turbulence intensity may be estimated from the concentration distribution of helium (obtained by sampling) downstream of a fine 'point source' injection tube immersed in the main turbulent flow. The concentration distribution measured perpendicular to the flow is essentially Gaussian, and its standard deviation $(\overline{y^2_{\text{turb}}})^{1/2}$ (after correction for molecular diffusion) is related to the absolute turbulence intensity $(\overline{v^2})^{1/2}$ by

$$(\overline{y^2_{\text{turb}}})^{1/2}/x=(\overline{v^2})^{1/2}/U$$

where x is the axial distance from the source and U is the mean flow velocity. $(\overline{y^2_{\text{turb}}})^{1/2}/x$ is thus equated to the relative turbulence intensity. Ref. 1 reported results using this technique with the helium source at a single location (approximately point B_4 in *Figure 1*) in highly turbulent flames stabilized on various baffles in a 2 in. × 8 in. rectangular duct. The present note contains results of additional experiments carried out for the purpose of studying the interaction of flame and turbulence at other positions in the duct.

EXPERIMENTAL RESULTS

The experiments were carried out at the APL Propulsion Research Facility with the same equipment as that described in ref. 1. The burner duct is

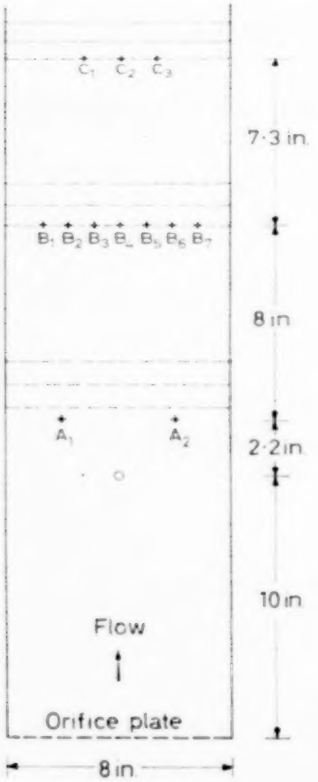

Figure 1. Schematic drawing of burner test section showing combustion efficiency traverses (dotted lines) and positions of turbulence measurement (A_1, A_2, etc.)

shown schematically in *Figure 1*. The only important change from the previous arrangement is the location of the flameholder, which was placed closer to the entrance of the test section for the present work to allow a greater length for flame spreading and study. Since it was shown that the flameholder size (not shape) had important bearing on the turbulence level, the smallest diameter consistent with stable burning near the lean blowoff limit was chosen. This was a $\frac{1}{4}$ in. cylindrical rod extending across the 2 in. duct dimension. The helium injection tube was placed so that its exit tip was successively at each of the twelve locations designated as A_1, A_2, B_1, etc. in *Figure 1*. All of these points were centred midway between front and back walls of the duct. Premixed pentane–air at 400°K and an equivalence ratio of 0·70 stoichiometric was the combustible used. The duct pressure was maintained at 0·85 atm. The approach velocity to the flameholder was 33 m/sec.

The measurements included heat release combustion efficiency traverses along the nine dotted lines shown in *Figure 1*, and turbulence intensities at the twelve locations indicated under both cold and burning conditions. Temperatures were obtained from the combustion efficiency values[1]. A complete set of such data was taken at each of two different turbulence levels. The so-called 'high turbulence' measurements were made with a multiply-perforated choking plate at the entrance to the test section, while the 'low turbulence' measurements were made with this plate removed.

By cross-plotting the combustion efficiency (or temperature) traverses, a reproduction of the flame could be obtained as a set of contours of constant efficiency (or isotherms). These are shown in *Figures 2* and *3* for the low and high turbulence cases. At each of the helium injection points the measured relative turbulence intensity is given as per cent of the mean stream velocity at that point. In each case the upper number in parentheses is the cold flow value and the lower is the value with flame present.

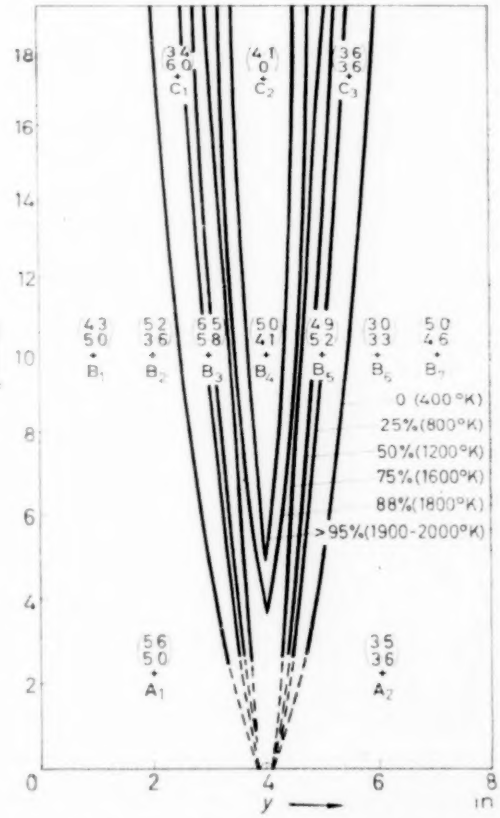

Figure 2. Reproduction of flame at LOW TURBULENCE. Lines are isotherms, or lines of constant heat release efficiency. Numbers in parentheses above the + points are the measured relative turbulence intensities in per cent of mean flow velocity with flame present (lower number) and without flame (upper number)

DISCUSSION

As discussed in ref. 1, the values of flame turbulence intensity measured by the diffusion method should be regarded only as estimates, since they are subject to unavoidable and rather large uncertainties. The main difficulty is in the correction for molecular diffusion. The interaction between molecular and turbulent diffusive processes has been summarized recently by G. K. BATCHELOR and A. A. TOWNSEND[2]. They show that the assumption of additivity of molecular and turbulent contributions to the total measured variance (i.e. $\overline{y^2} = \overline{y^2_{\text{mol}}} + \overline{y^2_{\text{turb}}}$) of a diffusing fluid is valid for measurements near the source where the Lagrangian correlation

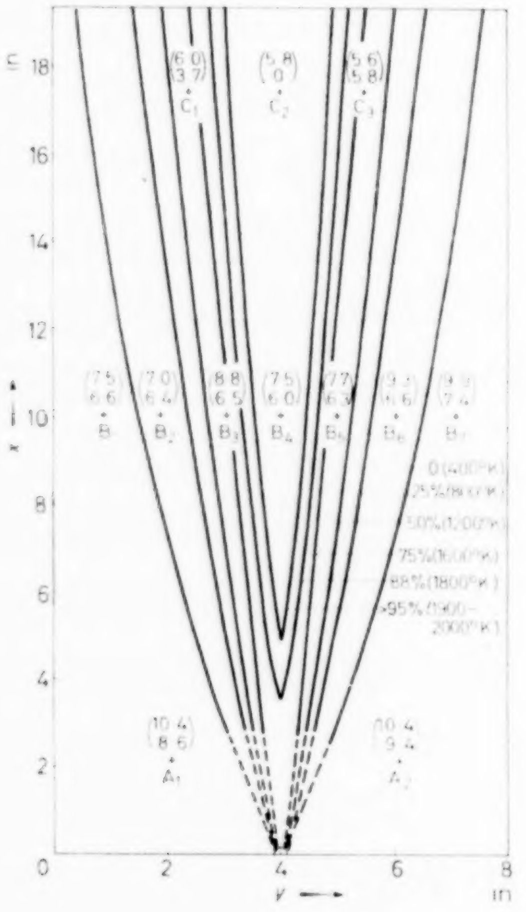

Figure 3. Reproduction of flame at ***HIGH TURBULENCE.*** *Lines are isotherms, or lines of constant heat release efficiency. Numbers in parentheses above the · points are the measured relative turbulence intensities in per cent of mean flow velocity with flame present (lower number) and without flame (upper number)*

coefficient is essentially unity. The latter condition was shown to obtain[1] in these experiments, so that this assumption is not the source of uncertainty in the molecular diffusion correction. Instead, it lies in the values of molecular diffusion coefficient for helium used in calculating y^2_{mol} at high temperatures. As discussed[1], it is necessary to rely on kinetic theory calculations for the diffusion coefficient since there are no experimental data at these temperatures*. Under such circumstances, the possibility of introducing errors is apparent. This applies particularly to the flame results where the contribution of molecular diffusion to the total variance of helium is comparable to that of turbulence. The cold flow intensities are more reliable since the molecular correction is much smaller—although not negligible—and the diffusion coefficient of helium (regarded as a binary mixture with nitrogen in this case) is known with some precision at ordinary temperatures.

Another source of error in the flame results is the temperature assigned to a particular point of turbulence measurement. Even if the molecular

---

*Since this paper was prepared, measurement of the diffusion coefficient of helium–nitrogen up to 1 200°K has been performed using a new technique (discussed fully in two papers by R. E. Walker and A. A. Westenberg published in the *Journal of Chemical Physics*, 1958, **29**, 1139 and 1147. The results indicate that the theoretical calculations used for the molecular diffusion coefficient were fairly reliable (within about 20 per cent at the highest temperatures), so that this source of uncertainty has been somewhat reduced.

diffusion coefficient of helium were known with confidence as a function of temperature, the use of this information in correcting the diffusion measurements obviously requires reliable temperature measurement. The technique employed of obtaining the temperature from combustion efficiency analysis of the sampled flame gases is probably as good as other common methods[3]. However, there remain unanswered questions about the process of sampling from regions of active burning where the probe 'sees' random pockets of partially burned gas, and about the interpretation of the 'average' temperature measured in such a case. Measurements in regions of completely burnt gas are free from this objection, of course. The diffusion technique is very useful in comparing different levels of turbulence, since it is quite sensitive to changes in turbulence intensity even though absolute values may be uncertain for the reasons cited above.

It should also be pointed out that at least some components of the fluctuating flow in a turbulent flame zone are perhaps not properly called 'turbulence' at all, in the strict sense. Thus it is possible that instabilities may be present which are of a periodic, non-random nature. However, in view of the practical impossibility of separating such effects from true turbulence, this paper will consider any fluctuation which contributes to the measured diffusion of helium as being turbulence.

With these considerations in mind certain aspects of the data are worth noting. First, the effect of the increased turbulence level on the rate of flame spreading in *Figure 3* over that in *Figure 2* is readily apparent. This is, of course, well known. Using a simple flame width criterion, the rate of flame spreading in the high turbulence case is about 1·5 to 2 times greater than in the low turbulence case. The actual intensities of cold flow approach turbulence are (positions A_1 and A_2) about 10 per cent and 4 to 5 per cent, respectively, so that very roughly speaking, doubling the approach turbulence intensity doubles the rate of flame spreading in this case. Further correlations of this type from these data are neither fruitful nor warranted.

Note that the cold flow intensities are not very uniform at a given cross section. This is most noticeable at low turbulence (*Figure 2*) where, for example, the intensities on either side of the flameholder at A_1 and A_2 are 5·6 and 3·5 per cent, respectively. Values at the B and C positions are somewhat more uniform. As might be expected, the presence of the turbulence-generating choking plate smooths out the variations in turbulence considerably, as the high turbulence cold flow values in *Figure 3* indicate. The decay of the turbulence in going from the A traverse, to the B and C traverses is clearly shown. The high and low turbulence intensities differ by a factor of from 1·5 to 3 at most positions.

The first thing to be noted about the relative intensities measured when the flame was present is that the values are generally either lower or about the same as the corresponding cold flow data. (There is no ready explanation for the apparent exception at C_1 at low turbulence. It may be an error, as there seems to be no reason why this point should be different.) At all positions, however, the mean flow velocity is accelerated when flame is present, so that a direct comparison of relative intensity should be made with caution—a point discussed at some length in ref. 1. In that paper it was suggested that a more informative comparison might be made of the *absolute* turbulence intensities with and without flame, as this would be indicative of the effect of the combustion process on turbulence. Such a comparison for all of the data shown in *Figures 2* and *3* is given in *Table 1*.

Table 1. Comparison of absolute turbulence intensities measured with and without burning

Position	*Low turbulence* $(v^2)^{\frac{1}{2}}$ *(cm/sec)*		*High turbulence* $(v^2)^{\frac{1}{2}}$ *(cm/sec)*	
	Cold	*Flame*	*Cold*	*Flame*
A_1	180	190	330	330
A_2	140	160	320	320
B_1	140	180	250	290
B_2	160	140	240	320
B_3	210	280	290	450
B_4	160	200	270	400
B_5	160	230	230	380
B_6	100	130	280	290
B_7	160	180	300	280
C_1	110	220	200	140
C_2	140	0	170	0
C_3	120	150	180	230

Some increase in absolute turbulence intensity is generally indicated for points where active combustion is going on. Thus for the low turbulence condition there is definite increase at points B_3, B_4, B_5, C_3 and probably C_1, and for the high turbulence condition at B_2, B_3, B_4, B_5 and C_3. The percentage increase caused by the flame seems to be somewhat larger at high turbulence than at low. No speculation as to the mechanism of this flame-generated turbulence is offered here, except to say that it seems plausible that it may be a result of shear flow set up by the combustion process farther upstream[1, 5]. The influence of the flameholder itself was negligible in the regions where measurement was taken, since it was shown previously[1] that baffles smaller than ½ in. diameter did not alter the turbulence level measurably.

One very interesting thing shown by these data is that where combustion is complete there is a striking tendency for the turbulence to be decreased. This is shown to some degree by point B_4 in both *Figures 2* and *3* where the flame-induced increase of turbulence is less than at points B_3 and B_5 on either side where burning is still proceeding, and the effect is very marked at C_2 in both cases where no turbulence at all can be measured by this technique. This is a point of 100 per cent combustion efficiency, as is nearly the whole centre-line from the flameholder. Possibly this drastic decrease in turbulence is due to greatly increased viscous damping when flame is present. Kinematic viscosity increases (very approximately) as the 1·5 power of temperature, and in the present example this means an increase of at least a factor of 11 in changing from cold flow to completely burnt gas. This might easily be enough to overcome the effect of increased mean flow velocity (a factor of about 2) which lowers the time available for decay of turbulence, so that the overall effect is a decrease to essentially laminar flow by the time the point C_2 is reached.

There seems to be little effect of the combustion process on those points, such as A_1, A_2, B_1 and B_7, which lie in the cold gas just adjacent to the flame zone. In terms of the absolute intensity, all these points give essentially the same result whether flame is present or not, as *Table 1* clearly indicates.

The facts brought out by this investigation may be summarized as follows: (*a*) Measurements of heat release combustion efficiency and transverse turbulence intensity in ducted flames are presented. An approximately twofold increase in approach intensity caused an approximately twofold increase in the rate of flame spreading, using the simple criterion of flame width. (*b*) Comparisons are made of turbulence measurements at various points in the duct under both burning and non-burning conditions. In general, the *relative* turbulence intensity was either decreased or practically unchanged by the presence of the flame. (*c*) In regions of actively burning gas the *absolute* turbulence intensity was generally higher than in the same region with no burning. (*d*) In regions of completely burnt gas the increase in *absolute* intensity due to combustion was somewhat less pronounced at one point, while farther downstream the flame actually caused the flow to become laminar. It is concluded that the effects of combustion on a turbulent flow may be either to increase or decrease the absolute intensity, depending upon whether one considers a zone of active burning or one which is simply burnt out, hot gas, and depending upon the location of the zone. (*e*) The *absolute* turbulence intensity in the unburnt gas close to the flame zone appeared to be affected only slightly or not at all by the presence of the flame.

Finally, it should be stated that turbulent combustion is much too complex a process to warrant the uncritical application of the foregoing conclusions to turbulent flames in general.

This work was supported by Contract NOrd 7386 with the Bureau of Ordnance, Department of the Navy.

Applied Physics Laboratory,
Johns Hopkins University,
Silver Spring, Maryland

(*Received September 1958*)

REFERENCES

[1] WESTENBERG, A. A. *J. chem. Phys.* 1954, **22**, 814

[2] BATCHELOR, G. K. and DAVIES, R. M. (editors). *Surveys in Mechanics.* Cambridge University Press: London, 1956. See chapter on 'Turbulent diffusion' by BATCHELOR, G. K. and TOWNSEND, A. A.

[3] GRUNFELDER, C. *Rep. appl. Phys. Lab. Johns Hopk. Univ. No. CM-768* (January 1953)

[4] WILLIAMS, G. C., HOTTEL, H. C. and SCURLOCK, A. C. *Third Symposium on Combustion, Flame and Explosion Phenomena,* p 21. Williams and Wilkins: Baltimore, 1949

[5] BLACKSHEAR, P. L. *Tech. Note Nat. Adv. Comm. Aero., Wash., No. 3830* (November 1956)

The Cooperative Mechanism in the Ignition of Dust Dispersions

H. M. CASSEL and I. LIEBMAN

Ignition temperatures, defined as the minimum ambient temperatures required to initiate luminous combustion, were determined for single particles of magnesium and of 50/50 magnesium aluminium alloy (10 to 80 microns in diameter) burning in air or oxygen, and for corresponding monodisperse dust clouds, at various concentrations, burning in air. In agreement with theoretical expectation, the ignition temperature of single particles generally increases with decreasing size. However, at high enough concentrations, the ignition temperatures of fine particles are lower than those of coarser particles. Also, depending on concentration, the ignition temperature of clouds is lower than that of the corresponding single particle. This is explained by the cooperative effect of heat transfer from neighbouring reacting particles. Ignition in clouds of low concentration originates from sporadically distributed flamelets. These are interpreted as evidence for thermal density fluctuations in the otherwise uniform aerosol.

SINCE the early work of E. A. GULBRANSEN[1] recent investigations of the oxidation of metals, particularly magnesium, aluminium and their alloys, have revealed a much more complex situation[2–4] than had been anticipated on the basis of the classical 'parabolic' diffusion law[5]. This is due partly to chemisorption and/or absorption of oxygen in the interior of the metal, subsequent to superficial oxidation, as indicated by considerable swelling of the oxidizing metal. Whether the binding of oxygen is merely an oxidation of particle boundaries or whether it results from the formation of crystalline solutions probably could be established by X-ray diffraction analysis. However, as this information is lacking, the kinetics of these processes requires further clarification. With this in mind, it may appear premature to attempt to interpret the ignition of metal particles dispersed in an oxidizing atmosphere. Nevertheless, the encouraging results of the experimental study initiated by I. HARTMANN[6–9] have prompted a systematic investigation of the ignition of certain metal dust clouds as a function of particle size and concentration.

A. THEORETICAL CONSIDERATION OF IGNITION OF SMALL METAL PARTICLES

In considering the oxidation of metal particles, it is helpful to distinguish two régimes: (*1*) A sufficiently low-temperature range where the rate of reaction is negligibly small, from T_u to T_m; and (*2*) a medium-temperature range where reaction proceeds, according to an Arrhenius-type law, from T_m to T_i.

(*1*) For a single small, spherical fuel particle of radius r and temperature T_u injected into an oxidizing atmosphere of temperature $T_0 > T_u$, the time required to heat it to a temperature $T_m < T_0$ can be estimated if the heat

transfer is solely conductive. If ρ is the density and c the specific heat of the fuel, the rise in surface temperature T is

$$(4\pi r^3/3)\,\rho c\,\partial T/\partial t = 4\pi r^2 k\,\partial T/\partial r \qquad \ldots . [1]$$

provided that the thermal conductivity of the metal is very great compared with that of the ambient gas, k. At the surface

$$\partial T/\partial r = (T_w - T)/r \qquad \ldots . [2]$$

and by integration

$$t_m = (c\rho r^2/3k)\ln[(T_w - T_0)/(T_w - T_m)] \qquad \ldots . [3]$$

Taking as an example, magnesium of $r = 2 \times 10^{-3}$ cm, $\rho = 1{\cdot}74$ g/cm^3, $c = 6/24{\cdot}3$ cal/g in air of $k = 7 \times 10^{-5}$ cal/(sec × cm), for $T_w - T_m = (T_w - T_0)/100$, one obtains $t \simeq 0{\cdot}04$ second. If the oxidizing gas is contained in an electric furnace of wall temperature T_w this time is obviously overestimated, because at lower particle temperatures radiation must contribute substantially to the heat transfer. On the other hand, when a dust cloud is heated in a furnace, it can be expected to take more time than a single particle to reach temperature T_m, because the inner parts of the cloud are shielded by surrounding particles against direct radiation from the furnace, and the gas carrying the particles must also be heated.

(2) In the régime of chemical reaction, the rate of heat generation per unit area is given by

$$G = fC_sQ\exp(-E/RT_s) \qquad \ldots . [4]$$

where f is a slightly temperature-dependent frequency factor, C_s is the superficial concentration of oxygen, Q is the molar heat of reaction, E is the free energy of activation per mole of fuel, R is the molar gas constant, and T_s is the surface temperature of the particle. The rate of heat loss per unit area is

$$L = (k/r)(T_s - T_0) \qquad \ldots . [5]$$

Therefore, the temperature of the particle surface rises according to

$$(4\pi r^3/3)\,\rho c\,\partial T/\partial t = 4\pi r^2(G - L) \qquad \ldots . [6]$$

Near the ignition point the LHS of this equation becomes zero.

The situation is illustrated by plotting the heat generation (heat loss) against the particle-surface temperature in *Figure 1*, where G denotes rate of heat generation per square centimetre, L is rate of heat loss per square centimetre, T_{s1} is the limit particle temperature for ambient temperature T_{01}, T_{s2} is the minimum particle temperature for ignition and T_{02} is the minimum ambient temperature for ignition. At room temperature the heat-generation curve G is convex to the temperature axis; according to the Arrhenius reaction-rate law, it straightens out when oxygen consumption begins to become rate-controlling and becomes concave against the temperature axis at higher temperatures where oxygen diffusion is predominantly the rate-determining factor[10].

Rate-of-heat-loss curves L start from the temperature axis at the ambient furnace temperature (when temporarily heat loss is zero) as straight lines

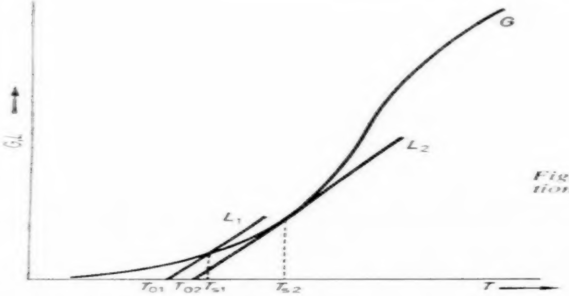

Figure 1. Rate of heat generation and heat loss versus temperature

that bend upward (not shown in figure) when heat loss by radiation contributes to heat loss by conduction and convection. If the heat-loss and heat-generation curves do not intersect, the temperature of the particle surface may rise close to a theoretical maximum. However, at an intersection the particle temperature is limited (T_{s1}). To avoid such a limit, it is necessary to reduce the heat loss by raising the ambient temperature. Since the slope of heat-loss lines remains virtually unchanged for a wide range of ambient temperatures, the heat-loss line must be shifted parallel to itself until it becomes a tangent to the heat-generation curve, L_2. This condition defines the 'ignition temperature,' T_{02}, for a given particle size. As the slope of the heat-loss line is inversely proportional to the particle radius, higher ambient temperatures must be attained for ignition of smaller particles.

The described 'ignition temperature' conditions are expressed from equation 6 by

$$G = L \text{ and by } dG/dT_s = dL/dT_s \qquad \ldots\ [7]$$

so that

$$C_s f Q \exp(-E/RT_s) = k(T_s - T_0)/r \qquad \ldots\ [6a]$$

and

$$C_s f Q \exp(-E/RT_s) \times E/RT_s^2 = k/r \qquad \ldots\ [7a]$$

Dividing equation 6a by 7a gives

$$RT_s^2/E = T_s - T_0 \qquad \ldots\ [8]$$

It is convenient to write equation 4 for the temperature range under discussion as

$$G = QC_s BT_s^x \qquad \ldots\ [9]$$

so that equation 6a becomes

$$QC_s BT_s^{x-2} = k(T_s - T_0)/rT_s^2 \qquad \ldots\ [10]$$

transfer is solely conductive. If ρ is the density and c the specific heat of the fuel, the rise in surface temperature T is

$$(4\pi r^3/3)\,\rho c\,\partial T/\partial t = 4\pi r^2 k\,\partial T/\partial r \qquad \ldots [1]$$

provided that the thermal conductivity of the metal is very great compared with that of the ambient gas, k. At the surface

$$\partial T/\partial r = (T_0 - T)/r \qquad \ldots [2]$$

and by integration

$$t_{min} = (c\rho r^2/3k)\ln[(T_0 - T_a)/(T_0 - T_m)] \qquad \ldots [3]$$

Taking as an example, magnesium of $r = 2 \times 10^{-3}$ cm, $\rho = 1{\cdot}74$ g/cm^3, $c = 6/24{\cdot}3$ cal/g in air of $k = 7 \times 10^{-5}$ cal/(sec × cm), for $T_0 - T_m = (T_0 - T_a)/100$, one obtains $t \simeq 0{\cdot}04$ second. If the oxidizing gas is contained in an electric furnace of wall temperature T_0 this time is obviously overestimated, because at lower particle temperatures radiation must contribute substantially to the heat transfer. On the other hand, when a dust cloud is heated in a furnace, it can be expected to take more time than a single particle to reach temperature T_m, because the inner parts of the cloud are shielded by surrounding particles against direct radiation from the furnace, and the gas carrying the particles must also be heated.

(2) In the régime of chemical reaction, the rate of heat generation per unit area is given by

$$G = fC_sQ\exp(-E/RT_s) \qquad \ldots [4]$$

where f is a slightly temperature-dependent frequency factor, C_s is the superficial concentration of oxygen, Q is the molar heat of reaction, E is the free energy of activation per mole of fuel, R is the molar gas constant, and T_s is the surface temperature of the particle. The rate of heat loss per unit area is

$$L = (k/r)(T_s - T_0) \qquad \ldots [5]$$

Therefore, the temperature of the particle surface rises according to

$$(4\pi r^3/3)\,\rho c\,\partial T/\partial t = 4\pi r^2(G - L) \qquad \ldots [6]$$

Near the ignition point the LHS of this equation becomes zero.

The situation is illustrated by plotting the heat generation (heat loss) against the particle-surface temperature in *Figure 1*, where G denotes rate of heat generation per square centimetre, L is rate of heat loss per square centimetre, T_{s1} is the limit particle temperature for ambient temperature T_{01}, T_{s2} is the minimum particle temperature for ignition and T_{02} is the minimum ambient temperature for ignition. At room temperature the heat-generation curve G is convex to the temperature axis; according to the Arrhenius reaction-rate law, it straightens out when oxygen consumption begins to become rate-controlling and becomes concave against the temperature axis at higher temperatures where oxygen diffusion is predominantly the rate-determining factor[10].

Rate-of-heat-loss curves L start from the temperature axis at the ambient furnace temperature (when temporarily heat loss is zero) as straight lines

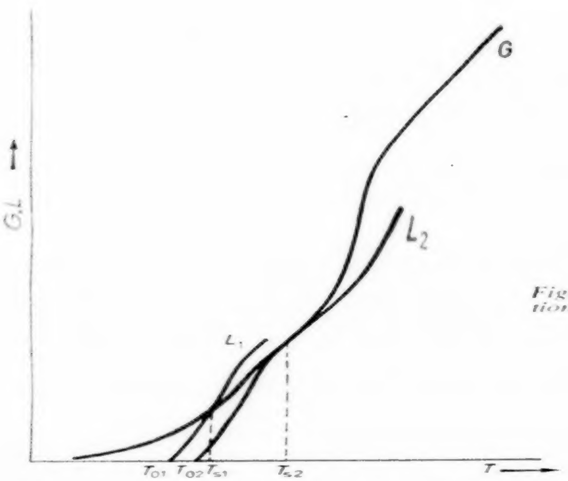

Figure 1. Rate of heat generation and heat loss versus temperature

that bend upward (not shown in figure) when heat loss by radiation contributes to heat loss by conduction and convection. If the heat-loss and heat-generation curves do not intersect, the temperature of the particle surface may rise close to a theoretical maximum. However, at an intersection the particle temperature is limited (T_{s1}). To avoid such a limit, it is necessary to reduce the heat loss by raising the ambient temperature. Since the slope of heat-loss lines remains virtually unchanged for a wide range of ambient temperatures, the heat-loss line must be shifted parallel to itself until it becomes a tangent to the heat-generation curve, L_2. This condition defines the 'ignition temperature,' T_{02}, for a given particle size. As the slope of the heat-loss line is inversely proportional to the particle radius, higher ambient temperatures must be attained for ignition of smaller particles.

The described 'ignition temperature' conditions are expressed from equation 6 by

$$G = L \text{ and by } \mathrm{d}G/\mathrm{d}T_s = \mathrm{d}L/\mathrm{d}T_s \qquad \ldots.[7]$$

so that

$$C_s f Q \exp(-E/RT_s) = k(T_s - T_0)/r \qquad \ldots.[6a]$$

and

$$C_s f Q \exp(-E/RT_s) \times E/RT_s^2 = k/r \qquad \ldots.[7a]$$

Dividing equation 6a by 7a gives

$$RT_s^2/E = T_s - T_0 \qquad \ldots.[8]$$

It is convenient to write equation 4 for the temperature range under discussion as

$$G = QC_s BT_s^x \qquad \ldots.[9]$$

so that equation 6a becomes

$$QC_s BT_s^{x-2} = k(T_s - T_0)/rT_s^2 \qquad \ldots.[10]$$

transfer is solely conductive. If ρ is the density and c the specific heat of the fuel, the rise in surface temperature T is

$$(4\pi r^3/3)\,\rho c\,\partial T/\partial t = 4\pi r^2 k\,\partial T/\partial r \qquad \ldots.[1]$$

provided that the thermal conductivity of the metal is very great compared with that of the ambient gas, k. At the surface

$$\partial T/\partial r = (T_0 - T)/r \qquad \ldots.[2]$$

and by integration

$$t_{um} = (c\rho r^2/3k)\ln[(T_0 - T_u)/(T_0 - T_m)] \qquad \ldots.[3]$$

Taking as an example, magnesium of $r = 2 \times 10^{-3}$ cm, $\rho = 1{\cdot}74$ g/cm^3, $c = 6/24{\cdot}3$ cal/g in air of $k = 7 \times 10^{-5}$ cal/(sec × cm), for $T_0 - T_m = (T_0 - T_u)/100$, one obtains $t \simeq 0{\cdot}04$ second. If the oxidizing gas is contained in an electric furnace of wall temperature T_0 this time is obviously overestimated, because at lower particle temperatures radiation must contribute substantially to the heat transfer. On the other hand, when a dust cloud is heated in a furnace, it can be expected to take more time than a single particle to reach temperature T_m, because the inner parts of the cloud are shielded by surrounding particles against direct radiation from the furnace, and the gas carrying the particles must also be heated.

(2) In the régime of chemical reaction, the rate of heat generation per unit area is given by

$$G = fC_s Q \exp(-E/RT_s) \qquad \ldots.[4]$$

where f is a slightly temperature-dependent frequency factor, C_s is the superficial concentration of oxygen, Q is the molar heat of reaction, E is the free energy of activation per mole of fuel, R is the molar gas constant, and T_s is the surface temperature of the particle. The rate of heat loss per unit area is

$$L = (k/r)(T_s - T_0) \qquad \ldots.[5]$$

Therefore, the temperature of the particle surface rises according to

$$(4\pi r^3/3)\,\rho c\,\partial T/\partial t = 4\pi r^2 (G - L) \qquad \ldots.[6]$$

Near the ignition point the LHS of this equation becomes zero.

The situation is illustrated by plotting the heat generation (heat loss) against the particle-surface temperature in *Figure 1*, where G denotes rate of heat generation per square centimetre, L is rate of heat loss per square centimetre, T_{s1} is the limit particle temperature for ambient temperature T_{01}, T_{s2} is the minimum particle temperature for ignition and T_{02} is the minimum ambient temperature for ignition. At room temperature the heat-generation curve G is convex to the temperature axis; according to the Arrhenius reaction-rate law, it straightens out when oxygen consumption begins to become rate-controlling and becomes concave against the temperature axis at higher temperatures where oxygen diffusion is predominantly the rate-determining factor[10].

Rate-of-heat-loss curves L start from the temperature axis at the ambient furnace temperature (when temporarily heat loss is zero) as straight lines

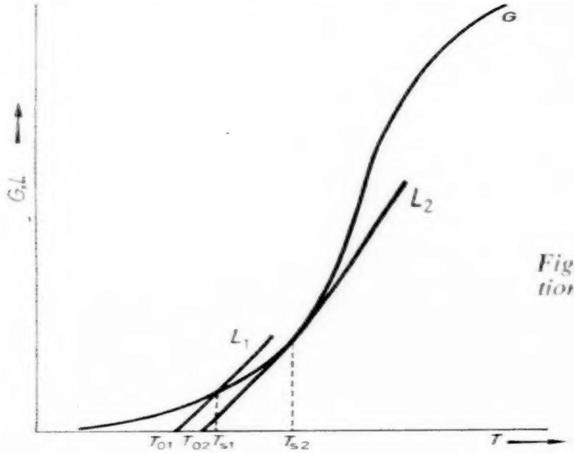

Figure 1. Rate of heat generation and heat loss versus temperature

that bend upward (not shown in figure) when heat loss by radiation contributes to heat loss by conduction and convection. If the heat-loss and heat-generation curves do not intersect, the temperature of the particle surface may rise close to a theoretical maximum. However, at an intersection the particle temperature is limited (T_{s_1}). To avoid such a limit, it is necessary to reduce the heat loss by raising the ambient temperature. Since the slope of heat-loss lines remains virtually unchanged for a wide range of ambient temperatures, the heat-loss line must be shifted parallel to itself until it becomes a tangent to the heat-generation curve, L_2. This condition defines the 'ignition temperature,' T_{02}, for a given particle size. As the slope of the heat-loss line is inversely proportional to the particle radius, higher ambient temperatures must be attained for ignition of smaller particles.

The described 'ignition temperature' conditions are expressed from equation 6 by

$$G = L \text{ and by } dG/dT_s = dL/dT_s \qquad \ldots.[7]$$

so that

$$C_s f Q \exp(-E/RT_s) = k(T_s - T_0)/r \qquad \ldots.[6a]$$

and

$$C_s f Q \exp(-E/RT_s) \times E/RT_s^2 = k/r \qquad \ldots.[7a]$$

Dividing equation 6a by 7a gives

$$RT_s^2/E = T_s - T_0 \qquad \ldots.[8]$$

It is convenient to write equation 4 for the temperature range under discussion as

$$G = QC_sBT_s^x \qquad \ldots.[9]$$

so that equation 6a becomes

$$QC_sBT_s^{x-2} = k(T_s - T_0)/rT_s^2 \qquad \ldots.[10]$$

or, on account of equation 8,

$$T_s^{\alpha-2} r = kR/EC_0QB \qquad \ldots.[11]$$

From equations 4 and 9 it follows that

$$\exp\,(T_2-T_1)E/RT_1T_2) = (T_2/T_1)^{\alpha} \qquad \ldots.[12]$$

or

$$(T_2-T_1)E/RT_1T_2 = \alpha \ln\,(T_2/T_1) \qquad \ldots.[13]$$

Hence, for a temperature interval T_2-T_1, which is small compared with T_1,

$$\alpha = E/RT_i \qquad \ldots.[14]$$

where $T_1 < T_i < T_2$ characterizes the temperature range. To replace T_s in equation 11 by T_0 we approximate T_s^2 in equation 8 by T_sT_i so that

$$T_s = T_0/(1-RT_i/E)$$

Because of equation 14

$$T_s = T_0\alpha/(\alpha-1) \qquad \ldots.[15]$$

and thus equation 11 becomes

$$T_0^{\alpha-2} r = (kR/EC_0QB)\,[(\alpha-1)/\alpha]^{\alpha-2} \qquad \ldots.[16]$$

This relation represents the 'ignition temperature' of single particles as a function of particle radius. In other words, the dependence of ignition temperature on particle size is quasi-hyperbolic. The minimum ambient temperature that must be attained to enable isolated particles to ignite decreases with increasing particle size.

Conditions differ for dust clouds. For a monodisperse dust cloud the ignition temperature can be expected to be lower than for a single particle of equal size, because the interior of the cloud is shielded against heat loss by the surrounding particles and the heat generated on the reacting particles is transferred to neighbouring particles.

B. EXPERIMENTAL PROCEDURES AND RESULTS

In the present experiments dried air or pure oxygen was used as oxidant. It is known that solid aluminium forms a protective oxide layer[11]. It might have been expected that melting would crack this layer, owing to the 6 per cent expansion of the metal which occurs in the phase transition (melting point, 659·7°C). However, it was not possible to ignite single aluminium particles travelling through a silicon carbide furnace, even at 1 400°C. This indicates that the molten liquid also is protected by oxidation, so that luminous combustion is inhibited unless the growing oxide layer does not reach a critical thickness before the ignition temperature is attained. Similar observations have been reported by H. C. Anderson and L. H. Belz, who studied the combustion of zirconium powders[12].

On the other hand, the oxide layer of magnesium is non-protective[11], and, according to W. M. Fassell *et al.*[2], the ignition temperature of 623°C (melting point, 651°C) is independent of layer thickness. Therefore, magnesium and 50–50 magnesium–aluminium alloy particles measuring

5 to 75 microns in diameter were chosen for the present work. The magnesium particles were obtained in spherical form from Picatinny Arsenal. The alloy particles were spheriodized by being heated above the melting point in an argon atmosphere as they fell through a vertical furnace.

To reduce the time of exposure to oxidation the particles were carried directly into the hot zone of the vertical furnace through a water-cooled tube. This furnace was 65 cm long and had an evenly heated length of about 35 cm, with an inner diameter of 2·7 cm. The particles were pre-classified by elutriation, and the maximum size fed from the top of the furnace was limited by controlling the flow velocity, as measured by a rotameter, of the gas that carried them. In this way the particle diameter did not vary more than ±15 per cent. The gas issued as a jet from a hypodermic needle directed against a horizontal rotating dust layer of constant height. To 'fluidize' the dust and to prevent particles from being deposited on tube walls, the disperser and attached feedline were tapped by a 120 c/s electromagnetic vibrator. The particles were kept floating in the hot zone by a rising stream of hot gas. Temperatures inside the furnace were measured by a platinum/platinum-rhodium thermocouple. The potentiometer reading gave an accuracy of ±2·5°C. To determine particle

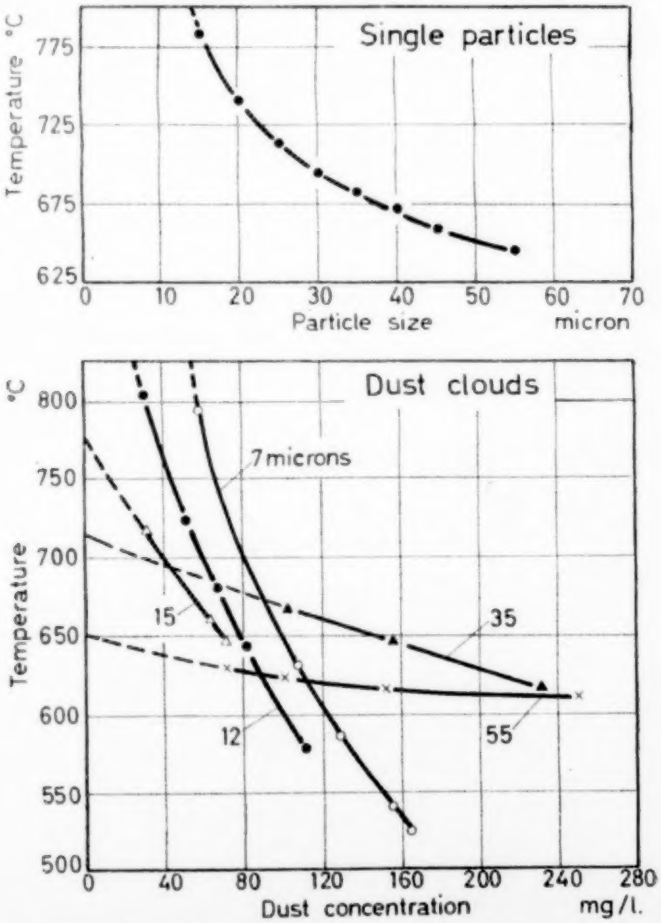

Figure 2. Ignition temperatures of magnesium particles

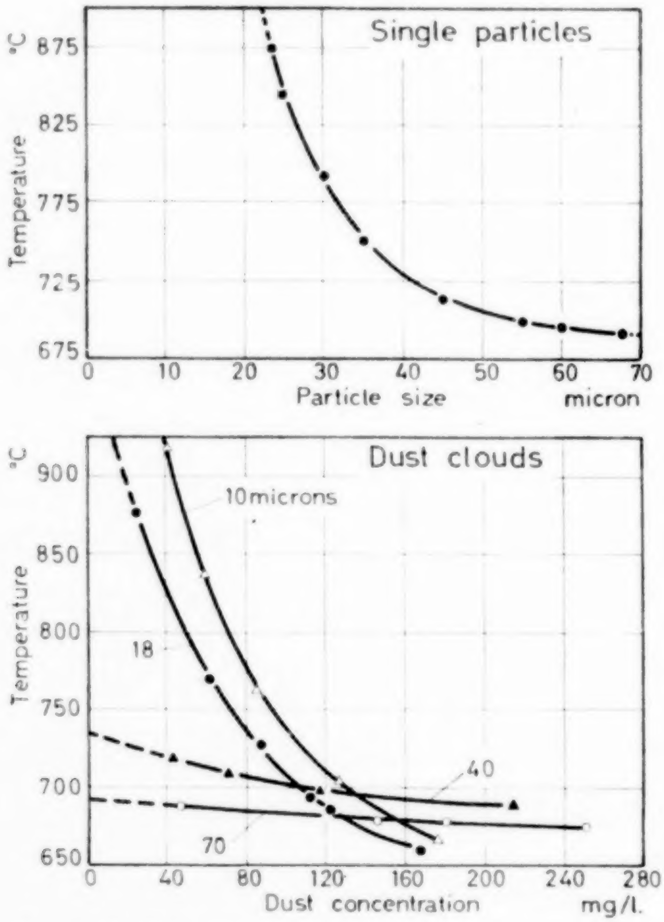

Figure 3. Ignition temperatures of 50–50 magnesium aluminium particles

size and concentration the dust stream was diverted from the furnace and collected either on greased microscope slides for inspection of particle size or the whole dust stream aspirated for a given period (15 seconds) through a glasswool filter and weighed. The volume of gas was derived from the flowmeter reading. A mirror at the bottom of the furnace was used to observe ignitions.

The time required to heat single particles to ignition increases from less than 0·1 second to 0·3 second as the particle diameter goes from 10 to 75 microns. This agrees approximately with equation 3 in regard to the proportionality of time lag before ignition and surface area of the particles. Evidently surface reactions predominate over volume reactions in the initial period of oxidation, the latter becoming competitive only in the slow oxidation of larger metal bodies. For clouds of large particles, the times observed were longer than for small particle clouds, exceeding the time requirement for single particles by up to 50 per cent.

The data recorded in the graphs of *Figures 2* and *3* present ignition temperatures as a function of particle size and concentration for magnesium and the 50–50 aluminium alloy, respectively, burning in air.

The theoretical deductions presented above depend on the assumption that, in the ignition stage, the rate of the chemical reaction is governed, not by diffusion, but by the rate of the heterogeneous surface reaction. To check this assumption, ignition temperatures of single particles were measured in pure oxygen. *Table 1* lists the results obtained.

Table 1

Fuel	*Particle diameter, × 10^4 cm*	*Ignition temperature, °C* *In air*	*In oxygen*
Mg	30	695	695
	45	660	655
	70	645	640
Mg-Al (50-50)	40	740	730
	50	710	705
	80	685	675

Hence, within the experimental error the ignition temperature remains unchanged for a fivefold increase in oxygen concentration. This finding supports the assumption that the reaction rate near the ignition temperature is not governed by oxygen diffusion.

DISCUSSION OF RESULTS

The ignition temperatures of the alloy are higher than those of pure magnesium, for the same particle size and concentration; the difference becomes greater with decreasing size. For both fuels the observed values of single-particle ignition temperatures as a function of particle size are in good agreement with equation 16; that is, the temperature increases with diminishing particle size*. From the experimental data for single particles, $\alpha_{Mg} = 8{\cdot}6$ and $\alpha_{alloy} = 8{\cdot}2$ are obtained. Thus from equation 14, $E_{Mg} = 17\,700$ cal/mole and $E_{alloy} = 18\,600$ cal/mole. These values appear reasonable when compared with the value determined from rate-of-oxidation experiments by Gulbransen[1] for aluminium, that is, 41 800 cal/mole, for which ignition of single particles could not be achieved in our experiments.

The rule that isolated small particles ignite at higher temperatures than large ones does not conflict with the fact that clouds of small particles require lower ignition temperatures than large single particles. The explanation lies in the cooperative mechanism of the ignition of dust dispersions. In the cloud each particle is close to heat-generating particles and thus loses less heat than an isolated particle. As the density of monodisperse dust clouds increases, the ignition temperature is greatly reduced, owing to the reduced distance between particles and to the increase of the total heat-generating area†. This decrease is steeper for fine particles than for coarse particles, so that the ignition temperature/concentration curves intersect. At a fixed ambient temperature, particles which cannot be ignited when isolated do ignite in a dust cloud of sufficiently high concentration.

---

*The same behaviour was observed with Pittsburgh coal particles containing 36 per cent volatile combustibles.

†If w = dust concentration, measured in g/cm^3, the number of particles of radius r in a monodisperse dust cloud per unit cloud volume is $n = 3w/4\pi\rho r^3$. Therefore, the average distance between particles is $(1/n)^{1/3} = (4\pi\rho/3w)^{1/3} \cdot r$, and the total surface area of the particles per unit cloud volume is $A = 3w/\rho r$.

Regarding dust clouds, it is clear from the concept of the cooperative mechanism as exemplified in the present results that the measured 'ignition temperatures' do not represent absolute values, characteristic of the fuel mixtures. For a given dust concentration of the cloud, cooperation must start at temperatures that are lower as the surface/volume ratio of the dust cloud is smaller.

This seems to be the reason why the present data are partly in contradiction with findings reported in the literature. For instance, in the work of G. COSTANTINIDES[13], ignition temperatures of sulphur, titanium and magnesium dust are found to be higher with coarse than with fine particles for all concentrations investigated. I. HARTMANN and coworkers[14] found that the ignition temperatures of dust clouds of synthetic resins, coal, starch and metal powders decreased with decrease in particle size and with increase in oxygen concentration; for metal powders the latter effect is small. In the range of sufficiently high concentrations, due to crossing of ignition temperature/concentration curves, our findings are not at variance with these data.

With small concentrations it is observed that ignition is not achieved uniformly throughout the cloud but originates from sporadically distributed centres in the form of flamelets, which then engulf the whole cloud. This phenomenon is also observed in the luminous zone of flat, laminar dust flames of aluminium and graphite, the number of flamelets per unit area increasing with dust concentration. This is illustrated by the photographs in *Figure 4*, taken with a focal-plane shutter camera having a 0·001 second exposure.

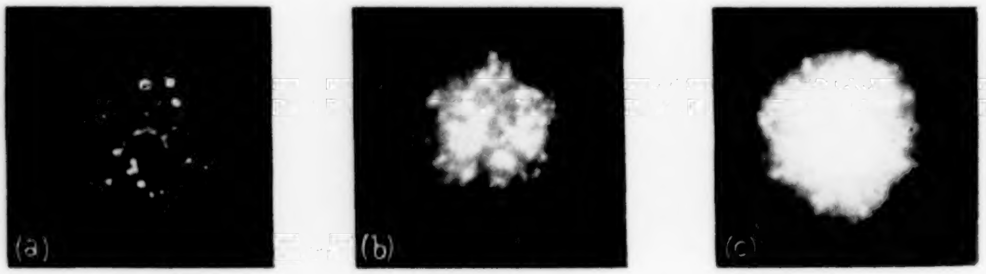

Figure 4. Top view of flat aluminium dust flames burning in air, showing distribution of flamelets. Dust particle size: 4 to 6 microns. Dust concentration: (a) 175 mg/l. (b) 200 mg/l. (c) 225 mg/l.

Flamelet formation is attributed to the existence of clusters in the dust clouds. The clusters are not particle agglomerations as considered in Smoluchowski's theory of rapid coagulation, based on the assumption that collisions between particles lead to polymerization. In the dispersions studied here only a very small fraction of the collisions can be successful, owing to the repellant electric double layers that coat the particles[5]. It rather appears that the cluster formation evidenced by flamelets is the natural consequence of statistical density fluctuations within the otherwise uniform cloud, typical of aerosols subject to Brownian motion. The situation corresponds to that in aqueous gold sols, well known from the work of H. WESTGREN[15].

The authors are indebted to Dr I. Hartmann, Chief, Branch of Dust Explosions, and to E. L. Litchfield, Division of Explosives Technology, Bureau of Mines, Pittsburgh, Pa, for valuable criticism and discussion, as well as to R. G. Walton, Jr, for building the dust disperser.

This work was in part sponsored by the Office of Ordnance Research, Durham, N.C.

Branch of Dust Explosions,
Division of Explosives Technology,
U.S. Bureau of Mines, Pittsburgh, Pa

(*Received June 1958*)

REFERENCES

[1] GULBRANSSEN, E. A. 'Kinetic and structural factors in the oxidation of metals'. *Industr. Engng Chem. (Industr.)*, 1949, **41**, 1385

[2] FASSELL, W. M. *et alii*. 'Ignition temperatures of magnesium and magnesium alloys'. *J. Metals, N.Y.* 1951, **3**, 522

[3] FLANDERS, H. E. 'Oxidation of magnesium powders'. University of Utah, Department of Metallurgy, *Status Reports I* to *XI*, September 1957

[4] 'Metal oxidation and ignition'. *Rep. ANL No. 5789*. Argonne National Laboratory, Chemical Engineering Division, September 1957

[5] WAGNER, C. and GRÜNEWALD, K. *Z. phys. Chem. B*, 1938, **40**, 455

[6] HARTMANN, I., NAGY, J. and BROWN, H. R. 'Inflammability and explosibility of metal powders'. *Rep. Invest. U.S. Bur. Min. No. 3722*, 1943, 44 pp; 'Explosibility of metal powders: *Metal Progr.* May 1944, **45**, pp 886–887, 930 and 932

[7] HARTMANN, I. and GREENWALD, H. P. 'The explosibility of metal powder dust clouds'. *Min. & Metall., N.Y.* 1945, **26**, 331

[8] HARTMANN, I. 'Dust explosions', p 795. *Marks' Mechanical Engineers' Handbook*, 1951

[9] HARTMANN, I., NAGY, J. and JACOBSON, M. 'The explosive characteristics of titanium, zirconium, thorium, uranium, and their hydrides.' *Rep. Invest. U.S. Bur. Min. No. 4835*, 1951, 16 pp

[10] SMITH, F. W. *Meteor Rep. No. 6*. Massachusetts Institute of Technology, 1947

[11] SEITZ, F. *The Physics of Metals*. McGraw-Hill: New York, 1943

[12] ANDERSON, H. C. and BELZ, L. H. *J. electrochem. Soc.* 1953, **100**, 240

[13] COSTANTINIDES, G. *Ann. Chim., Roma*, 1952, **42**, 383

[14] HARTMANN, I. 'Recent research on the explosibility of dust dispersions'. *Industr. Engng Chem. (Industr.)*, April 1948, **40**, 752-758

[15] WESTGREN, H. *Ark. Mat. Astr. Fys.* 1916, **11**, No. 8

Flame Quenching in Converging Rectangular Channels

A. L. BERLAD, R. D. ROWE* and C. H. YANG

A converging rectangular channel flame quenching apparatus is described, suitable for use with a dynamic flame quenching technique which is stated to be particularly useful for high reactivity systems. The application of apparatus and technique to the study of a stoichiometric oxygen–acetylene flame is outlined.

IT IS the purpose of this paper to describe a *dynamic* flame quenching technique which yields a highly precise quenching datum. The datum is obtained from a streak photograph of the flame propagating in and being extinguished in a converging rectangular channel. The technique simultaneously yields instantaneous spatial flame propagation velocities as well as other features of the flame structure prior to and during quenching.

The essential features of the quenching apparatus are indicated in *Figure 1*. The quenching chamber employs two steel channel dividers to define three short converging rectangular channels. Above these three quenching channels is an ignition section. The ignition section of the quenching chamber is separated from a large plenum by a fast acting gate

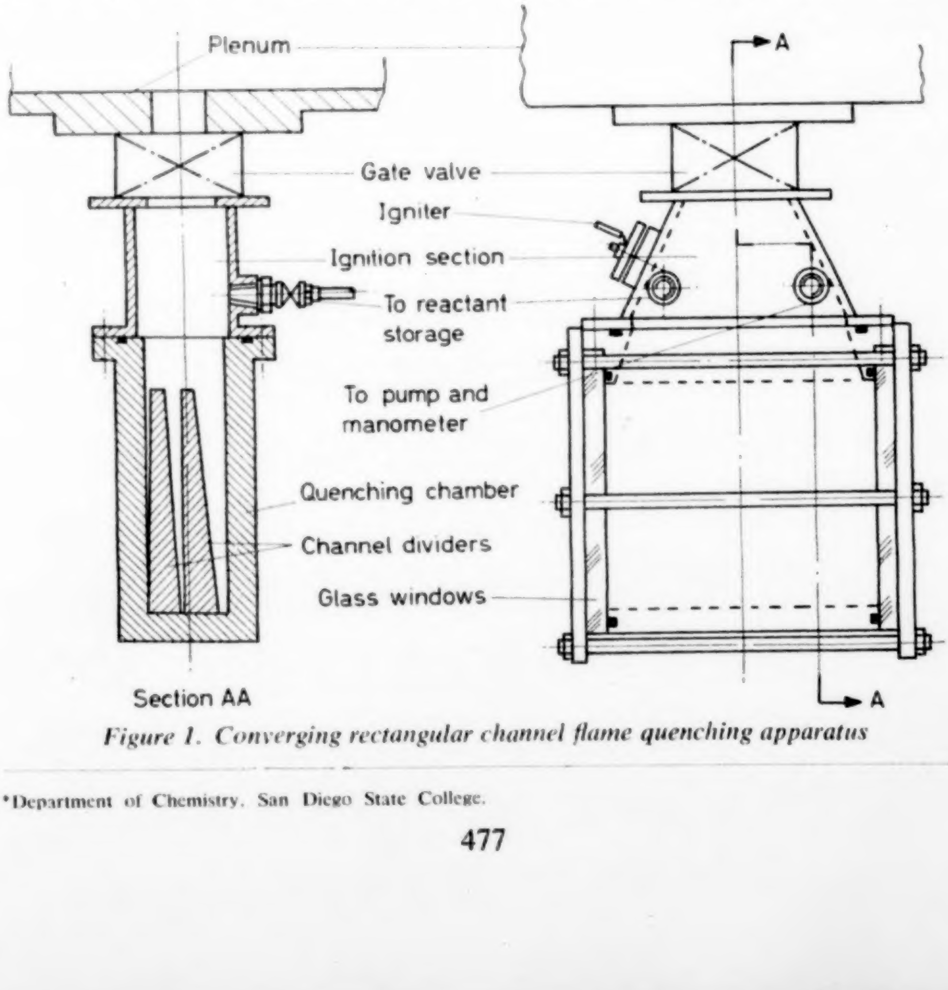
Plenum
A
Gate valve
Igniter
Ignition section
To reactant storage
To pump and manometer
Quenching chamber
Channel dividers
Glass windows
Section AA
A

Figure 1. Converging rectangular channel flame quenching apparatus

valve. The free volume of the plenum is about 5 000 times that of the quenching chamber. The 1·5 in. gate valve is electrically actuated and is coupled, through a variable time delay circuit, to the igniter. It takes about 0·5 sec for the gate valve to be opened fully. The three convergent rectangular channels employed were all 9·95 cm high, 12·62 cm deep and varied in width, respectively from 1·522 cm to 0·761 cm, from 0·780 cm to 0·260 cm and from 0·280 cm to zero (*Figure 1*).

---

*Department of Chemistry, San Diego State College.

A distinguishing feature of the apparatus centres about the fact that the flame under study propagates downward into a system of mildly *converging rectangular channels*, rather than in rectangular channels or cylindrical tubes of *constant* cross section. Consequently, the flame is quenched when it reaches a sufficiently narrow portion of a channel. Specifically, the converging channel quenching apparatus is used in the following manner. The quenching chamber is evacuated, then filled with the fuel–oxidant mixture to the pressure of interest. The plenum on the other side of the closed gate valve is filled with inert (e.g. nitrogen) to the identical pressure. The igniter delay is set so that 'ignition' and 'full open' for the gate valve are approximately coincident. Thus, upon 'firing', the gate valve opens, ignition occurs and the progress of the flame in a given channel is recorded by streak (visible or schlieren) photography. A streak photograph of the extinction history of a stoichiometric acetylene–oxygen flame propagating within the narrowest of the three wedges at a pressure of 11 mm of mercury is shown in *Figure 2*. The 'wedge quenching distance', d_w, is reproducible to better than one per cent and is easily calculated from the streak photograph. A very quick, less precise and less detailed quenching datum can be obtained by taking a time exposure of the entire event with a Polaroid Land Camera.

INTERPRETATION OF d_w

Strictly speaking, the observed flame extinction phenomenon is a highly time-dependent flame process. Of course, the transition of a stable flame

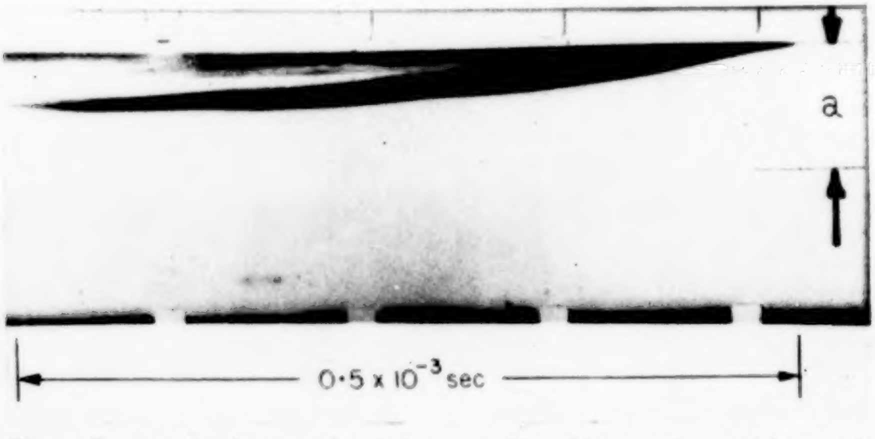

Figure 2. Streak photograph of the quenching history of a stoichiometric acetylene oxygen flame in the narrowest of the three channels. $p=11$ *mm* Hg, $d_w=0{\cdot}168$ *cm*, a = *channel height* = 9·95 *cm, film speed* = 204 *ft/sec*

to one which is quenched in a *constant* area duct is also a highly time-dependent flame process. The fact that the flame front decays over a finite, non-zero time suggests a degree of arbitrariness in deciding a critical value of d_w. However, for mildly convergent channels, this process should be expected to yield values of d_w which are very nearly those[1] for a long rectangular channel of constant separation d_c. The experimental observations reported[1–3] indicate that $d_w = d_c$ to a high degree of approximation. This is implied by the fact that very shallow constant area channels give quenching data equivalent to those obtained in deep, constant area channels. It appears, then, that the quenching instability of a flame is primarily determined by the wall separation in the *immediate* neighbourhood of the reaction zone.

A series of sub-atmospheric propane–air flames have been quenched in the converging rectangular channel system described above and the fact that $d_w = d_c$, within the limits of accuracy of previous data[2,3] has been confirmed.

GENERAL CHARACTERISTICS AND UTILITY OF STREAK PHOTOGRAPHY STUDIES OF FLAME EXTINCTION IN CONVERGING CHANNELS

(*1*) A *very precise* quenching datum is obtained quickly.

(*2*) *Dynamics* of the extinction process are observable. For example, the acetylene–oxygen flame of *Figure 2* was extinguished in less than 0·4 msec. Use of more refined techniques should yield additional information regarding the flame's history and structure *during* extinction.

(*3*) (Velocity) distinctions between deflagrations and detonations as well as steady versus non-steady state flames are simple. Thus, close-lying detonation and deflagration limits are easily distinguished. For example, the deflagration extinction process of *Figure 2* (stoichiometric acetylene–oxygen) may become a pre-detonation flame when the pressure is increased but a few millimetres of mercury. Thus the technique permits a check of the validity of a quenching datum. For highly reactive systems, such a check is necessary.

(*4*) The technique is particularly useful for *high reactivity* systems. This usefulness is implied by the aforementioned characteristics as well as by the fact that the no-flow, small reactant volume features of the technique allow a high degree of safety and economy. Streak photography observation of high reactivity systems (e.g. acetylene–oxygen) is particularly useful in that these systems frequently give rise to non-steady state phenomena.

(*5*) The technique permits observation of the detailed *effects of imposed physical influences on the dynamics* of flame propagation and extinction. For example, work in progress indicates that strong transverse electric fields have a destabilizing effect on acetylene–oxygen flames. That is, they quench at larger values of d_w. Similarly, the effects of sound fields, microwave fields, etc. on extinction phenomena may be investigated.

Convair Scientific Research Laboratory,
San Diego, California

(*Received November 1958*)

REFERENCES

[1] FRIEDMAN, R. *Third Symposium on Combustion and Flame and Explosion Phenomena*, pp 110–120. Williams and Wilkins: Baltimore, 1949

[2] BERLAD, A. L. *J. phys. Chem.* 1954, **58**, 1023

[3] FRIEDMAN, R. and JOHNSTON, W. C. *J. appl. Phys.* 1950, **21**, 791

[4] BERLAD, A. L. and POTTER, A. E., Jr. *Fifth Symposium (International) on Combustion*, pp 728–735. Reinhold: New York, 1955

The Effect of External Factors on the Formation of Detonation in Saturated Knallgas-Steam Mixtures*

L. B. ADLER†, E. C. HOBAICA‡ and J. A. LUKER

The formation of detonation in saturated mixtures of knallgas and steam at 100°C was studied with respect to spark and hot-wire modes of ignition and geometry (diameter) of the reaction vessel. Reaction pressures and the amount of knallgas consumed by reaction in each experimental mixture were measured. The data indicate that the ease with which detonation is formed is affected by both of the primary variables in a dual manner which is strongly dependent upon heat and wall effects related to the reactor size. The controlling effects observed are apparently accentuated due to the 'weak' nature of the pre-detonation reactions and the 'slow' transition to detonation which are characteristic of the majority of saturated knallgas-steam mixtures.

THE period of formation preceding the establishment of detonation in gaseous media is known to be influenced by certain external features of the detonation system. Two external factors which have been shown to affect the formation of detonation in gases are the mode and strength of the initiating source used to ignite the gas[1-5], and, in the case of plane waves, the detonation tube diameter[6, 7]. Some of the important aspects of shock-type ignition, most effective in accelerating the development of detonation, have recently been studied by a number of investigators[8-12]; however, 'weaker' methods of ignition, those which initiate detonation by flame rather than by shock wave, have received limited treatment. It is generally not clear, for instance, if the reaction initiated by a spark will transform into detonation any more readily than the reaction initiated by a hot-wire igniter. An additional question of interest is whether the pre-detonation flame corresponding to ignition methods of this type will be selectively influenced by the diameter of the detonation tube through which it is propagated. As with most points related to the formation of detonation in gases, such questions can be answered only by experiment.

The object of this study was to provide information regarding the effects of ignition and reactor diameter on the formation of detonation in saturated mixtures of knallgas and steam at 100°C. The basic method of attack employed was the same as that of a previous study made by L. B. ADLER and J. A. LUKER[13], in which detonation 'overpressures' in the saturated knallgas-steam system were of primary interest: experimental mixtures of varying knallgas content were ignited in a reaction tube; reflected reaction pressures were then measured at a fixed distance from the source of ignition with a piezoelectric quartz pressure transducer. Pressure/time records obtained in this manner corresponded to successive stages of development of the pre-detonation flame. The amount of knallgas reacted in each experimental mixture was also determined. Primary experimental conditions were varied by employing two modes of ignition, spark and hot wire, and three different reaction tubes. The strength of the spark mode of ignition was varied.

---

*Stoichiometric mixture of hydrogen and oxygen ($2H_2+O_2$).

†Present address: Brookhaven National Laboratory, Upton, New York.

‡Present address: Electric Boat Division, General Dynamics Corpn., Groton, Connecticut.

APPARATUS AND PROCEDURE

The apparatus and procedure employed in this investigation were essentially the same as those described in detail in an earlier paper[13]. Reference should thus be made to the previous work for all of the basic experimental details of the present study, with the exception of the modifications described here. The modifications made involved the use of two types of ignition and three different tubular vessels. These provided the desired primary experimental variables of ignition and of geometry (reactor diameter).

The three reaction tubes employed were 1·10, 2·43 and 7·37 cm in inner diameter. Positioning of the ignition source and of the pressure transducer was the same for each reactor; the distance between the two was 2·35 m.

Ignition was effected in either of two ways: by a spark, or by a hot-wire igniter. Two spark energy levels, 180 millijoules and 360 millijoules (mJ), were investigated. The 180 mJ spark was created by the discharge of a 0·01 microfarad capacitor maintained at a firing potential of 6 kV; the 360 mJ spark was created by the similar discharge of a 0·02 microfarad capacitor.

The hot-wire igniter was constructed from a 2 ohm strand of 28-gauge Nichrome wire wound into a helical coil and activated with d.c. power through a manually operated timing unit. Power was supplied to the igniter for a time sufficient to cause reaction, or for a maximum time of thirty seconds. The mean power input to the hot wire for all runs was 9·4 W with a mean deviation of ±0·7 W.

The particular combinations of reactor size and source of ignition studied are indicated in *Table 1*.

Table 1. Primary experimental conditions

Source of ignition	*Reactor inner diameter cm* 1·10	2·43	7·37
Spark (180 mJ)		×	
Spark (360 mJ)	×	×	×
Hot wire	×	×	

RESULTS AND DISCUSSION

Certain factors related to the presentation and discussion of the experimental results of this study are similar to those previously treated at length[13]. These include an analysis of errors, a discussion of the adequacy of the experimental pressure measurements, and an outline of the calculations made to define the theoretical combustion properties which are re-employed here. Such material will not be reiterated, and reference should be made to the earlier work for these details.

The experimental results are presented in two graphical forms, each of which relates an important measured reaction parameter to the experimental composition in terms of mole per cent knallgas. One of these important parameters is the peak reaction pressure, as evaluated by a 'static' or dead-weight calibration of the experimental pressure transducer; the other is the amount of knallgas consumed by reaction. These data are supplemented by typical reaction pressure/time records which aid in an analysis of the results.

The most effective means of representing the experimental data is a plot relating the ratio of peak reaction pressure/initial mixture pressure to the mixture composition, and the pertinent comparisons made will be based on data represented in this manner. Specific points of comparison are illustrated in *Figure 1*, a typical reaction pressure ratio curve obtained in the 2·43 cm reactor with a spark ignition energy level of 180 mJ. The particular features of this curve which are of interest are the *no-reaction limit*, the *pre-detonation region*, and the *induction composition*. The no-reaction limit, which is the origin of the experimental curve, denotes the mixture composition below which no reaction will occur. This limit serves as the lower boundary of the pre-detonation region, which is arbitrarily

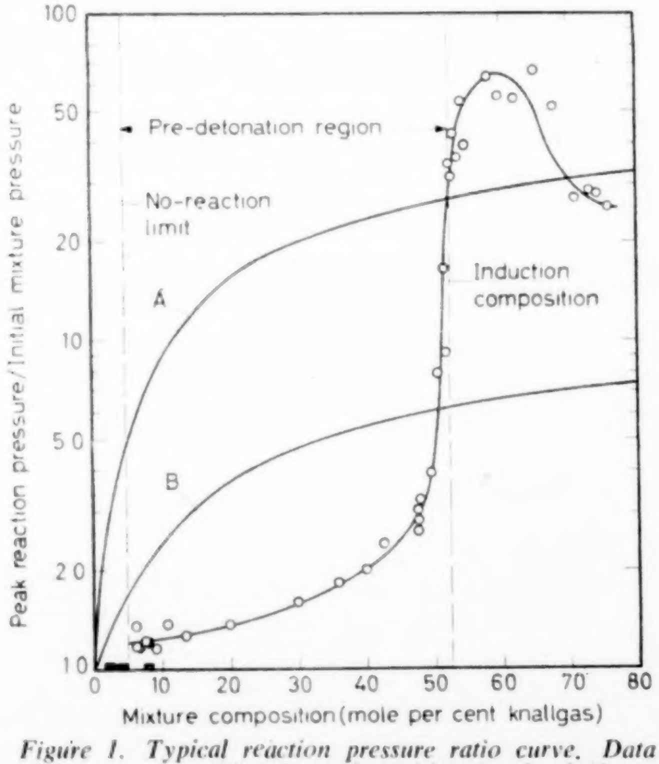

Figure 1. Typical reaction pressure ratio curve. Data shown are for 180 mJ spark ignition in the 2·43 cm reactor. ■ *No reaction;* A *Theoretical reflected detonation;* B *Theoretical explosion*

defined as the range of mixture compositions extending from the no-reaction limit to the intersection of the experimental curve and the theoretical curve corresponding to reflected detonation (curve A). The mixture composition at this point of intersection is the induction composition, or the leanest experimental mixture composition which will result in a reaction pressure equal to the theoretical detonation pressure under the conditions studied. While the majority of mixtures below the induction composition are characterized by relatively low reaction pressures, mixtures above the induction composition initially exhibit the 'overpressures' associated with unstable detonation[13]. With further enrichment, the transition to stable detonation is indicated. Curve B in this figure represents the theoretical pressure ratios for constant-volume explosion; it is presented solely for purposes of comparison. Both theoretical curves shown were taken from the previous paper.

Prior to further discussion, it should be noted that the experimental pressure ratios reported in this study are not to be taken as absolute measures of the actual reaction pressures developed, particularly in those mixtures exhibiting the high pressure ratios characteristic of extremely transient detonation reactions. This is due primarily to frequency limitations of the experimental pressure transducer. The induction composition, as defined above, is thus not a 'true' induction composition in that it is the mixture composition where actual reaction pressure ratios first

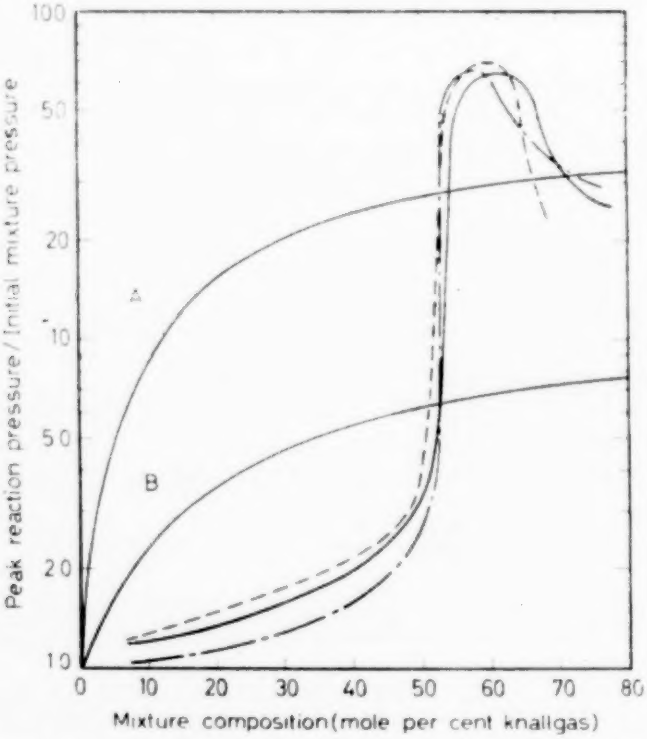

Figure 2. Effect of ignition on reaction pressure ratios in the 2·43 cm reactor. ——— 180 mJ spark; — — —360 mJ spark; — · — hot wire; **A** *Theoretical reflected detonation;* **B** *Theoretical explosion*

equal those of theoretical reflected detonation; however, the experimental pressures measured are correct in a relative sense, and since the same pressure-measuring device was used in obtaining all of the experimental data, the induction compositions based on these data should be just as valid for purposes of comparison as those based on the true pressures.

IGNITION

The results which illustrate the effect of ignition on the formation of detonation in the 2·43 cm reactor are given in *Figures 2, 3* and *4*. For clarity, smoothed curves are presented in *Figures 2* and *3;* this is done in each subsequent graph included in this paper. Representative scatter of actual experimental points is indicated by the 'sample' curve of *Figure 1*.

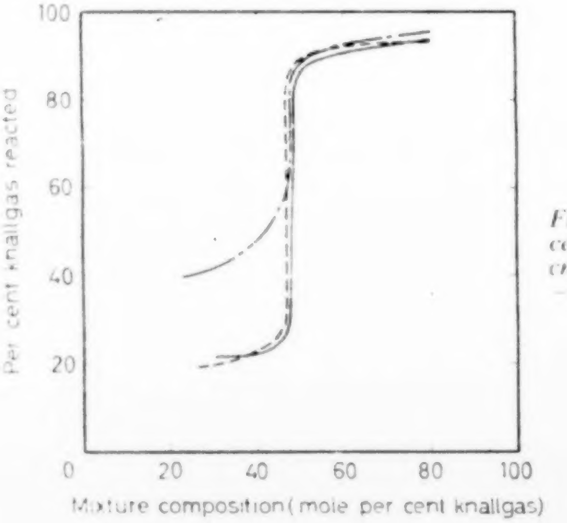

Figure 3. Effect of ignition on per cent knallgas reacted in the 2·43 cm reactor. ——— *180 mJ spark;* — — — *350 mJ spark;* — · — *hotwire*

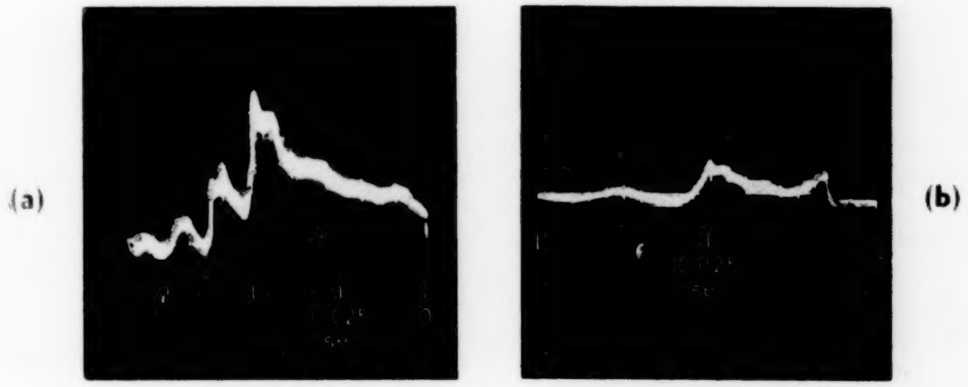

(a) *Hot wire ignition. Mixture composition = 6·9 mole per cent knallgas; peak reaction pressure = 1·16 atm; knallgas reacted = 18 per cent*

(b) *360 mJ spark ignition. Mixture composition = 8·7 mole per cent knallgas; peak reaction pressure = 1·39 atm; knallgas reacted = 57 per cent*

Figure 4. Pressure/time records of reaction in the 2·43 cm reactor. Vertical axis = pressure; horizontal axis = time

The curves shown in the pressure ratio plot of *Figure 2* correspond to each of the three sources of ignition employed in the 2·43 cm reactor. Differences between the three curves at the no-reaction and induction compositions are slight, and relative to possible errors in predicting mixture composition due to fluctuations in reactor temperature (see L. B. ADLER and J. A. LUKER[13]), these differences are not significant. The extent of the pre-detonation region for each curve can thus be considered the same, and detonation in this reactor is apparently formed with equal readiness by spark (either energy level) or hot wire.

Figure 3 provides additional information of interest. In this figure, the amount of knallgas consumed by reaction in each of the experimental mixtures is plotted versus the mixture composition for the three means of ignition employed in the 2·43 cm reactor. The curves shown are not extended to the no-reaction limit due to considerable scatter in the per cent reacted at the lower mixture compositions. This was due to mixture pressure variation caused by reactor temperature control[13]. At the lower compositions, such variation was quite significant with respect to the reaction pressure drop measured. The sharp rise in each of the per cent reacted curves indicates a change in the dominant reaction mechanism occurring within the experimental system. The amount of knallgas which is consumed by reaction is obviously related to this mechanism: in mixtures where weak reaction predominates (deflagration), the per cent reacted is low; in mixtures where more intense reaction predominates (shock-propagated reaction characteristic of the transition to detonation), the per cent reacted is high. Since each experimental curve in *Figure 3* rises abruptly at essentially the same mixture strength, the mixture composition at which a change in dominant reaction mechanism occurs is then the same for each curve. This gives further indication that the formation of detonation in the 2·43 cm reactor is independent of the three means of ignition studied.

It is interesting to note the pre-detonation pressure ratios. Although the extent of the pre-detonation region in the 2·43 cm reactor is not affected by ignition, the reaction pressures observed in this region are functions of the manner in which the experimental mixture is ignited. As indicated in *Figure 2*, the peak reaction pressures in the pre-detonation region were a maximum for the 360 mJ spark, lower for the 180 mJ spark, and a minimum for hot-wire ignition. This order corresponds to the relative strength of each ignition source if spark ignition is considered as being 'stronger' than hot-wire ignition by virtue of its instantaneous release of ignition energy; it is also possible that the generation of an auxiliary shock wave by the passage of the spark in these mixtures plays a significant role in the pre-detonation process. Pressure/time records of such reactions did reveal marked differences in form, the basic difference being in reaction rise time. In general, the rise times in mixtures ignited by hot wire were slower than those in mixtures ignited by spark. This is illustrated for comparable mixtures in *Figures 4*(a) and *4*(b). Note the existence of a leading pressure pulse in the reaction ignited by spark, and also the difference in the time base of the photographs. The horizontal segment of the spark trace preceding the initial pressure rise in *Figure 4*(b) represents the time interval between the passage of the spark and the arrival of the experimental pressure pulse at the transducer end of the reactor.

Further photographic evidence indicated that a series of weak combustion waves followed the initial pressure pulse when hot-wire ignition was employed. This is attributed to the fact that the hot-wire power was not terminated immediately when initial reaction was achieved; it was left 'on', and this was undoubtedly responsible for the multiple reactions observed. Presumably, this also accounts for the fact that experimental mixtures ignited by hot wire consumed a much larger amount of knallgas in the pre-detonation region than did those ignited by either of the two spark energies (see *Figure 3*).

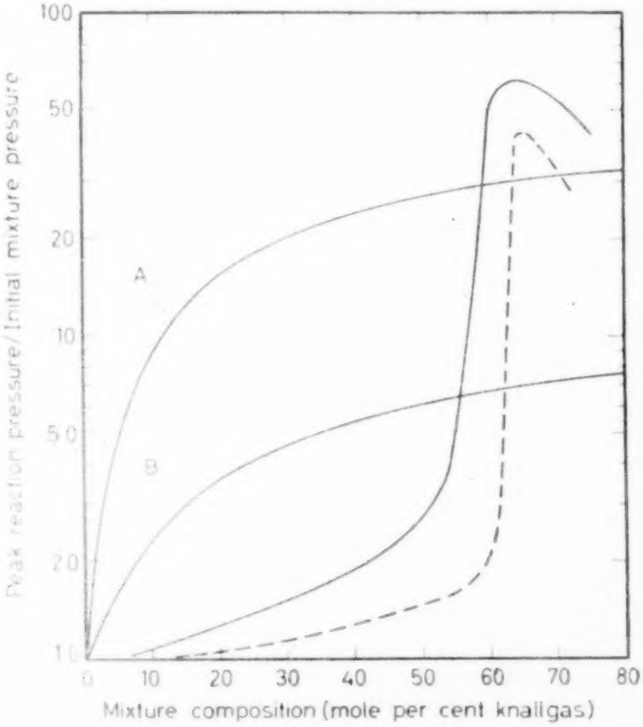

Figure 5. Effect of ignition on reaction pressure ratios in the 1·10 cm reactor, —— 360 mJ spark; – – – hotwire; A Theoretical reflected detonation; B Theoretical explosion

The results of the ignition study in the 1·10 cm reactor are presented in *Figures 5* and *6*. Two modes of ignition, spark (360 mJ) and hot wire, were employed in this smaller reactor, and thus only two data curves are available; however, these are sufficient to provide the necessary comparisons.

The data obtained in the 1·10 cm reactor, in contrast to those obtained in the 2·43 cm reactor, show the influence of ignition quite markedly. With respect to *Figure 5*, differences occur in the no-reaction limit (13 mole per cent knallgas for hot wire, as opposed to 6 mole per cent knallgas for spark) and in the induction composition (63 mole per cent knallgas for hot wire, as opposed to 57 mole per cent knallgas for spark). Differences in the pre-detonation reaction pressures for each type of ignition are also apparent.

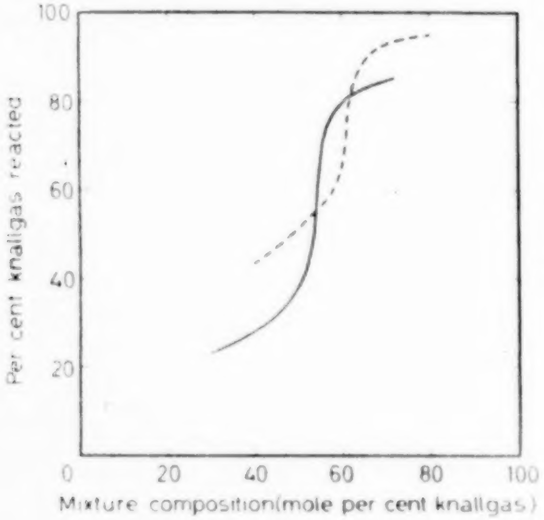

Figure 6. Effect of ignition on per cent knallgas reacted in the 1·10 cm reactor. ——— *360 mJ spark;* - - - - *hotwire*

The upward shift in induction composition with hot wire is corroborated by the per cent reacted plot of *Figure 6*, in which the hot-wire curve experiences a change in the dominant reaction mechanism at a higher mixture composition than that for spark. Detonation is thus formed more readily in this reactor with spark ignition than with hot-wire ignition.

The pertinent differences in the 1·10 cm reactor are undoubtedly related to the small reactor size. This is initially indicated by the higher no-reaction limit obtained with hot-wire ignition. Since reaction was achieved at a significantly lower mixture composition with spark, the change in this parameter can logically be attributed only to heat effects which abstract a part of the energy released by the hot wire at a rate sufficient to inhibit the initiation of reaction. These effects are presumably accounted for by the high surface/volume ratio of the 1·10 cm reactor (3·64 cm^{-1}, as opposed to 1·65 cm^{-1} for the 2·43 cm reactor) and thus, the more effective heat sink provided by the reactor walls. Spark ignition, characterized by a much faster and more intense release of ignition energy, would be expected to function more efficiently than hot-wire ignition in forming detonation in this reactor, which it apparently does. This result is then attributed to the large surface/volume ratio of the 1·10 cm reactor and consequent heat effects which inhibit the reactions initiated by hot wire. The exact mechanism by which the formation of detonation is affected cannot be ascertained with these experimental data.

GEOMETRY

The effect of reactor diameter on the formation of detonation in the experimental system is shown in *Figures 7, 8* and *9*. A fixed ignition source (360 mJ) was employed.

The three curves shown in the pressure ratio plot of *Figure 7* correspond to each of the three reactor diameters studied: 1·10, 2·43 and 7·37 cm. No significant difference in no-reaction limit is evident for these curves; the possible variation in mixture composition due to reactor temperature

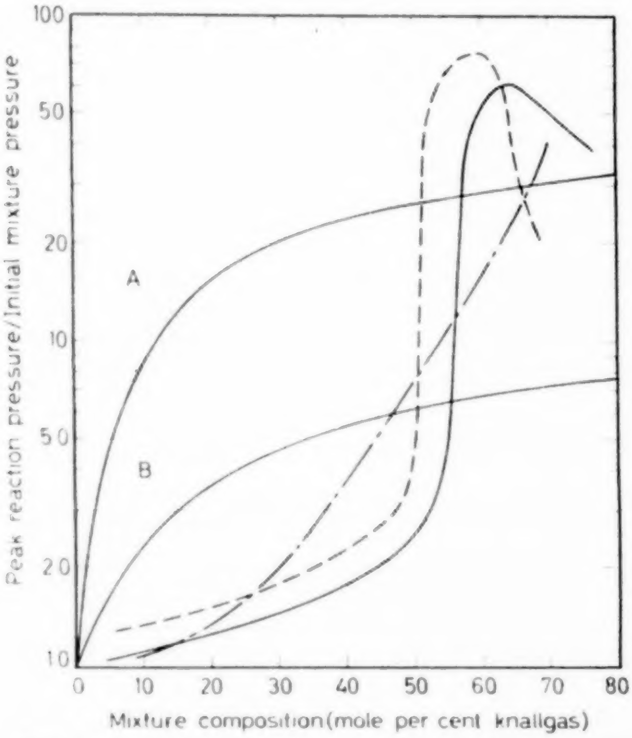

Figure 7. Effect of geometry (reactor diameter) on reaction pressure ratios obtained with 360 mJ spark ignition. ——— 1·10 cm; — — — 2·43 cm; —·— 7·37 cm: **A** *Theoretical reflected detonation;* **B** *Theoretical explosion*

Figure 8. Effect of geometry (reactor diameter) on per cent knallgas reacted with 360 mJ spark ignition. ——— 1·10 cm; — — — 2·43 cm; —·— 7·37 cm

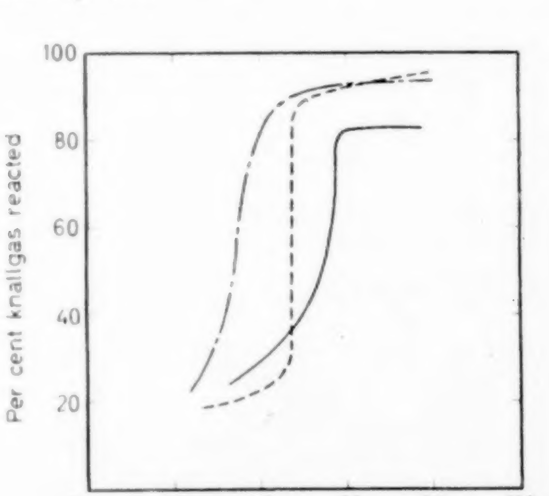

control at the no-reaction compositions shown is about ±3·5 per cent knallgas. Significant differences do exist, however, in the three induction compositions. These occur at 57, 51 and 67 mole per cent knallgas, respectively, and indicate that detonation is formed most readily in the

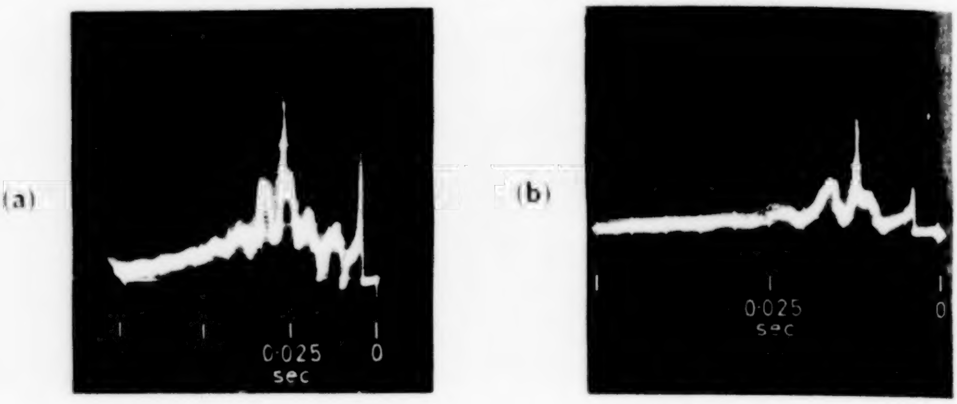

(a) *Mixture composition = 43·1 mole per cent knallgas: peak reaction pressure = 7·76 atm: knallgas reacted = 83 per cent*

(b) *Mixture composition = 53·7 mole per cent knallgas: peak reaction pressure = 23·1 atm: knallgas reacted = 93 per cent*

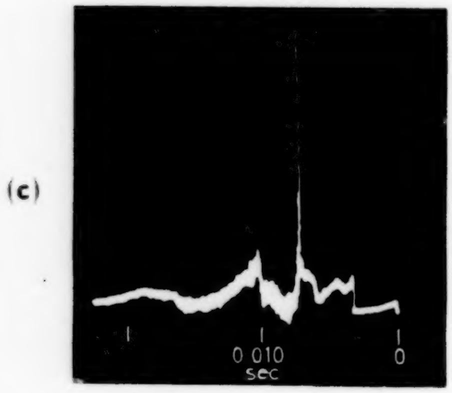

(c) *Mixture composition = 63·6 mole per cent knallgas: peak reaction pressure 104 atm: knallgas reacted = 99 per cent*

Figure 9. Pressure time records of reaction in the 7·37 cm reactor with 360 mJ spark ignition. Vertical axis = pressure; horizontal axis = time

2·43 cm reactor and least readily in the 7·37 cm reactor for this system: furthermore, the ease of forming detonation in the 1·10 cm reactor lies between these two extremes.

The particular dependence of the induction composition on reactor diameter shown in *Figure* 7 can be explained in the light of two possible diameter effects. The first of these concerns the role played by the reactor wall in controlling the extent of the pre-detonation region. As discussed with respect to the 1·10 cm reactor in the ignition study, small diameter (high surface/volume ratio) provides a more effective heat sink for the experimental gases, and results in a greater abstraction of reaction energy due to heat losses. If such heat losses significantly affect the pre-detonation period, it should be more difficult to form detonation in smaller tubes, i.e. here, the induction composition should increase with a decrease in reactor diameter. The overall situation is complicated, however, by a second diameter effect which is opposite in result to that based on reactor heat losses. It has been shown, initially by P. LAFFITTE[7], that the distance which a pre-detonation flame must travel before detonation is formed is proportional to the tube diameter. This effect has been attributed to interaction between the reacting gases and the tube walls, and particularly to the velocity gradient which is established during the pre-detonation gas flow (see G. B. KISTIAKOWSKY[11]). On this basis, detonation is formed more readily in a smaller tube, and the result of this diameter effect should be a decrease in induction composition with decrease in reactor diameter.

The data presented in *Figure 7* indicate that both of the diameter effects discussed above influence the formation of detonation in the experimental system. It also appears that a different effect is dominant for each reactor size studied. The first diameter effect discussed apparently controls in the case of the 1·10 and 2·43 cm reactors. Here, the induction composition is higher for the smaller tube. This must be attributed to its higher surface/volume ratio and the corresponding increase in heat losses which inhibit the development of reaction and reaction pressures in the pre-detonation region. If no other effect were present, the induction composition for the 7·37 cm reactor would then be the lowest of the three reactors because of its low surface/volume ratio (0·54 cm^{-1}); however, it is not the lowest, but the highest. This indicates that the formation of detonation in the 7·37 cm reactor is not a primary function of heat losses; rather, it is apparently governed by the diameter wall interaction effect which makes detonation harder to form in a larger vessel. Evidently, while not controlling in the two smaller reactors, where heat losses predominate, this effect is controlling in the large reactor, where the action of heat losses is greatly lessened.

Figure 8 does indicate that the pre-detonation reactions in the 7·37 cm reactor are affected less by heat losses: the per cent reacted curve for this reactor experiences the change indicative of a transition to more intense reaction at a mixture composition which is the lowest of the three curves shown. Shock-propagated reactions then occur at relatively low compositions in the large reactor; this is undoubtedly responsible for the high pre-detonation pressure ratios denoted by the 7·37 cm curve.

Differences in the formation of detonation in the three experimental reactors are emphasized by the manner in which the transition to detonation takes place. Referring again to *Figure 7*, the 7·37 cm pressure ratio curve is seen to rise rather gradually. This is markedly different from the abrupt rise in reaction pressure which occurs in both the 1·10 and 2·43 cm reactors. Apparently, the manner in which detonation is formed in the large reactor is then quite different from that in the two smaller reactors. This is taken as a further indication that the formation of detonation in the system studied is governed by two separate controlling effects which are related to the reactor size. A cross point must exist where one or the other of these diameter effects becomes controlling; however, this is not determinable from the data.

The gradual transition to detonation in the 7·37 cm reactor is illustrated in *Figure 9*. Discrete stages of the formation of detonation in the pre-detonation region are shown. The pre-compressional shock fronts which precede the flame front during the formation of detonation are clearly visible in each of the three photographs. As the experimental mixture strength is increased, the flame front and leading shock waves coalesce and tend to form a stable detonation wave. Stable detonation was not achieved in this reactor in the composition range of interest. Reactions in the 1·10 and 2·43 cm reactors were also evidenced by pressure/time records similar to those shown; however, these occurred in a much narrower range of mixture compositions.

CONCLUSIONS

The data obtained in this study indicate that the formation of detonation in saturated mixtures of knallgas and steam at 100°C is significantly dependent upon both mode of ignition (spark or hot wire) and reactor diameter. The particular extent to which important differences occur, however, is apparently controlled by heat and wall effects which are directly related to the reactor size. Ignition is seen to be a factor in forming detonation, but only in small tubes (high surface/volume ratio) where the increased action of heat losses evidently inhibits reactions initiated by the hot wire to a greater degree than those initiated by the spark. Reactor diameter (constant source of ignition) also affects the formation of detonation: in small tubes (1·10 and 2·43 cm in diameter), heat loss is indicated as the governing factor. In a larger tube (7·37 cm), heat losses are greatly lessened, and a reactor diameter–wall interaction effect is apparently dominant.

Perhaps the most significant information to be gained from this study is represented by the nature of the phenomena which apparently affect the formation of detonation in these mixtures. These same phenomena must play some part in the pre-detonation process of any detonatable gas; they are accentuated here because the majority of saturated knallgas–steam mixtures are 'slow' detonators, evidenced by 'weak' pre-detonation reactions as well as long detonation induction and stabilization distances which expand the time scale of the pre-detonation process. The effects shown here should then be useful in clarifying some of the phenomena associated with the pre-detonation period of detonatable gases in general.

The authors wish to express their grateful acknowledgement to Oak Ridge National Laboratory and the Union Carbide Nuclear Company, under whose auspices this work was performed.

Syracuse University Research Institute,
Syracuse 10, New York, U.S.A.

(Received November 1958)

REFERENCES

[1] PAYMAN, W. *Proc. Roy. Soc. A*, 1928, **120**, 90
[2] BONE, W. A. and FRASER, R. P. *Phil. Trans. A*, 1932, **230**, 363
[3] MANSON, N. and FERRIÉ, F. *Fourth Symposium (International) on Combustion*, p 486. Williams and Wilkins: Baltimore, 1953
[4] FREIWALD, H. and UDE, H. *Z. Elektrochem.* 1953, **57**, 629
[5] WAYMAN, D. H. and POTTER, R. L. *Combustion & Flame*, 1957, **1**, 321
[6] CAMPBELL, C. *J. chem. Soc.* 1922, **121**, 2483
[7] LAFFITTE, P. *C. R. Acad. Sci., Paris*, 1924, **179**, 1394; *Ann. Phys., Paris*, sér. 10, 1925, **4**, 587

[8] Shepherd, W. C. F. *Third Symposium (International) on Combustion, Flame and Explosion Phenomena*, p 301. Williams and Wilkins: Baltimore, 1949

[9] Berets, D. J., Greene, E. F. and Kistiakowsky, G. B. *J. Amer. chem. Soc.* 1950, **72**, 1086

[10] Mooradian, A. J. and Gordon, W. E. *J. chem. Phys.* 1951, **19**, 1166

[11] Fay, J. A. *Fourth Symposium (International) on Combustion*, p 501. Williams and Wilkins: Baltimore, 1953

[12] Fay, J. A. and Lekawa, E. *J. appl. Phys.* 1956, **27**, 261

[13] Adler, L. B. and Luker, J. A. *Combustion & Flame*, 1959, **3**, 157

[14] Kistiakowsky, G. B. *Industr. Engng Chem. (Industr.)*, 1951, **43**, 2794

The Burning Velocity of Hydrogen–Air Mixtures and Mixtures of Some Hydrocarbons with Air

T. G. Scholte and P. B. Vaags

An apparatus is described by which the burning velocity of gas air mixtures can be measured with an accuracy of about five per cent. The apparatus has been used for measuring the burning velocity of hydrogen air mixtures and mixtures of methane, ethane, propane, n-*butane, acetylene, ethylene, propylene and* n-*butylene with air as a function of the gas air ratio.*

By the term 'burning velocity' of a gas mixture is meant the velocity with which a very large, flat flame front propagates relatively to the unburnt gas in the direction of the normal. With the various existing methods for determining the burning velocity experimentally[1], it is not possible to start from a flat flame front with an infinitely large surface area. In the most favourable case one may attain a flat flame front with a limited surface area, as has been used for example by J. P. Botha and D. B. Spalding for determining the burning velocity of propane–air mixtures[2]. This method, however, is very laborious and not suited for series of measurements.

A suitable method for measuring the burning velocity makes use of a bunsen flame. Frequently, cylindrical burners are employed in this method. As the velocity of the laminar stream is greater along the centre than along the wall, a bent flame cone is formed which as a rule is very difficult to measure. This drawback can be obviated by causing the burner to terminate in a nozzle of such a shape that the gas mixture will issue at a uniform rate over the entire outlet area.

If we assume that inside the conical flame front the unburnt gas is not preheated and is still flowing completely parallel to the burner axis, it follows that the flame cone is completely straight and the following relation will be valid

$$S = V \sin \tfrac{1}{2}\alpha \qquad \ldots.[1]$$

where S denotes burning velocity, V is the outflow velocity, and α is the apex angle of the flame cone.

The outflow velocity from a nozzle of suitable design can be calculated directly from the total gas flow and the size of the burner mouth. In our measurements the flame front is visualized and photographed by a modified schlieren method.

APPARATUS AND MEASURING TECHNIQUE

Gas mixture

The rates of flow were measured with capillary flowmeters. First the gas was filtered by means of a tube filled with cotton wool. It was then led through a capillary tube about 20 cm long, the pressure drop across the tube being measured with a water manometer. During the experiments the room temperature was kept constant (about 20° C). All capillary tubes were gauged with a soap film flowmeter. The accuracy of the measurements of the gas streams was about one per cent.

The burner

The diameter of the burner tube was about 5·8 cm and its length, 80 cm. Near the bottom, at intervals of 1 cm, three metal gauzes were placed in the tube to suppress irregularities in the flow profile.

By preference the mouth of the burner has such a shape that, with all gas mixtures and with all flow velocities, the gas has a constant velocity profile over the entire cross section of the burner mouth. For this purpose axially symmetrical nozzles were provided, the vertical section of each consisting of two circular segments, the lower one joined to the burner tube, and the upper one to a short cylinder. As it was not possible to construct one nozzle, giving a completely uniform gas flow with different gases and different velocities, the upper cylinder was made variable, as

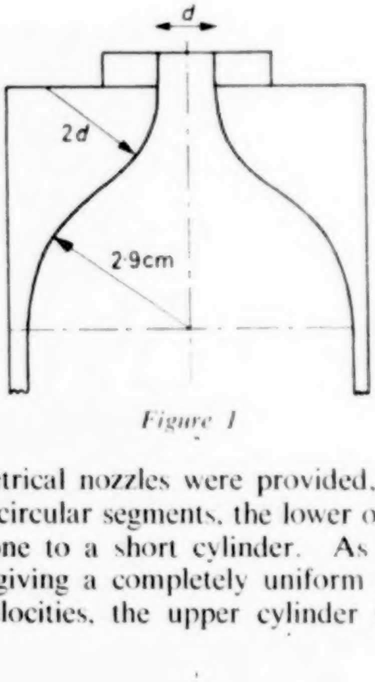

Figure 1

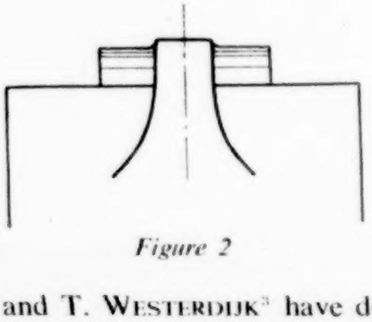

Figure 2

A. N. J. VAN DE POLL and T. WESTERDIJK[3] have done previously. If the velocity of the gas at the periphery is too high, which is indicated by a convex shape of the flame cone, the cylinder can be lengthened in order to retard the outermost part of the gas flow. If the cone is concave in shape, on the other hand, it is necessary to shorten the cylinder. In practice this is done by placing on the nozzle opening a number of rings having the same inner and outer diameters but differing in height. By means of a special holder, the rings were placed one above the other, the inner surfaces forming together a smooth cylinder. With a number of rings with heights of $\frac{1}{2}$, 1, 2, 4 and 8 mm, we could obtain all necessary lengths of the cylinder.

With a given gas mixture and a given velocity the length of the cylinder was so chosen that a completely straight flame cone was obtained. The nozzles could be cooled with running water. The determination of the burning velocity with the burner method using a nozzle involves some uncertainties. For instance, the influence of a boundary layer is not known exactly. Also, it is not certain that the gas flow is parallel from the nozzle opening to the flame cone and that the gas does not diverge in this region. A good check of the nozzle would be a measurement of the velocity profile just over the nozzle opening. Such checks have been made by F. H. GARNER *et al.*[1] and by F. R. CALDWELL *et al.*[2], who used very small Pitot tubes. However, it is very difficult to obtain accurate results in this way.

An indication of the reliability of the experimental method is a completely straight flame cone, the lower part of which is well joined on to the burner opening. Another check is obtained by measuring the burning velocity with nozzles of different diameters and at different flow velocities. If in this way the same results are obtained, this constitutes a further confirmation of the correctness of the method.

The optical apparatus

The flame cone was made visible by means of a modified schlieren method. Immediately behind the light source (a high-pressure mercury lamp) there was a variable vertical slit, $\frac{1}{2}$ to 2 mm wide. It was placed in the focus of a hollow mirror (focal length 45 cm, diameter 7 cm). The parallel light beam falls on to a positive lens, in the focus of which is placed a vertical strip, 1 mm wide. The slit is so adjusted that it is imaged completely on the strip. Of a flame placed in the parallel light beam, a schlieren image is formed by this method.

This image is photographed, and afterwards the top angle of the image of the flame cone is determined with a measuring microscope. The accuracy of the measured angle is highly dependent upon size and sharpness of the image and is mostly about one degree. With a top angle of, for instance, 50°, it is about two per cent of the measured burning velocity.

RESULTS

We measured the burning velocity of mixtures of the following gases with air: hydrogen, ethane, propane, *n*-butane, acetylene, ethylene, propylene and *n*-butylene-1.

Ethylene and propylene were prepared from ethylether and propylalcohol respectively by absorption of water with an aluminium catalyst at a temperature of about 350°C. Ethane and propane were prepared by hydrogenation of ethylene and *trans*butylene-2 with a palladium catalyst at room temperature. The other gases were commercial products. The compositions of the gases used are shown in *Table 1*.

Table 1. Composition of the fuel gases

Gas	H_2	CO	CH_4	C_2H_2	C_2H_4	C_2H_6	C_3H_6	C_3H_8	*n*-C_4H_8
Hydrogen	98·8	0·1	0·1						
Methane			99		< 0·1	< 0·1			
Acetylene				98·5					
Ethylene					99	0·4	0·1		
Ethane	0·15				1·9	97·0		0·1	
Propylene	0·1			0·2		0	98·7		
Propane						3·2		96	
n-*Butylene–1*							0·1		99·8
n-*Butane*	0					0·1		0·9	0·1

Gas	*cis*-C_4H_8	*trans*-C_4H_8	*n*-C_4H_{10}	*iso*-C_4H_{10}	*Acetone*	O_2	N_2	CO_2
Hydrogen							0·9	0·1
Methane						*Trace*	1·0	
Acetylene					0·5		1·0	
Ethylene						*Together* 0·3		
Ethane							0·3	
Propylene							1·0	
Propane				0·6		*Together* 0·1		
n-*Butylene–1*							0·1	
n-*Butane*	1·5	0·5	95	0·3		*Together* 1·2		0·1

The combustion velocity of hydrogen–air mixtures was measured on two nozzles of different diameters and at different outflow velocities:

Nozzle diameter: 3 mm, velocity 900 and 1 550 cm/sec
Nozzle diameter: 5 mm, velocity 850 and 1 100 cm/sec

The results of the measurements are illustrated in *Figure 3*. The maximum burning velocity was attained at 42·4 per cent hydrogen and amounted to 280 cm/sec. The burning velocity of methane–air mixtures was measured on nozzle diameters of 5, 7 and 10 mm at outflow velocities of 60, 80 and 100 cm/sec, respectively. The results are shown in *Figure 4*. The maximum burning velocity of 40·0 cm/sec was attained with a mixture

Table 2. Maximum burning velocity and composition of gas–air mixtures

Fuel gas	$S_{max.}$ *(cm/sec)*	g *at* $S_{max.}$ (% *by volume)*	$g_{stoich.}$ (% *by volume)*
Hydrogen	280	42·4	29·7
Methane	40·0	10·05	9·56
Acetylene	150·2	9·45	7·81
Ethylene	70·0	7·3	6·57
Ethane	43·3	6·25	5·73
Propylene	45·6	4·95	4·51
Propane	41·4	4·3	4·07
n-*Butylene–1*	46·0	3·5	3·39
n-*Butane*	39·2	3·45	3·19

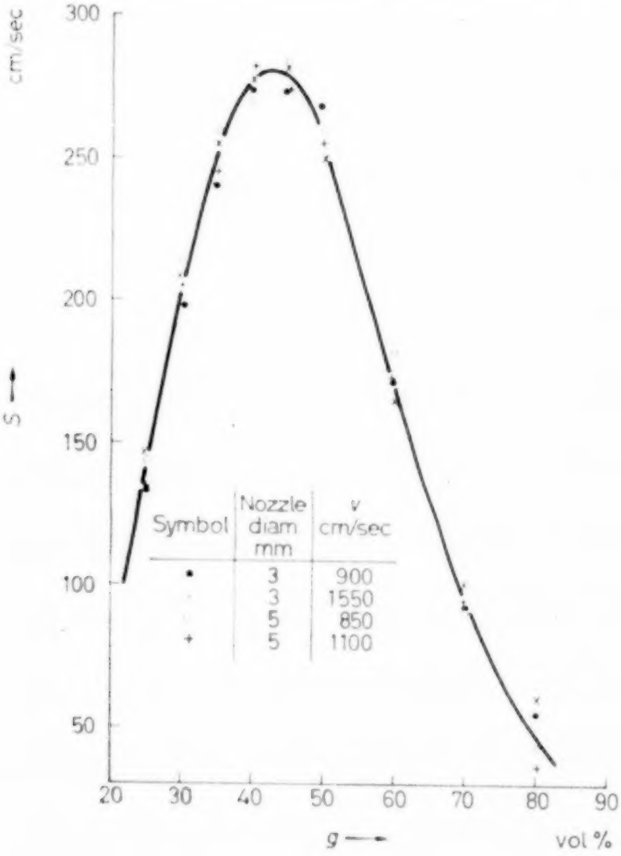

Figure 3. Burning velocity of hydrogen: g denotes amount of gas added

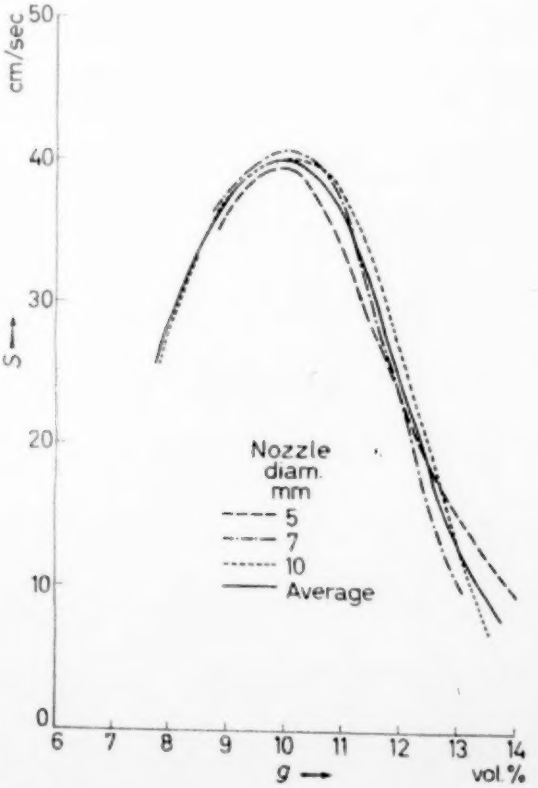

Figure 4. Burning velocity of methane (average values for gas velocities of 60, 80 and 100 cm/sec

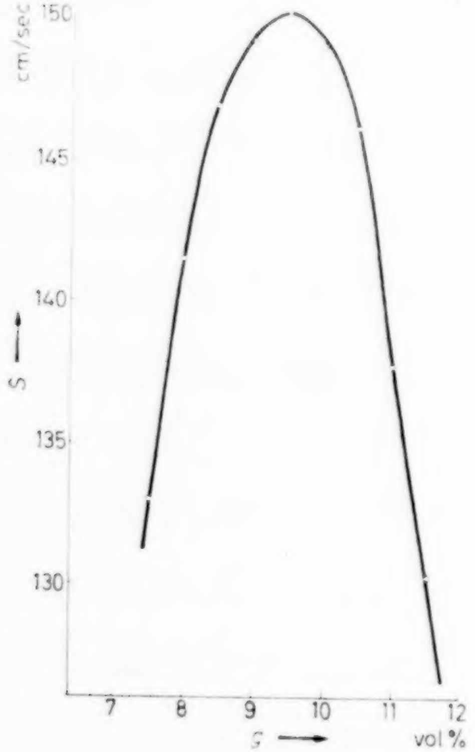

Figure 5. Burning velocity of acetylene

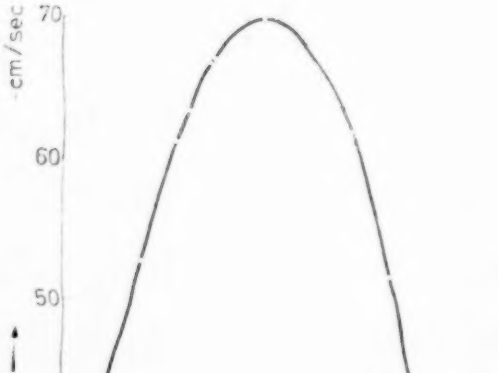

Figure 6. Burning velocity of ethylene

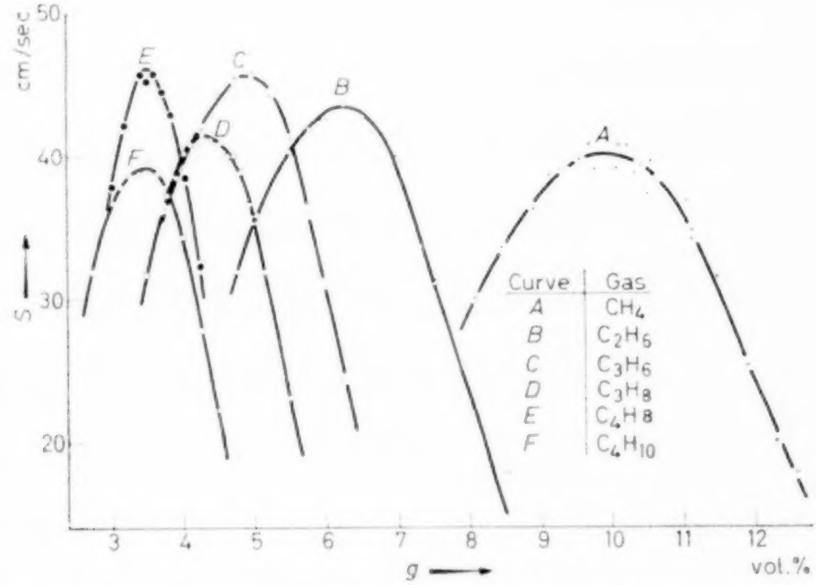

Figure 7. Burning velocities of ethane, propylene, propane, n-butylene-1 and n-butane

containing 10·05 per cent methane. The results of the measurements on mixtures of acetylene and ethylene with air are represented in *Figures 5* and *6*. The results for the other hydrocarbons are shown in *Figure 7*.

Table 2 gives the values of the maximum burning velocity and the corresponding gas percentages, *g*, for all the gases examined in addition to the gas percentages of the stoichiometric mixtures.

Centraal Laboratorium,
Staatsmijnen in Limburg,
Geleen, The Netherlands

(Received December 1958)

REFERENCES

[1] LINNETT, J. W. *Fourth Symposium (International) on Combustion*, pp 20–35. Williams and Wilkins: Baltimore, 1953
[2] BOTHA, J. P. and SPALDING, D. B. *Proc. Roy. Soc. A*, 1954, **225**, 71
[3] VAN DE POLL, A. N. J. and WESTERDIJK, T. *Z. tech. Phys.* 1941, **22**, 29
[4] GARNER, F. H., LONG, R. and THORLEY, B. *Fuel, Lond.* 1954, **33**, 394
[5] CALDWELL, F. R., BROIDA, H. P. and DOVER, J. J. *Industr. Engng Chem. (Industr.)*, 1951,**43**, 2731

The Influence of Small Quantities of Hydrogen and Hydrogen Compounds on the Burning Velocity of Carbon Monoxide–Air Flames

T. G. SCHOLTE and P. B. VAAGS

The dependence of the burning velocity of carbon monoxide–air mixtures on small admixed quantities of hydrogen, hydrogen compounds and deuterium has been measured. It was found with carbon monoxide–hydrogen mixtures that the square of burning velocity equals the sum of the square of the burning velocity of pure carbon monoxide and a term proportional to the hydrogen content. With added hydrogen compounds or deuterium a similar relation is valid.

IT IS a well known fact that the burning velocity of carbon monoxide–air mixtures increases sharply upon addition of small quantities of hydrogen, water vapour or other hydrogen compounds. This phenomenon has been experimentally studied by several investigators$^{1-13}$. However, the carbon monoxide used in many of the experiments was not completely pure, so that the results were generally badly scattered.

In our own experimental work we therefore used carbon monoxide of high purity prepared by reaction between formic acid and concentrated sulphuric acid. Prior to being fed to the test assembly, the carbon monoxide was very intensely dried, as was the combustion air with which it was mixed and, in some cases, also the air in the immediate vicinity of the flame.

Our investigation was undertaken first and foremost for the purpose of making an accurate determination of the increase of the burning velocity of carbon monoxide–air mixtures caused by small amounts of hydrogen (0·2 to 3 per cent by volume of the gas–air mixture) and the compounds water vapour, methane and propane. For comparison with the influence of hydrogen, the influence of small amounts of deuterium on the burning velocity was measured. Since hydrogen and deuterium differ only in atomic weight and not much in their chemical properties, this comparison can give some idea of the part played by hydrogen in the combustion of carbon monoxide.

EXPERIMENTAL

The burning velocities were determined by the burner method. The apparatus and measuring technique have been described in our previous paper^{14}.

For the determination of the burning velocity of pure carbon monoxide and also of the carbon monoxide–hydrogen mixtures and the carbon monoxide–deuterium mixtures containing little hydrogen or deuterium, the carbon monoxide was prepared by reaction between formic acid and concentrated sulphuric acid at 80°C, and stored in a container. This carbon monoxide was completely free of hydrogen and was very intensely dried by leading the gas stream successively through two flasks with calcium chloride, two wash-bottles with concentrated sulphuric acid, two tubes with potassium hydroxide tablets and a small flask with phosphorus pentoxide. In these experiments the air to be mixed with carbon monoxide was dried in the same manner. In addition, in some experiments the air immediately around the flame was dried. In these cases another tube with a diameter of about 6 cm was placed on the burner tube. This tube contained two diametrically placed glass windows; the completely dry air was led in through the lower end. The tube was 12 cm high and its top was covered with a metal gauze to prevent streams of outside air from entering. It appeared, however, that even with the pure carbon monoxide–air mixtures, drying of the air around the flame had no influence on the burning velocity.

The hydrogen used was practically pure. The deuterium was prepared by electrolysis of heavy water and contained, besides D_2, about 4 per cent of HD. The methane contained more than 97 per cent of CH_4. The propane contained, besides 92 per cent of C_3H_8, about 7 per cent of C_2H_6.

To obtain mixtures of carbon monoxide, air and water vapour, the carbon monoxide–air mixture was led through two wash-bottles filled with a mixture of sulphuric acid and water of known composition at a temperature of 20°C. By applying mixtures with different sulphuric acid/water ratios, gas mixtures containing different amounts of water vapour (0 to 2·3 per cent by volume) could be obtained.

RESULTS

(a) *Burning velocity of pure carbon monoxide*

From a dozen measurements of the burning velocity of carbon monoxide–air mixtures with 45 per cent by volume of carbon monoxide at different nozzle diameters (7 and 10 mm) and different gas velocities, we found a mean value of 14·5 cm/sec. With 40, 50 and 55 per cent of carbon monoxide we found the same burning velocity. None of the values deviated by more than 1 cm/sec from the mean.

(b) *Burning velocity of carbon monoxide mixed with hydrogen*

In these experiments with small amounts of hydrogen (<3 per cent), we used carbon monoxide prepared from formic acid and concentrated sulphuric acid, to which hydrogen and air were admixed. With greater amounts of hydrogen we used carbon monoxide from B.A.S.F. (Ludwigshafen, Germany) which contained 0·55 per cent of hydrogen, to which an additional amount of hydrogen was admixed.

The burning velocity was determined as a function of the hydrogen concentration. These series of measurements were carried out with different gas/air ratios, viz. with 35, 40, 45, 47·5, 50, 52·5, 55, 60 and

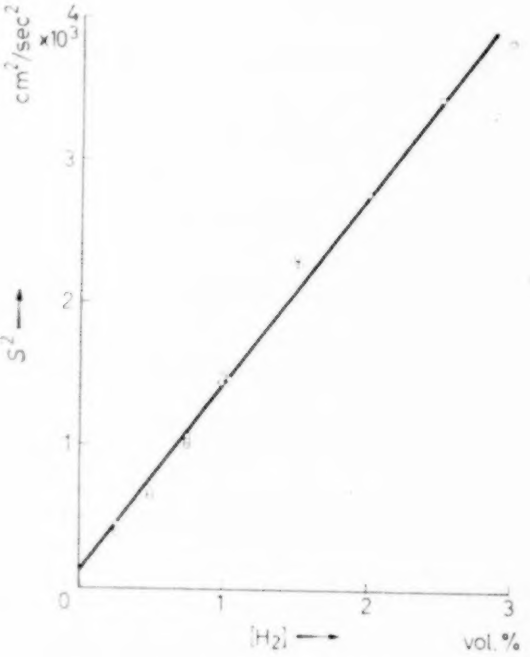

Figure 1. Burning velocity of carbon monoxide with hydrogen at 45 vol. % gas

65 per cent of gas. The relation between the burning velocity and the percentage of hydrogen for all gas–air ratios could best be described by

$$S^2 = a[\mathrm{H_2}] + b \qquad \ldots.[1]$$

where S is the burning velocity, $[\mathrm{H_2}]$ is the percentage of hydrogen in the gas–air mixture and a and b are constants (see, for example, *Figure 1*, with 45 per cent of gas). The relation

$$S = a[\mathrm{H_2}]^{\frac{1}{2}} + b \qquad \ldots.[2]$$

also agrees with our measuring results, excepting those for pure carbon monoxide.

The coefficients a and b of formula 2 for all gas/air ratios were calculated by the method of least squares. The results and also $S_0 = b^{\frac{1}{2}}$ are summarized in *Table 1*. Notwithstanding some spread in the values of S_0, the mean value agrees well with the experimentally determined value of 14·5 cm/sec. The value of a has a maximum at 45 to 55 per cent of gas.

Table 1

% gas	*a* (*cm²/sec²*)	*b* (*cm²/sec²*)	*S₀* (*cm/sec*)
35	1 030	340	18
40	1 350	190	14
45	1 320	130	11
47½	1 370	200	14
50	1 460	130	11
52½	1 300	210	14
55	1 410	120	11
60	1 000	220	15
65	450	210	14
		Mean value	14

The relation between S^2 and $[H_2]$ for greater amounts of hydrogen is given in *Figure 2* (with 50 per cent of gas). It appears that the linear relationship is valid to about 4 per cent of hydrogen in the total gas mixture (8 per cent of hydrogen in the carbon monoxide–hydrogen mixture).

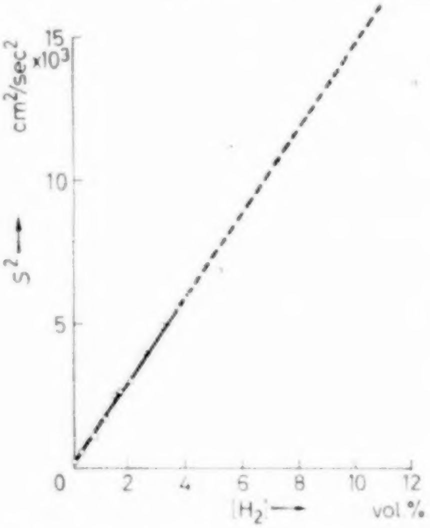

Figure 2. Burning velocity of carbon monoxide with hydrogen at 50 vol. % gas

(c) *Burning velocity of carbon monoxide mixed with water vapour*

By leading carbon monoxide–air mixtures of given composition (carbon monoxide with 0·55 per cent of hydrogen) through two wash-bottles filled with aqueous sulphuric acid solutions, gas mixtures were obtained with 0, 1·20, 1·87 and 2·30 per cent of water vapour. The burning velocities of these mixtures are given in *Figure 3*. The maximum burning velocities are obtained at 47 to 50 per cent of gas and amount to 23·6, 43·4, 49·2 and

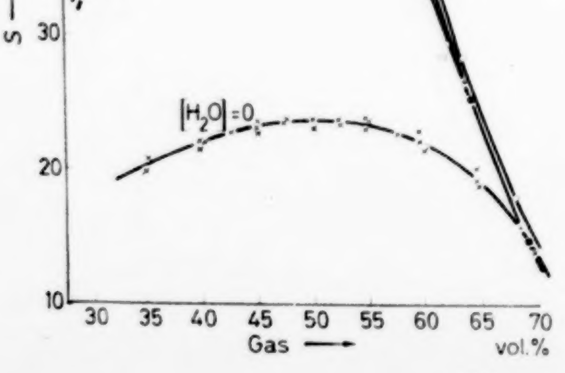

Figure 3. Burning velocity of carbon monoxide with water vapour

52·1 cm/sec. respectively (with an accuracy of 1 cm/sec). Also in this case there appears to be a quadratic relationship between the burning velocity and the concentration of water vapour. Water vapour has less influence on the burning velocity than hydrogen, however. The foregoing observations enable us to draw up the formula

$$S^2 = S_0^2 + a\left([\mathrm{H_2}] + \tfrac{2}{3}[\mathrm{H_2O}]\right) \qquad \ldots.[3]$$

Supposing $S_0^2 = 200\ \mathrm{cm^2/sec^2}$ the value of a for all measurements made with carbon monoxide and water vapour can be calculated. *Figure 4* shows these values in relation to the gas/air ratios.

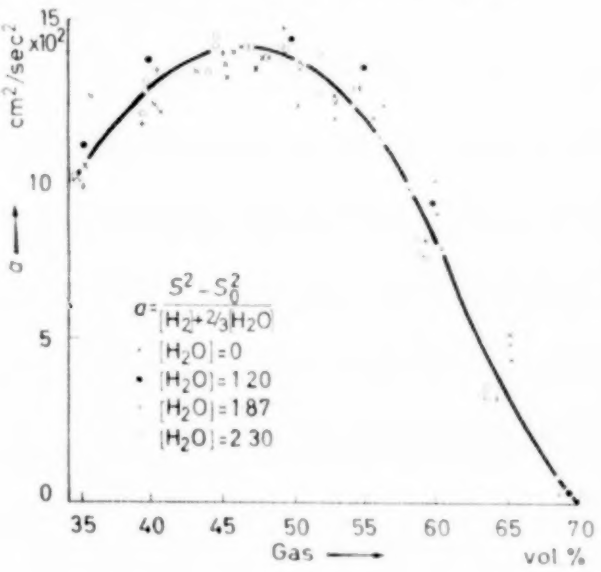

Figure 4. Burning velocity of carbon monoxide with water vapour

(d) *Burning velocity of carbon monoxide mixed with methane and with propane*

Figure 5 shows the burning velocity of mixtures of carbon monoxide and ½, 1, 2 and 3 per cent of methane as a function of the gas/air ratio.

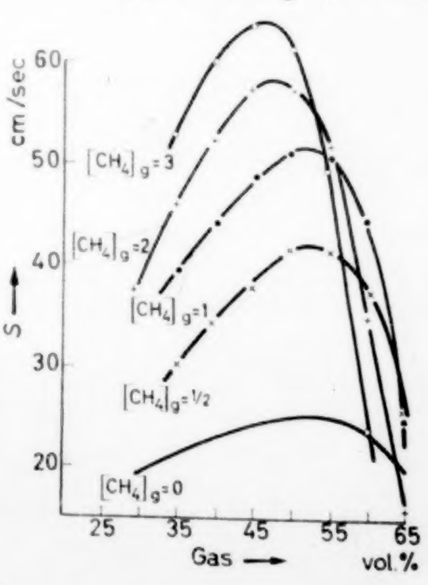

Figure 5. Burning velocity of carbon monoxide with methane

Especially with greater amounts of methane, the maximum moves to smaller gas/air ratios. Similar curves for mixtures of carbon monoxide with $\frac{1}{2}$, 1, $1\frac{1}{2}$ and 2 per cent of propane are given in *Figure 6*. On account of the shifting of the maximum we can only compare the values of the maximum burning velocity (the tops of the curves) with the maximum values of the carbon monoxide–hydrogen curves. The influence of methane on the burning velocity appears to be about twice as great as the influence of hydrogen. With propane this influence is about four times as great as with hydrogen.

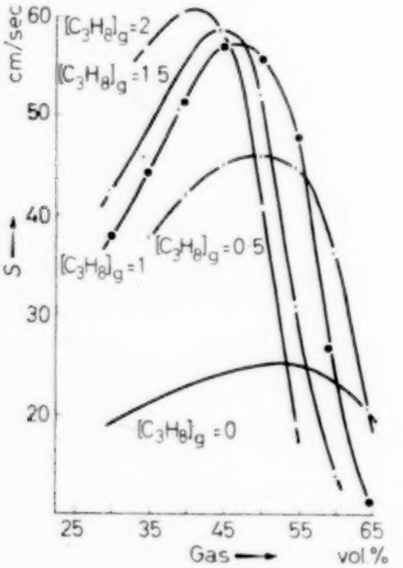

Figure 6. Burning velocity of carbon monoxide with propane

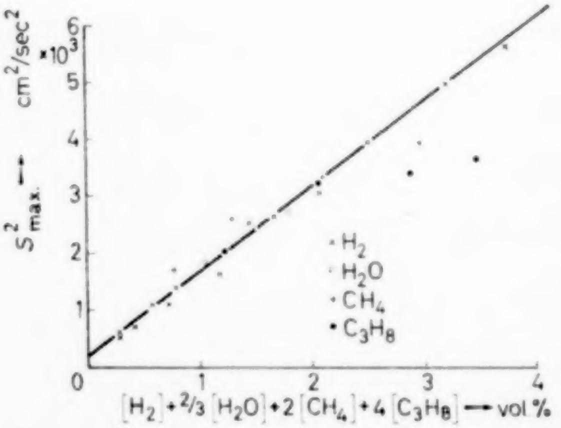

Figure 7. Maximal burning velocity of carbon monoxide with various hydrogen compounds in air

In *Figure 7* $S^2_{\text{max.}}$ is plotted as a function of the 'effective amount of hydrogen' in the total gas–air mixture, viz. of

$$[H_2] + \tfrac{2}{3}[H_2O] + 2[CH_4] + 4[C_3H_8] \qquad \ldots.[4]$$

Up to about $2\frac{1}{2}$ per cent all points are situated on a straight line. The increase of S^2 appears to be proportional to this sum.

(e) *Burning velocity of carbon monoxide mixed with deuterium*

The burning velocities have been measured of carbon monoxide–air mixtures with 45 per cent of carbon monoxide, to which at most 3 per cent of deuterium was added. The results are given in *Figure 8*, in which S^2 is plotted as a function of the amount of deuterium. For purposes of comparison the same graph also shows the value of S^2 found when hydrogen was added. The ratio between the increase of S^2 caused by hydrogen and the increase of S^2 caused by deuterium is 1 : 0·54.

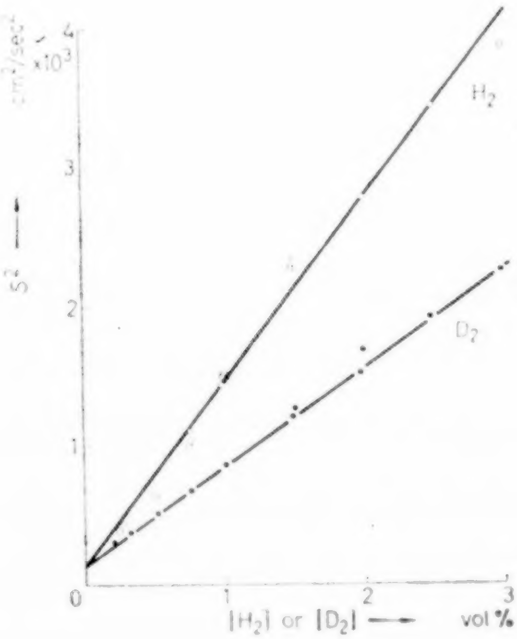

Figure 8. Influence of hydrogen and deuterium on the burning velocity of a carbon monoxide–air mixture (45 vol. % CO)

CONCLUSIONS

From our experiments we can draw the following conclusions:

(*1*) Pure carbon monoxide is combustible, even if, as far as possible, all traces of hydrogen and hydrogen compounds are removed. The burning velocity is about 14·5 cm/sec at 20°C and in the region between 40 and 55 per cent of carbon monoxide does not change with the gas/air ratio.

(*2*) With small amounts of admixed hydrogen (up to 4 per cent in the mixture) the square of the burning velocity at any gas/air ratio is equal to the sum of a constant and a quantity proportional to the amount of admixed hydrogen. This proportionality constant reaches its maximum at 45 to 55 per cent of carbon monoxide.

(*3*) With small amounts of admixed hydrogen compounds a similar relation is valid. In this case the constant is approximately proportional to the number of hydrogen atoms in the molecules of the admixed gas.

(4) With small amounts of admixed deuterium a similar relation as for hydrogen holds good. With 45 per cent of carbon monoxide the proportionality constant is 0·54 of that for hydrogen.

Centraal Laboratorium,
Staatsmijnen in Limburg,
Geleen, The Netherlands

(*Received December 1958*)

REFERENCES

[1] Traube, M. *Ber. dtsch. chem. Ges.*, 1885, **18**, 1890
Dixon, H. B. *J. chem. Soc.*, 1886, **49**, 94
[2] Ubbelohde, L. and Donner, O. *J. Gasbeleucht.* 1914, **57**, 757
[3] Bunte, K. and Litterscheidt, W. *Gas- u. Wasserfach*, 1930, **73**, 837, 871 and 890
[4] Hartmann, E. *Diss. Karlsruhe*, 1931
[5] Bunte, K. *Gas- u. Wasserfach*, 1932, **75**, 213
[6] Passauer, H. *Z. phys. Chem. A*, 1932, **161**, 299
[7] Jahn, G. *Der Zündvorgang in Gasgemischen*. Oldenbourg: Berlin, 1934
[8] Price, T. W. and Potter, J. H. *Fourth Symposium (International) on Combustion*, p 313. Williams and Wilkins: Baltimore, 1953
[9] Fiock, E. F. and King, H. K. *Tech. Rep. Nat. Adv. Comm. Aero., Wash., No. 531* (1935)
[10] Walker, P. L. and Wright, C. C. *Fuel, Lond.* 1952, **31**, 45
[11] McDonald, G. *J. chem. Phys.* 1956, **20**, 1497
[12] Friedman, R. and Cyphers, J. A. *J. chem. Phys.* 1956, **25**, 448
[13] Watermeier, L. A. *J. chem. Phys.* 1957, **27**, 1118
[14] Scholte, T. G. and Vaags, P. B. *Combustion & Flame*, 1959, **3**, 495

Burning Velocities of Mixtures of Hydrogen, Carbon Monoxide and Methane with Air

T. G. SCHOLTE and P. B. VAAGS

The burning velocities of mixtures of hydrogen–carbon monoxide, hydrogen–methane and carbon monoxide–methane with air were determined. These are maximum at a given gas/air ratio. The maximum burning velocities and the corresponding gas percentages are given as functions of the gas composition. The burning velocities of the various hydrogen–carbon monoxide–methane mixtures with air were also measured. The maximum burning velocities and the corresponding gas percentages of all hydrogen–carbon monoxide–methane mixtures are presented in a triangular diagram. Furthermore a determination was made of the effect of smaller amounts of nitrogen, carbon dioxide and oxygen on the maximum burning velocity and on the corresponding gas percentage.

THE principal components of most technical fuel gases manufactured from coal are hydrogen, carbon monoxide and methane. As several combustion properties of gas mixtures are governed largely by the burning velocity, it is useful to know the burning velocity of mixtures of the above components with air and also the effect which small amounts of nitrogen, carbon dioxide and oxygen have on the burning velocity. When these data have been collected, the burning velocity of many fuel gases in common use can be calculated. We determined the burning velocities by the burner method; the apparatus and measuring technique are described in our previous paper[1]. Flow-metered currents of gases and air are mixed and fed to a burner. Fitted on the burner mouth is a nozzle of such a design that the outflow velocity is uniform over the entire cross sectional area. The combustion velocity can then be calculated from the velocity of the gas flow, the surface area of the nozzle outlet and the top angle of the straight flame cone.

The burning velocities of hydrogen–air, methane–air and carbon monoxide–air mixtures have been presented in two previous papers[1, 2]. The present article first gives the burning velocities of several binary mixtures of hydrogen–carbon monoxide, hydrogen–methane and carbon monoxide–methane with air for various gas/air ratios. For the gas/air ratio at which the burning velocity is a maximum, the burning velocity is represented as a function of the fuel gas composition. In addition, for each of the three series of binary mixtures the gas percentages are given at which the burning velocity is maximum.

The results for the hydrogen–carbon monoxide–methane mixtures with air are presented in a triangular diagram. These results were obtained by preparing, in addition to the above binary mixtures, a set of ternary mixtures and measuring their burning velocities as functions of the gas/air ratio. All these data are represented in the triangular hydrogen–carbon monoxide–methane diagram by lines of constant maximum burning velocity (burning velocity at the gas/air ratio at which the burning velocity is a maximum).

In another triangular diagram the gas/air ratio of maximum burning velocity has been plotted in an analogous manner. As to the inert gases an examination was made of the effects of nitrogen, carbon dioxide and oxygen admixtures. When these gases are present in small amounts, the maximum burning velocity changes in proportion with the volume of the admixture. The effect of one part of oxygen on the maximum burning velocity with air is opposed to that of 79/21 parts of nitrogen. The effects of these gases were determined for various points of the triangle.

BINARY MIXTURES

(a) *Hydrogen–carbon monoxide mixtures*

The mixture was prepared from pure hydrogen and carbon monoxide containing 0·6 per cent nitrogen, 0·3 per cent oxygen, 0·02 per cent methane and 0·55 per cent hydrogen.

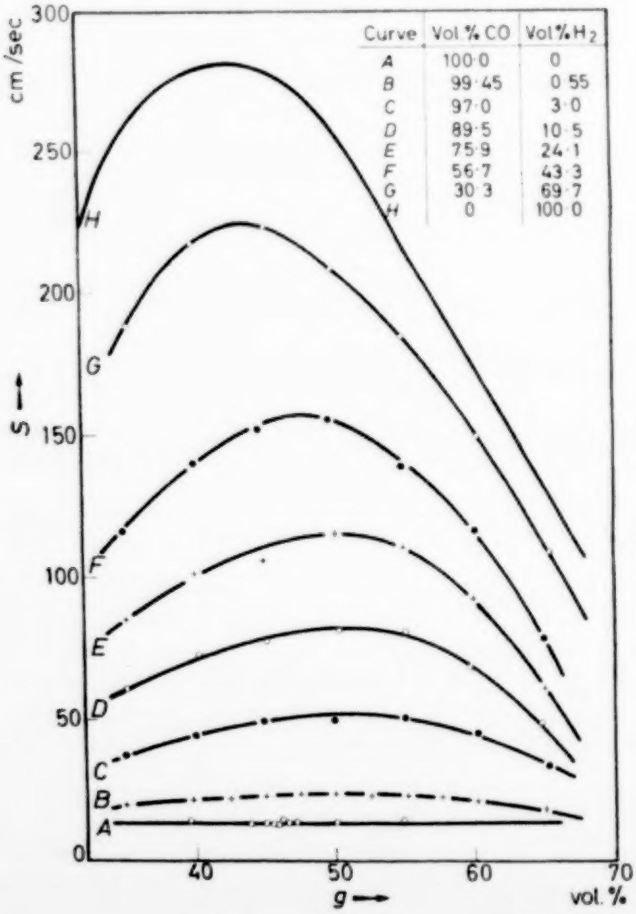

Curve	Vol % CO	Vol % H_2
A	100·0	0
B	99·45	0·55
C	97·0	3·0
D	89·5	10·5
E	75·9	24·1
F	56·7	43·3
G	30·3	69·7
H	0	100·0

Figure 1. Burning velocities of carbon monoxide–hydrogen mixtures

The measurements were made on 6 hydrogen–carbon monoxide samples containing 0·55, 3·0, 10·5, 24·1, 43·3 and 69·7 per cent hydrogen by volume. In the experiments with 0·55 and 3·0 per cent hydrogen, the gases were dried with concentrated sulphuric acid. The effect of small amounts of water vapour on the burning velocity of the other mixtures is negligible. For the mixture with 0·55 per cent hydrogen we used a nozzle of 10 mm diameter; the nozzle used for the other mixtures was 7 mm in diameter. The outflow velocities in the burner mouth were 65, 100, 200, 300, 400 and 500 cm/sec respectively.

The values of the burning velocity of gas/air mixtures as a function of the fuel gas percentage are given in *Figure 1*. The burning velocities of pure hydrogen and pure carbon monoxide with air, known from previous measurements[1, 2], are also plotted in this graph. The burning velocity of every hydrogen–carbon monoxide–air mixture reaches a maximum ($S_{max.}$) at a given gas percentage ($g_{S_{max.}}$). These maximum values and the corresponding gas percentages have been compiled in *Table 1*.

Table 1. Maximum burning velocities and compositions of hydrogen–carbon monoxide–air mixtures

Fuel gas composition		$S_{max.}$	$g_{S_{max.}}$	S_0	g_0
Hydrogen % *by volume*	*Carbon monoxide* % *by volume*	*cm/sec*	% *by volume*		
0	100	13·6	—	13·6	—
0·55	99·45	23·5	52	23·6	51·1
3·0	97	52	51	52·7	50·1
10·5	89·5	82·5	51	82·8	50·2
24·1	75·9	115·5	50	115·9	49·4
43·3	56·7	157	48	157·4	47·5
69·7	30·3	224·5	44	225·0	43·7
100	0	281	42·2	281	42·2

As the basic gases contained some impurities, such as nitrogen and oxygen, a correction was made by means of the data mentioned below.

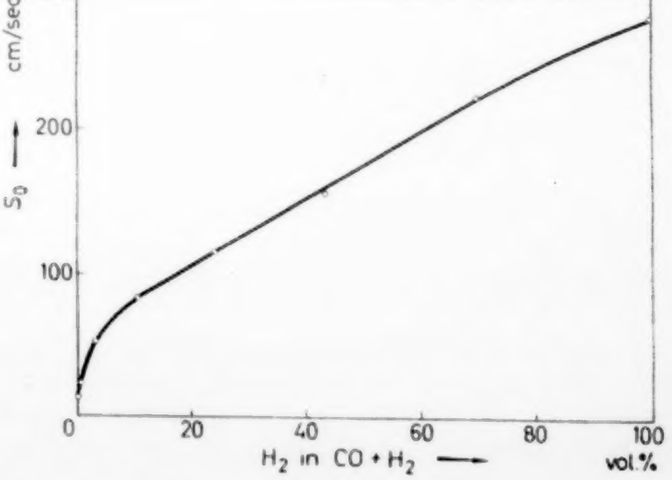

Figure 2. Maximum burning velocities of carbon monoxide–hydrogen mixtures

The corrected values for S_{max} and $g_{S_{max}}$, which will be called S_0 and g_0 are given in the last two columns of *Table 1*.

In *Figures 2* and *3* these values of S_0 and g_0 are presented as functions of the hydrogen percentage of the hydrogen–carbon monoxide mixture.

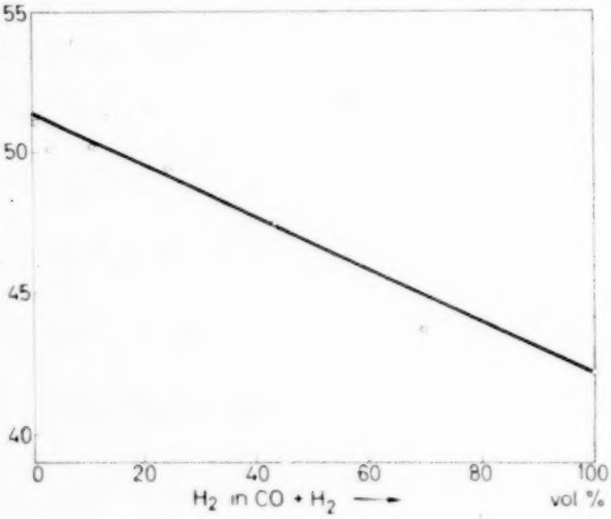

Figure 3. Gas concentrations in the ***gas–air*** *mixture at the* ***maximum*** *burning velocity of* ***carbon*** *monoxide–****hydrogen*** *mixtures*

(b) *Hydrogen–methane mixtures*

These experiments were made on the four hydrogen–methane mixtures mentioned in *Table 2*.

Table 2. Percentage composition of the hydrogen–methane mixtures

Mixture No.	H_2	CH_4	CO	N_2	O_2	CO_2	*Unsaturated hydro-carbons*
1	43·9	53·2	0·3	2·3	0	0·1	0·2
2	63·9	34·2	0·3	1·4	0	0·1	0·1
3	79·9	19·4	0·1	0·5	0	0·1	0
4	88·2	10·1	0·1	1·6	0	0	0

We used a burner with a 5 mm diameter nozzle and determined the burning velocity of each mixture at two different outflow velocities, viz. at 115 and 230 cm/sec, 305 and 615 cm/sec, 460 and 765 cm/sec and 460 and 770 cm/sec. The outflow velocity proved to have no effect on the value of the burning velocity.

In *Figure 4* the burning velocities of the four mixtures with air have been plotted as functions of the gas percentage. The values for mixtures of pure hydrogen and pure methane with air (known from earlier measurements[1]) are also plotted in this graph.

The maximum burning velocities (S_{max}) and the corresponding gas percentages $g_{S_{max}}$ are compiled in *Table 3*. The table also gives the values found after correction for nitrogen, carbon dioxide and carbon monoxide (S_0 and g_0).

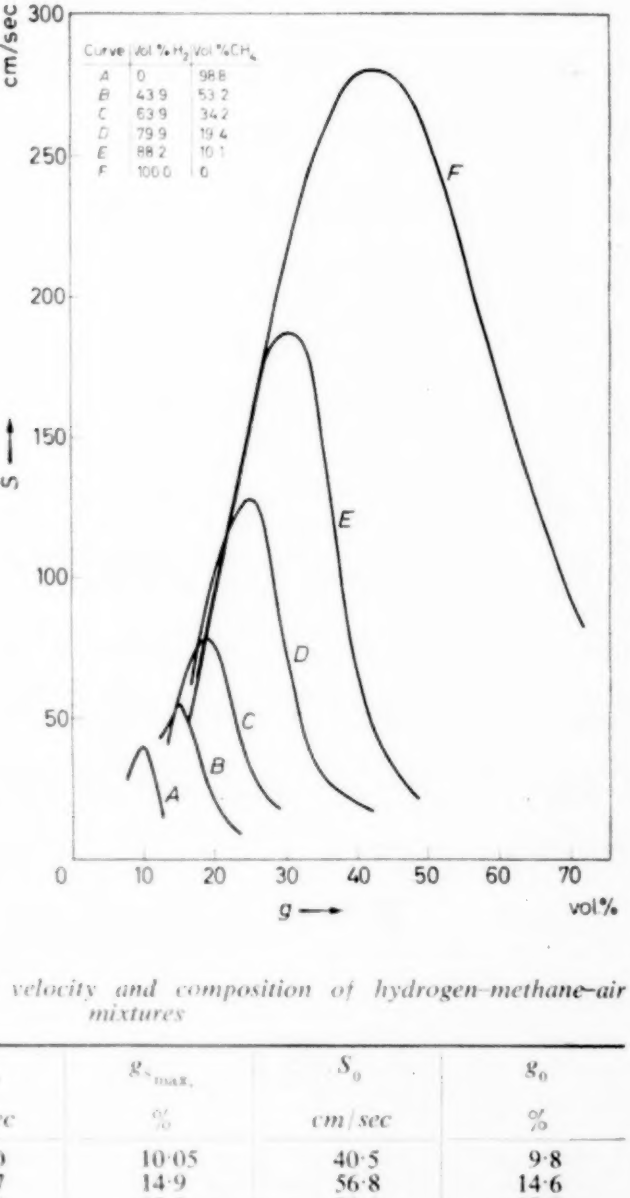

Figure 4. Burning velocities of hydrogen–methane mixtures

Table 3. Maximum burning velocity and composition of hydrogen–methane–air mixtures

Gas	$S_{\max.}$ *cm/sec*	$g_{S_{\max.}}$ %	S_0 *cm/sec*	g_0 %
Methane	40·0	10·05	40·5	9·8
Mixture 1	55·7	14·9	56·8	14·6
Mixture 2	80·1	19·1	81·1	18·9
Mixture 3	128·9	25·0	129·6	24·9
Mixture 4	188·0	30·6	190·4	30·3
Hydrogen	281	42·2	281	42·2

In *Figures* 5 and 6 S_0 and g_0 respectively have been given as functions of the hydrogen percentage of the hydrogen–methane mixture.

(c) *Carbon monoxide–methane mixtures*

The compositions of the basic gases are given in *Table 4*.

We prepared eleven different mixtures of these components and determined the burning velocities as functions of the gas/air ratio. The

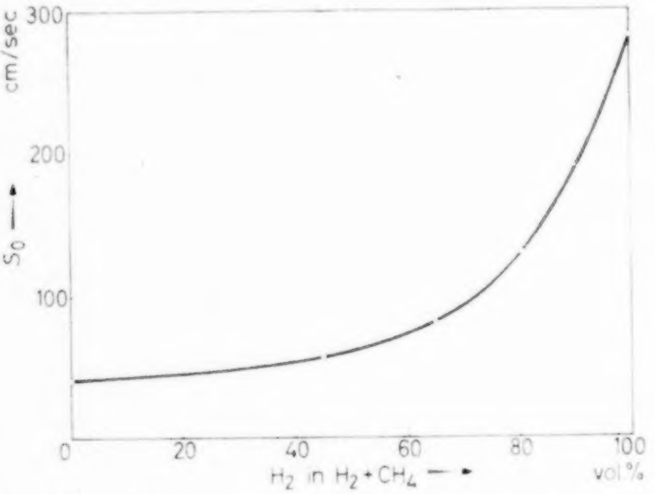

Figure 5. Maximum burning velocities of hydrogen–methane mixtures

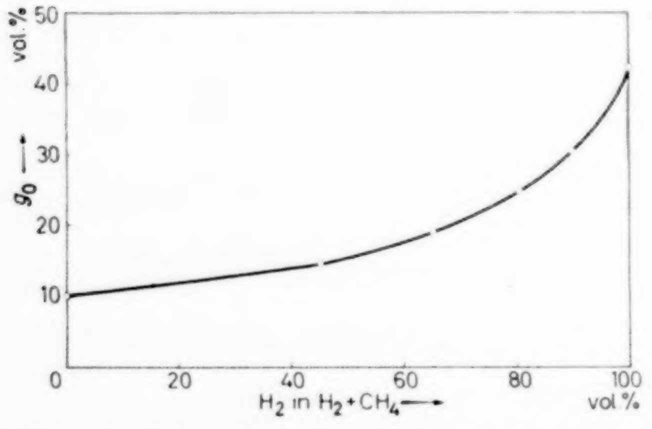

Figure 6. Gas concentrations in the gas–air mixture at the maximum burning velocity of the hydrogen–methane mixture

Table 4. Percentage composition of carbon monoxide and methane

Gas	CO	CH_4	H_2	*Unsaturated hydro-carbons*	N_2	CO_2	O_2
Carbon monoxide	98·8	0·30	0·49	0	0·5	0·2	0
Methane	0·3	97·3	0·0	0·2	2·0	0·1	0·1

composition of the mixtures and their outflow velocities have been compiled in *Table 5*.

When the fuel gas contained less than 5 per cent methane, the air was dried beforehand. With the other mixtures, drying of the air had no effect on the burning velocity and was therefore omitted. For all mixtures we used a 10 mm nozzle; for pure methane 10, 7 and 5 mm nozzles.

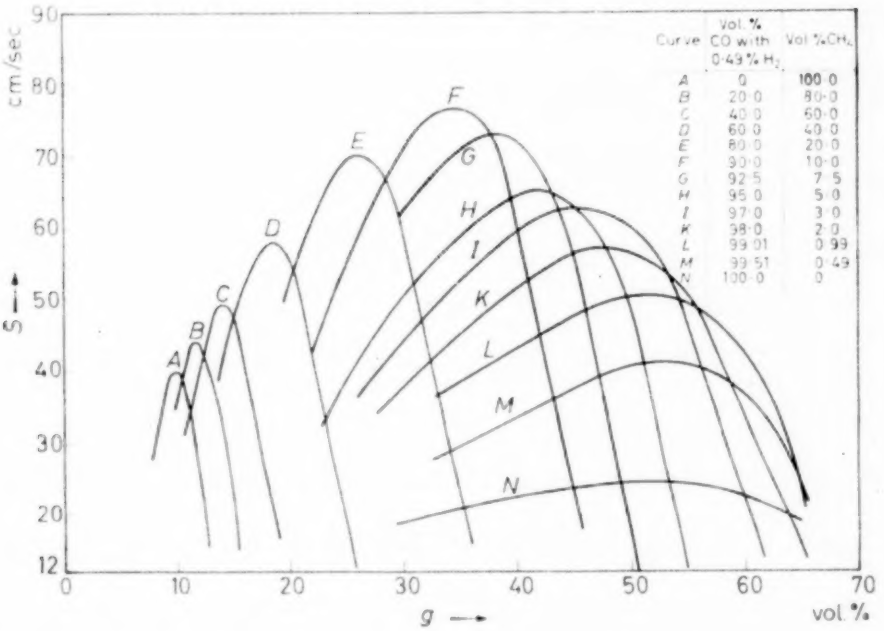

Figure 7. Burning velocities of carbon monoxide–methane mixtures

Figure 7 shows the burning velocities of the carbon dioxide–methane mixtures as functions of the gas/air ratio. The values for carbon monoxide and methane found from earlier measurements[1, 2] have also been plotted in this graph.

Table 5 gives the values of the maximum burning velocities ($S_{max.}$) and the gas percentages at which the burning velocity is maximum ($g_{S_{max.}}$), as well as the values corrected for impurities (S_0 and g_0) (not for hydrogen).

Table 5. Maximum burning velocities and compositions of methane–carbon monoxide–air mixtures

Gas comp. (% by vol.)		*Outflow velocity cm/sec*	$S_{max.}$ *cm/sec*	$g_{S_{max.}}$ *% by volume*	S_0 *cm/sec*	g_0 *% by volume*
Methane	*Carbon monoxide*					
0	100	80	24·2	52	24·4	51·8
0·49	99·5	160	41·2	52	41·5	51·8
0·99	99·0	160	50·7	52·5	51·1	52·3
2·0	98·0	160	57·2	47	57·6	46·8
3·0	97·0	160	62·8	46	63·3	45·8
5·0	85·0	155	65·1	42	65·6	41·8
7·5	92·5	155	73·1	38·5	73·7	38·3
10·0	90·0	155	76·3	35	76·9	34·8
20·0	80·0	155	70·2	26	70·8	25·8
40·0	60·0	100	58·5	18·5	59·1	18·3
60·0	40·0	100	49·4	14	50·0	13·8
80·0	20·0	100	44·3	11·7	44·9	11·5
100	0	60 80 100	40·0	10·05	40·5	9·8

Figures 8 and *9* give the values for S_0 and g_0 as functions of the methane content of the inert-free carbon monoxide–methane mixture. Note that upon addition of methane the burning velocity of carbon monoxide first increases sharply to reach its maximum at about 10 per cent methane, and then decreases slowly to the burning velocity of pure methane.

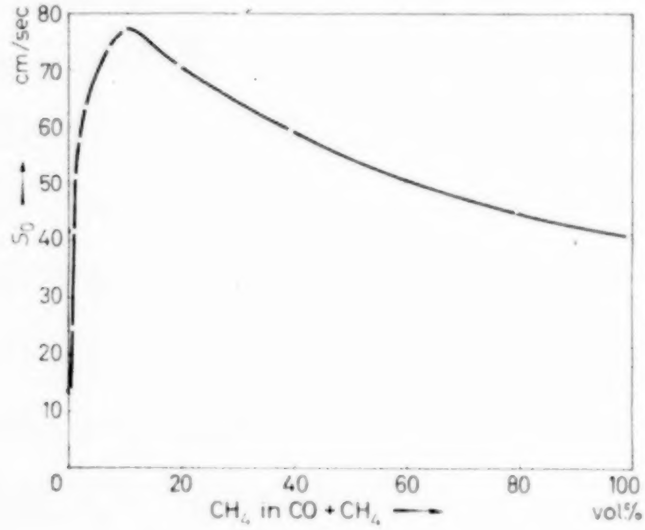

Figure 8. Maximum burning velocities of carbon monoxide–methane mixtures

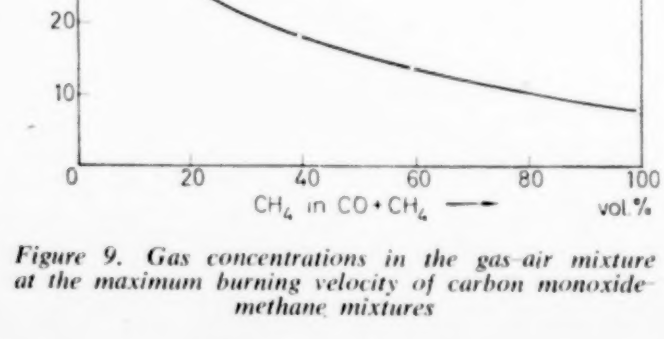

Figure 9. Gas concentrations in the gas–air mixture at the maximum burning velocity of carbon monoxide–methane mixtures

TERNARY MIXTURES

By compressing the separate components we prepared six ternary mixtures of the compositions shown in *Table 6*.

In *Figure 10* the burning velocities of these mixtures with air are presented as functions of the gas percentage.

Table 6. Compositions of hydrogen–carbon monoxide–methane mixtures

Mixture No.	*Gas composition, % by volume*						
	H_2	CO	CH_4	*Unsaturated hydro-carbons*	N_2	CO_2	O_2
1	35·6	35·0	28·1	0	1·3	0	0
2	28·1	55·2	14·8	0·2	1·5	0	0·2
3	21·8	69·5	6·6	0	1·9	0	0
4	57·9	26·4	14·2	0	1·5	0	0
5	45·5	45·9	6·5	0	1·9	0·2	0
6	70·0	23·2	5·9	0	0·9	0	0

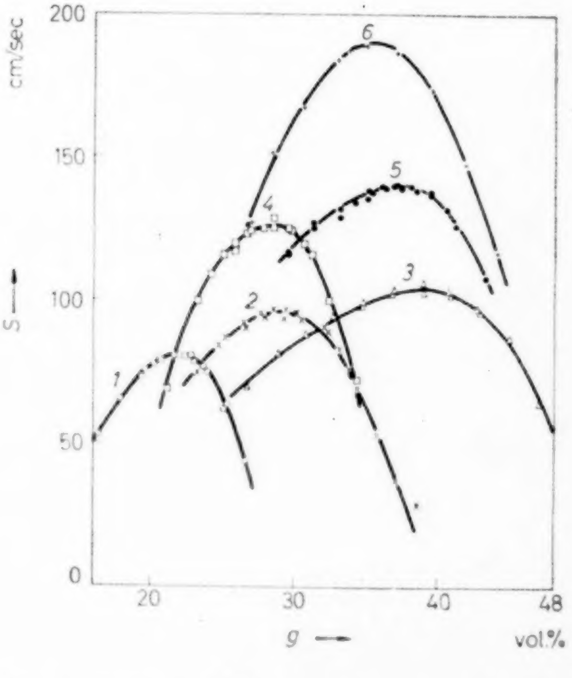

Figure 10. Burning velocities of some ternary mixtures of hydrogen, carbon monoxide and methane

The values corresponding with the maxima in these curves are given in *Table 7*. The values corrected for small amounts of nitrogen, carbon dioxide and oxygen (S_0 and g_0) have also been included in this table.

Table 7. Maximum burning velocities and compositions of hydrogen–carbon monoxide–methane–air mixtures

Mixture No.	$g_{S_{max.}}$ *% by volume*	$S_{max.}$ *cm/sec*	g_0 *% by volume*	S_0 *cm/sec*
1	21·9	81	21·7	81·2
2	29·0	96	28·6	97·4
3	38·9	105	38·2	105·7
4	28·5	127	28·2	128·1
5	37·1	141	36·6	144·3
6	35·3	190	35·1	192·0

TRIANGULAR DIAGRAMS

All data of the binary and ternary mixtures have been compiled in two triangular diagrams, one of which shows the maximum burning velocities and the other the gas percentages at which the burning velocity is a maximum. The diagrams were constructed by interpolating between the experimental points and drawing lines connecting the points of equal maximum burning velocity and the points of equal gas percentage at maximum burning velocity respectively. These diagrams are shown in *Figures 11* and *12*.

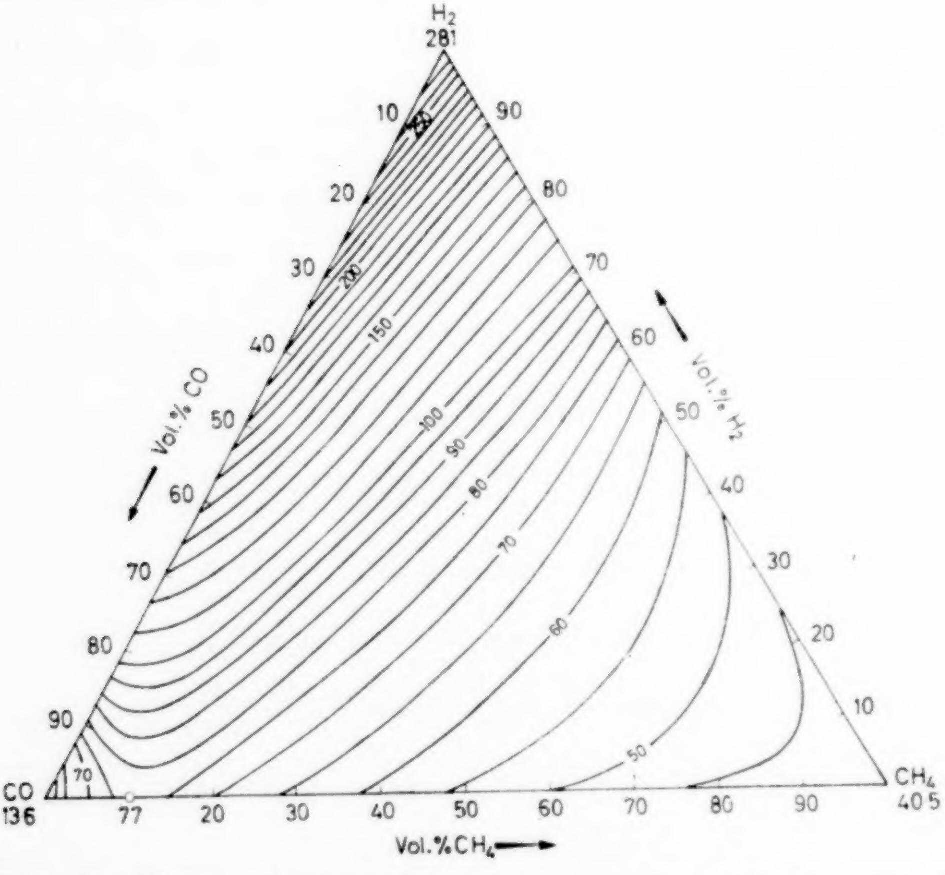

Figure 11. Maximum burning velocities (cm/sec) of hydrogen carbon monoxide methane mixtures

The maximum burning velocity and the corresponding gas percentage of any hydrogen–carbon monoxide–methane mixture of known composition can be read from these diagrams.

EFFECT OF NITROGEN, OXYGEN AND CARBON DIOXIDE

To determine the effect of small amounts of nitrogen, oxygen and carbon dioxide on the maximum burning velocity of the mixtures, 5 per cent (by volume) nitrogen, 10 per cent nitrogen, 2½ per cent oxygen and 5 per cent carbon dioxide were added to methane, hydrogen, hydrogen–methane and the ternary mixtures respectively. We wish to point out that addition of

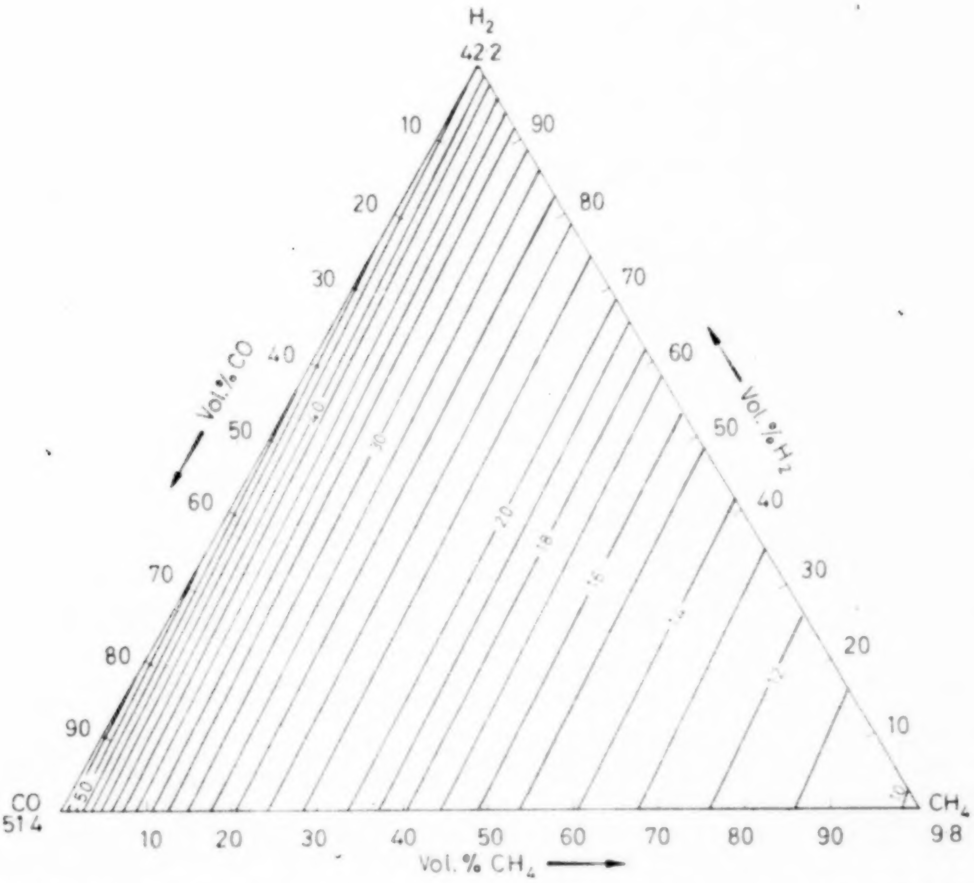

Figure 12. Gas concentrations in the gas-air mixture (vol. %) at the maximum burning velocity of hydrogen–carbon monoxide–methane mixtures

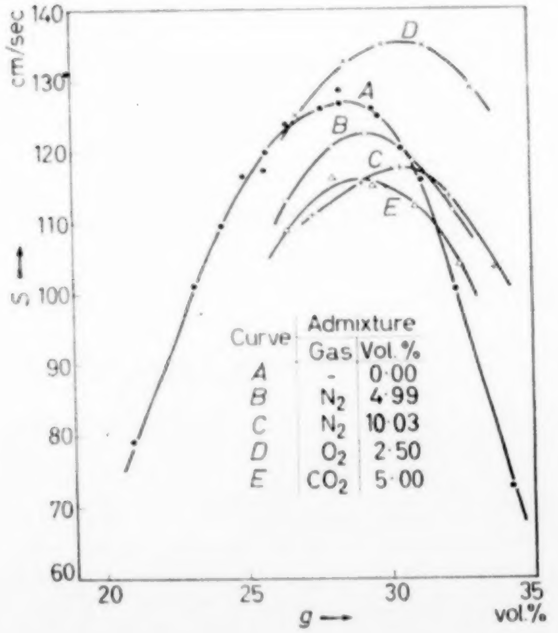

Figure 13. Burning velocity of ternary mixture No. 4 (Table 6) upon addition of nitrogen, oxygen or carbon dioxide

one part of oxygen has the same effect as elimination of 79/21 = 3·76 parts of nitrogen.

For an example we refer to the experiments with ternary mixture No. 4. This mixture contains, in addition to hydrogen, carbon monoxide and methane, 1·5 per cent of nitrogen. Upon addition of the amounts of nitrogen, oxygen or carbon dioxide mentioned in *Table 8*, we measured the burning velocities given in *Figure 13*.

The values corresponding with the maxima are given in the last two columns of *Table 8*.

If now the maximum burning velocities of the original gas and of the gas to which nitrogen or oxygen has been added are plotted versus the nitrogen content (in the case of oxygen addition: the effective nitrogen content) of the gas, it will be seen that the points are indeed located on a straight line (see *Figure 14*).

Table 8. Effect of inert gas on maximum burning velocity and composition of gas mixture No. 4

Amounts of inert gas added	*Content of inert gas upon addition*		$S_{max.}$ *cm/sec*	$g_{S_{max.}}$ *% by volume*
	N_2 *(effective) % by volume*	CO_2 *% by volume*		
—	1·50	—	126·9	28·5
4·99% N_2	6·42	—	122·4	29·2
10·03% N_2	11·38	—	117·5	30·5
2·50% O_2	−7·95	—	135·2	30·7
5·00% CO_2	1·43	5·00	116·0	28·9

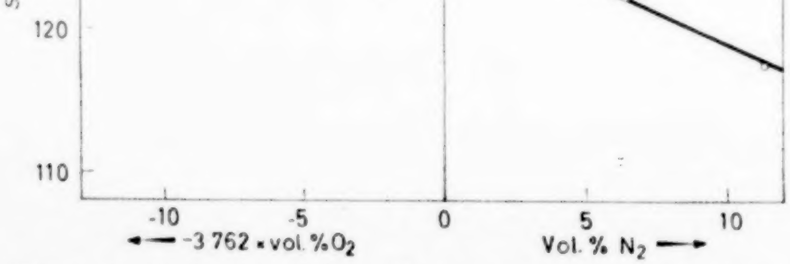

Figure 14. Maximum burning velocity of ternary mixture No. 4 (Table 6) upon addition of nitrogen and oxygen

This straight line satisfies the equation

$$S_{max.} = 128{\cdot}1 - 0{\cdot}932\,[N_2] \qquad \ldots.[1]$$

where $[N_2]$ is the nitrogen content of the gas (per cent by volume). With addition of carbon monoxide we get

$$S_{\text{max.}} = 128{\cdot}1 - 2{\cdot}085\,[CO_2] \qquad \ldots.[2]$$

The general formula is

$$S_{\text{max.}} = S_0 - a_B\,[B] \qquad \ldots.[3]$$

where S_0 denotes the maximum burning velocity of the original gas; $S_{\text{max.}}$ is the maximum burning velocity of the gas to which nitrogen, oxygen or carbon dioxide has been added; $[B]$ is the concentration of the gas B added; and a_B is a constant depending on the type of gas B.

For all the gas mixtures examined the values of these factors have been compiled in *Table 9*.

Table 9. Effect of nitrogen and carbon dioxide on the maximum burning velocities of gas–air mixtures

Gas		S_0	a_{N_2}	a_{CO_2}	$\frac{a_{CO_2}}{a_{N_2}}$	$A_{N_2} = \frac{100\,a_{N_2}}{S_0}$	$A_{CO_2} = \frac{100\,a_{CO_2}}{S_0}$
Hydrogen		280·7	2·318	3·311	1·43	0·825	1·18
Methane		40·6	0·186	0·412	2·22	0·457	1·02
Hydrogen–methane mixture	1	55·4	0·486	0·891	1·84	0·878	1·61
	2	83·0	0·712	1·411	1·98	0·858	1·70
	3	135·9	1·087	2·469	2·27	0·800	1·82
	4	183·9	1·532	3·016	1·97	0·833	1·64
Ternary mixture	1	81·2	0·496	1·191	2·40	0·611	1·47
	2	97·4	0·798	1·817	2·27	0·820	1·87
	3	105·7	1·070	1·831	1·71	1·012	1·73
	4	128·1	0·932	2·085	2·24	0·728	1·63
	5	144·3	1·234	2·739	2·21	0·859	1·90
	6	192·0	1·778	3·608	2·03	0·926	1·88
Mean value					2·05	0·801	1·64

It was found that all gas mixtures approximately satisfy the equation

$$S_{\text{max.}} = S_0\,\{100 - A_B\,[B]\}\,/\,100 \qquad \ldots.[4]$$

where the constant A_B has the following values:

$$A_{N_2} = +0{\cdot}8 \qquad A_{O_2} = -3{\cdot}0 \qquad A_{CO_2} = +1{\cdot}6$$

When these gases are present in the hydrogen–carbon monoxide–methane mixture, the maximum burning velocity can be found by multiplying the value read from the triangular diagram by

$$\{100 - 0{\cdot}8\,[N_2] + 3{\cdot}0\,[O_2] - 1{\cdot}6\,[CO_2]\}\,/\,100$$

We also determined the effect of admixed nitrogen, oxygen and carbon dioxide on the gas percentage at the maximum burning velocity.

With regard to mixtures of several gases with air it will be obvious that the reciprocal value of the stoichiometric gas percentage varies linearly with the gas composition. Experiments have shown that with binary gas mixtures this proportionality is also valid for the gas percentage at the maximum burning velocity. If a gas mixture containing *A* per cent by volume of component A and *B* per cent of component B, is mixed with air, the gas percentage at maximum burning velocity, g_{AB}, can be found from

$$100/g_{AB} = \{[A]/g_A + [B]/g_B\} \qquad \ldots.[5]$$

where g_A and g_B denote the gas percentages in mixtures of gas A with air and gas B with air at maximum burning velocity.

Equation 5 also holds for more complicated gas mixtures. For our hydrogen–carbon monoxide–methane mixtures with nitrogen, oxygen and carbon dioxide, g_{N_2} and g_{CO_2} must be put equal to unity, because nitrogen and carbon monoxide do not consume air. As oxygen does not consume air, but on the contrary one part of oxygen is equivalent to 100/21 parts of air, g_{O_2} must be put equal to $-21/79 = -1/3{\cdot}76$. If g_u is the gas percentage at maximum burning velocity of a mixture of pure hydrogen–carbon monoxide–methane with air, g_{max} for the mixture containing nitrogen, carbon dioxide and oxygen can be derived from

$$\frac{100}{g_{max}} = \frac{[H_2]+[CO]+[CH_4]}{g_u} + \frac{[N_2]+[CO_2]-3{\cdot}76[O_2]}{100} \qquad \ldots.[6]$$

CHECKING OF THE TRIANGULAR DIAGRAM AND THE CORRECTIONS

The diagrams were checked by measurements on four gas mixtures; these were prepared from the separate components and their compositions were as much as possible equal to those of technical gases: coal gas, town gas, Pintsch gas and blue watergas.

The compositions of these gases, the experimental and calculated values of the burning velocity (calculated by means of the triangular diagram and corrected) and the corresponding gas percentages have been compiled in *Table 10*.

Table 10. Measured and calculated burning velocities of some gases

Gas	*Gas composition, % by volume*							S_{max}, *cm/sec*		$g_{S_{max}}$, %	
	H_2	CO	CH_4	*Unsat. hydrocarbons*	N_2	CO_2	O_2	*Meas.*	*Calc.*	*Meas.*	*Calc.*
Coal gas	50·4	7·8	31·5	0	6·2	4·1	0	71	70·8	20·7	20·5
Town gas	50·8	21·5	17·4	0	5·1	5·2	0	97·5	99·4	27·3	27·5
Pintsch gas	51·6	28·5	11·2	0	6·2	2·8	0·1	121	122·7	31·8	32·2
Blue water-gas	50·6	37·8	1·2	0	5·0	5·3	0·1	163·5	163·5	45·5	46·0

Centraal Laboratorium,
Staatsmijnen in Limburg,
Geleen, The Netherlands

(Received December 1958)

REFERENCES

[1] SCHOLTE, T. G. and VAAGS, P. B. *Combustion & Flame*, 1959, **3**, 495
[2] SCHOLTE, T. G. and VAAGS, P. B. *Combustion & Flame*, 1959, **3**, 503

Notes on Gaseous Nitric Acid–Hydrocarbon Flames

J. MERTENS and R. L. POTTER

Substitution of argon for nitrogen as shielding fluid about nitric acid–hydrocarbon flames does not change the spectra involving CN *and* NH *radicals. Photographs in colour of these flames show qualitative differences between low and high temperature inlet gases.*

RECENTLY J. MERTENS and R. L. POTTER[1] published the results of an extensive study of gaseous nitric acid–hydrocarbon flames. Two topics mentioned there deserve further attention, and it is the purpose of this note to report the results of new work on these flames.

The first topic concerns the experimental technique used to take spectrograms of the flames. A great deal of emphasis was placed upon the prominence of CN and NH radical spectra, leading to the deduction that in these flames some of the nitrogen in the nitric acid breaks all its original bonds in the first combustion wave. However, it should be pointed out that all these flames were studied with nitrogen gas flowing around the flame. Hence it is possible that the nitrogen shield provided the nitrogen that appeared in the CN and NH, demonstrated to be present in the spectrum. If this were so, the conclusions brought forward by Mertens and Potter[1] would naturally be vitiated concerning radical mechanisms in these flames.

In order to ascertain whether the nitrogen appearing as CN and NH comes from the nitric acid or the nitrogen shield, further experiments were carried out using argon as the shielding fluid. The argon was high purity material, with an argon content of 99·995 mole per cent, and a nitrogen content of 0·003 mole per cent. The spectra obtained were identical with those obtained with the nitrogen shield, and hence it may be stated that the nitrogen present in the radicals CN and NH comes from the nitric acid and not from the nitrogen shield.

The second topic to be discussed is the qualitative appearance of the flames and the spectra of the flames. It was reported by Mertens and Potter[1] that the flames changed appearance when the inlet gases were preheated. They reported that a new combustion wave, blue in colour, appeared over the first combustion wave, in a Smithells separator. In the fuel rich region, the same behaviour is exhibited with nitrogen shielding. M. H. BOYER and P. E. FRIEBERTSHAUSER[2] have published black and white photographs of nitric acid–hydrocarbon flames in air and in secondary nitrogen. The temperature of the combustible gases is not directly reported by them; however, they say that their evaporator temperatures never exceeded about 450 K. As they remark, the photographs do not do justice to the flames. Photographs in colour taken by **Mr Glenn Pabst**, are presented in *Figure 1*. These show nitric acid propane flames surrounded by nitrogen at three mixture strengths and at both high and low initial gas temperatures. These are at atmospheric pressure; the low temperature is 450 K and the high temperature is just below 700 K. In the figure, the low temperature flames are in the top row while just below are the high temperature flames. From left to right, the photographs represent fuel rich, maximum burning velocity mixtures and oxidizer rich flames.

There is a striking contrast between the low and high temperature flames. The difference in the fuel rich case is especially plain as the low temperature flame consists solely of the inner cone, while the high temperature flame shows two distinct reaction zones. At the other mixture strengths the high temperature flames show more combustion taking place than do the low temperature flames. The spectra of these flames show much more structure in the high temperature case. *Figure 2* shows a comparative spectrum of the fuel rich flames at both low and high temperatures. The low temperature flame shows practically no structure while the high temperature flame shows a profusion of radical bands in addition to the continuum in the visible. Note that most of the radical bands are in the inner cone. There are two exceptions; the hydroxyl bands occur all the way to the top of the flame, and what appear to be carbon monoxide flame bands appear in the second combustion wave. They cease before the top of the flame is reached. These bands do not appear in the stoichiometric mixtures very strongly and they are absent in the oxidizer rich mixtures. In the fuel rich mixtures the NO + O continuum waxes and wanes as do the carbon monoxide flame bands. There is less difference between the spectra in the other mixture strength regions, the major difference being in the variation in the strength of the continuum in the visible.

It is remarkable that so little radical spectra occur over the inner cone of these flames; only OH and the NO + O continuum seem to be present right to the top of the flame. Clearly, reactions producing radicals occur early in the first reaction zone. Presumably there is carbon monoxide formed on passage through the first combustion wave, and resultant reaction with thermally decomposing nitric oxide in the second combustion wave may give rise to the carbon monoxide flame bands. According to A. G. **Gaydon**[3] flame bands are observed when carbon monoxide burns with nitrous oxide, and it seems reasonable to assume that nitric oxide would also produce them. It appears that the simplest explanation for the observations recorded here is that the major jump toward equilibrium occurs in the first combustion wave, and that slow adjustments toward equilibrium take place in the later combustion waves. When the initial gas temperature is low, the heat generated in the first wave must not be sufficient to enable the thermal reactions to be completed before the hot gases are cooled by the surrounding gases. In the high temperature flames, the partially burnt gases issuing from the first combustion wave are hot

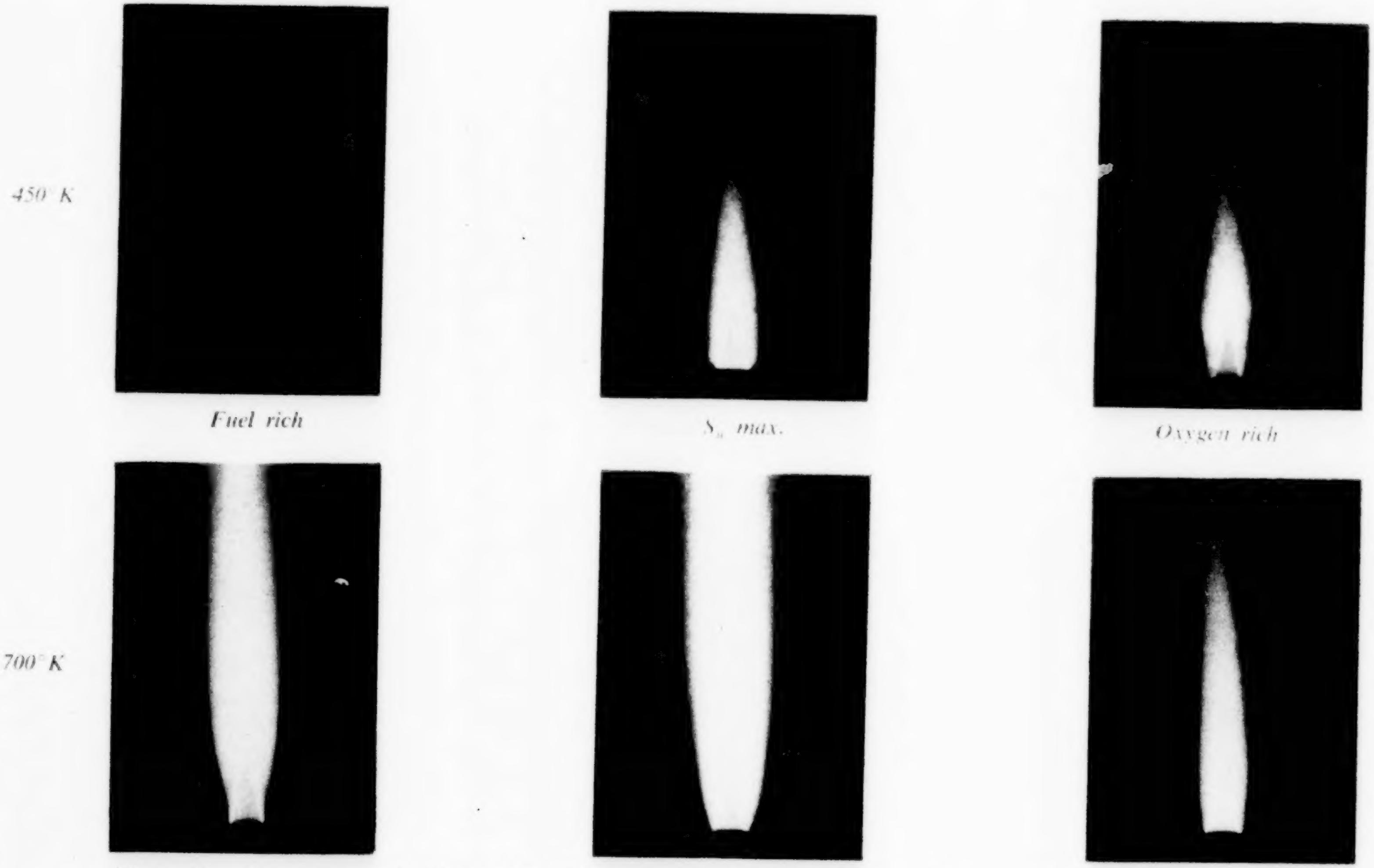
450° K
Fuel rich
S_u max.
Oxygen rich
700° K

Figure 1. Appearance of HNO_3–C_3H_8 *flames at* **450 K** *and* **700 K**. *(Atmospheric pressure nitrogen shield)*

Initial gas temperature 400°K

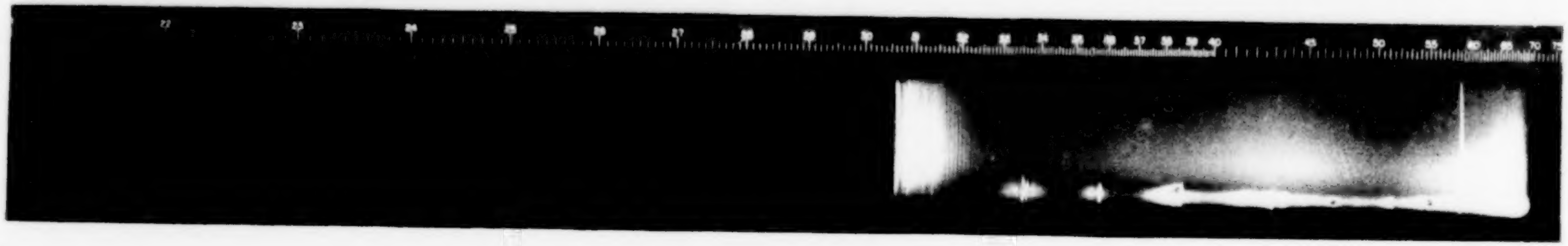
30
37
40
45
50
55
60
65
70
75

Initial gas temperature 700°K

Figure 2. Spectra of fuel rich HNO_3–C_3H_8 *flames*

(Atmospheric pressure—nitrogen shield)

enough to force the completion of the reactions which are essentially thermal in nature.

Bell Aircraft Corpn.
Post Office Box One,
Buffalo 5, N.Y

(Received June 1958)

REFERENCES

[1] MERTENS, J. and POTTER, R. L. *Combustion & Flame*, 1958, **2**, 181
[2] BOYER, M. H. and FRIEBERTSHAUSER, P. E. *Combustion & Flame*, 1957, **1**, 264
[3] GAYDON, A. G. *The Spectroscopy of Flames*. Wiley: New York, 1957

Theory of the Burning of Monopropellant Droplets[*]

F. A. Williams

The steady-state burning of a single liquid monopropellant droplet in an infinite inert atmosphere is considered in detail, including allowances for thermal conduction, diffusion and chemical kinetic effects. Simplified forms of the governing equations are developed, and theoretical predictions compared with experimental results.

We shall investigate in detail the steady-state burning of a single liquid monopropellant droplet in an infinite inert atmosphere. The case considered is that in which the arrangement is spherically symmetrical and the only coordinate of importance is r, the distance from the centre of the drop. Thermal conduction, diffusion, and chemical kinetic effects are included in predicting the burning rate of the droplet and other physical properties of the system. This problem is similar to the one-dimensional premixed laminar flame problem[1], but the spherical symmetry introduces some additional complications. Solution is necessary for a basic understanding of the combustion mechanism in liquid monopropellant rocket motors.

While the diffusion flame burning of single fuel droplets has been exhaustively studied in the literature[2], it appears that the only published theoretical investigation of the monopropellant counterpart of this problem is that of J. Lorell and H. Wise[3] who solved numerically the governing equations for a first-order chemical reaction. In addition to carrying out numerical solutions for second-order reactions similar to those of Lorell and Wise, we obtain approximate analytical expressions for the steady-state mass burning rate in limiting cases for arbitrary reactions. Since D. W. Kiley[4] was unable to produce the steady-state burning of monopropellant droplets in an inert atmosphere, we shall compare our theory with the experimental results given by M. Barrère and H. Moutet[5] who tested ethyl nitrate, propyl nitrate, hydrogen peroxide and some composite propellants, and by W. A. Rosser[6] who used ethyl nitrate, nitromethane and hydrazine.

After expressing the basic equations in a suitable dimensionless form, we discuss the methods by which exact and approximate solutions can be obtained. An approximate analytical expression for the burning rate is derived for the case in which the activation energies of all important reactions are large. In the third section simplified forms of the governing equations are given for one-step reactions with specific boundary conditions and a Lewis number of unity. A numerical integration of the governing equations for second-order reactions has been performed for adiabatic burning, and an analytical correlation of the resulting burning rate as a function of droplet radius at low activation energies is presented. Finally in the fourth section we compare the theoretical predictions with experiments.

---

[*] Paper presented at January 1958 meeting of Western States Section of Combustion Institute.

FORMULATION AND SOLUTION FOR ARBITRARY CHEMICAL KINETICS

(1) *Description of the system*

Let us consider a system which contains an arbitrary number s of different chemical constituents. The reactants evaporate from the droplet surface at its boiling point T_l. The subscript l refers to the conditions at the surface of the droplet while f will denote final conditions after burning is completed $(r=\infty)$. The reactants diffuse radially outward from the droplet surface, are continuously heated, and begin to react rapidly. Energy liberated by the reaction is conducted to the droplet surface and causes more reactants to evaporate. After completion of the reaction the products flow toward infinity.

Throughout the analysis the assumption of steady-state conditions will be made, i.e. all partial derivatives with respect to time are zero. This is rigorously true only if the droplet is continually supplied with monopropellant from an internal source in order to maintain a constant diameter. The conventional hypothesis that the solution thus obtained applies even when no mass is being added to the droplet is questionable in some cases[7].

(2) *Basic equations*

We shall consider systems which obey the ideal gas law in the gaseous phase surrounding the droplet: $p=\rho RT/\overline{M}$ where p is the pressure, ρ represents the mass density, R is the universal gas constant, and T signifies temperature. Here the average molecular weight is defined as $\overline{M}=\sum_{j=1}^{s} M_j X_j$, where M_j is the molecular weight of species j and X_j denotes the mole fraction of component j which obeys the equation

$$\sum_{j=1}^{s} X_j=1 \qquad \ldots.[1]$$

For deflagration problems it is justifiable to assume that p is constant.

The most important unknown quantity is the mass burning rate $m=4\pi r^2\rho v$ which must be constant in a steady-state situation. Here v represents the mass-average (radial) velocity. It is convenient to define the flux fraction of species j by the relation $\varepsilon_j=Y_j[1+(V_j/v)]$ where V_j is the diffusion velocity of species j and $Y_j=M_jX_j/\overline{M}$ is the mass fraction of component j. It is clear from these definitions that $\sum_{j=1}^{s} Y_j=1$, $\sum_{j=1}^{s} Y_jV_j=0$, and therefore

$$\sum_{j=1}^{s} \varepsilon_j=1 \qquad \ldots.[2]$$

If ω_j is the rate of production (mass per unit volume) of species j, then the conservation of mass in chemical reactions is expressed by the relation[8]

$$\omega_j=M_j\sum_{r=1}^{t}(\nu''_{j,r}-\nu'_{j,r})B_r\mathrm{e}^{-T_r/T}\prod_{i=1}^{s}\left(\frac{pX_i}{RT}\right)^{\nu'_{i,r}}=\frac{m}{4\pi r^2}\frac{\mathrm{d}\varepsilon_j}{\mathrm{d}r}\quad j=1,2,\ldots,s \qquad \ldots.[3]$$

Here T_r is the activation temperature for the rth chemical reaction, B_r is the reaction rate frequency factor, the quantities $\nu''_{j,r}$ and $\nu'_{j,r}$ are the stoichiometric coefficients of species j appearing as product and reactant, respectively, in the rth process, and t is the total number of reactions.

The values of X_j appearing in equation 3 are determined by the diffusion equation. If thermal diffusion is neglected, then it is found that to first order in a Sonine polynomial expansion the relation[9]

$$\frac{\mathrm{d}X_j}{\mathrm{d}r} = \frac{m}{4\pi r^2}\frac{RT}{p}\sum_{i=1}^{s}\frac{1}{D_{ij}}\left(\frac{X_j\varepsilon_i}{M_i} - \frac{X_i\varepsilon_j}{M_j}\right) \quad j = 1, 2, \ldots, s \qquad \ldots.[4]$$

is valid, where D_{ij} is the binary diffusion coefficient for species i and j.

The energy equation is obtained by equating the constant total energy flux across a shell of radius r to its value at $r = r_l$, viz.

$$4\pi r^2\lambda\frac{\mathrm{d}T}{\mathrm{d}r} = m\left[\Delta l + \bar{c}_p(T - T_l) + \sum_{j=1}^{s}(\varepsilon_j - \varepsilon_{j,l})h_j^0\right] \qquad \ldots.[5]$$

where λ is the thermal conductivity of the gas mixture, h_j^0 represents the (constant) standard heat of formation of species j, and Δl is the specific heat of vaporization of the mixture within the droplet. In equation 5 the average specific heat of the mixture has been defined as

$$\bar{c}_p \equiv \frac{1}{T - T_l}\sum_{j=1}^{s}\left[\varepsilon_j(h_j - h_j^0) - \varepsilon_{j,l}(h_{j,l} - h_j^0)\right] \qquad \ldots.[6]$$

where h_j denotes the total enthalpy of species j per unit mass. The boundary condition which physically determines m is the steady-state requirement that the energy entering the droplet by conduction must be equal to that needed to vaporize the propellant which flows outward [see equation 5], since it is assumed that the droplet is at a constant temperature.

Equations 3, 4 and 5 provide $2s+1$ equations in the $2s+1$ unknowns X_j, ε_j and T. In view of equations 1 and 2, only $2s-1$ of these equations are independent. The composition and evaporation characteristics of the droplet determine the boundary values $\varepsilon_{j,l}$ and T_l, while the nature of the surrounding atmosphere determines T_f and $X_{j,f}$. The requirement of chemical equilibrium at the temperature T_f at $r = \infty$ provides a relation between the quantities $\varepsilon_{j,f}$ and thereby ensures that the two-point boundary value problem has an eigenvalue m.

(3) *Dimensionless form of the governing equations*

It is convenient to introduce a dimensionless temperature $\theta \equiv T/T_f$ and radial coordinate $\sigma \equiv r/r_l$. If the dimensionless heat of vaporization is defined as $\alpha \equiv \Delta l/\bar{c}_pT_f$ and the quantity $h_j^0/\bar{c}_pT_f \equiv H_j$ is the dimensionless enthalpy of formation, then equation 5 may be written in the form

$$\frac{\mathrm{d}\theta}{\mathrm{d}\sigma} = \frac{m\bar{c}_p}{4\pi r_l\lambda\sigma^2}\left[\alpha + \theta - \theta_l + \sum_{j=1}^{s}H_j(\varepsilon_j - \varepsilon_{j,l})\right] \qquad \ldots.[7]$$

It is possible to select a characteristic species and to denote it by the subscript P. A Lewis number for species j may then be defined as $\mathscr{L}_j \equiv \lambda RT/\bar{c}_p pM_jD_{jP}$, and a dimensionless diffusivity will be denoted by

$\gamma_{ji} \equiv D_{iP}/D_{ji}$. By dividing equation 4 by equation 7 we now obtain the relation

$$\frac{\mathrm{d}X_j}{\mathrm{d}\theta} = \mathscr{L}_j \frac{\sum\limits_{i=1}^{s} \gamma_{ji}(\mathscr{M}_{ji} X_j \epsilon_i - X_i \epsilon_j)}{\alpha + \theta - \theta_l + \sum\limits_{i=1}^{s} H_i(\epsilon_i - \epsilon_{i,l})} \qquad j = 1, 2, \ldots, s \qquad \ldots.[8]$$

where the molecular weight ratio has been defined as

$$\mathscr{M}_{ij} \equiv M_i/M_j$$

By letting $r = 1$ denote an important reaction in which species P is formed, we may define a dimensionless frequency factor for the jth species and rth reaction by the relation

$$\beta_{j,r} \equiv \frac{(\nu''_{j,r} - \nu'_{j,r}) B_r (p/RT)^{O_r} M_j \lambda_l \bar{c}_{p,l}}{(\nu''_{P,1} - \nu'_{P,1}) B_{1,l} (p/RT_l)^{O_1} M_P \lambda \bar{c}_p} \qquad j = 1, 2, \ldots, s; \quad r = 1, 2, \ldots, t,$$

where $O_r \equiv \sum\limits_{i=1}^{s} \nu'_{i,r}$ is the order of the rth chemical reaction. Since B_r is proportional to a simple power of T, the temperature dependence of the quantities λ and $\bar{c}_p$ is included in $\beta_{j,r}$ for convenience. We define the constant dimensionless mass burning rate eigenvalue by the expression

$$\Lambda^\star \equiv (4\pi r_l^2/m)^2 (\lambda_l/\bar{c}_{p,l}) M_P (\nu''_{P,1} - \nu'_{P,1}) B_{1,l} (p/RT_l)^{O_1}$$

In view of these definitions, by dividing equation 3 by equation 7 we find that

$$\frac{\mathrm{d}\epsilon_j}{\mathrm{d}\theta} = \Lambda^\star \frac{\sigma^{-4} \sum\limits_{r=1}^{t} \beta_{j,r} e^{-\theta_r/\theta} \prod\limits_{i=1}^{s} X_i^{\nu'_{i,r}}}{\alpha + \theta - \theta_l + \sum\limits_{i=1}^{s} H_i(\epsilon_i - \epsilon_{i,l})} \qquad j = 1, 2, \ldots, s \qquad \ldots.[9]$$

where $\theta_r = T_r/T_l$ is the dimensionless activation energy for the rth reaction.

If we define the parameter $V^\star(\theta)$ by the equation

$$V^\star \equiv r_l^2 (\bar{c}_p/\lambda)^2 (\lambda_l/\bar{c}_{p,l}) M_P (\nu''_{P,1} - \nu'_{P,1}) B_{1,l} (p/RT_l)^{O_1}$$

then equation 7 may be rewritten in the form

$$\frac{\mathrm{d}\sigma}{\mathrm{d}\theta} = -\sigma^2 \left\{\frac{\Lambda^\star}{V^\star}\right\}^{\frac{1}{2}} \left[\alpha + \theta - \theta_l + \sum_{j=1}^{s} H_j(\epsilon_j - \epsilon_{j,l})\right]^{-1} \qquad \ldots.[10]$$

Equations 8 to 10 inclusive compose the desired dimensionless formulation.

(4) *General methods of solution*

The $2s+1$ first-order relations given in equations 8 to 10 above may be solved by stepwise numerical integration techniques. All coefficients are known simple functions of θ. If σ is replaced by the distance variable $\eta = 1/\sigma$, then all variables remain within a finite range. The eigenvalue $\Lambda^\star$ is determined by an approximation procedure (the integration is performed for an assumed value of $\Lambda^\star$; if the correct boundary conditions are not obtained then $\Lambda^\star$ is changed and the integration is repeated). Some differential equations can often be eliminated by physical considerations[10].

Since accurate iterative methods of solution lead to complicated numerical integrations, we find it necessary to use expansion procedures to obtain analytical results. By expanding the governing equations suitably about the end points, accurate functions $\theta(\sigma)$, $X_j(\sigma)$ and $\varepsilon_j(\sigma)$ will be obtained in the neighbourhood of these points and a useful analytical approximation for the burning rate eigenvalue $\Lambda^{\star}$ will be found.

(5) *An approximate expression for $\Lambda^{\star}$ and its validity*

By integrating the form of equation 9 for which $j=P$ from the droplet surface to the hot boundary ($\sigma=\infty$) we find that

$$\int_{\varepsilon_{P,1}}^{\varepsilon_{P,f}} f(\varepsilon_P)\, d\varepsilon_P = \Lambda^{\star} g \qquad \ldots.[11]$$

where the function $f(\varepsilon_P)$ has been defined by the equation

$$f(\varepsilon_P) \equiv \frac{1}{\sigma^2(1-\theta)}\left[\alpha+\theta-\theta_1+\sum_{j=1}^{s} H_j(\varepsilon_j-\varepsilon_{j,1})\right] \qquad \ldots.[12]$$

and the quantity g is given by the expression

$$g \equiv \sum_{r=1}^{t} \int_{\theta_1}^{1} \frac{B_{P,r}\, e^{-\theta_{a,r}/\theta}}{1-\theta} \prod_{j=1}^{s} X_j^{\nu'_{j,r}}\, d\theta \qquad \ldots.[13]$$

When θ_1 is reasonably large for all reactions which have rates large enough to contribute appreciably to the summation in equation 13, nearly all of the contributions to the important integrals will come from the range $\theta \approx 1$. By expanding equation 8 about $\theta=1$ we obtain approximate expressions for $X_j(\theta)$ which are valid near $\theta=1$. Substituting two-term expansions into equation 13 yields an accurate approximation for the quantity g, viz.

$$g = \sum_{r=1}^{t} \int_{\theta_1}^{1} \frac{B_{P,r}\, e^{-\theta_{a,r}/\theta}}{1-\theta} \prod_{j=1}^{s} \left[X_{j,f} - (1-\theta)\, \mathscr{L}_{j,f} \frac{\sum_{i=1}^{s} \gamma_{ji,f}(\mathscr{L}_{ii} X_{i,f}\varepsilon_{i,f} - X_{i,f}\varepsilon_{i,1})}{\alpha_f+1-\theta_1+\sum_{i=1}^{s} H_{i,f}(\varepsilon_{i,f}-\varepsilon_{i,1})} \right]^{\nu'_{j,r}} d\theta$$

$$\ldots.[13a]$$

Here it is understood that limiting procedures are to be used for evaluating indeterminate ratios if necessary. Since all X_js are linear functions of θ for one-step reactions in adiabatic systems with $\mathscr{L}_j=1$ (see third section), it is expected that equation 13a will often be valid for relatively small values of θ_1. All integrals involved in equation 13a may be evaluated in terms of tabulated integrals.

It is necessary to obtain a reasonable approximation for the function $f(\varepsilon_P)$ in order to determine $\Lambda^{\star}$. It is apparent from equation 12 that

$$f(\varepsilon_{P,1}) = \alpha_1/(1-\theta_1) \qquad \ldots.[14]$$

For non-adiabatic systems the heat transfer by thermal conduction does not vanish at $\sigma=\infty$. In this case the quantity $[\alpha+\theta-\theta_1+\sum_{j=1}^{s} H_j(\varepsilon_j-\varepsilon_{j,1})]$ therefore remains non-zero at $\theta=1$ and equation 10 shows that $(1-\theta)\sim 1/\sigma$ near $\theta=1$. By substituting this result into equation 12 we find that

$f(\epsilon_p) \sim 1/\sigma^4$ which approaches zero at $\epsilon_p = \epsilon_{p,f}$. In adiabatic cases the asymptotic behaviour of $f(\epsilon_p)$ is governed by the nature of the reaction through equation 9. For non-adiabatic systems and also for the adiabatic cases in which $f(\epsilon_{p,l}) = 0$, the largest contribution to the integral in equation 11 will usually come from the neighbourhood of the cold boundary. By differentiating equation 12 we obtain the equation

$$\frac{\mathrm{d}f}{\mathrm{d}\epsilon_p} = -\frac{4}{\sigma^5(1-\theta)}\left[\alpha+\theta-\theta_l+\sum_{j=1}^{s} H_j(\epsilon_j-\epsilon_{j,l})\right]\frac{\mathrm{d}\sigma}{\mathrm{d}\theta}\,\frac{\mathrm{d}\theta}{\mathrm{d}\epsilon_p}$$
$$+\frac{1}{\sigma^4(1-\theta)^2}\left[1-\theta_l+\alpha+\sum_{j=1}^{s} H_j(\epsilon_j-\epsilon_{j,l})\right]\frac{\mathrm{d}\theta}{\mathrm{d}\epsilon_p}+\frac{1}{\sigma^4(1-\theta)}\sum_{j=1}^{s} H_j\,\frac{\mathrm{d}\epsilon_j}{\mathrm{d}\theta}\,\frac{\mathrm{d}\theta}{\mathrm{d}\epsilon_p} \quad \ldots[15]$$

which, by equations 9 and 10, may be evaluated at $\epsilon_p = \epsilon_{p,l}$ with the result

$$\left(\frac{\mathrm{d}f}{\mathrm{d}\epsilon_p}\right)_{\epsilon_{p,l}} = \left\{\frac{1-\theta_l+\alpha_l}{(1-\theta_l)^2}-\frac{4}{1-\theta_l}\left(\frac{\Lambda^\star}{V^\star_l}\right)^{\frac{1}{3}}+\frac{\Lambda^\star}{\alpha_l(1-\theta_l)}\right.$$
$$\left.\sum_{r=1}^{f}\left[\left(\sum_{j=1}^{s} H_{j,l}\beta_{j,r,l}\right)e^{-\theta_r/\theta_l}\prod_{i=1}^{s} X_{i,l}^{\nu'_{i,r}}\right]\right\}\left[\frac{\Lambda^\star}{\alpha_l}\sum_{r=1}^{f}\beta_{P,r,l}\,e^{-\theta_r/\theta_l}\prod_{i=1}^{s} X_{i,l}^{\nu'_{i,r}}\right]^{-1}$$
$$\ldots.[16]$$

Here the small variation of $\bar{c}_p$ with θ has been neglected. Since m will decrease and hence $\Lambda^\star$ will increase as θ_l is increased at a given value of r_l, it follows that for sufficiently large values of θ_l the quantity in the curly brackets in equation 16 will be negative. For exothermic reactions the third term in equation 16 is negative. On the other hand, for θ_l sufficiently small and particularly for large droplets (large $V^\star_l$), the first term in equation 16 will be dominant and $(\mathrm{d}f/\mathrm{d}\epsilon_p)_{\epsilon_{p,l}}$ will be positive. It therefore follows that $f(\epsilon_p)$ behaves somewhat as shown in *Figure 1*. It is seen from *Figure 1* that for intermediate and large activation energies there is little error in the integral in equation 11 if a linear expansion of $f(\epsilon_p)$ about the end point $\epsilon_p = \epsilon_{p,l}$ is used. From a two-term expansion for $f(\epsilon_p)$ the relation*

$$\int_{\epsilon_{p,l}}^{\epsilon_{p,f}} f(\epsilon_p)\,\mathrm{d}\epsilon_p = f(\epsilon_{p,l})(\epsilon_{p,f}-\epsilon_{p,l})+\tfrac{1}{2}\left(\frac{\mathrm{d}f}{\mathrm{d}\epsilon_p}\right)_{\epsilon_{p,l}}(\epsilon_{p,f}-\epsilon_{p,l})^2 \quad \ldots.[17]$$

is obtained. By substituting equations 14 and 16 into equation 17 and equating the results to the RHS of equation 11, we obtain the relation

$$\left[\frac{\Lambda^\star}{\alpha_l}\sum_{r=1}^{f}\beta_{P,r,l}\,e^{-\theta_r/\theta_l}\prod_{i=1}^{s} X_{i,l}^{\nu'_{i,r}}\right]\left[\frac{\alpha_l(\epsilon_{p,f}-\epsilon_{p,l})}{(1-\theta_l)}-\Lambda^\star g\right]+\frac{(\epsilon_{p,f}-\epsilon_{p,l})^2}{2(1-\theta_l)}$$
$$\left\{\frac{(1-\theta_l+\alpha_l)}{(1-\theta_l)}-4\left(\frac{\Lambda^\star}{V^\star_l}\right)^{\frac{1}{3}}+\frac{\Lambda^\star}{\alpha_l}\sum_{r=1}^{f}\left[\left(\sum_{j=1}^{s} H_{j,l}\beta_{j,r,l}\right)e^{-\theta_r/\theta_l}\prod_{i=1}^{s} X_{i,l}^{\nu'_{i,r}}\right]\right\}=0$$
$$\ldots.[18]$$

Equation 18 with the quantity g given approximately by equation 13a determines $\Lambda^\star$ in terms of the physical properties of the system.

---

*When the linear approximation for f yields $f < 0$ at $\epsilon_p = \epsilon_{p,f}$, equations 17 and 18 are invalid, but similar manipulations show that equation 19 is valid.

(6) *Properties of the burning rate*

In the derivation of equation 18 the assumption was made that θ_r is large for the dominant reaction steps. From this it follows that if the value of

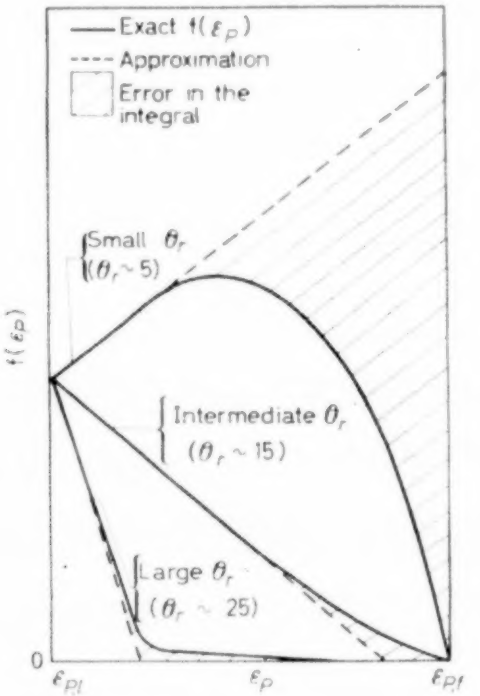

Figure 1. Schematic representation of error in $\Lambda^\star$ resulting from linear approximation of $f(\varepsilon_p)$ for various values of θ_r

θ_l is somewhat less than unity, then the terms involving the exponential factors in equation 18 are negligibly small. The resulting simplified form of equation 18 is

$$(\Lambda^\star / V^\star{}_l)^{1} = (1 - \theta_l + \alpha_l)/4\,(1 - \theta_l) \qquad \ldots . [19]$$

Equation 19 will be valid in most cases for which equation 18 is quantitatively applicable. In view of the definitions of $V^\star$ and $\Lambda^\star$, equation 19 implies that

$$m = 4\pi r_l \frac{\lambda_l}{\bar{c}_{p,l}} \frac{4\,(1 - \theta_l)}{(1 - \theta_l + \alpha_l)} = 16\pi r_l \frac{\lambda_l\,(T_f - T_l)}{\bar{c}_{p,l}\,(T_f - T_l) + \Delta l} \qquad \ldots . [19a]$$

If ρ_l is the density of the liquid droplet, then

$$m = -4\pi\rho_l r_l^2\, \mathrm{d}r_l / \mathrm{d}t \qquad \ldots . [20]$$

provided no mass is being added internally to the droplet. It follows from equations 20 and 19a that $\mathrm{d}r_l^2/\mathrm{d}t = \text{constant}$. If $d \equiv 2r_l$ is the droplet diameter, then the integration of equation 20 yields the relation

$$d_0^2 - d^2 = 32 \frac{\lambda_l}{\rho_l \bar{c}_{p,l}} \frac{(1 - \theta_l)}{(1 - \theta_l + \alpha_l)} (t - t_0) \equiv K\,(t - t_0) \qquad \ldots . [21]$$

where the subscript 0 refers to an initial condition of the droplet. Equation 21 determines the droplet evaporation constant K.

It is also seen from equation 19a that m increases as T_l and λ_l increase and $\bar{c}_p$ and Δl decrease. These results are expected from physical considerations. Furthermore it is seen that m is independent of the reaction rate parameters B_r and θ_r for large values of θ_r. The reason for this is that for large activation energies the reaction rate is strongly temperature-dependent and is therefore practically zero except at the surface $\theta = 1$ where the reaction proceeds rapidly to completion. The resulting flame surface is similar to that encountered in diffusion flame problems[2, 11] for which the burning rate is independent of the chemical reaction rate and $m \sim r_l$. The flame surface model can be used to obtain a complete analytical solution[12] for the burning of monopropellant droplets for large θ_r.

Because of the exponential factors in equation 18, for small values of θ_r and large r_l (i.e. large $V^{\star}{}_l$) the term involving $V^{\star}{}_l$ in the equation becomes much smaller than the other terms. It can be verified by substituting typical values into equation 18 that only the terms involving g and $(1 - \theta_l + \alpha_l)$ are non-negligible when T_l is less than approximately 12000 K. The resulting form of equation 18 shows that $\Lambda^{\star}$ is independent of the parameter $V^{\star}{}_l$, i.e. $m \sim r_l^2$. This conclusion is expected in the limit of large droplet radii and low activation energies because the reaction then goes nearly to completion in a layer small compared to r_l; the geometry becomes effectively one-dimensional in which case the burning rate is proportional to the surface area, $4\pi r_l^2$. It thus follows from equation 18 that, if no mass is added internally to the liquid drop, then

$$(d_0^k - d^k) \sim (t - t_0) \quad 1 \leq k \leq 2 \qquad \ldots . [22]$$

where k varies from 1 at small activation energies to 2 at large activation energies.

For one-step reactions the approximate form of equation 18 valid for θ_1 small shows that $\Lambda^{\star} \sim \exp(\theta_1)$, which implies that m is approximately proportional to the square root of the reaction rate. This result is also characteristic of one-dimensional premixed laminar flames and therefore provides further evidence that the effects of the spherical geometry disappear for large r_l and small θ_r. Although these trends are correct, the magnitude of $\Lambda^{\star}$ obtained from equation 18 is not accurate for small θ_r because of the error in the integral in equation 11 (see *Figure 1*).

SIMPLIFICATIONS AND RESULTS FOR ONE-STEP REACTIONS

(1) *Simplified governing equations*

For one-step chemical reactions the summation over r in equation 9 can be reduced to a single term, the subscript r becomes unnecessary, and we shall denote the single dimensionless activation energy by θ_1. Equation 9 then shows that all flux fractions can be expressed as linear functions of ε_P

$$\varepsilon_j = a_j \varepsilon_P + b_j \qquad j = 1, 2, \ldots, s \qquad \ldots . [23]$$

where the constants a_j are determined by the stoichiometry of the reaction $[a_j = (\nu''_j - \nu'_j) M_j / (\nu''_P - \nu'_P) M_P$ and $b_j = \varepsilon_{j,l} - a_j \varepsilon_{P,l}]$. The standard heat of reaction per unit mass of species P is given by $q = \bar{c}_p T_l Q$ where the dimensionless heat of reaction has been defined as $Q \equiv -\sum_{j=1}^{s} a_j H_j$. Equation 23 and the definition of b_j then show that $\sum_{j=1}^{s} H_j(\varepsilon_j - \varepsilon_{j,l}) = -Q(\varepsilon_P - \varepsilon_{P,l})$. The total number of differential equations is reduced to $s+2$, and the dependent variables are θ, X_j, and ε_P.

If it is reasonable to assume that $M_j = M$ and $D_{ij} = D$ for all species, then all Lewis numbers become equal ($\mathscr{L}_j = \mathscr{L}$) and $\gamma_{ij} = \mathscr{K}_{ij} = 1$. In this case equations 1 and 2 show that equation 8 takes on the simplified form

$$\mathrm{d}X_j/\mathrm{d}\theta = \mathscr{L}(X_j - \varepsilon_j)[\alpha + \theta - \theta_l - Q(\varepsilon_P - \varepsilon_{P,l})]^{-1} \quad j = 1, 2, \ldots, s \quad \ldots.[8a]$$

If equation 8a is divided by equation 10 and equation 23 is used to eliminate ε_j, then the relation

$$\frac{\mathrm{d}}{\mathrm{d}\sigma}\left(\frac{X_j - b_j}{a_j} - \frac{X_P - b_P}{a_P}\right) = \frac{\mathscr{L}}{\sigma^2}\left(\frac{V^\star}{\Lambda^\star}\right)^{\frac{1}{2}}\left(\frac{X_j - b_j}{a_j} - \frac{X_P - b_P}{a_P}\right) \quad j = 1, 2, \ldots, s \quad \ldots.[24]$$

is easily obtained. Since $a_P = 1$ and $b_P = 0$ by definition, the solution of equation 24 is

$$X_j = b_j + a_j X_P + (X_{j,\infty} - b_j - a_j X_{P,\infty}) \exp\left\{-\int_\sigma^\infty \frac{\mathscr{L}}{\sigma^2}(V^\star/\Lambda^\star)^{\frac{1}{2}}\,\mathrm{d}\sigma\right\} \quad j = 1, 2, \ldots, s \quad \ldots.[25]$$

where the constant of integration has been evaluated in terms of the known mole fractions at infinity. For the special case in which $D \sim T$, the product $\mathscr{L}[V^\star]^{\frac{1}{2}}$ is constant and the integration in equation 25 can be performed explicitly to determine all X_js in terms of X_P and σ.

If $\mathscr{L} = 1$ and $\bar{c}_p$ is constant then an expression similar to equation 25 relates θ to X_P. By subtracting the reciprocal of equation 10 from the ratio of equations 8a and 10, we obtain the relation

$$(\mathrm{d}/\mathrm{d}\sigma)(QX_P - \theta + \theta_l - \alpha - Q\varepsilon_{P,l}) = (1/\sigma^2)(V^\star/\Lambda^\star)^{\frac{1}{2}}(QX_P - \theta + \theta_l - \alpha - Q\varepsilon_{P,l}) \quad \ldots.[26]$$

The solution of equation 26 is

$$QX_P = \theta - \theta_l + \alpha + Q\varepsilon_{P,l} + (QX_{P,\infty} - 1 + \theta_l - \alpha - Q\varepsilon_{P,l}) \exp\left\{-\int_\sigma^\infty (1/\sigma^2)(V^\star/\Lambda^\star)^{\frac{1}{2}}\,\mathrm{d}\sigma\right\} \quad \ldots.[27]$$

If λ is independent of T then $V^\star$ is constant and the integral in equation 27 may be evaluated to determine X_P in terms of θ and σ. In this special case it is necessary to solve simultaneously only equations 10 and 9 with $j = P$ to obtain a complete solution. The number of governing differential equations cannot be decreased further without destroying essential features of the problem.

(2) *Characteristics of the solutions*

In practical experimental arrangements the mixture is often uniform at infinity, i.e. $\lim_{\sigma\to\infty}(\sigma^2\,\mathrm{d}X_j/\mathrm{d}\sigma)=0$ for all species j. It then follows from equations 8a and 25 that $X_{j,\infty}=\varepsilon_{j,\infty}=a_jX_{P,\infty}+b_j$ and all mole fractions are linear functions of X_P. In these cases the assumption that $D\sim T$ is therefore not needed for the explicit solution of equation 25. For a neutral species N ($a_N=0$), equation 25 then shows that $X_N=b_N=\varepsilon_N=$ constant. On the other hand, when burning occurs in an inert atmosphere $\varepsilon_N=0$, X_N is approximately an exponential function of $1/\sigma$, and at $\sigma=\infty$ there is relative diffusion of species N and the components evaporating from the droplet[13].

For cases in which $\mathscr{L}=1$, $\bar{c}_p$ is constant, and all X_js depend linearly upon X_P, by substituting equation 27 into equations 10 and 9 for $j=P$, we can deduce the qualitative behaviour of the temperature profile. If the resulting differential equations for ε_P and θ are expanded about the end points $\sigma=1$ and $\sigma=\infty$, then it is found that the dependence of T upon σ is approximately as illustrated in *Figure 2*. The critical adiabatic value of the final temperature T_{fa} is determined by the requirement that there is no thermal conduction of heat to the surrounding atmosphere, i.e. $\lim_{\sigma\to\infty}(\sigma^2\,\mathrm{d}\theta/\mathrm{d}\sigma)=0$. Since $X_{j,\infty}=\varepsilon_{j,\infty}$, equation 27 implies that T_{fa} is determined by the relation $Q(\varepsilon_{P,\infty}-\varepsilon_{P,l})=1-\theta_l+\alpha$, i.e.

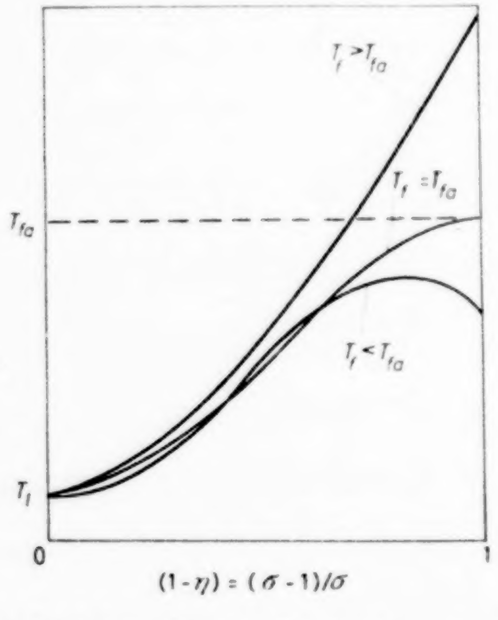

Figure 2. Temperature profiles when heat transfer to the surrounding atmosphere occurs

$$T_{fa}=T_l+(\varepsilon_{P,\infty}-\varepsilon_{P,l})(q/\bar{c}_p)-(\Delta l/\bar{c}_p) \qquad \ldots\ldots[28]$$

When Δl is small equation 28 shows that T_{fa} is very nearly the ordinary adiabatic flame temperature.

If $T_f=T_{fa}$, equations 27 and 25 show that all mole fractions are linear functions of the temperature, viz.

$$QX_j=Q\varepsilon_{j,l}+a_j(\theta-\theta_l+\alpha) \qquad j=1,2,\ldots,s \qquad \ldots\ldots[29]$$

It is seen from equation 29 that for adiabatic burning the assumption $\lambda=$constant is not needed to reduce the total number of differential equations to two. The result expressed by equation 29 also applies to one-dimensional flame problems with $\mathscr{L}=1$ if the heat conducted across the cold boundary is zero ($\alpha=0$)[11, 12].

(3) *Numerical results*

Numerical calculations have been performed with an electronic digital computing machine for a three-component system with a second-order reaction of the type $F+O\rightarrow 2P$ where F represents fuel, O denotes oxidizer, and P stands for products. An adiabatic arrangement with $M_i=M$, $D_{ij}=D\sim T^2$, $\lambda\sim T$, $\bar{c}_p=$ constant, $\mathscr{L}=1$, and no diffusion at infinity was considered. Equations 17 with $j=P$ and 18 were solved simultaneously for $\varepsilon_P(\sigma)$ and $\theta(\sigma)$ as described earlier. Equations 23 and 29 determine all variables in terms of ε_P and θ. Stoichiometric and oxidizer-rich systems were treated, in which case $\varepsilon_{F,f}=0$. Actually the problem is symmetrical in F and O. It was assumed that no liquid-phase reaction occurs and that $\varepsilon_{P,l}=0$. A fuel/oxidizer ratio can be defined as $\delta\equiv\varepsilon_{F,l}/\varepsilon_{O,l}\leqslant 1$, in which case the relations $\varepsilon_{F,l}=\delta/(\delta+1)$, $\varepsilon_{O,l}=1/(\delta+1)$, $\varepsilon_{O,f}=(1-\delta)/(\delta+1)$, and $\varepsilon_{P,f}=2\delta/(\delta+1)$ can be deduced from equations 2 and 23.

Table 1. Physical constants for numerical calculations

Quantity	*Value for non-stoichiometric case* ($\delta=0{\cdot}818$, $\epsilon_{P,f}=0{\cdot}9$)	*Value for stoichiometric case* ($\delta=1$, $\epsilon_{P,f}=1$)
B/M	$0{\cdot}834\times10^{16}$ cm^3/g.sec	$0{\cdot}834\times10^{16}$ cm^3/g.sec
$\bar{c}_p$	0·580 cal/g.°K	0·580 cal/g.°K
λ_f	5×10^{-4} cal/cm.sec.°K	5×10^{-4} cal/cm.sec.°K
ρ_f	$3{\cdot}12\times10^{-4}$ g/cm^3	$3{\cdot}04\times10^{-4}$ g/cm^3
Δl	380 cal/g	380 cal/g
q	1 000 cal/g	1 000 cal/g
T_l	387°K	387°K
T_f	1 283°K	1 457°K
θ_l	0·302	0·266
α	0·510	0·450

The numerical solutions were carried out for systems with the physical constants listed in *Table 1*. The variation of ε_P with θ was found to be similar to that for a one-dimensional laminar flame (see *Figure 3*). The location of the 'flame front', $r=r_c$, may be defined as the point at which $\varepsilon_P=\frac{1}{2}\varepsilon_{P,f}$ in which case it is found from *Figure 3* to vary from $r_c=1{\cdot}005\,r_l$ at $\theta_1=3{\cdot}9$ to $r_c=42\,r_l$ at $\theta_1=23{\cdot}4$ (see *Table 2*).

Table 2. Position σ_c at which the reaction is half complete, $\epsilon_P=\frac{1}{2}\epsilon_{P,f}$

δ	θ_1	σ_c
1·000	20·6	27
0·818	23·4	42
0·818	11·7	1·23
0·818	3·9	1·005

The dependence of m upon r_l derived from both analytical and numerical results is shown in *Figure 4*. From the slope of the numerical curve for large θ_1, it can be seen that $m \sim r_l^{1 \cdot 1}$, which is very nearly the variation

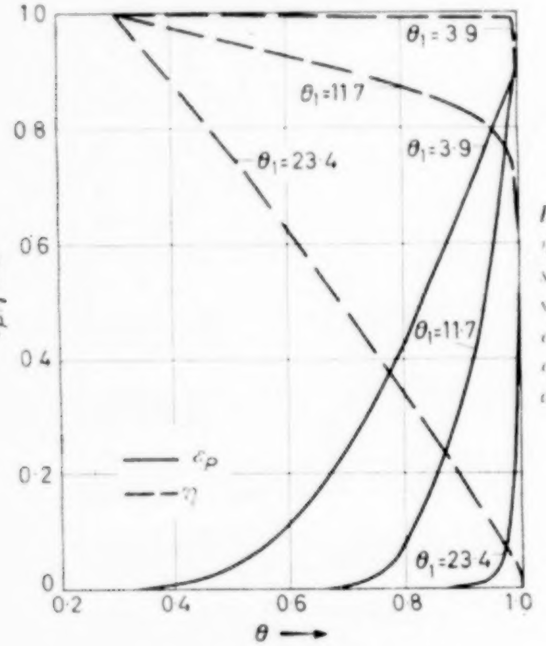

Figure 3. The flux fraction ϵ_p and $\eta = r_l/r$ as functions of the dimensionless temperature θ for non-stoichiometric mixtures with fuel/oxidizer ratio $\delta = 0·818$ ($\epsilon_{p,l} = 0·9$) at a droplet radius $r_l = 0·02$ cm and various activation temperatures

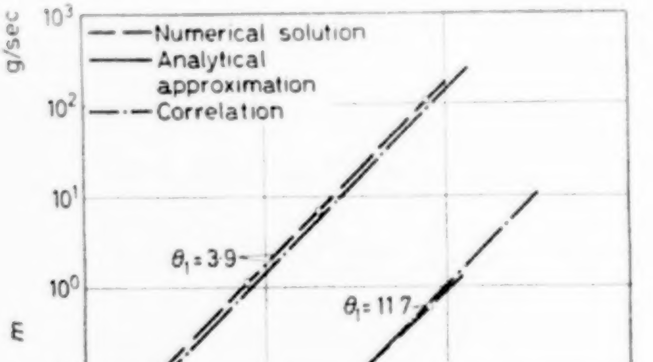

***Figure 4.** Mass flow rate m as a function of droplet radius r_l for non-stoichiometric mixtures with fuel/oxidizer ratio $\delta = 0·818$ ($\epsilon_{p,l} = 0·9$) and various activation temperatures*

$m \sim r_l$ predicted above. The average difference between the numerical and analytical results for the magnitude of m is less than 10 per cent for large θ_1. The large discrepancies occur only at large values of r_l where the second term in the curly brackets in equation 18 begins to become small invalidating the approximation used to obtain equation 19. For $\theta_1 = 11{\cdot}7$ and $\theta_1 = 3{\cdot}9$, in the range of values of r_l of practical interest the large activation energy approximation is no longer valid. The numerical results illustrated in *Figure 4* indicate that $m \sim r_l^2$ here as predicted by the reasoning presented above. It is also seen that m increases rapidly as θ_1 decreases at a given droplet radius for small activation energies.

The numerically obtained dependence of m upon r_l can be correlated quite well for θ_1 less than about 15 by the following method. If we assume that

$$(1/\sigma^1)[\alpha - Q(\varepsilon_P - \varepsilon_{P,l}) + \theta - \theta_l] \approx \alpha \qquad \ldots.[30]$$

then the RHS of equation 9 becomes independent of σ and ε_P. By using equation 29 for X_j, equation 9 with $j = P$ can now be integrated from $\varepsilon_P = 0$, $\theta = \theta_l$ to $\varepsilon_P = \varepsilon_{P,l}$, $\theta = 1$. For the present system the integration yields

$$\Lambda^{\star} = 2\alpha(1 - \theta_l + \alpha)/h \qquad \ldots.[31]$$

where the function h is defined by the equation

$$h \equiv \int_{\theta_l}^{1} e^{-\theta_1/\theta} \frac{1-\theta}{\theta}\left[1 - \varepsilon_{P,l} + \frac{\varepsilon_{P,l}(1-\theta)}{2(1-\theta_l+\alpha)}\right] d\theta \qquad \ldots.[32]$$

By performing the integration in equation 32 we obtain the expression

$$h = (1-\varepsilon_{P,l})\{(1+\theta_1)[-\mathrm{Ei}(-\theta_1)] - e^{-\theta_1} - (1+\theta_1)[-\mathrm{Ei}(-\theta_1/\theta_l)] + \theta_l e^{-\theta_1/\theta_l}\}$$
$$+ \frac{\varepsilon_{P,l}}{2(1-\theta_l+\alpha)}\{(1+2\theta_1+\theta_1^2/2)[-\mathrm{Ei}(-\theta_1)] - [(3+\theta_1)/2]e^{-\theta_1}$$
$$-(1+2\theta_1+\theta_1^2/2)[-\mathrm{Ei}(-\theta_1/\theta_l)] + \theta_l(2+\theta_1/2-\theta_l/2)e^{-\theta_1/\theta_l}\} \qquad \ldots.[33]$$

where $\mathrm{Ei}(x)$ is the exponential integral. Equation 31 for $\Lambda^{\star}$ is consistent with the relation $m \sim r_l^2$. It is seen from *Figure 4* that the average discrepancy between the numerical results and the values of m predicted by equation 31 is about 8 per cent. Since the function in equation 30 is nearly equal to $f(\varepsilon_P)$, *Figure 1* indicates that by equating this function to its value at the droplet surface we have caused a cancellation of the error in the integral at small and large values of ε_P in order to obtain a useful correlation of the burning rate for small activation energies.

COMPARISON WITH EXPERIMENT

The theory predicts that the functional dependence of the burning rate on droplet diameter is determined by θ_1. Overall activation energies for ethyl nitrate and similar compounds (ethyl nitrite, amyl nitrate, etc.) have been measured by B. P. MULLINS[16]. By an interpolation procedure the overall activation energy of propyl nitrate can be deduced from these data. It is thus found that, for adiabatic combustion [see equation 28], $T_{fa} = 1\,970°\mathrm{K}$, $\theta_1 = 6{\cdot}5$ and therefore $m \sim r_l^2$ for ethyl nitrate, while $T_{fa} = 800°\mathrm{K}$, $\theta_1 = 13{\cdot}7$ and therefore roughly $m \sim r_l^{1{\cdot}3}$ for propyl nitrate. For non-adiabatic burning with T_l in the range corresponding to the experiments of ref. 5, θ_1 varies from 15 to 26 for ethyl nitrate and from 13 to 22 for propyl nitrate. For most of these values of θ_1 the theory predicts that $m \sim r_l$, and, if no mass is added to the droplet, $(d_0^2 - d^2) \sim (t - t_0)$ for both ethyl nitrate and propyl nitrate.

The predictions in the preceding paragraph have been verified by experiments. M. BARRÈRE and H. MOUTET[5] suspended droplets on quartz fibres and measured the rate of decrease of droplet diameter during burning. It was observed that $(d_0^2 - d^2) \sim (t - t_0)$ for both ethyl nitrate and propyl nitrate. W. A. ROSSER[6] used a porous sphere apparatus in which r_l was held constant and the rate of flow of propellant into the sphere was measured. The results show that $m \sim r_l^2$ for ethyl nitrate as predicted from the theory for adiabatic systems.

Rosser also observed that $m \sim r_l^2$ for the hydrazine decomposition flame. This is in agreement with the theory provided use is made of the overall activation energy[17, 18] of 36 kcal/mole which leads to $\theta_1 \approx 12$ for the adiabatic case. Rosser's results seem to indicate that for a given fuel $m \sim r_l$ for sufficiently small spheres, while $m \sim r_l^2$ for large droplets as predicted above. The overall activation energy for hydrogen peroxide decomposition is about 45 kcal/mole for the homogeneous gas-phase reaction[19, 20] and the calculated value of θ_1 for adiabatic burning is 47·7 (see *Table 3*). Here $(d_0^2 - d^2) \sim (t - t_0)$ is unambiguously predicted by the analysis and agrees with experiment[5].

Table 3. Comparison of theoretical and experimental burning rates for the adiabatic combustion of hydrogen peroxide and propyl nitrate

Quantity	H_2O_2	$C_3H_7ONO_2$
λ_l *(cal/cm.sec.°K)*	$1{\cdot}0 \times 10^{-4}$	$1{\cdot}5 \times 10^{-4}$
ρ_l *(g/cm³)*	1·465	1·058
Δl *(cal/g)*	373	101
c_p *(cal/g.°K)*	0·40	0·42
T_l *(°K)*	425	384
T_f *(°K)*	472	803
T_1 *(°K)*	22 500	11 000
θ_1	47·7	13·7
θ_l	0·900	0·478
α	1·970	0·300
Theoretical K (cm²/sec)	$2{\cdot}6 \times 10^{-4}$	$0{\cdot}66 \times 10^{-2}$
Experimental[5] K (cm²/sec)	3×10^{-4}	$1{\cdot}3 \times 10^{-2}$

The burning rate constant, K, has been calculated for hydrogen peroxide and propyl nitrate by using equation 21. It is seen from *Table 3* that the theoretical adiabatic values differ from the corresponding experimental values for K by factors of 1·2 for hydrogen peroxide and 1·9 for propyl nitrate. The theoretical burning rates agree more closely with experiment for hydrogen peroxide, which has a large value of θ_1, than for propyl nitrate, which has a value of θ_1 very near the limit of validity of equation 19 (see *Table 3*). The largest sources of error in the theoretical calculations are the uncertainties in the values of λ and $\bar{c}_p$. Although these uncertainties are sufficiently large to cause the observed differences, the fact that the calculated value of K is always less than the observed value may be traceable to non-spherically-symmetrical natural convection effects which were neglected in the analysis and are important at atmospheric pressure for bipropellants[21-24].

Table 4. Data used in theoretical calculation of nitric acid amyl acetate monopropellant burning rate

ϕ	0·6	0·8	1·0	1·4	2·0
λ_l (*cal/cm.sec.°K*)	$1{\cdot}84\times10^{-1}$	$1{\cdot}84\times10^{-1}$	$1{\cdot}84\times10^{-1}$	$1{\cdot}84\times10^{-1}$	$1{\cdot}84\times10^{-1}$
ρ_l (*g/cm*^{3})	1·05	1·05	1·05	1·05	1·05
ΔI (*cal/g*)	140	140	140	140	140
c_p (*cal/g.°K*)	0·39	0·39	0·39	0·39	0·39
T_l (°*K*)	420	420	420	420	420
T_f (°*K*)	2 030	2 510	2 590	2 080	1 370
Theoretical					
K (*cm*^{2}/*sec*)	$1{\cdot}18\times10^{-2}$	$1{\cdot}23\times10^{-2}$	$1{\cdot}235\times10^{-2}$	$1{\cdot}185\times10^{-2}$	$1{\cdot}05\times10^{-2}$
Experimental[5]					
K (*cm*^{2}/*sec*)	$1{\cdot}37\times10^{-2}$	$1{\cdot}60\times10^{-2}$	$1{\cdot}74\times10^{-2}$	$1{\cdot}735\times10^{-2}$	$1{\cdot}47\times10^{-2}$

The burning rate as a function of equivalence ratio, ϕ, has been measured for droplets consisting of a mixture of amyl acetate as fuel and nitric acid as oxidizer[5]. The experimental results presented in *Table 4* are to be compared with the theoretical adiabatic burning rate which was calculated from the data in *Table 4*. The theoretical results are inaccurate here because ρ_l, ΔI and T_l are not accurately known for liquid propellant mixtures. It is also difficult to ascertain experimentally the mixture ratio because of the possibility of preferential evaporation of one component. The burning rates have maxima for $\phi \sim 1{\cdot}05$ theoretically and $\phi \sim 1{\cdot}15$ experimentally. Here again the magnitude of the theoretical burning rate is 20 to 30 per cent lower than the experimental value. In order to obtain a better comparison experiments which eliminate convective effects are needed.

The author is deeply indebted to Dr S. S. Penner for many helpful discussions relating to the formulation and solution of this problem. Thanks are also extended to Dr Barrère for some discussions concerning this problem and his experimental work during the summer of 1956. This work was supported, in part, by the Office of Ordnance Research, U.S. Army, under Contract No. DA 04–495–Ord–446 with the California Institute of Technology. A detailed discussion of the theory of burning of monopropellant droplets has been given by the author in Technical Report No. 21 of this contract, February 1958.

Pierce Hall, Harvard University,
Cambridge 38, Mass.

(Received September 1958)

REFERENCES

[1] von Kármán, T. and Penner, S. S. *Selected Combustion Problems*, pp 5–41. AGARD; Butterworths: London, 1954
[2] Goldsmith, M. and Penner, S. S. *Jet Propulsion*, 1954, **24**, 245
[3] Lorell, J. and Wise, H. *J. chem. Phys.* 1955, **23**, 1928
[4] Kiley, D. W. 'On the burning of single drops of monopropellants'. *Thesis*, California Institute of Technology: Pasadena, 1955
[5] Barrère, M. and Moutet, H. *Rech. aéro.* 1956, **9**, No. 50, 31
[6] Rosser, W. A. 'The decomposition burning of monopropellant drops; hydrazine, nitromethane, and ethyl nitrate'. *Progr. Rep. No. 20 305*. California Institute of Technology, Jet Propulsion Laboratory: Pasadena, 1957
[7] El Wakil, M. M., Uyehara, O. A. and Meyers, P. S. *Tech. Note Nat. Adv. Comm. Aero., Wash., No. 3179*, 1954
[8] See Sect. I E of ref. 1
[9] Hirschfelder, J. O., Curtiss, C. F. and Bird, R. B. *Molecular Theory of Gases and Liquids*, Section 7.4 e i. Wiley: New York, 1954
[10] See Sect. III B of ref. 1
[11] Williams, F. .A. 'Problems in combustion', Chap. II, Sect. C, *Ph.D. Thesis* California Institute of Technology: Pasadena, 1958
[12] See Chap. I, Sect. B 14 of ref. 11
[13] See Chap. I, Sect. B 16c of ref. 11
[14] See Sect. I G(b) of ref. 1
[15] Semenov, N. *Adv. phys. Sci., Moscow*, 1940, **24**, 433; English translation: *Tech. Memor. Nat. Adv. Comm. Aero., Wash., No. 1026*
[16] Mullins, B. P. *Fuel, Lond.* 1953, **32**, 327 and 451
[17] Gray, P. *et al. Sixth Symposium (International) on Combustion*, pp 255–263. Reinhold: New York, 1957
[18] Gilbert, M. 'The hydrazine flame'. *Progr. Rep. No. 20 318*. California Institute of Technology, Jet Propulsion Laboratory: Pasadena, 1957
[19] Schumb, W. C., Satterfield, C. N. and Wentworth, R. L. *Hydrogen Peroxide*. Reinhold: New York, 1955
[20] McLane, C. K. *J. chem. Phys.* 1949, **17**, 379
[21] Spalding, D. B. *Fourth Symposium (International) on Combustion*, pp 847–864. Williams and Wilkins: Baltimore, 1953
[22] Agoston, G. A., Wood, B. J. and Wise, H. 'Influence of pressure on the combustion of liquid spheres'. Presented at American Rocket Society Semi-Annual Meeting, San Francisco, June 1957
[23] Kumagai, S. *Jet Propulsion* 1956, **26**, 786
[24] Kumagai, S. and Isoda, H. *Sixth Symposium (International) on Combustion* pp 726–731. Reinhold: New York, 1957

Recent Developments and Notes

SHOCK TUBES

A comprehensive review of shock tubes and their applications has been published by the University of Toronto Institute of Aerophysics [*Rep. 12*, May 1958; Part I, 115 pp + 19 tables + 179 figs + 1 plate; Part II, 117 pp + 5 tables + 103 figs].

The first part, by I. I. GLASS, deals with the theory and performance of simple shock tubes. After consideration of flow in shock tubes of constant area, a treatment of continuous simple waves and shock waves in a perfect gas is given, including the use of the p/u plane and the treatment of wave interaction problems. A number of results for imperfect gases, relaxation and dissociation are given. The one-dimensional inviscid theory is compared with experimental results. The wave system due to diaphragm rupture and the effect of boundary-layer growth in the shock tube is discussed in this context.

The second part, by J. G. HALL, deals with the production of strong shock waves, the design of shock tubes, their applications and instrumentation. The production of strong shocks by heating the driver gas, double diaphragm technique and converging tubes is described. Theoretical and experimental data on the performance of these devices are supplied. Shock-wave attenuation is discussed briefly. Various applications of shock tubes are reviewed. Among these are hypersonic shock tunnels, gun tunnels, use of shock tubes for aerophysical research (wave interaction and high-temperature effects) and for combustion and chemical kinetics studies. The last sections are on the construction of shock tubes, including data on the selection of diaphragms and on instrumentation for pressure, density, temperature, wave speed and other measurements.

Many references are given in these reports and a large amount of information on ideal and real gas flow is presented in the form of numerous graphs and tables [from review by L. J. F. BROER, *Appl. mech. Rev.* 1959, **12**, 558].

COMBUSTION OSCILLATIONS

An experimental study of high-frequency combustion pressure oscillations has been described by M. J. ZUCROW and J. R. OSBORN [*Jet Propulsion*, 1958, **28**, 654]. Mixtures of hydrogen, methane, ethane, ethylene, or propane were made with air and injected into an instrumental rocket combustion chamber of 3·375 in. diameter and variable length, to 28 in. Nozzle size and shape and equivalence ratio were also varied, and their effects upon high-frequency combustion pressure oscillations were studied. Combustion-chamber pressure was varied in the range from 25 to 130 lb/in^2 absolute, peak-to-peak oscillation amplitudes being as large as 35 lb/in^2 in one case. Wave shape varied from a sinusoidal to a shock type. The longitudinal mode was found to occur only when the chamber length exceeded two or three diameters, at 45 lb/in^2 absolute. However, increase of pressure caused a shift from longitudinal to transverse modes, at a given chamber length. Nozzle shape affected wave shape. Instability regions are plotted as a function of equivalence ratio and pressure, for various fuels. A tentative theoretical interpretation of the results is offered, involving a type of detonation wave. L. Crocco has published some interesting comments on the theoretical aspects of this paper [*Jet Propulsion*, 1958, **28**, 843] [from review by R. Friedman, *Appl. mech. Rev.* 1959, **12**, 357].

CARBON FORMATION IN TURBOJET COMBUSTORS

E. R. Jonash, J. D. Wear and W. P. Cook, have described an investigation on the effect of fuel variables on carbon formation in turbojet-engine combustors [*Rep. Nat. Adv. Comm. Aero., Wash., No. 1352*, 1958].

Three empirical fuel factors, smoke-volatility index, smoke point, and NACA *K* factor were found to be satisfactorily correlated with combustor deposit and exhaust-gas smoke under one operating condition in a single tubular turbojet combustor and in several full-scale engines. None could be satisfactorily correlated at higher pressure and temperature in the single combustor. A number of organometallic compounds, commercial additives, and oxygen-bearing compounds markedly reduced deposits in the single combustor. The most effective additive, di*cyclo*pentadienyliron, reduced base-fuel deposits approximately 80 per cent. None of the additives affected exhaust-gas smoke.

DENSITY RATIO IN DETONATION WAVES

A new approach to the investigation of the mechanism of gaseous detonation is described by R. E. Duff, H. T. Knight and J. P. Rink [*Physics of Fluids*, 1958, **1**, 393] who set out to determine precisely the density ratio across detonation waves using a flash x-ray densitometer [cf. H. T. Knight and D. Venable, *Rev. sci. Instrum.* 1958, **29**, 92]. Measurements were made for two mixtures of acetylene, oxygen and krypton, one of hydrogen, oxygen and krypton, and two of cyanogen, oxygen and krypton. Detonation tube diameters and initial pressures were varied to permit extrapolation of the density ratios to infinite diameters and pressures. The values thus obtained are not in agreement with those calculated from detonation theory. For example, the mixture $0{\cdot}3\,C_2H_2+0{\cdot}3\,O_2+0{\cdot}4\,Kr$ gave an observed density ratio of 1·70 at infinite diameter while the tangent point on the equilibrium Hugoniot from the initial state corresponds to 1·79. The experimental results are regarded as being accurate to within one per cent [J. W. Givens, *Appl. mech. Rev.* 1959, **12**, 361].

INJECTION AND COMBUSTION OF LIQUID FUELS

Under this heading a note was published in an earlier issue of *Combustion and Flame* [1958, **2**, 307] with reference to a monograph on the *Injection and Combustion of Liquid Fuels*, prepared by the Battelle Memorial Institute for the Aeronautical Research Laboratory, Wright-Patterson Air Force Base, Ohio. This comprehensive guide to literature on fundamental research on liquid fuels combustion has now been reprinted in an enlarged form of 789 pages. The initial printing was announced as being available primarily to contractors conducting combustion research for the U.S.

Defense, Department, but copies of the second printing, designated as *Publication BP 131008*, may be obtained for $9. each from the Office of Technical Services, U.S. Department of Commerce, Washington 25, D.C.

PERGAMON INSTITUTE

Pergamon Institute, a non-profit foundation, was formed in Washington, D.C., in 1957 for the purpose of making available to English-speaking scientists the results of scientific, technological and medical research and development in the Soviet Union and other countries in the Soviet orbit. The President of the Board of Governors is Sir Robert Robinson, O.M., F.R.S. The Institute has offices in Oxford, London and Washington, D.C.

Several projects have already been started or are being planned by the Institute in association with and with the financial assistance of various government departments, learned societies and private organizations. These include: (*i*) a series of review volumes covering broad areas of Russian scientific, medical and technical progress, (*ii*) World Technical Press Digest based on the Express Information Service of the U.S.S.R. Academy of Sciences, (*iii*) Russian-English scientific and technical dictionaries, (*iv*) English editions of U.S.S.R. journals, (*v*) translations of important Russian books.

In addition to the above, a considerable number of Institute services are available to learned societies, government departments, trade associations and individual scientists. These include listing and abstracting of articles, bibliographical information, critical evaluation of Russian publications, provision of Russian books, journals and microfilms, translations, and Soviet patents. Full information on the services of the Pergamon Institute may be obtained from the Executive Director, Captain I. R. Maxwell, Headington Hill Hall, Oxford.

HIGHER TECHNOLOGICAL EDUCATION

The London and Home Counties Regional Advisory Council for Technological Education issues annually a *Bulletin of Special Courses in Higher Technology*. This is published in two parts, Part I, giving details of courses held in the autumn term, is issued in July, and Part II, containing information about courses held in the spring and summer terms is printed in December. An annual subscription of 6s secures one copy of Parts I and II, and application should be made to The Secretary, Regional Advisory Council, Tavistock House South, Tavistock Square, London, W.C.1.

The purpose of this *Bulletin* is to give publicity to special advanced courses held in the London and home counties region which do not regularly appear in college calendars or prospectuses as part of a grouped course or as subjects offered for endorsement on Higher National Certificates. They are usually part-time evening courses, but full-time courses which are specially arranged and are not of longer than three months duration are also included. Amongst courses concerned with combustion, flame, and power generation, the following are being held in the present term: Oil burning technology, at Borough Polytechnic; Gas turbines, at Enfield Technical College; (*i*) Gas dynamics of reactive propulsion, (*ii*) Gas-to-gas heat exchangers, (*iii*) The engineering design of nuclear power plant, at chamber length. Nozzle shape affected wave shape. Instability regions are plotted as a function of equivalence ratio and pressure, for various fuels. A tentative theoretical interpretation of the results is offered, involving a type of detonation wave. L. Crocco has published some interesting comments on the theoretical aspects of this paper [*Jet Propulsion*, 1958, **28**, 843] [from review by R. Friedman, *Appl. mech. Rev.* 1959, **12**, 357].

CARBON FORMATION IN TURBOJET COMBUSTORS

E. R. Jonash, J. D. Wear and W. P. Cook, have described an investigation on the effect of fuel variables on carbon formation in turbojet-engine combustors [*Rep. Nat. Adv. Comm. Aero., Wash., No. 1352*, 1958].

Three empirical fuel factors, smoke-volatility index, smoke point, and NACA *K* factor were found to be satisfactorily correlated with combustor deposit and exhaust-gas smoke under one operating condition in a single tubular turbojet combustor and in several full-scale engines. None could be satisfactorily correlated at higher pressure and temperature in the single combustor. A number of organometallic compounds, commercial additives, and oxygen-bearing compounds markedly reduced deposits in the single combustor. The most effective additive, di*cyclo*pentadienyliron, reduced base-fuel deposits approximately 80 per cent. None of the additives affected exhaust-gas smoke.

DENSITY RATIO IN DETONATION WAVES

A new approach to the investigation of the mechanism of gaseous detonation is described by R. E. Duff, H. T. Knight and J. P. Rink [*Physics of Fluids*, 1958, **1**, 393] who set out to determine precisely the density ratio across detonation waves using a flash x-ray densitometer [cf. H. T. Knight and D. Venable, *Rev. sci. Instrum.* 1958, **29**, 92]. Measurements were made for two mixtures of acetylene, oxygen and krypton, one of hydrogen, oxygen and krypton, and two of cyanogen, oxygen and krypton. Detonation tube diameters and initial pressures were varied to permit extrapolation of the density ratios to infinite diameters and pressures. The values thus obtained are not in agreement with those calculated from detonation theory. For example, the mixture $0{\cdot}3\,C_2H_2+0{\cdot}3\,O_2+0{\cdot}4\,Kr$ gave an observed density ratio of 1·70 at infinite diameter while the tangent point on the equilibrium Hugoniot from the initial state corresponds to 1·79. The experimental results are regarded as being accurate to within one per cent [J. W. Givens, *Appl. mech. Rev.* 1959, **12**, 361].

INJECTION AND COMBUSTION OF LIQUID FUELS

Under this heading a note was published in an earlier issue of *Combustion and Flame* [1958, **2**, 307] with reference to a monograph on the *Injection and Combustion of Liquid Fuels*, prepared by the Battelle Memorial Institute for the Aeronautical Research Laboratory, Wright-Patterson Air Force Base, Ohio. This comprehensive guide to literature on fundamental research on liquid fuels combustion has now been reprinted in an enlarged form of 789 pages. The initial printing was announced as being available primarily to contractors conducting combustion research for the U.S.

Defense Department, but copies of the second printing, designated as *Publication BP 131008*, may be obtained for $9. each from the Office of Technical Services, U.S. Department of Commerce, Washington 25, D.C.

PERGAMON INSTITUTE

Pergamon Institute, a non-profit foundation, was formed in Washington, D.C., in 1957 for the purpose of making available to English-speaking scientists the results of scientific, technological and medical research and development in the Soviet Union and other countries in the Soviet orbit. The President of the Board of Governors is Sir ROBERT ROBINSON, O.M., F.R.S. The Institute has offices in Oxford, London and Washington, D.C.

Several projects have already been started or are being planned by the Institute in association with and with the financial assistance of various government departments, learned societies and private organizations. These include: (*i*) a series of review volumes covering broad areas of Russian scientific, medical and technical progress, (*ii*) World Technical Press Digest based on the Express Information Service of the U.S.S.R. Academy of Sciences, (*iii*) Russian–English scientific and technical dictionaries, (*iv*) English editions of U.S.S.R. journals, (*v*) translations of important Russian books.

In addition to the above, a considerable number of Institute services are available to learned societies, government departments, trade associations and individual scientists. These include listing and abstracting of articles, bibliographical information, critical evaluation of Russian publications, provision of Russian books, journals and microfilms, translations, and Soviet patents. Full information on the services of the Pergamon Institute may be obtained from the Executive Director, Captain I. R. Maxwell, Headington Hill Hall, Oxford.

HIGHER TECHNOLOGICAL EDUCATION

The London and Home Counties Regional Advisory Council for Technological Education issues annually a *Bulletin of Special Courses in Higher Technology*. This is published in two parts, Part I, giving details of courses held in the autumn term, is issued in July, and Part II, containing information about courses held in the spring and summer terms is printed in December. An annual subscription of 6s secures one copy of Parts I and II, and application should be made to The Secretary, Regional Advisory Council, Tavistock House South, Tavistock Square, London, W.C.1.

The purpose of this *Bulletin* is to give publicity to special advanced courses held in the London and home counties region which do not regularly appear in college calendars or prospectuses as part of a grouped course or as subjects offered for endorsement on Higher National Certificates. They are usually part-time evening courses, but full-time courses which are specially arranged and are not of longer than three months duration are also included. Amongst courses concerned with combustion, flame, and power generation, the following are being held in the present term: Oil burning technology, at Borough Polytechnic; Gas turbines, at Enfield Technical College; (*i*) Gas dynamics of reactive propulsion, (*ii*) Gas-to-gas heat exchangers, (*iii*) The engineering design of nuclear power plant, at

Northampton College of Advanced Technology; Internal combustion engines, at Willesden Technical College; (*i*) Principles of flame structure, shape and stability in flowing gases, (*ii*) Flame spectroscopy, (*iii*) Optics of flames, (*iv*) Measurement of temperature in flames, (*v*) Analytical methods in combustion research, (*vi*) Infra-red spectroscopy, (*vii*) Modern methods of gas analysis, (*viii*) Explosion prevention and control, (*ix*) Fire prevention and control, (*x*) Combustion of atomized liquid fuels, at the Imperial College of Science and Technology.

NATIONAL FIRE PROTECTION CONFERENCE

Since the preliminary announcement [see *Combustion and Flame*, 1959, **3**, 403] of the National Fire Protection Conference to be held by the Fire Protection Association further particulars are now available. The Conference will be held at the Connaught Rooms, Kingsway, London, W.C.2, on 25 and 26 February 1960. The titles of the papers to be presented to the Conference are: Fire prevention in the motor car industry; Fire protection in retail department stores; Insurance and fire prevention; The Fire Brigade and fire prevention; The architect and fire prevention; The industrial fire prevention officer.

The fee for admission to the Conference, including a copy of the proceedings, is 50s. Applications should be made not later than 22 January 1960 to the Secretary, Fire Protection Association, 31–45 Gresham Street, London, E.C.2.

INDUSTRIAL SOLVENTS AND FLAMMABLE LIQUIDS

The Fire Protection Association has published a revised edition of its booklet *Industrial Solvents and Flammable Liquids* which first appeared in 1954. Intended primarily as a work of reference, the booklet is set out in tabular form and provides information on the physical properties of some 400 liquids, under the headings of: flash point, specific gravity, solubility in water, flammability limits, auto-ignition temperature, susceptibility to spontaneous heating, vapour density, melting point, boiling point, vapour pressure, suitable extinguishing agent.

The information on flash points and flammability limits has been extensively revised, while the alternative names of some liquids are now incorporated in the main table.

Copies of this booklet are obtainable from the Fire Protection Association, 31–45 Gresham Street, London, E.C.2. Price to non-Members 3*s*.

INSTRUMENTS EXHIBITION

An International Instruments, Electronics and Automation Exhibition, under the patronage of H.R.H. The Duke of Edinburgh, will be held at Olympia, London, in May 1960. It will be double the size of the last Exhibition held in 1958. The Grand Hall, the Extension and the National Hall will be occupied by more than 450 firms. Over 100 of these will represent a dozen foreign countries.

FIRST GAS TURBINE TANKER

The Shell tanker *Auris* of 12 000 tons deadweight, originally a motor ship, has now been fitted with gas turbine machinery and has successfully completed sea trials; she thus becomes the first tanker to be driven entirely by a gas turbine. The *Auris* was built in 1948. In 1951, a small experimental gas turbine was fitted which helped the main diesel engines to drive the ship. The success of the first turbine led to the present installation in which a much larger gas turbine is the only means of propulsion. The turbine of 5 500 h.p. was designed by the British Thomson-Houston Co. and was built by them and by Cammell Laird and Co. of Birkenhead.

The object of the *Auris* experiment was to find out whether gas turbines can be used with advantage in preference to steam turbines or diesel engines for driving merchant ships. During the trials gas oil was used as the fuel and it was found that the thermal economy of the present unit in *Auris* is about the same as a comparable steam turbine and at a disadvantage compared with a modern marine diesel engine.

Maintenance costs should be somewhat lower, but it is clear that this advantage could never be of sufficient extent to offset the high capital cost of a gas turbine unit of this particular design. Accordingly, it is not Shell's intention to repeat the installation of this type of machinery in any other ships, but the *Auris* will be run to gain additional experience with this type of machinery together with the transmission system incorporating a new means of going astern, which might well be applied to a conventional steam turbine power plant. It is, however, recognized that the gas turbine may still find a place in the commercial marine field, for example, it might prove to be eminently suitable for employment in methane carriers or possibly be teamed up with nuclear propulsion.

CONGRESS ON I.C.E.

The Congrès International des Machines à Combustion (CIMAC), Paris, was founded in 1950 with the object of promoting the international exchange of scientific and technical knowledge on internal combustion engines. The Congrès International is a federation of the national organizations of manufacturers of engines in eleven European countries, in the United States of America and in Japan. Meetings have been arranged in past years in Paris, Milan, The Hague and Zürich. The fifth international congress was held at Wiesbaden from 14 to 19 June last, and dealt with current problems of diesel engines and gas turbines up to 1 500 h.p. Thirty five papers were presented [*Engineer, Lond.* 1959, **208**, 119].

One of the papers, by J. F. ALCOCK and R. WATTS, of Ricardo and Co., Shoreham-by-Sea, dealt with the combustion process in high-speed diesel engines and described research on a special two-stroke engine, the valve-less cylinder head of which allowed almost complete freedom of combustion chamber design. Cylinder heads were fitted with transparent Perspex windows, a high-speed ciné-camera was used to record ignition and the propagation of flame, and indicator diagrams were taken simultaneously. So far two combustion systems have been used, the conventional four-spray direct injection with swirl, and the Ricardo 'Comet' swirl chamber.

It is said that the work has already shown that current views on diesel combustion require considerable modification. It was found, for instance, that the fuel jet strikes the walls and the resulting 'splash' can spread some distance along the wall, thus playing an important part in the fuel–air distribution. A substantial proportion of the spray appears to be vaporized before ignition. Ignition is said to occur in small, separate nuclei which later coalesce, and in direct-injection engines the point of initial ignition can vary considerably from cycle to cycle without noticeable effect on the engine performance or on the indicator diagram. The nuclei do not occur in the visible spray, but usually near it or in the 'wall splash'. In a divided-chamber engine ignition normally occurs just on the cell side of the throat, and flame spreads at about the same rate within the cell and through the throat into the main chamber. This is not in accord with the usually accepted view that precombustion takes place in the cell and is followed by expulsion of the burning gases into the cylinder.

GLASS TECHNOLOGY

The Society of Glass Technology has recently announced that from February 1960 its *Journal* will be published bi-monthly in two parts. These will be called: *(i) Glass Technology* and *(ii) Physics and Chemistry of Glasses*. The editor is Professor R. W. DOUGLAS.

Glass Technology will contain papers on, amongst other subjects, the design, operation and performance of furnaces and several contributions dealing with this subject are expected to be published in the first number.

In *Physics and Chemistry of Glasses* will be published reports of experimental and theoretical studies of, for example, electrical properties, infrared absorption and relaxation processes.

Further information on these publications may be obtained from The Editor and Honorary Secretary, Society of Glass Technology, 20 Hallam Gate Road, Sheffield, 10.

NEW ROCKET COMPONENT

At the recent inauguration of the headquarters of Atlantic Research Corporation, near Alexandria, Va, it was disclosed that its new propellant, arcite, contains aluminium mixed with polyvinyl chloride and ammonium perchlorate. The use of aluminium increases the boost velocity of rockets by 10 to 30 per cent and range or altitude by 20 to 60 per cent. The Polaris sea-to-air missile is driven by an aluminized propellant. About 20 per cent of aluminium will be required to ensure a reducing system with no risk of dissociation reactions [*Chem. Engng*, 1959, **66**, No. 16, 56].

FIRE RESEARCH

In *Fire Research 1958: Report of the Fire Research Board with the Report of the Director of Fire Research* [Department of Scientific and Industrial Research and Fire Offices' Committee: Her Majesty's Stationery Office: London, 1959] which has recently been issued, it is stated that whereas the open fire has for many years been regarded as the greatest domestic fire risk, it is not now the most hazardous. The newer types of heaters are even more prone to cause fire, electricity seven times and oil four times for an equivalent amount of useful heat. Detailed fire reports of electrical origin in the U.K. have been called for throughout the year and it is expected that these will point the way to halting the upward trend which must otherwise take place as the nation makes greater use of electricity.

During the year the new Models Laboratory at the Fire Research Station, Boreham Woods, Herts, was formally opened. This marks an important stage in the development of fire research. There are so many variables involved in a fire that a comprehensive study using full-scale experiments is not feasible and it is only by examining the factors controlling fires in models that a balanced approach to the problem of fire protection can be achieved. Modelling techniques will be extended to the extinction of fires.

In researches on ignition and growth of fire, it has been previously found possible from a consideration of their physical constants to forecast the circumstances under which heated vertical wooden surfaces will ignite provided the ignition time is relatively short. During the period under review attention has been given to two classes of problem which are not, as yet, generally amenable to a theoretical solution: the ignition of heated vertical surfaces surrounded by an enclosure, a practical application of which would be the ignition of the contents of a room by radiation entering a window, and the ignition of materials when the rate of heating is so low that ignition time is long. Examples of the latter would be ignition of dusts and wood near to steam pipes and the self-heating of stored materials.

In connection with the use of water sprays to extinguish fully developed fires in rooms, tests, in which nozzle pressures of 80 to 500 lb/in^2 and rates of flow of 5 to 25 gal/min were used, showed that only a small amount of water is necessary to control and extinguish this type of fire. The results suggest that such fires could be dealt with most effectively by an equipment providing a spray for control, whereby the major flames are subdued, and a jet for the extinction of the small remaining pockets of fire.

With regard to the extinction of fires in large buildings or basements, the possibility of achieving this by replacing the atmosphere by one incapable of supporting combustion is being investigated. For this purpose it is proposed to use jet engines to generate the inert gas at rates up to 50 000 ft^3/min, and a standard engine is now being modified to supply gas of about 8 per cent oxygen content for use in full-scale experiments.

FURNACE TEMPERATURE CONTROL

The United Steel Companies Ltd together with Winston Electronics Ltd have developed a very sensitive temperature controller for furnaces used for testing over long periods, maybe years, the creep characteristics of alloy steels. Temperatures up to 1 200°C can be maintained with an accuracy of ±0·25°C continuously over very long periods. A string of 56 controllers has been in continuous use for three years and the total time out of operation for maintenance has been only three hours.

The high standard of operation is regarded as being chiefly due to relieving the switching relay of any other function than its primary one. A platinum resistance thermometer serves as an a.c.-powered Wheatstone bridge, the pre-set arm being a potentiometer graded in 4 000 steps of 0·25°C. Out-of-balance voltage from the bridge is amplified and fed to a phase-sensitive bridge which gives a positive or negative output according to a rise or fall in temperature. This output is amplified and communicated to one section of the relay controlling the furnace relay to alter its current provided its signal is more positive than that of the other section of the furnace relay which is governed by a time-interval generator [*The New Scientist*, 1959, **6**, 232].

OPEN-HEARTH FURNACE FLAMES

With the use of liquid fuel for firing open-hearth furnaces, driving rates have been increased and this has meant substantial increase in fuel flow and flame momentum. In addition to the momentum determining the rate of combustion, the amount of recirculation of the waste gases at the higher values of thrust involved becomes appreciable, and the general furnace flow pattern is influenced. The magnitude and direction of the flame velocity at the bath surface will affect convective heat transfer, mixing of the slag and metal, and the oxidation rate. These considerations indicate the importance which must be attached to flow pattern and to the shape, length and velocity of flame in the open-hearth furnace fired by oil, and they form the subject of a paper presented by C. HOLDEN, of the Research and Development Department of The United Steel Companies Ltd, to the 'Conference on Major Developments in Liquid Fuel Firing 1948–59', organized by The Institute of Fuel and held in Torquay, 11 to 14 May 1959.

It is concluded that as regards the effect of flame position on furnace output, the optimum on one furnace was achieved by inclining the burner 25° to 28° to the bath. An examination has been made of the relationship

$$L_s = k(15M_o + M_s + M_r)/G^{1/2}$$

where L_s is the stoichiometric mixing length for a free flame assuming constant density, M_o, M_s and M_r are the mass flows of oil, steam and recirculating gases respectively, G is jet momentum, and k is a constant. Using results obtained on a model it is found that this relationship holds over a fairly wide range. On applying this formula to the furnace it is deduced that at high levels of momentum a change in momentum has very little effect on the flame length.

W. A. KIRKBY

IN MEMORIAM

It is with profound sorrow that we note the death on 29 July of Dr JAMES STODDART WATSON, of the National Research Council of Canada. For the past three years Dr WATSON had served as Chairman of the Canadian Section of The Combustion Institute. Under his leadership, the Section has played an increasingly important part in the work of the Institute. He will be sorely missed by those associated with him in Institute affairs.

FUEL

Readers of *Combustion and Flame* may like to know that *Notes* in the October issue of *Fuel* dealt with:

Use of liquid fuel in the gas turbine
Oil-fired boiler plants

Letters to the Editors

Letters to the Editors on points of scientific interest related to combustion and flames are invited. The Editors do not hold themselves responsible for opinions expressed in correspondence. Anonymous contributions cannot be accepted.

Experimental Demonstration of the Existence of Two Flame Speeds

A RECENT theory[1] of inflammability limits predicts the existence of two different burning velocities for a given fuel/air ratio, the higher value normally being the stable one. The use of a porous flat-flame burner[2] with heat extraction makes it possible to stabilize flames with the lower burning velocity as well; the plot of burning velocity S_u versus the heat extracted Q reveals this feature.

This was first found experimentally for propane–air at reduced pressure by J. P. BOTHA[3], on a porous flat-flame burner. However, his results for atmospheric pressure did not show a similar effect. Some experiments with the same type of burner were conducted to determine whether the prediction of the theory still holds true at atmospheric pressure and for other combustible mixtures.

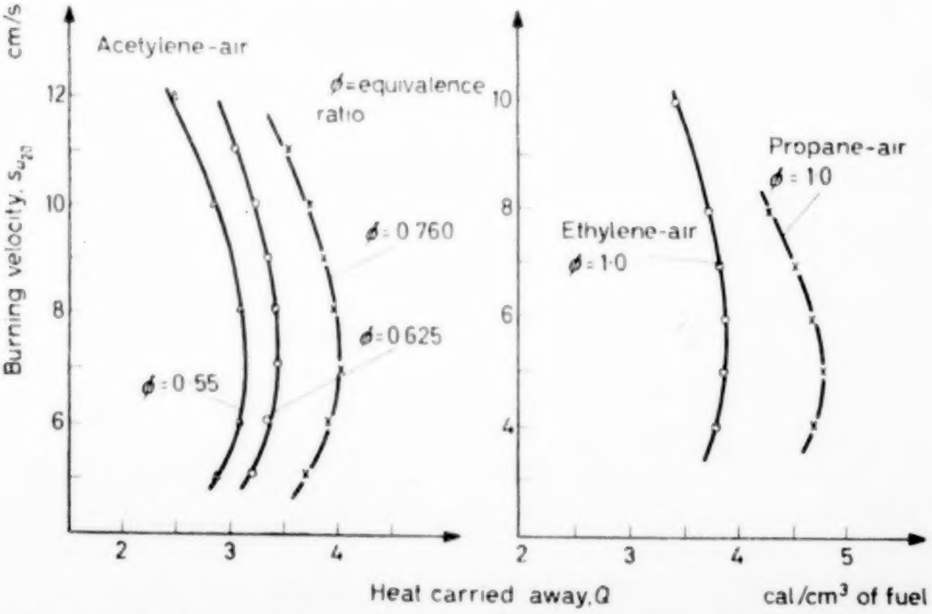

Figure 1. Experimental determination of critical velocity with acetylene–air on 1 in. diameter burner

Figure 2. Critical velocity, with ethylene–air and propane–air mixtures

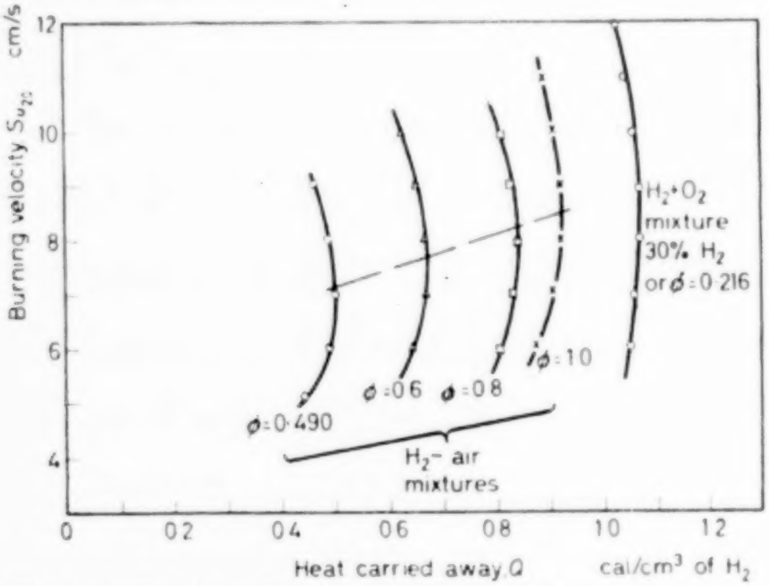

Figure 3. Burning velocity as a function of heat carried away (hydrogen–air and hydrogen–oxygen mixtures)

The results of the present investigation are given in *Figures 1, 2* and *3*. During the experiments a 1 in. diameter burner was used as compared with the 2 in. diameter burner used by Botha. It can be seen that there exists a maximum value of Q for each gas mixture at which the two burning velocities coincide (critical burning velocity S_{u_c}); either decrease or increase of S_u is accompanied by a decrease of Q. However, as it was not possible to stabilize velocities lower than 4 cm/s, the bottom portion of the curve could not be wholly determined.

It is worth while to note that S_{u_c} for propane–air is about 4·9 cm/s which is very close to the value for the flame speed at the inflammability limit reported by A. C. EGERTON and S. K. THABET for a different type of flat-flame burner[4].

It was considered possible that the reduction of Q at low values of S_u was brought about by diffusion of air from the surroundings. Diffusion was therefore prevented by provision of a cylindrical mica screen, fitting closely over the top of the burner. This measure resulted in an increase in Q at low values of S_u (compare *Figures 2* and *5*) but did not alter the trend of the curve.

We therefore conclude that a combustible mixture of fixed equivalence ratio, pressure and initial enthalpy (determined by Q) is capable of supporting a one-dimensional laminar flame of two different flame speeds, as is predicted by the theory.

The theory also predicts that the value of S_u for maximum Q should increase with the volumetric rate of radiative heat loss from the gases. *Figure 3* confirms this trend.

Since it is not easy to vary the radiative properties of the combustion gases in a known manner, the influence of conductive heat loss to a downstream cooled plug was investigated experimentally. The apparatus is shown in *Figure 4*(a).

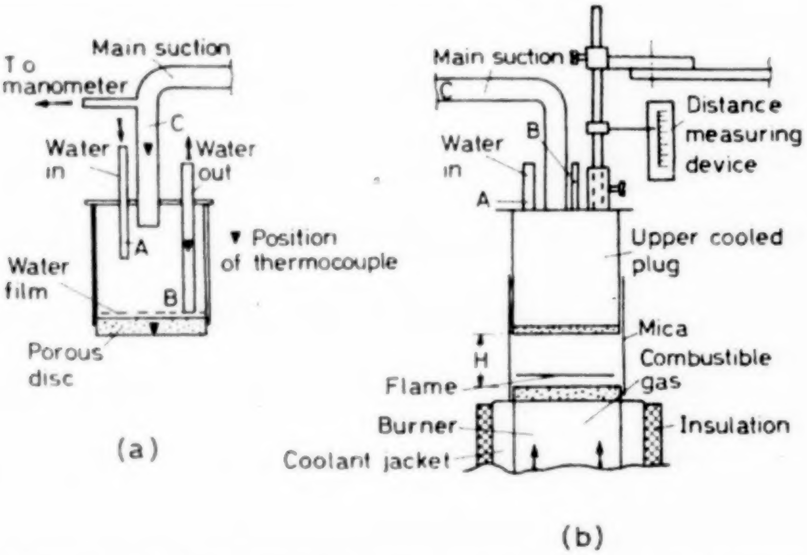
To manometer
Main suction
C
Water in
Water out
A
B
Water film
Porous disc
▼ Position of thermocouple
(a)
Main suction
C
B
Water in
A
Distance measuring device
Upper cooled plug
Mica
H
Combustible gas
Flame
Burner
Insulation
Coolant jacket
(b)

Figure 4. (a) Construction of upper cooled plug (b) 1 in. diameter burner with upper cooled plug

It consists of a sintered porous disc, of the same material as the burner, soldered to a cylindrical metal tube about one inch long. The cooling of the plug is achieved by a thin layer of water on top of the disc, supplied by a small diameter pipe A and constantly sucked away by a water filter pump through B. Another more powerful water filter pump was used to suck the product gases through the porous plug and through pipe C.

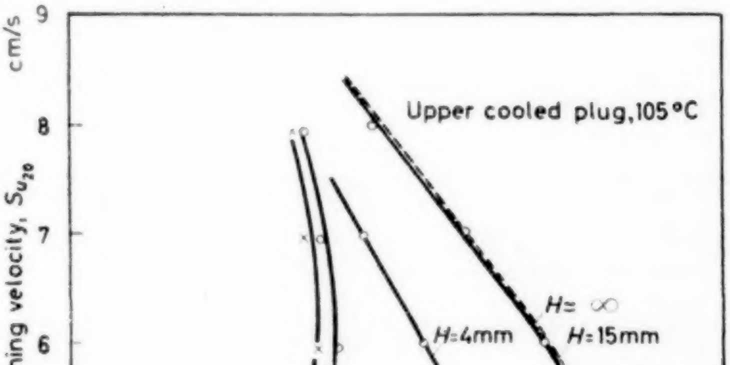

Figure 5. Effect of increased heat losses on critical burning velocity

With this arrangement the one-dimensional flow character of the flame was not impaired by the presence of the cooled plug [see *Figure 4*(b)] and also the plug temperature could be maintained at a desired value. The diffusion of the atmospheric air into the combustion zone was prevented by the use of mica. The pressure inside the mica was observed by means of a Chattock gauge and maintained equal to atmospheric pressure by varying the suction rate. The distance of the upper cooled plug from the lower one could be varied.

In *Figure 5*, the burning velocities S_u are plotted against Q, for fixed heights of the upper cooled plug, for propane air and acetylene air mixtures. It appears that an increase in downstream heat losses (reduced plate separation) reduces Q (raises initial enthalpy) for a given flame speed. The presence of the maximum Q value for each curve is clearly shown.

Although the results are qualitatively in accord with the theory, no quantitative comparison can be made, since the boundary conditions of the theory differ somewhat from those of the experimental arrangement. The appropriate adjustments to the theory are currently being made: the equations are being solved by digital computer.

The above work has been supported by the National Engineering Laboratory, East Kilbride. Permission for publication has been given by the Director.

Department of Mechanical Engineering,
Imperial College of Science and Technology

D. B. Spalding
V. S. Yumlu

(*Received June 1959*)

REFERENCES

[1] Spalding, D. B. *Proc. Roy. Soc. A*, 1957, **240**, 83
[2] Botha, J. P. and Spalding, D. B. *Proc. Roy. Soc. A*, 1954, **225**, 71
[3] Botha, J. P. *Ph.D. Thesis*, University of Cambridge, 1956
[4] Egerton, A. C. and Thabet, S. K. *Proc. Roy. Soc. A*, 1952, **211**, 445

A 'One-dimensional' Pulverized Fuel Flame with Controlled Mixing

THE complexity of the combustion mechanism of flames is greatly increased by their aerodynamic flow pattern. The jet pattern involves the variation of all important characteristics, as e.g. flow velocities, concentrations, temperatures, etc. in any cross section at right angles to the axis of the flame, and makes a better understanding of the fundamentals of combustion mechanisms difficult.

The present note describes an attempt to obtain an experimental pulverized fuel flame of simplified pattern—a so called 'One-dimensional' flame*—in which the characteristics of the flame and the histories of fuel particles vary in one dimension only: along the flame. The mixing of the secondary air with the flame is controllable in this experimental furnace so that the secondary air can be mixed in at various points along the flame, in contrast to jet flames, where the mixing cannot be controlled directly; it is governed by the laws of entrainment. Also, effects of recirculation in jet flames can be studied under controlled conditions on the experimental furnace by the deliberate introduction of hot combustion products into the primary air–fuel mixture before its ignition.

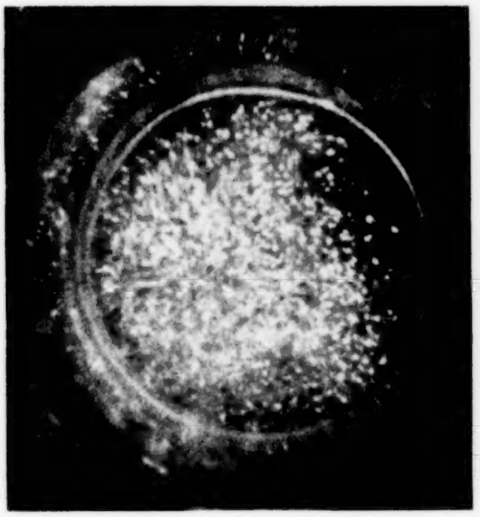

Figure 1

Figure 2

The assumptions made in connection with the experimental 'One-dimensional' flame were as follows:

(*a*) The velocity profile of the primary mixture is flat and the concentration of the dust cloud is uniform in order to obtain a flat flame front.

(*b*) Mixing both of hot combustion products in the pre-ignition zone and secondary air in the flame is instantaneous so that time for macro mixing can be neglected compared with time for reaction. (Reaction is taken to include micro mixing and surface diffusion as well as chemical reaction.)

---

*Strictly speaking it should be called a 'one-dimensional' turbulent flame with controlled mixing of secondary air and adiabatic combustion products.

(*c*) As a result of assumptions (*a*) and (*b*) the history of coal particles is independent of place in any cross section of the flame and varies only in the length of the furnace, i.e. along the flame.

(*d*) The reaction is adiabatic. (Later on a deliberate controlled heat removal along the flame will be introduced.)

In order to obtain the flat velocity profile and the uniform concentration of the primary mixture, water model experiments were carried out and a 'one-dimensional' burner was designed. The burner—a cooled truncated cone of 5° half angle—sits on the top of the vertical furnace. The primary jet which transports the pulverized fuel, is directed upwards in the cone and the jet bouncing on to the top plate of the cone produces there highly turbulent conditions and good mixing. The flow then spreads out following the walls of this diffuser and approaches the flame front in uniform concentration and with a flat, turbulent velocity profile. Photographs taken of

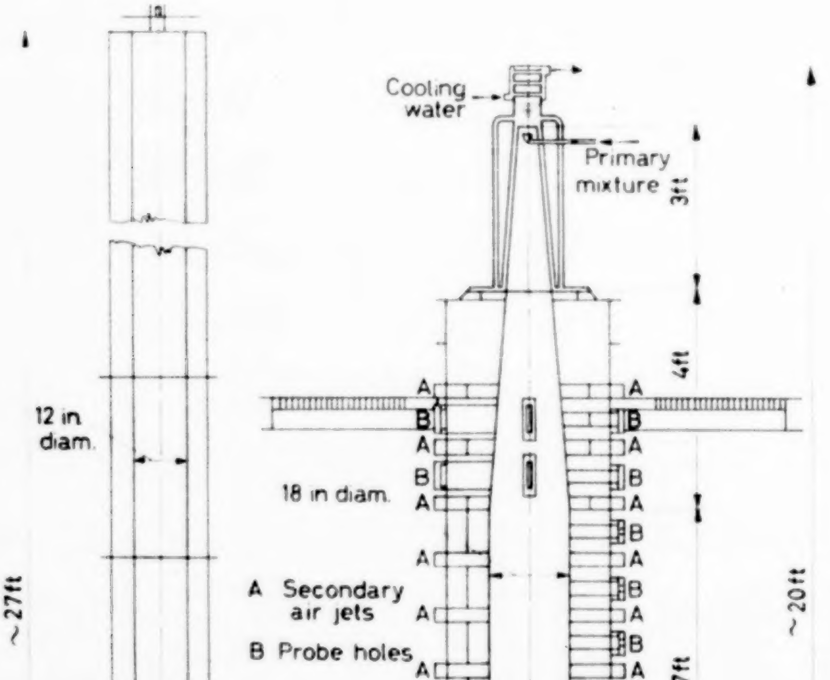

Figure 3

the flow pattern in the water model can be seen in *Figures 1* and *2*. These were taken by using the slit light technique and the tracers are <2 mm polystyrene spheres.

The furnace is cylindrical, of 18 in. internal diameter, 20 ft high, with 9 in. thick insulation brick walls. The top section of the furnace joins the burner with a 4 ft high conical part. The furnace consists of rings, which contain alternately arrays of air nozzles and sampling holes. *Figure 3* shows the diagrammatic arrangement.

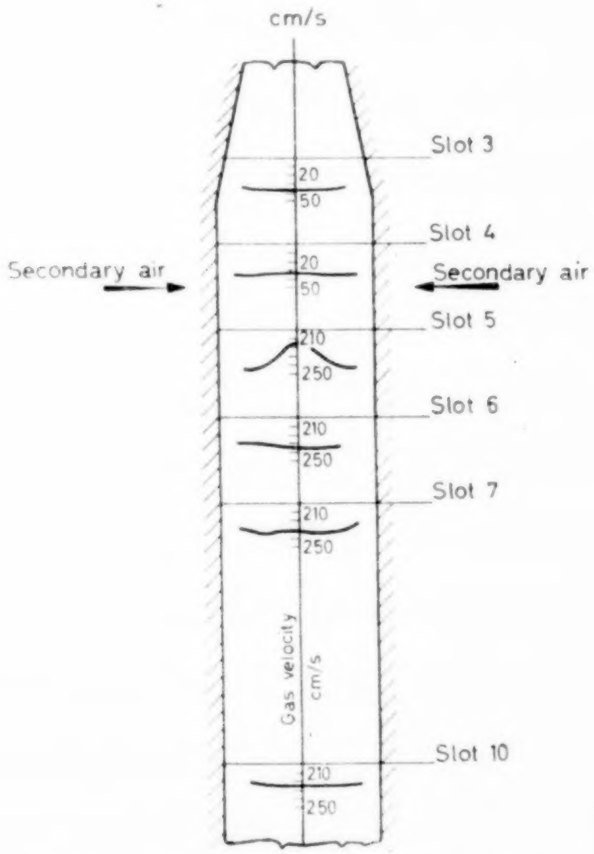

Figure 4. Calculated velocity traverses in the flame

The first experiments were carried out while burning a South Wales anthracite (ash: 3 per cent, volatile: 6 per cent). Fineness and size distribution of the pulverized coal: 80 per cent < 60 microns and 99·6 per cent <240 microns. Coal input: 40 lb/h. Carbon dioxide of the waste gases at the end of the 9 ft long flame: 13 per cent. Primary/secondary air ratio: 1/7. Temperature of combustion air: 21°C.

Because of the low flow velocities in the flame, suction pyrometer and gas composition traverses were taken and gas velocities were calculated instead of direct velocity measurements (*Figure 4*). These traverses show also the rapidity of mixing of the secondary air. The suction pyrometer traverses taken at various points along the flame are plotted in *Figure 5* (gas temperature versus width of the furnace). The secondary air, which amounted to 83 per cent of the cold combustion air, was introduced between slots 4 and 5 (see *Figure 5*).

These experimental results seem to prove the validity of our assumptions inasmuch as the flame front is flat, suction pyrometer traverses in the ignited primary mixture show a flat temperature, and hence velocity profile (see *Figure 5*, slots 3 and 4), and the macro mixing is sufficiently rapid (traverses taken at slots 5 and 6).

CONCLUSION

Preliminary experiments on a 'one-dimensional' pulverized fuel flame indicate that assumptions stated in connection with velocity profiles, concentrations and mixing in the flame are applicable, and show that an experimental 'one-dimensional' pulverized fuel flame can be obtained. Investigations on the combustion mechanism of this flame are in progress and results will be reported later.

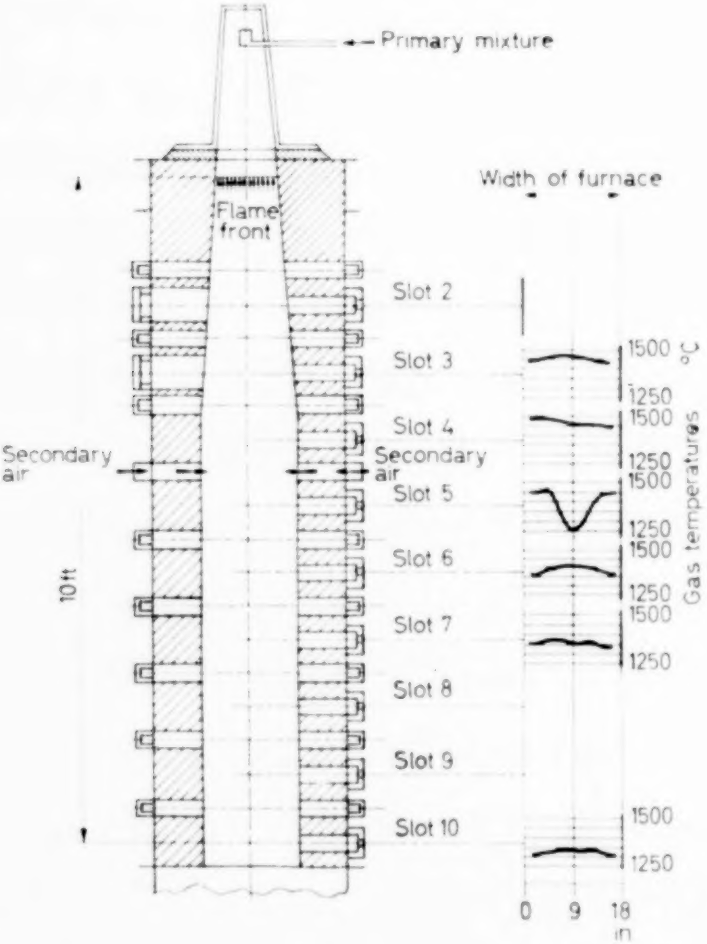
Primary mixture
Width of furnace
Flame front
Slot 2
Slot 3
Slot 4
Secondary air
Secondary air
Slot 5
Slot 6
Slot 7
Slot 8
Slot 9
Slot 10
10ft
1500
1250
1500
1250
1500
1250
1500
1250
1500
1250
1500
1250
°C
Gas temperatures
0
9
18
in

Figure 5

We are most grateful to the Electricity Supply Research Council for permission to publish this note.

J. M. Beér
M. W. Thring
R. H. Essenhigh

Department of Fuel Technology,
University of Sheffield

(Received September 1959)

Classified Contents

Addition of air in stages to a perfectly stirred reactor, 125
Afterburner combustion, effect of combustion length on, 339
Ammonium nitrate, a model describing combustion of solid composite propellants containing, 301
Ammonium nitrate propellants, application of a thermal layer mechanism to, 285

Blockage effects in bluff-body flame stabilization, 319
Bluff-body flame stabilization: blockage effects, 319
Burning velocity of hydrogen–air mixtures and mixtures of some hydrocarbons with air, 495
Burning velocities of mixtures of hydrogen, carbon monoxide and methane with air, 511

Carbon monoxide, excess radical concentrations and the disappearance of, in flame gases from some lean flames, 49
 radiation from explosion flames of, 169
Carbon monoxide–hydrogen–air flames, source of the continuum in, 39
Combustion Institute interests, 265
Comparative study of flame propagation in compounds containing nitrogen oxides, 187
Considerations pertaining to spherical-vessel combustion, 437
Cooperative mechanism in the ignition of dust dispersions, 467

Determination of the burning velocity of a gas mixture, modified analysis for the, in a spherical constant volume combustion vessel, 201
Detonation, effect of external factors on formation of, in saturated knallgas–steam mixtures, 481
Detonation overpressures in saturated knallgas steam mixtures, 157
Deviation from chemical equilibrium in gas flow, 273
Diffusion flame, effect of the electric field upon the spectra of the hydrocarbon, 277
Diverging reactor, heterogeneous burning in, 355
Dust dispersions, cooperative mechanism in ignition of, 467

Effect of combustor length on afterburner combustion, 339
Effect of the electric field upon the spectra of the hydrocarbon diffusion flame, 277
Effect of external factors on formation of detonation in saturated knallgas–steam mixtures, 481
Ethylene–air flames, examination of reaction rate laws in lean, 229
Examination of reaction rate laws in lean ethylene–air flames, 229
Excess radical concentrations and the disappearance of carbon monoxide in flame gases from some lean flames, 49
Existence of steady state flames, 447
Experimental demonstration of the existence of two flame speeds, 553

Factors affecting the mixing of gas and air, model investigations into, in coke oven flues, 97
Fast flames, quenching diameters of some, at low pressures, 453
Flame propagation, theory of, 61
— through kerosine foams, 347
Flame quenching in converging rectangular channels, 477
Flame with controlled mixing, one-dimensional pulverized fuel, 557
Furnace flames, similarity criteria for the study of, by means of cold models, 373
Further measurements of turbulence intensity in flame zones, 459

Gaseous nitric acid–hydrocarbon flames, 525

Heterogeneous burning in a diverging reactor, 355
*cyclo*Hexane, low-temperature vapour-phase oxidation of, 75

Hydrocarbon products from rich hydrocarbon flames, 133
Hydrogen air mixtures, burning velocity of, 495, 503, 511

Inductive break sparks of high incendive power, 131
Influence of small quantities of hydrogen and hydrogen compounds on the burning velocity of carbon monoxide-air flames, 503

Kerosine foams, flame propagation through, 347

Limits of the eigenvalue of the laminar flame equation in terms of the reaction rate-temperature centroid, 389
Low-temperature vapour-phase oxidation of *cyclo*hexane, 75

Magnesium sodium nitrate Laminac system, pre-ignition and ignition reactions of the propagatively reacting, 3
Mean temperature of burnt gases, 419
Model describing combustion of solid composite propellants containing ammonium nitrate, 301
Model investigations into the factors affecting the mixing of gas and air in coke oven flues, 97
Modified analysis for the determination of the burning velocity of a gas mixture in a spherical constant volume combustion vessel, 201
Molecular spectra arising from combustion processes, transition probability parameters of, 13, 276
Monopropellant droplets, theory of the burning of, 529

Nitrogen oxides, comparative study of flame propagation in compounds containing, 187
Notes on gaseous nitric acid-hydrocarbon flames, 525

One-dimensional pulverized fuel flame with controlled mixing, 556
Optical flame structure studies: examination of reaction rate laws in lean ethylene-air flames, 229

Perchloryl fluoride flames, studies of, 147
Pre-ignition and ignition reactions of the propagatively reacting system magnesium sodium nitrate Laminac, 3
Propane as an engine fuel, studies of autoignition and knock with, 421

Quenching diameters of some fast flames at low pressures, 453
Quenching, flame, in converging rectangular channels, 477

Radiation from explosion flames of carbon monoxide, 169
Recent developments and notes, 105, 254, 398, 545

Saturated knallgas steam mixtures, detonation overpressures in, 157
— effect of external factors on formation of detonation in, 481
Similarity criteria for the study of furnace flames by means of cold models, 373
Source of the continuum in carbon monoxide hydrogen air flames, 39
Sparks, inductive break, of high incendive power, 131
Spherical-vessel combustion, considerations pertaining to, 437
Spray combustion theory, 215
Stirred reactor, addition of air in stages to a perfectly, 125
Studies of autoignition and knock with propane as an engine fuel, 421
Studies of perchloryl fluoride flames, 147

Theory of flame propagation, 61
Theory of the burning of monopropellant droplets, 529
Theory, spray combustion, 215
Thermal layer mechanism of combustion of solid composite propellants: application to ammonium nitrate propellants, 286
Transition probability parameters of molecular spectra arising from combustion processes, 13, 276
Turbulence intensity, further measurements of, in flame zones, 459
Two flame speeds, experimental demonstration of the existence of, 553

Author Index

Acton Taylor, R. A.: review of *The Kinetics of Chemical Reactions in Gases*, 416

Adams, G. K.: review of *The Science of High Explosives*, 122

Adler, J.: The limits of the eigenvalue of the laminar flame equation in terms of the reaction rate–temperature centroid, 389

Adler, L. B. and Luker, J. A.: Detonation overpressures in saturated knallgas–steam mixtures, 157

— Hobaica, E. C. and Luker, J. A.: The effect of external factors on the formation of detonation in saturated knallgas–steam mixtures, 481

Allen, D. H., Garner, F. H., Long, R. and Todd, J. R.: The low-temperature vapour-phase oxidation of *cyclo*hexane, 75

Anagnostou, Evelyn and Potter, A. E., Jr: Quenching diameters of some fast flames at low pressures, 453

Andersen, W. H., Bills, K. W., Mishuck, E., Moe, G. and Schultz, R. D.: A model describing combustion of solid composite propellants containing ammonium nitrate, 301

Aroeste, H.: *See* Rudin, M. and Aroeste, H.

Barenblatt, G. I.: *See* Zeldovich, J. B. and Barenblatt, G. I.

Bartkowiak, A., Lambiris, S. and Zabetakis, M. G.: Flame propagation through kerosine foams, 347

Beér, J. M., Thring, M. W. and Essenhigh, R. H.: A 'one-dimensional' pulverized fuel flame with controlled mixing, 556

Berlad, A. L. and Yang, C. H.: On the existence of steady state flames, 447

— Rowe, R. D. and Yang, C. H.: Flame quenching in converging rectangular channels, 477

Berz, I.: On inductive break sparks of high incendive power, 131

Bills, K. W.: *See* Andersen, W. H., Bills, K. W., Mishuck, E., Moe, G. and Schultz, R. D.

Cassel, H. M. and Liebman, I.: The cooperative mechanism in the ignition of dust dispersions, 467

Chaiken, R. F.: A thermal layer mechanism of combustion of solid composite propellants: application to ammonium nitrate propellants, 285

Cook, E. B.: *See* Grumer, J., Cook, E. B. and Kubala, T. A.

de Jaegere, S. and van Tiggelen, A.: Comparative study of flame propagation in compounds containing nitrogen oxides, 187

Eckel, E. F.: *See* Williams, F. A., Penner, S. S., Gill, G. and Eckel, E. F.

Egerton, Sir Alfred: Editorial, 1

Essenhigh, R. H.: *See* Beér, J. M., Thring, M. W. and Essenhigh, R. H.

Fraser, P. A.: *See* Nicholls, R. W., Fraser, P. A. and Jarmain, W. R.

Garner, F. H.: *See* Allen, D. H., Garner, F. H., Long, R. and Todd, J. R.

Gaydon, A. G.: review of *A Dictionary of Named Effects and Laws in Chemistry, Physics and Mathematics*, 123

— review of *Seventh Symposium (International) on Combustion*, 417

Gill, G.: *See* Williams, F. A., Penner, S. S., Gill, G. and Eckel, E. F.

Gordon, Saul: *See* Hogan, Virginia D. and Gordon, Saul

Grumer, J., Cook, E. B. and Kubala, T. A.: Considerations pertaining to spherical-vessel combustion, 437

Hobaica, S. C.: *See* Adler, L. B., Hobaica, E. C. and Luker, J. A.

Hogan, Virginia D. and Gordon, Saul: Pre-ignition and ignition reactions of the propagatively reacting system magnesium–sodium nitrate–Laminac, 3

Hulse, C.: *See* Jayaraman, V., Hulse, C. and Thring, M. W.

Jarmain, W. R.: *See* Nicholls, R. W., Fraser, P. A. and Jarmain, W. R.

Jayaraman, V., Hulse, C. and Thring, M. W.: Model investigations into the factors affecting the mixing of gas and air in coke oven flues, 97

Kaskan, W. E.: The source of the continuum in carbon monoxide hydrogen air flames, 39

— Excess radical concentrations and the disappearance of carbon monoxide in flame gases from some lean flames, 49

Kirkby, W. A.: Recent developments and notes, 105, 254, 398, 545

Kubala, T. A.: *See* Grumer, J., Cook, E. B. and Kubala, T. A.

Kydd, P. H.: Hydrocarbon products from rich hydrocarbon flames, 133

Lambiris, S.: *See* Bartkowiak, A., Lambiris, S. and Zabetakis, M. G.

Leah, A. Smeeton and Watson, H.: Radiation from explosion flames of carbon monoxide, 169

Levy, A. and Weinberg, F. J.: Optical flame structure studies: examination of the reaction rate laws in lean ethylene air flames, 229

Liebman, I.: *See* Cassel, H. M. and Liebman, I.

Lloyd, P.: review of *Aircraft and Missile Propulsion*, Vol. II: *The Gas Turbine Power Plant, Turboprop, Turbojet, Ramjet and Rocket Engines*, 271

Lodwig, R. M. and Margrave, J. L.: Studies of perchloryl fluoride flames, 147

Long, R.: *See* Allen, D. H., Garner, F. H., Long, R. and Todd, J. R.

Luker, J. A.: *See* Adler, L. B. and Luker, J. A.

— *See* Adler, L. B., Hobaica, E. C. and Luker, J. A.

Margrave, J. L.: *See* Lodwig, R. M. and Margrave, J. L.

Masdin, E. G.: *See* Thring, M. W. and Masdin, E. G.

Mertens, J. and Potter, R. L.: Notes on gaseous nitric acid–hydrocarbon flames, 525

Minkoff, G. J.: review of *Gas Chromatography 1958*, 271

— review of *Analytical Chemistry—Some New Techniques*, 416

Mishuck, E.: *See* Andersen, W. H., Bills, K. W., Mishuck, E., Moe, G. and Schultz, R. D.

Moe, G.: *See* Andersen, W. H., Bills, K. W., Mishuck, E., Moe, G. and Schultz, R. D.

Moore, N. P. W. and Roy, B. N.: Studies of autoignition and knock with propane as an engine fuel, 421

Nakamura, J.: Effect of the electric field upon the spectra of the hydrocarbon diffusion flame, 277

Nicholls, R. W., Fraser, P. A. and Jarmain, W. R.: Transition probability parameters of molecular spectra arising from combustion processes, 13, 276

O'Donovan, K. H. and Rallis, C. J.: A modified analysis for the determination of the burning velocity of a gas mixture in a spherical constant volume combustion vessel, 201

Penner, S. S.: *See* Williams, F. A., Penner, S. S., Gill, G. and Eckel, E. F.

Potter, A. E., Jr: *See* Anagnostou, Evelyn and Potter, A. E., Jr

Potter, R. L.: *See* Mertens, J. and Potter, R. L.

Railly, J. W.: review of *Axial Flow Compressors*, 124

Rallis, C. J.: Mean temperature of burnt gases, 419

— *See* O'Donovan, K. H. and Rallis, C. J.

Rice, J. L.: *See* Westenberg, A. A. and Rice, J. L.

Rowe, R. D.: *See* Berlad, A. L., Rowe, R. D. and Yang, C. H.

Roy, B. N.: *See* Moore, N. P. W. and Roy, B. N.

Rudin, M. and Aroeste, H.: Deviation from chemical equilibrium in gas flow, 273

Scholte, T. G. and Vaags, P. B.: The burning velocity of hydrogen–air mixtures and mixtures of some hydrocarbons with air, 495

— — The influence of small quantities of hydrogen and hydrogen compounds on the burning velocity of carbon monoxide–air flames, 503

— — Burning velocities of mixtures of hydrogen, carbon monoxide and methane with air, 511

Schultz, R. D.: *See* Andersen, W. H., Bills, K. W., Mishuck, E., Moe, G. and Schultz, R. D.

Spalding, D. B.: review of *Fundamentals of Advanced Missiles*, 272
— and Yumlu, V. S.: Experimental demonstration of the existence of two flame speeds, 553

Thring, M. W.: *See* Beér, J. M., Thring, M. W. and Essenhigh, R. H.
— *See* Jayaraman, 'V., Hulse, C. and Thring, M. W.
— and Masdin, E. G.: The addition of air in stages to a perfectly stirred reactor, 125
Thurlow, G. G.: Similarity criteria for the study of furnace flames by means of cold models, 373
Todd, J. R.: *See* Allen, D. H., Garner, F. H., Long, R. and Todd, J. R.

Ubbelohde, A. R.: review of *Fast Reactions in Solids*, 123
Useller, James W.: Effect of combustor length on afterburner combustion, 339

Vaags, P. B.: *See* Scholte, T. G. and Vaags, P. B.
van Tiggelen, A.: *See* de Jaegere, S. and van Tiggelen, A.

Watson, H.: *See* Leah, A. Smeeton and Watson, H.
Weinberg, F. J.: *See* Levy, A. and Weinberg, F. J.
Westenberg, A. A. and Rice, J. L.: Further measurements of turbulence intensity in flame zones, 459
Williams, F. A.: Spray combustion theory, 215
— Theory of the burning of monopropellant droplets, 529
— Penner, S. S., Gill, G. and Eckel, E. F.: Heterogeneous burning in a diverging reactor, 355
Wilson, M. J. G.: review of *The Efficient Use of Fuel*, 418
Wright, F. H.: Bluff-body flame stabilization: blockage effects, 319

Yang, C. H.: *See* Berlad, A. L. and Yang, C. H.
— *See* Berlad, A. L., Rowe, R. D. and Yang, C. H.
Yumlu, V. S.: *See* Spalding, D. B. and Yumlu, V. S.

Zabetakis, M. G.: *See* Bartkowiak, A. Lambiris, S. and Zabetakis, M. G.
Zeldovich, J. B. and Barenblatt, G. I.: Theory of flame propagation, 61

Name Index

Aberdeen, S. G. 110
Acton Taylor, R. A. 416
Adams, G. K. 123, 199, 263
Adler, J. 389
Adler, L. B. 157, 481, 486, 493
Agnew, J. T. 438, 439, 442, 446
Agoston, G. A. 265, 544
Agroskin, A. A. 104
Alcock, J. F. 549
Allen, C. 77, 96
Allen, D. H. 75, 96
Anagnostou, Evelyn, 453
Andersen, W. H. 266, 285, 289, 299–301, 317
Anderson, D. A. 12
Anderson, H. C. 470, 475
Andrews, E. G. D. 406
Anson, D. 255, 353
Arden, E. A. 199
Armstrong, D. L. 317
Armstrong, E. B. 37
Aroeste, H. 275
Atzwanger, H. 147, 156
Babbitt, J. A. 435
Badami, J. S. 151, 156
Bagley, C. H. 268
Bahn, G. S. 265
Baker, H. D. 185, 186
Baldwin, R. R. 399, 435
Ballentyne, D. W. G. 123
Bame, J. L. 408
Barber, R. 409
Barenblatt, G. I. 61, 74
Barrère, M. 264, 529, 542–544
Barrère, S. 264
Barsh, M. K. 317
Barth-Wehrenalp, G. 147, 156
Bartkowiak, A. 347
Basu, S. 261
Batchelor, G. K. 461, 465
Bateman, W. 409
Bates, D. R. 14, 37
Bawn, C. E. H. 96
Beér, J. M. 560
Belles, F. E. 457
Belz, L. H. 470, 475

Bennet, W. J. 265
Berets, D. J. 165, 167, 493
Berlad, A. L. 265, 447, 457, 477, 480
Berz, I. 132
Betz, A. 337
Bigler, J. E. 435
Bills, K. W. 285, 289, 300, 301, 317
Bird, R. B. 228, 253, 544
Bjerklie, J. W. 265
Blackman, A. U. 434, 435
Blackshear, P. L. 465
Blanc, M. V. 457
Bone, W. A. 164, 167, 492
Botha, J. P. 145, 495, 501, 553
Bowden, F. P. 123
Boyer, M. H. 525, 527
Boys, S. F. 452
Bragg, S. L. 129
Brazil, R. J. 266
Brinkley, S. R., Jr. 161, 167, 263
Broer, L. J. F. 545
Broida, H. P. 39, 48, 283, 497, 501
Brown, A. T. 435
Brown, H. R. 475
Browning, J. A. 353
Bruschweiler, H. 96
Bulewicz, E. M. 48, 60
Bunte, K. 510
Burgess, D. S. 256, 442
Burgholz, R. 109
Burgoyne, J. H. 92, 96, 115, 226, 228, 252, 253, 353
Burke, E. 253
Burnham, H. 96

Caffo, E. 107
Calcote, H. F. 283, 284
Caldwell, F. R. 202, 214, 497, 501
Campbell, C. 4, 12, 167, 492
Campbell, D. E. 61, 74
Carslaw, H. S. 300
Cassel, H. M. 467
Chaiken, R. F. 266, 285
Chamberlain, G. H. H. 433, 435
Chapman, D. L. 167
Cheaney, D. E. 259
Clark, T. P. 105
Cohen, L. 226, 228, 353
Cohen, P. M. 429, 435
Cohen de Lara, G. 106
Cole, R. H. 161, 167
Conan, H. R. 201, 213
Condon, E. U. 15, 37
Constantinides, G. 474, 475
Cook, E. B. 437, 446
Cook, M. A. 122, 263, 264
Cook, W. P. 546
Corbett, P. F. 112
Cornell, W. G. 337
Corner, J. 452
Corney, N. S. 435
Corzilius, M. W. 435
Cosslett, V. E. 414
Coulson, C. A. 145
Courant, R. 391, 397
Crocco, L. 546
Croft, H. O. 96, 156
Crosby, J. K. 268
Crotty, W. W. 47, 59
Crumley, P. H. 112
Cullis, C. F. 86, 96, 119
Curtet, R. 106
Curtiss, C. F. 61, 74, 122, 228, 253, 452, 454
Cyphers, J. A. 59, 60, 510

Dalgarno, A. 37
Daniel, W. A. 435
Daniels, F. 285, 300, 301, 317
Darlington, M. E. 96
Das, M. N. 77, 96
David, W. T. 185, 186
Davidson, J. E. 119
Davidson, R. R. 96
Davies, D. A. 259
Davies, R. M. 465
Davis, A. 259
DeBell, A. G. 408
Deckers, J. 200
de Hartoulari, R. 398
de Jaegere, S. 187, 199, 200, 398
DeJuhasz, K. J. 258
Dekker, A. O. 285, 289, 300, 302, 317
Delbourg, P. 107
Dennis, W. R. 255
Denton, W. 96
Desty, D. H. 271
Ditchburn, R. W. 33, 38
Dixon, H. B. 510
Dixon, R. N. 38
Doherty, H. 96
Donald, M. 96
Donaldson, W. F. 256
Donner, O. 510
Donovan, T. M. 403
Dorfman, H. 12
Douglas, R. W. 550
Dover, J. J. 501
Dow, R. B. 272
Downs, D. 429, 433–435
Duff, R. E. 546
Dumanois, P. 167

Echols, L. S. 408
Eckel, E. F. 355, 371
Egbert, R. B. 170, 185

Egerton, Sir Alfred, 115, 252, 253, 264, 418, 428, 435, 554, 556
Ellis, H. B. 265, 270
El Wakil, M. M. 544
Emmons, H. 452
Engelbrecht, A. 147, 156
Enikolopyan, N. S. 114
Eschenbach, R. 438, 439, 442, 446
Essenhigh, R. H. 560
Estradère, S. 96
Ettinger, M. B. 77, 96
Evans, M. G. 258
Evans, M. W. 253
Eyring, H. 312, 317

Farmer, E. H. 90, 96
Fassell, W. M. 470, 475
Faunce, B. G. 199
Fay, J. A. 261, 493
Feast, M. W. 33, 38
Feder, A. 266
Fenimore, C. P. 48–50, 58–60, 144, 145
Ferguson, R. E. 283, 284
Ferrié, F. 492
Filler, A. S. 264
Fiock, E. F. 202, 214, 510
Flamm, L. 437, 444, 446
Flanders, H. E. 475
Foster, J. R. 337
Fowler, A. 151, 156
Foxwell, G. E. 418
Franck, J. 15, 37
Frank, C. E. 434, 435
Frank-Kamenetsky, D. A. 62, 74, 115, 253
Fraser, P. A. 13–15, 37, 38, 276
Fraser, R. P. 164, 167, 492
Freeman, E. S. 10, 12
Freiwald, H. 492
Friauf, J. B. 165, 167
Friebertshauser, P. E. 525, 527
Friedman, R. 59, 60, 117, 253, 260, 299, 300, 457, 480, 510, 546
Fristrom, R. M. 253
Fuhs, A. E. 405

Garner, F. H. 75, 94, 96, 497, 501
Garner, W. E. 169, 185
Garton, W. R. S. 38
Gaydon, A. G. 13, 37–39, 41, 48, 60, 123, 149, 156, 283, 417, 418, 457, 526, 527
Geckler, R. D. 317
Gey, W. A. 263
Gibson, H. J. 407
Gilbert, M. 446, 544
Gilchrist, B. 167
Gill, G. 355, 371
Ginell, R. 287, 300
Givens, J. W. 546
Glass, I. I. 545
Gniewek, T. 160, 163, 166, 167
Godrich, J. 185
Godridge, A. M. 112, 388
Goldsmith, M. 544
Gordon, A. S. 39, 48, 266
Gordon, B. 77, 96
Gordon, S. 3, 4, 10, 12, 161, 167, 275, 457
Gordon, W. E. 167, 493
Goulding, Miss D. 37
Gouy, M. 156
Gray, F. A. 388, 412
Gray, J. A. 188, 190, 199
Gray, P. 199, 200, 399, 544
Graziotti, R. 399
Green, L., Jr. 260, 300
Greene, E. F. 165, 167, 493
Greenwald, H. P. 475
Gross, D. 401
Grover, J. 96
Grünewald, K. 475
Grumer, J. 256, 437, 446, 457
Grunfelder, C. 465
Gubergrits, M. Y. 104
Guedeney, F. 41, 48, 60
Guenault, E. M. 283, 284
Guénebault, H. 398
Guest, P. G. 457
Gulbransen, E. A. 467, 475

Hall, A. R. 199, 200
Hall, J. G. 545
Halpern, C. 59, 60
Harding, A. J. 253
Harris, E. 457
Hartmann, I. 467, 474, 475, 510
Hayner, C. L. 317
Heddle, D. W. O. 33, 38
Henderson, E. 167
Henderson, G. P. 37
Herbert, M. V. 130
Herzberg, G. 37
Hilbert, D. 391, 397
Hinshelwood, Sir Cyril N. 86, 96, 418
Hirschfelder, J. O. 61, 74, 122, 228, 253, 452, 544
Hirsh, H. 115
Hoare, D. E. 259
Hoare, M. F. 201, 213
Hobaica, E. C. 167, 481
Hogan, Virginia D. 3, 4, 12
Hogg, A. 388
Holden, C. 388, 552
Holliday, J. B. 129
Honda, K. 283, 284
Hoot, W. F. 92, 96

Hopfield, H. S. 48
Horlock, J. H. 124
Horn, G. 388
Hornbeck, G. A. 39, 48
Hottel, H. C. 170, 185, 465
Howe, H. 112
Hoy, H. R. 111
Huebler, J. 167
Huff, V. N. 161, 167, 275, 457
Hulse, C. 97, 387
Hush, N. S. 258
Husson, M. 107
Hutchisson, E. 15, 37

Isoda, H. 544

Jack, H. R. S. 185
Jacobson, M. 475
Jaeger, J. C. 300
Jahn, G. 156, 510
James, C. G. 48, 60
James, H. 119
Jarmain, W. R. 13, 15, 37, 38, 276
Jayaraman, V. 97
Jeans, J. 253
Jellinek, H. H. G. 317
Jennissen, J. 345
John, R. R. 264
Johnson, C. A. 160, 163, 166, 167
Johnston, W. C. 480
Johnstone, R. E. 388
Jonash, E. R. 546
Jones, A. G. 416
Jones, G. W. 48–50, 59, 60, 144, 145, 435
Jones, H. 402
Jones, L. 96
Jones, R. A. 60
Jones, W. Idris. 132
Jost, W. 96, 156
Jouguet, E. 167
Joyce, J. R. 410

Kandiner, H. J. 161, 167
Karlovitz, B. 263
Kaskan, W. E. 39, 48, 49, 59, 60, 145
Kaufman, F. 40, 48
Kear, R. W. 255
Kennedy, R. E. 353, 435
Keyes, R. J. 264
Khitrin, L. N. 113
Kiley, D. W. 529, 544
Kinbara, T. 283, 284
King, C. R. 346
King, H. K. 510
King, R. O. 96
Kirkby, W. A. 120, 262, 413, 552
Kissel, M. 106
Kistiakowsky, G. B. 164, 165, 167, 491, 493
Klibanov, T. M. 253
Knight, H. T. 546
Knipe, R. H. 39, 48
Knox, J. H. 258
Kobe, K. A. 92, 96
Kolmogorov, A. N. 74
Kondrat'yev, V. N. 416
Konschak, M. 167
Kozlov, G. I. 114
Krall, G. W. 353
Kriebel, R. 96
Kubala, T. A. 437
Kuesiner, A. 268
Kumagai, S. 544
Kydd, P. H. 133

Ladenburg, R. V. 457
Laffitte, P. 119, 167, 399, 490, 492
Lambiris, S. 347
Landau, L. 404
Lane, W. H. 96
Laserson, G. L. 185, 186
Lawrence, H. L. 96
Lawrence, R. W. 317
Lawton, H. 122
Layzer, D. 452
Leah, A. S. 169, 185
Lee, J. C. 399
Lekawa, E. 493
Lenihan, J. M. A. 414
Letort, M. 86, 96
Levine, R. S. 265
Levy, A. 229, 253
Lewis, B. 42, 48, 52, 60, 62, 74, 131, 132, 145, 156, 165, 167, 202, 203, 214, 263, 418, 446, 457
Liebman, I. 467
Ligett, W. B. 407
Linden-Bell, D. 385
Linnett, J. W. 156, 201, 213, 501
Lintin, D. R. 401
Lishka, R. J. 77, 96
Litchfield, E. L. 442, 475
Litterscheidt, W. 510
Littler, W. B. 167
Lloyd, P. 271
Lodwig, R. M. 147
Loeb, L. B. 284
Loison, M. 106
Long, R. 75, 94, 96, 497, 501
Long, V. D. 413
Longwell, J. P. 129, 253
Lorell, J. 529, 544
Lubny-Gertsyk, A. L. 118
Luker, J. A. 157, 160, 163, 166, 167, 481, 486, 493

McDonald, G. 510
McGill, P. L. 161, 167
McGowan, I. R. 95, 96
Mache, H. 437, 444, 446
McInerney, M. J. 412
McLane, C. K. 544
Magee, E. M. 256
Maklakov, A. I. 105
Makovky, A. 199
Malcor, M. 106
Malherbe, F. E. 93, 96
Malinowski, A. E. 404
Malmberg, E. W. 435
Manson, N. 492
Manton, J. 214, 446
Marble, F. E. 319, 337
Mardles, E. W. J. 92, 96
Margrave, J. L. 147, 156
Marr, G. V. 37, 38
Martin, F. J. 115
Marvin, C. F. 202, 214
Marx, E. 145
Masdin, E. G. 129
Mason, J. M. 427, 434
Mason, W. H. 353
Masterman, D. M. A. 406
Mattocks, G. R. 412
Matton, G. 325, 337
Mauss, F. 77, 96
Mayers, M. A. 255
Mayor, L. 399
Meachen, D. 409
Menkes, J. 395, 397
Merk, H. J. 254
Mertens, J. 525, 527
Meyers, P. S. 544
Miller, E. 199
Milliken, B. B. 446
Minkoff, G. J. 96, 272, 417
Mishuck, E. 285, 289, 300, 301, 317
Moberg, D. A. 269
Moe, G. 285, 289, 300, 301, 317
Mooradian, A. J. 167, 493
Moore, G. E. 49, 145
Moore, N. P. W. 421, 434, 435
Morrell, V. C. 457
Morrell, V. E. 161, 167, 275
Morris, H. E. 75, 96
Mottram, A. W. T. 406
Moutet, H. 529, 542, 544
Mulcahy, M. F. R. 86, 96
Mullaney, G. J. 105
Mulliken, R. S. 38
Mullins, B. P. 129, 541, 544
Murray, W. L. 413
Myerson, A. L. 199

Nagel, A. 446
Nagy, J. 475
Nakamura, J. 277, 283, 284
Neugebauer, C. A. 147, 156
Newby, M. P. 373, 387, 412
Newitt, D. M. 92, 96, 252, 435
Nicholls, R. W. 13, 37, 38, 276
Niclause, M. 86, 96
Nolan, W. J. 12
Norrish, R. G. W. 115, 119, 253
Nugent, G. G. 299, 300
Nugent, R. G. 117, 253

Oberdorfer, R. 433, 435
O'Brien, C. J. 268
O'Donovan, K. H. 201
Oldenberg, O. 56, 60
Oppenheim, A. K. 167, 262
Osborn, J. R. 545

Pabst, G. 526
Pack, D. C. 263
Pack, D. H. 263
Padovani, C. 107
Pahnke, A. J. 429, 435
Pannetier, G. 149, 156, 398
Parker, W. G. 199
Parlin, R. B. 312, 317
Passauer, H. 510
Payman, W. 492
Payne, K. G. 404
Pearce, K. W. 405
Pearse, R. W. B. 38, 156
Pease, R. N. 457
Penner, S. S. 74, 228, 275, 285, 300, 301, 317, 355, 371, 452, 543, 544
Perrin, J. R. 268
Perrine, J. 268
Peters, E. D. 96
Petersohn, E. 337
Phillips, J. G. 38
Pickering, H. S. 201, 213
Pietrovski, I. G. 74
Pignèguy, J. H. 434
Pilkington, S. 412
Piskunov, N. S. 74
Plumb, G. R. 92, 96
Pollard, F. H. 169, 185
Polyakov, M. V. 253
Pomerantsev, V. V. 253
Potter, A. E., Jr. 453, 457, 480
Potter, E. B. V. 406
Potter, J. H. 510
Potter, R. L. 492, 525, 527
Poulston, B. V. 410
Powling, J. 199, 253
Pratt, M. W. T. 190, 199
Price, E. W. 267
Price, T. W. 510

Protheroe, J. 259
Putnam, A. A. 255

Rabin, E. 269
Railey, J. W. 124
Rallis, C. J. 201, 420
Reck, J. 253
Reed, L. E. 109
Reid, R. C. 95, 96, 434, 435
Rice, J. L. 459
Rice, O. K. 287, 300
Richardson, J. M. 72, 74
Richmond, J. K. 256
Rieke, F. F. 56, 60
Rifkin, E. B. 427, 434
Rigg, M. W. 265
Rimarski, W. 167
Rimmer, W. B. 151, 156
Rink, J. P. 546
Rivière, M. 106
Roberts, A. G. 111
Robertson, A. D. 388, 412
Robertson, A. F. 401
Robinson, D. 38
Robinson, Sir Robert, 547
Roeder, C. H. 202, 214
Roselaar, L. C. 119
Rosen, B. 38
Rosen, B. H. 353
Rosen, J. B. 72, 74, 450
Rosenthal, D. 300, 452
Roshko, A. 337
Ross, J. 77, 96
Rosser, W. A. 295, 300, 529, 542, 544
Rossini, F. D. 253
Rotherham, L. 414
Rounthwaite, C. 171, 185
Rowe, R. D. 477
Roy, B. N. 421, 434
Rudin, M. 275
Ruegg, F. W. 59, 60
Rumbel, K. E. 299, 300
Rushhoft, C. C. 77, 96

Sänger, E. 118
Sandri, R. 120
Sarjant, R. J. 418
Sasiadek, M. 262
Sato, K. 268
Satterfield, C. N. 95, 96, 434, 435, 544
Scarborough, J. B. 161, 167
Scholte, T. G. 495, 503, 510, 511, 524
Schrivener, J. 199
Schryver, S. B. 76, 96
Schultz, R. D. 285, 289, 299–302, 317
Schumb, W. C. 544
Scurlock, A. C. 299, 300, 465
Seitz, F. 475
Semenov, N. N. 115, 544
Seltzer, H. J. 199
Shapiro, I. 268
Shepherd, W. C. F. 493
Siddall, R. G. 388
Silletto, G. P. 300, 317
Simmons, F. S. 408
Simon, D. M. 457
Simonis, E. A. 400
Simons, R. F. 435
Singer, J. M. 257, 446
Skidmore, I. C. 122
Skirrow, G. 116
Skull, A. 406
Slootmaekers, P. J. 200
Smith, A. F. 353
Smith, D. 446
Smith, F. L. 428, 435
Smith, F. W. 475
Smith, J. B. 167
Smith, M. L. 435
Smith, R. F. 258
Smith, S. R. 266
Smith, W. A. W. 199
Solovyeva, L. S. 113
Spakowski, A. E. 457
Spalding, D. B. 65, 74, 130, 145, 244, 253, 272, 389, 396, 397, 452, 495, 501, 544, 556
Spolan, I. 353, 435
Sprake, C. H. 406
Starkman, E. S. 265
Stern, R. A. 262
Stiles, R. B. 96
Stocks, G. W. 199
Stops, D. W. 253
Strasser, A. 199
Street, J. C. 433, 435
Sturgis, B. M. 429, 435
Style, P. W. G. 188, 199
Sugden, T. M. 48, 60
Sumi, K. 253
Summerfield, M. 264
Sunavala, P. D. 387
Sundralingham, A. 90, 96

Tamura, Z. 257, 258
Tanasawa, Y. 257, 258
Tang, T. L. 92, 96
Taylor, F. R. 199
Taylor, H. S. 457
Taylor, J. 300, 317, 414
Temple, R. G. 94, 96
Tesima, T. 257
Therneau, G. M. 317
Thring, M. W. 97, 129, 373, 387, 388, 560
Thabet, S. K. 115, 253, 554, 556
Thomas, A. 353
Thorley, B. 497, 501
Thornes, L. S. 435

Thornhill, D. W. 414
Thurlow, G. G. 112, 373, 388, 409
Tipper, C. F. H. 95, 96, 116
Tissander, M. 106
Todd, J. R. 75
Townsend, A. A. 461, 465
Toyoda, S. 257
Traube, M. 510
Trotman-Dickenson, A. F. 258
Trotsenko, M. A. 253
Tully, C. 385
Turin, J. J. 167
Turner, R. G. 38
Tyler, T. L. 353
Tyrrell, A. E. 110
Tyson, G. N., Jr. 268

Ubbelohde, A. R. J. P. 123, 264, 428, 435
Ubbelohde, L. 510
Ude, H. 492
Uri, N. 258
Useller, James W. 339
Uyehara, O. A. 544

Vaags, P. B. 495, 503, 510, 511, 524
Vaidya, W. M. 156
van de Poll, A. N. J. 496, 501
van der Wal, B. 96
van Langen, J. M. 410
van Leeuwen, H. B. 96
Vanpee, M. M. 261
van Tiggelen, A. 187, 199, 200, 398
van Wonterghem, J. 199, 200
Venable, D. 546
Vick, F. A. 414
Violett, T. D. 199
von Elbe, G. 42, 48, 52, 60, 62, 74, 96, 131, 132, 145, 156, 202, 203, 214, 446, 457
von Kármán, T. 64, 74, 452, 544
Vortmeyer, D. 402

Wagner, C. 403, 475
Wagner, C. D. 76, 96
Walcutt, C. 427, 434
Walker, L. E. Q. 123
Walker, P. L. 510
Walker, R. E. 462
Walsh, A. D. 93, 96, 259, 429, 433, 435
Wallace, L. V. 38
Wallis, J. 112, 388
Walton, R. G., Jr. 475
Warren, T. W. 407
Watermeier, L. A. 446, 510
Watson, H. 169, 186
Watts, R. 549
Wayman, D. H. 492
Wear, J. D. 546
Webber, W. T. 269
Weinberg, F. J. 229, 253, 404
Weiss, M. A. 129, 253
Wentworth, J. T. 435
Wentworth, R. L. 544
Westenberg, A. A. 253, 459, 462, 465
Westerdijk, T. 496, 501
Westgren, H. 475
Wharton, W. W. 199
Wheatley, P. J. 201, 213
Wheeler, R. V. 283, 284
Wheeler, R. W. 429, 433, 435
Wheeler, W. H. 164, 167
White, A. G. 156, 253
White, D. R. 115, 167
Whittaker, A. G. 403
Whitworth, C. 167
Wibaut, J. P. 76, 96
Wicke, E. 402
Widmaier, O. 76, 77, 96
Wilfong, R. E. 285, 300, 301, 317
Wilkins, D. M. 111
Williams, F. A. 215, 228, 355, 362, 371, 529, 544
Williams, G. C. 465
Williams, H. 261, 403
Wilson, D. S. 112
Wilson, J. S. 552
Wilson, M. J. G. 418
Wilson, R. E. 95, 96
Winkler, C. A. 60
Wise, H. 295, 300, 529, 544
Wolfhard, H. G. 13, 37, 199, 200, 261, 457
Wood, B. J. 544
Wooding, E. R. 401
Wopat, F. 96
Wright, C. C. 510
Wright, F. H. 319
Wyller, A. 38

Yang, C. H. 263, 447, 477
Yoffe, A. D. 123
Yumlu, V. S. 556
Yust, V. E. 408

Zabetakis, M. G. 259, 347, 353
Zeldovich, Y. B. 61, 74, 115
Zueva, N. M. 65
Zucrow, M. J. 271, 545
Zukoski, E. E. 265, 319, 337